Centrifugal and Axial Flow Pumps

2nd
Edition

Centrifugal and Axial Flow Pumps

THEORY, DESIGN, AND APPLICATION

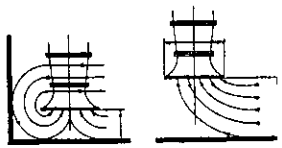

A. J. Stepanoff, Ph.D.
Melville Medalist, A.S.M.E.
Ingersoll-Rand Company

JOHN WILEY & SONS, INC.
New York • Chichester • Brisbane • Toronto

New York · London · Sydney

20 19 18 17 16 15 14

ISBN 0 471 82137 3

Library of Congress Catalog Card Number: 57–10815

Printed in the United States of America

Preface

Since publication of the first edition of this book, the application centrifugal pumps has been extended to new fields. At the same ti the ranges of head per stage, total pressure, temperature, speed, and s have moved to new high levels. This advancement presented n problems—hydraulic, mechanical, metallurgical, and manufacturing. considerable progress was achieved during the same period in the th retical aspects and design procedure based on a better understanding the flow processes through the parts comprising a centrifugal pun Thus a new edition of this book at this time seemed well justified.

The theoretical treatment of the impeller action and casing perfor ance and the method of presenting experimental information as used the first edition have been retained. These have withstood the test time very well. At the same time a successful application of the sa technique to the field of turboblowers in the last decade has furnish added assurance of the soundness of such methods of attack. A numb of new topics dealing with theory, design, and application are include On the other hand, a number of articles were eliminated or condens to save space.

The major changes and additions are listed below:

A new chapter, "Water-Hammer Problems in Centrifugal Pun Systems," has been added. With pump sizes and speeds increased, it impossible for a pump designer or application engineer to escape wat hammer problems. This chapter will serve as an introduction to t subject. Chapter 18, dealing with centrifugal-jet pump systems, h been expanded and rewritten to a great extent. This chapter has broug forth more comments from the readers than any other chapter. T majority of illustrations in Chapters 16 and 17 were replaced with ne ones. The problem of the shut-off head for axial and mixed flow ir peller pumps is expanded in light of new experimental evidence. Pri ciples of suction sump design for vertical propeller pumps are extende A new viscosity correction chart is introduced in Chapter 14 covering wider range of pump types. New complete characteristics of mixed flo and axial pumps are included in Chapter 13. Also a brief account of t progress in water storage pumps is given in the same chapter. A therm

cavitation criterion is introduced in Chapter 12 to correlate pump behavior with respect to cavitation when pumping liquids of different physical and thermal properties. New charts are given in Chapter 9 relating to impeller design for any discharge angle. At the same time a procedure is established to select the casing design elements to suit impellers. An improved method of the inlet velocity triangle construction is offered in Chapter 5.

A great number of minor improvements and refinements will be found throughout the book. Old chapter numbering and titles were retained for easy reference of readers familiar with the first edition. The first edition of this book has been translated into Japanese and arrangements are in progress to translate the second edition into German.

I am indebted to Ingersoll-Rand Company, Mr. R. H. Johnson, President, and to Mr. Hanns Hornschuch, Engineer-in-charge, Blower and Pump Engineering Department, whose support made this volume possible. Professor A. Hollander of the California Institute of Technology and Mr. H. A. Stahl of Ingersoll-Rand Company have furnished numerous corrections and helpful suggestions.

Although great care has been exercised to check the manuscript and proofs, errors may be discovered. I shall appreciate it if these are called to my attention. I also invite criticism of the views presented in the book or suggestions which may lead to its improvement.

A. J. S.

Phillipsburg, N. J.
April, 1957

Contents

Chapter 1

Selected Topics from Hydraulics

A theoretical treatment of the flow through hydraulic machines is very difficult because most of the channels comprising such machines have variable and irregular sections and a curved mean path. Some of the channels are in a circular motion with power applied to or taken from the flow. Simple relationships established in hydraulics for idealized conditions, if applied directly to such flow, may not only give an incorrect quantitative answer but may also result in a false qualitative mental pattern of flow.

An oversimplified view of some of the flow problems in hydraulics has, in the past, resulted in a number of fallacies which still persist although there is ample experimental evidence to prove the erroneous reasoning behind such views.

In this chapter a number of subjects are treated which are either missing or not sufficiently emphasized in books on hydraulics. In several instances limitations of principles established in hydraulics, when applied to conditions of flow as found in centrifugal pumps, are stressed. A few of the most common fallacies are clarified.

1.1 BERNOULLI'S EQUATION

When Bernoulli's equation is applied to the flow through various parts of hydraulic machines its limitations are frequently overlooked. Bernoulli's equation,

$$h + \frac{p}{\gamma} + \frac{v^2}{2g} = E = \text{constant} \tag{1.1}$$

represents the energy per unit of weight where h is the energy of position (or ability to do work when situated h feet above the arbitrary datum plane), p/γ is the pressure energy, and $v^2/2g$ is the kinetic energy, or velocity head. All three are expressed in feet. The quantity E is the total energy in foot-pounds per pound of liquid. It does not depend on the specific weight of the liquid, γ. When applied to two points of the same tube, Bernoulli's equation expresses the law of conservation

of energy for an *idealized* liquid. In actual liquids, variations of E between different streamlines occur and changes of the value of E may be produced by the action of viscosity. The following paragraphs deal with the limitations caused by actual liquids.

(*a*) Equation 1.1 is obtained from the power equation

$$Q\gamma h + Qp + Q\gamma \frac{v^2}{2g} = \text{constant} \tag{1.2}$$

by eliminating Q (volume per unit time) and γ (specific weight of the liquid).

Elimination of Q from equation 1.2, when applied to two points of the same stream tube, requires that continuity of volume be satisfied. This means that in a closed conduit no liquid escapes or is added between the two points. *Therefore, when Bernoulli's equation is applied to imaginary stream tubes or streamlines, this continuity requirement makes it necessary that the two points of comparison lie on the same streamline because the constant in Bernoulli's equation is not necessarily the same for different streamlines;* as, for example, in straight pipe flow the total energy carried by streamlines near the center of the pipe is greater than that at any point in the pipe section.

(*b*) Elimination of γ from equation 1.2 is possible only if γ is constant at all points of the flow. *This means that the liquid must be incompressible.* It is not sufficient that the product $Q\gamma$ be constant, because this product represents the weight of the liquid which is constant for gases. Bernoulli's equation, as given in equation 1.1, does not apply for gases because it does not include thermodynamic changes which take place in flowing gas. From the above it follows that *Bernoulli's equation cannot be used in cases where the gases are liberated or absorbed along the flow path, as either process involves an energy change.*

(*c*) A *streamline* is defined as the path of the liquid particle made up of prevailing flow direction from point to point. A fluid is in steady motion when its streamlines permanently maintain their position and relative arrangement and velocities at each point on the streamline are the same. *Bernoulli's equation applies only to a steady flow.*

(*d*) *Bernoulli's equation applies only to an "absolute" flow. In relative flow in a moving channel,* depending on the form of the channel and the nature of its motion, *energy is either applied to or absorbed from the flow.* Thus the constant in Bernoulli's equation varies along the streamline and from one streamline to another.

(*e*) *With actual liquids, Bernoulli's equation is not applicable to curvilinear motion* because inertia forces come into play and centrifugal forces are developed. Streamlines do not maintain their relative positions; secondary cross flows appear; and the liquid may leave the walls of the channel.

(*f*) *Even when applied to the average flow of the whole channel, Bernoulli's equation is invalid if the conduit contains bends and turns, or is in motion, because local pressures and velocities (as measured at two points) may differ greatly from the average values for the whole flow.* Besides, the velocity head in Bernoulli's equation based on mean velocity does not represent the true kinetic energy of the flow which is equal to a summation of the kinetic energy of individual streamlines [1] and

$$\frac{v_m^2}{2g} < \Sigma \frac{v^2}{2g}$$

This expression means that the square of the mean is smaller than the mean of the squares. This can be verified easily by a numerical example.

1.2 REYNOLDS NUMBER

Reynolds number $R = vd/\nu$, where v is the velocity, d the diameter of pipe, and ν the kinematic viscosity of liquid, is used as a criterion of the flow in closed conduits. The type of flow (laminar or turbulent) and the velocity distribution are similar for geometrically similar tubular sections, and the same friction coefficient f can be used in Darcy's formula

$$h = f \frac{L}{d} \frac{v^2}{2g}$$

if the Reynolds number is the same irrespective of the nature of the fluid or actual velocity or pipe size. A considerable amount of data on friction losses for round pipes has been accumulated and correlated with Reynolds number as a basis. Evaluation of the pipe roughness is the only factor which makes the results uncertain to within ± 10 per cent.

(*a*) **Hydraulic Radius.** For conduits other than circular, it has been customary to use the hydraulic radius m = area/wetted perimeter, and to select the friction coefficient from round pipe data for $d = 4m$, the existence of similarity of flow pattern under such conditions being assumed. *There is no theoretical justification for such an assumption because geometrical similarity is the first prerequisite for similarity of flow.* Thus, for laminar flow it has been shown theoretically and proved experimentally that the friction coefficient for a rectangular channel

section depends on the shape of the channel and is different from that for a round pipe.[2]

$$f = \frac{64}{R} \qquad \text{for a round pipe}$$

$$f = 0.89\,\frac{64}{R} \qquad \text{for a square channel}$$

$$f = 1.5\,\frac{64}{R} \qquad \text{for an annulus, or two flat plates}$$

Schiller [2] investigated the flow through conduits of different sections—round, square, rectangular, triangular, and star-shaped—and found that the coefficients of friction f, plotted on the basis of $d = 4m$, do not coincide with those for round pipe. In the turbulent region the difference is not great and, for lack of better means, round pipe data may be used for flow in channels of other shape as an approximation, although the theoretical justification of such procedure is lacking.

(*b*) **Curvilinear Flow and Channels of Variable Cross Section.** *Anything that disturbs the velocity distribution of flow, such as a change in area or direction of flow, changes the pattern of flow through a conduit, and the Reynolds number based on the average velocity of steady flow ceases to be a criterion of the flow in the sense that it is used for straight pipe flow.* That is to say, the same Reynolds number is no assurance of similarity of flow because the change from laminar to turbulent flow may take place at vastly different Reynolds numbers when the pipe axis is not straight.[3] There is no way to estimate the friction coefficient f for such a flow; in fact, in some cases determination of the exact channel length or sectional area is impossible (example: impeller and volute channels). Moreover, the skin friction loss becomes secondary to additional eddy losses incurred by the disturbing element. The eddy losses follow laws different from those followed by friction losses. In a straight pipe flow a length of 20 to 40 pipe diameters (or even more according to some investigators) is necessary for the flow to assume its final velocity distribution. No such length is available in the channels comprising a centrifugal pump. Most of these are of irregular section, mostly divergent, some are stationary, and others are in rotary motion. There are a number of Reynolds numbers that can be assigned to a given pump, depending on what channel and which section of a given channel are taken for calculation of velocity and characteristic length for the Reynolds number. Each of many possible Reynolds numbers, if used as a criterion of operation of a given type of pump, will reflect the summary effect of all channels comprising a pump. Properties of such criteria

have never been determined and are different from those established for a straight pipe flow. Fortunately, in a modern pump, hydraulic friction losses are but a small fraction of the pump power input and affect little the laws of similarity governing the head generation which are the basis of the pump design. For that reason the dearth of accurate information about hydraulic losses in centrifugal pumps has not retarded appreciably the progress in their design.

To summarize, it can be stated that the velocity distribution, the loss of head (friction and eddy losses), and the pattern of flow (laminar or turbulent) cannot be established from the knowledge of Reynolds number in curvilinear, divergent, or convergent flow. For some types of flow there is no generally accepted definition of Reynolds [1] number for others, properties of Reynolds number have never been determined in a sense commonly used for the straight pipe flow.

(*c*) **Convergent and Divergent Channels.** Figure 1.1 is reproduced from Nikuradse's work [4] to show the effect of channel section variation

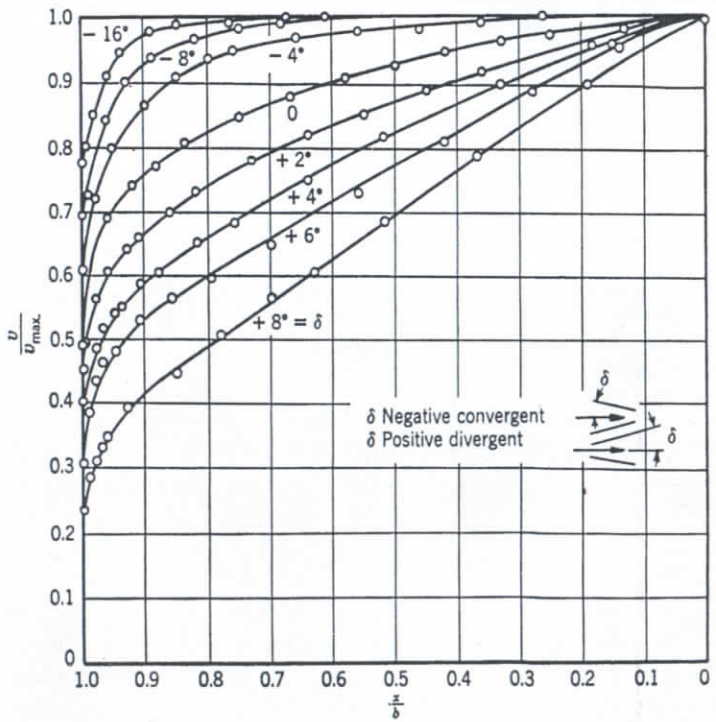

FIG. 1.1. Velocity distribution in convergent and divergent rectangular channels b is one half of channel width, x is location of the point from the axis of the channel (Nikuradse [4]).

on the velocity distribution. The most uniform velocity across the channel is obtained in a convergent channel. The beneficial effect of convergent flow is made use of in designing impeller approach channels for the purpose of producing uniform velocity distribution. The author has found that a reducing suction elbow is just as efficient as a straight taper, an indication that the bad effect of an elbow on the velocity distribution is fully neutralized by the steadying effect of a convergent channel.

1.3 FLOW THROUGH ELBOWS AND BENDS

(a) Velocity and Pressure Distribution. The majority of investigations on flow through pipe bends and elbows were concerned with the losses of pressure through these parts. A theoretical pattern of flow, vr = constant (where v is the velocity of a streamline and r is the radius of curvature of its path), was generally assumed. However, more recent studies [5] have shown that such a pattern of flow exists only at very low velocities or where the ratio of the mean radius of curvature to the pipe diameters, r/d, is very large. At high velocities, or low values of r/d, the flow shifts toward the outer wall of the elbow in the second half of the turn (Figs. 1.2 and 1.3). With ideal liquids a change in the velocity distribution is followed by a change in pressure distribution in such a manner that an increase in velocities near the inner walls is accompanied by a pressure drop, and a reduction in velocities at the outer wall of the turn is followed by a pressure increase. Such a velocity and pressure distribution begins to appear in the approach to the turn with low velocities and high r/d ratio.

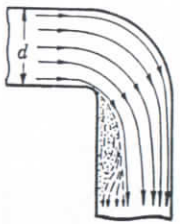

FIG. 1.2. Direction of streamlines in an elbow (Nippert [5]).

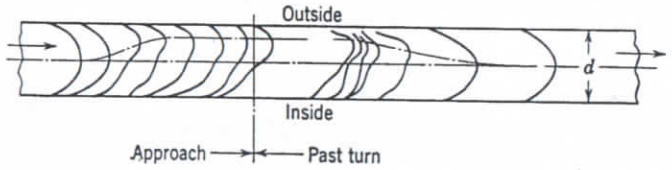

FIG. 1.3. Velocity distribution in an elbow; developed (Nippert [5]).

In high velocities and sharp turns, although high velocities shift toward the outer wall, the pressure distribution is affected little by this change, and *the maximum velocity and pressure both exist at the outer wall of the bend.* The low pressure zone extends somewhat downstream, resulting in a separation of flow from the inner wall and the formation of

pockets filled with eddies (Figs. 1.4 and 1.5). Such behavior of liquid in a turn is caused by inertia of the flowing mass or centrifugal forces. In addition, two spiral cross-flow motions appear in the stream which are directed, in the middle, toward the outer wall of the turn and along the side walls of the pipe, toward the inner wall of the turn (Fig. 1.6).

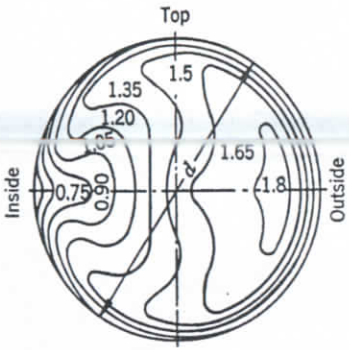

FIG. 1.4. Velocity distribution in the middle of an elbow; velocities in meters per second (Nippert [5]).

Yarnell [6] has obtained a similar velocity and pressure distribution experimenting with a standard 6-in. elbow. High pressures and velocities were observed at the outer wall by the end of the 90° turn, whereas at the beginning of the turn high velocities and low pressures occur at the inner wall of the elbow. Five feet beyond the turn pressures are equalized, but it takes up to 10 ft to restore the normal pipe velocity distribution.

Adler [7] observed higher velocities and pressures near the outer wall of the turn for laminar flow, very large radii of curvature r/d (25, 50, and 100), and Reynolds numbers 1930 to 3220. The critical values of

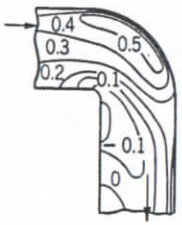

FIG. 1.5. Pressure distribution in an elbow. Pressures shown are in meters of water (Nippert [5]).

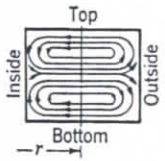

FIG. 1.6. Diagram of spiral cross flows in an elbow.

velocities or ratio of r/d at which the theoretical velocity and pressure distribution is destroyed were not definitely established.

In centrifugal pumps, all passages in the impeller and casing are curvilinear and velocities are high. Therefore a theoretical velocity and pressure distribution is hardly ever encountered.

(*b*) **Several Turns in Series.** When the flow of liquid follows several turns in succession in the same direction, which are located in different planes as shown in Fig. 1.7, the liquid acquires a spiral motion which is superimposed on its forward velocity.[8] Such motion does not cause any additional losses in a channel with a circular cross section; in fact, it has a definite tendency to stabilize the flow. However, if the channel is square or rectangular, losses of head result because of excessive eddies in the corners. In multistage centrifugal pumps of the volute type, such a succession of turns is found in the crossover passages from stage to stage. Round sections for the major portion of the crossovers should be used to reduce the losses.

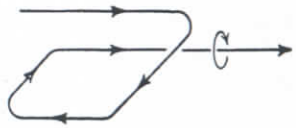

FIG. 1.7. Several elbows in series induce vortex motion.

1.4 ENERGY GRADIENT

To start and maintain flow in a channel, stationary or moving, there must be a drop in total energy content in the direction of flow below its initial level at zero flow. The graphical representation of the total energy along the path of flow is the energy gradient. This should be distinguished from the hydraulic gradient, which shows only static pressures at different points of the path (Fig. 1.8). The hydraulic gradient may have a local drop and rise along the path, but the energy gradient drops continually and it determines the direction of flow. In actual pipe flow the energy gradient drop represents hydraulic losses along the flow path.

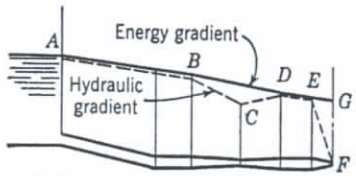

FIG. 1.8. Energy and hydraulic gradients.

An idealized flow can be imagined to be produced by hydraulic (or pressure) gradient drop with the energy content remaining constant; for instance, the discharge from a vessel through a nozzle. But in every case where real liquids are concerned the process will follow the direction indicated by the energy gradient drop.

The presence of a pump in a system of conduits produces a jump in the energy gradient, but the flow is still maintained by the energy gradient drop ahead of the pump, through the pump, and beyond the pump. *In a movable channel, such as an impeller of a pump, the energy gradient drop is referred to the energy level when there is no flow.* When the flow starts, energy is absorbed by the flow at such a rate that the total energy remains, at all times and at all points, below its zero flow level. The use of the energy gradient concept simplifies a number of problems connected with the flow through a pump and will be elaborated further in later chapters (Figs. 1.9, 1.11; Fig. 7.11).

1.5 TRANSITION OF PRESSURE IN LIQUID IN MOTION

In a stationary body of liquid, pressure intensity is transmitted equally in all directions. In moving liquids, a difference in pressure may exist along the path of the flow and also across the section of the channel as a result of the dynamic forces developed by the flow. Pressure changes along the path of flow are a result of a change in kinetic energy as given by Bernoulli's equation, the total energy of each streamline remaining constant.

Variation of pressure across a channel, however, can occur in such a manner that some streamlines will increase their pressure without decreasing their velocities, thus increasing their total energy, or the constant in Bernoulli's equation. But, since the total energy of the flow across the channel section remains the same, such an increase of pressure energy of one group of streamlines takes place at the expense of the pressure energy of the remaining streamlines. When the transition of pressure energy takes place in this manner without actual mixing of streamlines, pressure energy exchange might be called "conduction" by analogy to heat conduction. Both pressure energy and heat energy are due to molecular kinetic energy and are interchangeable, as is well known in thermodynamics of gases.

When the pressure energy exchange is effected by shifting or mixing of streamlines the process is similar to convection. There is still another mode of pressure transition which takes place without exchange of particles or mixing of streamlines, and that is by means of traveling pressure waves. Pressure waves follow all water-hammer phenomena and are treated in the extensive literature on the subject.

The flow of pressure energy from a higher to a lower level takes place naturally like heat flow from a higher to a lower temperature, whereas the flow of pressure energy in the reverse direction usually takes place under the dynamic forces developed in a curvilinear or rotary motion. As soon as the tangential component of the velocity is taken out of the flow by special means, such as guide vanes or a straight length of pipe, pressures are immediately equalized by a natural flow of the pressure energy from a higher to a lower level without mixing of the streamlines. Conduction is responsible for the constant pressure across the section of a channel with a steady flow assumed in hydraulics. Examples of conduction and convection of pressure energy follow. Figure 1.9

shows a straight pipe approach to an impeller of a centrifugal pump. At the section AB, sufficiently removed from the pump, pressure p_1 is uniform across the section and a normal pipe velocity distribution prevails. At section CD, near the pump, the pressure p_2, as measured at the pipe wall, is higher than at section AB. But since the energy gradient decreases from AB to CD, the higher pressure at CD can appear only at the expense of the middle streamlines. A paraboloid of pressure distribution is developed at CD with the pressure at the periphery higher (and lower at the center) than the average original pressure. The absolute velocities at the periphery are higher than those in

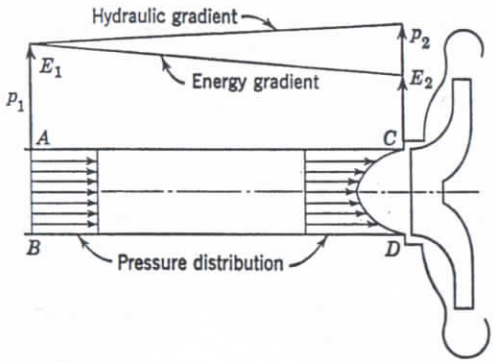

FIG. 1.9. Hydraulic and energy gradients along impeller approach.

the middle as a result of the addition of a tangential component due to rotation of the stream. This pressure exchange takes place without mixing of streamlines.

In Chapter 3, it will be shown that prerotation in the suction pipe is caused by the tendency of the liquid to follow a path of least resistance on its way to enter impeller channels. This becomes evident when the prerotation is in a direction opposite to that of the impeller. This occurs usually at pump capacities exceeding the normal capacity.

The process is reversed at the discharge of an axial flow pump. At the impeller discharge, pressure and velocities are higher at the periphery than at the hub. In the diffusion casing, part of the kinetic energy is converted into pressure, and pressures are equalized across the whole discharge pipe area. The exchange of pressure energy in the diffusion casing takes place without mixing of streamlines, as visually observed by Schmidt,[9] by introducing smoke and sparks at a blower inlet.

Higher velocities and pressures near the outer wall of a turn observed by Adler[7] for laminar flow may serve as an illustration of the pressure

transition by conduction, as there is no mixing of streamlines in the laminar flow.

Transition of pressure by convection takes place, for instance, in an elbow (Fig. 1.5). Beyond the turn, pressure and velocities are higher at the outer wall of the turn, the increase in energy being made at the expense of streamlines near the inner wall. This process is not efficient and is always followed by losses or degeneration of pressure energy into heat. Beyond the turn a uniform pressure is reestablished, partly by convection, partly by conduction.

1.6 PRESSURE ENERGY

(*a*) **Definition.** Pressure energy is defined by the term p/γ in Bernoulli's equation (1.1). It should be distinguished from the energy of compression as applied to gases. Energy of compression is due to the volume elasticity of fluids and is negligible for liquids. Both the pressure energy and the energy of compression are varieties of potential energy, which is stored energy. The difference between the two becomes apparent from the following example: a pound of water in an enclosed vessel under 100 psi static pressure possesses energy of compression only which is negligible; but a pound of water at the bottom of a standpipe 231 ft high possesses 231 ft-lb of pressure energy. The amount of potential energy of a pound of water in the standpipe is the same irrespective of its position in the standpipe but it is differently divided between the pressure energy and energy of position for different elevations in the standpipe. In both examples the amount of stored energy is equal to the amount of energy put in. Pressure is only an indication of the level at which energy is stored without any reference to the amount, in the same manner as temperature is no indication of the amount of heat in a body.

Pressure and pressure energy have been confused frequently.[10,11] Pressure p (pounds per unit area) may stand for pressure energy in expressions such as Bernoulli's equation, where it means energy (foot-pounds) per unit volume in the same manner as head h in feet represents energy in foot-pounds per pound of liquid.

(*b*) **Solid-Liquid Mixtures.** Centrifugal pumps are widely used for transporting solids in suspension in a liquid. Dredging operations and pumping of paper pulp, ashes, and cement are examples of moving solids in suspension. Both mechanical and hydraulic performances of pumps are greatly affected by the presence of solids in the liquid.

It is important to realize that solids in suspension in the liquid cannot absorb, store, or transmit pressure energy, which is a property of fluids.

Pressure exerted by a fluid on the walls of a container is caused by the bombardment of molecules freely moving in a confined space. Molecules of a solid being restricted in their movement by the molecular attraction cannot participate in maintaining or transmitting pressure energy, nor can they increase their own kinetic energy (disregarding the energy of compression) when surrounded with liquid carrying the pressure energy. A simple example will illustrate the point: in a standpipe a pound of solids at the top of the standpipe has as much potential energy of position as a pound of water (referred to the bottom of the standpipe). At the bottom of the standpipe a pound of water possesses as much potential energy as a pound of water at the top of the standpipe, but a pound of solids at the bottom of the standpipe does not possess any energy referred to the same datum. If a mixture of solids and water is pumped into the standpipe, a pound of solids would not carry any energy into the standpipe except a small amount of kinetic energy which is wasted at the discharge. In a standpipe filled with a solid-liquid mixture of an average specific gravity of, say, 1.1, the pressure gage at the bottom of the standpipe will register a pressure 1.1 times that of the clear water. But this pressure increase is due to the extra pressure energy of the liquid required to move and support solids in suspension. The potential energy of solids is all due to position and is all wasted when solids settle to the bottom of the standpipe.

Note that, having no part in maintaining or transmitting pressure energy, solids in suspension cannot convert their kinetic energy into pressure. This question becomes important and will be further elaborated in the discussion of pumping solids in suspension with centrifugal pumps in Chapter 4, Art. 4.4(*b*).

1.7 VORTEX MOTION

Movement of water in a circular path is known as a vortex motion. All particles of liquid describing circles of the same radius form stream cylinders. Particles of the same stream cylinder move with the same tangential and angular velocity. These velocities may vary from one cylinder to another. *Variation in the linear or angular velocity determines the pressure distribution along the radius, or the shape of the free surface if the vessel containing the liquid is open to atmosphere.*

The condition of equilibrium requires that, for each particle, the centrifugal force must be balanced by the pressure or static liquid column at the same point.

$$\frac{dp}{dr} = \frac{\gamma}{g}\frac{v^2}{r} = \frac{\gamma}{g}\omega^2 r \qquad (1.3)$$

TABLE 1. VORTEX MOTION

Curve No. on Figs. 1.10(*a*) and 1.10(*b*)	Angular Velocity Distribution $\omega = Cr^m$	Peripheral Velocity Distribution $vr^n = C$	Pressure Distribution $\int dp = \int \frac{\gamma}{g}\omega^2 r\,dr$	Type of Vortex	Remarks
1	$\omega = C_1 r^{-\infty}$	$vr^{\infty} = C_1$	$\frac{p}{\gamma} = C_1^2 + h_1 = \text{constant}$	$\omega = 0$, stationary	
2	$\omega = C_2 r^{-3/2}$	$vr^{3/2} = C_2$	$\frac{p}{\gamma} = -\frac{C_2^2}{3gr^3} + h_2$		ω is higher toward center for 1, 2, 3, 4, 5, and 6
3	$\omega = C_3 r^{-2}$	$vr = C_3$	$\frac{p}{\gamma} = -\frac{C_3^2}{2gr} + h_3$	$h_3 + \frac{p}{\gamma} + \frac{v^2}{2g} = \text{constant}$, free vortex	
4	$\omega = C_4 r^{-3/2}$	$vr^{1/2} = C_4$	$\frac{p}{\gamma} = -\frac{C_4}{gr} + h_4$		
5	$\omega = C_5 r^{-1}$	$vr^0 = C_5$	$\frac{p}{\gamma} = \frac{C_5^2}{g}\log r + h_5$	$v = \text{constant}$	
6	$\omega = C_6 r^{-1/2}$	$vr^{-1/2} = C_6$	$\frac{p}{\gamma} = \frac{C_6^2 r}{g} + h_6$	$\frac{v^2}{r} = \text{constant} = \text{centrifugal force}$	
7	$\omega = C_7 r^0$	$vr^{-1} = C_7$	$\frac{p}{\gamma} = \frac{C_7^2 r^2}{2g} + h_7$	$\omega = \text{constant}$, forced vortex	ω = constant
8	$\omega = C_8 r^{1/2}$	$vr^{-3/2} = C_8$	$\frac{p}{\gamma} = \frac{C_8^2 r^3}{3g} + h_8$	Superforced vortex	ω is higher toward periphery for 8, 9, and 10
9	$\omega = C_9 r$	$vr^{-2} = C_9$	$\frac{p}{\gamma} = \frac{C_9 r^4}{4g} + h_9$	Superforced vortex	
10	$\omega = Cr^m$	$vr^{-(m+1)} = C$	$\frac{p}{\gamma} = \frac{C^2 r^{2(m+1)}}{2(m+1)g} + h$	A general form of vortex equation	

where p is pressure at radius r, v is the tangential velocity, and ω is the angular velocity.

If the variation of angular velocity with radius is known, substitution of this value of ω into equation 1.3 will permit integration, and the pressure distribution along the radius will be obtained. In Table 1, results of the integration of equation 1.3 are tabulated for a velocity distribution given by an equation:

$$\omega = Cr^m \tag{1.4}$$

or

$$vr^n = C \tag{1.5}$$

where

$$n = -(m + 1)$$

Different values of m result in different types of vortices. The free vortex and forced vortex described in textbooks on hydraulics are special cases of this series. The first one is determined by a condition

$$vr = C_3 \tag{1.6}$$

and the pressure distribution is obtained from

$$h + \frac{p}{\gamma} + \frac{v^2}{2g} = E = \text{constant} \tag{1.7}$$

which states that all particles possess the same amount of energy. If such a vortex is superimposed upon an axial flow with a uniform velocity, equation 1.7 will require either that no energy be added to the liquid or that energy be added at a constant rate. Such a pattern of flow is sometimes assumed for axial flow pumps.

In a forced vortex the angular velocity is constant, or

$$\omega = \text{constant} \tag{1.8}$$

This means that the liquid is revolving as a solid body. After the liquid is set in motion, disregarding losses, no power is required to maintain such a vortex. The pressure distribution curve is a square parabola; see Fig. 1.10(*a*), curve 7. Forced vortex motion may be superimposed upon a radial outward flow; the resulting motion is a spiral forced vortex. Such a pattern of flow is found in centrifugal pumps. Disregarding losses, particles at the periphery carry the total amount of energy applied to the liuqid. *To make possible a radial outward flow against higher pressures the energy gradient must be below the forced vortex pressure paraboloid* (Fig. 1.11). The latter represents a state of static equilibrium for a forced vortex in the same manner as a horizontal plane does for a

stationary liquid. To produce flow the energy gradient must fall in the direction of flow below its value at zero flow.

If a forced vortex is superimposed upon a uniform axial flow in a cylindrical conduit an axial spiral forced vortex is obtained. This type

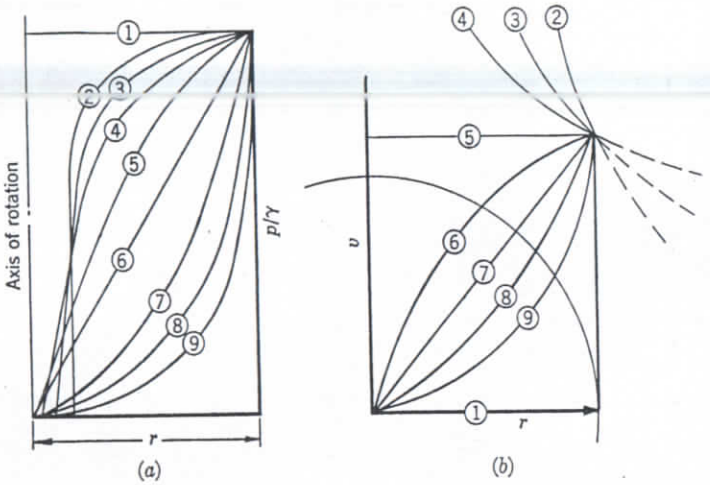

FIG. 1.10. (*a*) Vortex pressure distribution-elevation; (*b*) vortex velocity distribution, $vr^n = C$, plan view.

of flow is observed in axial flow pumps. Power is applied to maintain this flow. Particles carry different amounts of energy at different radii, with a maximum at the periphery.

A free spiral vortex motion is observed when water flows through a hole in the bottom of a vessel. The vortex usually starts naturally,

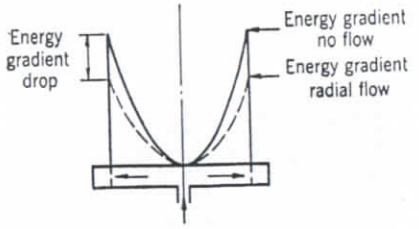

FIG. 1.11. Energy gradient, forced vortex.

some initial distrubance giving the direction of rotation. Water moves spirally toward the opening, friction limiting velocities near the axis to some finite values.

When large vertical pumps of the propeller type are operated with a low submergence, free spiral vortices are formed in the suction sump.

Air is drawn into the pump suction bell through the funnels formed at the axes of these vortices. A wooden board float around the pump column usually prevents formation of vortices under such circumstances. Also, suitable baffling of the pump suction bell or of the channel of approach will eliminate the tendency toward formation of vortices in the sump. Other forms of vortices can be produced with axial flow impellers having different vane curvature and vane twist along the radius. *All these vortices are stable and without cross flows as all satisfy equation 1.3*, but means of producing various vortices in this manner may not be equally efficient.

1.8 LOSSES

(a) Elbow Losses. Figure 1.12 is a compilation of information on hydraulic losses in elbows of various design. The losses are expressed by means of a dimensionless coefficient C in the equation

$$\text{Loss} = C\frac{v^2}{2g}\text{ ft} \tag{1.9}$$

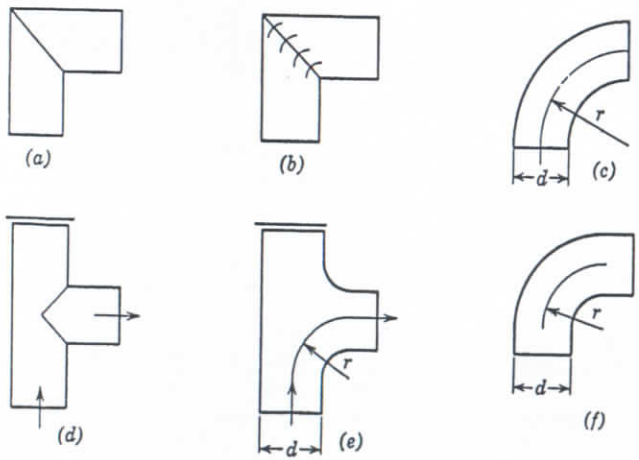

(a) $C = 1.0$

(b) $C = 0.136$ Airfoil baffles
0.24 Commercial baffles
0.40 (Stuart [14])

(c)

r/d	C
1.0	0.27
1.25	0.22
1.5	0.17
2.0	0.13

(d) $C = 0.88$

(e) $r/d = 1.5$; $C = 0.40$

(f) $r/d = 1$; $C = 0.24$

FIG. 1.12. Elbow losses. Data by N.A.C.A.,[13] Stuart,[14] Freeman,[15] Nordell,[16] and Madison.[17]

The data of several investigators are consistent and have an accuracy comparable to that observed on pipe friction experiments. Emphasis is placed on the relative value of several designs rather than on the absolute value of the losses. For example, a sharp 90° elbow with several short guide baffles of commercial design, Fig. 1.12(*b*), and with vanes of uniform thickness, has no advantage over a regular elbow with a radius ratio $r/d = 1.25$ or higher, Fig. 1.12(*c*). The primary function of such baffles is to maintain a uniform velocity throughout the section.

One wide baffle in the middle of the section of a regular elbow with a radius ratio of 1.5 or greater, Fig. 1.12(*f*), has little or no advantage over a plain elbow, Fig. 1.12(*c*). The effect of guide baffles in this case is to increase the radius ratio.

Nordell [16] has found that channels of square or rectangular section have the same total loss of head as circular turns of the same radius ratio.

(b) Sudden Enlargement or Reduction of the Channel Area. When the area of a channel is changed abruptly as in Fig. 1.13, the loss of head can be expressed by the equation

$$h_l = C\frac{(v_1 - v_2)^2}{2g} \tag{1.10}$$

The value of $C = 1.0$ for a sudden enlargement and the value of $C = 0.4$ to 0.5 for a sudden reduction of area.[12]

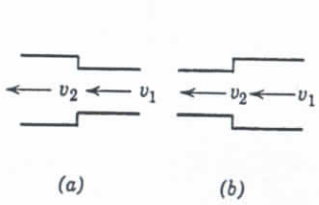

FIG. 1.13. Sudden enlargement and contraction.

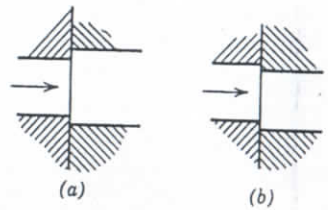

FIG. 1.14. Mismatched channel sections.

The loss due to a sudden reduction in area is about half that due to a sudden enlargement. It has been the practice in the past, when a channel is formed by two or more parts, to make the section of the upstream part slightly smaller to avoid liquid "hitting the corner," Fig. 1.14(*a*). Evidently such devices make the flow conditions worse instead of improving them. If two parts are of the same area, but sections are not matched because of manufacturing inaccuracies, Fig. 1.14(*b*), the hydraulic loss is smaller than in the case shown on Fig. 1.14(*a*).

REFERENCES

1. Boris Bakhmeteff, "Hydraulics," *Trans. A.S.M.E.*, 54–4, p. 57, Aug. 15, 1932.
2. Hugo Richter, *Rohrhydraulik*, pp. 130–133, 124–125, Berlin, Julius Springer, 1934.
3. L. Prandtl and O. G. Tietjens, *Applied Hydro- and Aeromechanics*, pp. 43, 52, 53, New York, McGraw-Hill Book Company, 1934.
4. J. Nikuradse, "Untersuchung über die Strömungen des Wassers in konvergenten und divergenten Kanälen," *Bull.* 289, Berlin, Verein Deutscher Ingenieure, 1929.
5. H. Nippert, "Über den Strömungsverlust in gekrümmten Kanälen," *Bull.* 320, pp. 1, 2, Berlin, Verein Deutscher Ingenieure, 1929.
6. David L. Yarnell, "Flow of Water through 6 Inch Pipe Bends," *Tech. Bull.* 577, U. S. Dept. of Agriculture, Washington, D. C., October 1937.
7. M. Adler, "Strömung in gekrümmten Rohren," *Z. angew. Math. Mech.*, Vol. 14, p. 257, October 1934.
8. H. Föttinger, "Hydraulische Probleme, Diskussion über Kavitation," p. 110, Berlin, Verein Deutscher Ingenieure, 1926.
9. Henry F. Schmidt, "Some Screw Propeller Experiments," *J. Am. Soc. Naval Engrs.*, Vol. XL, No. 1, p. 15, 1928.
10. A. F. Sherzer, *Trans. A.S.M.E.*, Vol. 64, p. 592, 1942.
11. Hunter Rouse, *Elementary Mechanics of Fluids*, p. 114, New York, John Wiley and Sons, 1946.
12. C. Pfleiderer, *Die Kreiselpumpen*, p. 29, Berlin, Julius Springer, 1955.
13. N.A.C.A. *Tech. Mem.* 722, p. 28.
14. M. C. Stuart et al., ASHVE Meeting, June 1942.
15. John F. Freeman, "Experiments upon the Flow of Water in Pipes," *Trans. A.S.M.E.*, p. 173, 1941.
16. Carl H. Nordell, "Curved Flow in Conduits of Constant Cross Section," *Oil Gas J.*, May 16 and June 13, 1940.
17. R. D. Madison and J. R. Parker, "Pressure Losses in Rectangular Elbows," *Trans. A.S.M.E.*, Vol. 58, No. 3, p. 167, April 1936.

Chapter 2

Definitions and Terminology

2.1 INTRODUCTION

Centrifugal pumps comprise a very wide class of pumps in which pumping of liquids or generation of pressure is effected by a rotary motion of one or several impellers. In the early stage of centrifugal pump development, pumping was ascribed to centrifugal forces. Later this class of pumps was extended to include axial flow pumps, and the conception of the centrifugal action of the impeller was inadequate to explain the operation of axial flow pumps. However, treatment of axial flow pumps as a class by themselves was not justified, because hydraulically they represent one extreme of a continuous series of pump types. This continuity applies to both theoretical treatment and design methods. Some intermediate types are called mixed flow pumps. In these, the flow through the impeller has both radial and axial components and the impeller resembles a ship propeller.

2.2 CLASSIFICATION AND TERMINOLOGY

The great variety of centrifugal pumps built for various applications may be reduced to a few fundamental hydraulic types. The difference in design details is dictated mostly by the application and mechanical requirements. Every pump consists of two principal parts: an impeller, which forces the liquid into a rotary motion by impelling action, and the pump casing, which directs the liquid to the impeller and leads it away under a higher pressure (Fig. 2.1). The impeller is mounted on a shaft which is supported by bearings and driven through a flexible or rigid coupling by a driver. The pump casing includes suction and discharge nozzles, supports the bearings, and houses the rotor assembly. The casing has to be packed around the shaft to prevent external leakage. Closely fitted rings, called wearing rings (Fig. 2.2), are mounted on the impeller and fitted in the casing to restrict leakage of high-pressure liquid back to the pump suction. Liquid is directed to the impeller eye by the suction nozzle and is brought into a circular motion by the impeller vanes. The impeller vanes and impeller side walls, or shrouds, form the impeller channels. In a double-suction impeller, liquid

introduced at both sides (Fig. 2.3). Frequently impellers are built "open," that is, with the front shroud removed. Impeller vanes are

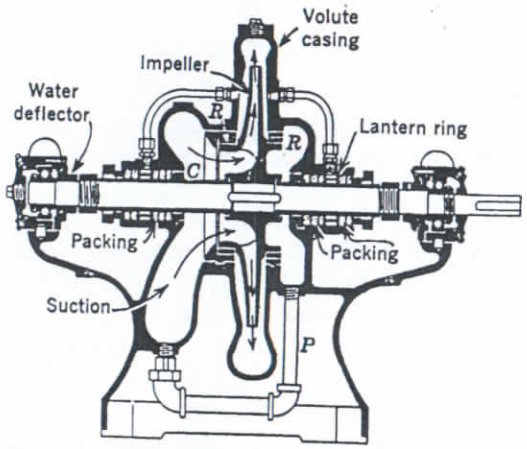

FIG. 2.1. Single-suction pump.

always curved backwards and are called plain or radial (erroneously) if they are of single curvature (Fig. 2.4). Wider impellers have vanes of double curvature, the suction ends being twisted. Such vanes are also

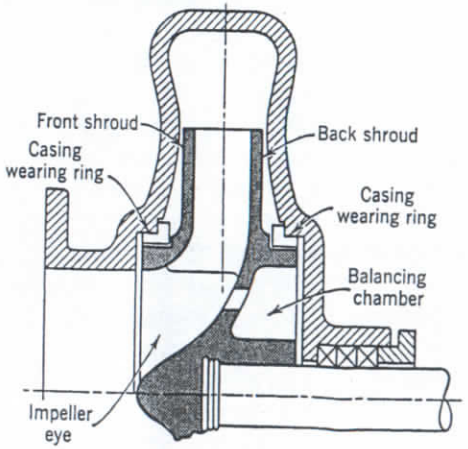

FIG. 2.2. Single-suction impeller with a balancing chamber on the back.

called mixed flow vanes or Francis type, after James B. Francis, who introduced double-curvature vanes for water turbines known as Francis' turbines.

An impeller is designated as radial if the shrouds are essentially normal to the shaft axis, being only slightly curved at the entrance. These

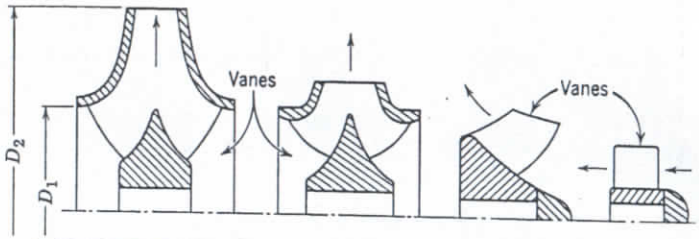

Type	Centrifugal Double-Suction	Mixed Flow Double-Suction	Mixed Flow Propeller	Axial Flow Propeller
n_s	1250	2200	6500	13500
gpm	2400	2400	2400	2400
Head ft	70	48	33	20
rpm	870	1160	1750	2600
D_2 in.	19	12	10	7
D_1/D_2	0.5	0.7	0.9	1.0

FIG. 2.3. Impellers of different specific speeds.

impellers usually have plain vanes. In an axial flow pump, liquid approaches the impeller axially and the forward component of velocity through the impeller is parallel to the shaft axis. Mixed flow impellers occupy an intermediate position in the continuous range of types from radial to axial flow. These always have Francis-type vanes. Extreme

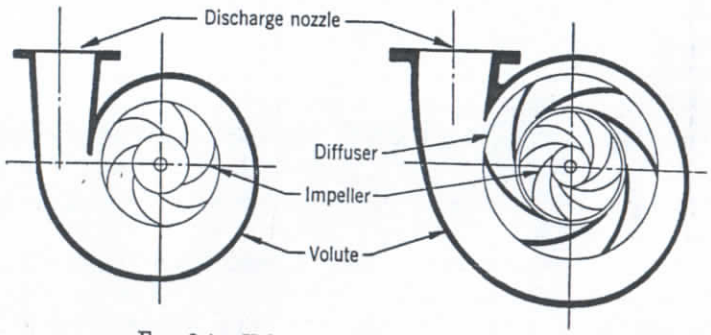

FIG. 2.4. Volute and diffusion casing pumps.

mixed flow and axial flow pumps are also called propeller pumps. Both types are built almost exclusively with open impellers.

As a result of the impeller action, liquid leaves the impeller at a higher pressure and higher velocity than exist at its entrance. The velocity

is partly converted into pressure by the pump casing before it leaves the pump through the discharge nozzle. This conversion of velocity into pressure is accomplished either in a volute casing or in a diffusion casing. In a volute casing (Fig. 2.4) the impeller discharges into a single casing channel of gradually increasing area called a volute, and the major part of the conversion takes place in the conical discharge nozzle. When the impeller discharges into a channel provided with vanes, a major part of the conversion of velocity into pressure takes place between the diffusion vanes (Fig. 2.4). The diffusion vane casing was introduced into pump design from water turbine practice where diffusion vanes are indispensable. Early pumps equipped with diffusion vanes were known as turbine pumps. For vertical pumps of the mixed flow and axial flow types, the diffusion casing gives a more compact design and is predominant (Fig. 16.17).

Presently a great majority of single-stage horizontal pumps are built with volute casings. In Europe there are examples of large single-stage pumps with diffusion vane casings. Multistage pumps in this country are perhaps equally divided between the volute and diffusor types, whereas abroad practically all multistage pumps are of the diffusor type.

When the total pressure cannot be efficiently produced by one impeller, several impellers are arranged in series; the result is a multistage pump (Figs. 17.9 and 17.20). In some designs, for hydraulic reasons, the total pump capacity is divided among two or three impellers operating in parallel. Such pumps are rarely used today because modern propeller pumps are particularly suited for low head and high capacity.

Any centrifugal pump can be arranged with either a horizontal or a vertical shaft, depending on the application, type of driver, and other requirements. But there is one type of pump—the vertical turbine pump (Figs. 7.25 and 16.17)—which was specifically developed for vertical operation. Originally these pumps were designed to fit deep wells of limited inside diameter. Considering the space limitations, these pumps have reached a high degree of perfection and, owning to their efficient hydraulic performance, are now used widely for a variety of services for which horizontal pumps have been used in the past.

2.3 FIELD OF APPLICATION AND LIMITATIONS

There are few limits to maximum or minimum head or capacity produced by modern centrifugal pumps. Centrifugal pumps developing 5400 psi are used for operation of hydraulic presses.

The largest pumps installed in the United States are those of the Grand Coulée project (Fig. 17.23), 12 in number, rated each 607,000 gpm at 310-ft head and driven by 65,000-hp motors at 200 rpm. These are exceeded only by the pump-turbine unit of the pumped storage project at Hiwassee Dam, in North Carolina, rated 1,750,000 gpm at 205-ft head, at 106 rpm, requiring 102,000 hp. Centrifugal pumps leave a very small field for reciprocating pumps, a field where capacities are too low and pressures too high to permit a favorable type for a centrifugal pump. However, this field is being gradually reduced.

Such progress in the development and application of centrifugal pumps is due to several factors: (1) their high adaptability for high-speed electric motor and steam turbine drive; (2) minimum of moving parts; and (3) small size and low cost for the amount of liquid moved.

2.4 PUMP CHARACTERISTICS

(*a*) **Capacity.** The volume of liquid pumped is referred to as capacity and is generally measured in gallons per minute (gpm). Large capacities are frequently stated in cubic feet per second, or millions of gallons per day. When referring to the pumping of petroleum oils, the capacity is sometimes specified in barrels (42-gal) per day. The following are the conversion factors.

1 cu ft per sec = 448.8 gpm

1,000,000 gallons per day = 694.4 gpm

1,000 barrels per day = 29.2 gpm

The height to which liquid can be raised by a centrifugal pump is called head and is measured in feet. This does not depend on the nature of the liquid (its specific gravity) so long as the liquid viscosity is not higher than that of water. Water performance of centrifugal pumps is used as a standard of comparison because practically all commercial testing of pumps is done with water. When a pump is not used for actual lifting of the liquid but for generation of pressure, the head can also be expressed in feet of liquid, or pounds per square inch. Determination of the pump total head depends on the method of measuring pressures ahead and beyond the pump, and varies for several types of pumps.

(*b*) **Total Dynamic Head.** For a horizontal pump the total dynamic head is defined as

$$H = H_d - H_s + \frac{v_d^2}{2g} - \frac{v_s^2}{2g} \tag{2.1}$$

H_d is the discharge head as measured at the discharge nozzle and referred to the pump shaft center line, and is expressed in feet; H_s is the suction

head expressed in feet as measured at the suction nozzle and referred to the same datum. If the suction head is negative, the term H_s in equation 2.1 becomes positive.

The last two terms in equation 2.1 represent the difference in the kinetic energy or velocity heads at the discharge and suction nozzles.

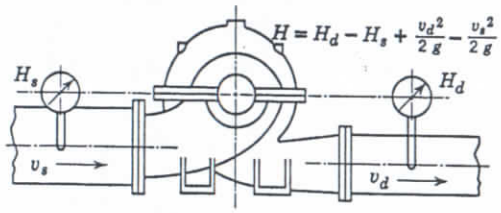

FIG. 2.5. Total dynamic head of horizontal pumps.

As expressed by equation 2.1, the total dynamic head is the energy imparted to liquid by the impeller between the points where suction and discharge heads are measured (Fig. 2.5). Note that the losses in the suction pipe are not charged against the pump.

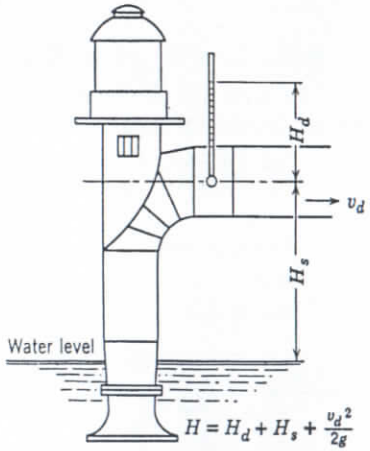

FIG. 2.6. Total dynamic head of vertical pumps.

For a vertical pump with the pumping element submerged (Fig. 2.6), the total dynamic head is given by

$$H = H_d + H_s + \frac{v_d^2}{2g} \qquad (2.2)$$

where H_s is the distance from the suction liquid level to the center line of the discharge elbow and H_d is the discharge head in feet referred to the center of the discharge elbow. The last term in equation 2.2 represents the velocity head at the discharge. In this case the loss in the suction bell and the discharge column, up to the point where the discharge head is measured, is charged against the pump.

The method of arriving at the total dynamic head varies for different pump arrangements and means used for measuring head. The Hydraulic Institute Test Code gives a detailed procedure for head determination for all possible practical cases.

(c) Efficiency. The degree of hydraulic and mechanical perfection of a pump is judged by its efficiency. This is defined as a ratio of pump energy output to the energy input applied to the pump shaft. The latter is the same as the driver's output and is termed brake horsepower (bhp), as it generally determined by a brake test.

$$\text{Efficiency } e = \frac{\text{pump output}}{\text{bhp}} = \frac{Q\gamma H}{550 \times \text{bhp}} \qquad (2.3)$$

where Q is capacity in cubic feet per second, γ is the specific weight of the liquid (for cold water = 62.4 lb per cu ft), and $Q\gamma$ is the weight of liquid pumped per second. If the capacity is measured in gallons per minute, equation 2.3 for water becomes

$$e = \frac{\text{gpm} \times 8.33 \times H}{60 \times 550 \times \text{bhp}} = \frac{\text{gpm} \times H}{3960 \times \text{bhp}} \qquad (2.4)$$

In equation 2.4, (gpm $\times$ H)/3960 is the pump output expressed in horsepower and is referred to as water horsepower (whp). If a liquid other than cold water is used, the water horsepower should be multiplied by the specific gravity of the liquid to obtain the pump output or liquid horsepower.

The pump efficiency as defined by equations 2.3 and 2.4 is a gross efficiency. This is used by engineers for the comparison of performance of centrifugal pumps. Besides this there are a number of partial efficiencies used by designers and experts; these describe only one phase of pump performance—hydraulic, mechanical, volumetric—and are of no interest to the users of pumps but are important in the study of pump performance and will be defined in a later chapter.

(d) Performance Curves. Variation of the head with capacity at a constant speed is called the pump characteristic (Fig. 2.7). A complete characteristic includes also efficiency and brake horsepower curves. Head and capacity of a pump vary with the speed in such a way that the performance curves retain their characteristic features. The variation of head, capacity, and brake horsepower with speed follows definite rules known as affinity laws.* These were originally found experimentally but have a rigorous theoretical background. When applied to every point on the head-capacity curve these laws state: When speed is changed, capacity varies directly as the speed, the head varies directly

* See Chapter 5 for development of these laws.

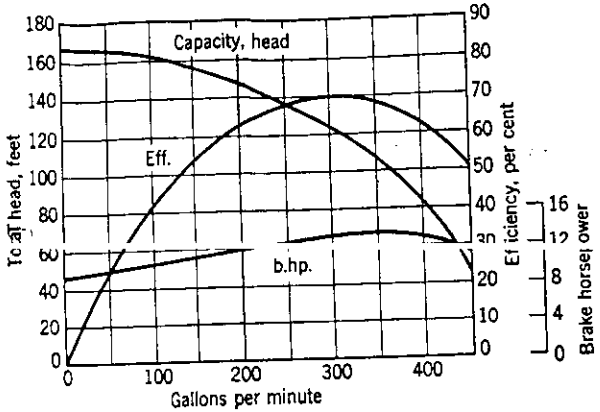

FIG. 2.7. Centrifugal pump characteristics; 3-in. pump at 1750 rpm.

as the square of the speed, and the brake horsepower varies directly as the cube of the speed. The cube of the speed is based on the assumption that efficiency stays constant with speed for each point. The affinity laws are expressed by the following equations

$$\frac{Q_1}{Q_2} = \frac{n_1}{n_2} \qquad \frac{H_1}{H_2} = \frac{{n_1}^2}{{n_2}^2} \qquad \frac{(\text{bhp})_1}{(\text{bhp})_2} = \frac{{n_1}^3}{{n_2}^3} \tag{2.5}$$

Figure 2.8 shows three head-capacity curves at speeds n_1, n_2, and n_3. Points connected by the affinity laws are called corresponding points

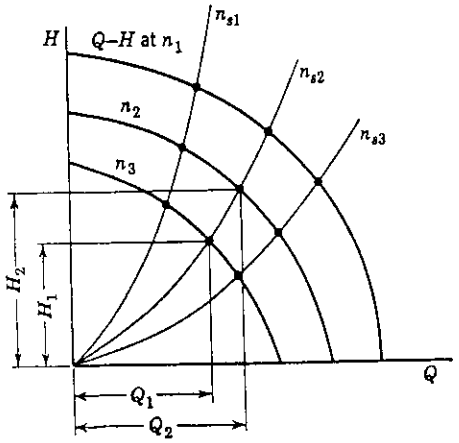

FIG. 2.8. Head and capacity variations with the speed.

and are connected by curved lines which are square parabolas. These points have the same efficiency and are of the same specific speed.

2.5 SPECIFIC SPEED

In the early stages of pump development it was customary to classify pumps according to their hydraulic-type ratios, such as a ratio of the impeller width at discharge to the impeller outside diameter (b_2/D_2). Ratios of the impeller eye diameter to the impeller outside diameter (D_1/D_2) were also used for the same purpose. Camerer † introduced a new characteristic to describe the hydraulic type of water turbines which was later applied to centrifugal pumps. It is called specific speed and is defined as

$$n_s = \frac{n\sqrt{Q}}{H^{3/4}} \tag{2.6}$$

where n is revolutions per minute, Q is capacity in gallons per minute, and H is head in feet. The physical meaning of specific speed is: revolutions per minute to produce 1 gpm at 1-ft head with an impeller similar to the one under consideration but reduced in size. The physical meaning of specific speed has no practical value and the number is used as a "type" number. The specific speed as a type number is constant for all similar pumps and does not change with the speed for the same pump. Figure 2.3 shows several impellers of different specific speeds. With each specific speed are associated definite proportions of leading impeller dimensions such as b_2/D_2 or D_1/D_2.

In the study of pump performance and classification of all important design constants, specific speed is a criterion of similarity for centrifugal pumps in the manner that Reynolds number is a criterion for pipe flow. When used as a type number, specific speed is calculated for the best efficiency point. For a multistage pump, specific speed is calculated on the basis of the head per stage. When the specific speed of a double suction impeller is compared with that of a single-suction impeller the capacity of the first should be divided by 2 or its specific speed should be divided by $\sqrt{2}$. All important pump design and performance characteristics are so closely connected with the specific speed that it is impossible to discuss certain features without reference to it.

From equation 2.6 it follows that, for the same head-capacity requirements, higher specific speed pumps will run at a higher speed and will be of smaller physical dimensions. Also, for the same speed and capacity, higher specific speed pumps will operate at a lower head or, for the same speed and head, a higher specific speed pump will deliver higher capacity.

† R. Camerer, *Z. ges. Turbinenwes.*, p. 217, 1915.

introduced at both sides (Fig. 2.3). Frequently impellers are built "open," that is, with the front shroud removed. Impeller vanes are

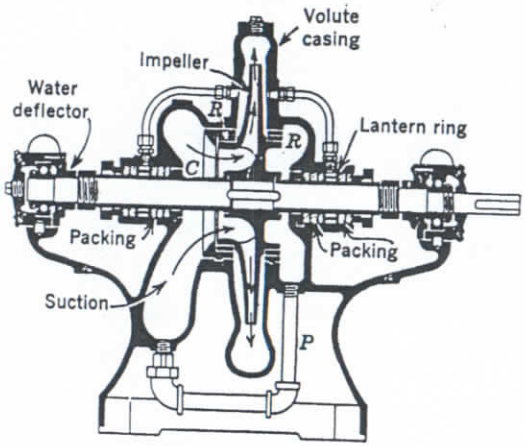

FIG. 2.1. Single-suction pump.

always curved backwards and are called plain or radial (erroneously) if they are of single curvature (Fig. 2.4). Wider impellers have vanes of double curvature, the suction ends being twisted. Such vanes are also

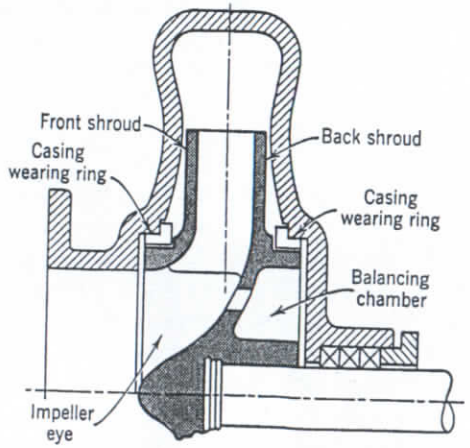

FIG. 2.2. Single-suction impeller with a balancing chamber on the back.

called mixed flow vanes or Francis type, after James B. Francis, who introduced double-curvature vanes for water turbines known as Francis' turbines.

An impeller is designated as radial if the shrouds are essentially normal to the shaft axis, being only slightly curved at the entrance. These

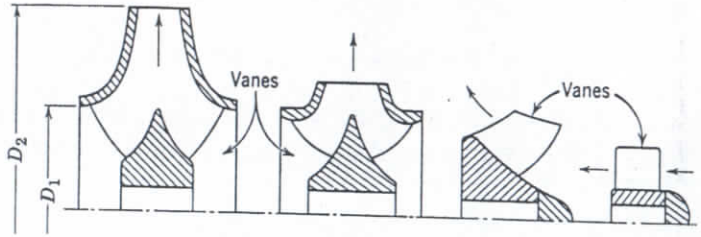

Type	Centrifugal Double-Suction	Mixed Flow Double-Suction	Mixed Flow Propeller	Axial Flow Propeller
n_s	1250	2200	6500	13500
gpm	2400	2400	2400	2400
Head ft	70	48	33	20
rpm	870	1160	1750	2600
D_2 in.	19	12	10	7
D_1/D_2	0.5	0.7	0.9	1.0

FIG. 2.3. Impellers of different specific speeds.

impellers usually have plain vanes. In an axial flow pump, liquid approaches the impeller axially and the forward component of velocity through the impeller is parallel to the shaft axis. Mixed flow impellers occupy an intermediate position in the continuous range of types from radial to axial flow. These always have Francis-type vanes. Extreme

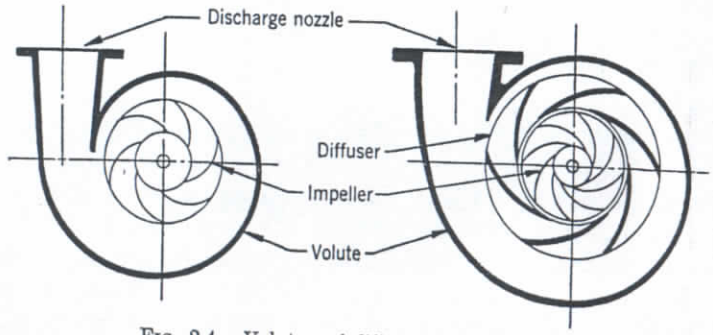

FIG. 2.4. Volute and diffusion casing pumps.

mixed flow and axial flow pumps are also called propeller pumps. Both types are built almost exclusively with open impellers.

As a result of the impeller action, liquid leaves the impeller at a higher pressure and higher velocity than exist at its entrance. The velocity

is partly converted into pressure by the pump casing before it leaves the pump through the discharge nozzle. This conversion of velocity into pressure is accomplished either in a volute casing or in a diffusion casing. In a volute casing (Fig. 2.4) the impeller discharges into a single casing channel of gradually increasing area called a volute, and the major part of the conversion takes place in the conical discharge nozzle. When the impeller discharges into a channel provided with vanes, a major part of the conversion of velocity into pressure takes place between the diffusion vanes (Fig. 2.4). The diffusion vane casing was introduced into pump design from water turbine practice where diffusion vanes are indispensable. Early pumps equipped with diffusion vanes were known as turbine pumps. For vertical pumps of the mixed flow and axial flow types, the diffusion casing gives a more compact design and is predominant (Fig. 16.17).

Presently a great majority of single-stage horizontal pumps are built with volute casings. In Europe there are examples of large single-stage pumps with diffusion vane casings. Multistage pumps in this country are perhaps equally divided between the volute and diffusor types, whereas abroad practically all multistage pumps are of the diffusor type.

When the total pressure cannot be efficiently produced by one impeller, several impellers are arranged in series; the result is a multistage pump (Figs. 17.9 and 17.20). In some designs, for hydraulic reasons, the total pump capacity is divided among two or three impellers operating in parallel. Such pumps are rarely used today because modern propeller pumps are particularly suited for low head and high capacity.

Any centrifugal pump can be arranged with either a horizontal or a vertical shaft, depending on the application, type of driver, and other requirements. But there is one type of pump—the vertical turbine pump (Figs. 7.25 and 16.17)—which was specifically developed for vertical operation. Originally these pumps were designed to fit deep wells of limited inside diameter. Considering the space limitations, these pumps have reached a high degree of perfection and, owning to their efficient hydraulic performance, are now used widely for a variety of services for which horizontal pumps have been used in the past.

2.3 FIELD OF APPLICATION AND LIMITATIONS

There are few limits to maximum or minimum head or capacity produced by modern centrifugal pumps. Centrifugal pumps developing 5400 psi are used for operation of hydraulic presses.

The largest pumps installed in the United States are those of the Grand Coulée project (Fig. 17.23), 12 in number, rated each 607,000 gpm at 310-ft head and driven by 65,000-hp motors at 200 rpm. These are exceeded only by the pump-turbine unit of the pumped storage project at Hiwassee Dam, in North Carolina, rated 1,750,000 gpm at 205-ft head, at 106 rpm, requiring 102,000 hp. Centrifugal pumps leave a very small field for reciprocating pumps, a field where capacities are too low and pressures too high to permit a favorable type for a centrifugal pump. However, this field is being gradually reduced.

Such progress in the development and application of centrifugal pumps is due to several factors: (1) their high adaptability for high-speed electric motor and steam turbine drive; (2) minimum of moving parts; and (3) small size and low cost for the amount of liquid moved.

2.4 PUMP CHARACTERISTICS

(*a*) Capacity. The volume of liquid pumped is referred to as capacity and is generally measured in gallons per minute (gpm). Large capacities are frequently stated in cubic feet per second, or millions of gallons per day. When referring to the pumping of petroleum oils, the capacity is sometimes specified in barrels (42-gal) per day. The following are the conversion factors.

1 cu ft per sec = 448.8 gpm

1,000,000 gallons per day = 694.4 gpm

1,000 barrels per day = 29.2 gpm

The height to which liquid can be raised by a centrifugal pump is called head and is measured in feet. This does not depend on the nature of the liquid (its specific gravity) so long as the liquid viscosity is not higher than that of water. Water performance of centrifugal pumps is used as a standard of comparison because practically all commercial testing of pumps is done with water. When a pump is not used for actual lifting of the liquid but for generation of pressure, the head can also be expressed in feet of liquid, or pounds per square inch. Determination of the pump total head depends on the method of measuring pressures ahead and beyond the pump, and varies for several types of pumps.

(*b*) Total Dynamic Head. For a horizontal pump the total dynamic head is defined as

$$H = H_d - H_s + \frac{v_d^2}{2g} - \frac{v_s^2}{2g} \tag{2.1}$$

H_d is the discharge head as measured at the discharge nozzle and referred to the pump shaft center line, and is expressed in feet; H_s is the suction

Development of the formula for the specific speed and further discussion are presented in Chapter 5.

2.6 NET POSITIVE SUCTION HEAD

NPSH, a term accepted by the pump industry, stands for "net positive suction head." It is defined as the gage reading in feet taken on the suction nozzle referred to the pump center line, minus the gage vapor pressure in feet corresponding to the temperature of the liquid, plus velocity head at this point. When boiling liquids are being pumped from a closed vessel, NPSH is the static liquid head in the vessel above the pump center line minus losses of head in the suction pipe. Hydraulic Institute Charts BF-11 to 17 give NPSH values recommended for boiler feed and condensate pumps (see Reference 7, Chapter 17). This subject is further discussed in Chapters 12 and 17.

Note that the NPSH requirements for a given pump, as determined experimentally, by definition are tied to a given size of the suction nozzle or suction pipe. Therefore, the available NPSH of a given installation should be based on the same size of suction pipe when selection of a pump is made.

Chapter 3

Theory of the Centrifugal Pump Impeller

3.1 VELOCITY TRIANGLES

A study of the several component velocities of flow through an impeller is best carried out graphically by means of velocity vectors. The shape of such vector diagrams is triangular and they are called velocity triangles. They can be drawn for any point of the flow path through the impeller, but usually attention is focused on the entrance and discharge part of the impeller vanes, and the velocity triangles are called entrance and discharge triangles.

It is necessary to distinguish between absolute and relative velocities. The relative velocity of flow is considered relative to the impeller. The absolute velocity of flow is taken with respect to the pump casing and is always equal to the vectorial sum of the relative velocity and the peripheral velocity of the impeller. Any point on the impeller will describe a circle about the shaft axis and will have a peripheral velocity

$$u = \frac{\pi D}{12} \times \text{rps} \qquad \text{or} \qquad u = \frac{D \times \text{rpm}}{229} \text{ ft per sec}$$

where D is the diameter of the circle in inches.

Figure 3.1(a) shows an entrance triangle and Fig. 3.1(b) a discharge triangle. The following notation is adopted.

u = peripheral velocity of impeller, feet per second

w = relative velocity of flow, feet per second

c = absolute velocity of flow, feet per second

Subscript 1 refers to the entrance; subscript 2 to the discharge. Tangential components of relative and absolute velocities are given another subscript, u. Components of the absolute velocity normal to the peripheral velocity are designated as c_{m1} and c_{m2} for entrance and discharge diagrams. This component is radial in a radial impeller and axial in a

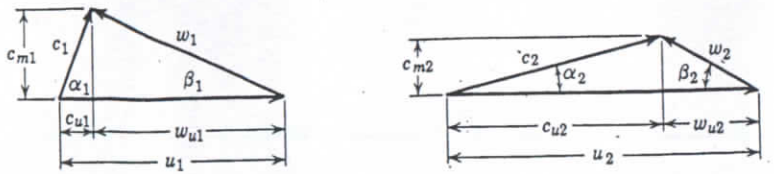

FIG. 3.1. (*a*) Entrance velocity triangle; (*b*) discharge velocity triangle.

axial impeller. It will be referred to, in general, as meridional, and will have the subscript m.

Unless specifically stated, all velocities are considered average velocities for the section normal to the general direction *of flow at a specified point. This is one of the approximations made for theoretical studies and practical design which is not true in practice. A uniform velocity across a channel section does not exist for actual liquids, even in the case of straight pipe flow.*

3.2 THEORETICAL HEAD OF CENTRIFUGAL PUMPS

An expression for the theoretical head of a centrifugal pump is obtained by applying the principle of angular momentum to the mass of liquid going through the impeller passages. This principle states that the time rate of change of angular momentum of a body with respect to the axis of rotation is equal to the torque of the resultant force on the body with respect to the same axis.

Let us consider a mass of liquid filling the space between two adjacent impeller vanes (Fig. 3.2). At time $t = 0$ its position is *abcd* and, after a time interval dt, its position has changed to *efgh*. Denote the mass of an infinitely thin layer of liquid *abef* just leaving the impeller channel dm. This is equal to the mass of liquid just entering the channel in the same interval of time dt, as represented by *cdgh*. The part *abgh* of the liquid contained between the two impeller vanes does not change its moment of momentum in time interval dt; thus the change in moment of momentum of the whole content of the channel is given by the change of moment of momentum of the mass dm entering the impeller (*cdgh*) and mass dm leaving the impeller (*abef*). This change of moment of momentum is equal to the moment of all external forces applied to the liquid contained between the two impeller vanes. The moment of external forces being denoted by T, the above is stated mathematically by

$$T = \frac{dm}{dt}(r_2c_2 \cos \alpha_2 - r_1c_1 \cos \alpha_1) \tag{3.1}$$

The external forces applied to the liquid contained between the vanes are: (1) the difference in pressure on two sides of each vane (p_f and p_b); (2) pressures p_d and p_s, on the faces *ab* and *cd* of the elementary liquid section respectively, which are radial forces and have no moment about the axis of rotation; and (3) hydraulic friction forces, which oppose the relative flow and produce torque in addition to that exerted by the impeller vanes. Friction forces are neglected in idealized flow.*

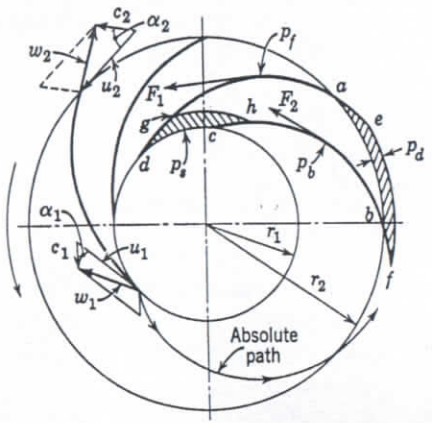

FIG. 3.2. Forces and velocities in an impeller.

The term dm/dt, when extended to all impeller channels, represents the constant time rate of mass flow through the impeller which is $Q\gamma/g$. Substituting this into equation 3.1 and multiplying both sides of it by ω, the angular velocity of the impeller, we obtain

$$T\omega = \frac{Q\gamma}{g}\omega(r_2c_2 \cos \alpha_2 - r_1c_1 \cos \alpha_1) \tag{3.2}$$

The left-hand side of equation 3.2 represents power input P applied to the liquid by the impeller vanes. Substituting $u_2 = \omega r_2$, $c_2 \cos \alpha_2 = c_{u2}$, $u_1 = \omega r_1$, and $c_1 \cos \alpha_1 = c_{u1}$ into equation 3.2, we obtain

$$P = \frac{Q\gamma}{g}(u_2c_{u2} - u_1c_{u1}) \tag{3.3}$$

Assuming that there is no loss of head between the impeller and th

* In an actual pump, friction forces F_1 and F_2 have a moment about the axis, thu requiring power from the shaft. Therefore, not all the applied torque is converte into head.

point where the total dynamic head is measured, this power is available as the pump output of an idealized pump.

$$Q\gamma H_i = \frac{Q\gamma}{g}(u_2c_{u2} - u_1c_{u1}) \tag{3.4}$$

Eliminating $Q\gamma$, we get an expression for head.

$$H_i = \frac{u_2c_{u2} - u_1c_{u1}}{g} \tag{3.5}$$

Since all hydraulic losses between the points where the actual total dynamic head of a pump is measured have been disregarded, the head H_i is a theoretical head; the equation is known as Euler's equation.

If the liquid enters the impeller without a tangential component, or if $c_{u1} = 0$ (radially for a radial pump and axially for an axial flow pump), Euler's equation reduces to

$$H_i = \frac{u_2c_{u2}}{g} \tag{3.6}$$

By geometric substitutions from the velocity triangles, Euler's equation 3.5 is transformed into another form more convenient for some discussions. From the velocity triangles we find

$$w_2^2 = c_2^2 + u_2^2 - 2u_2c_2\cos\alpha_2$$
$$w_1^2 = c_1^2 + u_1^2 - 2u_1c_1\cos\alpha_1$$

Making use of these, Euler's equation becomes

$$H_i = \frac{c_2^2 - c_1^2}{2g} + \frac{u_2^2 - u_1^2}{2g} + \frac{w_1^2 - w_2^2}{2g} \tag{3.7}$$

The first term represents a gain of the kinetic energy (K.E.) of the flow through the impeller. The second and third terms jointly represent an increase in pressure from the impeller inlet to the outlet. It is futile to attach any physical meaning to the second and third terms individually. Thus the second term does not represent entirely gain in pressure of the flow due to centrifugal force because there are no particles of the fluid moving with the peripheral velocities u_1 and u_2. Similarly, the third term does not represent an increase in pressure due to conversion of the relative velocity from w_1 to w_2, as it should be realized that no diffusion can take place in a curved channel, stationary or moving. In the case of axial flow impellers there is no definite channel containing velocities w_1 or w_2. Although the third term is

shown positive, it is really a subtractive term. Rearranging the secon and third terms, this becomes apparent.

$$H_i - \text{K.E.} = \frac{u_2^2 - w_2^2}{2g} - \frac{u_1^2 - w_1^2}{2g}$$

which can be transformed back to the form of equation 3.5.

$$H_i - \text{K.E.} = \frac{c_{u2}u_2 - c_{u1}u_1}{g} - \frac{c_2^2 - c_1^2}{2g}$$

In general, although a velocity can be represented by its component energy can be expressed only in terms of the resultant or absolut velocity (equation of momentum) because *energy is not a vector quantity*. According to equation 3.5 the head (both pressure and K.E.) built up gradually as both c_{u2} and u_2 are increased steadily.

If, in equations 3.1 and 3.2, c_1 and c_2 represent actual absolute velocitie of all liquid particles and α_1 and α_2 are their true directions, P in equation 3.3 will represent the actual power input to the liquid by the impelle In that case the theoretical head H_i, as given by equations 3.5, 3.6 and 3.7, will be the actual theoretical head of the pump, or the inpu head. The term input head will be used in preference to actual theoret ical head to avoid confusion, as different theories give different theoretica heads. However, for a given pump the input head H_i is a definite quan tity independent of the equations used for its calculation. In practice however, the true velocities of flow and their directions are never known Theoretical studies of impeller performance are based on the velocity triangles drawn on the vane angles, and the theoretical head is calcu lated by means of Euler's equations (3.5 or 3.7). Using velocities fron such velocity triangles leads to a considerably higher head than th input head. To distinguish the two theoretical heads, the velocity triangles drawn on the vane angles will be called Euler's velocity trian gles, and the head calculated by using velocities and angles from Euler' velocity triangles will be termed Euler's head and denoted by H_e.

If velocities from Euler's velocity triangles are inserted in equation 3.5 P will not represent the actual power input to liquid, the equality will b destroyed, and the equation will lose its meaning. Euler's velocity triangle are used mostly for graphical determination of the impeller vane shape particularly in mixed flow and axial flow impellers.

3.3 THEORETICAL CHARACTERISTIC CURVES

By taking Euler's head equation in its simplest form as given in equa tion 3.6, it can be shown that it is the equation of a straight line whicl

will give the variation of Euler's head with capacity. Substituting

$$c_{u2} = u_2 - w_{u2} = u_2 - \frac{c_{m2}}{\tan \beta_2}$$

into equation 3.6 we obtain

$$H_e = \frac{u_2^2}{g} - \frac{u_2 c_{m2}}{g \tan \beta_2} \tag{3.8}$$

In equation 3.8, c_{m2} is proportional to the capacity since Q is equal to the product of c_{m2} and the area normal to c_{m2}. Thus equation 3.8 is a

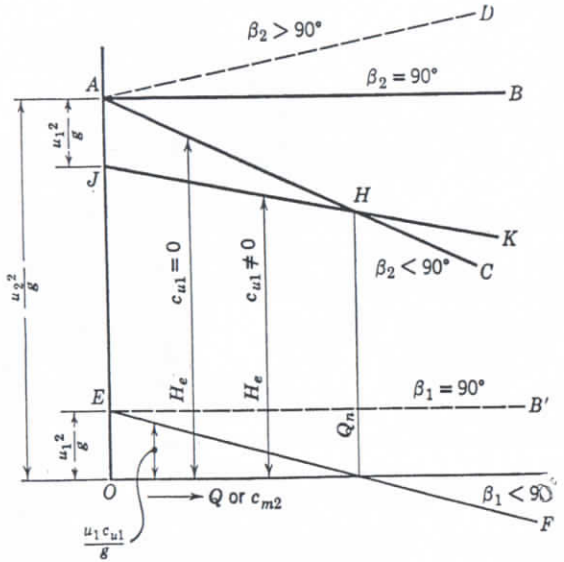

FIG. 3.3. Euler's head-capacity characteristics.

linear equation which intersects the head axis at u_2^2/g and the c_{m2} axis at $u_2 \times \tan \beta_2$ (Fig 3.3). The slope of this line depends on the value of the angle β_2. When $\beta_2 = 90°$, the head-capacity line is parallel to the axis of capacities, and $H_e = u_2^2/g$ = constant. For $\beta_2 < 90°$, the head decreases as the capacity increases. With $\beta_2 > 90°$, the head increases with the capacity. This can be realized only by impulse action with an impeller similar to the Pelton water wheel reversed, as the absolute velocity leaving the impeller c_2 is greater than the peripheral velocity u_2 (Fig. 3.4). It is impossible to devise a pump casing

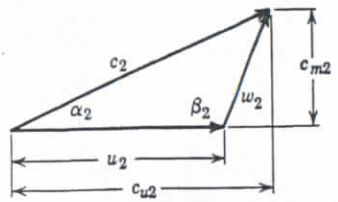

FIG. 3.4. Discharge triangle for $\beta_2 > 90°$.

which would catch the high-velocity jets, convert velocity into pressure, and permit impulse action.

When the approach to the impeller eye is such that liquid has prerotation before being acted upon by the impeller, the subtractive term in equation 3.5 is not equal to zero and the head-capacity curve is obtained as follows. Let $u_1 c_{u1}/g = H_1$. Applying the same trigonometric substitution as used in equation 3.8, we get

$$H_1 = \frac{u_1^2}{g} - \frac{u_1 c_{m1}}{g \tan \beta_1} \tag{3.9}$$

This equation is of the same type as equation 3.8 and represents a straight line cutting the head axis at u_1^2/g, which is parallel to axis of capacities for $\beta_1 = 90°$, and which decreases for $\beta_1 < 90°$ (line EF, Fig. 3.3). The Euler's head, line JK, is obtained by subtracting ordinates of the line EF from those of line AC.

When prerotation is in a direction opposite to that of the impeller, the second term of the numerator of equation 3.5 changes its sign and a higher head is obtained than with the meridional impeller approach. Although prerotation in a direction with the impeller rotation is sometimes unavoidable on account of the shape of the impeller approach (such as the shape of the suction nozzle of the horizontal double-suction pumps), there is nothing to be gained by the use of special means to provide prerotation in either direction; for that reason, inlet guide vanes are never used with centrifugal pumps.

In practice the discharge angles β_2 vary between 35° and 15°, the normal range being $25° > \beta_2 > 20°$. The entrance angle lies within the limits $50° > \beta_1 > 15°$.

In an idealized pump the input is equal to output, or brake horsepower equals water horsepower. The shape of the theoretical power curve is obtained by multiplying equation 3.8 by Q, or Kc_{m2}, where K is a constant for a given pump and can be accounted for by a proper selection of scales. Then

$$\frac{\text{whp}}{K} = \frac{u_2^2 c_{m2}}{g} - \frac{u_2 c_{m2}^2}{g \tan \beta_2} \tag{3.10}$$

When $\beta_2 = 90°$, equation 3.10 represents a straight line passing through the origin. For $\beta_2 < 90°$, it is a parabola tangent to the above straight line at the origin (Fig. 3.5). With $\beta_2 > 90°$ the

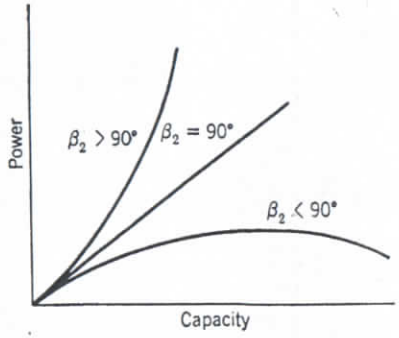

FIG. 3.5. Power to produce Euler's head.

power curve is also a parabola tangent to the first straight line but lies above it. The latter shape of the power curve is never realized in actual pumping machinery. Whereas the discharge angle β_2 is selected to meet the required head-capacity characteristics, the entrance angle is determined from the velocity triangle, depending upon the impeller capacity, profile, and speed as will be shown in Chapter 5.

3.4 EFFICIENCIES

All the head in a centrifugal pump is generated by the impeller. The rest of the parts contribute nothing to the head but incur inevitable losses—hydraulic, mechanical, and leakage. All losses of head which take place between the points where the suction and discharge pressures are measured constitute hydraulic losses. These include skin friction losses along the liquid path from the suction to the discharge nozzle, losses due to sudden change in area or direction of flow, and all losses due to eddies whatever their causes. Hydraulic efficiency is defined as a ratio of the available total dynamic head to the input head, or

$$e_h = \frac{H}{H_i} = \frac{H_i - \text{hydraulic losses}}{H_i} \tag{3.11}$$

The ratio of the input head to Euler's head will be referred to as vane efficiency, or

$$\frac{H_i}{H_e} = e_{va} \tag{3.12}$$

In Fig. 3.6, AED is Euler's velocity triangle and AFD the input velocity triangle. The area AFB is proportional to the impeller input because

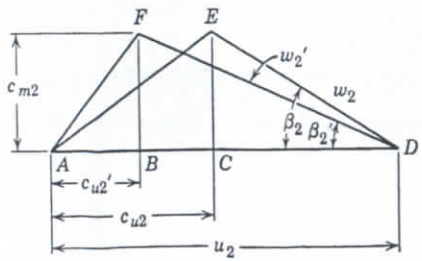

FIG. 3.6. Euler's and input velocity triangles.

$H_i = u_2c_{u2}'/g$ and $Q = c_{m2}A_2$, where A_2 is the impeller discharge area normal to c_{m2}. Then

$$P = Q\gamma H_i = \frac{u_2c_{u2}'}{g} \times c_{m2}\gamma A_2 = \frac{c_{u2}'c_{m2}}{2} \times K$$

In the above, K is a constant for a given pump and revolutions pe minute.

Similarly, the area AEC is proportional to the input to produce Euler head. Then the ratio of the two areas is the vane efficiency.

$$\frac{AFB}{AEC} = \frac{H_i}{H_e} = \frac{c_{u2}'}{c_{u2}} \tag{3.12a}$$

This is similar to the cylinder or indicated efficiency of a steam engi which is defined as the ratio of the actual indicator diagram (correspon to area AFB in our case) to the theoretical Rankine or Clausius pressur volume diagram (area AEC on Euler's triangle).†

Besides the losses of head there are *losses of capacity* in each pum known as leakage losses. These take place through the clearanc between the rotating and stationary parts of the pump. The capacit available at the pump discharge is smaller than that passed throug the impeller by the amount of leakage. The ratio of the two is calle the volumetric efficiency.

$$\frac{Q}{Q_i} = \frac{Q}{Q + Q_L} = e_v \tag{3.13}$$

where Q_L is the amount of leakage.

Mechanical losses include *loss of power* in bearings and stuffing boxe and the disk friction. The latter loss is hydraulic in nature but is groupe with the mechanical losses since it is external to the flow through th pump and does not result in a loss of head. The mechanical efficienc is the ratio of the power actually absorbed by the impeller and co verted into head and the power applied to the pump shaft, or

$$e_m = \frac{\text{Brake horsepower} - \text{mechanical losses}}{\text{Brake horsepower}} = \frac{Q_i\gamma H_i}{550 \text{ bhp}} \tag{3.14}$$

The relationship between the partial efficiencies defined above an the gross or total efficiency e can be obtained from

$$e = \frac{Q\gamma H}{550 \text{ bhp}} \tag{3.15}$$

† The product of $e_h e_{va} = e_{man}$ has been named manometric efficiency by sever writers and defined as $H/H_e = e_{man}$. This has no physical meaning and frequent has been confused with hydraulic efficiency.

The difference between Euler's head H_e and the input head H_i is not a loss, ther fore the ratio H_i/H_e could be termed vane effectiveness rather than vane efficienc However, the latter term will be used for convenience.

by substituting for Q its value $Q = e_v Q_i$, for H its equivalent $H = e_h H_i$, and for bhp its value from equation 3.14,

$$e = e_v e_h e_m \tag{3.16}$$

which is the expression sought.

3.5 IMPELLER APPROACH AND PREROTATION

To study the effect of the impeller approach channel upon the impeller performance it is better to take into consideration part of the suction pipe because impeller reaction on the flow may extend a considerable distance ahead of the impeller. *The flow toward the impeller, through the impeller, and beyond the impeller is caused by the drop of the energy gradient below its level at zero flow.*‡ The drop in energy gradient permits liquid to proceed through the impeller against a gradually increasing head. *Following the energy gradient the liquid selects a path of least resistance to get to and through the impeller and out of the pump.* The liquid acquires prerotation to enter the impeller passages with a minimum disturbance and the direction depends on the impeller vane entrance angle β_1, the capacity going through, and the impeller peripheral velocity—all three of which determine the entrance velocity triangle.§

It is evident that resistance to flow is a minimum if the liquid enters the impeller channel at an angle approaching the vane angle β_1. For a given impeller speed, there is only one capacity at which the liquid will approach the impeller meridionally, or without prerotation; see Fig. 3.7(*a*). At a capacity considerably smaller than normal, the liquid should acquire prerotation in the direction of impeller rotation to be able to enter the channel at an angle approaching β_1; see Fig. 3.7(*b*). But at a capacity greater than normal, a prerotation in the opposite direction is necessary for the liquid to satisfy the "least resistance" requirement. The behavior of the liquid in actual pumps follows this pattern, modified somewhat by the effect of the suction nozzle and suction pipe design. *Note that the rotation of the liquid in the impeller*

‡ It should be realized that liquids cannot transmit tension, therefore cannot be "pulled" or "sucked" but only "pushed" by the excess pressure from behind. Any devices that suck liquids accomplish only a local reduction of pressure, thus establishing an energy or hydraulic gradient necessary to produce flow.

§ The principle of least resistance is quite general when applied to the flow of energy; it is nothing more than a restatement of the second law of thermodynamics. Human beings and animals follow it by instinct; for instance, taking the shortest distance between two points, or boarding a moving train by running in the direction of the train motion. The latter is analogous to prerotation of flow in the impeller approach at partial capacities.

approach is not derived from the impeller, as it is evident that an impeller cannot impart liquid rotation opposite to its own—a condition frequently observed at capacities above normal.[1]

Stewart,[2] with a special instrument, the "rotometer," established prerotation in a 6-in. suction pipe 18 in. ahead of the impeller. At zero capacity the rotometer showed 233 rpm (impeller speed was 1135 rpm), which gradually decreased to zero as capacity approached the normal; then the rotometer speed increased again to 40 rpm for capacities over normal. At that time (1909) it was not realized that the direction of

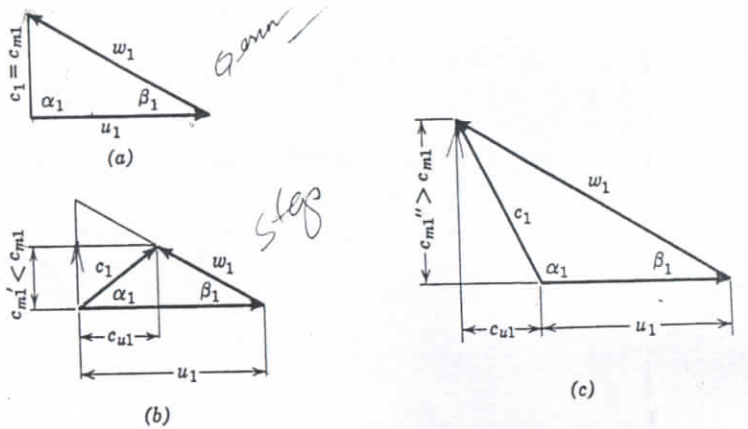

FIG. 3.7. Entrance velocity triangles.

prerotation changed when the best efficiency point was passed. Th rotometer could record revolutions but not direction of rotation.

In these tests it was observed that the suction pressure at the pum suction nozzle was 0.3 ft higher than the level in the suction tank (Fi 3.8). On the basis of the above speed of prerotation of 233 rpm and 6-in. pipe diameter, the centrifugal head inside the pipe figures out t be 0.58 ft = $u^2/2g$, which is the height of the paraboloid of pressur (Fig. 3.9). One half of it (0.29 ft) is above the average pressure h (tan level) and the second half below the average. The full meaning Stewart's tests was not appreciated at that time.

If the suction pipe of a single-stage pump is such that a forced vort can be set up and if the suction pressure is measured at the sucti flange, the total head based on the suction head obtained in this w will be lower than its true value. The error is more pronounced lower capacities, thus affecting the shape of the head-capacity a efficiency curves. With large pumps and Francis-type impellers op ating with low velocities in the suction pipe, a forced vortex may

velop in the suction pipe if no means are employed to prevent it. For instance, such a forced vortex was observed at the rated capacity during the field test on the large Colorado River Aqueduct pumps at Intake Station. These pumps take their suction from a lake through a long radius elbow. The suction head, measured at four points around the suction flange, was higher than the static level in the lake, indicating the presence of the paraboloid of pressures caused by the vortex.

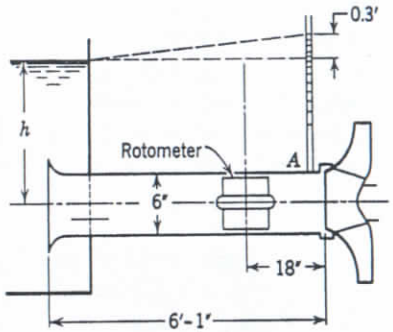

FIG. 3.8. Observation of prerotation in suction pipe by Stewart.[2]

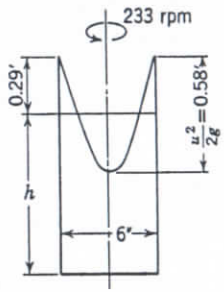

FIG. 3.9. Pressure rise in pipe due to rotation of liquid.

By referring to Figs. 3.8, 3.9 and 1.9, it will be observed that the energy gradient drop is greater along the streamlines in the middle of the suction pipe than along the streamlines near the pipe walls. Thus, higher velocities are expected in the middle of the impeller eye. At low capacities, approaching zero, the difference between the velocities in the suction pipe becomes more pronounced. This gives the impeller an opportunity to increase the tangential component of the velocity of flow near the periphery of the impeller eye by viscous drag of the liquid. *Thus, the energy of the streamlines near the pipe wall may increase and there may be no energy gradient drop available to maintain the flow along these streamlines. As a result, the flow near the impeller periphery may be reversed at capacities approaching zero. Such a back-flow has been observed by several investigators.*[3]

If the liquid approaching the impeller eye acquires prerotation in the direction of impeller rotation, the impeller will be deprived of the opportunity to impart that much of the tangential component to the flow and the entrance part of the impeller vanes will be inactive, taking no power from the shaft. This condition reduces the input head and, consequently, the available total head. It is immaterial whether prerotation is caused by the shape of the channel approach or by the exaggerated

vane entrance angle. Lower input head will result, and the subtractiv term in Euler's equation (3.5) will not equal zero.

An illustration of the above statements is given in Fig. 3.10 showin a water performance of a 4-in. paper stock pump shown in Fig. 3.11 This pump has a booster impeller in the suction nozzle ahead of th regular impeller. Comparison of the performance of this pump witl and without the booster impeller shows that, although the booste

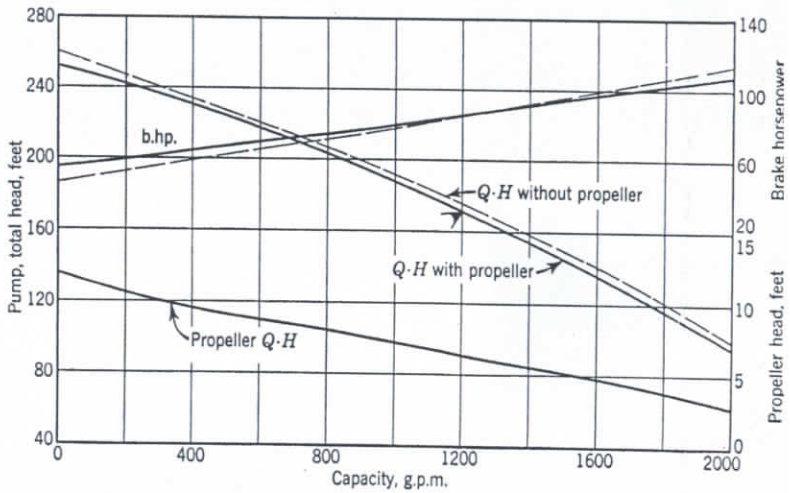

FIG. 3.10. Performance of 4-in. paper stock pump shown in Fig. 3.11, at 1750 rpm

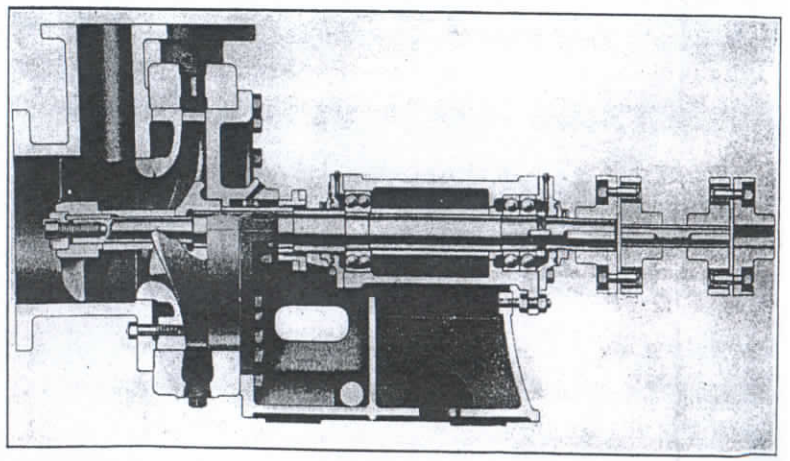

FIG. 3.11. Ingersoll-Rand 4-in. paper stock pump with a booster impeller in the suction nozzle. Performance in Fig. 3.10.

impeller produces an appreciable head, the total combined head is not any higher than that without this impeller; in fact it is slightly lower by the amount of the additional hydraulic losses. The brake horsepower at normal capacity is essentially the same in both cases. Thus the head of the regular impeller was reduced by the amount of head produced by the booster impeller, and the power demand by the first impeller was reduced in proportion to the reduced head.

The design of suction nozzle and impeller approach in modern pumps is such that prerotation is suppressed to a great extent. Thus, although liquid seeks a path of least resistance to enter impeller channels, it is not given sufficient time and space to adjust itself for a shockless entrance at all capacities. As a result, separation of liquid from the impeller vane takes place at capacities other than normal, causing vane pitting as shown in Figs. 12.5 and 12.12.

3.6 DISCUSSION OF EULER'S CHARACTERISTICS AND EULER'S VELOCITY TRIANGLES

(*a*) **Head-Capacity Characteristics.** For simplicity assume no prerotation in the impeller approach. Euler's equation of head (3.8) represents a straight line intersecting the head axis at $H_e = u_2^2/g$ and the axis of capacities at $Q_{max} = A_2 u_2 \tan \beta_2$. A_2 is the impeller discharge area normal to c_{m2} and, since it is constant for a given pump, it can be omitted from the above relationship by incorporating it in a proper scale selection. *The head-capacity characteristics, shown in Fig. 3.12(a), are plotted on suitable dimensionless scales for a given impeller discharge angle β_2 and apply to pumps of all specific speeds and sizes using the same angle β_2 and consistent in design elements.*

The specific speed is used here as a type number for actual pumps at the best efficiency point (b.e.p.) only and is determined by the conditions of minimum hydraulic losses. All points corresponding to the b.e.p. of different specific speeds (n_{s1}, n_{s2}, n_{s3}, etc.) are located on line BA, the specific speeds increasing from B to A. Similarly, Fig. 3.12(*b*) shows Euler's discharge velocity triangles OCB, ODB, OEB for several capacities and applies to several specific speeds with their b.e.p. at points C, D, E, and so on. Each point on line AB, Fig. 3.12(*b*), represents a different specific speed and fixes all important impeller characteristics.

(*b*) **Dimensionless Scales.** Thus line AB on Fig. 3.12(*b*) represents the head-capacity curve for pumps of all specific speeds using the same angle β_2 in the same manner as AB on Fig. 3.12(*a*), but to a different scale. Conversely, by connecting points C, D, E, and so on, to point O on Fig. 3.12(*a*), discharge velocity triangles OBC, OBD and OBE are

obtained if the scales for head and capacity are selected so that the angl OBA is equal to β_2. *By using suitable scales, Euler's head-capacity dia gram and the discharge velocity diagrams become identical.* This is a important property because certain features not clear on one diagra become more apparent on the other.

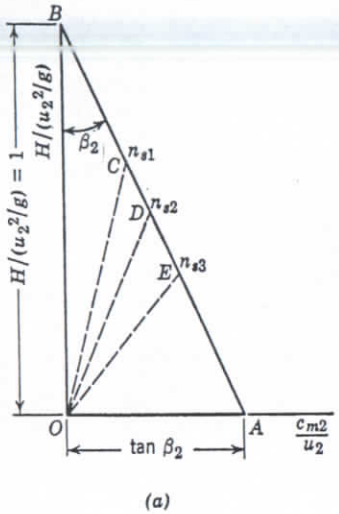

(*a*)

FIG. 3.12. (*a*) Euler's head-capacity characteristics.

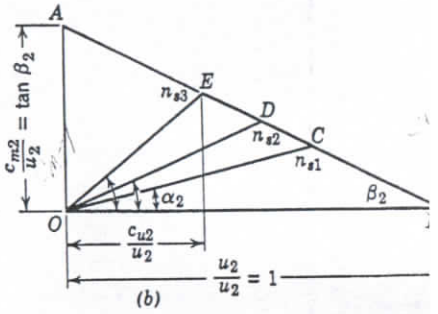

(*b*)

FIG. 3.12. (*b*) Euler's discharge veloc triangle.

The following dimensionless scales (ratios) will bring both the hea capacity and the discharge velocity diagrams to the same scale. T meridional velocity c_{m2} will represent the capacity. On the hea capacity diagram, Fig. 3.12(*a*), heads are expressed as ratios to shut-head, or

$$\psi_e = \frac{H_e}{u_2^2/g} = \frac{u_2 c_{u2} g}{g u_2^2} = \frac{c_{u2}}{u_2} \tag{3.}$$

which will be called the head coefficient. Then, on the velocity diagra heads will be represented to the same scale by use of the ratio

$$\frac{c_{u2}}{u_2} = \psi_e \tag{3.}$$

All velocities on the velocity diagram will be taken as ratios to u_2; t

$$\frac{c_{m2}}{u_2} = \phi_e \tag{3.}$$

will be the meridional velocity on the velocity diagram and will re

sent capacity on both diagrams. This ratio is called the capacity coefficient. The peripheral velocity will be $u_2/u_2 = 1$. The shut-off head on the head-capacity diagram is also equal to unity. The maximum capacity and maximum meridional velocity are equal to

$$\left(\frac{c_{m2}}{u_2}\right)_{\max} = \tan \beta_2 \tag{3.20}$$

(*c*) **Vane Efficiency.** The input head-capacity curve DA for a given β_2 is drawn on Fig. 3.13(*a*). Both Euler's head-capacity curve BA and input head-capacity curve DA meet at zero head.‖

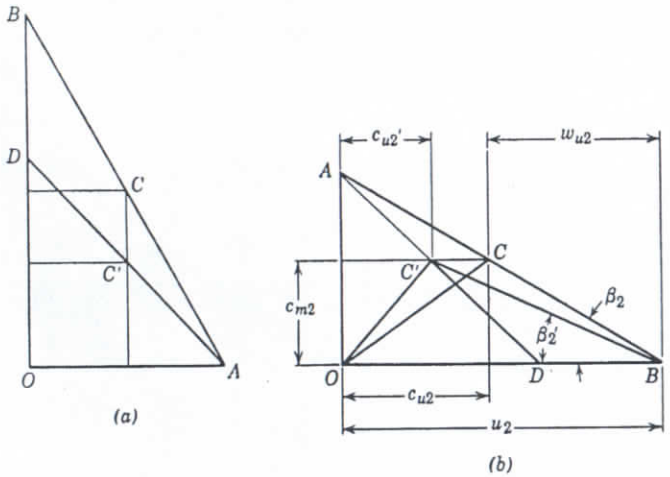

FIG. 3.13. (*a*) Euler's and input head-capacity curves; (*b*) Euler's and input discharge velocity triangles.

The direction of line DA can be determined by locating one point on this line. This point can be estimated, for instance, by assuming or calculating the hydraulic efficiency for the best efficiency point of one existing pump of any specific speed. Then line DA will represent the input head-capacity curve for this particular pump. Moreover, it will represent the input head-capacity characteristics of pumps of all specific speeds having the same discharge vane angle β_2.

The ratio of ordinates for any capacity will be the vane efficiency or $e_{va} = DO/BO$. This is equal for pumps of all specific speeds using the same β_2 and consistent otherwise. Figure 3.13(*b*) represents Euler's velocity triangle drawn to the same dimensionless scale as Fig. 3.13(*a*). By transferring point D from Fig. 3.13(*a*) to Fig. 3.13(*b*), line DA

‖ This assumption is made by several writers.[4]

becomes the locus of all c_{u2}' values for the input velocity triangl $OC'B$ shown for one point C. The vane efficiency then is

$$e_{va} = \frac{H_i}{H_e} = \frac{c_{u2}'}{c_{u2}} \tag{3.2}$$

and is constant for all capacities for pumps of all specific speeds forming continuous series in their hydraulic design.

3.7 FLOW THROUGH THE IMPELLER

The reason impeller vanes cannot apply, and liquid cannot absorb t power required to produce Euler's head, will be seen from the followi considerations.

(*a*) **Pressure Distribution.** In order to transmit power to the liqui pressure p_f on the leading or front face of the vane should be high than pressure p_b on the back of the vane (Fig. 3.14). Any force exert

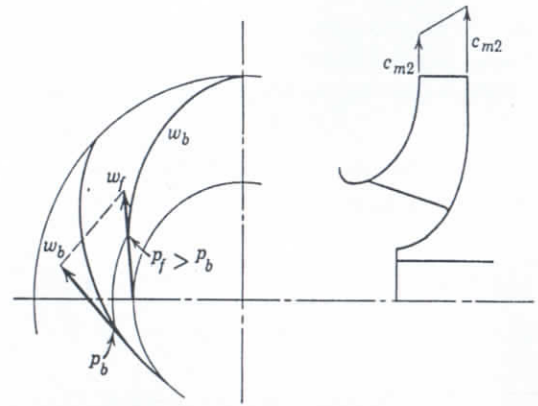

FIG. 3.14. Velocity distribution in an impeller channel.

by the vane on the liquid has an equal and opposing reaction fro the liquid and this can exist only as a pressure difference on two sid of impeller vanes. The immediate effect of such a pressure distribu tion is that relative velocities near the back of the impeller vanes a higher than those near the front of the vane. The velocity triangl Fig. 3.1(*b*), will show that, for a given vane angle, the head produce is lower with higher meridional velocities. Therefore the higher rel tive velocity at the back of the vane will result in lower heads and t total integrated head will be lower than that calculated for an averag velocity of flow, as will be shown later in this chapter.

(*b*) **Velocity Distribution.** Another cause for velocity distortion, which takes place even in an idealized pump, is the effect of turns in the impeller approach and impeller profile. In radial flow and mixed flow impellers the liquid must make nearly a full 90° turn before it is acted upon by the vane. An illustration of velocity distribution in a turn has been given in Chapter 1. The final result of uneven velocity distribution is again a reduction of the maximum head possible; see Fig. 3.14.

(*c*) **Relative Circulation.** The relative velocity distribution through an impeller channel is affected also by the relative circulation of the

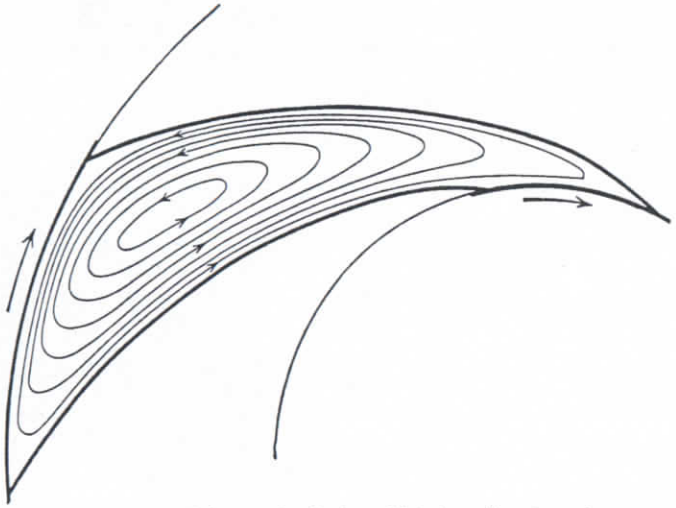

FIG. 3.15. Relative circulation within impeller channel.

liquid due to the inertia effect of frictionless liquid particles; see Figs. 3.15 and 3.16. The particles retain their orientation in space, as shown in Fig. 3.17. Here, particle AB, shown as a sphere, has an arrow AB marked on its body and pointing radially outward from the center. After half a revolution the same particle will have its arrow pointing toward the center, and after a complete revolution the arrow again will be pointing away from the center. The particle, while following the impeller in its translatory movement around the axis, fails to turn with the impeller. This results in a turning movement relative to the impeller. Superimposition of flow through the impeller increases the velocity at the back of the vane and reduces the velocity at the front face of the vane. The result is a component in the tangential direction opposite to c_{u2} at the discharge (Fig. 3.18) and an additional component in the direction of c_{u1} at the entrance (Fig. 3.19). All these

effects reduce the input head. Although the particle within the impeller channel remains irrotational, it travels in a translatory motion in a circular path and therefore is subject to a centrifugal force which causes outward flow through the impeller. Evidently the relative circulation

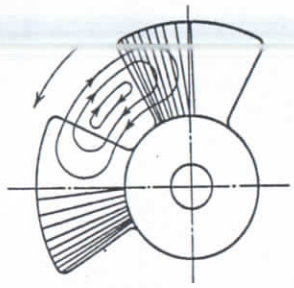

FIG. 3.16. Relative circulation within impeller channels of axial flow pump.

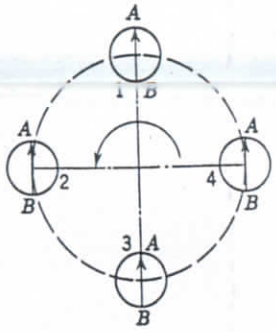

FIG. 3.17. Relative motion of particles is opposite to impeller rotation.

is less with a greater number of vanes, hence the input head and the pump useful head are higher for a greater number of vanes. Also, it is reasonable to expect that relative circulation is smaller in a narrow impeller than in a wide one. For the same impeller diameter, the tota head is greater with a narrow impeller (lower specific speed). The surface friction of shrouds has a decided effect on suppressing the relative circulation within the impeller channel and in imparting rotary motion to the liquid, thereby increasing the tangential component of the absolute

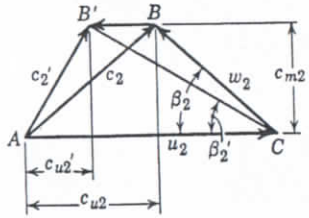

FIG. 3.18. Discharge velocity triangle.

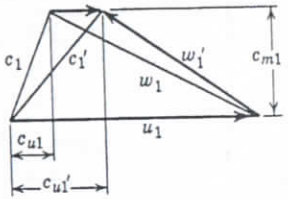

FIG. 3.19. Entrance velocity triangle.

velocity c_{u2} and the absolute velocity c_2. Special tests [5] have show that higher absolute velocities exist near the shrouds at the impelle discharge.

(*d*) **Actual Discharge Angle.** A study of Figs. 3.18 and 3.19 w reveal that the relative circulation of liquid within the impeller van

has the effect of decreasing the liquid discharge angle from vane angle β_2 to β_2'. The inlet angle β_1, on the other hand, is increased to β_1', allowing more prerotation than indicated on Euler's velocity triangle. With actual liquids, power cannot be applied by the vane if the liquid moves in a path having the same relative angle β_2 as the vane itself. In that case the liquid would move outward with the same velocity as the vane sweeps radial distances while turning. In an established flow, whether rotary or straight as in open channel flow, a body must move faster than the established velocity of flow in order to exert any force on the liquid flowing in the same direction. In other words, the vane must have "impelling" action.

It is important to realize that changing the vane angle from β_2 to β_2' will mean only that the liquid will again lag behind the vane and discharge at a smaller angle $\beta_2'' < \beta_2'$.

(e) Non-Active Part of Vane. In an actual pump or an idealized one, the pressure difference on the two faces of a vane disappears at the vane

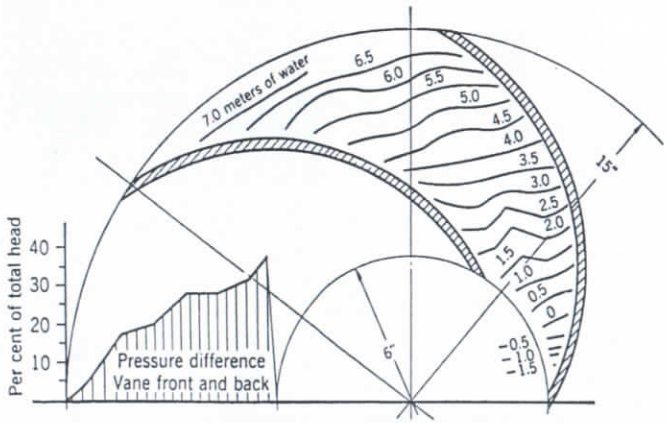

FIG. 3.20. Pressure distribution inside the impeller channel; 316 gpm, 28.6-ft head, 700 rpm, normal capacity 400 gpm (Uchimaru [6]).

tips where the two streams from adjacent impeller channels join. This means that not all of the vane is equally active; in fact, the vane discharge tips have to be inactive since no pressure difference exists there. To unload vane discharge ends the angle β_2 must be reduced. In actual pumps it has been found advantageous to taper off the vane discharge ends, which has the effect of reducing the vane discharge angle.

Pressures on the impeller vanes, as measured by Uchimaru,[6] show that the pressure difference on the two faces has a maximum near the suction end and tapers off to nothing near the discharge end (Fig. 3.20). Such pressure distribution in the actual pump does not entail any additional losses; it simply means that each vane can only transmit, and the liquid can only absorb, a fixed amount of energy. This is lower than that given by Euler's equation.

(f) Theoretical Head with Non-Uniform Meridional Velocity. It has been pointed out, in the previous article, that in an idealized pump the velocity distribution across the impeller channel is not uniform. Under such conditions the theoretical head H_t developed by the impeller is lower than that calculated on the basis of an average velocity.

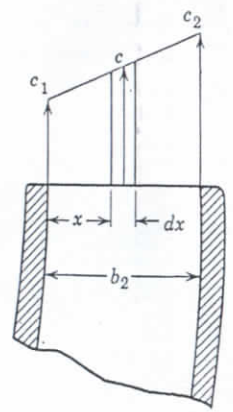

FIG. 3.21. Velocity distribution at impeller discharge.

Assuming that the radial velocity varies uniformly from c_1 at one shroud to c_2 at the other shroud (Fig. 3.21) and at some point located at a distance x from the shroud, the radial velocity is $c = c_1 + ax$ where $a = (c_2 - c_1)/b_2$, b_2 being the impeller width at the discharge. The head produced at this point is

$$H_t = \frac{u_2 c_{u2}}{g} = \frac{u_2}{g}\left(u_2 - \frac{c}{\tan \beta_2}\right) = \frac{{u_2}^2}{g} - \frac{u_2 c}{g \tan \beta_2} \tag{3.22}$$

The volume of water discharged by an element dx of the impeller width is equal to

$$dQ = c\pi D_2\, dx \tag{3.23}$$

The power output of this element is

$$dP = \gamma H_t\, dQ = \gamma H_t c \pi D_2\, dx \tag{3.24}$$

Substituting for H_t its value from equation 3.22, we get

$$dP = \left(\frac{{u_2}^2}{g} - \frac{u_2 c}{g \tan \beta_2}\right) \gamma \pi D_2 c\, dx \tag{3.25}$$

For brevity,

$$\frac{{u_2}^2}{g} = A \qquad \frac{u_2}{g \tan \beta_2} = B \qquad \gamma \pi D_2 = C$$

The equation then takes the form

$$dP = (A - Bc)Cc\, dx = C(Ac - Bc^2)\, dx$$

Substituting for c its value $c = c_1 + ax$,

$$dP = C[A(c_1 + ax) - B(c_1 + ax)^2]\, dx$$

Integrating between the limits 0 and b_2, we obtain the power output of the impeller.

$$P = \int_0^{b_2} CA(c_1 + ax)\,dx - \int_0^{b_2} CB(c_1 + ax)^2\,dx$$

$$= CA\left[\frac{(c_1 + ax)^2}{2a}\right]_0^{b_2} - BC\left[\frac{(c_1 + ax)^3}{3a}\right]_0^{b_2}$$

$$= CA\left[\frac{(c_1 + ab_2)^2}{2a} - \frac{c_1^2}{2a}\right] - BC\left[\frac{(c_1 + ab)^3}{3a} - \frac{c_1^3}{3a}\right]$$

But $c_1 + ab_2 = c_2$; then

$$P = CA\,\frac{(c_2^2 - c_1^2)}{2a} - CB\,\frac{(c_2^3 - c_1^3)}{3a}$$

Substituting for a its value $a = (c_2 - c_1)/b_2$ and letting c_m denote $(c_2 + c_1)/2$, the mean radial velocity, the expression for the power output takes the form

$$P = CA\,\frac{(c_2 - c_1)(c_2 + c_1)}{2a} - CB\,\frac{(c_2 - c_1)(c_2^2 + c_2c_1 + c_1^2)}{3a}$$

$$= CAb_2c_m - CBb_2\,\frac{(c_2^2 + c_2c_1 + c_1^2)}{3}$$

The average head produced by the impeller is obtained by dividing the impeller power output by the weight of liquid discharged W.

$$W = \gamma\int_0^{b_2} dQ = \gamma\int_0^{b_2} c\pi D_2\,dx$$

$$= \gamma\int_0^{b_2} D_2(c_1 + ax)\,dx = \gamma\pi D_2\left(c_1b_2 + \frac{ab_2^2}{2}\right)$$

$$= \gamma\pi D_2\left[c_1b + \frac{(c_2 - c_1)b_2^2}{2b_2}\right] = \gamma\pi D_2b_2\,\frac{c_2 + c_1}{2}$$

$$W = \gamma\pi D_2b_2c_m = Cb_2c_m \tag{3.26}$$

which could be written at once, since the velocity involved is a linear function of x.

$$H_t = \frac{P}{W} = A + \frac{B}{c_m}\left(\frac{c_2^2 + c_2c_1 + c_1^2}{3}\right)$$

$$= A + \frac{B}{c_m}\left[\frac{(c_2 + c_1)^2 - c_2c_1}{3}\right]$$

$$= A + \frac{B}{c_m}\left[\frac{3(c_2 + c_1)^2 + (c_2 + c_1)^2 - 4c_2c_1}{12}\right]$$

$$H_t = A + \frac{B}{c_m}\left[\left(\frac{c_2 + c_1}{2}\right)^2 + \frac{(c_2 - c_1)^2}{12}\right] \tag{3.27}$$

$$= A - \frac{B}{c_m}\left[c_m^2 + \frac{(c_2 - c_1)^2}{12}\right]$$

$$= A - Bc_m\left[1 + \frac{(c_2 - c_1)^2}{12c_m^2}\right]$$

$$H_t = \frac{u_2^2}{g} - \frac{u_2c_m}{g\tan\beta_2}\left[1 + \frac{(c_2 - c_1)^2}{12c_m^2}\right] \tag{3.28}$$

A comparison of this equation with 3.22, shows that the average theoretical head produced by an impeller with radial velocity varying from c_1 to c_2 is smaller than that for the mean radial velocity c_m.

The difference in the head is greater for a greater difference between c_2 and c_1, this difference disappearing when c_2 is equal to c_1. The effect of the variable radial velocity on the head produced will be understood more clearly if it is kept in mind that the elementary equation 3.2 gives the head per pound of liquid pumped and that more pounds per second of the low pressure liquid are discharged by the impeller when the radial velocity is greater, since the head developed is smaller for higher radial velocity.

From equation 3.28 it is seen that for the same ratio of c_2 to c_1 the correction factor is more effective for impellers for which the second term $u_2c_m/(g\tan\beta_2)$ is greater in comparison with the first or u_2^2/g. In normal designs the second term is greater for impellers of high specific speed; hence the correction affects more the theoretical head for these impellers. In addition, the factor $\left[1 + \frac{(c_2 - c_1)^2}{12c_m^2}\right]$ is greater for wide impellers, since the velocity distortion is greater and the length of the water path is smaller for impellers of high specific speed. This explains the reason for a greater discrepancy between the theoretical and the actual heads for impellers of higher specific speed.

It is evident that equation 3.28 holds for the velocity distribution with a linear relation between the maximum and minimum velocity

For any other relation between the minimum and maximum radial velocities the form of the expression for the correction factor will change, but the significance of the expression will remain the same.

REFERENCES

1. H. F. Schmidt, "Some Screw Propeller Experiments," *J. Am. Soc. Naval Engrs.*, Vol. XL, p. 16, February 1928.
2. C. B. Stewart, "Investigation of Centrifugal Pumps," *Univ. of Wisc., Bull.* 318, p. 119, September 1909.
3. Karl Fischer, "Untersuchung der Strömung in einer Zentrifugalpumpe," *Mitt. Hyd. Inst. Tech. Hochschule München, Bull.* 4, Berlin, Oldenbourg, p. 13, 1931.
4. Joseph Lichtenstein, "Method of Analyzing the Performance Curves of Centrifugal Pumps," *Trans. A.S.M.E.*, Vol. 50, No. 3, p. 3, 1928.
5. R. C. Binder and R. T. Knapp, "Experimental Determination of the Flow Characteristics in the Volutes of Centrifugal Pumps," *Trans. A.S.M.E.*, Vol. 58, No. 8, p. 649, November 1936.
6. Saichiro Uchimaru, "Experimental Research on the Distribution of Water Pressure in a Centrifugal Pump Impeller," *J. Faculty Eng. Tokyo Imp. Univ.*, Vol. XVI, No. 6, 1925.
7. A. J. Stepanoff, *Turboblowers: Theory, Design, and Application of Centrifugal and Axial Flow Compressors and Fans*, New York, John Wiley and Sons, Inc., 1955.

Chapter 4

Vortex Theory of Euler's Head

4.1 RADIAL IMPELLER

Flow through the impeller can be considered as consisting of two com ponents: a circular motion around the axis as a result of the impellin action of the vanes, and through-flow or meridional flow caused by the energ gradient drop. The circular component of flow forms a vortex motion The type of vortex depends on the velocity and pressure distributio and can be established from a study of Euler's equation. For sim plicity, consider first a straight radial impeller in which the flow ap proaches the impeller eye without prerotation. Euler's equation fo this case, Fig. 3.1(*b*), is

$$H_e = \frac{u_2 c_{u2}}{g} = \frac{u_2^2}{g} - \frac{u_2 c_{m2}}{g \tan \beta_2} = \frac{u_2^2}{g} - \frac{u_2 w_{u2}}{g} \qquad (4.1$$

Only tangential velocities appear in equation 4.1, indicating that a head is produced by vortex action in planes normal to the axis of rota tion. If will be shown that this is true, in general, for all centrifuga pumps, including straight axial flow pumps.

When the flow is zero ($w_{u2} = 0$), Euler's head becomes

$$H_e = \frac{u_2^2}{g} = 2\frac{u_2^2}{2g} \qquad (4.2$$

and the total head at any radius r is equal to

$$H = 2\frac{u^2}{2g} \qquad (4.2a$$

where u is the peripheral velocity at radius r. This head is equally divided between static and kinetic heads. Such energy distributio along the radius is typical for a forced vortex and is represented by a square parabola OA in Fig. 4.1. When flow starts, the head drops by an amount $u_2 w_{u2}/g$, where w_{u2} is proportional to the flow. *This drop of head is the energy gradient drop necessary to produce flow, because ever*

an idealized pump (no losses) cannot start flow against a head higher than or equal to its zero flow head. It is also evident that a further drop of energy gradient is necessary to increase the flow or produce a higher capacity. Thus the total head drops from AE to CE on Fig. 4.1. The value of u_2w_{u2}/g decreases with decreasing radii and the head variation along the radius is represented by a parabolic curve OC. In a straight radial impeller the relative velocity and vane angle vary little along

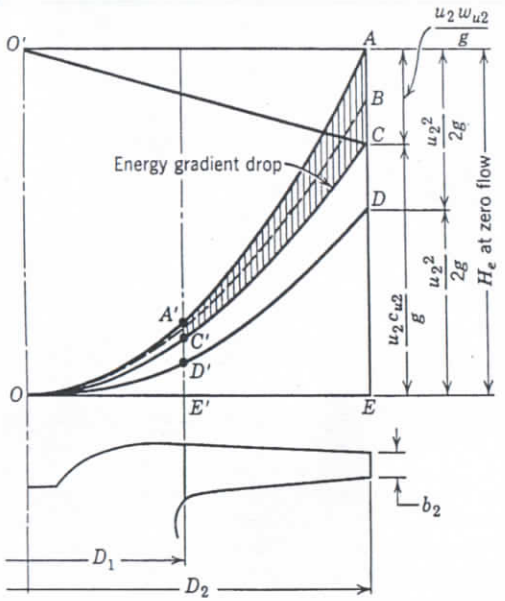

FIG. 4.1. Euler's head, radial flow impeller.

the radius, and the tangential component of the relative velocity (w_{u2}) will also vary little. Assuming the latter to be constant along the radius, the energy gradient drop u_2w_{u2}/g will vary as u_2 or will increase directly as the distance traveled by the flow ($O'C$ on Fig. 4.1.) This is analogous to the hydraulic gradient drop in pipe flow of constant velocity. However, in this case the drop in hydraulic gradient represents hydraulic loss along the pipe, whereas *in a centrifugal pump impeller the drop in energy gradient is a condition which is necessary to realize flow and which results in an equal reduction of the impeller input.* As the capacity increases, the energy gradient drop increases and Euler's head decreases.

The energy gradient drop u_2w_{u2}/g can be considered a turbine reaction of the pump impeller. While pumping, an impeller acts as a turbine

runner. With the head u_2w_{u2}/g applied to the impeller eye and the direction of flow as it exists in the pump impeller, the direction of rotation due to turbine reaction will be the same as that of the pump. The torque developed by the turbine action will act in the same sense as the applied torque. As a result the impeller power input is reduced by the value of u_2w_{u2}/g (Fig. 4.2). There being no losses in an idealized machine, the turbine reaction returns to the shaft the energy put into it by the flow caused by the energy gradient drop.

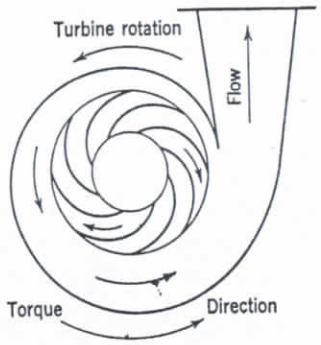

FIG. 4.2. Turbine reaction of impeller.

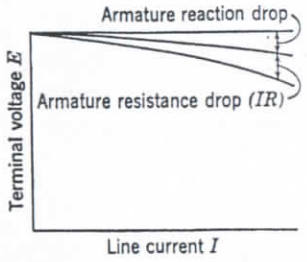

FIG. 4.3. Regulation curve of a direct-current generator.

The turbine reaction of a pump impeller is analogous to the armature reaction of a direct-current generator. Figure 4.3 shows a relationship between the voltage E (corresponding to the pump head) and current I (corresponding to the pump capacity) for a direct-current generator. The general appearance of E-I curves resembles that of the Q-H curve representing Euler's equation in Fig. 3.3.

For any rate of flow,

$$\frac{u_2^2}{g} = \frac{u_2c_{u2}}{g} + \frac{u_2w_{u2}}{g} \tag{4.3}$$

$$\frac{u_2^2}{g} = \text{pump action} + \text{turbine reaction}$$

Note the similarity of the algebraic expression for the first and second terms of the right-hand part of equation 4.3 representing pumping action and turbine reaction.*

* Applying the same reasoning to a hydraulic turbine runner, it can be stated that the runner, while rotating under applied head, generates a centrifugal head analogous to the back-electromotive force of an electric motor. The flow through th

If prerotation is allowed in the impeller approach, Euler's equation takes the form

$$H_e = \frac{u_2 c_{u2}}{g} - \frac{u_1 c_{u1}}{g} = \frac{u_2^2}{g} - \frac{u_2 w_{u2}}{g} - \frac{u_1 c_{u1}}{g}$$

hence

$$\frac{u_2^2}{g} = \left(\frac{u_2 c_{u2}}{g} - \frac{u_1 c_{u1}}{g}\right) + \left(\frac{u_2 w_{u2}}{g} + \frac{u_1 c_{u1}}{g}\right)$$

$$= \text{pump action} + \text{turbine reaction}$$

Figure 4.4 represents the same relationship graphically.

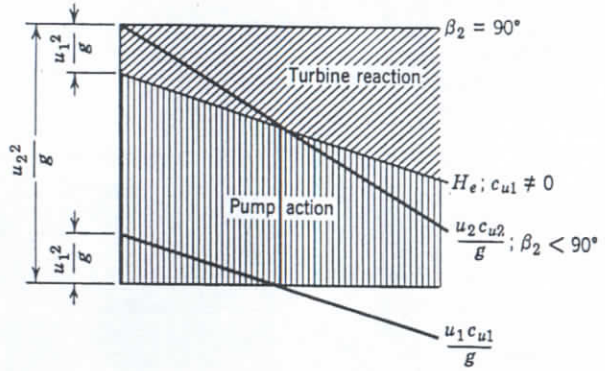

FIG. 4.4. Pump action and turbine reaction with prerotation allowed.

If the flow approaching the impeller eye is not radial, or prerotation is allowed, Euler's equation (4.1) will change to

$$H_e = \frac{u_2 c_{u2}}{g} - \frac{u_1 c_{u1}}{g} \tag{4.4}$$

It will be noticed that the second or subtractive term is similar to the first term. Following the same reasoning applied to the first term will reveal that the subtractive term represents the part OC' of the parabolic head curve OC (Fig. 4.1), and thus the total head will be obtained as the difference $CE - C'E' = H_e$.

For each capacity there is a parabolic curve located somewhere between OA and OE representing the head variation along the impeller radius. The line OE is reached at zero head or when $w_{u2} = u_2$ in equation 4.1.

runner is determined by the difference between the head applied and the centrifugal head developed by the runner. A further reference to this subject is found in Chapter 13.

By using Euler's head equation in the expanded form,

$$H_e = \frac{u_2^2 - u_1^2}{2g} + \frac{c_2^2 - c_1^2}{2g} + \frac{w_1^2 - w_2^2}{2g} \tag{4.5}$$

it can be shown that each component part of the total head as it appears in this equation represents a vortex motion. By making use of the geometrical relationships

$$c_1^2 = c_{u1}^2 + c_{m1}^2 \qquad w_1^2 = w_{u1}^2 + c_{m1}^2$$

$$c_2^2 = c_{u2}^2 + c_{m2}^2 \qquad w_2^2 = w_{u2}^2 + c_{m2}^2$$

equation 4.4 can be changed to

$$H_e = \frac{u_2^2 - u_1^2}{2g} + \frac{c_{u2}^2 - c_{u1}^2}{2g} + \frac{w_{u1}^2 - w_{u2}^2}{2g} \tag{4.6}$$

Only tangential velocities appear in this equation and the radial velocities at entrance and discharge, not equal in general, cancel out. This shows again that all changes in velocities as a result of impeller action take place in planes normal to the axis of rotation producing a vortex motion. With radial approach $c_{u1} = 0$ and $w_{u1} = u_1$, equation 4.5 reduces to

$$H_e = \frac{u_2^2}{2g} + \frac{c_{u2}^2}{2g} - \frac{w_{u2}^2}{2g} \tag{4.7}$$

As the capacity approaches zero, w_{u2} approaches zero, and c_{u2} approaches u_2. *So at zero flow,*

$$H_e = \frac{u_2^2}{g} = \frac{u_2^2}{2g} + \frac{c_{u2}^2}{2g} \tag{4.7a}$$

showing that at zero capacity the total head is equally divided between static head and kinetic energy. At zero head, $c_{u2} = 0$ and $w_{u2} = u_2$; then

$$H_e = \frac{u_2^2}{2g} - \frac{w_{u2}^2}{2g} = 0 \tag{4.7b}$$

showing that the flow is meridional, under energy gradient, and there is no vortex produced by the impeller.

4.2 AXIAL FLOW IMPELLER

In an axial flow pump, liquid particles leave the impeller at the same radius at which they enter. Applying Euler's equation (4.6) to a point on the impeller periphery and noting that $u_2 = u_1$, we get

$$H_e = \frac{c_{u2}^2 - c_{u1}^2}{2g} + \frac{w_{u1}^2 - w_{u2}^2}{2g} \tag{4.8}$$

Again assuming first that the liquid approaches the impeller without prerotation ($c_{u1} = 0$ and $w_{u1} = u_1$), equation 4.8 reduces to

$$H_e = \frac{u_2^2}{2g} + \frac{c_{u2}^2}{2g} - \frac{w_{u2}^2}{2g} \tag{4.8a}$$

Substituting $c_{u2} = u_2 - w_{u2}$, we obtain

$$H_e = \frac{u_2^2}{g} - \frac{u_2 w_{u2}}{g} \tag{4.9}$$

Because this is exactly the same as equation 4.1, it indicates that *the process of generating head is the same in axial flow pumps as it is in radial*

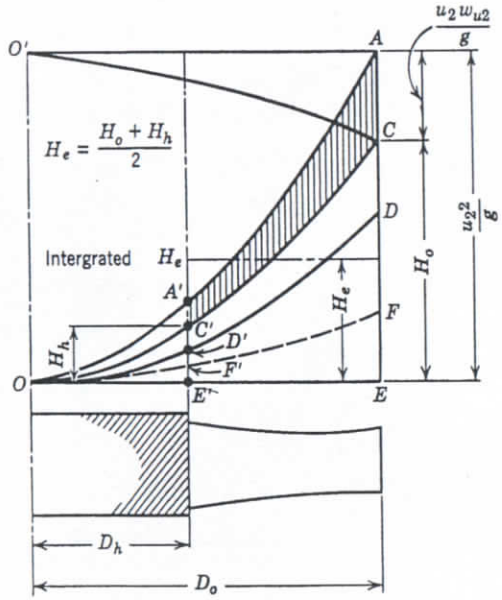

FIG. 4.5. Euler's head, axial flow impeller.

flow pumps. In both, head is generated through the vortex motion and the flow through the impeller is caused by the energy gradient drop $u_2 w_{u2}/g$. The head distribution along the radius is shown on Fig. 4.5, where curve AA' shows the head at different radii with zero flow. This is a square parabola. Curve CC' shows the head variation for one rate of flow (w_{u2}). AC is the energy gradient drop at the periphery. Ordinates between curves AA' and CC' represent the energy gradient drop for different radii. It will be shown later in this chapter that for a normal design both w_{u2} and u_2 vary directly as the radius. Therefore the energy gradient drop $u_2 w_{u2}/g$ varies directly as the square of the radius

(curve $O'C$), and the curve of heads OC is a square parabola. This is a characteristic of a forced vortex when all particles rotate with the same angular velocity.

Although the head distribution along the radii is similar for radial and axial pumps there is an important difference between the final results of the two. In a radial impeller all particles reach the same maximum head at the periphery of the impeller. In an axial flow pump, liquid particles enter and leave at the same radii and the head produced at different radii are different, being a maximum at the periphery and a minimum at the hub. The pump total head is an integrated average. The hydraulic integration of the head over the whole impeller area takes place in the discharge casing, where the tangential component of the absolute velocity is converted into pressure and the pressure is equalized over the whole area of the discharge pipe. In an efficient diffusion casing, this equalization of pressure occurs without mixing of streamlines, as demonstrated with axial blowers by admitting smoke and sparks into the suction.[1] Evidently the pressure equalization takes place by conduction. (See Chapter 1.) Figure 4.6 shows a diagram of hydraulic integration. The volume of the liquid in the two legs of the U-tube is the same. In the left leg, liquid is in rotation. The column of liquid at the center of the left leg supports a higher head H in the right-hand leg of the tube. The integrated head of the impeller in Fig. 4.5 is equal to the average of the head at the hub (H_h) and the head at the periphery (H_o). This follows from the geometrical properties of a square paraboloid.

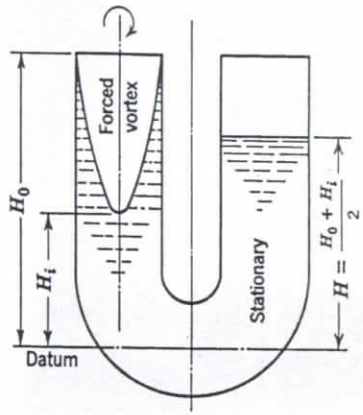

FIG. 4.6. Diagram of hydraulic integration.

$$H_e = \frac{H_h + H_o}{2} \tag{4.10}$$

If the liquid approaches the impeller with prerotation, Euler's head for an axial flow impeller is given by equation 4.4 which is the same as for the radial impeller. The subtractive term is of the same appearance as the first terms, and represents a square parabola of suction heads at different radii (FF', Fig. 4.5). The net Euler's head at different radii is represented by ordinates between the curves CC' and FF'. The curve of the net Euler's head will remain a square parabola.

4.3 FORCED VORTEX AXIAL FLOW IMPELLER

(*a*) **Inlet and Outlet Pitch, Pitch per Second.** All theoretical discussion and practical design of axial flow pumps are based on the assumption of constant axial velocity through the impeller. The axial velocity of approach to the impeller and beyond the impeller is assumed to be equal to that through the impeller. This assumption is reasonable with a normal design except for the effects of frictional drag at the casing and impeller walls. Such distribution has been actually observed on axial flow blowers. To maintain a uniform axial velocity the impeller vane

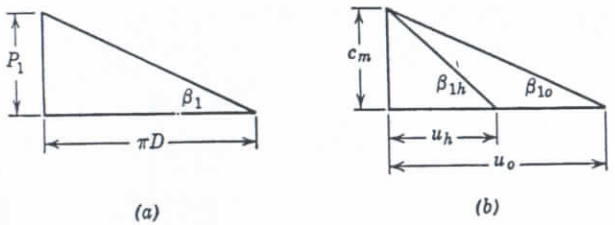

FIG. 4.7. (*a*) Inlet pitch; (*b*) inlet velocity triangle for axial flow pump.

should have the same inlet pitch at different radii. The latter is defined as $P_1 = \pi D \tan \beta_1$ where P_1 is inlet pitch, D is impeller diameter, and β_1 is the vane entrance angle, Fig. 4.7(*a*).

There is a definite relationship between the axial velocity c_m at normal capacity and pitch P_1. From the entrance velocity triangle, Fig. 4.7(*b*),

$$\frac{c_m}{u_o} = \tan \beta_{1o} \qquad \text{and} \qquad \frac{c_m}{u_h} = \tan \beta_{1h} \tag{4.11}$$

where subscript o refers to the outside diameter and h refers to the hub. But

$$u_h = \pi D_h \times \text{rps} \qquad u_o = \pi D_o \times \text{rps} \tag{4.12}$$

and

$$\tan \beta_{1h} = \frac{P_h}{\pi D_h} \qquad \tan \beta_{1o} = \frac{P_o}{\pi D_o} \tag{4.13}$$

$$c_m = P_h \times \text{rps} = P_o \times \text{rps} = P_1 \times \text{rps} = P_{1s} \tag{4.14}$$

Thus, to maintain a constant axial velocity c_m, the vane inlet pitch at all radii should be constant.

To provide impelling action, the impeller vane angles should increase gradually from inlet toward discharge or the vane pitch should increase. To maintain the same axial velocity along the radii the pitch for all radii should remain constant to assure the same degree of impelling

action for several streamlines of different radii. Thus, by definiti (Fig. 4.8),

$$P_2 = \pi D_h \tan \beta_{2h} = \pi D_o \tan \beta_{2o} \tag{4.1}$$

and, multiplying by the revolutions per second, we obtain (Fig. 4.1

$$P_2 \times \text{rps} = u_h \tan \beta_{2h} = u_o \tan \beta_{2o} = P_{2s} \tag{4.1}$$

P_{2s} may be called discharge pitch per second, a term which will be us in discussing axial flow impeller geometry. Similarly $P_1 \times \text{rps} = P$

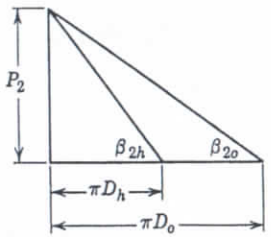

FIG. 4.8. Outlet pitch.

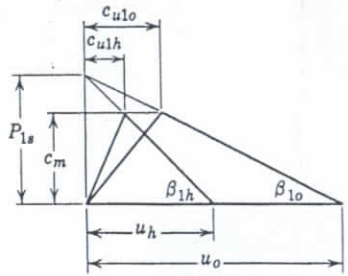

FIG. 4.9. Axial flow pump entrance triangle with prerotation.

may be called inlet pitch per second. With an axial inlet velocit $P_{1s} = c_m$ at normal capacity.

If some prerotation is allowed ahead of the impeller and the va entrance angles are so selected that the entrance pitch is constant alo the radius, the entrance velocity triangle will be as shown on Fig. 4.9 where $P_{1s} > c_m$ at normal capacity.

The differences $(P_{1s} - c_m)$ and $(P_{2s} - c_m)$ are frequently referred to as axial slip. This term is misleading as slip is usually associated with loss of capacity and corresponding drop in volumetric efficiency. However, with axial flow pumps there is no connection between $(P_{1s} - c_m)$ and volumetric efficiency. Thus at half-normal capacity the slip $[(P_{1s} - c_m)/c_m]$ may more than one half, but a pump gross efficiency considerably over 50 p cent is quite common. Also, at a capacity over the normal, $(P_{1s} - c$

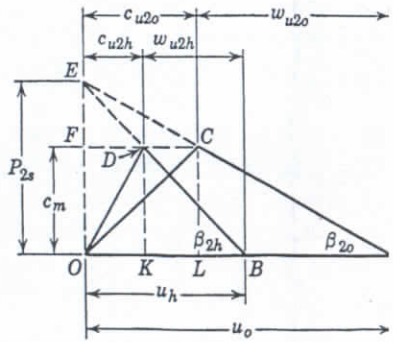

FIG. 4.10. Discharge velocity triangle, a flow pump.

is negative while the efficiency is decreasing after reaching a maximum at the normal capacity.

(*b*) **Forced Vortex Action.** A constant pitch P_1 at entrance and P_2 at discharge, where $P_2 > P_1$, assures a forced vortex motion of the liquid by the impeller. Assuming an axial inlet, it follows from consideration of two pairs of similar triangles *OEB* and *EFD*, *OEA* and *EFC* of Fig. 4.10, that

$$\frac{c_{u2h}}{u_h} = \frac{c_{u2o}}{u_o} = \frac{P_{2s} - c_m}{P_{2s}} \tag{4.17}$$

hence

$$\frac{c_{u2h}}{r_h} = \frac{c_{u2o}}{r_o} = \omega' \tag{4.18}$$

where ω' is the angular velocity of the absolute flow leaving the impeller which is constant for all streamlines at different radii. This is the requirement for a forced vortex.

From similar triangles *EBO* and *DBK*, *EAO* and *CLA* (Fig. 4.10),

$$\frac{w_{u2h}}{u_h} = \frac{w_{u2o}}{u_o} = \frac{c_m}{P_{2s}} \quad \text{and} \quad \frac{w_{u2h}}{r_h} = \frac{w_{u2o}}{r_o} = \omega''$$

also

$$\omega' + \omega'' = \omega \tag{4.19}$$

where ω'' is the relative angular velocity of flow, also constant for all streamlines.

The forced vortex regime is maintained at all capacities, or all values of c_m. Zero head ($c_u = 0$) occurs simultaneously at all streamlines at $c_m = P_{2s}$. Also, zero capacity takes place at the same time at all points on different radii when $c_m = 0$.

To summarize: *Euler's head in an axial flow pump can be generated by a forced vortex motion. To produce a forced vortex the impeller has to be of constant pitch along the radius, the pitch increasing from suction to discharge.* The pitch at the suction edge fixes the axial velocity at normal capacity. *The ratio of the pitch per second at discharge P_{2s} to the axial velocity c_m is a measure of the impelling action of the vane and will be referred to as an impelling ratio.*

$$\frac{P_{2s}}{c_m} = \text{impelling ratio} \tag{4.20}$$

For the axial flow impellers without prerotation, the impelling ratio becomes the pitch ratio, since

$$\frac{P_{2s}}{c_m} = \frac{P_{2s}}{P_{1s}} = \frac{P_2}{P_1} = \frac{\tan \beta_2}{\tan \beta_1} \tag{4.20a}$$

The impelling ratio varies with the capacity, increasing as the capacity c_m is decreasing. It is equal to unity at zero head point since the axial velocity c_m at that point is equal to P_{2s}. There is no impelling action when the impelling ratio is equal to unity.

Thus, when there is no slip ($P_{2s} - c_m = 0$), there is no impelling action, and impelling action is increasing as the slip is increasing.

(*c*) Mixed Flow Impellers. It has been shown that the action of impellers is the same in a straight radial flow and a straight axial flow pump. This action consists in producing a forced vortex which is superimposed on a radial outward flow in the first case and upon a uniform axial flow in the latter case. The mixed flow impellers occupy an intermediate position between the above two types. Therefore all the deductions for radial and axial flow pumps apply as well to the mixed flow types. The meridional velocity at the entrance c_{m1} is not equal to that at discharge; normally $c_{m1} > c_{m2}$. In drawing the discharge angles, the same procedure is followed as in Fig. 4.10 for axial flow impellers, the impelling ratio P_{2s}/c_m being selected. It should be noted that with mixed flow impellers a vane having a prescribed impelling ratio may have a discharge angle at the hub lower than the entrance angle $\beta_{2h} < \beta_{1h}$. This depends on the relative values of c_{m2} and c_{m1} and impeller profile.

With radial impellers $\beta_2 < \beta_1$ is a most frequent occurrence. The impelllng ratio as defined by equation 4.20 applies equally to the radial impellers. The pitch per second at discharge P_{2s} for radial impellers is defined in the same manner as for axial flow impellers.

$$P_{2s} = u_2 \tan \beta_2$$

and the impelling ratio is

$$\frac{P_{2s}}{c_{m2}} = \frac{u_2 \tan \beta_2}{c_{m2}} = \frac{\tan \beta_2}{c_{m2}/u_2} = \frac{\tan \beta_2}{\phi_e} \tag{4.20b}$$

where ϕ_e is capacity coefficient, defined by equation 3.19.

The impelling ratio increases as the specific speed at b.e.p. decreases. The impelling ratio is discussed further in Chapter 9, in connection with other design elements incorporated in the author's diagram of centrifugal pump characteristics represented in Fig. 9.13.

(*d*) Free Vortex Pattern of Flow through the Axial Flow Impeller. The forced vortex pattern of flow, as a basis of the impeller action on the liquid, is not the only one possible when applied to straight axial flow pumps. A free vortex pattern of flow for axial flow pumps is assumed by many writers on the subject mostly in connection with th

airfoil theory. According to this, the tangential velocity distribution along the radius follows the law

$$c_{u2}r = \text{constant} \tag{4.21}$$

This is arrived at by assuming that the same head is generated at all radii, or

$$uc_{u2} = gH = \text{constant} \tag{4.21a}$$

which is Euler's head equation with an axial inlet velocity. Both assumptions are motivated by reasoning that only at these conditions is

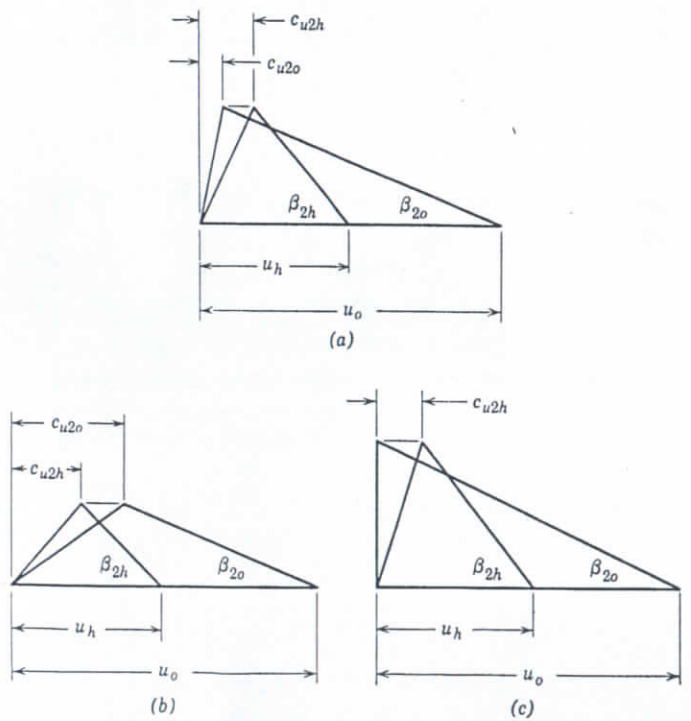

FIG. 4.11. (*a*) Discharge velocity triangle at rated point, free vortex; (*b*) velocity triangle at partial capacity; (*c*) velocity triangle at capacity over the normal.

the flow stable or free from cross flows. In Chapter 1 it has been shown that a free vortex is only one mode of circular motion of liquids out of a great many possible ones, all of which are stable. There are several objections to a free vortex flow pattern as a basis for the theoretical reasoning of the axial flow pump impeller action, some of which have been pointed out in more recent writings on the subject:[2]

1. Free vortex motion of liquid at the impeller discharge can exis at one point on the head-capacity curve only. If Fig. 4.11(*a*) represent Euler's velocity triangle, at the design point

$$c_{u2h}r_h = c_{u2o}r_o = \text{constant} = C \tag{4.22}$$

which means that the tangential component is inversely proportiona to the radius. Then at partial capacity c_{u2o} becomes greater tha c_{u2h}, and the regime approaches a forced vortex, Fig. 4.11(*b*). At zer capacity the flow becomes a forced vortex. At capacities over the rated, c_{u2o} will become zero, while c_{u2h} is not, Fig. 4.11(*c*). At a still greater capacity, c_{u2o} becomes negative.

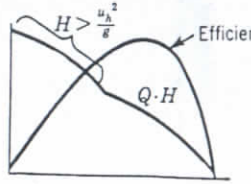

FIG. 4.12. Axial flow pum characteristics.

2. Acutal test curves show that at capacities below one half of normal (Fig. 4.12) the total head H is equal to or exceeds u_h^2/g. This is a maximum possible theoretical head at the hub. Evidently a theory assuming a constant head for all radii does not hold at capacities less than norma and some different assumption is required.

3. Since the tangential components vary inversely as the radius a the b.e.p., the angular velocity of the absolute flow will vary inversely as the square of radius, as the following relationships show. From equation 4.22

$$\omega_h = \frac{c_{u2h}}{r_h} = \frac{C}{r_h^2}$$

and

$$\omega_o = \frac{c_{u2o}}{r_o} = \frac{C}{r_o^2} \tag{4.23}$$

Such an angular velocity distribution is not easy to visualize in view of the constant angular velocity of the impeller which is responsible for all changes in velocities.

4. The advocates of the free vortex pattern of flow for axial flow pumps usually resort to selection of impeller vane sections from airfoil test data. This procedure is not applicable to extreme mixed flow impellers or straight radial flow impellers. Thus the pump designer is left to his own resources in filling the gap between the straight radial and straight axial impeller types.

The forced vortex reasoning of impeller action is free from these drawbacks because:

1. It applies equally well to straight centrifugal, mixed flow, and straight axial flow pumps.

2. With axial flow pumps the forced vortex regime is maintained for the whole head-capacity range. Zero head and zero capacity points occur at the same time at the hub and periphery of the impeller.

3. A constant absolute angular velocity is maintained at all capacities ahead, through, and beyond the impeller, this velocity increasing as the capacity decreases.

4. Head generated at different radii of the impeller expressed as a fraction of the maximum head at zero capacity is constant.

$$\psi_e = \frac{H_e}{u_2^2/g} = \frac{c_{u2}}{u_2} = \text{constant}$$

where ψ_e, the head coefficient defined by equation 3.17, is constant for all radii and at all capacities. Thus, at each radius the impeller vane elements transmit the same amount of energy (Hg) per foot of peripheral velocity or, stated differently, the "dimensionless head" ψ_e produced at different radii is constant at all capacities.

5. Using a forced vortex pattern of flow leads to a geometrical procedure of impeller vane layout which is valid for straight axial flow impellers as well as for mixed flow impellers of any profile.

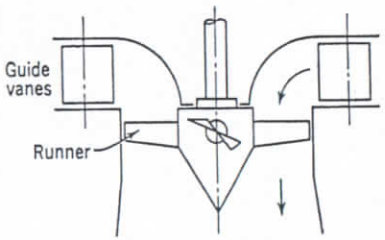

FIG. 4.13. Axial flow water turbine.

The use of a free vortex theoretical treatment of operation of hydraulic axial flow water turbines is the only one possible because the same head is actually applied to all streamlines. Radial guide vanes (Fig. 4.13) give the water the same tangential component for all streamlines. The flow between the guide vanes and the impeller follows closely the law $c_u r$ = constant.

4.4 REMARKS

(*a*) **Reverse Rotation.** Since the theoretical head at shut-off does not depend on the impeller vane angle, one may expect that an impeller running in a direction opposite to that of normal should develop the same head at zero capacity. In practice, however, it has been found that the pump develops only about one half of the shut-off head under normal operation. The difference is not in the impeller performance but in the casing and method of measuring heads. Thus, in a normally operated pump, losses being disregarded and an impeller developing full

u_2^2/g shut-off head being assumed, a gage at A, Fig. 4.14(*a*), will register only the static head $u_2^2/2g$. A gage at B will register both the static and the dynamic head or u_2^2/g.

When the impeller rotation is reversed, Fig. 4.14(*b*), the pressure at A will remain the same or $u_2^2/2g$, but pressure at B will be lower than at A because of a negative dynamic head or suction exerted by the flow

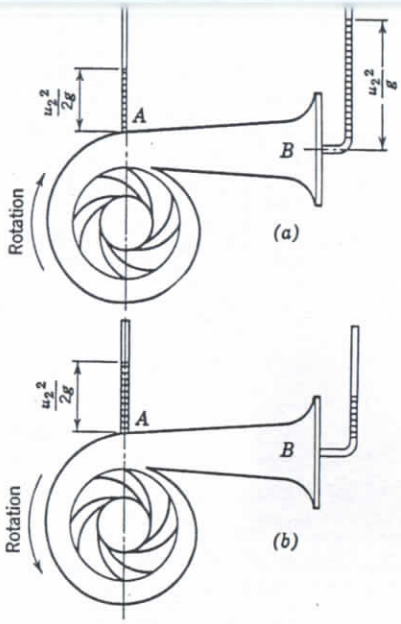

FIG. 4.14. Pump head at zero capacity with a correct and reverse rotation.

on the nozzle in the same manner as a pitot tube facing backwards will show a pressure lower than the static pressure by the amount of the velocity head. Thus the difference in the head at normal and backward rotation is caused by the casing, the impeller behavior being quite normal in both cases.

(*b*) **Pumping Solid-Liquid Mixtures.** In a centrifugal pump, power applied to the shaft is converted by the impeller into pressure energy and kinetic energy of the liquid. In Art. 1.6 it has been shown that *in solid-liquid mixtures solids cannot possess or transmit any pressure energy; therefore when solid-liquid mixtures are being pumped, solids can acquire only kinetic energy. But since solids cannot convert their kinetic energy into pressure the major part of the latter is wasted. Solids are moved through the pump and beyond almost entirely at the expense of the energy imparted to the liquid*

by the impeller. For that reason the energy per pound of mixture (total head) is considerably lower than that for the liquid alone. Transportation of solids in a liquid results in additional hydraulic losses due to the relative motion of the liquid with respect to the solids, which, in a sense, are obstructions to the flow of the liquid. These losses expressed as a percentage of the impeller input increase with the concentration of solids in the mixture. The pump gross efficiency decreases rapidly when concentration of solids in the mixture is increased.[3]

REFERENCES

1. Henry F. Schmidt, "Some Screw Propeller Experiments with Particular Reference to Pumps and Blowers," *J. Am. Soc. Naval Engrs.*, Vol. XL, No. 1, p. 15, February 1928.
2. C. W. Smith, Minutes of Axial Flow Compressor Meeting of 26 June, on German Articles primarily by Bruno Eckert and Group P.40, Navy Department, Code 445A, Bureau of Ships, Washington, D. C., 1946.
3. M. P. O'Brien and D. G. Folsom, "The Transportation of Sand in Pipe Lines," *Univ. of Calif. Pub. Eng.*, Vol. 3, No. 7, pp. 343–384, 1937; available in bulletin form.

Chapter 5

Specific Speed and Design Constants

5.1 CENTRIFUGAL PUMP CONSTANTS FROM GENERAL PRINCIPLES OF SIMILITUDE

Dimensional analysis applied to problems of similitude in hydraulic proved to be a useful tool in many instances. It disclosed the functional relationship among the quantities involved and established dimensionless criteria of flow, found already experimentally in many cases, for conditions known as dynamically similar. One of the important contributions of dimensional analysis to our knowledge of model testing is that it indicated the limitations of the theory of similitude, showed the way to evaluate the various factors affecting the flow and, sometimes, by destroying the geometrical similarity (one of the requisites for dynamic similarity), indicated how to obtain the desired information from model testing. *Applied to centrifugal pumps, the dimensional analysis did not contribute anything new*, but it established from the very general principle the constants in a dimensionless form and facilitated, from experience with water, the drawing of conclusions regarding the behavior of pumps when pumping liquids of different viscosities. The affinity laws follow from these constants.

Use will be made of the method of procedure proposed by Buckingham.* *The principle of dimensional analysis requires that all the terms of a correct and complete physical equation shall have the same dimensions. This implies that the object to be studied by dimensional analysis should be known well enough to permit assumption of the physical quantities expected to affect the phenomenon under consideration.* In the case of centrifugal pumps the quantities involved are

H	pump head (length)	l
Q	capacity (volume per unit time)	l^3/t
n	speed in revolutions per minute (number per unit time)	$1/t$

* E. Buckingham, "On Model Experiments and the Form of Empirical Equation," *Trans. A.S.M.E.*, Vol. 37, p. 263, 1915; or review by Alton C. Chick, *Hydraulic Laboratory Practice*, Appendix 15, A.S.M.E., 1929.

D	impeller diameter representing the pump size for a series of similar pumps	l
g	acceleration due to gravity, constant	l/t^2
ρ	liquid density (mass per unit volume)	m/l^3
μ	absolute viscosity (viscosity coefficient)	m/lt
E	energy applied (to the shaft) and obtained in the form of pump output measured in foot-pounds or $H \times$ mg, or per unit mass $E = gH$ which differs from the head by a constant g; its dimension is	l^2/t^2

Energy per unit mass $E = gH$ will be used instead of head because of its more general character and because it includes the effect of the acceleration due to gravity. It should be remembered that all equations for the head developed by an impeller are based on the law of conservation of energy which, for an incompressible fluid with a constant acceleration due to gravity, reduces to the height the liquid can be raised by the pump. Thus the number of quantities necessary to describe the operation of a centrifugal pump reduces to six: Q, E, n, D, ρ, and μ. These are measured by three fundamental units: length (l), time (t), and mass (m). The relation among these quantities may be expressed by a general functional equation

$$f(Q, E, n, D, \rho, \mu) = 0 \tag{5.1}$$

According to a theorem of dimensional analysis a complete equation describing the relation among n different quantities (six in this case) measured with k fundamental units (three here) can be reduced to the form

$$f(\Pi_1, \Pi_2, \cdots \Pi_{n-k}) = 0$$

or in this case

$$f(\Pi_1, \Pi_2, \Pi_3) = 0 \tag{5.2}$$

where II (Greek capital letter pi) represents a dimensionless product of the form

$$\Pi = Q^a E^b n^c d^d \rho^e \mu^g$$

where a, b, c, d, e, and g are whole numbers or fractions or equal to zero, in which case the corresponding factor is equal to unity; f is some unknown function to be found by experiment. If we select E, D, ρ as three independents, the dimensionless quantities Π_1, Π_2, Π_3 can be put in the form

$$\begin{aligned} \Pi_1 &= E^{x_1} D^{y_1} \rho^{z_1} Q \\ \Pi_2 &= E^{x_2} D^{y_2} \rho^{z_2} n \\ \Pi_3 &= E^{x_3} D^{y_3} \rho^{z_3} \mu \end{aligned} \tag{5.3}$$

where x_1, y_1, z_1, x_2, etc., are the unknown exponents to be determined now. To do this, we express E, D, ρ, Q, n, and μ in terms of their dimensional equations.

$$\Pi_1 = \left(\frac{l^2}{t^2}\right)^{x_1} (l)^{y_1} \left(\frac{m}{l^3}\right)^{z_1} \left(\frac{l^3}{t}\right) = l^{2x_1+y_1-3z_1+3} t^{-2x_1-1} m^{z_1}$$

$$\Pi_2 = \left(\frac{l^2}{t^2}\right)^{x_2} (l)^{y_2} \left(\frac{m}{l^3}\right)^{z_2} \left(\frac{1}{t}\right) = l^{2x_2+y_2-3z_2} t^{-2x_2-1} m^{z_2} \tag{5.4}$$

$$\Pi_3 = \left(\frac{l^2}{t^2}\right)^{x_3} (l)^{y_3} \left(\frac{m}{l^3}\right)^{z_3} \left(\frac{m}{lt}\right) = l^{2x_3+y_3-3z_3-1} t^{-2x_3-1} m^{z_3+1}$$

To make Π_1, Π_2, and Π_3 dimensionless the exponents of l, t, and m must be equal to zero. For Π_1 we obtain three simultaneous equations for determination of x_1, y_1, and z_1.

$$\begin{aligned} 2x_1 + y_1 - 3z_1 + 3 &= 0 \\ -2x_1 - 1 &= 0 \\ z_1 &= 0 \end{aligned}$$

from which we get

$$x_1 = -\tfrac{1}{2} \qquad y_1 = -2 \qquad z_1 = 0$$

Substituting these in the expression for Π_1 in equation 5.3, we obtain

$$\Pi_1 = E^{-\frac{1}{2}} D^{-2} \rho^0 Q = \frac{Q}{E^{\frac{1}{2}} D^2} = \frac{Q}{(gH)^{\frac{1}{2}} D^2} \tag{5.5}$$

Similarly, for Π_2 the equations for the determination of x_2, y_2, z_2 ar

$$\begin{aligned} 2x_2 + y_2 - 3z_2 &= 0 \\ -2x_2 - 1 &= 0 \\ z_2 &= 0 \end{aligned}$$

Hence

$$x_2 = -\tfrac{1}{2} \qquad y_3 = 1 \qquad z_2 = 0$$

and

$$\Pi_2 = \frac{nD}{E^{\frac{1}{2}}} = \frac{nD}{(gH)^{\frac{1}{2}}} \tag{5.6}$$

x_3, y_3, and z_3 are found from

$$\begin{aligned} 2x_3 + y_3 - 3z_3 - 1 &= 0 \\ -2x_3 - 1 &= 0 \\ z_3 + 1 &= 0 \end{aligned}$$

Hence

$$x_3 = -\tfrac{1}{2} \qquad y_3 = -1 \qquad z_3 = -1$$

and

$$\Pi_3 = \frac{\mu}{\rho D E^{1/2}} = \frac{\nu}{D(gH)^{1/2}} \tag{5.7}$$

where ν (kinematic viscosity) $= \mu/\rho$.

According to dimensional analysis, the relationship between Π_1, Π_2, and Π_3 can be established only experimentally. The II products remain constant for similar impellers and dynamically similar conditions, irrespective of the rotative speed or size of the impellers; they are "criteria" of the flow. For practical purposes these expressions will be transformed by making use of the fact that if any of the II functions are constant for similar impellers their products, or any power, also will remain constant and also will be "criteria" of operation of the impeller. Thus,

$$\Pi_4 = \Pi_1\Pi_2 = (D/\nu)(Q/D^2) = Q/\nu D \tag{5.8}$$

$$\Pi_5 = \Pi_2^{1/2}\Pi_3 = nQ^{1/2}/(gH)^{3/4} \tag{5.9}$$

$$\Pi_6 = \Pi_2/\Pi_3 = Q/nD^3 \tag{5.10}$$

The expressions Π_4, Π_5, and Π_6 are a new set of independent dimensionless criteria describing the operation of an impeller. To this will be added one more,

$$\Pi_7 = 1/\Pi_3^2 = gH/(n^2D^2) \tag{5.11}$$

This can be used alternately for Π_5 or Π_6. It is not an independent as

$$\Pi_6^{1/2}/\Pi_7^{3/4} = \Pi_5 = nQ^{1/2}/(gH)^{3/4} \tag{5.12}$$

Obviously an infinite number of dimensionless criteria can be obtained in a similar manner, but only three of them will be independent. The form of Π_4, Π_5, Π_6, and Π_7 was selected because these terms were already in use in dimensional form (mostly in the water turbine and centrifugal pump fields) long before they were developed by the use of the dimensional analysis.

(*a*) **Reynolds Number.** The expression 5.8 is a form of Reynolds number, in which the impeller diameter D represents the size of the machine and Q/D^2 the velocity, as for similar pumps Q/D^2 is proportional to the velocities at the corresponding point of channels comprising impeller and casing of the pump.† It is important to realize tha Reynolds number (equation 5.8 or any other of several Reynolds num bers possible for several sections of the channels comprising a pump does not possess the properties of a criterion of flow through the pum such as are usually associated with Reynolds number for pipe flow Thus the same Reynolds number does not assure the same pattern o velocity distribution or the same regime, viscous or turbulent. Th change from one regime to the other may take place at different rate of flow in different parts of the machine. Besides, very little is know about the significance of the Reynolds number of the flow throug curvilinear and convergent or divergent channels where some of th channels are in rotary motion with energy added or taken away fron the flow. For that reason all attempts in the past to calculate th hydraulic friction losses through pumps by applying the methods an data (correlated on the basis of Reynolds number) for flow in pipe never served any useful purpose. Moreover, in a pump, the skin friction loss becomes secondary to eddy losses caused by a lack of streamlinin and diffused flow prevailing in the impeller and casing. Note also tha identical Reynolds numbers can be obtained with pumps of differen physical configurations, or different specific speeds.

(*b*) **Specific Speed.** The expression for Π_5, equation 5.9, is a dimen sionless expression for specific speed first mentioned in Art. 2.5.

$$\Pi_5 = nQ^{1/2}/(gH)^{3/4} \tag{5.9}$$

To be dimensionless all terms have to be expressed in fundamenta units; i.e., n, in revolutions per second; Q, in cubic feet per second; H in feet; and g, in feet per second squared. However, for practical use the specific speed expression is used in the form as given by equation 2.6

(*c*) **Specific Capacity.** The expression for Π_6 is called "specifi capacity"

$$\Pi_6 = q_s = Q/nD^3 \tag{5.13}$$

This is also dimensionless if Q, n, and D are measured in fundamenta units. The physical meaning of the specific capacity q_s is volume c fluid per 1 rps with an impeller of 1-ft diameter. The specific capacit

† It may be of interest to point out that the velocity term Q/D^2 when divided b the impeller peripheral velocity u_2 to make it dimensionless becomes the specifi capacity q_s defined by the equation 5.13.

$$\frac{Q}{D^2}\frac{1}{u_2} = \frac{Q}{ND^3\pi} = \frac{q_s}{\pi}$$

Thus q/D^2 is a true criterion of flow rate.

remains constant for all similar impellers. The affinity laws follow from this property. Thus for a given pump (D = constant) Q varies directly as n to maintain q_s constant. Also, for similar pumps, if n is constant, Q varies directly as cube of the impeller diameter ratio. If both n and D are varied, both rules are applied simultaneously. Specific capacity q_s is used occasionally for plotting the pump performance in dimensionless form.

(d) Specific Head and Head Coefficient. Equation 5.11 is a dimensionless expression for head and may be termed "specific head"

$$\Pi_7 = h_s = gH/n^2D^2 \tag{5.14}$$

As it appears in this equation, specific head means input energy per unit mass per revolution and with an impeller of 1-ft diameter. It remains constant for all similar impellers. Affinity laws follow from this property of the specific head: for a given D, head varies directly as square of the speed to satisfy the above condition; also, if n is kept constant, then head H varies directly as the square of the impeller diameters.

As a dimensionless characteristic the specific head expression is slightly modified and is known as the "head coefficient"; it is denoted by ψ (Greek letter psi) ‡

$$\psi = \frac{H}{u_2^2/g} = \frac{gH}{\pi^2 n^2 D^2} = \frac{h_s}{\pi^2} \tag{5.15}$$

The head coefficient ψ expresses the head in feet as a fraction of the maximum theoretical head at zero capacity for meridional inlet (no prerotation) u_2^2/g.

For the flow to be dynamically similar while speed, size, and viscosity are varied, it is necessary that all three criteria remain constant. In a practical sense it is impossible to comply with this requirement, for, if the viscosity is kept constant and only speed and size are varied, the Reynolds number will vary while Π_2 and Π_3 remain constant. However, since Reynolds number affects similarity of flow only so far as hydraulic skin friction losses and velocity distribution are concerned, its effect is very small on the over-all performance of the impeller because in a good pump hydraulic losses are of the order of 5 per cent. The affinity laws hold true with an accuracy sufficient for practical purposes throughout a wide range of speeds and sizes and represent the basis of the design procedure of all pumps.

‡ Following Rateau, a Greek letter μ (mu) is used to some extent for the head coefficient.

(e) Remarks.

1. The function expressed by the equation 5.2 can be established only experimentally. For a given impeller operated at constant speed (D, n, ν, and g are constant), it represents a regular constant-speed head-capacity curve. When pumping liquids of different viscosities, the same function will furnish a series of Q-H curves to be determined by test. The problem of pumping viscous liquids is presented in Art. 14.4.

2. For any impeller the specific speed varies from 0 to ∞ for various points on the head-capacity curve, being zero when the capacity is zero and infinity when the head is zero. As a type number, specific speed is used to designate the operating characteristics for the best efficiency point only.

5.2 DESIGN PROCEDURE

The design of a pump impeller involves the following steps (the casing design procedure is discussed in Chapter 7):

(a) Selection of Speed. To meet given head-capacity conditions the rotative speed is selected first. This establishes the specific speed or type of the impeller. Selection of the speed is governed by a number of considerations:

1. Type of driver contemplated for the unit.
2. Higher specific speed results in a smaller pump and cheaper drivers.
3. Optimum hydraulic (and total) efficiency possible with each type varies with the specific speed. Fig. 5.1 shows efficiencies attained at various specific speeds by single-stage single-suction impellers for different capacities in gallons per minute.
4. If the total required head cannot be produced in one stage, it is divided between two or more stages. The head per stage also affects the final specific speed and, hence, the expected efficiency of the pump.

Having established the specific speed of the proposed impellers, the designer looks for a suitable "model" from existing impellers of the same specific speed which have satisfactory hydraulic performance, i.e., suitable slope of the head-capacity curve and acceptable efficiency. Besides the required specific speed the model should be of the same class of pump and be of suitable mechanical type. For instance, an impeller of a multistage pump (large shaft and impeller hub) would not be a suitable model for single-stage overhung construction with an end inlet. The reduction factor or multiplier to be applied to the existing model is found by the use of affinity laws. Design of an im-

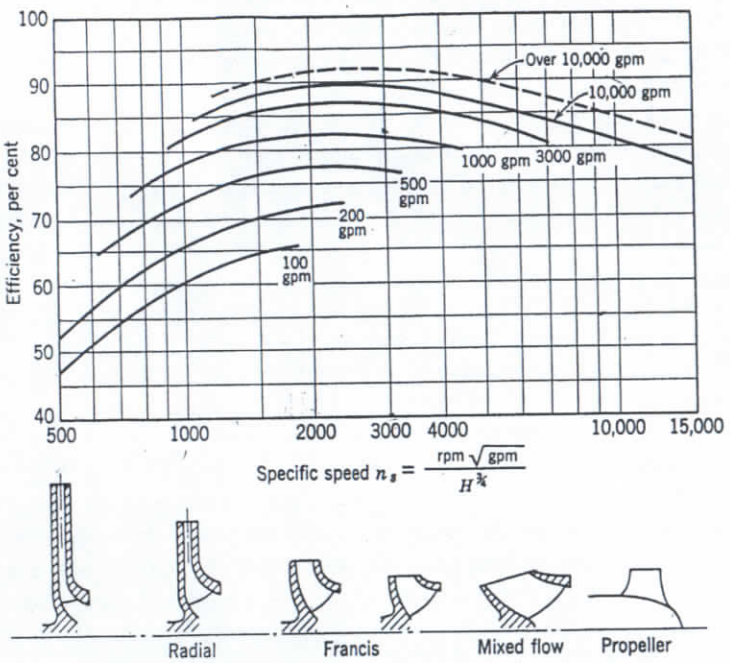

FIG. 5.1. Pump efficiency versus specific speed and pump size (Worthington).

peller for which no existing type is available is made from basic design constants discussed later in this chapter.

(*b*) **Reduction Factor or Multiplier.** If an impeller which is selected for a model is rated Q_1 gpm at H_1-ft head at n_1 rpm and its impeller diameter is D_1 and the new impeller is required to produce Q_2 gpm H_2-ft head at n_2 rpm, with an impeller diameter D_2, the specific speed of both should be the same,

$$n_1 Q_1^{1/2}/H_1^{3/4} = n_2 Q_2^{1/2}/H_2^{3/4} \tag{5.16}$$

In addition, the following relationships between model and the new capacities and heads can be written:

$$Q_2 = Q_1 f^3 (n_2/n_1) \tag{5.17}$$

$$H_2 = H_1 f^2 (n_2/n_1)^2 \tag{5.18}$$

where $f = D_2/D_1$ is the reduction factor or multiplier.

From equation 5.18 the following formula for the reduction factor f is obtained:

$$f = \frac{n_1/\sqrt{H_1}}{n_2/\sqrt{H_2}} = \frac{n_1}{n_2}\left(\frac{H_2}{H_1}\right)^{1/2} \tag{5.19}$$

Expression $n/\sqrt{H}$ is referred to as "unit speed," meaning revolution per minute, needed to produce 1 ft of head by a given impeller. It also possible to express the factor f in terms of capacities and speed fro equation 5.17

$$f^3 = \frac{Q_2/n_2}{Q_1/n_1} = \frac{n_1}{n_2}\frac{Q_2}{Q_1} \tag{5.2(}$$

Q/n is referred to as unit capacity and represents gallons per minut per revolution for a given impeller.

(*c*) **New Impeller Design.** To design a new impeller for which r model is available designers use "design factors" established exper mentally from successful designs that give direct relationships betwee the impeller total head and capacity at the design point and sever elements of Euler's velocity triangles. These are dimensionless velocit ratios, indpendent of the impeller size and speed, which are correlate on the basis of specific speed for different impeller discharge angle In addition a number of ratios of important linear dimensions, n directly related to velocities, are found helpful in perfecting hydraul design of impellers. These ratios, too, are entirely experimental ar do not lend themselves to theoretical treatment. The degree of perfe tion of a design is measured by the value of the pump hydraulic efficienc

The impeller profile and vane layout is possible if the following el ments are known:

1. Meridional velocities at inlet and outlet.
2. Impeller outside diameter.
3. Impeller vane inlet and outlet angles.

These same quantities determine both Euler's entrance and dischar triangles. For straight radial vanes, all particles of fluid enter ar leave the impeller at the same diameter, and the vane is "plain" or single curvature. Thus only one entrance and one discharge triang determine the impeller design. For mixed flow and axial flow impelle velocity triangles are drawn for several streamlines. Three streamlin usually suffice for average mixed flow and axial flow impellers. Variati of vane angles along the radius determines the vane curvature ar "twist." The graphical problems connected with an impeller layo are presented in detail in Chapter 6. This article will deal with the sele tion of the impeller design elements listed above. They are chosen f the design point only. The head-capacity curve is estimated from pr vious experience and based on typical curves for different specific speec

(*d*) **The Vane Discharge Angle.** This angle is the most importa single design element. It has been shown that the theoretical chara

teristics are determined by the vane angle alone. In actual pumps, β_2 is still the deciding factor in design. *All the design constants depend on the value of β_2. Therefore a choice of β_2 is the first step in selecting impeller design constants.* This selection is based on consideration of the desired steepness of the head-capacity curve and whether or not a maximum output is desired from the impeller of a given diameter as both normal head and capacity increase with the angle β_2. If there are no such limitations, selection of β_2 is made for an optimum efficiency, or normal design. An average value of 22½° can be called normal for all specific speeds. For forced output this may be raised to 27½° without affecting the efficiency appreciably. The lower limit of β_2, consistent with good design, is about 17½°.

(e) Speed Constants. A speed constant is a factor giving the relation between the pump total head and the impeller peripheral velocity. Several such constants are in use.

The most widely used speed constant is defined as follows.

$$K_u = \frac{u_2}{\sqrt{2gH}} \quad \text{or} \quad u_2 = K_u\sqrt{2gH} \quad \text{and} \quad H = \frac{1}{K_u^2}\frac{u_2^2}{2g} \tag{5.21}$$

This was originally introduced for hydraulic turbines and later adopted by centrifugal pump engineers. In this definition, K_u is a ratio of u_2 to the free jet velocity under head H. It is used for calculation of the impeller diameter when the head H is given and the speed is selected. K_u increases with the specific speed.

In Fig. 5.2, curves for K_u are drawn for an average normal design and an impeller discharge angle β_2 of approximately 22½°. K_u is affected by several design elements: (1) K_u increases for lower values of angle β_2 since the normal head H is decreased. (2) Greater ratio of D_1/D_{2o} requires a higher value of K_u. Figure 5.2 gives ratios of the impeller eye diameter (D_1) to the impeller discharge diameter (D_{2o} or D_m) for normal design. (3) K_u is also affected by the number of vanes. This number depends on the vane load. With low vane discharge angles β_2, six vanes are probably a minimum for specific speeds up to 5000, whereas eight vanes can be considered normal for the same range of specific speeds. For higher specific speeds, fewer vanes are used. Figure 8.7 shows the usual number of vanes for mixed and axial flow pumps. The number of vanes also depends on the pump size and the pump total head, smaller and lower head pumps requiring fewer vanes. For special services such as pumping paper stock or raw sewage, nonclogging impellers have frequently only two vanes.§

§ For centrifugal blower impellers discharge angles from 25° to 90° are in use. The following "rule of thumb" represents very accurately the number of impeller vanes in terms of impeller discharge angle in degrees: $z = \beta_2/3$, where z is the number of vanes. This rule is also applicable to centrifugal pump impellers.

The value of K_u depends on the pump size, smaller pumps requiring higher value of K_u. Any reduction in gross pump efficiency of small pumps as compared with large pumps of the same specific speed is caused by a reduction of hydraulic efficiency. To compensate for a

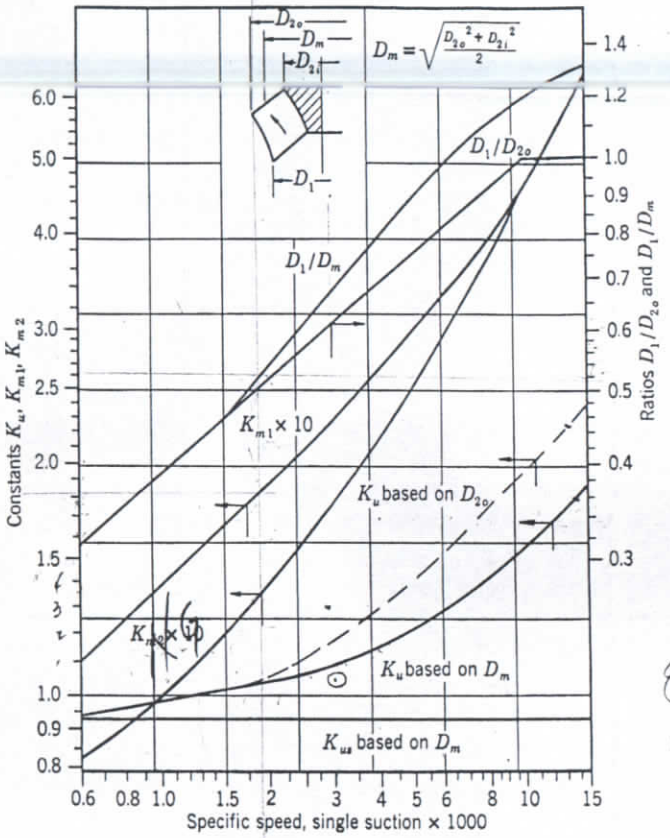

FIG. 5.2. Impeller constants.

reduction of head due to increased hydraulic losses in small pumps, larger impeller diameter or greater value of K_u is used.

(f) The Head Coefficient. The head coefficient defined by equatio 5.15 can also be used as a speed constant for determination of th impeller diameter. It can be shown that

$$\psi = \frac{1}{2K_u^2} \tag{5.2}$$

Figure 9.15 shows the values of the head coefficient for specific speeds up to 4000 and $\beta_2 = 20°$ to $90°$ is discussed in Chapter 9.

(g) Mean Effective Impeller Diameters. The correlation and plot of several design constants covering a complete range of impellers from

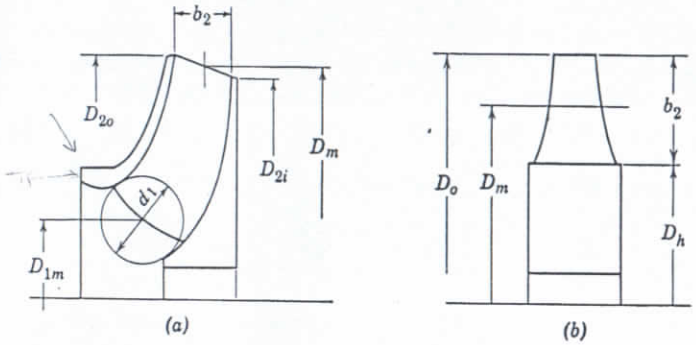

FIG. 5.3. Mean effective diameter.

straight radial to axial flow types becomes particularly simple if peripheral velocity at the impeller discharge is based on the "mean effective" impeller diameter defined as follows (Fig. 5.3):

$$D_m^2 = (D_{2o}^2 + D_{2i}^2)/2 \tag{5.23}$$

For axial flow impellers this reduces to:

$$D_m^2 = D_o^2(1 + \nu^2)/2 \tag{5.24}$$

where $\nu = D_h/D_o$ = the hub ratio (ν is Greek letter nu).

It can be shown that for mixed and axial flow impellers the mean effective diameter divides the flow through the impeller into two equal parts. It may be of interest to point out that, based on the mean effective diameter, the head coefficient for zero flow is the same ($\psi_o = 0.585$) irrespective of the angle β_2 or specific speed.

(h) The Capacity Constant. Capacity constant is defined by

$$K_{m2} = \frac{c_{m2}}{\sqrt{2gH}} \tag{5.25}$$

where c_{m2} is the meridional velocity at discharge. When c_{m2} is calculated from test data at the best efficiency point, the leakage is disregarded. Then, when a value of K_{m2} is selected from tabulated or plotted experimental data it is not necessary to consider the leakage.

For practical use, experimental values of K_{m2} are plotted against specific speed (Fig. 5.2) for a continuous line of pumps. The continuity

of type extends to the design of sealing rings. Any deviation from suc general trend will introduce some inaccuracy which probably will n be any greater than that involved in calculations of leakage volum

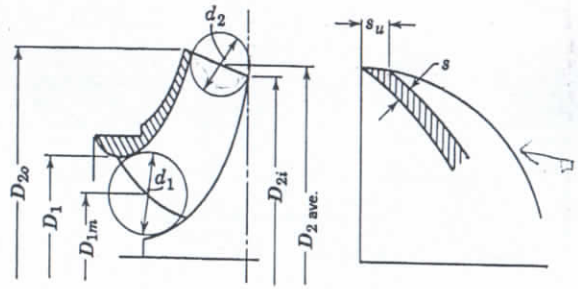

FIG. 5.4. Impeller inlet and outlet areas.

When c_{m2} or K_{m2} is calculated, the vane thickness should be cor sidered in arriving at a net area normal to c_{m2}. For example, in Fig. 5.

$$c_{m2} = \frac{Q}{A_2} = \frac{Q}{(D_{\text{ave}}\pi - zs_u)d_2} \tag{5.26}$$

where z is the number of vanes and s_u is the vane tangential thickness

(i) The Capacity Coefficient. This is used as a capacity design con stant and is defined as:

$$\phi = c_{m2}/u_2 \tag{5.27}$$

where c_{m2} is the meridional velocity at impeller discharge, for the bes efficiency point, based on the net discharge area (excluding vane and disregarding the leakage). After the pressure coefficient is selecte and u_2 is established, c_{m2} can be calculated. The capacity coefficien increases for higher specific speeds at constant values of β_2. Also, increases with the angle β_2 for a constant specific speed (Fig. 9.15) It is connected to K_{m2} as follows:

$$\phi = \frac{K_{m2}}{K_u} = \frac{c_{m2}}{u_2} \tag{5.28}$$

(j) The Entrance Velocity. In order to complete the impeller profile the meridional velocity at entrance should be also known. This is given by the ratio

$$K_{m1} = \frac{c_{m1}}{\sqrt{2gH}} \tag{5.29}$$

This is calculated for the area at the vane entrance tips, again omitting the leakage. The vane thickness can be disregarded as the vane tips

are usually tapered, and c_{m1} can be assumed to be the velocity just ahead of the vanes. Referring to Fig. 5.3,

$$c_{m1} = \frac{Q}{\pi D_{1m} d_1} \tag{5.30}$$

The velocity through the impeller eye is either equal to c_{m1} or slightly lower, depending on the impeller approach.

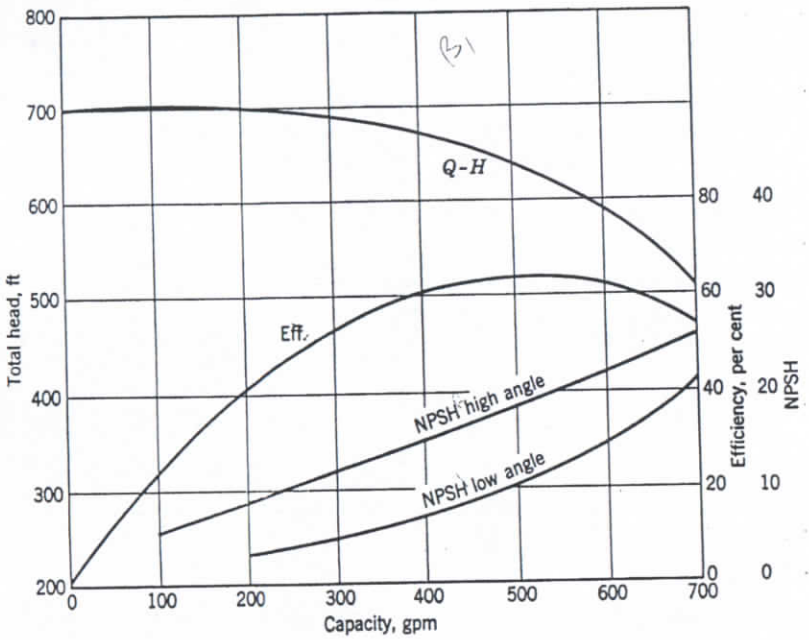

FIG. 5.5. Effect of impeller inlet angle on NPSH 3-in. pump, 3550 rpm.

Neglecting leakage introduces an error in vane angles β_1 and β_2 for several streamlines as determined from Euler's velocity triangles. This error is negligible, and never over one degree on normal designs, and is certainly far smaller than the inaccuracy resulting from the assumption of a uniform meridional velocity for several streamlines.

The inlet velocities as shown in Fig. 5.2 are about 1.5 times the impeller discharge velocities at low specific speeds and equal to those for the straight axial flow pumps. These entrance velocities should be considered as normal. They are suitable for the average suction conditions as represented by the Hydraulic Institute charts showing the NPSH requirements in terms of specific speed and maximum head. Deviations in both directions are possible with little or no sacrifice of

efficiency. Thus for multistage pumps, such as boiler feed, the ratio c_{m1}/c_{m2} may be as high as 1.625. On the other hand for services where low NPSH requirements are important, the entrance velocities are equal to or even lower than the impeller discharge velocities. Note that low entrance velocities lead to the low entrance angles. In the past it was customary to use "exaggerated" entrance angles with wide openings between the vanes normal to the relative flow, expecting in this way to reduce the NPSH requirements. Later experiments have demonstrated that lower vane entrance angles tend to reduce the NPSH requirements. This indicates that with high entrance angles a portion of the impeller channel is inactive due to separation as a result of a high angle of attack. Figure 5.5 shows a test of a 3-in pump with identical impellers except for the vane entrance angles.

(*k*) Entrance Velocity Triangle. The impeller vane entrance angles are established from the entrance velocity triangles. For these, some "nominal" prerotation is allowed, which will locate the "shockless" capacity slightly to the right of the b.e.p. (Fig. 5.6). The extent of

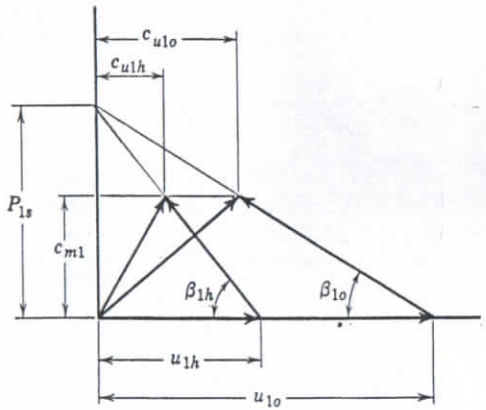

FIG. 5.6. Inlet velocity triangle.

prerotation can be specified by the ratio of the pitch per second to the inlet meridional velocity. A forced vortex pattern of flow is assumed in the impeller approach. This ratio varies within narrow limits.

$$R_1 = P_{1s}/c_{m1} = 1.15 \text{ to } 1.25$$

for single-suction pumps with an end suction. For double-suction horizontally split pumps where the shape of the suction nozzle induces some prerotation, higher values of R_1 are allowed

$$R_1 = 1.25 \text{ to } 1.35$$

For low NPSH conditions, lower values of R_1 are used. On the other hand, exceeding the above upper limits leads to a reduction of efficiency of a point or two, which was proved by special experiments. From inspection of Fig. 5.6 it is evident that R_1 is the ratio of the shockless capacity to the rated capacity. However, allowing for vane thickness, the true ratio may be somewhat lower. The conditions at the impeller entrance are only one item of several that contribute to the location of the b.e.p. on the head-capacity curve.

(*l*) Dimensionless Specific Speed. For analysing pump performance and correlating the experimental design constants (pressure and capacity coefficients), the expression for specific speed (equation 5.9) can be transformed to include the dimensionless capacity ϕ and dimensionless head ψ rather than the measured gallons per minute and head in feet.

Make the following substitutions into equation 2.6.

$$Q = \text{gpm} = (c_{m2} b_2 \pi D_{\text{ave}}) \times 60 \times 7.48 \tag{5.31}$$

$$n = 60u_2/\pi D_m \tag{5.32}$$

$$H = \psi u_2^2/g \tag{5.33}$$

$$\phi = c_{m2}/u_2 \tag{5.34}$$

and segregating all constants into one, we obtain

$$\frac{(\text{rpm})\sqrt{\text{gpm}}}{H_{\text{ft}}^{3/4}} = n_s = 9675 \left(\frac{b_2}{D_m}\right)^{1/2} \left(\frac{D_{\text{ave}}}{D_m}\right)^{1/2} \frac{\phi^{1/2}}{\psi^{3/4}} \tag{5.35}$$

where b_2 is impeller width at discharge.

D_m is mean effective diameter.

D_{ave} is an average of the two impeller shroud diameters at discharge $(D_{2o} + D_{2i})/2$.

The ratio D_{ave}/D_m is equal to unity for centrifugal impellers and is only slightly less than one for high specific speed axial flow impellers, for instance

$$(D_{\text{ave}}/D_m)^{1/2} = 0.965 \quad \text{for} \quad n_s = 12{,}500$$

For axial flow pumps $b_2 = (D_o - D_h)/2$ (Fig. 5.3) and equation 5.35 becomes

$$n_s = 6830 \left[\frac{1 - \nu^2}{1 + \nu^2}\right]^{1/2} \frac{\phi^{1/2}}{\psi^{3/4}} \tag{5.35a}$$

where $\nu = D_h/D_o$ is the hub ratio, an important criterion for the axial

flow impeller. Since for all similar impellers the ratio b_2/D_m is constan the ratio

$$\omega_s = \phi^{1/2}/\psi^{3/4} \tag{5.3(}$$

can be used as a type number or another form of dimensionless specif speed.

In Fig. 9.13, lines of constant ω_s can be calculated for any desire value of ω_s by assuming ψ and calculating ϕ. Thus lines of constar ω_s are part of the network, having an absolute scale not dependir upon any test points. It will be observed from equation 5.35 that f a given b_2/D_m, which fixes the impeller profile, lines of constant ω are lines of constant specific speed n_s.

Also note that by using different impeller discharge angles β_2 th same performance specific speed n_s (in terms of revolutions per minut gallons per minute, and head in feet) can be obtained with impelle of different ω_s, but the impeller profile b_2/D_m will be different for th two cases.

5.3 REDUCTION OF IMPELLER DIAMETER

In order to reduce the head and the capacity of a given centrifug pump, the impeller diameter is generally reduced. Rules for estimatin the performance of a pump for a given reduction in impeller diamet are closely associated with the affinity laws but are not so accurat The error becomes greater the more the impeller diameter is reduce The effect of reducing the impeller diameter is not the same for straigh centrifugal, mixed flow and axial flow pumps, and each type will b discussed separately.

(*a*) Radial Impellers. When the impeller diameter is cut in a straigh centrifugal pump a new but similar Euler's velocity triangle at the di charge is obtained which is constructed on a reduced peripheral velocit vector u_2' (Fig. 5.7). All velocities of this new diagram are reduced i

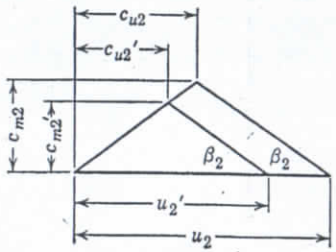

FIG. 5.7. The discharge velocity triangles for full and reduced impeller diameters.

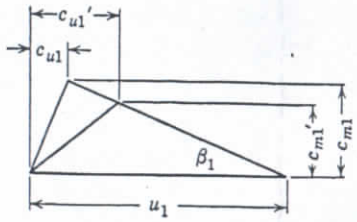

FIG. 5.8. Inlet velocity triangles for full and reduced impeller diameters.

the ratio of the impeller diameters D_2'/D_2. If the subtractive term in Euler's equation (u_1c_{u1}/g) is omitted, the following rules for predicting performance are obtained. The head varies directly as the square of the diameter ratio, capacity varies directly as diameter ratio, and brake horsepower varies directly as the cube of the impeller diameter ratio. However, as the impeller diameter is reduced the rules become approximate only, because: (1) the hydraulic efficiency decreases with cut impellers (appearing as a loss in head) instead of remaining constant as assumed in the above rules; (2) the subtractive term in Euler's equation is seldom if ever zero, and when the impeller diameter is reduced, c_{u1} increases to c_{u1}' (Fig. 5.8), and the subtractive term u_1c_{u1}/g becomes greater. The reduction in gross efficiency due to reduced impeller diameters is caused by several factors.

1. Cutting impellers with streamlined tapered vanes results in blunt vane tips which cause more disturbance in the volute. This effect may

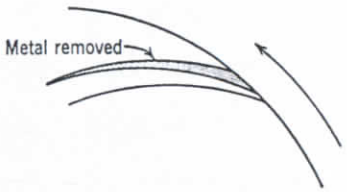

FIG. 5.9. Impeller vane overfiling.

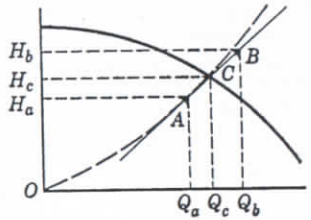

FIG. 5.10. Determination of impeller diameter cut.

be partly or entirely eliminated by again tapering the vanes after cutting by "overfiling" or removing the metal on the leading face of the vane (Fig. 5.9).

2. A reduced impeller diameter results in a longer path for the liquid to travel in the volute casing before reaching the discharge nozzle.

3. In general, in the case of exaggerated entrance vane angles, cutting the impellers moves the best efficiency point away from the "shockless" entrance conditions.

4. A reduction in mechanical efficiency occurs with cut impellers because the mechanical losses, such as bearing and stuffing box losses, remain the same while the power output drops as the cube of impeller diameters.

o

The following procedure eliminates trial and error methods in calculating the impeller diameter required for a given head-capacity point. In Fig. 5.10, the specified point A is below the head-capacity curve Q-H.

Take an arbitrary capacity Q_b higher than the given capacity Q_a, and calculate the head H_b by applying the affinity laws.

$$H_b = H_a\left(\frac{Q_b}{Q_a}\right)^2$$

Connect points B and A to obtain the point of intersection C on the Q-H curve. The required impeller diameter ratio is Q_a/Q_c. The line AB is a part of a parabola connecting corresponding points or points of the same specific speed. The efficiency at point A will be approximately the same as that at point C.

The calculated impeller diameter ratio Q_a/Q_c should be increased somewhat to compensate for the inaccuracy of the above established rules. Figure 5.11 gives the actual impeller diameter ratio in per cent

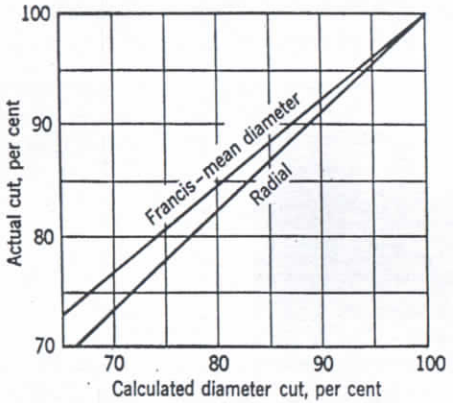

FIG. 5.11. Correction for calculated impeller diameter cut.

plotted against calculated impeller diameter ratios. This correction again is approximate only, the accuracy decreasing with increased specific speed.

(*b*) **Axial Flow Impellers.** Reducing the outside diameter of an axial flow impeller would require a new casing or a liner to accommodate the reduced diameter. For that reason it is rarely used in practice. Referring to the preceding chapter and Fig. 4.5, the variation of the head and the capacity with cut impellers can be established: (1) the capacity varies directly as the net area swept by the impeller vane, the axial velocity remaining the same; (2) the head at the outside diameter will be reduced directly as the square of the diameters. The integrated head H' will be equal to the average of the head at the

hub H_h (unchanged) and the new reduced head at the outside diameter $= H_o(D_o'/D_o)^2$.

$$2H' = H_h + H_o\left(\frac{D_o'}{D_o}\right)^2 \tag{5.37}$$

Axial flow impellers designed for a constant head at all radii at the design point will produce the same head as the full diameter impellers if cut.

It will be shown in Chapter 8 that the head produced by an axial flow impeller depends on the vane length. Cutting the vane length is unpractical because the streamlining of the vane is impaired to such a degree that the efficiency drop becomes excessive.

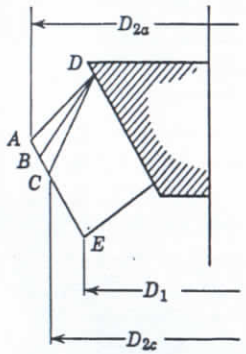

Fig. 5.12. Mixed flow impeller cutting.

(c) Mixed Flow Impellers. Mixed flow impellers can stand less reduction in diameter than radial impellers because the vane overlap is a great deal less. In calculating the impeller diameter ratio, an average of the diameters of the outer and inner shrouds can be taken as an approximation and both diameters cut in the same ratio. With mixed flow propeller pumps it is better to cut more at the outside diameter and nothing at the hub. Figure 5.12 shows impeller cuts *BD*, *CD*. The head and capacity reduction calculated on the basis of outside diameter ratios is not reliable. For a given profile, the vane length ratio *BE/AE*, *CE/AE* may serve as a guide for estimating the necessary vane cut.

Remarks.

1. In connection with the design procedure outlined in this chapter it should be noted that if all new impellers were built by multiplication of existing types there would be no progress in performance of pumps. Designing new impellers from basic design elements always involves some degree of experimentation. It depends upon the skill of the designer to sort out values leading to the optimum efficiency.

2. Curves of design constants in Fig. 5.2 and Figs. 9.13 and 9.14 are based on the test data of a great many centrifugal pumps and blowers covering a wide range of specific speeds and impeller discharge angles. Deviations from these curves are expected as there are always some factors which vary from those constituting a continuous row of types. This is particularly true of high specific speed pumps of mixed and axial flow propeller type. There are a number of design elements, such

as hub ratio, number of vanes, vane length, and hub profile angle which do not enter directly into the calculation of design constants but all of these elements have a marked effect on the pump performance

3. The measured shut-off head of a pump is different from that of the impeller as it is affected by the amount of leakage and the slope of the head-capacity curve. Figure 5.13 shows this very clearly. Also, impellers with an unstable head-capacity characteristic near shut-off (drooping head-capacity curve) have a lower shut-off head than impellers

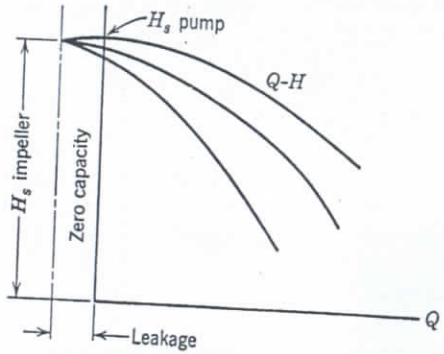

Fig. 5.13. Effect of leakage on shut-off head.

of the same diameter having a steadily rising head-capacity curve. The first show excessive losses at the impeller discharge at and near zero capacity which do not occur with normal design. The above reasons partly explain the scatter of the K_{us} values about their average level.

4. The shut-off head is also affected by the casing design. The same impeller in a casing having a smaller volute will show a higher shut-off head. Also, a smaller diffusion vane angle results in a higher shut-off head. This is always followed by moving of the b.e.p. to a lower capacity and higher head. Figure 14.19 illustrates this point. In this example the pump casing is provided with adjustable diffusion vanes. Evidently the impeller shut-off head is the same for different diffusion vane angles. With smaller volute sections and lower diffusion vane angles (and hence a smaller net area between the diffusion vanes), a greater portion of the dynamic head is registered on the discharge pressure gage.

Chapter 6

Design of Mixed Flow Impellers for Centrifugal Pumps

6.1 STATEMENT OF THE PROBLEM

The layout of a mixed flow impeller on the drawing board is the most complicated drafting problem in centrifugal pump design. Two methods are in use. The first, or old, method is one in which the vane entrance and discharge tips are developed on a cone as a plain cylindrical vane and then transferred to the plan view from which the vane pattern sections are constructed. In the second, or new, method, the vane plane development with true angularity, vane length, and thickness is assumed, and then the vane flow lines are replotted on the plan view. This method, called by Kaplan "the method of error triangles," will be discussed in this chapter as it has definite advantages over the old cone development.

The design of a centrifugal impeller can be divided into two parts. The first is the selection of proper velocities and vane angles needed to obtain the desired performance with the best possible efficiency. The second is the layout of the impeller for the selected angles and areas. The first phase of the design will not be discussed here. For a given set of basic design elements it is possible to make several layouts that will differ in performance. Therefore, for best results, experience and skill are necessary to represent graphically the requirements for best efficiency.

The following are the minimum basic design elements necessary to define the impeller proportions; see Figs. 3.1(*a*) and 3.1(*b*).

1. Radial velocity at the impeller eye, c_{m1}.
2. Radial velocity at the impeller discharge, c_{m2}.
3. The impeller peripheral velocity u_2 at the discharge or impeller diameter D_2.
4. The vane angle at entrance, β_1.
5. The discharge angle β_2.

These quantities are sufficient to construct Euler's velocity triangles, the impeller profile, and the vane plan view.

6.2 GEOMETRICAL RELATIONSHIPS

Before the development of mixed flow vanes is described, several geometrical definitions and statements will be given. These are necessary for further discussion.

(*a*) The angle α between two intersecting planes A and B (Fig. 6.1) is equal to the angle between the two normals CO and DO drawn at any point on the common line of intersection of the two planes. Evidently both of these normals lie in a plane normal to both plane A and plane B. Traces of the normal plane on planes A and B (lines EO and FO) form an angle α.

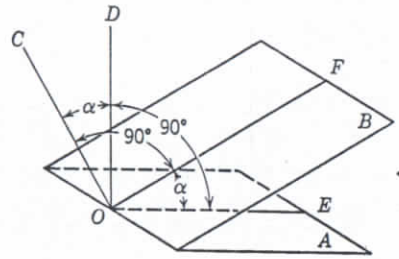

FIG. 6.1. Angle between two planes.

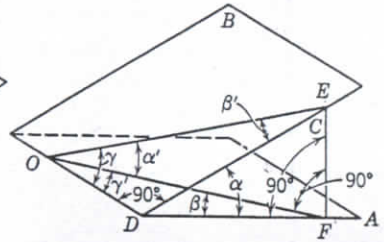

FIG. 6.2. Angle projections on a plane.

(*b*) If two planes A and B (Fig. 6.2) have an angle α between them and are sectioned with another plane C normal to plane A, the traces of plane C on planes A and B (lines OF and OE respectively) will form an angle α' which is related to the angle α in the following way:

$$\tan \alpha' = \tan \alpha \cos \beta \tag{6.1}$$

where β is an angle between the plane C and a plane normal to both plane A and plane B. If EDF lies in a plane normal to both A and B, then

$$\tan \alpha = \frac{EF}{DF} \qquad \tan \alpha' = \frac{EF}{OF} \qquad OF \cos \beta = DF$$

Hence

$$\frac{\tan \alpha'}{\tan \alpha} = \frac{DF}{OF} = \cos \beta$$

(*c*) If an angle γ on a plane B (Fig. 6.2) is projected on plane A, its projection angle γ' will be given by the relation

$$\tan \gamma' = \tan \gamma \cos \alpha \tag{6.2}$$

because

$$\frac{DE}{OD} = \tan\gamma \qquad \frac{DF}{OD} = \tan\gamma' \qquad \frac{DF}{DE} = \cos\alpha$$

and

$$\frac{\tan\gamma'}{\tan\gamma} = \cos\alpha$$

(*d*) Similarly, it can be shown that

$$\tan\beta\cos\alpha = \tan\beta' \tag{6.3}$$

Note that when one side of the angle is parallel to or coincides with OD, the common line of intersection of planes A and B, the angles in projection are smaller; but if none of the angle sides is parallel to the line of plane intersection OD, the angle in projection (β on plane A) is greater than the projected angle β' on plane B.

The same definitions and theorems apply when one or both of the planes are replaced by curved surfaces except that tangent planes drawn at a common point on both surfaces are substituted for curved surfaces.

6.3 PLAIN VANE FAULTS

If the vane shown in Fig. 6.3 is laid out so that the entrance angle is β_1 on the plan view for the flow lines near the front and back shrouds,

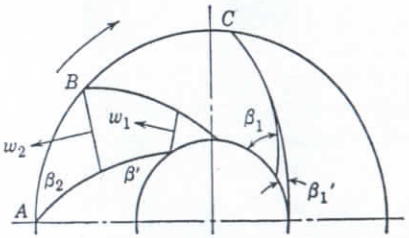

FIG. 6.3. Plain vane impeller.

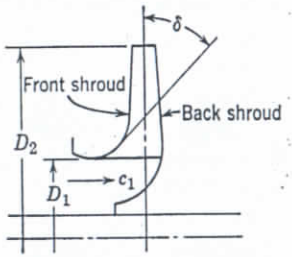

FIG. 6.4. Profile of a plain vane impeller.

the true angle between the vane and peripheral velocity at the entrance edge near the front shroud will be considerably greater than β_1, and is given, according to (c) in Art. 6.2, by the equation

$$\tan\beta_{1f}\cos\delta = \tan\beta_1 \tag{6.4}$$

where δ is the angle between the tangent to the front shroud at the entrance edge (Fig. 6.4) and the plane normal to the impeller shaft axis. Thus, if $\beta_1 = 20°$ and $\delta = 45°$, which is quite usual for a plain vane

impeller, $\beta_{1f} = 27°$. But, since the peripheral velocity is constant f all points along the entrance edge, the vane angle should be consta for all points on the entrance edge to agree with the velocity triangl To be equal in space the angle β_1' at the front shroud should be small on the plan view, so that

$$\tan\beta_1' = \tan\beta_1\cos\delta \tag{6.}$$

This is shown in Fig. 6.3, vane C. It means that the vane should ha a double curvature. *Thus a plain vane impeller should have both shrou*

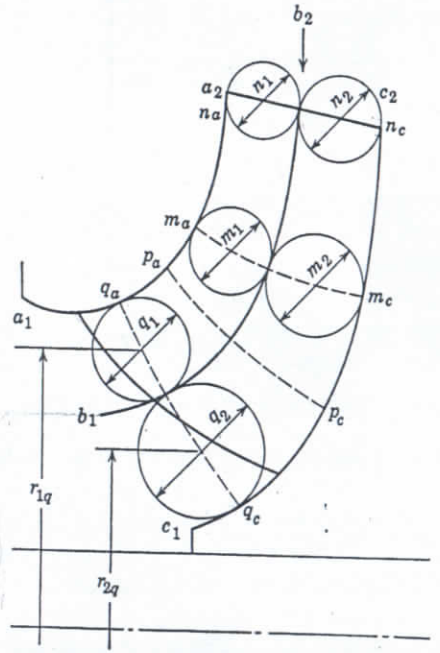

FIG. 6.5. Mixed flow impeller profile.

normal to the shaft axis; such a condition seldom exists. With curve shrouds a mixed flow vane is necessary for "shockless entrance" even i the vane entrance edge is parallel to the axis.

In addition, if the front shroud is curved it is impossible to avoid sharp corners between the vane and the shroud with a plain vane; therefore the vane is extended into the impeller eye (Fig. 6.5) so that the entrance edge is no longer parallel to the axis, and the vane is curved so that the angles between the vane and the shrouds are nearly 90°.

With such a vane, different entrance angles will be required for several flow lines, such as a_1a_2, b_1b_2, and c_1c_2 (Fig. 6.5), for shockless entrance.

The entrance angle varies in such a way that the vane becomes more nearly normal to both shrouds. The higher entrance angles required with mixed flow vanes result in wider openings between the vanes which are necessary for high specific speed impellers. Thus it follows that plain, single-curvature vanes can be used only with narrow impellers with both shrouds nearly normal to the axis and curved very little at the impeller eye. Such impellers are suited only to small pumps.

6.4 MIXED FLOW IMPELLERS

To make a mixed flow vane pattern it is necessary to have drawings of the impeller and vane profile showing the layout of the front and back shrouds, the impeller vane entrance and exit edges, and the vane sections along contour lines on several planes drawn normal to the axis.

The following points will be given consideration in developing the profile of an impeller of the mixed flow type.

(*a*) Extending the impeller vanes at the entrance into the impeller eye tends to improve efficiency by giving a greater overlap to the vanes and reducing the impeller outside diameter required for a given normal head. Shock losses take less power when the shock occurs at a smaller diameter, and disk friction will be less.

The effect of the impeller eye diameter on the total head will be seen from a consideration of the equation for the input head.

$$H_i = \frac{u_2 c_{u2} - u_1 c_{u1}}{g}$$

In a normal pump design it is impossible and inadvisable to suppress completely liquid prerotation at the impeller entrance; therefore c_{u1} is not equal to zero. In that case the subtractive term is smaller for lower values of u_1, and for a fixed outside diameter of the impeller the total head will be higher for smaller impeller entrance diameters. However, there is a limit to extending the vanes into the impeller eye beyond which further extension will reduce rather than improve the efficiency. This is because it is difficult to avoid sharp corners between the vanes and shrouds and, since vanes take up a considerable portion of the eye area, unnecessary vane friction is added, and the cleaning of the impeller casting becomes difficult. To provide the necessary entrance area a larger eye diameter is required.

(*b*) The profile of the impeller is drawn for given radial velocities c_{m1} at the entrance and c_{m2} at the discharge and in such a way that the change from c_{m1} to c_{m2} is gradual.

(*c*) The entrance edge of the vane on the profile is a circular projection of points which are not in one plane, but which are brought into the plane of the drawing by rotation about the axis of the impeller shaft. Similarly, the flow lines a_1a_2, b_1b_2, and c_1c_2 (Fig. 6.5) are circular projections of the paths of the water particles if they follow the vane in the manner prescribed by the design. The flow lines a_1a_2 and c_1c_2 represent the true radial sections through the impeller shrouds at the same time. The shroud curvature should be as gradual as possible to minimize uneven pressure and velocity distribution.

The edge of the vane is drawn so that the angles formed with the shrouds on the elevation view are about 90°.

(*d*) The flow lines are one set of construction lines used for the vane development on the drawing. The number of flow lines necessary to define accurately the vane surface depends on the width of the impeller and the actual impeller size. This is a matter of experience. The flow lines are drawn in such a way that the surfaces of revolution formed by these lines divide the flow into equal parts. Following water turbine practice, where mixed flow impellers were first developed, it is assumed that the meridional velocity is constant along normals to the flow lines (n_an_c, m_am_c, p_ap_c, and q_aq_c, Fig. 6.5) and equal to the average velocity. From this it follows that the meridional velocities for several points along the entrance edge of the vane are the same only if the entrance edge coincides with one of the normals.

The normals are drawn first by eye. Then these are divided into parts (Fig. 6.5): n_1, n_2; m_1, m_2; q_1, q_2; so that

$$2\pi r_{1q} q_1 = 2\pi r_{2q} q_2 \tag{6.6}$$

or

$$r_{1q} q_1 = r_{2q} q_2$$

where r_{1q} and r_{2q} are the radii of the centers of gravity of sections q_1 and q_2. This is repeated for every normal.

For wide and large impellers requiring four or five flow lines, the work of adjusting the sections to comply with equation 6.6 requires much time and a great deal of patience. Accuracy within 3 to 5 per cent should be considered satisfactory.

6.5 METHOD OF ERROR TRIANGLES

The principle of this method of plotting the flow lines on the plan view will be described now. In Fig. 6.6(*a*), suppose a flow line c_1c_2 is shown in perspective on a surface of the back shroud of an impeller. By cutting the surface with a number of parallel planes, the curve c_1c_2

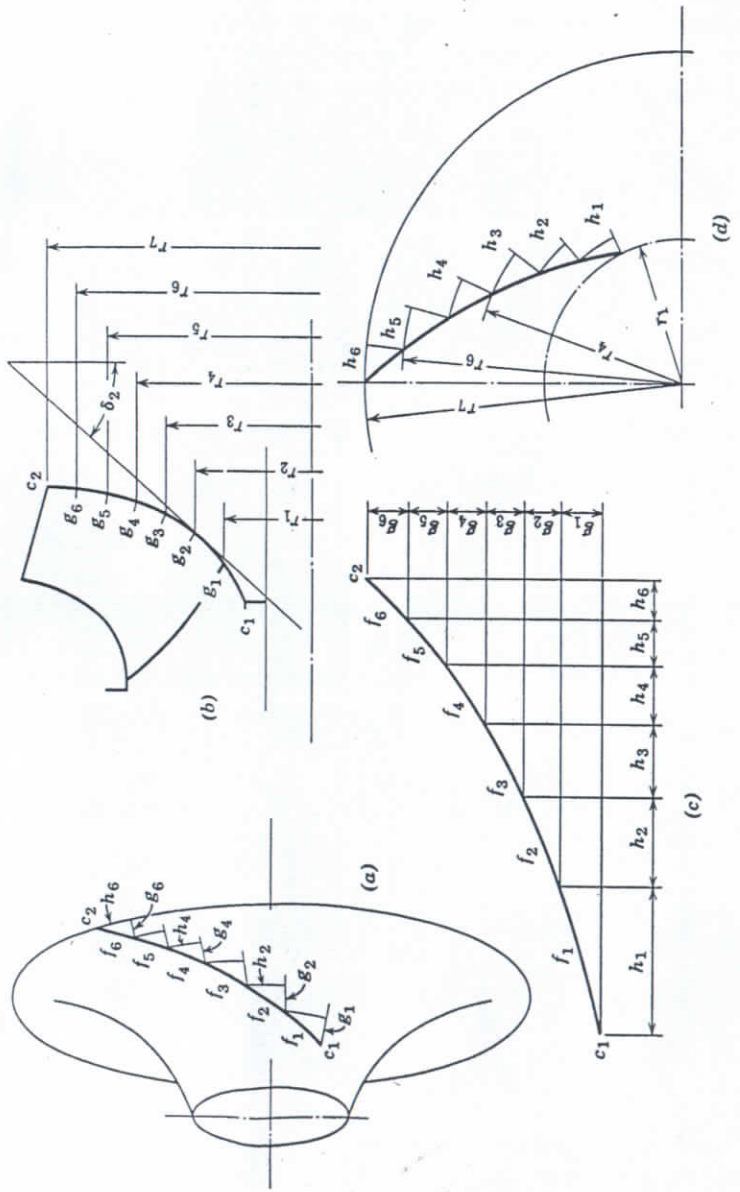

FIG. 6.6. Impeller flow line development on a plane.

can be divided into sections $f_1, f_2, \cdots, f_6$. The intersection of the plane with the surface of the shroud will form a number of parallel circles. Through the points of intersection of the curve c_1c_2 with the parallel circles, a number of meridional planes may be drawn which will section the shroud surface along the curved lines $g_1, g_2, \cdots, g_6$. These lines together with the sections of the parallel circles $h_1, h_2, \cdots, h_6$ and the curve c_1c_2, form a number of curved triangles called by Kaplan "error triangles." Now suppose all these curved triangles are cut and transferred to a plane so that sections $h_1, h_2, \cdots, h_6$ of the parallel circles are arranged along horizontal parallel lines. The sections $g_1, g_2, \cdots, g$ of the curved vertical sides will become flat vertical lines, and the curve $f_1, f_2, \cdots, f_6$ will form a plane development of the curve c_1c_2, Fig. 6.6(*c*). Obviously the greater the number of sections drawn through the flow line, the more accurate the plane development of the curve will be. The angles the curve c_1c_2 makes with the parallel circles are the same on the plane development. Also, the length of the flow line c_1c_2 in the development is very nearly equal to the true length of the flow line in space.

On the elevation view, the flow line c_1c_2 will appear as shown in Fig. 6.6(*b*) where $r_1, r_2, \cdots, r_6$ are the radii of the parallel circles. A plan view of the flow line c_1c_2 can now be drawn; Fig. 6.6(*d*). Each point of the curve in the plan view is located by radii $r_1, r_2, \cdots, r_6$. The displacement $h_1, h_2, \cdots, h_6$ of one meridional plane with respect to an adjacent one along the parallel circle is shown without distortion on the plane development, Fig. 6.6(*c*), and appears in full length on the plan view, Fig. 6.6(*d*). The intersections of the meridional planes with the parallel circles determine the points of the curve in the plan view.

To apply the method of error triangles to the impeller vane layout the following procedure is followed.

(*a*) The elevation view, or profile, of the impeller is drawn as described previously. The flow lines are drawn and checked in the same manner, Fig. 6.7(*a*).

(*b*) The vane development on a plane, Fig. 6.7(*b*), is drawn to correspond to the profile and the vane angles at entrance and discharge. The vane thickness is shown on the plane development, s on Fig. 6.7(*b*).

To draw the vane development divide one of the flow lines a_1a_2 into a number of parts and then lay out the same distances along the rest of the flow lines, points $1_a, 2_a, \cdots, 8_a$; $1_b, 2_b, \cdots, 10_b$; $1_c, 2_c, \cdots, 11_c$. In this way all the error triangles on the development will be of the same height. Parallel lines spaced g_1, g_2, g_3, etc., apart are drawn for the vane development on a plane, Fig. 6.7(*b*). The vane development is

first sketched in between the parallel lines limiting the flow lines on profile 1_a, 8_a; 1_b, 9_b; and 1_c, 10_c for the flow lines a_1a_2, b_1b_2, and c_1c_2 respectively. The vane thickness is also shown for the flow line c_1c_2 on

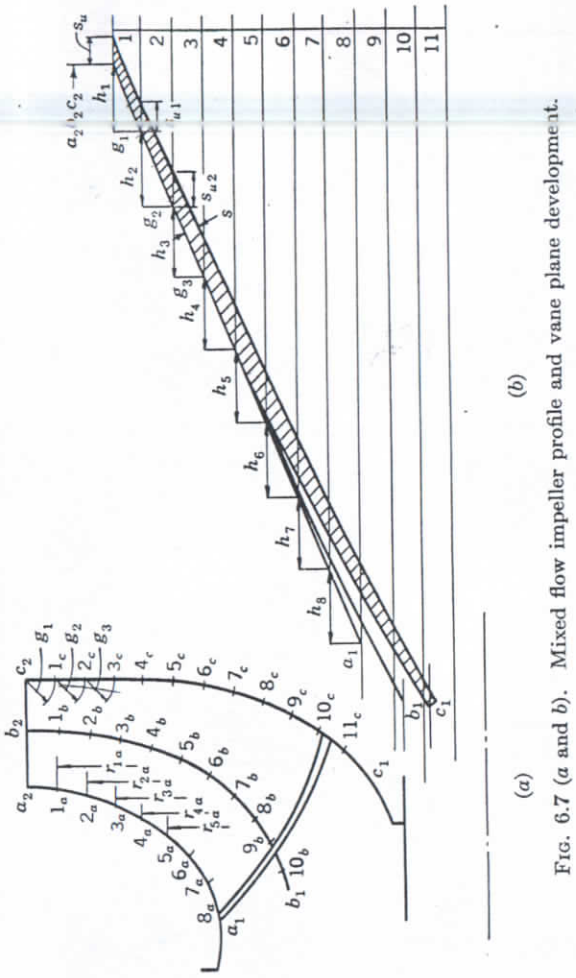

(a) (b)

FIG. 6.7 (*a* and *b*). Mixed flow impeller profile and vane plane development.

Fig. 6.7(*b*). This does not have to be the same for all flow lines or constant along the same flow line. The desired degree of streamlining can be given to the vane. Also, for molding reasons or strength, the vane thickness may vary from one flow line to the other. Although for the development it is more convenient to draw vane sections a certain distance apart, it is found helpful to put the vane development of several flow lines into their true relative positions, Fig. 6.7(*b*). The suction

ends of the developed flow lines should arrange themselves evenly spaced and the tips of flow lines should form a smooth curve to assure that the edge projection on the plan view will also be a smooth curve. Then the triangles are drawn for one side of the vane only, say the leading face, a_1a_2, Fig. 6.7(*b*).

(*c*) The vane sections are transferred from the development to the plan view, Fig. 6.7(*c*). An arbitrary starting point having been chosen,

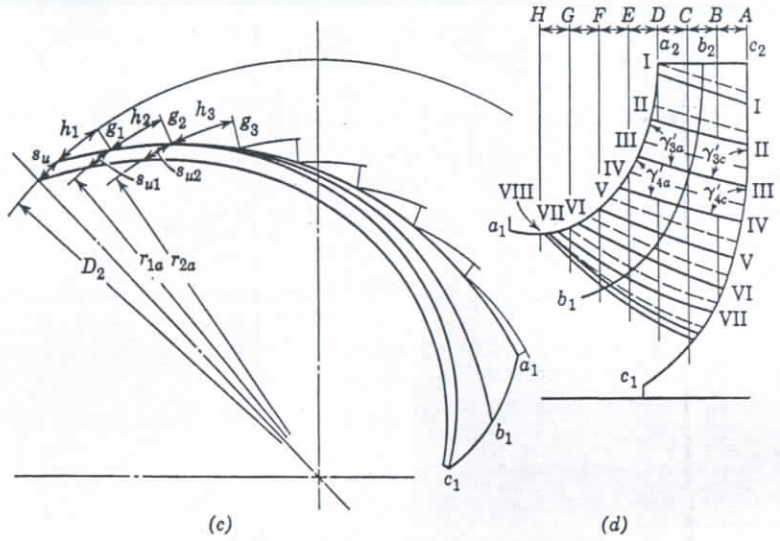

(c) (d)

FIG. 6.7. (*c*) Impeller vane plan view; (*d*) radial sections on profile view.

curved triangles are drawn. The arcs of parallel circles are drawn with radii taken from the elevation view for points 1_a, 2_a, $\cdots$, 8_a, etc. The displacement of one point with respect to the other is taken from the vane development (h_1, h_2, $\cdots$, h_8). By joining the points with a curved line the plan projection of the flow line is obtained.

To draw the back side of the vane, the vane thickness is laid off from points 1_a, 2_a, $\cdots$, 8_a along the parallel circle arcs taken from the vane development (s_{u1}, s_{u2}, etc.). The flow lines b_1b_2 and c_1c_2 are plotted on the plan view in the same way.

(*d*) The flow lines on the elevation and plan view are the first set of construction lines used for plotting the vane pattern sections. As a second set of construction lines, a number of uniformly spaced (I, II, III, etc.) radial sections are drawn on the plan view, Fig. 6.7(*e*). The intersections of the flow lines, with the radial sections for both front and back of the vane, are plotted on the elevation view from the plan

view, Fig. 6.7(*d*). If the radial sections on the elevation view do not form smooth lines, uniformly spaced, it is an indication that the change in vane angularity on the vane developments was too abrupt for one or more of the flow lines.

An alternate method of drawing the second set of construction lines may be mentioned. In this, the flow lines on the elevation view are divided into an equal number of parts and the corresponding points 1_a, 1_b, 1_c; 2_a, 2_b, 2_c, etc., Fig. 6.7(*a*), should form smooth curves on the plan view also. These curves are used for the second set of construction lines for plotting the vane pattern sections. The advantage of this method is that no additional points are plotted, and those already on the drawing are utilized.

(*e*) The next step is to draw the vane pattern sections $A, B, C, \cdots, H$, Fig. 6.7(*d*). The vane is divided into a suitable number of boards, the number depending on the vane dimensions. Vane sections are

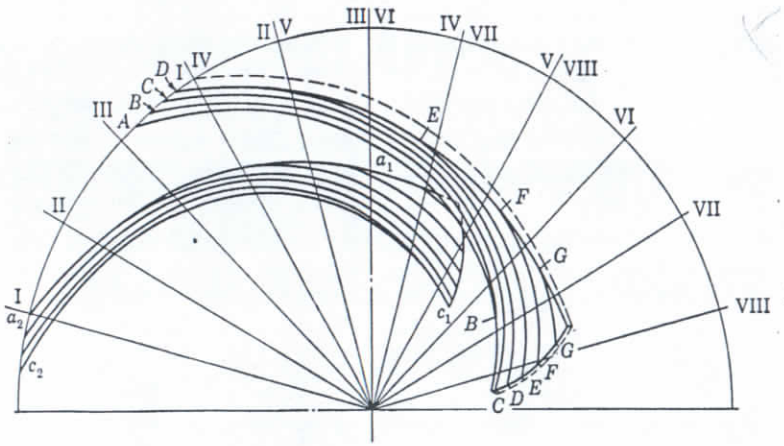

FIG. 6.7(*e*). Vane pattern sections.

drawn on the elevation view and then plotted on the plan view, the intersections of the board planes being located with the radial sections or any other construction lines. To avoid confusion of lines it may be advisable to separate the views of the front and back sides of the vane by showing the front side of one vane and back side of the next vane, Fig. 6.7(*e*). In this way the channel between the two vanes will be defined.

The contour lines or the vane pattern sections on the plan view completely determine the shape of the vanes. If boards of the proper thickness are cut along these lines and stacked in the proper order and the

corners of the boards are shaved off, the vane surface will be obtaine for the front and back sides.

There are two ways to use these vane sections for building the im peller pattern. In one, a sectional core box is made for a single-van channel. A number of cores equal to the number of vanes are mad and assembled into one core, for the whole impeller. For this arrange ment, views of the front and back sides of the vane as shown on Fig 6.7(*e*) are sufficient.

In the second method, used mostly for smaller impellers, one core i made for the whole impeller. This core is usually baked with meta

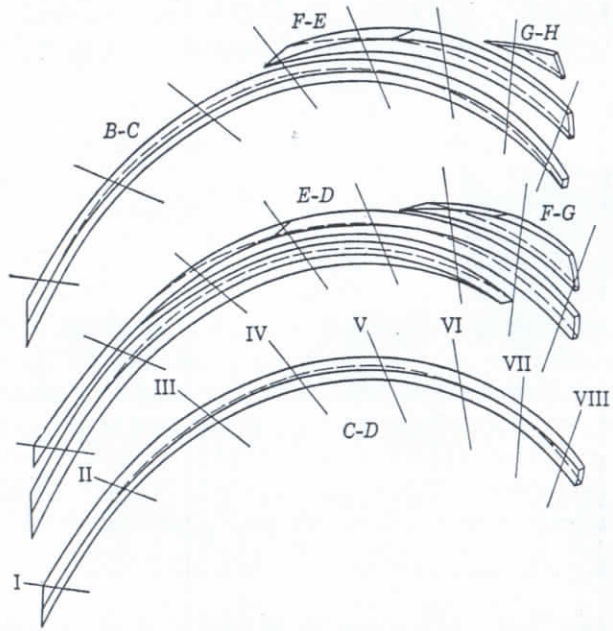

FIG. 6.7(*f*). Vane pattern sections.

vanes in place and is then broken to remove the vanes, after which the parts of the core are pasted together. For a pattern of this type a wooden vane is first made, from which metal vanes are cast for the core box. To build the wooden vane, the vane sections are cut to the proper shape and thickness and, when they are glued together in the proper order and their corners are shaved off, they will give the vane shape.

The vane section drawings are obtained by placing the two views of the front and back sides of the vane in their proper relative position, one on top of the other. From this the vane sections can be picked out for each board; Fig. 6.7(*f*). Although only outer contour lines are

necessary to cut the boards, the inside lines are also shown because they assist in locating the boards in their correct position. Also the radial lines I, II, III, etc., are shown on the vane section as additional guides in the assembly of the vane from the board sections.

(*f*) Hydraulically, the best form of the impeller channel is obtained when the true angles between the impeller vanes and shrouds are close to 90°. When the impeller profile is curved considerably, this becomes difficult to accomplish. *The channel form may be improved by tilting the vane with respect to the shrouds. This is done by moving the flow lines on the plan view, Fig. 6.7(c), through a certain angle, which will change the angle between the vane and the impeller shrouds without changing the vane angularity.*

When heavy vanes are used, a slight inclination of the vanes to both impeller shrouds at the discharge results in quieter pump operation because the discharge from the individual impeller channels against the volute tongue is smoother. With thin streamlined vanes and ample space between the impeller and volute tongue, this consideration becomes unimportant.

To obtain a true picture of the impeller channel normal to the flow, the channel section should be drawn normal to some average flow line which passes somewhere in the middle of the channel. This section is not normal to either of the shrouds or vanes, as neither the shrouds nor two adjacent vanes are parallel. It is difficult to draw such a section on the drawing. However, to find the angles between the vanes and both shrouds, the radial sections I, II, III, etc., Fig. 6.7(*e*), will give a satisfactory approximation. *It will be shown that the angles between the shrouds and the vane radial sections on the elevation view—*γ_{4a}' *and* γ_{4c}', *Fig. 6.7(d)—are very nearly equal to the true angles in space between the vane and shroud surfaces* γ_{4a} *and* γ_{4c} or, more accurately,

$$\tan \gamma_{4a}' = \tan \gamma_{4a} \times \cos \beta_{4a}$$

$$\tan \gamma_{4c}' = \tan \gamma_{4c} \times \cos \beta_{4c} \qquad (6.7)$$

where β_{4a} and β_{4c} are the vane angles at section IV, Fig. 6.7(*d*), taken for illustration.

This follows from the fact that the plane normal to the flow line a_1a_2 intersects the plane normal to the peripheral velocity (radial plane) at an angle β, according to the definition of the angle between the two planes. Thus the true angle γ_{4a} between the vane and shroud taken in the plane normal to the flow line, if projected on the radial plane IV making an angle γ_{4a} to the normal plane, will be reduced as given by equation 6.7. It should be noticed that if γ is 90° (tan $\gamma = \infty$) or

near it, its tangent is a very large number and $\gamma' \approx \gamma$. Below are tabulated several values of γ and γ' for different values of β.

γ / γ'	$\beta = 20°$	$\beta = 30°$	$\beta = 45°$	$\beta = 60°$
85°	84.7	84.3	83.0	80.0
80°	79.4	78.5	76.0	70.6
75°	74.1	72.8	69.3	61.8

Because the shrouds are not parallel it is impossible to make angles between one vane and both shrouds 90° without excessive vane bending. But, since β seldom exceeds 30° and γ is seldom smaller than 75°, γ' on the elevation view always will be, within a few degrees, equal to γ the true angle between the vane and shrouds in space.

When laying out a vane with high angles, such as are used on diffusion casings of vertical turbine pumps, the profiles of both shrouds enclosing the vanes are very nearly parallel, in which case there is no difficulty in keeping γ near 90°; but γ' on the elevation view will be considerably lower than γ in space, as cos β is decreasing rapidly when vane angle β is approaching 90°.

(*g*) The vane angle β for any point on the flow lines appears on the plan view reduced to β' so that

$$\tan \beta' = \tan \beta \cos \delta \qquad (6.8$$

where δ is the angle between the tangent to the flow line at that point on the elevation view and the plane normal to the impeller axis. Thus for instance, on Figs. 6.7(*a*), (*b*), (*c*), (*d*) for triangle (3),

$$\tan \beta = \frac{g_3}{h_3} \qquad \tan \beta' = \frac{r_{2a} - r_{3a}}{h_3}$$

but

$$\frac{r_{2a} - r_{3a}}{g_3} = \cos \delta_3$$

hence

$$\tan \beta' = \tan \beta \cos \delta_3$$

It has been found that for centrifugal pumps three flow lines will be sufficient for a vane layout in the majority of cases. *Furthermore, the vane construction can be simplified by drawing the middle flow line as a curve equally spaced from both shrouds. For small and narrow impeller*

the middle flow line can be omitted. In that case the radial vane sections —lines I, II, III, etc., Figs. 6.7(*d*) and 6.7(*e*)—are drawn as straight lines or curves by eye on the elevation view. The accuracy of vane construction is not impaired by these short cuts, as can be proved by comparing layouts made with and without these simplifications.

6.6 APPLICATION OF METHOD OF ERROR TRIANGLES TO THE DESIGN OF PLAIN VANES

For a given entrance angle β_1 and discharge angle β_2 it is always possible to draw a vane as a circular arc with a single radius. However, such a vane has serious disadvantages. Figure 6.8 shows the construction. From an arbitrary point A on the circle of the impeller outside diameter, draw one line AM at an angle β_2 to the radius AC. At

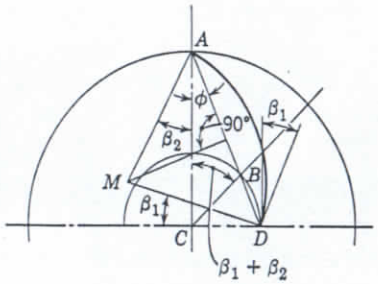

FIG. 6.8. Plain vane drawn as a circular arc.

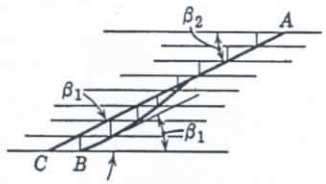

FIG. 6.9. Development of the vane in Fig. 6.8.

point C, construct an angle $\beta_2 + \beta_1$ to the radius AC. The line will intersect the impeller eye circle at B. Draw a line AB to intersect the impeller eye circle at D. Draw a perpendicular line in the middle of AD to intersect line AM at M. MA will be the radius of the arc to give an angle β_2 at discharge and an angle β_1 at entrance.

The proof of this construction may be of interest.

$$\beta_1 + \beta_2 + \phi = \angle CBD = \angle CDB$$

$$\beta_2 + \phi = \angle MAD = MDA$$

By subtraction

$$\beta_1 = \angle CDB - \angle MDA = \angle MDC$$

The method of error triangles can be advantageously applied to the analysis and construction of the plain vane. On Fig. 6.9, AB is the development on a plane of the vane in Fig. 6.8 obtained by the use of

error triangles. It will be noticed that the change in vane angularity is irregular. First, the vane angle increases rapidly, then slowly decreases to the discharge angle. This form of vane is not considered the most efficient. A vane with a gradual change in the vane angle, AC in Fig. 6.9, is preferred. To get a better vane shape for the plain vane impeller, it pays to draw first the vane development on a plane and then to replot it on a plan view by the method of error triangles. Although this method takes more time, its systematic use permits improving the vane shape to get the best performance.

6.7 DIFFUSION CASING VANE LAYOUT FOR VERTICAL PUMPS

Figure 6.10(*a*) shows a profile of the diffusion casing vane of a vertical pump of the deep-well type similar to that shown on Fig. 7.25. Figure 6.10(*b*) shows the plan view of the vane looking in the direction of the arrow, and Fig. 6.10(*c*) represents the plane vane development with the true vane angularity and length along the three streamlines, a_1a_2, b_1b_2, and c_1c_2. The vane thickness is shown only for the streamline a_1a_2. On Fig. 6.10(*a*) and (*b*) AA, BB, CC, $\cdots$, MM are the pattern board sections, all of the same thickness. If the method of error triangles is used and the procedure outlined in Art. 6.5 is followed exactly, it will be found that the radial sections I, II, III, etc., on Fig. 6.10(*b*) do not give sufficient intersections with board sections AA, BB, CC, etc., and therefore cannot serve as a second set of auxiliary construction lines to draw the board sections. (The streamlines a_1a_2, b_1b_2, and c_1c_2 could have been plotted on the plan view in a regular manner, as was demonstrated on Fig. 6.8 for a mixed flow impeller.) For that reason the procedure is modified as follows:

1. The board thicknesses are drawn on the elevation Fig. 6.10(*a*), AA, BB, CC, etc., being equally spaced.
2. The board thicknesses measured along the streamlines, ab, bc, cd, de, $\cdots$, lm, for the streamline a_1a_2 are used as the heights of the error triangles on the vane development, Fig. 16.10(*c*). Thus the spacing of the lines, AA, BB, CC, etc., on Fig. 6.10(*c*) is not uniform.
3. The error triangles for the streamlines b_1b_2 and c_1c_2 are drawn in the same manner. The triangle heights are different for the three streamlines.
4. The streamlines are plotted on the plan view in the regular manner, starting from an arbitrary point A, and advancing progressively distances a, b, c, etc., along the arcs of radii r_a, r_b, r_c, etc. The plotted points for the streamlines a_1a_2, b_1b_2, and c_1c_2 are shown with heavy dots.

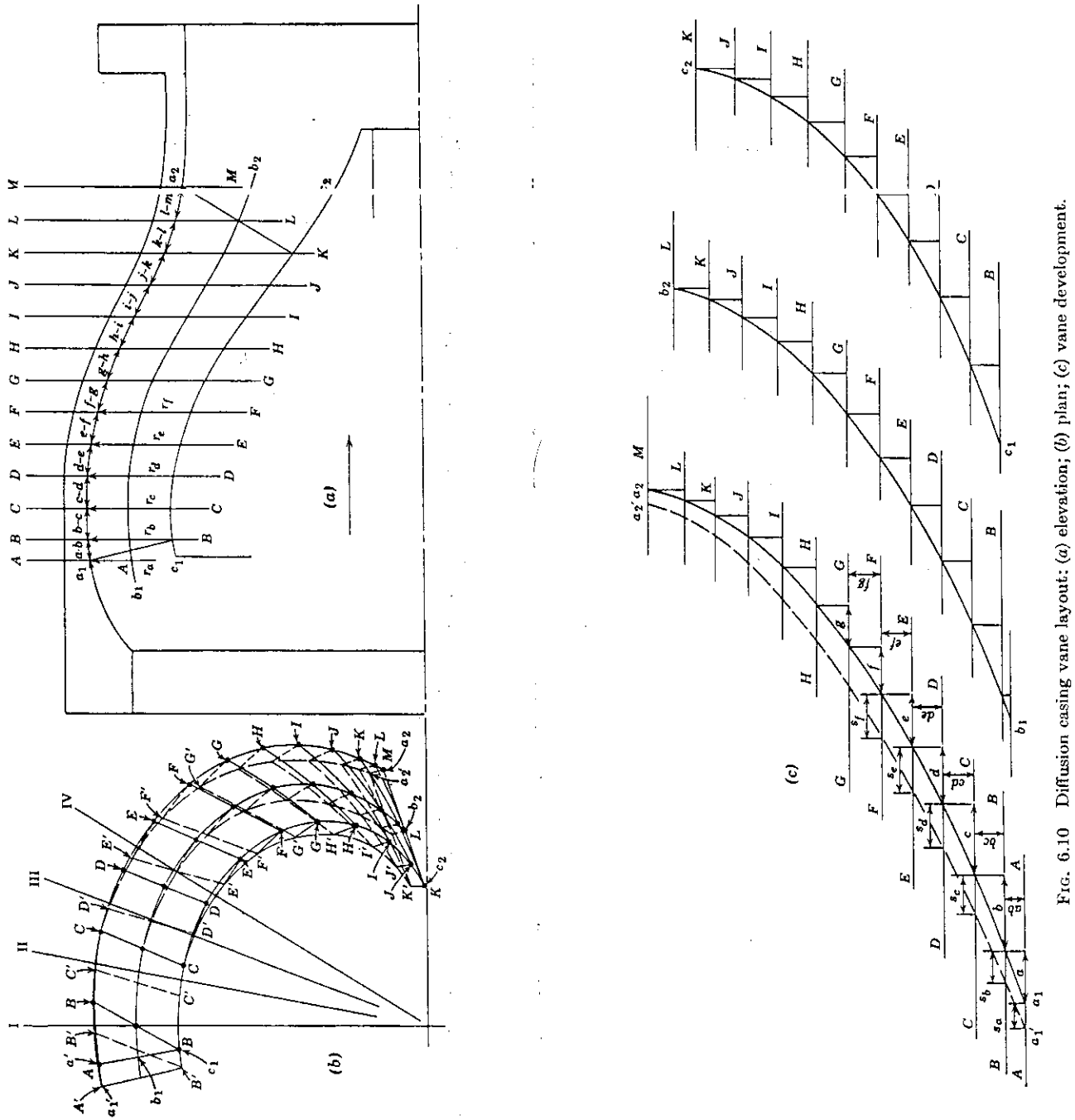

FIG. 6.10 Diffusion casing vane layout: (*a*) elevation; (*b*) plan; (*c*) vane development.

5. By joining the three points on the three streamlines belonging to the same board sections (marked with the same letters A, B, C, etc.), the board sections are obtained for one face of the vane shown by solid lines (back side).

6. Then true vane thickness is drawn for streamlines a_1a_2, b_1b_2, and c_1c_2; only a_1a_2 thickness is shown on Fig. 6.10(c). Now, the vane thickness can be transferred on the plan view by laying out the tangential vane thickness (s_a, s_b, s_c, etc., for a_1a_2) along the arcs of the corresponding radii r_a, r_b, r_c, etc., for all three streamlines. These are shown by dashed lines. By connecting the points plotted in this way, the board section lines are obtained for the other face (front) of the vane marked A', $B'B'$, $C'C'$, $D'D'$, etc.; (see Fig. 6.10(b)).

This completes the pattern drawing of the diffusion casing vane.

REFERENCES

1. Victor Kaplan and Alfred Lechner, *Theorie und Bau von Turbinen-Schnellläufern*, pp. 125–129, Munich, R. Oldenbourg, 1931.
2. Herman Schaefer, *Kreiselmaschinen*, pp. 29–37, Berlin, Julius Springer, 1930.
3. L. Quantz, *Kreiselpumpen*, pp. 18–20, Berlin, Julius Springer, 1930.
4. C. Pfleiderer, *Die Kreiselpumpen*, pp. 266–279, Berlin, Julius Springer, 1932.
5. R. Camerer, *Vorlesungen über Wasserkraftmaschinen*, pp. 274, 275, 369, Leipzig, Wilhelm Engelman, 1929.

Chapter 7

Pump Casing

The purpose of the pump casing is to guide the liquid to the impeller convert into pressure the high velocity kinetic energy of the flow from the impeller discharge, and lead the liquid away. *The casing takes n part in the generation of head, and all theoretical discussion of the casing deals with losses.*

7.1 SUCTION NOZZLE

Since the liquid path between the suction flange and the impeller eye is short, and velocities in the suction nozzle are relatively low, the loss of head due to friction in the suction nozzle is very small. However the design of the suction nozzle has an important bearing on the velocity distribution immediately ahead of the impeller, and in this way it may affect the impeller efficiency and pump cavitation characteristics. These effects are more pronounced in low head, high specific speed pumps. *With vertical pumps having only a short suction bell ahead of the impeller, the shape of the suction sump becomes an important part of the impeller approach and has a direct bearing on the hydraulic and mechanical performance of the pump.* There are numerous cases on record where large propeller pumps failed to meet the performance indicated by model tests, or by tests of similar pumps in different installations, owing entirely to the suction sump design.[1]

A straight, tapered suction nozzle known as end suction nozzle is the best in every respect for single-inlet impellers. Such a nozzle, the area of which gradually reduces toward the impeller eye, has a definite steadying effect on the flow and assures a uniform liquid feed to the impeller.

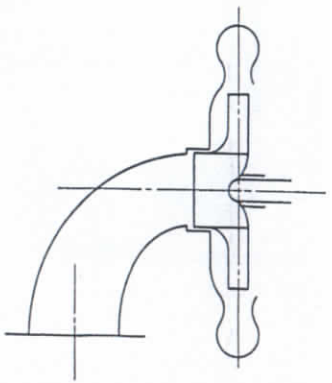

FIG. 7.1. Reducing suction elbow

A tapered, long-radius elbow is next best (Fig. 7.1). For low specific speeds (below 1500), the two are equivalent hydraulically; however, fo

higher specific speeds and *particularly for propeller pumps, the optimum efficiency and maximum heads will be appreciably reduced with the elbow suction.* A flat elbow, or volute suction, as used with horizontally split pumps of multistage type (Fig. 7.2), is almost as efficient as a tapered elbow for low specific speed pumps, but for high specific speed pumps the bad effects of the sharp 90° turn become most pronounced. Propeller pumps are never built with flat elbow suction. In an elbow of this type it is essential to have the flow accelerated gradually, in order to suppress the tendency toward velocity distortion due to a double turn just in front of the impeller eye. To effect a better distribution

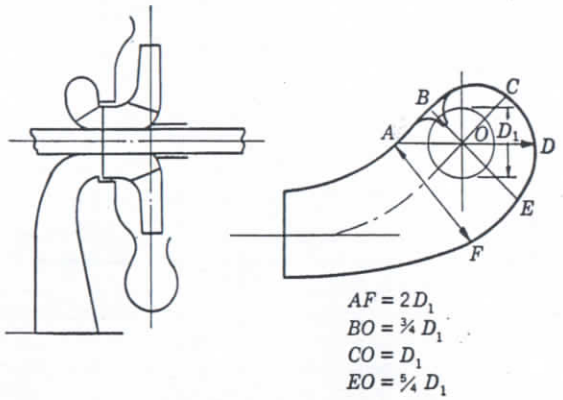

FIG. 7.2. Volute suction nozzle.

around the impeller eye section AF, Fig. 7.2, is given an area some 50 per cent or more greater than that of the impeller eye. At the same time the width of the nozzle at AF is about twice the impeller eye diameter. As a result of the turn, most of the flow shifts to the outer side; therefore the suction baffle or stop at B is placed about 90° past the middle line of the nozzle OC.

7.2 VOLUTE

Except for vertical pumps of the turbine type, the majority of single-stage pumps built in the United States are of the volute type. The main advantage of the volute casing, as compared with a casing having diffusion vanes, is its simplicity. However, the casing with the diffusion vanes is the more efficient of the two. This has been proved experimentally for single-stage pumps and single-stage turboblowers.[2,3] In Europe, except for small sizes, all single-stage pumps and all multistage pumps are equipped with vaned diffusers. In this country, high pressure

multistage pumps are perhaps equally divided between the diffuser type and the double-volute type.

There are several design elements of volute casings which determine their hydraulic characteristics, namely volute areas, volute angle α_v, volute width b_3, and volute base circle D_3 (Fig. 7.3). The selection of these elements is governed by theoretical considerations given below, but their actual values have been established experimentally for best hydraulic performance.

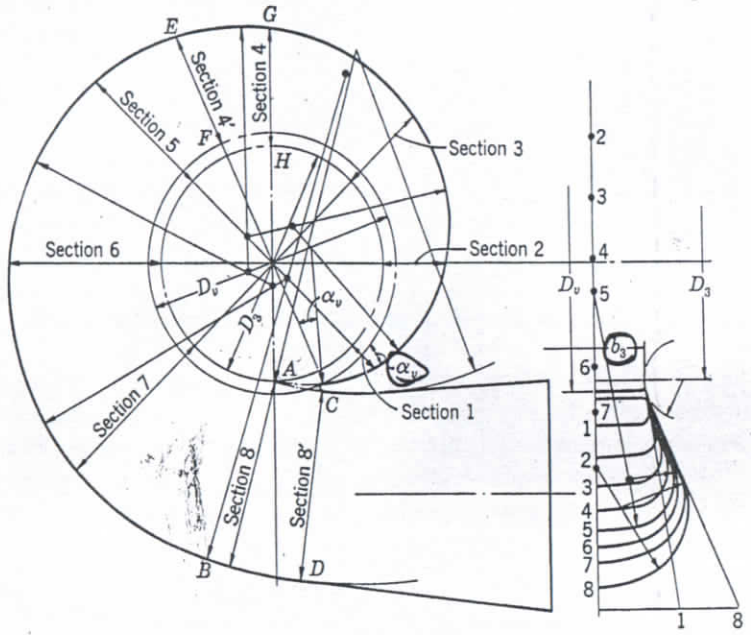

FIG. 7.3. Pump volute casing.

(a) Volute Areas. Reference to Fig. 7.3 will show that the tota pump capacity passes through the volute throat AB, Section 8; only part of pump capacity passes at any other section, the amount depend ing on the location of the section from the dividing wall. Thus, volut areas are graually increased from a point A, called the volute tongu or cut-water, toward the volute nozzle to accommodate the discharg along the impeller periphery. A certain amount of liquid will be recircu lated between the cut-water and the impeller diameter and also betwee the impeller shrouds and casing side walls. The velocity in the volut varies with the pump capacity; therefore the analysis will be confine to the b.e.p., or design capacity only. The capacity through the volut is lower than that discharged from the impeller by the amount of leakag

but the latter will be disregarded and taken care of later by an experimental factor.

The velocity distribution across any volute section is not uniform. This is easy to visualize by having in mind the flow pattern in a pipe under the most favorable conditions. There the mean velocity of flow is from 0.78 to 0.92 of the maximum velocity at the center of the pipe. With small pipe diameters still lower ratios are possible. In a volute the maximum velocity is at the impeller periphery but is not uniform across the width of the impeller. Also, the velocity decreases toward the volute walls. In contrast with pipe flow, the high velocity core in the volute is driven by the impeller and, under such circumstances, the ratio of mean velocity to the maximum discharge velocity from the impeller is lower than that which can be expected in straight pipe flow. The flow pattern is complicated further by the radial outward component of the absolute velocity which causes a spiral motion along the volute. This motion is outward in the middle and inward near the walls of the volute (Fig. 7.4). Such a velocity distribution and spiral motion in the volute were visually observed by Kranz.[4]

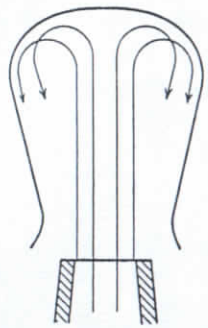

FIG. 7.4. Spiral flow in volute casing.

The ratio of the mean volute velocity c_3 to the impeller discharge velocity c_2' is lower for higher specific speed pumps, as shown in Fig. 9.14 and discussed in Chapter 9. The absolute velocity angle α_2' at impeller discharge represents specific speed on this figure, higher specific speeds having higher values of α_2'. The best modern pumps are designed for a constant average velocity for all sections of the volute; this means that volute areas are increased in proportion to their angular advancement from the cut-water.* The average volute velocity c_3 is determined experimentally from the relationship

$$c_3 = K_3\sqrt{2gH} \tag{7.1}$$

where K_3 is an experimental design factor. This varies with the specific speed. Figure 7.5 shows values of K_3 for volute pumps. Considerable deviations from these average values are possible and take place when

* Tests on centrifugal fans by Polikovsky and Abramovitch of the Central Aero-Hydrodynamical Institute, U.S.S.R., reveal that "the measured tangential velocity components did not follow the law of constant angular momentum. Instead of this, the measurements showed an almost constant value for the tangential velocity component." Review by A. Nekrassov, *Mech. Eng.*, p. 628, Aug. 1937.

The same results were confirmed later by F. Krisam,[12] p. 322.

the impeller diameter is cut or when several impellers are used wit the same casing. However, if volute areas are too small in compariso to the optimum values, the peak efficiency will decrease slightly an move toward a lower capacity or, if volute areas are too large, the pea efficiency may increase but will move toward a higher capacity. Th efficiency at partial capacities will be lower in the latter case.

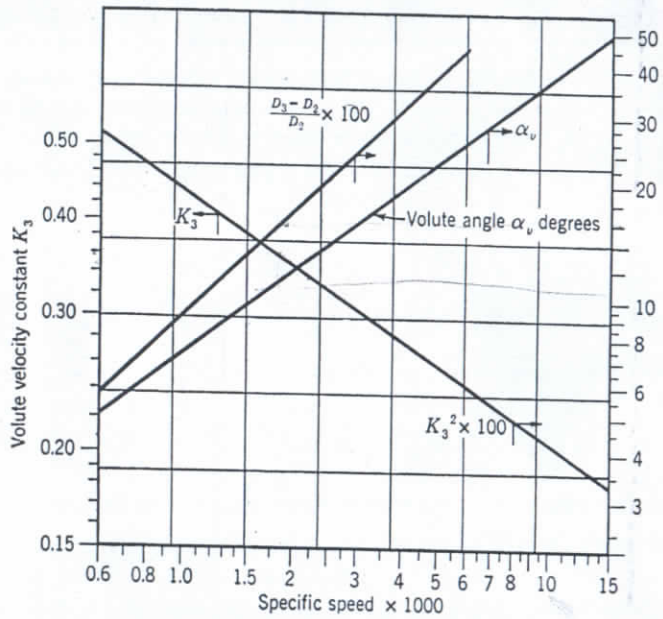

FIG. 7.5. Volute constants.

Volute areas are measured above or outside the base circle. The fact that there is an additional gap between the volute tongue and base circle has no bearing on the method of measuring the volute areas, as the increment of volute area for a given angular displacement remains unchanged, and this is the governing consideration.

(b) Volute Angle. To avoid shock and separation loss at the volute tongue, the volute angle α_v is made to correspond to the direction of the absolute velocity vector at the impeller discharge α_2', as given by Fig. 7.5. Considerable deviation from the angle α_2' is possible in practice without any harmful effects on the efficiency at low and medium specific speeds. First, it cannot be expected that one vane (volute tongue) can exert much guiding effect on the total flow from the impeller; second, no loss is incurred when the flow enters the vane with a small angle of attack. Usually there is an ample gap provided between the impeller

and the volute tongue for the flow to adjust itself for a minimum loss. At higher specific speeds the volute angle α_v and the length and shape of the tongue become more important. Thus, on a mixed flow pump of specific speed 7500, the author has found that removal of a portion of the tongue (high angle part of it) reduced the efficiency from 85 to 81 per cent. Restoring the tongue to the original shape brought the efficiency back to 85 per cent.

It should be realized that at volute sections removed from the volute tongue the flow from the impeller is "bent" or deflected from its direction as it leaves the impeller, and near the outer wall the radial component of flow c_{m2} is reversed, thus starting a spiral flow along the volute as mentioned above. The radial component is not lost, as the energy corresponding to the $(c_{m2}^2/2g)$ is greater than the total combined hydraulic losses of the whole pump.

(*c*) **Volute Width.** Volute width b_3, Fig. 7.3, is determined by the following considerations:

1. In view of the flow pattern in the volute as presented above, less loss is incurred at the impeller outlet if the high velocity flow is discharged into a body of rotating liquid rather than against stationary walls.
2. The volute casing should be able to accommodate impellers of different diameters and widths.
3. In multistage pumps, a liberal clearance is necessary between the impeller shrouds and casing walls to take care of possible inaccuracies of castings and shrinkage. With small pumps of six or eight stages this becomes a problem. For pumps of medium specific speeds, $b_3 = 1.75b_2$, where b_2 is the impeller width at discharge. For small pumps of lower specific speeds (b_2 is small), including multistage pumps, $b_3 = 2.0b_2$. For high specific speed pumps ($n_s > 3000$ double suction) b_3 can be reduced to $b_3 = 1.6b_2$.

(*d*) **Base Circle.** The base circle is used for drawing the volute layout, and the cut-water diameter D_v, fixed by the base circle diameter, determines the physical limitations of the maximum impeller diameter. If a certain minimum gap between the casing and the impeller outside diameter is not maintained, the pump may become noisy and the efficiency may be impaired. Figure 7.5 shows the minimum diametrical gap at the base circle expressed as a fraction of the impeller diameter, or

$$\rho = \frac{D_3 - D_2}{D_2} \tag{7.2}$$

which is plotted against specific speed. These values increase when

the impeller diameter is cut. It has been found by special tests that an unnecessarily large base circle for a given impeller diameter reduces the pump optimum efficiency as extra power is required to circulate liquid through the gap between the cut-water and the impeller.

To satisfy the continuity equation several of the volute design elements are connected by the following relationship:

$$A_v = b_2 D_2 \pi \sin \alpha_v \tag{7.3}$$

where A_v is the volute throat area (Section 8, Fig. 7.3).

(*e*) **Volute Areas versus Specific Speed.** Referring to the chart in Fig. 7.5, it will be noticed that for a given head H and capacity Q, the volute velocity decreases for higher specific speeds. This has been indicated from considerations of Euler's velocity triangles in Chapter 3, Fig. 3.12(*b*), and is shown in Fig. 9.13, Chapter 9, for "actual" velocity triangles. *This means that if a higher specific speed is selected the volute areas will be increased irrespective of the actual rotative speed,* as

$$c_3 = K_3\sqrt{2gH} \qquad \text{and} \qquad A_8 = \frac{Q}{c_3}$$

The kinetic energy contained in the flow in the volute, expressed as a ratio of the velocity head, $c_3^2/2g$, to the pump total head is also decreased. This follows from

$$K_3 = \frac{c_3}{\sqrt{2gH}} \qquad \text{and} \qquad \frac{c_3^2}{2g}\frac{1}{H} = K_3^2 \tag{7.4}$$

and is shown in Fig. 7.5. The average pressure in the volute casing above the suction pressure at b.e.p. is equal to $H(1 - K_3^2)$, disregarding the loss of head due to friction in the volute casing and the velocity head in the suction nozzle.

The physical over-all dimensions of the pump casing are determined by the size of the volute areas and the diameter of the base circle. For a given head and capacity, the areas increase as the specific speed is increased, but the base circle and the impeller diameter decrease. At a certain specific speed the two will balance each other and a further increase in specific speed will not reduce the size and weight of the casing.

Note that the gap between the impeller and cut-water is greater for higher specific speed pumps. This is necessary to minimize the losses in the process of turning the flow from the impeller (c_{m2} component of it), leaving impeller at a higher absolute angle α_2', and also to reduce the shearing loss when the impeller absolute velocity c_2' is reduced to

an average volute velocity c_3. The ratio of the two $R_{c3} = c_3/c_2'$ is lower for high specific speed pumps (Fig. 9.14).

7.3 PRESSURE DISTRIBUTION AND RADIAL THRUST IN THE VOLUTE CASING

(*a*) **Radial Thrust.** *That a constant average velocity in the volute casing is the most favorable for the pump performance is shown by the fact that in actual pumps, at and near the b.e.p., the pressure is the same in all volute*

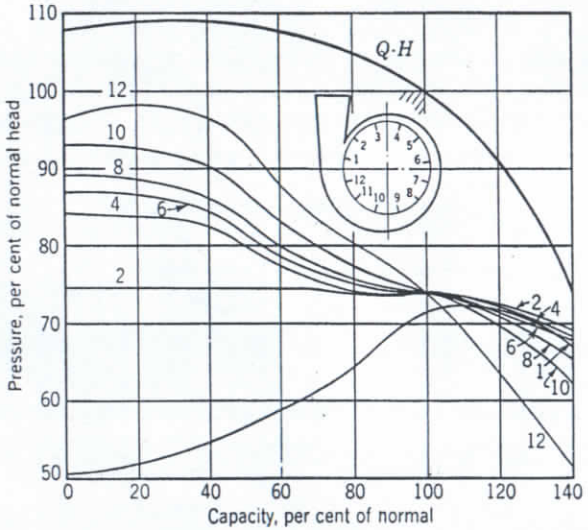

FIG. 7.6. Volute pressure distribution, 6-in. single-suction pump; $n_s = 1700$.

sections around the impeller. Evidently this is the most desirable condition for the impeller discharge. However, on both sides of the b.e.p. this equilibrium of volute pressure is destroyed. Figure 7.6 shows a typical volute pressure distribution. Figure 7.7(*a*) shows results of radial thrust measurements on a 4-in. pump. The magnitude of the forces was determined by measuring the shaft deflections and calibrating the shaft by dead weights. The radial thrust can be expressed by

$$P = \frac{KHD_2B_2}{2.31} \tag{7.5}$$

where P = radial resultant force, in pounds
H = head, in feet
D_2 = impeller diameter, in inches

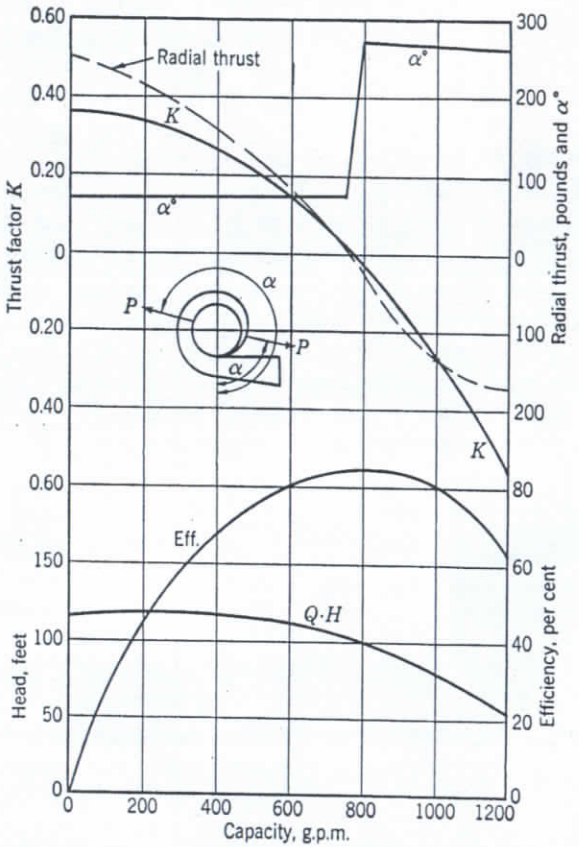

FIG. 7.7(*a*). Radial thrust in a single-volute 4-in. pump. $D_2 = 10\frac{1}{2}$ in., $B_2 = 1\frac{1}{4}$; 1760 rpm.

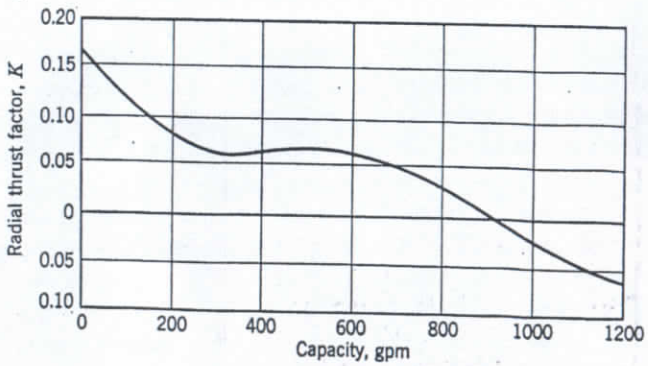

FIG. 7.7 (*b*). Radial thrust in a double-volute 4-in. pump at 1760 rpm. The impeller is the same as that in Fig. 7.7 (*a*).

B_2 = impeller over-all width including shrouds, in inches
K = a constant which varies with capacity as given by the following equation arrived at experimentally.

$$K = 0.36\left[1 - \left(\frac{Q}{Q_n}\right)^2\right] \qquad (7.6)$$

where Q is any capacity and Q_n is the normal capacity. This equation gives zero radial thrust at normal capacity and maximum radial thrust at zero capacity when $K = 0.36$. The value of K depends on the pump type. Higher values than that given by equation 7.6 have been observed ($K = 0.6$ at zero capacity).

The immediate effect of radial forces in the volute casing is excessive shaft deflection, which results in the rapid wear of the wearing rings

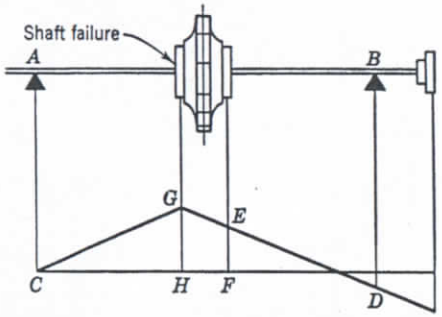

FIG. 7.8. Moment diagram of a pump shaft.

and shaft breakage due to fatigue failure of the shaft material. Shaft failures mostly occur in double-suction pumps having a large bearing span. One peculiar feature of shaft failures due to this cause is that, in a great majority of cases, the shafts fail immediately beyond the impeller on the outboard side where torque stresses do not exist. The explanation lies in the fact that the weight of the coupling (Fig. 7.8) sets up a negative bending moment at the inboard bearing B, which results in a greater bending moment and flexural stress in the plane GH than in the plane EF. In every case of shaft failure in the manner described it has been found that the pump was operating at partial capacities. The increase in operating speeds of modern pumps has aggravated the conditions as heads and the frequency of flexure reversals have increased. For long life, a shaft material with a high endurance limit should be used; also, threads should be removed from the middle portion of the shaft, and the key seat should be milled out with a proper fillet. Note that shrinking the impeller on the shaft reduces the endurance limit.[5]

(b) Double Volute. To eliminate radial thrust, double-volute casings have been introduced. In such a casing the flow is divided into two equal streams by two cut-waters 180° apart (Fig. 7.9). Although the volute pressure inequalities remain as in a single-volute casing, owing to symmetry there are two resultants of radial forces opposing each other.

Actual measurements of pressure distribution along the volutes of a double-volute casing by Knapp[6] and *direct measurements of radial forces by Ingersoll-Rand Company (1936, not published) show that a complete elimination of the radial thrust is not accomplished by the double volute.*

Figure 7.7(*b*) shows the values of radial thrust factors for a 4-in. single-suction pump with a double-volute casing. It will be noticed that for a double-volute casing the radial thrust variation for different capacities is of the same type, but on a reduced scale, as that for a single-volute pump, as shown in Fig. 7.7(*a*). *The direction of the radial thrust in a double-volute casing is approximately the same as it is in a single-volute casing.* The same impeller was used in both cases.

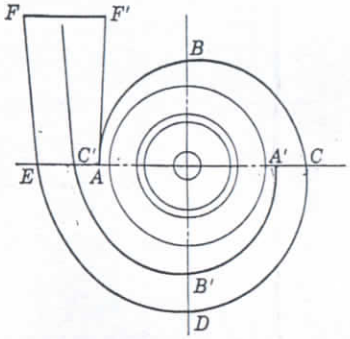

FIG. 7.9. Double-volute casing reduces but does not eliminate radial thrust.

The reason radial thrust exists in a double-volute casing is that the outlets from the two volutes are not identical. The outer volute path, $ABCDEF$ (Fig. 7.9), is approximately twice as long as that of the inner volute $A'B'C'F'$. *The energy gradient drop along the first volute is greater than that along the second. But, since the final pressures and velocities at the discharge flange are the same, the pressure in the volute ABC is lower than that in the volute $A'B'C'$.* Variation of radial thrust with the capacity is better understood from the study of the energy gradient in the volute casing given later in this chapter.

For a complete symmetry of impeller discharge pressure distribution the suction impeller approach should be also symmetrical. Any deviation from symmetry at the impeller eye results in different heads produced by different portions of the impeller periphery. There are cases on the record of shaft failures in large, high speed, double-suction pumps with double-volute casings.

The efficiency of the double-volute casing pumps approaches within one point that of single-volute pumps. But for optimum performance, double-volute pumps require more work in matching passages of split-

casing pumps, and cleaning of double-volute passages is very difficult. The efficiency curve of double-volute pumps is flatter and the improvement over single-volute pumps appears more at capacities over the normal than at partial capacities. The reason for such an improvement of pump efficiency on both sides of the peak efficiency point lies in the fact that the impeller is discharging against a more uniform pressure in a double volute than in a single volute.

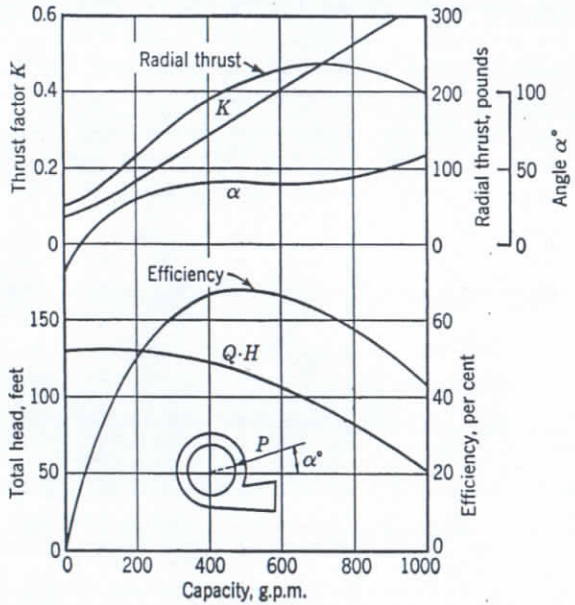

FIG. 7.10. Radial thrust in a circular casing. $D_2 = 10\frac{1}{2}$ in., $B_2 = 1\frac{1}{4}$ in., 1760 rpm.

In the double-volute casing the conversion of the velocity into pressure takes place only in the discharge nozzle. The channel leading the discharge from the first volute (ABC, Fig. 7.9) around the second volute ($A'B'C'$) is made of constant area. Attempts to utilize this channel for the conversion of velocity from the first volute were penalized by a loss of efficiency of one point or more.

Besides, having halves of the discharge nozzle of different area and under different pressures may lead to mechanical difficulties in large pumps, such as vibration of the discharge pipe or even a failure of the partition of the double-volute casing.[7]

(c) Circular Casing. Figure 7.10 shows the performance and radial thrust of a 4-in. pump with a circular casing having constant volute areas. Such designs have been used in the past for small pumps. The

maximum radial forces are developed at the b.e.p. and the radial thrust is always directed away from the cut-water. The factor K in formula 7.5 for the circular casing, as determined experimentally, can be expressed by

$$K = 0.36\frac{Q}{Q_n} \qquad (7.6a)$$

Pumps with circular casings, besides being larger, were inferior in efficiency to pumps with constant velocity volute casings and were discontinued.

(d) Radial Thrust in Volute Casing. *The pressure distribution in the volute casing, the location of the resultant of all radial forces acting on the*

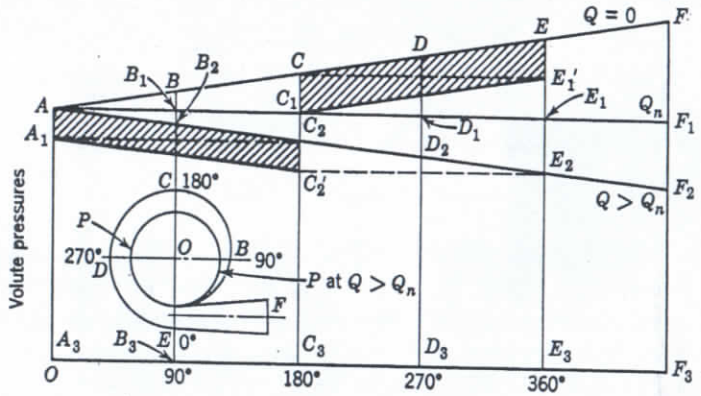

FIG. 7.11. Energy gradient and radial thrust in a single-volute casing.

impeller, and reversal of its direction can be explained by the energy gradient variation along the liquid path from the impeller periphery to the casing discharge nozzle. In a volute casing designed for a constant velocity, the pressure gradient will parallel the energy gradient. On Fig. 7.11, line AF represents the static pressure gradient along the periphery of the impeller for zero flow and developed on a straight line. Point A is at or near the cut-water. Pressure rises steadily toward the discharge flange. This can be easily visualized because, with the discharge blocked, liquid is crowded toward the discharge nozzle and cut off by the cut-water; or, the conditions in the casing can be looked upon as an eccentric forced vortex in which particles on a larger radius develop higher pressure. Pressures along AC oppose those along CE because they are 180° apart. The resultant pressure forces are proportional to the areas on the diagram. The pressure area AA_3CC_3 will balance the area $C_1C_3E_1'E_3$. The unbalanced radial forces will be represented by the

area CC_1EE_1'. The direction of the resultant is along a radial line toward the center and 270° from the cut-water.

When flow starts in the volute, the hydraulic gradient drops below AF and at normal capacity it reaches a position AF_1, where pressures are equal all around the impeller. The hydraulic gradient drop increases along the volute from zero at A to BB_1, CC_1, and so on. At normal capacity the resultant of all radial forces is zero.

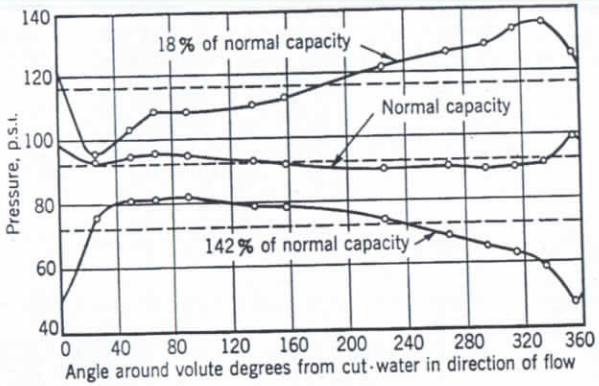

FIG. 7.12. Pressure distribution around the volute casing; 8-in. pump, 2500 rpm (California Institute of Technology).

As the flow increases further to $Q > Q_n$, the hydraulic gradient continues to drop from BB_1 to BB_2, from CC_1 to CC_2, and so on. Now pressures are higher along AC than along CE. Pressure area $A_1A_3C_2'C_3$ balances area $C_2C_3E_2E_3$ and the unbalanced radial forces are represented by the area $AA_1C_2C_2'$. The direction of the resultant of these forces is from smaller volute sections toward larger sections. Note that pressure at the nozzle F_2 is lower than at any point in the volute.

Figure 7.7(*a*) shows that the directions of the resultant radial force vary slightly from those arrived at on the diagram in Fig. 7.11. In Fig. 7.12 is shown a pressure distribution for three capacities of an 8-in. pump at 2500 rpm tested at the California Institute of Technology.[8] From this it is seen that the pressure distribution along the volute deviates from the straight line assumed on Fig. 7.11, particularly at and near the cut-water where two regions with different pressures meet. The general trend of the pressure curves, however, substantiates the reasoning underlying the construction of Fig. 7.11.

The energy gradient diagram for the double volute would have the same appearance as that for the single volute in Fig. 7.11. By referring to Fig. 7.9, it will be seen that pressures in the two volutes are equalized

beyond the discharge flange. They are also equal just ahead of the inner volute cut-water A'. At all intermediate points the pressures will be indicated by the direction of the energy gradient drop, giving a diagram similar to Fig. 7.11. Therefore, variation of the radial thrust and its direction in the double volute are of the same nature as they are in the single volute, Fig. 7.7(*b*).

7.4 CROSSOVER

In multistage pumps, the channel leading from the discharge volute of one stage to the impeller eye of the next stage is called a crossover. This channel must perform several important functions:

1. Convert high velocity energy prevailing in the volute into pressure by reducing the velocity sufficiently to perform the next function with a minimum loss.
2. Make a 180° turn to direct the flow into the eye of the next impeller. (Depending on the stage arrangement this flow may travel axially through one or more stage spacings.)
3. Change the shape of the channel so that it will distribute the flow uniformly around the eye of the next impeller (Fig. 7.13).

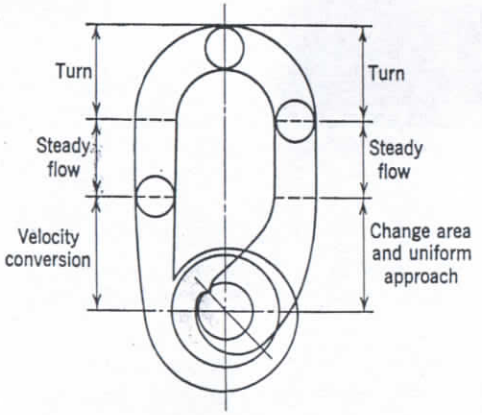

FIG. 7.13. Diagram of a crossover.

For efficient operation, each of these functions should be completed independently or one at a time. Velocity cannot be converted efficiently by diffusing and making a turn simultaneously because, during the turn, higher velocities are shifted to the outer side of the elbow and no conversion will result. Also, while changing the shape of the passage, equal areas will not result in uniform velocity if a change in direction of flow

is made at the same time. In each plane the diffusion rate must be kept within permissible limits. When the channel is being shifted from one stage to the other, turns are not in one plane; therefore there will be a spiral motion set up in the flow. A circular section is best suited for such turns. Figure 7.13 shows a diagram of an ideal crossover. The

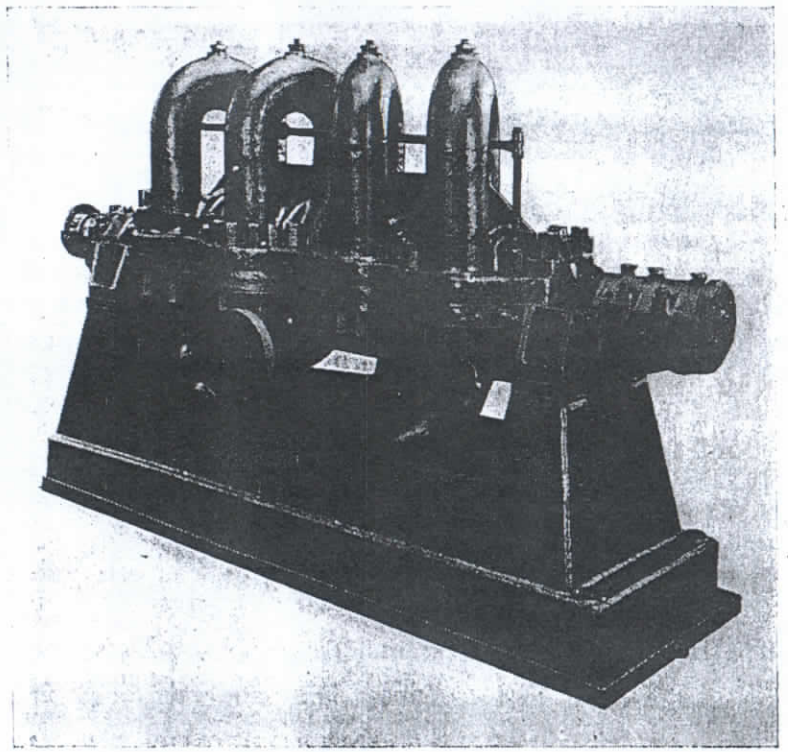

FIG. 7.14. Eight-stage pump with all-external crossovers (United Pumps).

immediate approach to the impeller eye is developed in the same manner as the first-stage suction discussed in Art. 7.1.

Efficiencies of 85 per cent have been obtained commercially with pumps of this type in three and four stages, 1200 gpm at 3500 rpm, and specific speeds of 1500 to 1800. In six and eight stages and lower specific speeds (1250), efficiencies of 81 to 82 per cent are obtainable for the same size of pumps.

The practical limit for the number of stages for multistage pumps with external crossovers is eight. However, the pattern and core work for eight-stage units becomes extremely complicated. Any unnatural

bend or twist of the crossover (to clear each other) defeats the purpose of high efficiency conversion.

Figure 7.14 shows an eight-stage pump with all external crossovers, four short one-stage crossovers in the upper half of the casing and three long (more than one-stage) in the lower half. The sectional drawing of this pump appears on Fig. 17.19. The stage arrangement from right to left is: 1–2–5–6–8–7–4–3. The crossover 4–5 is hidden below the 2–3 and 6–7 crossovers. The multistage pumps with external crossovers are practically unknown in Europe. In the sizes and specific speeds stated above, equal efficiencies are obtained with the modern, vaned diffuser designs.

Small-volute multistage pumps are frequently built with crossovers "cast-on" in the abbreviated form as a part of the casing (Fig. 7.15).

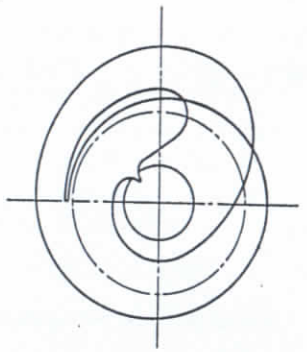

FIG. 7.15. Cast-on crossover.

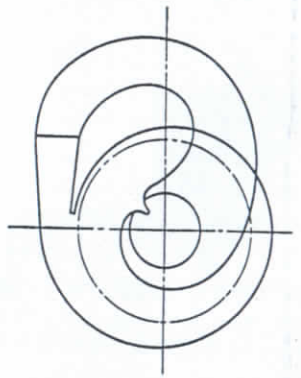

FIG. 7.16. Cast-on crossover with a straight nozzle.

Two or more points of efficiency are sacrified by such simplification, depending on the shape of the crossover passages. To achieve any degree of velocity recovery in a cast-on crossover, a small, straight nozzle should be provided for this purpose immediately following the volute throat (Fig. 7.16). Circular sections of the channel should be adapted as much as possible.

7.5 DIFFUSION CASING

(*a*) Single-Stage Pumps. Although peak efficiency of pumps with vaned diffusion casings is higher to the extent of two points than that of the volute pumps, there are only a few single-stage pumps with diffusers built in this country (Fig. 17.12). Low cost and mechanical simplicity are the deciding factors in favor of volute casings. In Europe,

owing to a higher evaluation of efficiency, a great majority of large pumps are provided with the diffusion vanes.[9] The Grand Coulee pumps, referred to in Art. 2.3 and shown on Fig. 17.23, have four vanes added to their double-volute casings, thus giving the appearance of vaned diffusers. However, the number of vanes and their shape (profile) are such that they serve only as guide vanes introduced for strength reasons. The conversion of velocities into pressure is accomplished in the long discharge nozzles.

(*b*) **Multistage Horizontal Pumps.** Figures 17.9, 17.10, and 17.13 show three types of high pressure multistage pumps with diffusion vane casings. The hydraulic elements of all three are alike—each consisting of the individual stage diffusion vane ring and vaned return channel. In the first, the pumping element is enclosed within a horizontally split casing capable of withstanding the total discharge pressure. In the second, the individual stage elements are held together with strong anchor bolts, whereas in the third, the pumping element is enclosed into a forged barrel with a circular cover on each end. Both Fig. 17.10 and Fig. 17.13 are used for the highest pressures encountered in the boiler feed application. The Fig. 17.9 design is limited to 1200 psi pressure.

Hydraulic design of vaned diffuser is guided by the same considerations as that of the volute casing. The total throat (inlet) area of the diffuser is made equal to that of a volute casing for the same conditions. Although the restrictive action for through-flow in the vaned diffuser is greater than that of the volute casing, the flow through the diffuser and in the collecting chamber (volute) is more orderly and the same capacities are realized in both designs for the same total throat area.

The base circle D_3 and the vane entrance angle for the vaned diffuser are established in the same manner as for the volute casing. The diffuser width b_3 is made slightly greater than the impeller width b_2, so that $b_3 \approx 1.1\, b_2$. For small multistage pumps $b_3 = (b_2 + 1/16)$ in., which is a minimum to allow for inaccuracy of the casing casting.

The number of vanes should be a minimum necessary to realize the required throat area and maintain the shape of the channel between two vanes as discussed below. The outside diameter of the vaned part of the diffuser is not a criterion by itself, but depends on the number of vanes and channel proportions and the gap between the impeller and diffuser vanes. In a well-designed diffuser the outside diameters vary from $1.35D_2$ to $1.6D_2$.

The optimum shape of the channel between two vanes of a diffuser has been established by several investigators here and abroad. This shape should satisfy the following conditions:

1. For a given area, the hydraulic radius of the channel should be a minimum. The best practical approach to this is a square section at or near the entrance to the diffuser. Round sections have proved more efficient, but are difficult to adopt for practical use, except in special designs.

2. The diffuser channel, confined between the two adjacent vanes, should be straight-walled conical.

3. The number of vanes should be a minimum required to form a good channel, the optimum length of the confined channel being fixed in a rather narrow limit.

4. The angle of divergence of the diffuser channel should be equal to or smaller than those established for straight channels with a uniform velocity of approach. For a straight, circular conical diffuser an included angle of divergence of 8° was already quoted in connection with volute discharge nozzles. For a square section the optimum divergence angle is about 6°. For a rectangular diffuser section, formed between two parallel walls, the divergence angle is about 11°. These figures, established experimentally, are not inconsistent if compared on the basis of the rate of area expansion.

5. The correct diffuser entrance angle is secondary to the optimum diffuser channel proportions, although, as a starting point, this angle should be taken from the input discharge velocity triangle.

6. The diffuser depth $(D_4 - D_3)/2$ or the diffuser ratio D_4/D_2 (Fig. 7.17) is not a controlling factor. The number of vanes and D_4 are adjusted to obtain the desired shape of the diffuser channel.

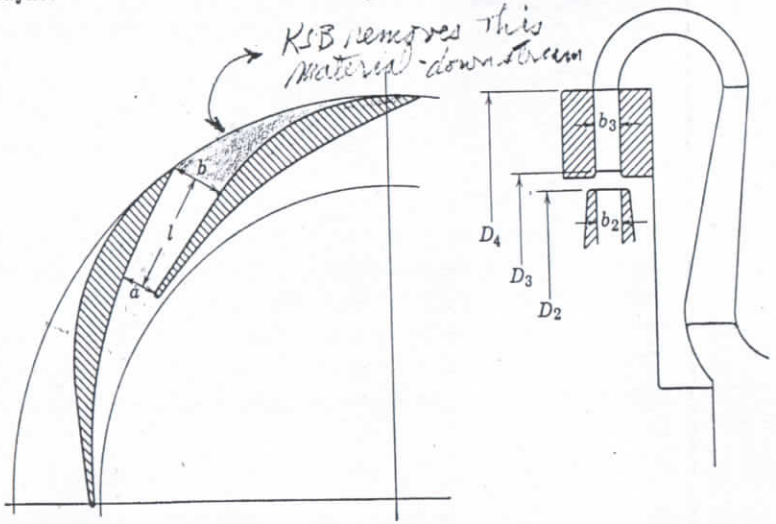

FIG. 7.17. Diffuser proportions.

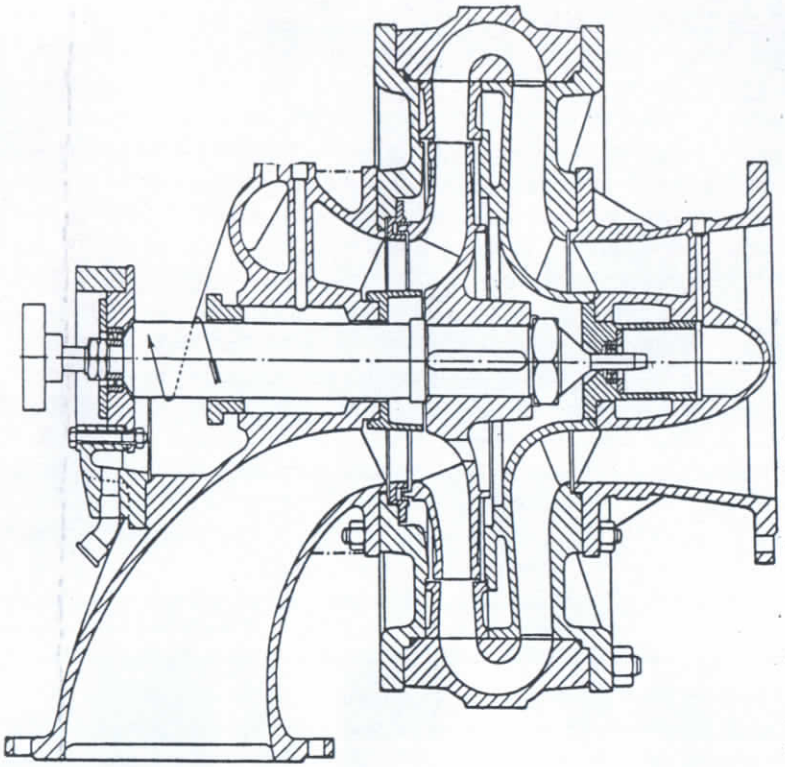

FIG. 7.19. Sulzer model pump.

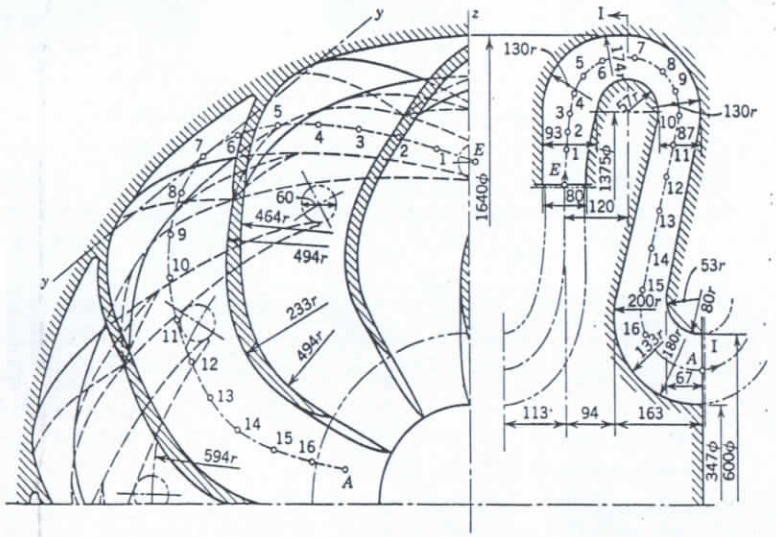

FIG. 7.20. Diffuser and return channel with continuous vanes of pump shown in Fig. 7.19 (Sulzer [10]).

passage length, the friction loss is insignificant in this part of the flow passages. Dividing the channel from stage to stage into a combination of two vaned parts (diffuser and return channel) and a vaneless U turn is done for manufacturing reasons both in the blower and centrifugal pump field at the expense of perhaps two to three points in efficiency.

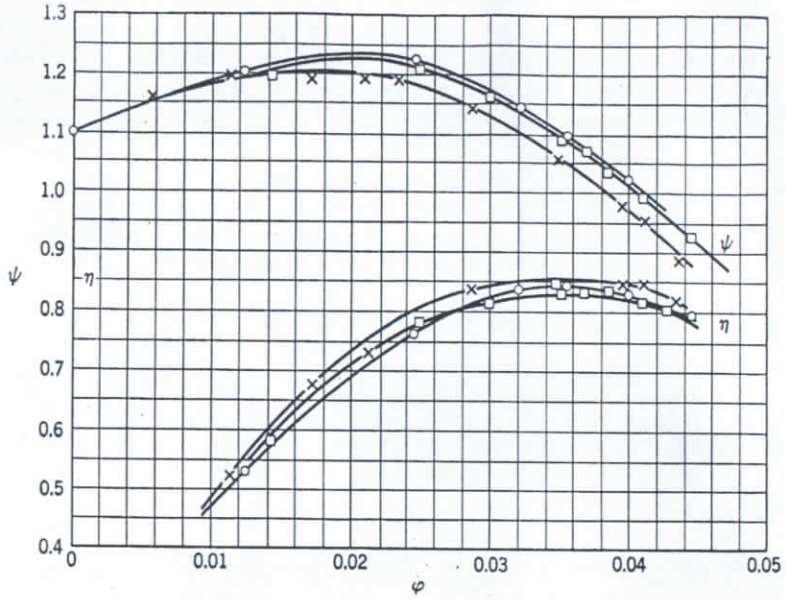

FIG. 7.21. Characteristic of the model pump with an impeller diameter of 550 mm (Sulzer [10]). The head coefficient ψ as shown is twice the value as used in this book, equation 5.15. The capacity coefficient ϕ as shown should be divided by $4/\pi^2$ to obtain the specific capacity q_s as defined by equation 5.13. N is power input.

Figure 7.19 shows an assembly of a Sulzer one-stage pump [10] with 21¾ in. impeller diameter which is a model for a five-stage water storage pump for 42,700 gpm (5700 cfm), 1620-ft head, 500 rpm, 20,500 bhp; specific speed is 1400. This includes the return channel, with continuous vanes shown in Fig. 7.20, manufactured in three parts. Tested on water and air this model has shown 85 per cent efficiency (Fig. 7.21).

Very extensive tests on air fix the length of the confined diffuser passage as four times the opening between the two adjacent inlet vane tips, or $l = 4a$ (Fig. 7.17). The preferred area expansion ratio is $b/a = 1.6$. This corresponds to about 8½° of divergence for a diffuser with parallel side walls.

To extend the length of the channel beyond $l/a > 4$ does not improve the performance of the diffuser. Apparently what is gained by a further velocity recovery is lost in additional diffuser loss and eddy losses accompanying the joining of two streams from the two adjacent diffuser channels.

Long and curved diffuser channels (mean path) cannot perform conversion of velocity into pressure effectively as the flow becomes crowded toward the outer wall of the channel where local high velocities are restored. On one occasion the author observed that increasing the number of diffuser vanes (slightly curved) from seven to nine, thus increasing the vane overlap, reduced the efficiency of a unit by three points.

It should be pointed out that the relative position of the impellers and diffusers in a multistage pump has a marked effect on the pump efficiency and the shape of the head-capacity curve near the shut-off. The best efficiency is obtained when the front shroud (impeller inlet shroud) is lined up with the diffuser wall. The shut-off head tends to rise at the same time. When the back shroud is lined up with the diffuser wall, the head-capacity curve tends to show a "droop" toward zero capacity and efficiency is measurably impaired. With the impeller in the mid-position in respect to the diffuser channel the effects on performance are intermediate between those in the first two cases. The above observations suggest that the flow through the impeller discharge shifts toward the back shroud. In one example of a pump of $n_s = 1700$, the peak efficiency variation between the extremes was two points, with the shut-off head variation of 10 per cent. These effects are less pronounced with lower specific speed impellers.

(c) Return Channel. Return channels receive the flow from the diffuser at a reduced velocity, turn it 180° toward the inlet of the next impeller, and take out what is left of the tangential component. To perform this function efficiently, the flow should be gradually accelerated. To arrive at a proper curvature of the return channel vane, it is better to assume the development of a one-piece vane combining the diffuser and return channel vanes (Fig. 7.18) and then transfer one half of it into the diffuser and the other half into the return channel, using the "error triangle" method presented in detail in Chapter 6. The diffuser vanes can be further modified by taking out some of the curvature of the channel and incorporating the favorable proportions discussed above. The number of return channel vanes is established from the same considerations as that of the impeller and is lower than the latter by two to three vanes.

While experimenting with return channels of different design, the author found a spread of 8.5 points in efficiency between the best and worst channels.

Utilization of the kinetic energy of the preceding stage in the following stage is the important guiding principle, established experimentally. The recovery of pressure should proceed not more than necessary to a slight acceleration in the U turn and next-stage impeller approach. A quite common fault of the return channels of the older design was that the fluid was "dumped" from the diffuser into the return channel without any attempt to guide the flow or control the velocities.

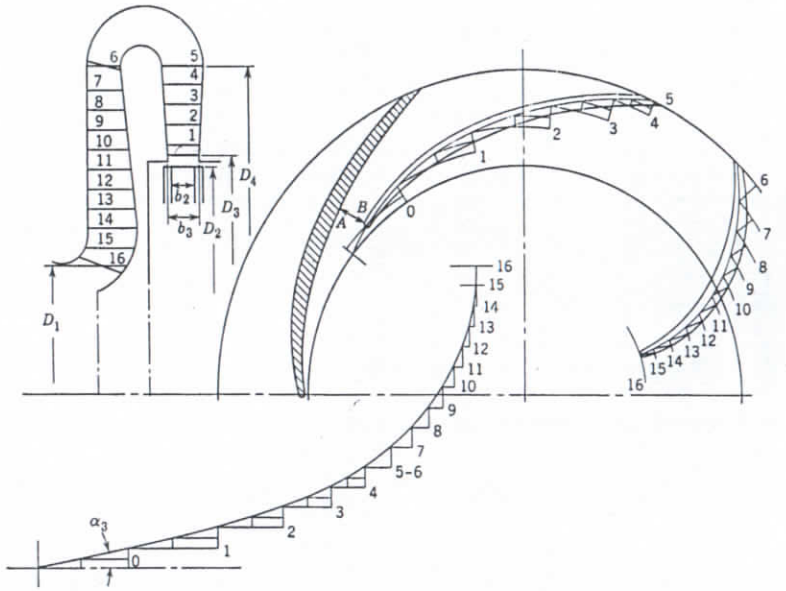

FIG. 7.18. Diffuser and return channel vanes layout.

(d) Continuous Diffuser Channel. A comparison of performance of multistage pumps with that of single-stage pumps (with vaned diffusers) of the same specific speed indicates that there is an excessive hydraulic loss in the sharp 180° turn between the diffuser and return channel vanes. This loss is of the nature of eddy losses due to the abrupt change in velocity and direction of flow. Because of the short

This design is typical of the latest European multistage pumps showing appreciable improvement in efficiency, as compared with older separate diffuser rings, return channel, and unvaned U-turn.

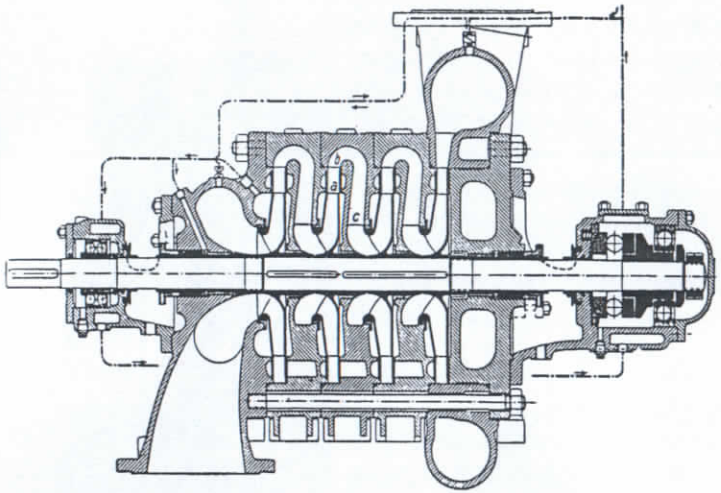

FIG. 7.22. Multistage pump with a continuous diffuser and return channel (Rütschi [11]).

Figure 7.22 shows another example of a multistage pump with a continuous diffuser and return channel. Figure 7.23 shows the core work ready for the mold, and Fig. 7.24 shows a straight-walled part of the

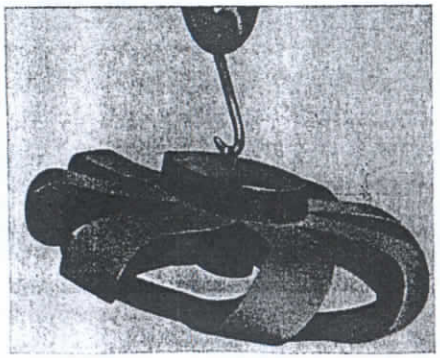

FIG. 7.23. Corework of the diffuser and return channel of pump shown in Fig. 7.22 (Rütschi [11]).

diffuser proper. In size of 1000 gpm, specific speed $n_s = 1600$, efficiencies of 82 to 83 per cent were obtained with the above design.[11]

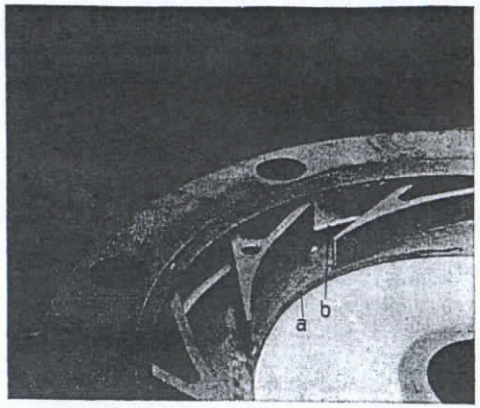

FIG. 7.24. Diffuser of pump shown in Fig. 7.22 (Rütschi [11]).

(*e*) Diffusion Casing of Vertical Turbine Pumps. To this clas belong all vertical pumps of a wide range of specific speeds (1000 t 15,000). In smaller sizes and in low and medium specific speeds (150 to 4500), these pumps have been used mostly on irrigation projects i West Coast states for pumping from drilled wells. They have bee perfected to a high degree and, at the present, represent the most efficien type of multistage centrifugal pump. Laboratory pump efficiencie up to 90 per cent for 1200-gpm pumps at 1760 rpm are on the record Several factors contributed to this progress: (1) selection of favorabl specific speeds of 2500 to 4000, not used in any other multistage pumps (2) use of open impellers, which reduce the disk friction loss and per mit better cleaning and polishing of the impeller vanes; (3) improve hydraulic design of the casing with a liberal stage spacing; (4) kee competition of a score of companies, simple, cheap patterns, and larg sales volume, which permit continuous improvements and change i design; (5) owing to the stage arrangement, absence of (*a*) interstat leakage, (*b*) leakage from balancing devices, as hydraulic thrust is take up by the motor thrust bearing, (*c*) high pressure stuffing boxes in ope shaft designs.

Hydraulically, the casing design involves several features resultin from the vertical arrangement: (1) the diffusion vanes are arrange more in an axial direction; (2) the diffusion vanes are developed in on piece and without sharp turns (Fig. 7.25), thus allowing more spac between the impeller and the diffusion vanes; (3) it is possible to us impellers of different diameters and widths. With increasing specifi speed the impeller profile gradually changes from a straight radial to a conical mixed flow, and finally to a straight axial flow (Fig. 7.26).

Selection of diffusion vane angles and velocities follows the same guiding considerations. Much higher velocities through the diffuser are possible with vertical pumps than with volute pumps of the same specific speed, particularly in the high specific speed range, because all turns are gradual and, in axial and mixed flow types, little or no turns in the meridional velocities are present.

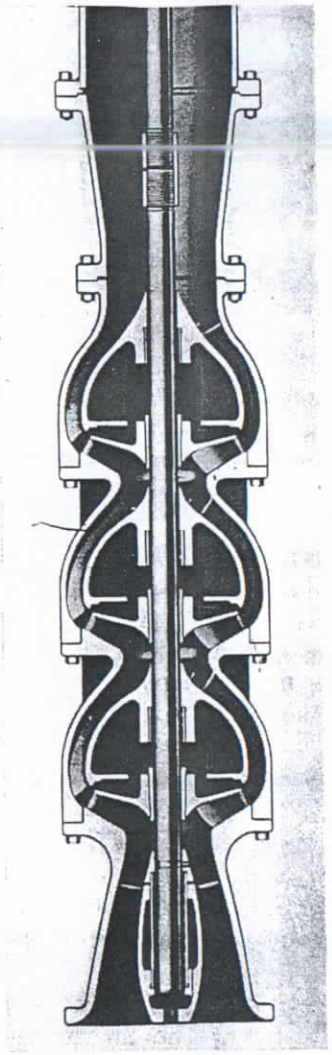

FIG. 7.25. Vertical turbine pump (Ingersoll-Rand).

In order to obtain a maximum capacity for a given diameter of pump casing, considerably higher diffusion vane angles α_v are used in vertical turbine pumps than in horizontal volute pumps.

Figure 7.26 gives limits of α_v values for turbine pumps.

(f) Effect of Speed on Casing Performance. If pump speed (and hence head per stage) is steadily increased, and assuming that there is ample NPSH at any speed to prevent cavitation, experience has shown that the peak efficiency, having reached a maximum, begins to fall off. A gradual increase in efficiency up to the optimum is explained by a reduction of losses at higher Reynolds numbers. A reduction of efficiency beyond the optimum point is caused by the fact that high velocities through the pump parts, as found at high speeds, require a greater degree of refinement in hydraulic design than is found in normal good designs based on moderate speeds and heads per stage. In general, a great degree of streamlining is required at higher speeds. This includes: (1) less curved impeller approach; (2) less curved impeller profile; (3) better streamlining of impeller vanes, approaching airfoil profiles; (4) larger gap between the impeller and the diffuser vanes or volute cut-water; and (5) a smaller discharge nozzle diffusion angle of the volute casing.

There is ample evidence in the field of turboblowers that at high speeds and heads per stage the advantage of the vaned diffuser over the volute casing is more pronounced. It is believed that the spiral motion in the volute casing, as shown on Fig. 7.4, at high volute velocities incurs

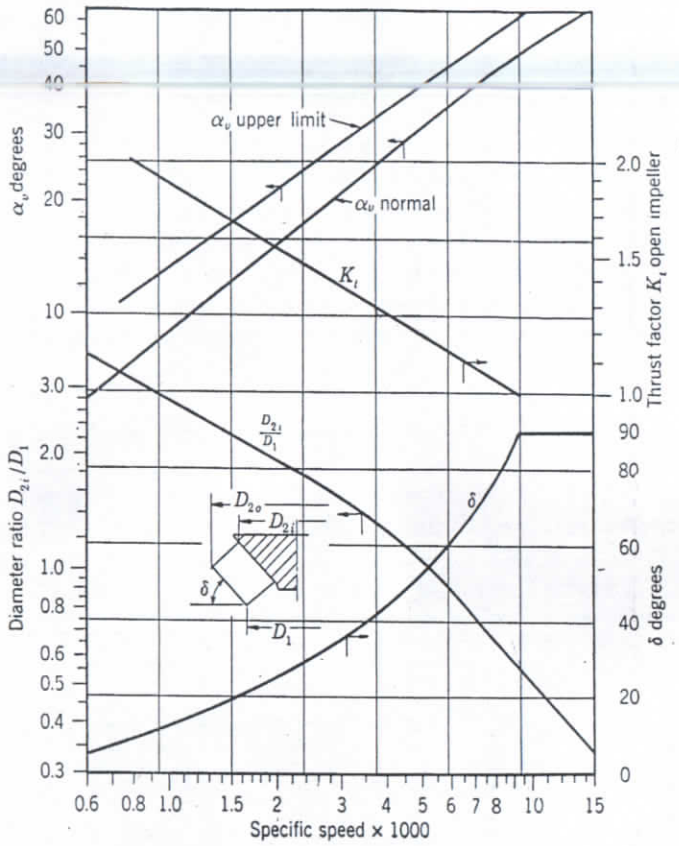

FIG. 7.26. Vertical turbine pump constants.

additional losses. Besides, the dual spin of the fluid in this volute impairs the specific capacity (the through-flow ability at b.e.p.). The b.e.p. moves to the left and the head-capacity curve at capacities over the normal becomes steeper.

(g) Remarks on Volute Casings. Although volute casings have only a few controlling design elements and a very simple shape of the flow passages, a very accurate manufacturing procedure is required to obtain the optimum hydraulic efficiency in high speed, high head pumps. The most common faults in casing manufacturing are:

1. Failure to clean the volute passages may reduce the pump efficiency up to four points in small pumps. Cleaning of the casing side walls reduces the disk friction loss appreciably.

2. Displacement of the impeller central plane with respect to the volute casing plane of axial symmetry, Fig. 7.27(*a*), or angular displacement, Fig. 7.27(*b*) impairs the efficiency measurably. Thus angular displacement of the impeller plane of symmetry of 1° reduced the peak efficiency by 1.5 points in one example and 2.7 points in another case.

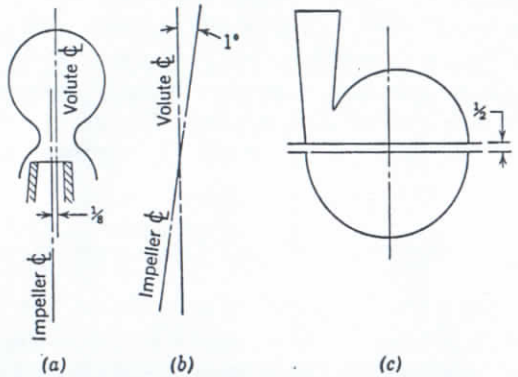

FIG. 7.27. Volute casing manufacturing faults.

3. Mismatching of the two halves of horizontally split pumps or failure to remove all the metal allowed for finish on the split flange (resulting in the "spreading" apart of the two hydraulic halves of the volute) affects the pump efficiency, Fig. 7.27(*c*).

4. Any deviation from the symmetrical volute with respect to the impeller central plane is accompanied with a reduction of efficiency.[12]

The conversion of velocity into pressure can be accomplished only in a straight conical discharge nozzle. No conversion can be expected in a discharge nozzle incorporating a gooseneck bend which is sometimes provided to bring the discharge flange into the shaft central plane to make the pump "symmetrical."

REFERENCES

1. R. W. Allen, "Some Experiences of the Use of Scale Models in General Engineering," *Engineering*, p. 313, Sept. 9, 1938.
2. A. J. Stepanoff, "Volute vs. Diffuser Casings for Centrifugal Pumps," *Proc. Natl. Conf. Ind. Hydraulics*, pp. 55-74, 1950.
3. A. J. Stepanoff, *Turboblowers*, p. 166, New York, John Wiley and Sons, 1955.

4. H. Kranz, "Strömung in Spiralgehäusen," *Bull.* 370, Berlin, Verein Deutsche Ingenieure, 1935.
5. Battelle Memorial Institute, *Prevention of the Failure of Metals under Repeate Stress*, p. 44, New York, John Wiley and Sons, 1941. (Out of print.)
6. R. T. Knapp, "Centrifugal Pump Performance as Affected by Design Features, *Trans. A.S.M.E.*, Vol. 63, No. 3, p. 254, April 1941.
7. J. Parmakian, "Vibration of the Grand Coulee Pump-Discharge Lines," *Tran A.S.M.E.*, Vol. 76, p. 783, 1954.
8. R. C. Binder and R. T. Knapp, "Experimental Determination of the Flo Characteristics in the Volutes of Centrifugal Pumps," *Trans. A.S.M.E.*, Vo 58, No. 8, p. 659, November 1936.
9. H. Lepique, "Kreiselpumpen im Wasserwerk Getrieb," *Z. Wasserwirts.*, N 12, 1942.
10. Sulzer, *Tech. Rev.* (Switz.), No. 3, 1951.
11. A. Stingelin and K. Rütschi, "Hockdruck-Zentrifugalpumpe von hohem Wi kungsgrad," *Schweiz. Bauz.*, Vol. 106, No. 19, Nov. 9, 1935.
12. F. Krisam, "Neue Erkentnisse im Kreiselpumpenbau," *Z. Ver. deut. Ing.*, Vo 95, No. 11/12, p. 320, Apr. 15, 1953.

Chapter 8

Axial Flow Pumps

8.1 INTRODUCTION

The useful range of specific speeds covered by axial flow pumps extends from 10,000 to 15,000. Axial flow pumps having specific speeds lower than 10,000 have been designed but they cannot compete with mixed flow impeller design in efficiency.[1] Besides they lead to very high values of shut-off brake horsepower and undesirable cavitation characteristics. Specific speeds above 15,000 are possible but the peak efficiency will not be higher than that of pumps with a specific speed of 15,000 operating at capacities above the normal. Axial flow air blowers are designed for specific speeds as low as 5000, but they are built as multistage units to obtain a maximum possible pressure to compete with centrifugal compressors in price, size, and efficiency. Multistage axial flow pumps, however, would not be commercially valuable.

8.2 TERMINOLOGY AND GEOMETRY OF THE AXIAL FLOW IMPELLER VANES

(*a*) **Vane Cascades.** To discuss the action of the impeller vanes in an axial flow pump it is convenient to represent vanes on the development of several cylindrical sections. Three such developments are of particular interest: at the outside impeller diameter D_o; at the impeller hub D_h and at the mean effective diameter D_m. It will be recalled that the mean effective diameter is defined by equations 5.23 and 5.24.

On the cylindrical development, vanes appear equally spaced at a distance $t = \pi D/z$, sometimes referred to as "pitch," where z is the number of vanes and D is the diameter of the cylindrical section. The ratio of the vane chord length to the vane spacing (l/t) is an important design element, being an index of the "vane solidity." Vane solidity is a descriptive term relating the vane area (actual or projected) to the area of the annulus normal to the flow. The chord-spacing ratio generally increases from the vane tip to the hub (Fig. 8.1).

To exert effectively any driving action on the fluid, the vane angle is gradually increased from β_1 to β_2. The difference between the two,

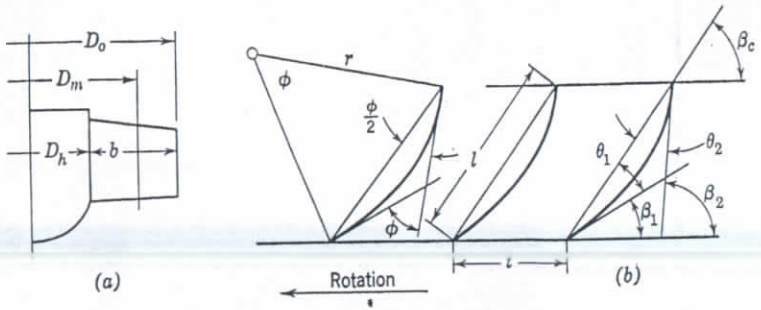

FIG. 8.1. Cascade notation.

$\beta_2 - \beta_1$, is a measure of the vane curvature along any particular vane section. From the geometry of Fig. 8.1, the following relationships between the several angles can be written:

(*a*) Vane curvature

$$\beta_2 - \beta_1 = \phi = \theta_1 + \theta_2 \tag{8.1}$$

(*b*) Chord angle

$$\beta_c = \beta_1 + \theta_1 \tag{8.2}$$

$$\beta_c = \beta_2 - \theta_2$$

(*c*) Circular arc vane

$$\theta_1 = \theta_2 = \theta = \phi/2 \tag{8.3}$$

$$\beta_2 - \beta_1 = \phi = \text{central angle}$$

$$l = 2r \sin \theta$$

(*b*) **Airfoils.** In view of the very low head produced by an axial flow impeller, the skin friction loss, or what is known as drag, acquires a greater importance than in centrifugal or mixed flow impellers. For that reason a high degree of impeller vane streamlining and polishing is required to obtain the optimum peak efficiency. To satisfy this requirement and that of mechanical strength, the impeller vane profiles take the form of airfoils. Although developed primarily for the airplane supporting wing application, airfoils have found wide use in the field of axial flow turbomachines and, therefore, familarity with the properties of airfoils is essential.

A great many airfoil sections have been tested in several countries for the last 30 years in order to determine the profile which, when applied to airplane wing design, will support a maximum load with minimum expenditure of power. In *N.A.C.A. Report* 460 (1935) all useful airfoil sections have been classified according to their curvature and thickness. For this purpose, airfoils are considered as made up of a certain profile thickness form disposed about certain mean lines (Fig. 8.2

The form of the mean line determines completely most of the important hydraulic properties of airfoils, whereas thickness is dictated by the strength requirements. All good airfoils have nearly the same thickness variation along the mean line, the maximum thickness being different

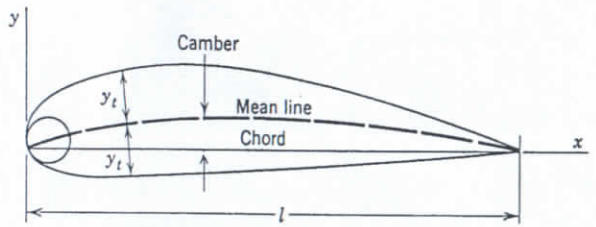

FIG. 8.2. Airfoil nomenclature.

for different profiles. The maximum distance from the chord to the mean line is called "camber" and is usually expressed in per cent of the chord length or c/l, Fig. 8.2.

Each N.A.C.A. profile is assigned a four-digit number such as 4312. The first number indicates the camber of the mean line; the second, the location of the camber from the leading edge in tenths of the chord length. The last two digits show the maximum vane thickness in per cent of the chord.

The angle of attack is the acute angle (α, Fig. 8.3) between the vane chord and the direction of the relative velocity of the flow. The aspect ratio is the ratio of the length of the airfoil to the length of the chord.

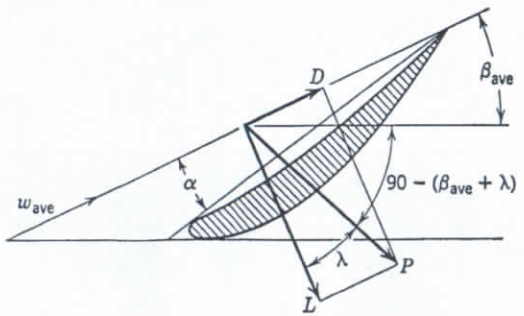

FIG. 8.3. Forces acting on an airfoil.

All N.A.C.A. sections were tested with an aspect ratio 6 to 1, but results were also recalculated for an infinite aspect ratio. Since, in a pump, fluid is confined between the hub and casing side walls and is not free to escape radially, use of the airfoil data for infinite aspect ratio is justified.

(*c*) **Lift and Drag: Gliding Angle.** If an airfoil is exposed to an a flow, the forces acting upon it can be resolved into two component component L, normal to the direction of the approaching undisturbe flow which is called the lift, and component D, in the direction of tl air flow which is called the resistance or drag (Fig. 8.3). The magnitu of these forces can be represented by the following equations:

$$L = C_L b l \rho \frac{w_{ave}^2}{2} \tag{8.}$$

and

$$D = C_D b l \rho \frac{w_{ave}^2}{2} \tag{8.}$$

where C_L and C_D are experimental coefficients of lift and drag.
b is the width of the airfoil.
l is the length of the chord of the airfoil.
w_{ave} is the undisturbed relative air velocity.
ρ is the density of the fluid.

Both C_L and C_D depend upon the profile of the airfoil, the angle attack α, and the aspect ratio. Their values have been experimentall determined for a great number of profiles. C_D is very small in con parison with C_L. The ratio C_D/C_L defines λ which is called the glidir angle. At this angle an airplane can perform a steady gliding fligh The drag force D includes (1) the skin friction, which depends greatl on the smoothness of the surface, and (2) losses due to eddies in th wake behind the wing. This part of the drag is greater for thick pr files. A well-rounded nose and a sharp tail edge reduce this part of th drag.

Figure 8.4 shows performance of airfoils 4306 and 4312 replotte from *N.A.C.A. Report* 460 to show the effect of the thickness upon th lift and drag coefficient C_L and C_D respectively. For the useful rang C_L is identical for both airfoils. The ratio L/D serves as an index the airfoil efficiency. This is better for the thin airfoil. The max mum value of the lift coefficient C_L is obtained with 12 per cent airfo thickness. Airfoils 4315, 4318, and 4321 have a lower maximum lif

For this plot the scale for the angle of attack α was deliberatel reversed from that of *N.A.C.A. Report* 460 to show the resemblanc of curve C_L versus α to the ordinary head-capacity curve of an axi flow pump; C_L standing for head; the angle of attack α, for capacity; an the ratio L/D representing efficiency.

Figure 8.5, plotted in the same manner, shows the effect of the van camber. Higher lifts at a lower angle of attack are obtained with 6 pe

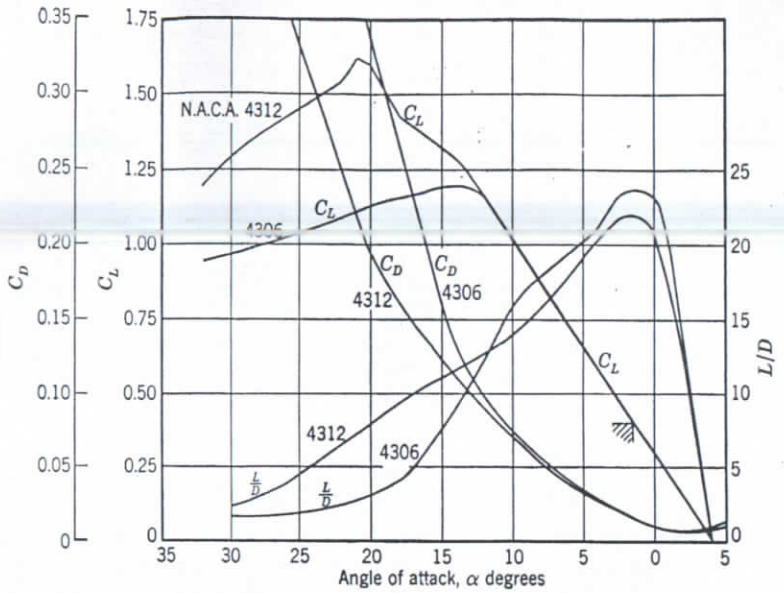

FIG. 8.4. Effect of vane thickness on airfoil performance (*N.A.C.A. Report* 460).

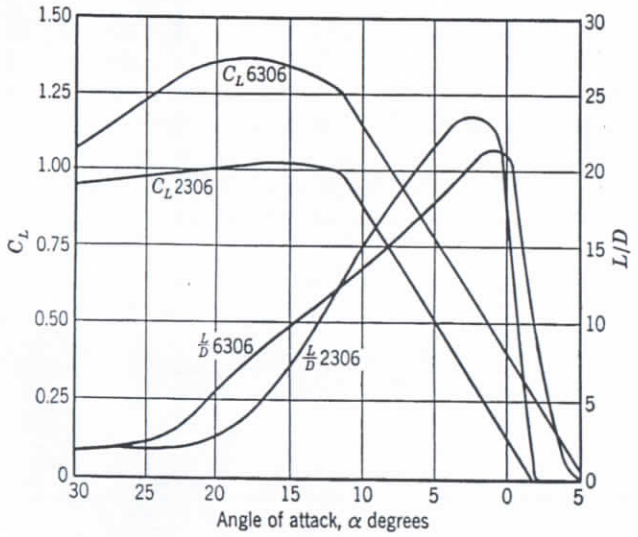

FIG. 8.5. Effect of vane camber (curvature) on airfoil performance (*N.A.C.A. Report* 460).

cent camber than with 2 per cent camber at the optimum L/D ratio, but the airfoil with 2 per cent camber is the more efficient of the two.

(*d*) Airfoil Profiles, Munk Method. Munk [2] has shown that the mean camber lines of the N.A.C.A. four-digit airfoil profiles and their aerodynamic properties are completely defined by two tangents with their points of contact to the leading and trailing ends of the mean line (AC and BC in Fig. 8.6). This follows from the properties of parabolic curves comprising the mean camber lines of this family of airfoils. Tangents AC and BC may be given by specifying angles θ_1 and θ_2 between the

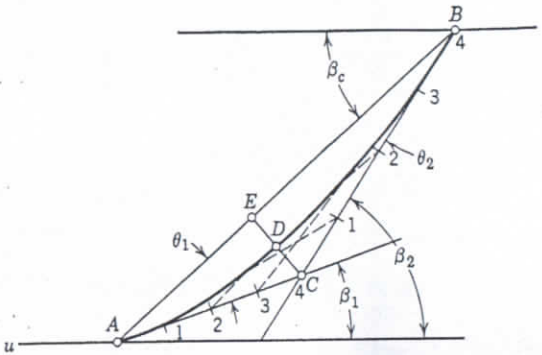

FIG. 8.6. Airfoil characteristics in terms of curvature $\beta_2 - \beta_1 = \theta_2 + \theta_1$.

chord and the tangents. Additional tangents can be drawn by dividing the tangents AC and BC into a number of equal parts and joining the corresponding points (1, 2, 3, 4, 5, and 6). The point C of the intersection of the two tangents determines the location of the maximum camber station, and the value of the camber ED is equal to one half of the distance EC. It is evident that Munk's geometrical method of drawing the mean camber line of airfoils parallels the author's procedure of drawing axial flow impeller sections based on the inlet and discharge angles β_1 and β_2 established from Euler's velocity triangles. From Fig. 8.6 the following relationships between angles β_1, β_2, θ_1, and θ_2 are evident.

$$\beta_2 - \beta_1 = \theta_2 + \theta_1 \qquad (8.$$

The vane curvature $(\beta_2 - \beta_1)$ can be expressed in terms of camber and its location. From Fig. 8.6, $\tan \theta_1 = 2ED/AE = 2c/l_c$ and $\tan = 2ED/EB = 2c(l - l_c)$ where c is the camber and l_c is its location relative to the leading edge, both expressed as fractions of the airfoil chord length. Since angles θ_1 and θ_2 are usually small, the values the angles in radians are approximately equal to their tangents. Th

the vane curvature becomes

$$\beta_2 - \beta_1 = \frac{2c}{l_c} + \frac{2c}{l - l_c} = \frac{2cl}{l_c(l - l_c)} \tag{8.7}$$

Equation 8.7 shows that the vane curvature $(\beta_2 - \beta_1)$ establishes the hydrodynamic properties of the airfoil just as completely as the camber and its location in the N.A.C.A. classification.

8.3 EXPERIMENTAL DESIGN FACTORS

There are a number of design elements of axial flow pumps which do not enter into the theoretical discussion although they affect directly the performance of the axial impeller. These include: (1) hub ratio, (2) number of vanes, (3) vane thickness, (4) turning of vanes on the hub as it occurs in adjustable vane impellers, and (5) pump casing, with or without diffusion vanes. Selection of any of these design elements depends upon experience. Correlation of test information, on the basis of specific speed, shows a definite pattern consistent with that of lower specific speed centrifugal and mixed flow pump. As more test data are accumulated, it depends upon the skill of the designer to discern the effects of these several variables, leading to the optimum hydraulic performance.

(a) Impeller Hub Ratio. The ratio of the impeller hub diameter to the impeller outside diameter is directly connected with the specific speed of axial flow pumps. This ratio is established experimentally. Higher specific speed pumps have smaller hubs, which give a greater free area for the flow and a smaller diameter to the average streamline, resulting in a greater capacity and a lower head. Figure 8.7 gives hub ratios for various specific speeds compiled from a number of modern axial flow pumps and blowers. Note that the ratio D_{2i}/D_1 (in Fig. 7.26) becomes the hub ratio for axial flow pumps above $n_s = 9350$. The hub ratio is the most important design element controlling specific speed of the axial flow impeller. The scatter of the points resulted from the attempt to use several impellers in the same pump casing. When more than one point is shown at the same hub ratio, a black mark indicates the better point of this group.

Figure 8.8 shows the ψ-ϕ characteristics of three fans having the same number of impeller vanes (seven) and approximately the same vane setting (20 to 23° at outside diameter). The b.e.p. based on the total head are marked A, B, and C. The hub ratios, efficiency, and specific speeds in terms of gallons per minute and head in feet are tabulated be-

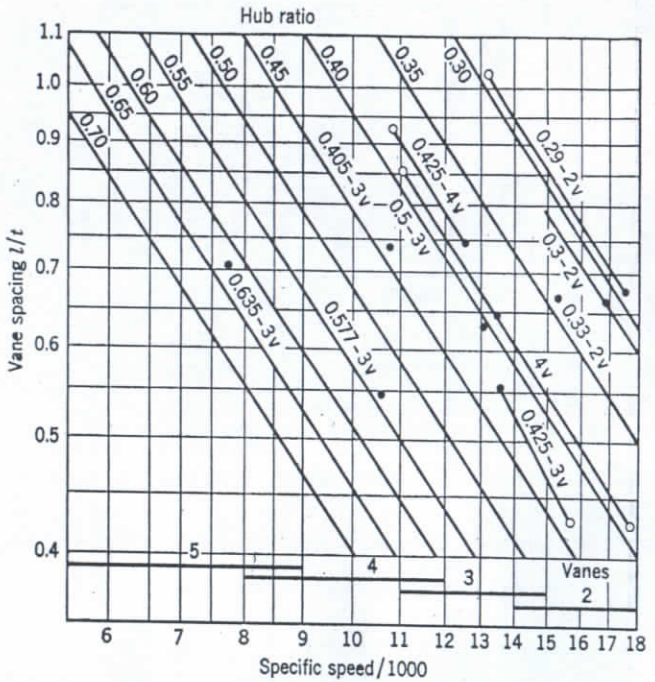

FIG. 8.7. Hub ratio, number of vanes, and l/t ratio for axial flow pumps.

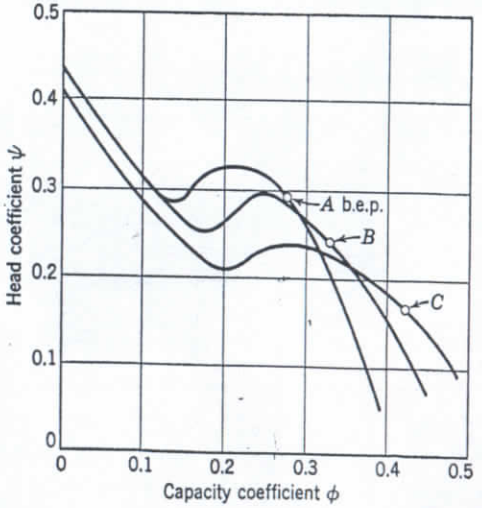

FIG. 8.8. Effect of hub ratio on specific speed; data by Buffalo Forge.

low. The formula connecting the dimensionless coefficients ψ and ϕ with the performance specific speed is given by equation 5.35(*a*).

PERFORMANCE DATA FOR FIGURE 8.8

B.e.p.	*A*	*B*	*C*
Hub ratio	0.702	0.573	0.426
Total efficiency, per cent	84	85	82
Vane setting degrees at outside diameter	20	21	23
Specific speed n_s	5550	8500	14,750
Dimensionless specific speed ω_s	1.133	1.70	2.46

It should be pointed out that the hub ratio depends also upon the selection of the capacity coefficient ϕ which in turn depends upon the impeller discharge angle and specific speed ω_s (Fig. 9.13). This is because the continuity equation

$$Q = c_m \pi D_o^2 (1 - \nu^2)/4 \qquad (8.8)$$

has to be satisfied. Thus the impeller design involves adjustment of several variables to agree with the above requirements.

(*b*) **Chord-Spacing Ratio.** The chord-spacing ratio l/t is another important design element which is selected on the basis of previous experience. For axial flow pumps of specific speeds of 10,000 and higher, the ratio l/t is less than unity. For impellers cast in one piece, non-overlapping vanes are mostly used, as they require a very simple molding procedure without any core work. The ratio l/t varies along the radius, increasing toward the hub. This increase in l/t at the hub is desirable for mechanical reasons.

Figure 8.7 shows values of the l/t ratio for the section at the periphery of the impeller for various hub ratios. The value of l/t at the hub is 1.25 to 1.30 times that at the outside diameter of the impeller, depending on the hub ratios. Higher l/t ratios at hub have been used but are less suitable for the adjustable vane design, and may complicate the molding method for a one-piece casting. It is possible to obtain the same values of l/t with a different number of vanes. The actual hub ratios and number of vanes for different specific speeds are marked for each point on Fig. 8.7.

(*c*) **Number of Vanes.** Basing his opinion on the extensive tests with hydraulic turbines, Kaplan [3] has found that for a given wetted area of the vane (l/t) the number of vanes should be a minimum. This was also confirmed by Schmidt's tests [4] which showed that a two-vane impeller is most efficient with a projected vane area of about 63 per cent.

With heavy vanes and a low chord angle, the maximum number of vanes is almost fixed since adding vanes will restrict the free area of the

flow. The normal capacity will decrease and efficiency will drop. In one example a good performance was obtained with three and four vanes only. With two vanes, the ratio l/t was too low for good efficiency and

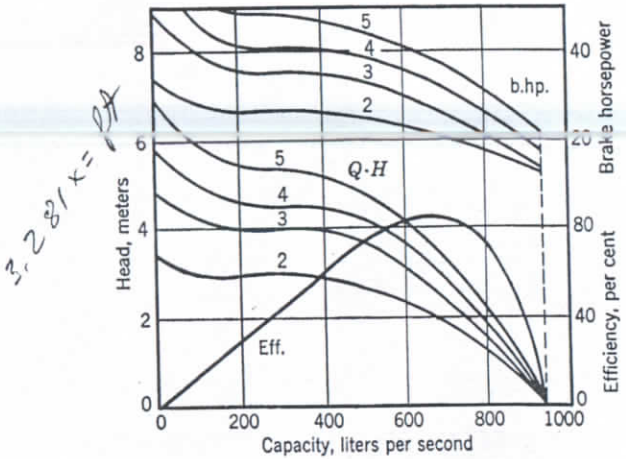

FIG. 8.9. Effect of number of vanes on performance (Schlimbach [5]).

with five both head capacity and efficiency dropped. Figure 8.9 shows a test of a pump with identical vanes numbered from 2 to 5. Note that:

1. The capacities at normal and zero head are the same for the several impellers. This is determined mainly by the vane entrance angle.
2. The heads increase with the number of vanes. This is entirely due to the increase in the l/t ratio.

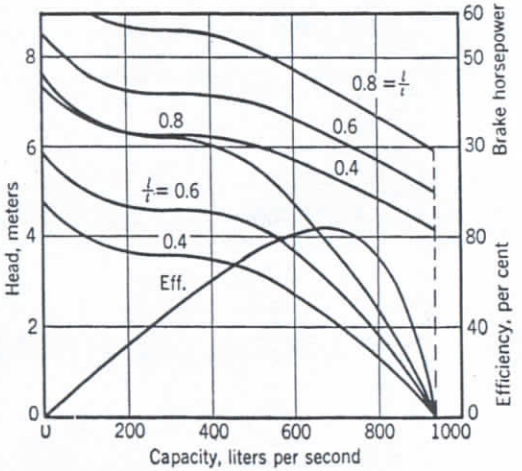

FIG. 8.10. Effect of l/t on performance; 730 rpm; $\beta_2 = 20°$ average (Schlimbach [5]).

Figure 8.10 shows tests of three impellers having four vanes each, but with l/t ratios of 0.4, 0.6, and 0.8. The curves are similar to the ones shown in Fig. 8.9, as in both cases l/t was varied.

Figure 8.11 shows results of Schmidt's tests for two-vane impellers of the same inlet and outlet angles and of different projected area. Note

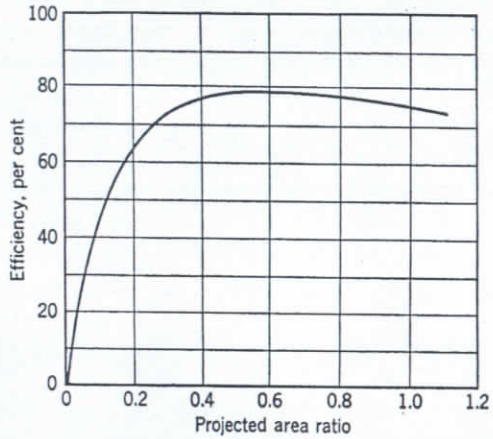

FIG. 8.11. Effect of the projected area on the impeller efficiency (Schmidt [4]).

that there is an optimum vane area, on both sides of which the efficiency drops. This is to be expected, although it does not appear on Schlimbach's tests [5] (Fig. 8.10).

(*d*) **Vane Curvature and Vane Setting.** Figure 8.12 shows the performance of a four-vane impeller with different vane settings, i.e., the vane curvature $\beta_2 - \beta_1$, or vane camber, remained the same, the dis-

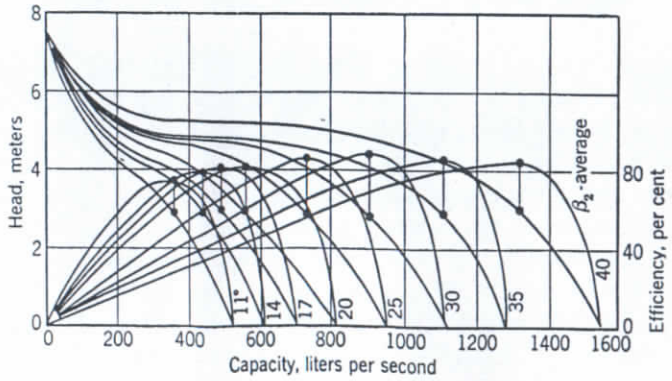

FIG. 8.12. Performance 4-vane impeller, 500-mm diameter, at different vane angles, 650 rpm (Schlimbach [5]).

charge angle β_2 and the inlet angle β_1 being changed by the same amount. The point of interest is that the head produced is essentially the same for all vane settings and thus is a function of the vane curvature $(\beta_2 - \beta_1)$ alone. This means that although the tangential component at the impeller discharge (c_{u2}) is higher at higher values of β_2, the tangential component at inlet (c_{u1}) is increased by approximately the same amount.

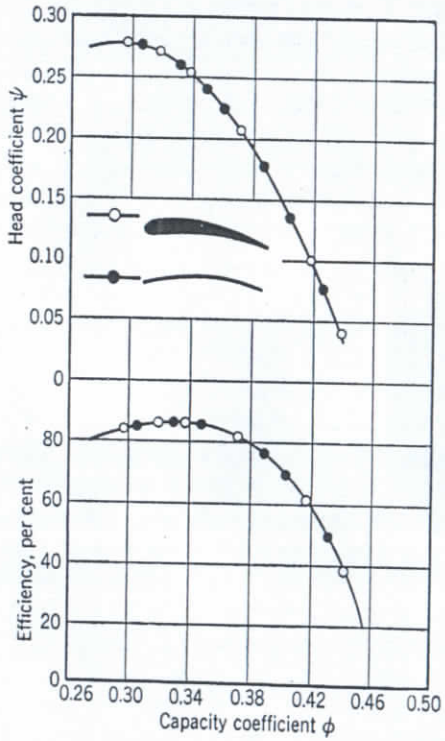

FIG. 8.13. Performance of a thin vane and an airfoil (Eckert [6]).

The peripheral velocity being the same at inlet and outlet—no change in head results. Efficiency is good over a wide range of capacities. In fact if the casing vanes could be changed for every impeller vane setting, the decrease in efficiency on both sides of the optimum setting would be still smaller. Capacity varies approximately directly as the inlet pitch or $\tan \beta_1$. This particular point was also proved by Schmidt's tests.[4]

(*e*) **Vane Thickness.** Figure 8.13 shows test results by Eckert [6] of two impellers, one with airfoil vanes well streamlined and polished, the other of the same solidity and camber line but made of stamped steel sheet vanes welded to the hub. The performance of the two impellers is identical. Similar results were obtained by several investigators.

Eckert also found by test that another impeller of the same airfoil pattern but made of cast iron with the trailing edge about ⅛ inch thick was five points lower in efficiency. Part of the efficiency reduction was caused by the greater relative roughness of the cast-iron vane as compared to the polished alloy vane. For cast vanes it is necessary to add metal to the trailing edge to be removed after machining. Excessive vane thickness results in separation and noise with high pressure high speed impellers. Thus *the advantages of airfoil sections lie in the fact that they permit the desired mechanical strength with a minimum sacrifice of efficiency.**

8.4 AXIAL FLOW IMPELLER DESIGN PROCEDURE

The design procedure for a single-stage axial flow impeller is essentially the same as for a centrifugal impeller. In fact, in the centrifugal pump field, the axial flow impeller is the high specific speed extreme of a continuous row of types from low specific speed plain centrifugal types through the various types of mixed flow impellers with conical hubs to the straight axial flow impeller. The design procedure involves the following steps:

1. To meet a given set of head-capacity requirements, the speed (revolutions per minute) is selected; thus the specific speed of the impeller is fixed. Due consideration should be given to the head range the proposed pump should cover in future applications under the most adverse suction conditions.
2. For the specific speed thus obtained, the hub ratio and vane spacing l/t are selected, Fig. 8.7 being used as a guide. The number of vanes is assumed at the same time.
3. The speed constant and the capacity constants are chosen next. The chart in Fig. 5.2 gives these constants for an average impeller discharge angle of approximately 22½°. For values at different discharge angles the diagram in Fig. 9.13 can be used (see Chapter 9). These constants having been established, the meridional velocity and impeller diameter can be calculated and the impeller profile can be drawn.
4. The impeller vane profiles, both vane curvature and vane twist, are drawn after the entrance and discharge vane angles for several streamlines are established from Euler's entrance and exit velocity triangles. Chapter 4 gives guiding principles for the drawing of these

* *N.A.C.A. Report* 460 makes a very clear statement to that effect on p. 3: "The thickness form is of particular importance from a structural standpoint. On the other hand, the form of the mean line determines almost independently some of the most important aerodynamic properties of the airfoil section."

triangles. The diagram in Fig. 9.13 establishes the impelling ratios in terms of specific speed. In drawing the vane profiles for several streamlines, airfoil shapes are good examples to follow, but the vane thickness should be kept to a minimum consistent with the vane mechanical strength and good foundry practice.

The design procedure as outlined is applicable to mixed flow and radial impellers. When used for extreme mixed flow and axial flow impeller design, Euler's entrance and exit velocity triangles determine completely the impeller vane profile sections for all radii.

8.5 AIRFOIL THEORY

(*a*) **Introduction.** A lack of reliable test and design data on axial flow pumps in the early stages of their development is responsible for the attempts of several investigators to make use of the extensive test data on airplane airfoil profiles for axial flow blower and pump impellers. The airfoil theory of axial flow impeller design establishes a connection between the lift coefficients of airfoil test data and the impeller total head. The design procedure consists of the selection of suitable airfoil profiles for several radii of the impeller and determination of the vane setting on the hub, or chord angle β_c for each radius. A constant head for several streamlines is usually assumed in this method even though other assumptions are possible. The other important impeller design elements, such as (1) hub ratio, (2) l/t ratio at each radius, (3) revolutions per minute or specific speed, (4) axial velocity, and (5) impeller diameter are selected on the basis of previous experience. There is nothing in the airfoil theory to help or guide in making such selections. Thus the impeller design is still entirely experimental, air foil experimental knowledge being used for establishing the vane curvature only. It is only natural that after sufficient experience was accumulated on efficient axial flow fans, blowers, and pumps the interest in the airfoil theory subsided. In the meantime, other more direct methods of design were advanced based on the experience with rotating profiles in suitable casings.

(*b*) **Total Head Equation.** If a cylindrical cut is made through an axial flow impeller and the cylinder is developed onto a plane, a row of vane profiles will result. The action of fluid on the profile can be considered similar to that taking place on an airfoil in a wind tunnel, provided the relative velocity w_{ave} is an average value of the relative velocity of approach and discharge w_1 and w_2 which exist before and after the vane at a distance where the effect of the flow through the

row of vanes is equalized (Fig. 8.3). The effect of the cascade arrangement of vanes on the lift coefficient C_L is little known and has been neglected by several advocates of the airfoil theory for axial flow impellers.[7]

The total force P exerted by the fluid per unit of vane length is a resultant of lift L and drag D and makes an angle λ with L (Fig. 8.3). P forms an angle $90° - (\beta_{ave} + \lambda)$ with the peripheral velocity of the impeller. The tangential component of P is

$$P \cos [90° - (\beta_{ave} + \lambda)] = P \sin (\beta_{ave} + \lambda) \tag{8.9}$$

The work per second is

$$E = Pu \sin (\beta_{ave} + \lambda) \tag{8.10}$$

Considering a slice of vane between two concentric cylindrical surfaces of radius r and $r + dr$, the corresponding work per second for z vanes is

$$z\,dE = zP\,dr\,u \sin (\beta_{ave} + \lambda) \tag{8.11}$$

If dQ denotes the volume of fluid included between the two cylindrical surfaces, the work per pound of fluid is

$$H_t = \frac{z\,dE}{dQ\,\gamma} = \frac{Pu \sin (\beta_{ave} + \lambda) z}{dQ\,\gamma}\,dr \tag{8.12}$$

But $dQ = zt\,dr\,c_m$, $P = L/\cos \lambda$, and $L = C_L(\gamma w_{ave}^2 F)/2g$, where $F = l \times 1 = l$, area per unit length. Then,

$$P = C_L(\gamma l w_{ave}^2/2g \cos \lambda) \tag{8.13}$$

and equation 8.12 becomes

$$H_t = C_L \frac{l}{l} \frac{u}{c_m} \frac{w_{ave}^2}{2g} \frac{\sin (\beta_{ave} + \lambda)}{\cos \lambda} \tag{8.14}$$

or

$$C_L \frac{l}{l} = H_t \frac{2g}{w_{ave}^2} \frac{c_m}{u} \frac{\cos \lambda}{\sin (\beta_{ave} + \lambda)} \tag{8.15}$$

The theoretical head H_t is obtained from $H_t = H/e_h$, where e_h is the hydraulic efficiency and has to be assumed.

w_{ave} and β_{ave} are obtained from the velocity diagram (Fig. 8.14) constructed for an average tangential component $(c_{u2} - c_{u1})/2$. The value of c_{u2} is obtained from

$$c_{u2} - c_{u1} = \frac{gH_t}{u} \tag{8.16}$$

Usually c_{u1} is assumed to be equal to zero.

From equation 8.15 it is seen that for a greater value of u and w_{ave} the value of $C_L(l/t)$ is lower; that is, at larger radii l/t and C_L are lower than at the hub. Equation 8.15 includes the l/t ratio, and does not give any indication of the number of vanes. For higher heads, higher values of C_L and l/t are required; or, more vane area and a higher cambered profile are required.

Equation 8.15 is used for the calculation of $C_L(l/t)$ for several radii of the impeller. It is assumed that H_t and c_m are constant along a radius. Next l/t is assumed. For a fixed hub ratio, l/t can vary only

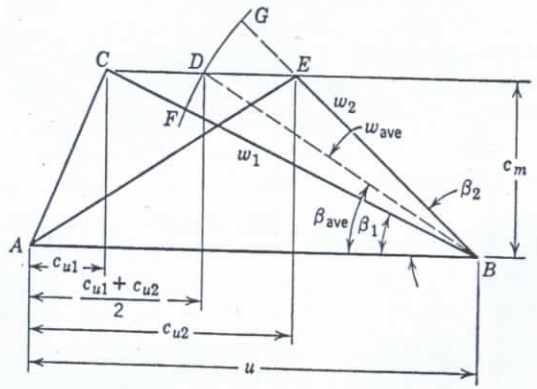

FIG. 8.14. Velocity diagrams of flow ahead of and past the airfoil.

within narrow limits for a given specific speed. Vane profiles are selected for a chosen l/t ratio. Experience is necessary to select proper values of l/t to obtain C_L and the vane profile in order to produce an efficient impeller and head-capacity and efficiency curves of good shape.

(c) Lift Coefficient versus Head Coefficient. The right-hand side of equation 8.15 can be further simplified by the following approximations:

$$\cos \lambda \approx 1 \qquad c_m/w_{ave} \approx \sin \beta_{ave}$$

since λ is of the order of 1°. Also substituting for $H_t = uc_{u2}/g$, equation 8.15 becomes

$$C_L l/t = 2c_{u2}/w_{ave} \tag{8.17}$$

The right-hand side of this equation can be transformed to express the lift coefficient C_L for an assumed value of the chord-spacing ratio l/t in terms of (1) vane curvature $(\beta_2 - \beta_1)$, (2) camber and its location, and (3) head and capacity coefficients ψ and ϕ.

In Fig. 8.14 the area of triangle $CEB = \frac{1}{2}c_m(c_{u2} - c_{u1}) = \frac{1}{2}c_m c_{u2}$ if $c_{u1} = 0$. This is approximately but very closely equal to the area of the

sector $FGB = \frac{1}{2}w_{ave}^2(\beta_2 - \beta_1)$. Hence

$$c_m c_{u2} = w_{ave}^2(\beta_2 - \beta_1)$$

and

$$C_L l/t = 2(\beta_2 - \beta_1)/\sin \beta_{ave} \tag{8.18}$$

By referring to Fig. 8.6 we notice that $\tan \theta_1 = 2ED/AE = 2c/l_c$ and $\tan \theta_2 = 2ED/EB = 2c/(l - l_c)$, where c is the camber and l_c is its location relative to the leading edge, both expressed as fractions of the airfoil chord length. Since values of θ_1 and θ_2 are usually small, the values of the angles in radians can be substituted as an approximation for their tangents. Then the vane curvature becomes

$$\beta_2 - \beta_1 = 2cl/l_c(l - l_c) \tag{8.19}$$

and equation 8.18 can be further modified to

$$C_L l/t = \frac{4cl}{l_c(l - l_c)\sin \beta_{ave}} \tag{8.20}$$

To express the lift coefficient in terms of ψ and ϕ the following substitutions are made in equation 8.17

$$\frac{c_{u2}}{u} = \psi \quad \text{and} \quad w_{ave} = \frac{c_m}{\sin \beta_{ave}} = \frac{u\phi}{\sin \beta_{ave}}$$

then

$$C_L l/t = \frac{2\psi \sin \beta_{ave}}{\phi} \tag{8.21}$$

Note that w_{ave} as defined in Fig. 8.14 is not an exact average of w_1 and w_2 and, similarly, β_{ave} is not an exact average of β_1 and β_2. It can be shown that

$$\beta_{ave} = \beta_c + \frac{\theta_2 - \theta_1}{2} \tag{8.22}$$

and thus $\beta_{ave} = \beta_c$ when $\theta_2 = \theta_1$, as is the case with a circular arc mean camber line. In general $\beta_{ave} \approx \beta_c$ and represents the profile position in respect to the hub for each radius. Equations 8.18 and 8.21 show that the lift coefficient in equation 8.15 does not reveal any new relationship between the head produced and the design elements which could not be expressed in terms of familiar design elements used for centrifugal and mixed flow impellers.

By substituting for ψ its value from equation 5.22 and for ϕ its value from equation 5.28 we obtain

$$C_L l/t = \sin \beta_{ave}/K_u K_{m2} \tag{8.21a}$$

Thus a selection of C_L and l/t is equivalent to a selection of the speed constant K_u and capacity constant K_{m2}, which is a normal procedure for straight centrifugal and mixed flow impeller design.

(d) Discussion of the Airfoil Theory. The airfoil data available for selection of axial flow impeller profiles following the airfoil theory were obtained under conditions vastly different from the flow pattern existing in a pump. A number of simplifying assumptions were necessary to make possible a comparison of the flow of the two. In practice, corrective factors had to be applied after tests of units designed on the basis of airfoil theory in order to bring the test results to some kind of agreement with the anticipated design performance. There are a number of factors responsible for such a state of affairs, the most important of which will be listed below:

1. The mutual vane interference under the conditions prevailing in the impeller is not sufficiently known. Even when the cascade test data of several airfoils with a required chord-spacing ratio are available, the performance of a vane of variable profile and at different vane settings along the radius is greatly different from that of a cascade in the straight flow of a wind tunnel.
2. Profiles selected on the basis of "over-all" performance may produce the assumed axial velocity only by accident. Axial velocity (or in general meridional velocity) results from the proper selection of the impeller entrance and discharge angles. Besides, the through-flow velocity and specific capacity q_s depend upon the hub ratio and vane solidity. All these factors fix the specific speed of the impeller. In the airfoil theory and design procedure little or no consideration is given to all these factors.
3. N.A.C.A. data are limited to cambers of 0, 2, 4, and 6 per cent. In practice, higher and intermediate cambers may be required. Thus either new profiles have to be drawn for which test data are not immediately available, or the nearest existing profile has to be used, thus impairing continuity of the vane surface and the flow along the radius.
4. Airfoil cascade tests do not provide for the effects of the impeller approach and casing beyond the impeller. Thus the same impeller will perform differently in different casings, such as one with straightening vanes, the other without.

5. The effect of the end conditions of the vane (running clearance between the outside diameter and stationary wall, and revolving hub wall) are impossible to estimate accurately from the cascade tests.

6. The method becomes less accurate and workable for lower specific speed axial flow impellers and fails entirely for mixed flow types such as are in use in the mixed flow propeller pump field. A continuity of mental pattern of flow, theoretical reasoning, and geometrical design procedure is indispensable for a pump designer to enable him to interpret the test results and to correlate the experimental design constants for the whole field of specific speeds. The airfoil theory does not satisfy this requirement.

7. The airfoil theory method of axial impeller design is invariably associated with a free vortex energy distribution along the radius, i.e., vane sections at different radii are designed for the same head (at design point only). Two reasons could be discerned for this: (1) At the time the airfoil theory of the axial flow impeller was introduced it was a general belief that only the free vortex pattern provides a stable flow radially; (2) the theory was originally proposed for axial flow water turbines where a constant head is actually applied at all radii. There is nothing in the airfoil theory to prevent any desired head distribution along the vane radius; later designs with other than free vortex pattern of flow were applied in connection with a different theoretical treatment. The high pressure multistage axial compressors for gas turbines imposed such severe requirements as to performance size and weight that all theory and practice heretofore employed were reviewed critically.

As a result, new design methods evolved which are based on inlet and outlet velocity triangle considerations and corrective factors determined from cascade airfoil tests and actual impeller performance in a suitable casing. There has been a steady drift away from the free vortex hypothesis of flow in the direction of the forced vortex. A detailed account of the later methods of axial flow impeller design, as developed for high pressure multistage axial flow compressors, is given in reference 8.

8.6 THE AXIAL FLOW PUMP CASING

The purpose of the diffusion casing of an axial flow pump is to convert into pressure the tangential component of the absolute velocity leaving the impeller. This is accomplished by "straightening" the flow as it leaves the impeller and by reducing the velocity.

The diffusion vane curvature is selected so that the liquid enters th diffusion vanes with a minimum loss and leaves the casing axially. Wit an impeller designed for a forced vortex pattern of flow, the angul velocity of the flow leaving the impeller is constant. The diffusion var angularity is adjusted so that the flow continues with the constar angular velocity, the value of which is decreased until all the tangenti component is taken out of the flow. To accomplish this the diffusic vane entrance angles should be laid out for a constant pitch P_{3s} (Fi 8.15).

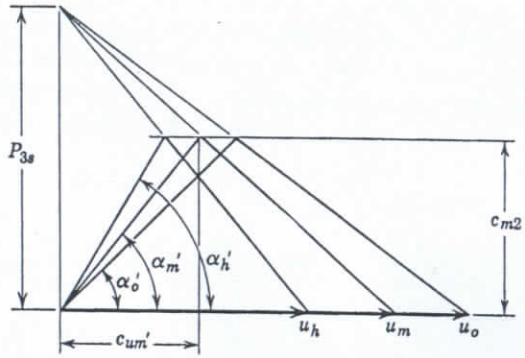

FIG. 8.15. Velocity diagram at entrance to diffusion casing.

The design of the casing involves the following steps.

(a) Mean Effective Impeller Diameter. First, the direction of th absolute velocity at the impeller exit, at least at one point, is deter mined. *It is advantageous to select this point at the mean effective diameter which is defined as*

$$D_m = \sqrt{\frac{D_o^2 + D_h^2}{2}} \tag{8.23}$$

It will be shown that the head produced at this diameter is equal to the tota integrated head. In Chapter 4, equation 4.10 and Fig. 4.5, it has beer shown that the integrated head is equal to the arithmetical average o the heads generated at the hub and at the periphery, and

$$H_e = \frac{u_o c_{uo} + u_h c_{uh}}{2g} = \frac{u_m c_{um}}{g} \tag{8.24}$$

where u_m is the peripheral velocity at diameter D_m and c_{um} is the tangential component at the same diameter. From equation 8.24

$$2 = \frac{u_o c_{uo}}{u_m c_{um}} + \frac{u_h c_{uh}}{u_m c_{um}} \tag{8.25}$$

In a forced vortex, peripheral and tangential velocities vary as the diameters; therefore

$$2 = \frac{D_o^2}{D_m^2} + \frac{D_h^2}{D_m^2}$$

or

$$D_m = \sqrt{\frac{D_o^2 + D_h^2}{2}} \tag{8.26}$$

Note that the mean effective diameter as defined by equation 8.26 is directly connected with the forced vortex pattern of head generation in the axial flow pump.

(*b*) **Head at Impeller Exit.** Next, the head at the impeller exit is estimated. The total head H and the pump gross efficiency e are considered as known. Taking the hydraulic efficiency as $e_h = \sqrt{e}$, the input head H_i is determined from

$$H_i = \frac{H}{\sqrt{e}} \tag{8.27}$$

The head at the impeller exit is less than H_i by the amount of the hydraulic losses in the impeller. If the casing losses are equal to those of the impeller (each part represents a set of vanes), the head at the impeller exit H_d is

$$H_d = \frac{H_i + H}{2} = \frac{\dfrac{H}{\sqrt{e}} + H}{2} \tag{8.28}$$

This head can be expressed as

$$H_d = \frac{u_m c_{um}'}{g} \tag{8.29}$$

hence c_{um}' can be determined giving the direction of flow at the diameter D_m. The direction of flow at any other diameter is found from

$$\frac{c_{uo}'}{D_o} = \frac{c_{uh}'}{D_h} = \frac{c_{um}'}{D_m} = \frac{\omega'}{2} \tag{8.30}$$

or may be found graphically as shown on Fig. 8.15 where the absolute velocity angles α_o', α_h', and α_m' are indicated.

To deflect liquid from these directions the diffusion vane angles should be greater by a few degrees, or an angle of attack should be allowed. Without this the vane tips would be inactive. To maintain a forced vortex pattern of flow the vane should be of constant pitch. The angle of attack can be allowed by reducing pitch per second, P_{3s}.

In addition to the reduction obtained by converting the tangential velocity component into pressure, the axial velocity is also reduced by increasing the diffuser diameter at the discharge. A small divergence angle of the diffuser cone (8° total) is essential for an effective conversion.

The number of vanes in the diffuser casing varies from five to eight, a smaller number of vanes being used for smaller pumps. The vane length at the hub can be reduced ($DC < AB$, Fig. 8.16) because the vane spacing is closer at the hub than it is at the outside diameter. The axial distance d between the impeller vanes and the diffusion vanes has some bearing on the performance, and the most favorable value of the ratio d/D_o is about 0.05. When the value of d is being selected, provision should be made for accommodating an impeller with a higher vane angle setting, which requires more axial space. The impeller hub length should be fixed with this idea in mind.

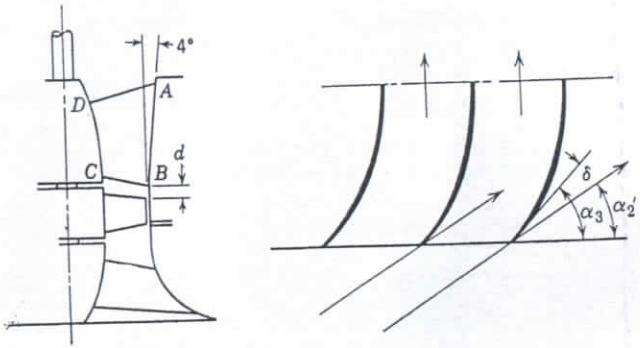

FIG. 8.16. Axial flow pump diffusion casing.

The value of the diffusion vane angle is not very critical, and variation as great as ±5° from the optimum value have hardly any noticeable effect on the pump performance. This is rather fortunate as usually one pump casing is used with several impellers requiring different diffusion vane angles. When the diffusion angle is reduced, the b.e.p. is moved toward a lower capacity. Figure 7.26 gives the average values of the diffusion vane angle α_v based on the mean effective diameter D_m for different specific speeds. In Chapter 9, a new method of the graphical determination of the diffusion vane angle or volute angle is given (in Fig. 9.13).

REFERENCES

1. Morrough P. O'Brien and Richard G. Folsom, "The Design of Propeller Pumps and Fans," *Univ. of Calif. Publ.*, Vol. 4, No. 1, pp. 1–18, 1939.
2. Max M. Munk, "On the Geometry of Streamlining," Theodore von Kármàn Anniversary Volume, p. 8, *Calif. Inst. of Tech.*, 1941.
3. Victor Kaplan and Alfred Lechner, *Theorie und Bau von Turbinen-Schnellläufern*, p. 145, Munich, R. Oldenbourg, 1931.
4. Henry F. Schmidt, "Some Screw Propeller Experiments with Particular Reference to Pumps and Blowers," *J. Am. Soc. Naval Engrs.*, Vol. XL, No. 1, Feb. 1928.
5. A. Schlimbach, "Der Man-Schraubenschaufler," *Mitt. Forsch. Anstalt.* GHH-Konzern, p. 54, October 1935 (Maschinenfabrik Augsburg-Nürnberg).
6. B. Eckert, "Neuere Erfahrungen an Überdruck-Axialgebläsen," *Bull.* 88, No. 37/38, Berlin, Verein Deutscher Ingenieure, p. 516, Sept. 16, 1944.
7. C. Pfleiderer, *Die Kreiselpumpen*, p. 320, Berlin, Julius Springer, 1955.
8. A. J. Stepanoff, *Turboblowers*, New York, John Wiley and Sons, Inc., p. 277, 1955.

Hydraulic Performance of Centrifugal Pumps

A study of losses in centrifugal pumps may be undertaken for one o the following reasons: (1) information about the nature and magnitud of losses may indicate the way to reduce these losses; (2) if the losse are known, it is possible to predetermine the head-capacity curve of a new pump by first assuming or establishing in some other manner the head-capacity curve of an idealized pump; (3) since the Q-H curve of an idealized pump is a straight line, the shape of the head-capacity curve of an actual pump is determined by the hydraulic losses. Thus it would seem possible, when something is known about the losses, to change the shape of the head-capacity curve to suit some special requirement.

Considering the high degree of perfection of modern pumps, as demonstrated by pump gross efficiencies of over 90 per cent, it is remarkable that so little exact knowledge is available on the losses of centrifugal pumps. None of the three above objectives has been achieved to any appreciable degree because of the present lack of knowledge of losses.

The progress in pump design has been accomplished mostly in an experimental way, the pump gross efficiency being the only criterion of improvement in performance. In this book all losses are grouped under the headings: hydraulic, leakage, mechanical, and disk friction losses. Only hydraulic losses will be discussed in this chapter.

9.1 HYDRAULIC LOSSES

These are the least known of all the losses in pumps and, at the same time, they are the most essential ones for the attainment of the three objectives set forth above. The reason for this is that there are so many factors contributing to the hydraulic losses. Even the combined effect of these factors cannot be ascertained accurately. In general it can be said that hydraulic losses are caused by: (1) skin friction and (2) eddy and separation losses due to changes in direction and magnitude of the velocity of flow. The latter group includes the so-called shock loss and diffusion loss.

In the channels from the suction to the discharge nozzle, there is not a single stretch of the path where either the direction of flow or the area and shape of the channel is constant; besides, part of the channel is rotating, thus upsetting the velocity distribution and further complicating the study of hydraulic losses. Under such conditions it is impossible to calculate the friction loss through the pump with a degree of accuracy sufficient to serve any useful purpose.

In the following discussion no attempt will be made to give equations or methods for calculating hydraulic losses in various parts of centrifugal

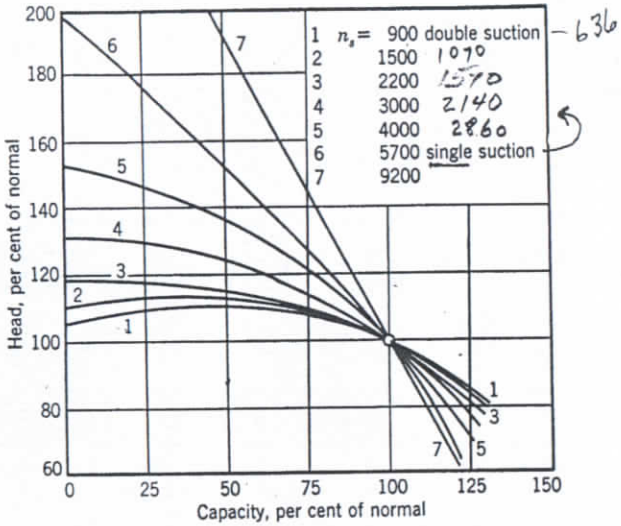

FIG. 9.1. Head-capacity curves for several specific speeds.

pumps. The need for prediction of head-capacity characteristics of a pump has long passed because, when new types are contemplated, sufficient data are available for designers to estimate the characteristics from existing types.

Figure 9.1 shows typical head-capacity curves, Fig. 9.2 shows efficiency curves, and Fig. 9.3 shows brake-horsepower curves for several specific speeds. The head-capacity, efficiency, and brake-horsepower curves are so interrelated that a change in the form of one is followed by a change in the form of the other two. The responsibility for the change in the pump characteristics to incorporate a maximum of desirable features with a minimum sacrifice in efficiency rests upon the skill of the designer. This phase of the subject is treated in Chapter 14. However, a general discussion of hydraulic losses, without any attempt to evaluate individual losses, will show the relation between the characteristics of an actual and those of an idealized pump, and will illustrate the manner in which different types of characteristics are obtained.

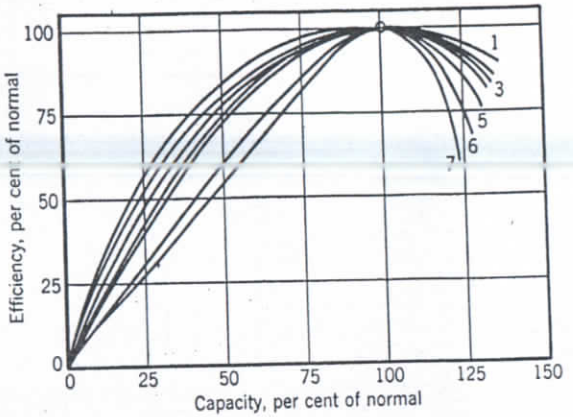

FIG. 9.2. Efficiency curves for different specific speeds.

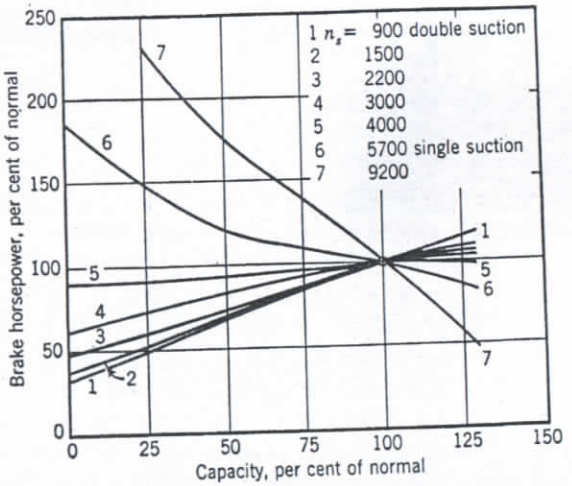

FIG. 9.3. Brake-horsepower curves for different specific speeds.

(a) Friction and Diffusion Losses. The general equation for friction loss is

$$h_f = f\frac{L}{4m}\frac{v^2}{2g} \qquad (9.1)$$

where f is a friction coefficient.
L is the length of the channel.
m is the hydraulic radius of the channel section.
v is the velocity at the section with the hydraulic radius m.

This could be applied to the several parts of the total path, as the suction nozzle, impeller channel, volute, and discharge nozzle. However, actual measurements of the length L, and the hydraulic radius m may present difficulty in many cases (extreme mixed flow impeller or suction nozzle of a double-suction pump, for instance). The selection of a suitable friction coefficient is a problem in itself. For these reasons several investigators combine all the friction losses in one term, expressing it by a simplified equation:

$$h_f = K_1' \frac{v_1^2}{2g} = K_1 Q^2 \tag{9.2}$$

where K_1 is a constant for a given pump and includes all lengths, areas and area ratios, and friction coefficients. Thus K_1 covers all the unknown factors and also any errors caused by the inability to find a better expression for the several items contributing to the friction losses. Similarly an expression can be set up for the diffusion loss in the impeller channel or discharge nozzle and stated by

$$h_d = f_2 \frac{v_2^2}{2g} \tag{9.3}$$

Again, selection of the coefficient f_2 for the impeller channel presents difficulty. Therefore, for simplicity it is customary to express all diffusion losses by

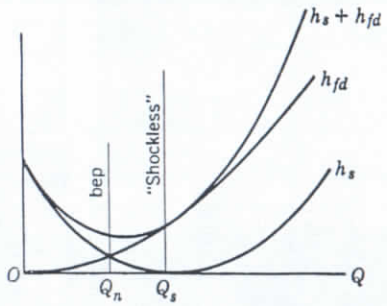

FIG. 9.4. Hydraulic losses.

$$h_d = K_2' \frac{v_2^2}{2g} = K_2 Q^2 \tag{9.4}$$

where K_2 is a constant for a given pump.

Since the losses expressed by equation 9.2 and 9.4 both vary as the square of the capacity they can be combined into one equation

$$h_{fd} = h_f + h_d = K_3 Q^2 \tag{9.5}$$

which is a square parabola with its axis on the axis of heads (Fig. 9.4).

(*b*) **Eddy and Separation Losses.** Losses at the impeller entrance and exit are usually called shock losses. *The author accepts this term very reluctantly because in mechanics "shock" or impact does not necessarily mean a loss, and in hydraulics, if impact is in the direction of flow, most of the energy of impact is recoverable (impulse action). Liquid flow in a pump tends to avoid shock by acquiring prerotation at the impeller*

inlet and by establishing a velocity gradient in the volute casing at the in peller discharge, thus cushioning the shock. The nature of the hydraul loss at the impeller entrance, when liquid approaches at a high angle attack, is that caused by a sudden expansion or diffusion after separati (Fig. 9.5). At the impeller discharge the loss is mostly caused by high rate of shear due to a low average velocity in the volute and hig velocity at the impeller discharge. It should be noted that even at tl b.e.p., the average volute velocity is considerably lower than the ta gential component of the absolute velocity at the impeller dischar

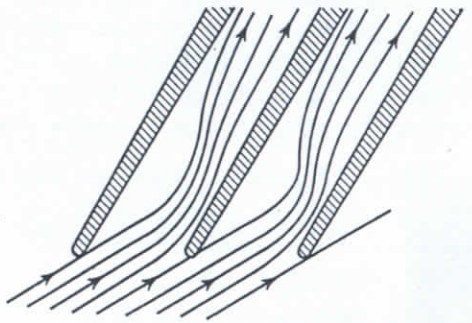

FIG. 9.5. Shock loss is a diffusion loss.

(c_{u2}'), and since this is the optimum condition it cannot be improv by changing the volute area (Chapter 7). Besides this, there is a sho loss at the cut-water of a volute pump and at the entrance of diffusi vanes when a diffusion vane casing is used. These losses are of t same nature as shock loss at the entrance to the impeller; i.e., they a diffusion losses.

If we assume that the impeller design is such that at a capacity (shockless) the direction of flow agrees with the vane angles at bo entrance and discharge, thus incurring no additional losses at the points, then at capacities above and below Q_s there will be a sudd change in the direction and magnitude of the velocity of flow. Th change results in losses which can be expressed as

$$h_{s1} = K_4 \frac{\Delta c_{u1}^2}{2g} \tag{9.}$$

for the entrance, and

$$h_{s2} = K_5 \frac{\Delta c_{u2}^2}{2g} \tag{9.}$$

for the exit of the impeller.

In Fig. 9.6 at capacity Q_s the meridional velocity at impeller entran is c_{m1}, the flow is approaching the impeller under an angle α_1 with

tangential component of the absolute velocity c_{u1}. When the capacity is reduced ($c_{m1}' < c_{m1}$), the liquid should have a tangential component c_{u1}' to enter the vanes at an angle β_1, and

$$\Delta c_{u1} = c_{u1}' - c_{u1}$$

Similarly, at the discharge (Fig. 9.7) at capacity Q_s, the meridional velocity is c_{m2}, the tangential component of the absolute velocity is c_{u2}. At a reduced capacity, the tangential component will increase to c_{u2}', and the increment of the tangential component is the difference between the two: $\Delta c_{u2} = c_{u2}' - c_{u2}$. At capacities greater than Q_s, both Δc_{u1} and Δc_{u2} are negative. Note that, in Figs. 9.6 and 9.7, for equal increments of c_{m1} or capacity, Δc_{u1} increases the same amount.

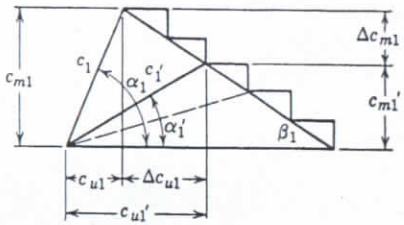

FIG. 9.6. Shock component of peripheral velocity at entrance to impeller.

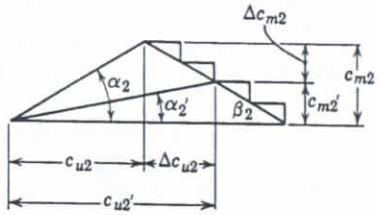

FIG. 9.7. Shock component of velocities at discharge.

Similarly, for the same steps in c_{m2} the value of Δc_{u2} increases by an equal amount. Thus both items increase on both sides of Q_s as the square of the capacity increments. In this way it is possible to combine both equations 9.6 and 9.7 into one expression, or

$$h_s = K_6(Q - Q_s)^2 \tag{9.8}$$

This represents a square parabola with its apex at Q_s (Fig. 9.4).

9.2 TOTAL HEAD-CAPACITY CURVE

(*a*) **The Head-Capacity Curve Equation.** The head-capacity curve of an idealized pump is a straight line. For a given discharge vane angle, a single line will represent the characteristics of pumps of all specific speeds when plotted to dimensionless scales. When the essential design elements are selected, the location of the b.e.p., and hence the specific speed, are fixed. Hydraulic losses for the selected proportions of essential passages will determine the head-capacity curve of the actual pump. In general, for a constant speed, the head-capacity curve can be obtained by subtracting losses from the input head of an idealized

pump. For a given capacity the actual head may be expressed by

$$H = H_i - K_3Q^2 - K_6(Q - Q_s)^2 \tag{9.9}$$

To draw the H_i line the knowledge of one point only on this line is necessary since, at zero head, H_i and H_e lines intersect at a capacity given by $\phi = c_{m2}/u_2 = \tan \beta_2$. Such a point is shown in Fig. 9.13 (point B) and is discussed later. The procedure for the determination of one point on the H_i line is outlined in Chapter 10.

Constants K_3 and K_6 are determined from an actual Q-H curve by selecting several points on the head-capacity curve, substituting the values of Q and H into equation 9.9, and obtaining any desired numbe

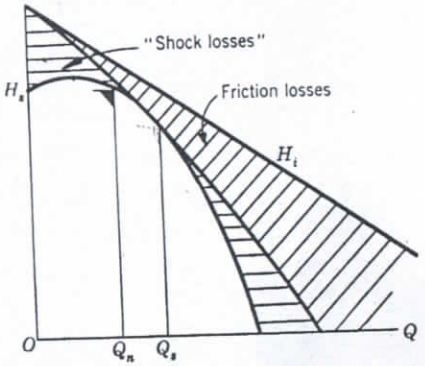

FIG. 9.8. Q-H curve is obtained by subtraction of hydraulic losses from input he

of simultaneous equations which can be solved for K_3 and K_6. As shou be expected, the value of the constants thus found are different fr pump to pump and are inconsistent along the same curve. For th reason there has been no serious attempt to establish such constan Graphically the total head-capacity curve is obtained by subtracti the friction and shock losses, as shown in Fig. 9.4 from the H_i cu (Fig. 9.8). By referring to Fig. 9.4 it will be noticed that *the b.e will always occur at a capacity lower than the shockless capacity* Q_s *beca the sum of the friction and shock losses determines the location of the p efficiency. The impeller vane entrance angle at the b.e.p. is exaggera or laid out for a meridional inlet (without prerotation) for a capacity gre than the normal capacity; this means that at the b.e.p. prerotation is allo*

The Q-H curve on Fig. 9.8 is a parabola with its apex displaced to right of the axis of heads. Such curves are observed on low and med specific speed pumps. But, when found objectionable, the droop of Q-H curve at shut-off can be eliminated by special design, as discu

in Chapter 14. On medium and high specific speed pumps the Q-H curve rises constantly toward zero capacity, thus indicating the inaccuracy of the method outlined for establishing the total head-capacity curve from the input head-capacity characteristics.

(*b*) **General Pump Characteristics.** By expressing the constants K_3 and K_6 of equation 9.9 in terms of the pump physical dimensions (ratios) and angles it is possible to transform equation 9.9 to the form

$$H = An^2 + BnQ + CQ^2 \qquad (9.10)$$

where A, B, and C are constants depending on the pump design. For a constant speed n, this is an equation of the head-capacity curve. Since equation 9.10 has no practical application and its development does not reveal anything new or instructive, it is omitted from this discussion.*

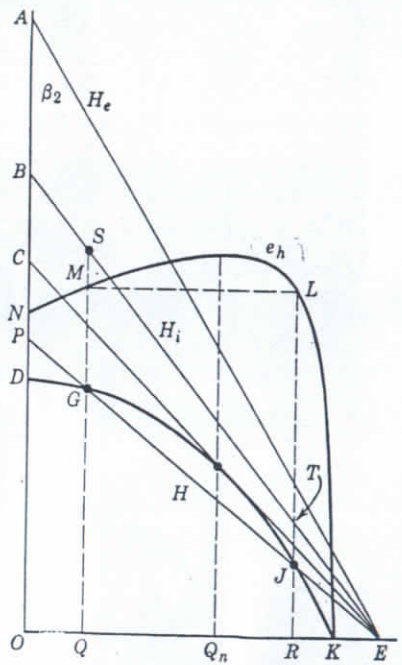

FIG. 9.9. Hydraulic efficiency.

In Chapter 13, a more detailed study of complete pump characteristics is made. Figures 13.1 and 13.2 give charts showing the actual pump characteristics plotted for constant n, Q, or H.

9.3 HYDRAULIC EFFICIENCY

(*a*) **Hydraulic Efficiency at Zero Capacity.** In Chapter 5 it was shown that the shut-off head of actual pumps, expressed in dimensionless coordinates, is essentially constant for all specific speeds. This is expressed by the fact that ψ_s, the head coefficient at shut-off, is constant for all specific speeds (point D, Fig. 9.11). This in turn means that the hydraulic efficiency at shut-off is constant for all specific speeds and all angles β_2.

$H_s = 0.585u_2^2/g$ and $e_{hs} = H_s/H_i$

From Fig. 9.13

$$e_{hs} = DO/BO = 0.585/0.725 = 0.808 = \text{constant} \qquad (9.11)$$

* The development of equation 9.10 is given by Pfleiderer,[1] Spannhake,[2] LeConte,[3] and others.

(*b*) **Hydraulic Efficiency versus Specific Speed.** On Fig. 9.9 BE the input head line; $DGHJK$ is the actual total head-capacity cur and $NMLK$ is the hydraulic efficiency curve. If a line PE is dra through E, intersecting the total head-capacity curve at two points, and J, these points will be found to be points of equal hydraulic efficien since

$$GQ/SQ = JR/TR$$

This follows from the relation of the two sets of similar triangles, EC and EJR, and ESQ and ETR. As line PE is moved toward line CE, will always cut the total head-capacity curve at two points of equ hydraulic efficiency, and, in the limiting case, line PE will become ta gent to the total head-capacity curve at the point of maximum hydra lic efficiency.†

If several total head-capacity curves for pumps of different speci speeds are intersected by a line PE (Fig. 9.10), all the points of int

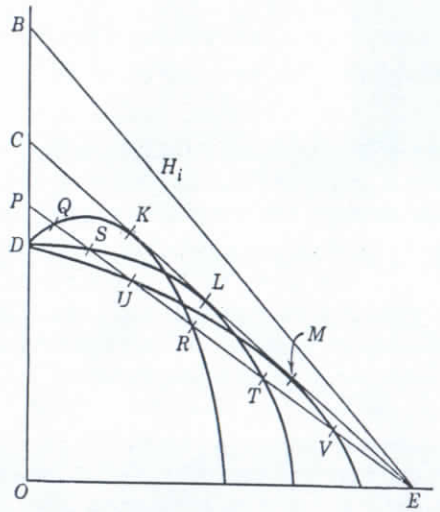

FIG. 9.10. Hydraulic efficiency is the same for all specific speeds.

section, Q, R, S, T, U, and V, will be points of the same hydraul efficiency. Now, if line PE is moved toward line BE, it will become ta gent to the several total head-capacity curves at the points of best h draulic efficiency K, L, and M.

Experimental evidence with centrifugal pumps indicates that a head-capacity curves for a continuous row of pumps within the usef

† Lichtenstein [4] has proved analytically that a tangent to the total head-capaci curve at the point of best hydraulic efficiency will pass through the point E, i tersection of the input head line with the axis of capacities.

range of specific speeds will have a common tangent CE at the point of best hydraulic efficiency.

In Fig. 9.11 are plotted several head-capacity points representing the b.e.p. of pumps of different specific speeds. These pumps are of consist-

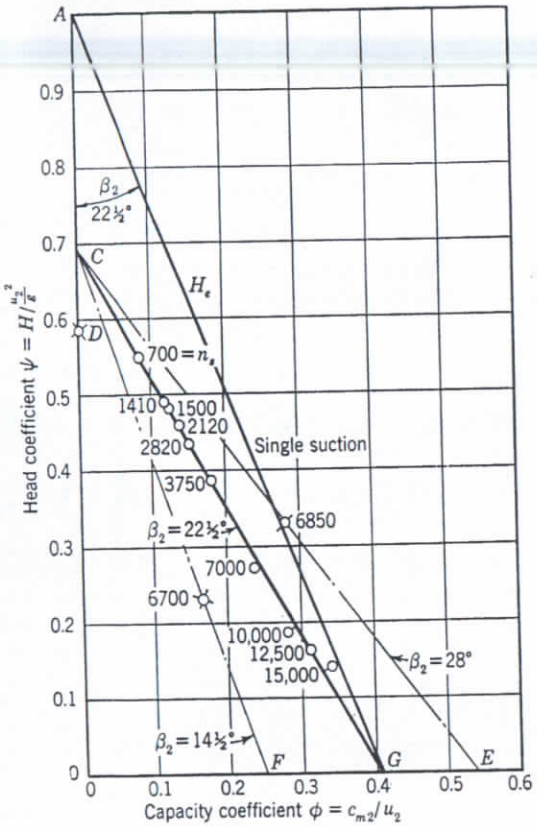

FIG. 9.11. B.e.p. of pumps of different specific speeds on ϕ-ψ chart.

ent design, the same impeller discharge angle, about 22½°, being used. The points show a definite trend to align themselves along the line passing through the point of zero input head ($c_{m2}/u_2 = \tan 22\frac{1}{2}°$). Now, if it is assumed that all total head-capacity curves have a common tangent, *the optimum peak hydraulic efficiency is the same for pumps of all specific speeds.* Such a conclusion can be justified by the following reasoning and qualifications:

1. It is assumed that all machines are of such sizes that the scale effect can be disregarded.

2. For a continuous and consistent row of machines of different specific speeds it will be assumed that the hydraulic losses are divided between the impeller and casing in the same ratio. Then, confining discussion to the impeller only, it can be stated with more confidence that the impeller hydraulic efficiency is the same for all specific speeds. At the b.e.p., hydraulic losses are almost entirely friction losses. These losses are proportional to the number of impeller channels and their lengths, but the head produced also increases with the number of channels and length. If both maintain the same ratio, the optimum hydraulic efficiency of the impeller will remain constant for all specific speeds. At zero capacity, hydraulic friction losses are zero and the hydraulic efficiency is determined by the shock losses only. These losses bear a constant ratio to the total head for several specific speeds, and a constant hydraulic efficiency at shut-off results. This has been proved experimentally.

3. *For axial flow and mixed flow pumps, angle β_2 is taken at the mean effective diameter $D_m = \sqrt{(D_{2o}^2 + D_{2i}^2)/2}$. The peripheral velocity u_2 for the dimensionless head and capacity coefficients is based on the mean effective diameter. For straight axial flow pumps, β_2 is the discharge angle of the mean line and not a chord angle.*

(c) Effect of Discharge Angle β_2 on Impeller Hydraulic Efficiency. Figure 9.12 shows Euler's head H_e and input head H_i, lines AE and

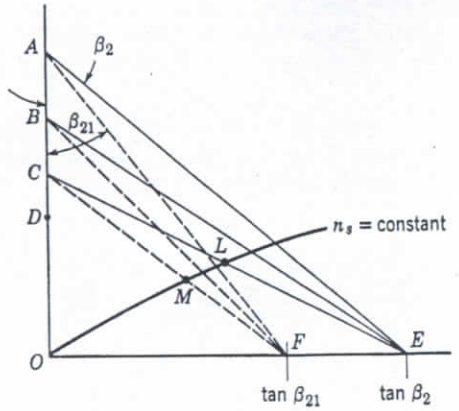

FIG. 9.12. Hydraulic and vane efficiency are independent of discharge angle β_2

BE respectively, for a given discharge angle β_2. Line CE is the locus of the best hydraulic efficiency points of actual total head curves for all specific speeds. The point D, the actual shut-off head, is common for all total head-capacity curves. Location of the maximum capacity

point E is fixed by the angle β_2 and $OE = \tan \beta_2$. The optimum hydraulic efficiency of the impellers of all specific speeds is CO/BO.

If the impeller discharge angle is changed from β_2 to β_{21}, the maximum capacity point F will be given by the relationship $OF = \tan \beta_{21}$. Points A, B, C, and D remain the same, and H_e, H_i, and H lines can be drawn as shown by dotted lines. The line CF now becomes the locus of heads for the optimum hydraulic efficiency of the impeller. The hydraulic efficiency itself stays unchanged and is still equal to CO/BO. Thus the optimum impeller hydraulic efficiency is constant for all specific speeds and does not depend on the discharge vane angle β_2. There is sufficient experimental evidence to corroborate this conclusion.

Referring to Fig. 9.12 it will be noticed that the vane efficiency, $e_{va} = BO/AO$, being constant for impellers of all specific speeds and at all capacities, does not change when the discharge angle β_2 is varied. It has been found that when the discharge angle is varied the head and capacity change in such a way that the specific speed remains constant.

$$\omega_s = \phi^{1/2}/\psi^{3/4} = \text{constant} \qquad (9.12)$$

It follows also from the equation 5.35, for a constant impeller profile b_2/D_2, that specific speed n_s remains constant for different values of β_2.

9.4 AUTHOR'S DIAGRAM OF PUMP CHARACTERISTICS

(*a*) **Construction of Diagram.** In Fig. 9.13 the author has prepared a master diagram covering essential design and performance features of impellers of all specific speeds and impeller discharge angles β_2, for the optimum b.e.p. The fact that the points line up along a straight line on Fig. 9.11 for one value of $\beta_2 = 22\frac{1}{2}°$, which intersects the axis of ϕ at a point where $\phi = \tan 22\frac{1}{2}°$, strongly suggested to the author that for any other values of β_2 the values of ϕ and ψ for the b.e.p. will also arrange themselves on the lines connecting point C with points of $\phi = \tan \beta_2$ on the axis of ϕ. This was substantiated by the test values of ϕ and ψ, covering a complete range of specific speeds and values of β_2 of centrifugal and axial flow pumps and blowers.

Point B on Fig. 9.13 was obtained by calculating the hydraulic efficiency CO/BO at b.e.p. of a representative centrifugal pump, as discussed in detail in Chapter 10. Point D represents the shut-off value of ψ_s which, as stated earlier, is common for all machines.

(*b*) **Properties of the Diagram.**

1. Lines radiating from point C are loci of the head-capacity b.e.p. for different impeller discharge angles and specific speeds, the latter increasing from top to bottom of the chart. Since the shut-off (point D) common to all angles and specific speeds, location of the b.e.p. fixes t slope of the head-capacity curve.

2. By connecting any point on the chart, say F', with points O a A, the *actual* velocity triangle is obtained with angles and velociti approximately (but very closely) equal to those at the impeller di

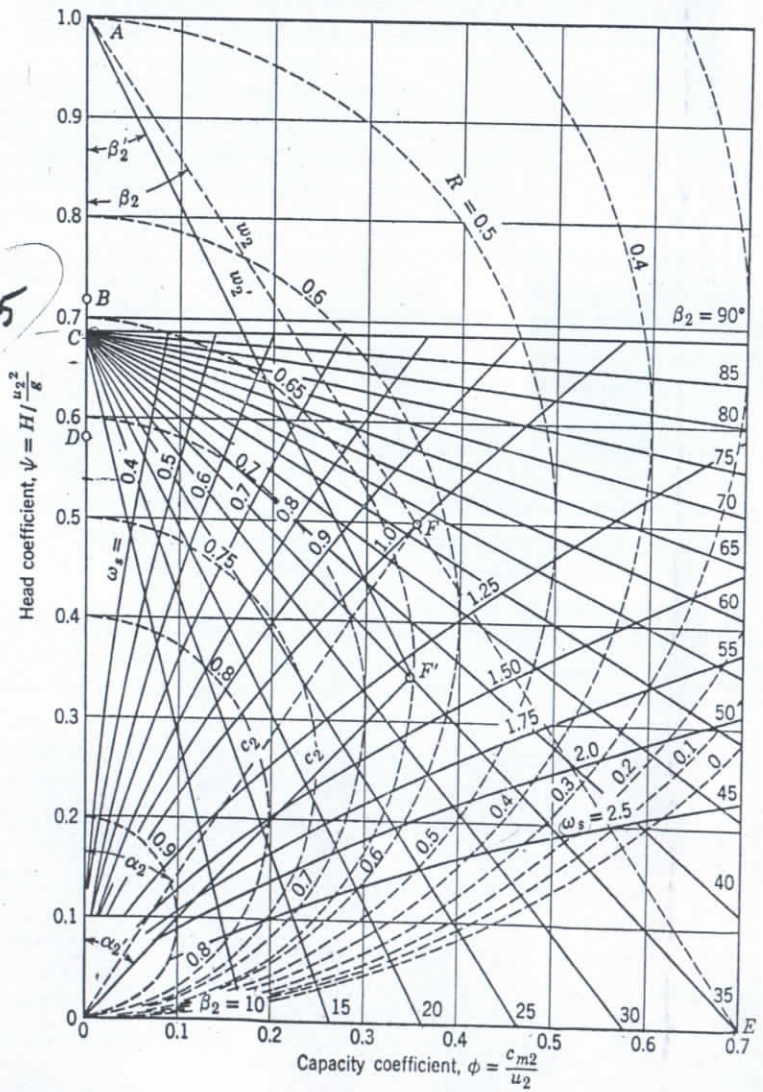

FIG. 9.13. Author's chart of centrifugal and axial pump characteristics.

charge. Any inaccuracy results from the effects of the hydraulic losses in the casing.

3. The Euler's velocity triangle AFO is obtained by connecting point A with E to obtain F at a given capacity ϕ.

4. The chart gives the basic impeller design data—impeller diameter, width, and discharge angle; also the casing velocity (volute or diffusion vanes) and volute or discharge diffusion casing vane angle α_2'. To obtain the average casing velocity, the value of the absolute velocity

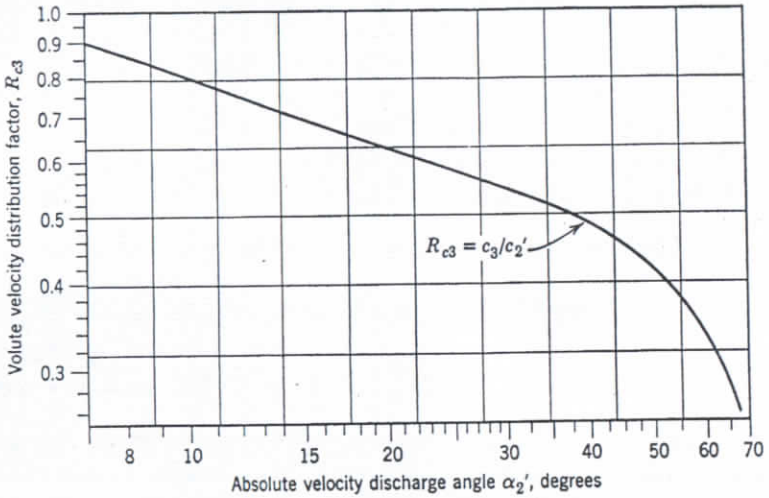

α_2' and c_2' from Fig. 9.13

FIG. 9.14. Volute velocity distribution factor.

c_2', as given by the input (actual) velocity triangle, is multiplied by a velocity distribution factor given in Fig. 9.14 which is plotted as a function of the discharge angle α_2'.

5. The functional relationship of controlling desgin elements is clearly shown on the diagram. (*a*) When impeller discharge angle β_2 is changed without changing the impeller profile, the operating point moves along the constant specific speed curve. (*b*) If the operating point is moved along the constant head line (ψ = constant) the chart will give variation of the meridional velocity c_{m2}, for different β_2 and hence the impeller width, to meet a given capacity. (*c*) If, for a given impeller, the casing area (volute) is changed, the operating point moves along the constant β_2 line until the impeller capacity ($A_2 \times c_{m2}$) is equal to the volute capacity ($A_v \times c_2' \times R_{c3}$), where A_v is the volute throat area and $c_2' \times R_{c3}$ is the average casing velocity c_3. (*d*) For a given

pump casing and fixed impeller profile, variation of the impeller discharge angle moves the b.e.p. along the line of constant absolute velocity angle α_2'.‡ (*e*) The ratio $OE/\phi = \tan\beta_2/\phi$ is the "impelling ratio," defined by equation 4.20, which is an important factor for the determination of vane discharge angles for several streamlines when that for the mean effective diameter is selected (axial and mixed flow impellers).

6. The chart in Fig. 9.13 gives only essential elements of the discharge velocity triangles for a continuous row of hydraulic types. In addition to those represented on the chart, there are a number of design elements, such as the impeller hub ratio, number of vanes, and casing design, which have a bearing upon the pump performance. If these secondary design elements deviate considerably from the normal average values, the points of ψ and ϕ will not fall in their proper places on the chart. It is the designer's problem to recognize such deviations from normal designs and anticipate their effect on the pump performance.

7. Figure 9.13 is prepared for pumps having no means to produce or prevent prerotation at the impeller inlets. When prerotation is allowed, Fig. 9.13 can be used, but the actual head (specified) should be either reduced or increased by the value $c_{u1}'u_1/g$. The value of c_{u1}' is obtained by multiplying the value of c_{u1}, as given on the Euler's entrance triangle drawn on the entrance guide vane angle α_1, by a factor 0.691 = CO/AO in Fig. 9.13, thus allowing the same vane effectiveness of the guide vanes as was established experimentally for the impeller vanes

8. The input head lines can be drawn by connecting points for different discharge angles β_2 ($\phi = \tan\beta_2$ on the axis of ϕ) with point B instead of C. This is determined by $CO/BO = e_h$, where e_h is the hydraulic efficiency. Once determined for one value of the discharg angle and specific speed, e_h remains the same for the whole chart fo pumps approaching optimum performance, for which $e_h = 0.95$ ha been found experimentally. However, the input head is of academi interest only—the value of Fig. 9.13 is that it contains actual hea capacity, velocities, and angles.

9. A number of half-circles in Fig. 9.13 marked $R = 0.1, 0.2 \cdots 0$. represent the degree of reaction defined as the ratio of the pressure ri in the impeller to the total head produced by the impeller. Obvious $(1 - R)$ will represent the kinetic energy as a fraction of the total hea

The degree of reaction concept is not used in connection with centrif gal pumps. The chart Fig. 9.13 in its present form was prepared apply to turboblowers also.

‡ Note that all velocities in Fig. 9.13 appear in the dimensionless form. To obt velocities in feet per second, the values from the chart should be multiplied by value of the peripheral velocity u_2 in feet per second.

(*c*) **Use of Fig. 9.13.** The chart in Fig. 9.13 can be used for the selection of the impeller head and capacity coefficients (ψ and ϕ), and for the determination of the volute average velocity c_3 and volute angele α_v (or α_2') for impeller discharge angles different than 22½°. For practical use, values of ψ and ϕ are given in Fig. 9.15 as a function of the performance specific speed n_s for different values of the impeller discharge angle β_2.

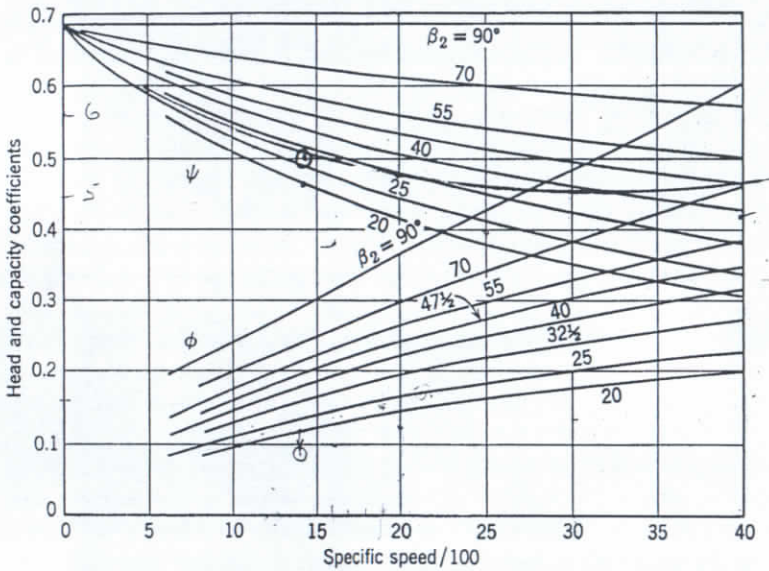

FIG. 9.15. Head coefficient ψ and capacity coefficient ϕ versus specific speed n_s.

The details of the procedure of plotting Fig. 9.15 are given in reference 5. For specific speeds over 4000, which are outside the range of Fig. 9.15, the chart in Fig. 9.13 can be entered by calculating the dimensionless speed ω_s with the use of equation 5.35. For this the value of b_2/D_m for mixed flow impellers, or the hub ratio $\nu = D_h/D_o$ are assumed. This procedure may require two approximations to obtain consistent impeller proportions.

If performance of a pump with one value of the impeller discharge angle β_2 is known, the chart in Fig. 9.13 can be entered by locating the known design point on the chart and, by following the line of ω_s = constant, values of design constants for other values of the impeller discharge angle β_2 can be determined.

(*d*) **The Dimensionless Pump Casing Criterion.** By simple algebraic substitutions it can be shown that head coefficint ψ, capacity coefficient ϕ, and dimensionless specific speed ω_s are functions of the impeller discharge angle β_2' and the absolute velocity at discharge angle α_2' only. Thus, by referring to Fig. 9.16, it can be written

$$\psi = \frac{c_{u2}'}{u_2} = \frac{c_2' \cos \alpha_2'}{u_2} = \frac{\sin \beta_2' \cos \alpha_2'}{\sin (\alpha_2' + \beta_2')}$$

or,

$$\psi = \frac{1}{1 + \tan \alpha_2' \cot \beta_2'} \tag{9.13}$$

and

$$\phi = \frac{c_{m2}}{u_2} = \frac{c_2' \sin \alpha_2'}{u_2} = \frac{1}{\cot \alpha_2' + \cot \beta_2'} \tag{9.14}$$

Hence,

$$\omega_s = f(\alpha_2', \beta_2') = \phi^{1/2}/\psi^{3/4} \tag{9.15}$$

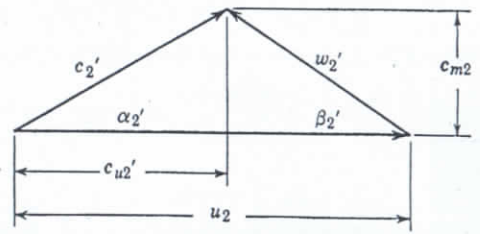

FIG. 9.16. Discharge velocity triangle.

The importance of the impeller discharge angle β_2 as a single controllin design element has been emphasized already. Attention is called t the fact that the absolute velocity angle at impeller discharge α_2 represents the casing criterion in the above relationships.

The affinity laws and several criteria of performance of pumps estab lished in Chapter 5 really apply to the impeller only. Pump casing desig deals with two variables: velocity of flow from the impeller and its direc tion. Since velocity varies with the speed, the angle α_2' is the onl criterion which can be used as an independent variable to correlate th casing design data for pumps of different specific speed. Figure 9.1 shows the casing "velocity distribution factor" plotted against th angle α_2', and not against specific speed.

(*e*) **Specific Capacity and Through-Flow Ability of a Pump.** It i important to grasp the physical meaning of specific capacity q_s define by equation 5.13, and referred to the b.e.p. It represents the "through flow ability" § of a complete pump. It has been shown in Chapter 4 tha the flow through a pump is produced by the energy gradient, the valu of which is determined by the impeller discharge angle. The location o

§ A translation of German word "Durchschluckfähigkeit."

the b.e.p., and hence of q_s, is determined by the combined restrictive action of the impeller and casing which, in turn, jointly locate the point of minimum combined losses of the system. The restrictive action of the pump passages may be differently divided between the impeller and casing, i.e., a tight (narrow) impeller and a rather liberal casing, or vice versa. Finding the optimum flow condition of a pump is the objective of every designer. The restrictive action of the pump passages should not be connected in any way with the combined resistance to the flow which results in a loss of head but should be thought of as an efficient nozzle that determines the rate of flow. Thus, two pumps of different specific speed may be equally efficient, but their specific capacity q_s may be greatly different. Any changes in the casing such as reduction of the volute area, reduction of the diffuser casing vane angle, or increase in number of vanes above normal will reduce the specific capacity. But, since head is produced by the impeller alone, it will not change near the b.e.p., but the b.e.p. will move to a lower capacity and higher head. Or, if impeller width is increased, the specific capacity will increase but not in proportion to the impeller outlet area increase because impeller passages are only one link in a series of passages from the inlet to the outlet. In normal designs a higher specific capacity (which means also a higher specific speed) leads to lower hydraulic friction losses and a better gross efficiency.

(*f*) **Absolute Velocity at Impeller Discharge.** The values of the head coefficient ψ and capacity coefficient ϕ on the chart (Fig. 9.13) are based on the measured head and capacity. The capacity of the impeller is higher than the measured capacity by the amount of leakage. Also, the tangential component of the absolute velocity (c_{u2}') is higher at impeller discharge than that corresponding to ψ by the amount of hydraulic losses beyond the impeller discharge. The true value of the absolute angle at the impeller discharge (α_2') differs little from that given by the chart. The value of the average volute velocity $c_3 = R_{c3} \times c_2'$ is corrected by the experimental factor R_{c3} based on the actual volute areas.

Thus, although the chart (Fig. 9.13) involves several minor approximations, the values contained in the chart can be used with confidence for design of impellers and volute and vaned diffuser casing as long as the hydraulic design does not deviate appreciably from the continuous types on which the chart is based.

(*g*) **Optimum Pump Efficiency.** The design constants and basic relationships derived from Fig. 9.13 are based on the test data of a great many successful pumps and blowers, covering a wide range of specific speeds and impeller discharge angles β_2. It is believed that these

design constants represent values leading to an optimum pump efficiency. A different combination of several design elements of the impeller and casing than those derived from Fig. 9.13 may produce different values of the head and capacity coefficients for the b.e.p. but at some sacrifice in efficiency. Such deviations from standard designs are frequently required in practice to extend the operating range of pumps by providing several impellers for the same casing, or by using the same impeller in two different casings. Both cases result in mismatching of impellers

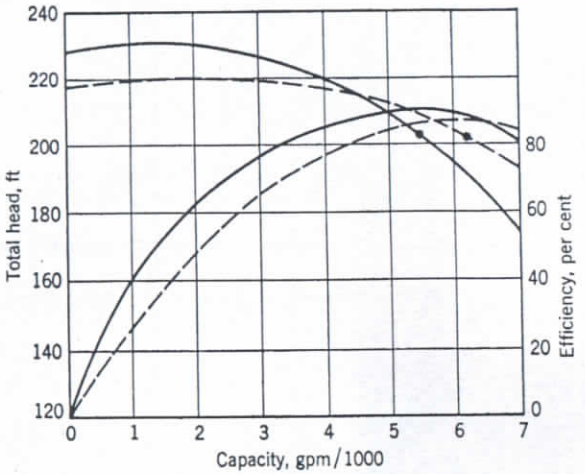

FIG. 9.17. Performance of the same impeller in two different volute casings, 1450 rpm.

and casings. It has been pointed out in Art. 9.4(*b*) how the location of the b.e.p. can be estimated in such cases. Below are given several examples.

Figure 9.17 shows the performance of the same impeller in two different volute casings. The ratio of the volute throat areas is 1.30. Note that the smaller volute results in a higher shut-off head and a steeper head-capacity curve.

Figure 9.18 shows the performance of two impellers in the same volute casing. Both impellers have the same outside diameter (13½ in.), the same profile, the same impeller discharge angle $\beta_2 = 20°$, and the same number of vanes $z = 7$. The impeller width at discharge b_2 of one is 1 in. and for the other $b_2 = \frac{1}{2}$ inch. The b.e.p. of both fall on the same β line on Fig. 9.13, i.e., $\beta_2 = 20°$. The loss in head and efficiency with the narrow impeller is caused by head loss at impeller discharge (eddy loss) since the volute areas are too large for this impeller. Note that the capacity at b.e.p. of the narrow impeller is about 75 per cent of that for

the wide (normal) impeller and not 50 per cent as the impeller discharge area would indicate. This illustrates that the b.e.p. location is determined by specific capacity, fixed by impeller and casing through-flow ability.

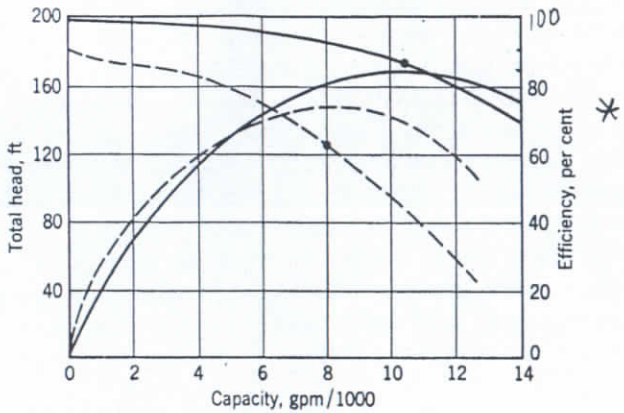

FIG. 9.18. Performance of 5-in. double-suction pump, 1750 rpm; full-line impeller, 1 in. wide; dotted-line impeller, ½ in. wide.

If the impeller profile is kept the same but the impeller discharge angle is changed, the head and capacity coefficients fall on their respective lines of β_2 and the same line α_2' on Fig. 9.13. For an illustration see Chapter 17, reference 10, p. 68.

Figure 9.19 shows the effect of reducing the gap between the impeller and volute cut-water or tongue. The solid lines show the head-capacity

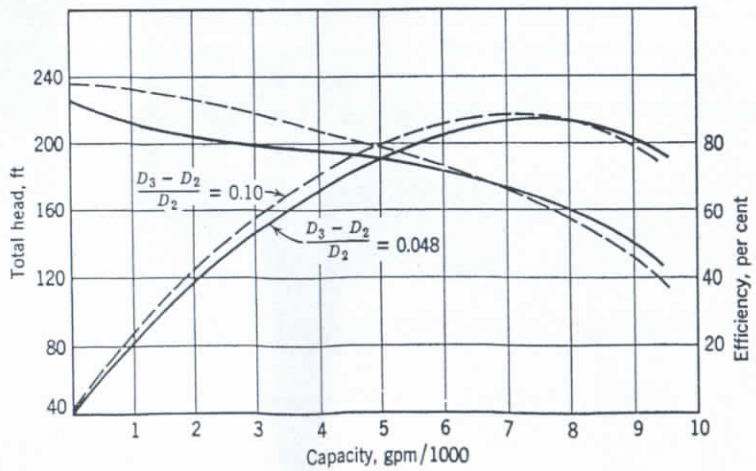

FIG. 9.19. Effect of clearance between impeller and volute tongue, 1200 rpm.

and efficiency of the pump with a gap $(D_3 - D_2)/D_2 = 0.048$, whereas a normal gap for a pump of this specific speed ($n_s = 1560$) is 0.135 according to Fig. 7.5. The dotted lines show the performance of the same impeller with volute cut-water removed to increase the gap to about 0.10. With normal values of gap between the impeller and casing cut-water, a further increase of the gap by removing a portion of cut-water will have little or no effect on performance. An excessive gap between the impeller outside diameter and volute tongue leads to reduction of efficiency. It has been pointed out in Art. 7.2(*b*) that for high specific speed pumps ($n_s = 7500$, double-suction) removal of a part of the volute tongue resulted in a loss of four points in efficiency.

REFERENCES

1. C. Pfleiderer, *Die Kreiselpumpen*, p. 376, Berlin, Julius Springer, 1955.
2. Wilhelm Spannhake, *Centrifugal Pumps*, p. 152 (translation), Cambridge, Mass. Inst. of Tech., 1934.
3. Joseph N. LeConte, *Hydraulics*, p. 314, New York, McGraw-Hill Book Company, 1926.
4. Joseph Lichtenstein, "Method of Analyzing the Performance Curves of Centrifugal Pumps," *Trans. A.S.M.E.*, Vol. 50, No. 3, p. 3, 1928.
5. A. J. Stepanoff, *Turboblowers*, Chapter 6, New York, John Wiley and Sons, 1955.

type #

*

$Q = 1050$
$H = 170$
$N = 1750$
$N_s = 1205$
$\beta_2 = 20°$
$D_2 = 13\frac{1}{2}$
$U_2 = \frac{13\frac{1}{2} \times 1750}{229} = 103$ ft/sec

$C_{m_2} = \phi \times U_2$

$C_{m_2} = \frac{1050 \times .321}{b_2}$

ϕ_{step}	
0.11	0.09
11.3'	9.3
$b_2 = 0.84''$	1.02''

amazing even Steps doesn't mean what the

Chapter 10

Leakage, Disk Friction, and Mechanical Losses

10.1 LEAKAGE LOSS

(*a*) **Volumetric Efficiency.** Leakage loss is a loss of capacity through the running clearances between the rotating element and the stationary casing parts. Leakage can take place in one or several of the following places, according to the type of pump: (1) between the casing and the impeller at the impeller eye; (2) between two adjacent stages in multistage pumps; (3) through the stuffing box; (4) through axial thrust balancing devices; (5) through bleed-off bushings when used to reduce the pressure on the stuffing box; (6) past vanes in open impeller pumps; and (7) at any bleed-off used for bearing and stuffing box cooling.

The capacity through the impeller is greater than the measured capacity of the pump by the amount of leakage, and the ratio of the measured capacity Q to the impeller capacity $Q + Q_L$ is the volumetric efficiency.

$$\frac{Q}{(Q + Q_L)} = e_v \tag{10.1}$$

Usually the volumetric efficiency takes into account only the leakage between the impeller and casing at the impeller eye for multistage and single-stage pumps. The interstage leakage in multistage pumps and leakage through the balancing devices or any other point should be treated separately. In each case the amount of such leakage should be multiplied by the pressure drop across the clearance to obtain the power loss caused by leakage. Although the actual pressure at the clearance may be reduced as a result of the vortex action of the impeller, the full-stage pressure, or a multiple of the stage pressure, depending on the stage at which the loss occurs, should be used to calculate the loss of power caused by leakage since the amount of leakage is given full input head when it passes through the impeller. Thus $(\text{hp})_L = Q_L \gamma H / e_h$ is the power loss due to leakage.

Figure 10.1 shows several popular designs of impeller and casing rings. These may be modified by including a step instead of one continuous

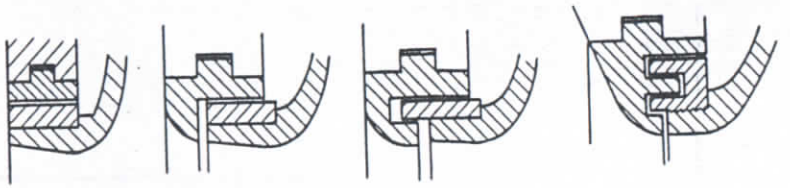

FIG. 10.1. Wearing-ring types.

throttling surface. The bleed-off devices consist of long throttling surfaces (Fig. 10.2), continuous or interrupted by steps, grooves, or arranged as a labyrinth, in which case there are really several throttling surfaces in series.

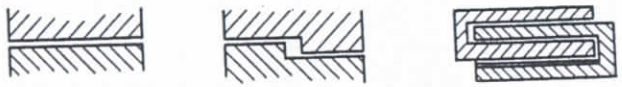

FIG. 10.2. High pressure sealing arrangements.

For a known pressure drop across the clearance, the amount of leakage can be calculated by

$$H_L = f\frac{L}{d}\frac{v^2}{2g} + 0.5\frac{v^2}{2g} + \frac{v^2}{2g} = \left(f\frac{L}{d} + 1.5\right)\frac{v^2}{2g} \tag{10.2}$$

where H_L is the head across the clearance in feet.
f is a friction coefficient, dimensionless.
v is velocity through the clearance in feet per second.
L is the length of the throttling surface, or width of the wearin ring, in feet.
d is the diameter of a circular pipe, in feet, having the sam hydraulic radius m as the annular channel of the clearanc

Hydraulic radius is defined as

$$m = \frac{d}{4} = \frac{\text{area of clearance}}{\text{wetted perimeter}} = \frac{\pi D a}{2\pi D \times 2} = \frac{a}{4} \tag{10.}$$

where D is the average diameter of the throttling surfaces and a is tl diametrical clearance, both in feet. Note from the above that $d =$

The first term in equation 10.2 represents the friction loss, the seco the entrance loss, and the last the velocity head at discharge from t clearance. The diameter d of a circular pipe having the same hydrau radius as the annular channel of the clearance is introduced to ma possible comparisons of friction coefficients found on special tests close annular clearances with those for circular pipes. Figure 1

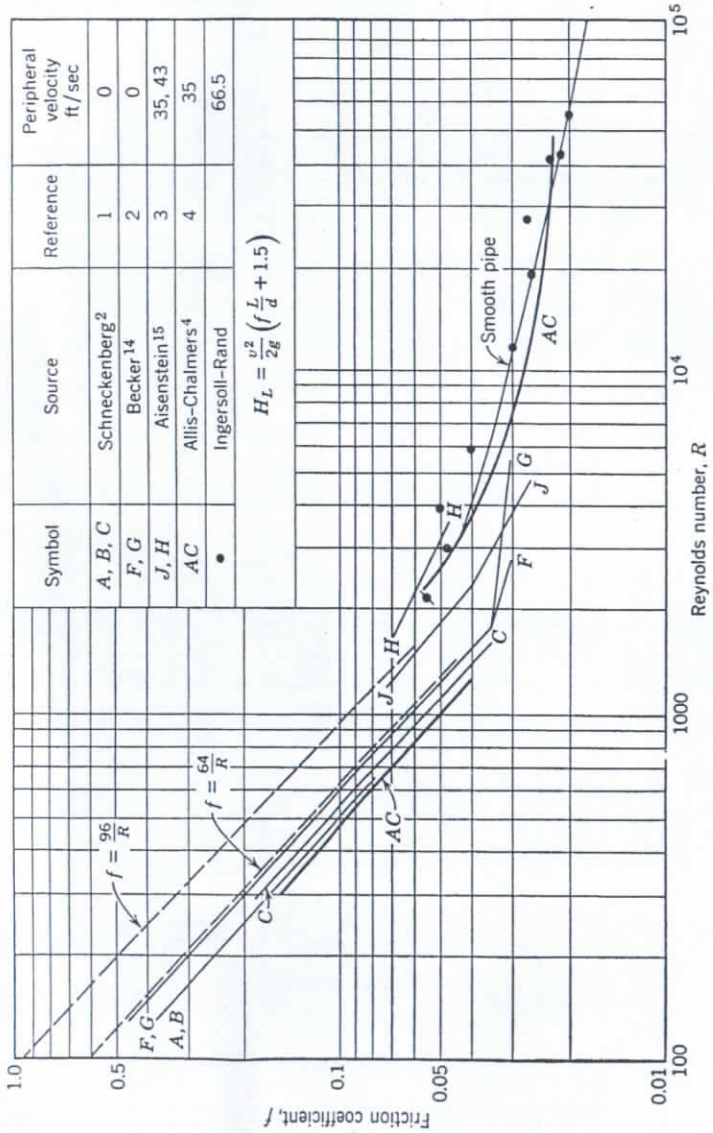

FIG. 10.3. Friction coefficient for flow through annular clearances.

shows the values of f calculated by equation 10.2 from test results o several investigations. The values of f are plotted against the Reynold number $R = vd/\nu$, where ν is the kinematic viscosity of liquid in squar feet per second.

In the turbulent flow region ($R > 2500$), the values of f for smal annular channels with revolving rings follow the curve for smoot round pipes.[1] This is merely a coincidence, because there is no geo metrical similarity of the channels or velocity distribution between th two patterns of flow. In the turbulent region of flow the amount o flow does not depend on the shaft speed (Ingersoll-Rand tests witl 4¼-in. shaft at 0 to 3600 rmp).

In the laminar region, the experimental points for both a stationar and revolving ring arrange themselves nearer the line $f = 64/R$ (deter mined theoretically for circular pipes) than the line $f = 96/R$ for th annular channels. The value of f for laminar flow is affected by th speed of rotation, and will be found to increase with the speed. It i also sensitive to the eccentricity of the clearance. Thus, according t Schneckenberg,[2] maximum eccentricity may increase the amount o leakage to 2.5 times the amount for a concentric annular channel. I the turbulent region of flow the increase of flow due to eccentricity i only about 30 per cent.

Values of f for narrow rings in the viscous flow regime will be foun to be higher than those on Fig. 10.3 as there is not sufficient time fo the flow to assume its final velocity distribution. It takes a length o 30 to 40 pipe diameters for the flow to develop its steady pattern o velocity distribution. The matter is further complicated by the effec of heat (produced by friction) on the viscosity of the liquid. Thi becomes an important factor for viscous liquids where long throttlin surfaces and small clearances are involved. Calculation of the amoun of leakage under such conditions becomes very uncertain. The autho has run very extensive tests on leakage through rings of different de signs under actual operating conditions of the pump. The chart i Fig. 10.4 is compiled from the original report,[3] and the comparative merit of different designs are evident from this tabulation. Blackwell an Murdock's tests[4] show that the amount of leakage is reduced 20 to 2 per cent when either the stationary bushing or the revolving sleeve i grooved.

(b) Pressure at the Wearing Rings. The pressure H_L across th clearance at the impeller eye is lower than the pressure in the volut casing H_v. The reduction in pressure at the wearing ring is caused b rotation of the liquid in the space between the impeller and casing walls It is usually assumed that the liquid in this space rotates at half th

		a In.	b In.	Leakage per cent at r.p.m.			
				1400	1700	2000	2500
1	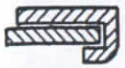	0.012	1 1/16	1.52	1.80	2.00	2.18
2		0.012	1 1/16	2.85	3.32	3.52	3.70
3	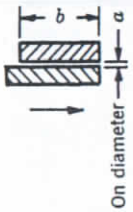	0.012	1 1/16	3.52	4.03	4.33	4.50
4		0.017	11/16	6.06	6.65	6.70	6.70
5		0.020	11/16	7.92	8.62	8.86	8.60
6		0.029	11/16	13.2	13.9	14.0	14.0
7		0.039	11/16	18.7	19.6	19.8	20.0
8		0.017	11/16	4.83	5.38	5.58	5.52
9	Circular groove 1/16 × 1/16 1/8 apart	0.029	11/16	12.7	13.5	13.7	13.6
10		0.011	11/16	3.18	3.68	3.94	4.08
11		0.021	11/16	8.53	9.04	9.15	9.19
12		0.011	11/16	2.52	2.88	2.92	2.98
13	1/16 × 1/16 spiral groove	0.021	11/16	6.24	6.68	6.89	6.82
14		0.010	11/16	2.55	3.03	3.28	3.44
15		0.010	11/16	2.07	2.34	2.45	2.52

FIG. 10.4. Leakage loss in per cent of normal capacity at several speeds; 3-in. pump, $n_s = 1090$, $D_2 = 10\frac{1}{8}$ in., ring diameter = $4\frac{1}{8}$ in.

impeller angular velocity. The pressure in the volute can be obtained by subtracting from the pump total head the kinetic energy of flow in the volute (the loss of head due to friction in the volute casing and the velocity head in the suction nozzle being disregarded).

$$H_v = H - \frac{{c_3}^2}{2g} = H(1 - {K_3}^2) \tag{10.4}$$

where c_3 is the volute velocity and K_3 is determined from $c_3 = K_3\sqrt{2gH}$, one of the design constants. The pressure at the wearing rings is given by

$$H_L = H(1 - {K_3}^2) - \frac{1}{4}\frac{{u_2}^2 - {u_r}^2}{2g} \tag{10.5}$$

where u_r is the peripheral velocity of the impeller ring. From actual pressure measurements on one pump of $n_s = 1090$, using two impeller diameters, the author has developed an empirical formula for the pressure at the ring for b.e.p. The equation is

$$H_L = \frac{3}{4}\frac{{u_2}^2 - {u_1}^2}{2g} \tag{10.6}$$

where u_1 is the peripheral velocity of the vane entrance tip. The development of this equation is given in the original report.[3]

(c) Leakage Loss versus Specific Speed. Using coefficients from Fig. 10.3, the author has calculated the leakage loss for a number of double-suction horizontally split pumps of different specific speeds, and the results are shown in Fig. 10.5. In all cases, actual clearances and wearing-ring widths for plain flat rings were used. It will be observed that leakage loss decreases rapidly with increasing specific speed.

For the purpose of further discussion it is important to establish some general relationships between leakage loss and specific speed. It will be shown that the power loss due to leakage is constant for pumps of the same specific speed, irrespective of pump size and speed. Equation 10.2 will be used for calculation of the amount of leakage.

$$Q_L = CA\sqrt{2gH_L} \tag{10.7}$$

where

$$C = \frac{1}{\sqrt{f\frac{L}{d} + 1.5}}$$

$A = \frac{a\pi D}{2}$, the clearance area

$$H_L = K_r H$$

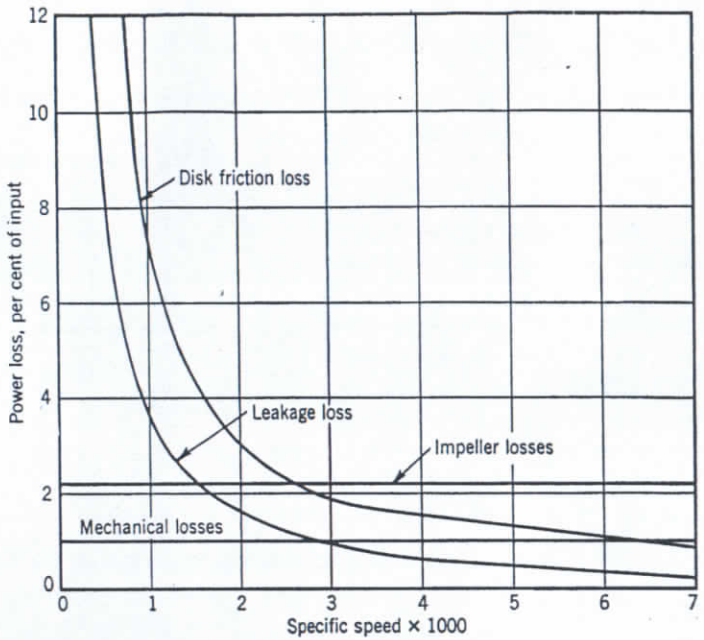

FIG. 10.5. Losses versus specific speed for double-suction pumps.

The coefficient of discharge C and the factor K_r, expressing H_L as a fraction of the pump total head, are assumed to be constant for similar pumps. The power lost because of the back-flow through the clearance is

$$(\text{hp})_L = \frac{Q_L \gamma H}{e_h 550} \tag{10.8}$$

where γ is the weight of 1 cu ft of water. The ratio of power lost due to leakage of two pumps is equal to

$$\frac{(\text{hp})_{L1}}{(\text{hp})_{L2}} = \frac{a_1 D_1 H_1^{3/2}}{a_2 D_2 H_2^{3/2}} \tag{10.9}$$

If similarity of the two pumps is extended to the wearing-ring diameters and clearances,

$$\frac{a_1 D_1}{a_2 D_2} = \frac{D_{1o}^2}{D_{2o}^2} \tag{10.10}$$

where D_{1o} and D_{2o} are the outside impeller diameters of the two pumps. Substituting this into equation 10.9, we obtain

$$\frac{(\text{hp})_{L1}}{(\text{hp})_{L2}} = \frac{D_{1o}^2 H_1^{3/2}}{D_{2o}^2 H_2^{3/2}} \tag{10.11}$$

Making use of equation 10.12, which gives the type-unit-capacity re tionships for similar pumps, we can change equation 10.11 to 10.13.

$$\frac{Q_1}{\sqrt{H_1}\, D_{1o}^2} = \frac{Q_2}{\sqrt{H_2}\, D_{2o}^2} = \text{constant} \tag{10.1}$$

$$\frac{(\text{hp})_{L1}}{(\text{hp})_{L2}} = \frac{Q_1 H_1}{Q_2 H_2} = \text{constant} \tag{10.1}$$

This equation states that *the power lost in leakage is proportional to pump output. Hence, if expressed as a percentage of the pump outp this loss is constant for all similar pumps.** In practice, however, t leakage loss is greater for smaller pumps, because the clearances cann be reduced below a certain minimum; also because the wearing rings larger pumps are wider, and the coefficient of discharge C is small

In order to compare the leakage loss horsepower for pumps of t same output but of different specific speed, revolutions per minute, a size, we may write equation 10.9 as before,

$$\frac{(\text{hp})_{L1}}{(\text{hp})_{L2}} = \frac{a_1 D_1 H_1^{3/2}}{a_2 D_2 H_2^{3/2}} = \frac{D_1^2 H_1^{3/2}}{D_2^2 H_2^{3/2}} \tag{10.}$$

assuming that the width of the wearing rings and the coefficient have the same value, and that the clearances vary in the same ratio the impeller wearing-ring diameters. The radial velocity at the impel eye varies with the impeller type and speed, and a ratio of radial vel ities may be expressed in terms of the head as follows:

$$\frac{c_{m1}}{c_{m2}} = \frac{K_{m1} H_1^{1/2}}{K_{m2} H_2^{1/2}} \tag{10.}$$

Assuming that the full impeller eye area = $\pi D^2/4$ is available the flow, i.e., the pump is of the overhung impeller construction, that the effect of the presence of the shaft in the impeller eye upon ratio of the impeller eye areas may be neglected, we can write

$$\frac{Q_1}{Q_2} = \frac{c_{m1} D_1^2}{c_{m2} D_2^2} = \frac{K_{m1} H_1^{1/2} D_1^2}{K_{m2} H_2^{1/2} D_2^2} \tag{10.}$$

Combining this equation with equation 10.14, we obtain

$$\frac{(\text{hp})_{L1}}{(\text{hp})_{L2}} = \frac{Q_1 H_1 K_{m1}}{Q_2 H_2 K_{m2}} = \frac{K_{m2}}{K_{m1}} \tag{10.}$$

* The relationship represented by equation 10.13 (and later by equation 10 is approximate only and is intended to show the trend of variation of the leakage with specific speed, pump size, and speed. In addition to depending on the phys dimensions of the throttling surfaces, the amount of leakage also depends on Reynolds number, as shown by Fig. 10.3.

Since the water horsepower (whp) is the same for both pumps, the ratio of the leakage loss horsepower, expressed in per cent of water horsepower, will be given by equation 10.17. The value of factor K_m increases with an increase of specific speed; hence for the same pump output the leakage loss is higher for the lower specific speed pump. For example, for $n_s = 1000$ the factor $K_{m1} = 0.138$, and for $n_s = 2000$ the factor $K_{m2} = 0.188$, and the ratio of the leakage loss horsepower is equal to

$$\frac{(\text{hp})_{L1}}{(\text{hp})_{L2}} = \frac{0.188}{0.138} = 1.35$$

10.2 DISK FRICTION LOSS

(a) Disk Friction Loss Formulas. Of all external mechanical losses the disk friction is by far the most important. Considerable test data are available on the disk friction loss for cold water, and several formulas are in use. All of these stem from one fundamental equation:

$$(\text{hp})_d = Kn^3D^5 \tag{10.18}$$

where $(\text{hp})_d$ is the power absorbed by disk friction.

K is an experimental factor which also takes care of the units used.

n is the revolutions per minute.

D is the disk diameter in feet.

Several formulas use fractional exponents for n and D, the authors claiming that only in that case is K a real constant. The derivation of equation 10.18 follows. Referring to Fig. 10.6, a disk of diameter D, or radius r, is revolved at an angular speed of ω. Assuming turbulent flow at the disk surface, the friction force at radius r exerted on a ring having width dr can be expressed as

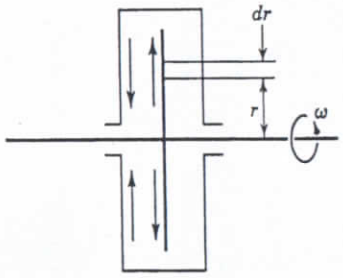

FIG. 10.6. Disk friction loss.

$$F = KAv^2 = K2\pi v^2 r\,dr$$

The power required to overcome this resisting force is found by multiplying it by the velocity v, or

$$(\text{hp})_d = K2\pi\int_0^r v^3 r\,dr = K2\pi\omega^3\int_0^r r^4\,dr = \frac{K2\pi\omega^3 r^5}{5}$$

If we combine all constants into one, include the power loss for both

sides of the disk, use n = rpm instead of angular velocity ω, and diameter D instead of the radius, we obtain the equation

$$(\text{hp})_d = Kn^3D^5 \tag{10.18}$$

The particles of liquid in the space between the disk and stationary walls acquire a rotary motion. As a result of centrifugal forces, particles start moving outward in the immediate neighborhood of the disk and new particles approach the disk near the center. Thus a circulation is established. If the path of circulation is short, or the volume of the liquid surrounding the disk is small, particles approaching the disk will retain part of their rotary motion, thus requiring less power from the disk. Gibson and Ryan [5] and LeConte [6] have found experimentally that the power to drive a disk increases as the clearance between the disk and walls is increased. For instance, when the clearance was increased from 1.03 to 17.7 per cent of the disk diameter, the power increased by 4 to 12 per cent. The same investigators have also established that: (1) painting a rough cast-iron casing reduces disk friction power by 16 to 20 per cent; (2) polishing the disk reduces the loss by 13 to 20 per cent; (3) badly rusted cast-iron disks take 30 per cent more power than the same disks newly machined; (4) increase of water temperature from 65°F to 150°F decreased the disk friction power by 7 to 19 per cent, depending on the combination of the disk and casing finish.

Based on works of Zumbusch and Schultz-Grunow,[7] Pfleiderer [8] has prepared a chart of the friction coefficients for calculating the disk friction loss (reproduced in Fig. 10.7) to be used in connection with the following equation (two sides)

$$\text{hp}_d = KD^2\gamma u^3 \tag{10.19}$$

where K is a numerical coefficient plotted against Reynolds number Re

Re is the Reynolds number equal to ur/ν, dimensionless.

u is the outside peripheral velocity in feet per second.

r is the impeller radius in feet.

ν is the kinematic viscosity in feet squared per second.

D is the impeller diameter in feet.

γ is the fluid density in pounds per cubic foot.

The values of the coefficient K are given for three values of the sid clearance B/D, where B is the distance between the disk and stationar walls of the casing. For normal designs B/D is from 2 to 5 per cen This falls within the region of minimum disk friction loss, as is evider from a curve of K versus B/D drawn for $Re = 1.8 \times 10^6$.

It has been a common assumption that the fluid between the disk and stationary walls rotates with one half of the impeller angular velocity. This can be justified by theoretical reasoning and has been confirmed by the Schultz-Grunow [7] experiments quoted above.

The values of the disk friction loss as determined from Fig. 10.7 should be increased by 5 to 10 per cent as the actual area of the revolving impeller shrouds is appreciably greater than that of a flat disk of

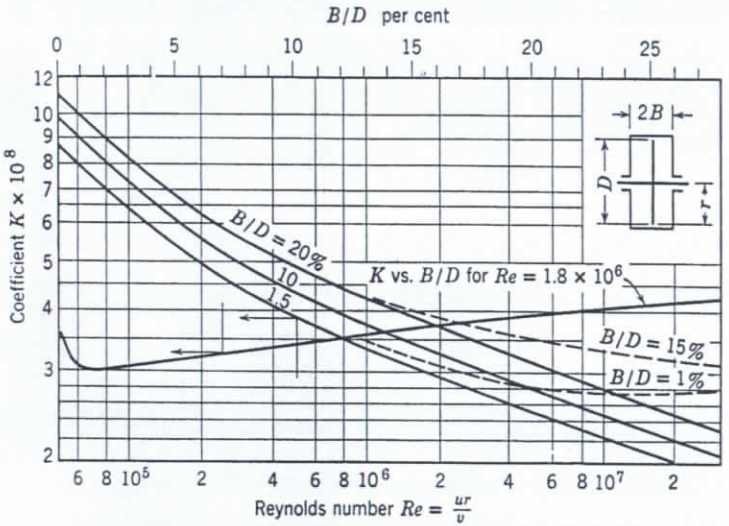

FIG. 10.7. Disk friction coefficient versus Reynolds number; full lines, smooth disk; dashed lines rough disk.

the same diameter used by the experimenters. Two dotted curves show values of the coefficient K for rough disks for B/D ratio of 1 and 15 per cent. A considerable increase of K is observed at higher Reynolds numbers, where turbulent flow prevails at all radii of the impeller.

(*b*) **Actual Disk Friction Loss versus Specific Speed.** By using Pfleiderer's equation (10.19), the disk friction loss was computed for a number of double-suction pumps of different specific speeds. This loss expressed as percentage of pump brake horsepower is plotted in Fig. 10.5. Attention is called to the rapid rise of disk friction loss at specific speeds below 2000. It is interesting to note that, almost throughout the entire range of specific speeds, leakage loss is approximately equal to one half of the disk friction loss.

For pumps of the same specific speed but of different size and speed, both the pump output and the power consumed by the disk friction are proportional to n^3D^5 and their ratio remains the same. This consideration disregards the effect of Reynolds number on the value of the coefficient K in equations 10.18 and 10.19 and on the hydraulic efficiency of the pump, as it affects the pump output.

10.3 MECHANICAL LOSSES

(*a*) **Stuffing Box and Bearing Losses.** Although the nature o mechanical losses in the bearings and stuffing boxes is well understood very little actual data on the values of these losses are available. The difficulty lies in their being small and difficult to measure with ordinary testing facilities. On the other hand, it is felt that such tests will be o only slight value to pump manufacturers in so far as improvement o pump performance is concerned. Both stuffing box and bearing designs are governed by requirements for satisfactory mechanical performance The matter of friction loss in both is of secondary importance. Besides friction loss in the stuffing boxes is affected by a number of factors, fo example, size and depth of stuffing box, pump speed, pressure, and method of packing and lubrication, so that any actual values will be illustrative of a certain type of stuffing box application only.

Although ball bearing sizes are well standardized, the friction loss in the ball bearings varies for the same size and load for different makes o bearings. Also, the method of lubrication affects the losses in ball bearing, as shown by bearing running temperatures. It has been found tha the type of coupling between the pump and driver affects the bearing behavior and, hence, losses, as some couplings impose an axial load on the thrust-type ball bearings.

Figures 10.8 and 10.9 show stuffing box friction power loss obtained by Mockridge.[9] Note that the frictional torque is very high with a tight gland and small leakage, but decreases rapidly as the gland is loosened and the leakage increases. A slight increase in torque follows on further loosening of glands, as packing pulls away from the bottom of the stuffing box. In Fig. 10.9 the power loss varies approximately as the square of the speed. Assuming that the shaft as tested is good for 1250 hp at 3000 rpm, the loss at the stuffing boxes at that speed will be only 0.22 per cent. At 1500 rpm, the same pump would require only 156 hp, and the stuffing box loss will be 0.48 per cent. Allowing an equal loss for the bearings, the mechanical losses for both items will be only about 1 per cent in the last example. However, in small pumps under unfavorable conditions, mechanical losses may be 2 or 3 per cent or more of the brake horsepower.

Recently tests were run by Ingersoll-Rand Company on a special rotor equipped with two stuffing boxes having nine ½ by ½ rings o

packing, 4⅞-in. outside diameter of shaft sleeves, two sleeve bearings, and a Kingsbury thrust bearing. When the boxes were sealed against 300 psi of water at 350°F, and allowing about ½ gpm of leakage from

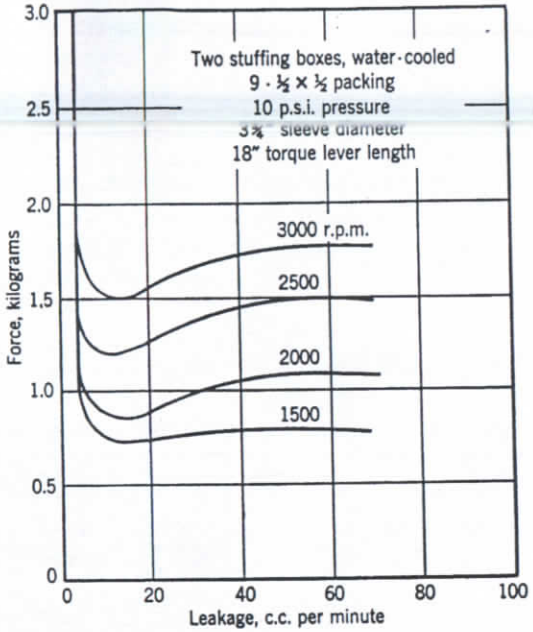

FIG. 10.8. Stuffing box friction loss (Mockridge).

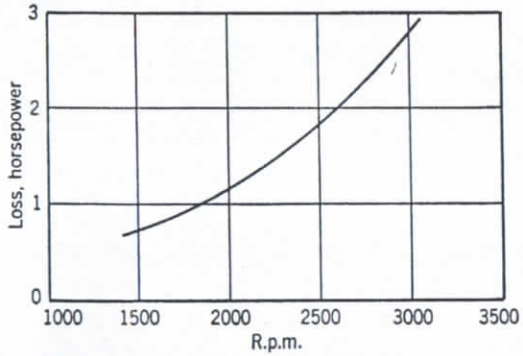

FIG. 10.9. Stuffing box friction loss. Data from Fig. 10.8 (Mockridge [9]).

two stuffing boxes at 3500 rpm, the stuffing box friction horsepower was found to vary from 7.5 at the start of run to 2.5 after several hundred hours of operation. The bearing friction horsepower, with no thrust

load on the bearing, was found to be 1.5. This size of shaft was used for high pressure boiler feed pumps requiring up to 1500 hp. Thus the stuffing box friction for such a pump would vary from 0.5 to 0.2 per cent of the brake horsepower and the bearing loss would be probably 0.2 per cent, which is double the loss actually measured in the tests to allow for some axial thrust load on the thrust bearing. In the above tests the sleeves were new, the packing was properly adjusted, the stuffing boxes were water-cooled, and glands were quenched. On the basis of the above figures, a 1 per cent loss for bearings and stuffing boxes of high speed pumps would appear to be a good estimated average value. For the purpose of this discussion it will be assumed that the stuffing box and bearing friction will be equal to 1 per cent of the brake horsepower and will be independent of the specific speed. This is also shown in Fig. 10.5.

(*b*) Power Balance versus Specific Speed. If the mechanical, disk, and leakage losses for the b.e.p. for different specific speeds are known, it is possible to determine the hydraulic losses for the same points. Double-suction pumps will be considered here with their optimum efficiencies for different specific speeds as given in Fig. 16.12. Taking the lowest specific speed at which a maximum efficiency of over 90 per cent is reached ($n_s = 2000$), the known losses from Fig. 10.5 are: disk friction 3.0 per cent, leakage 1.5 per cent, and mechanical loss 1.0 per cent, making a total of 5.5 per cent of the power input. Since the pump output is 90 per cent, this leaves 4.5 per cent for all hydraulic losses. The hydraulic losses are essentially all friction losses and will be assumed to be equally divided between the impeller and the casing. Impeller hydraulic losses of 2.25 per cent will be assumed constant for all specific speeds.

In Fig. 10.10, a power balance is drawn for double-suction pumps of different specific speeds. The casing hydraulic losses are obtained by subtraction from the pump input of all known losses and the pump output. For specific speeds below 2000 the casing hydraulic losses remain constant and equal to the impeller losses by assumption. For higher specific speeds the casing losses increase. In Fig. 10.10 the pump output is numerically equal to the pump gross efficiency, as all values are percentages of the pump input. The output of vertical pumps is shown by a broken line. The difference between the casing losses of the two types of pumps is ascribed to the effect of the suction approach in double-suction pumps. This does not necessarily mean extra hydraulic losses in the suction nozzle as the loss also includes the detrimental effect of the 90° turn ahead of the impeller eye on the impeller efficiency. This effect is also evidenced by the impaired cavitation characteristics, as

compared with pumps of the same specific speed having a straight suction approach.

The hydraulic efficiency in terms of power is expressed as

$$e_h = \frac{Q\gamma H}{Q\gamma H + (Q\gamma h_l)/e_v} = \frac{H}{H + h_l/e_v} \tag{10.20}$$

where h_l is the sum of all hydraulic losses and e_v is the volumetric efficiency. The hydraulic efficiency of pumps of specific speeds below

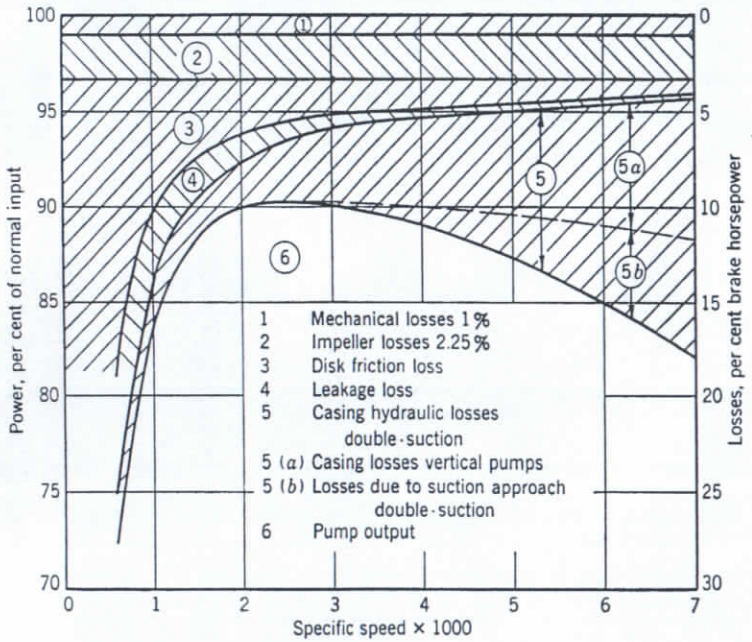

FIG. 10.10. Power balance for double-suction pumps at b.e.p.

2000 is approximately constant. Although the hydraulic losses in per cent of power input are constant for pumps of specific speeds below 2000, the volumetric efficiency decreases with the specific speed and the hydraulic efficiency will also decrease, as equation 10.20 shows.

At specific speed $n_s = 2000$, the hydraulic efficiency as calculated from the data in Fig. 10.10 is equal to $e_h = 95.3$ per cent. This is taken as an optimum hydraulic efficiency for all specific speeds and is marked as point B on the author's diagram, Fig. 9.13. *It follows from Fig. 10.10 that the hydraulic efficiency decreases for specific speeds above 2000, and this is entirely due to the increased pump casing hydraulic losses. At lower specific speeds the reduction of the gross efficiency is caused by the increased disk friction and leakage losses.*

10.4 LOSSES VERSUS CAPACITY AT CONSTANT SPEED

A power balance for a pump operating at a constant speed and variable capacities can be drawn, as shown in Fig. 10.11, in the following manner. This will be done for a 12-in. double-suction pump of $n_s = 1900$,

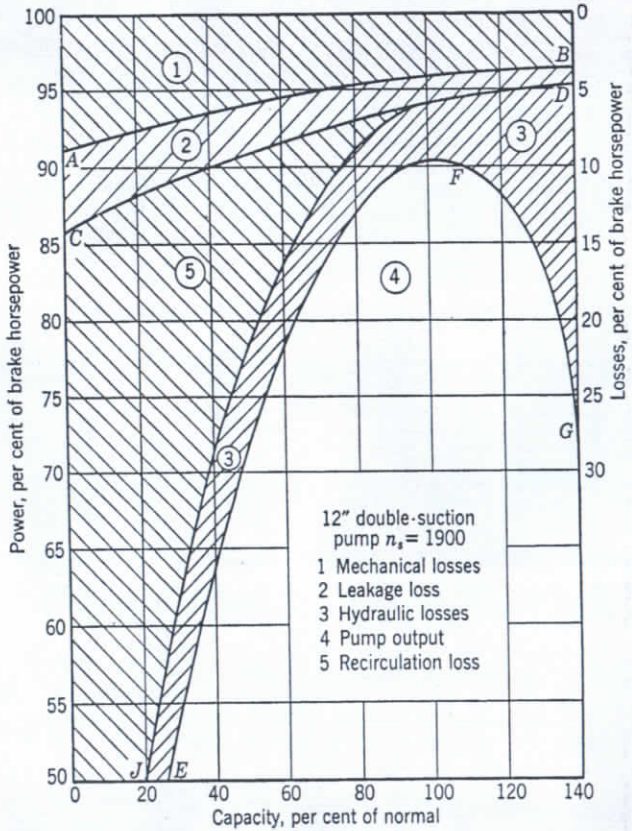

FIG. 10.11. Power balance versus capacity at constant speed.

performance for which is shown in Fig. 10.12. In the same figure, the hydraulic efficiency curve is drawn. For this three points are known. For the b.e.p. the hydraulic efficiency was estimated above to be 95.3 per cent. At shut-off the hydraulic efficiency is obtained from Fig. 9.13 and is equal to

$$e_h = \frac{DO}{BO} = \frac{58.5}{72.5} = 0.808 \tag{10.21}$$

The third point is the zero efficiency point which is zero head poin

on the head-capacity curve. The hydraulic efficiency for two points A and B being known, the input head line DE can be drawn, and hydraulic efficiency $e_h = H/H_i$ can be plotted for every point. To draw the input head line, the zero input head point can be used as one of the points. The capacity for this point can be obtained from

$$\phi = \frac{c_{m2}}{u_2} = \tan \beta_2$$

The points of equal hydraulic efficiency on the head-capacity curve should fall on a straight line joining these points and the point of zero input head, as shown in Fig. 10.11.

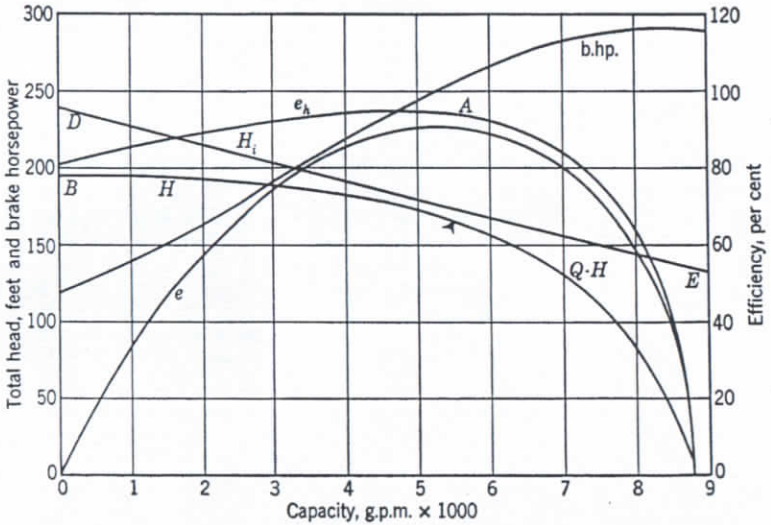

FIG. 10.12. Performance of 12-in. double-suction pump, 1180 rpm; n_s = 1900.

The difference between H_i and H curves represents hydraulic losses h_l. The power loss due to hydraulic losses can be calculated from

$$(\text{hp})_h = (Q + Q_L)\gamma h_l = \frac{Q\gamma h_l}{e_v} \qquad (10.22)$$

The pump output in Fig. 10.11 is represented by the curve EFG, which is the gross efficiency curve, since

$$e = \frac{Q\gamma H}{\text{bhp}} \qquad (10.23)$$

Although mechanical losses, including the disk friction loss, are constant for any capacity in Fig. 10.11, when expressed as a percentage of the brake horsepower, the percentage will increase for lower capacities since the brake horsepower decreases toward zero capacity. Also the percentage of leakage loss horsepower increases for the same reason. Besides, leakage in gallons per minute increases as the capacity decreases on account of the increasing head toward shut-off.

$$(\text{hp})_L = Q_L\gamma H_i = \frac{Q_L\gamma H}{e_h} \qquad (10.24)$$

All known losses and the output of the pump having been drawn on Fig. 10.11, a considerable loss of power remains unaccounted for at

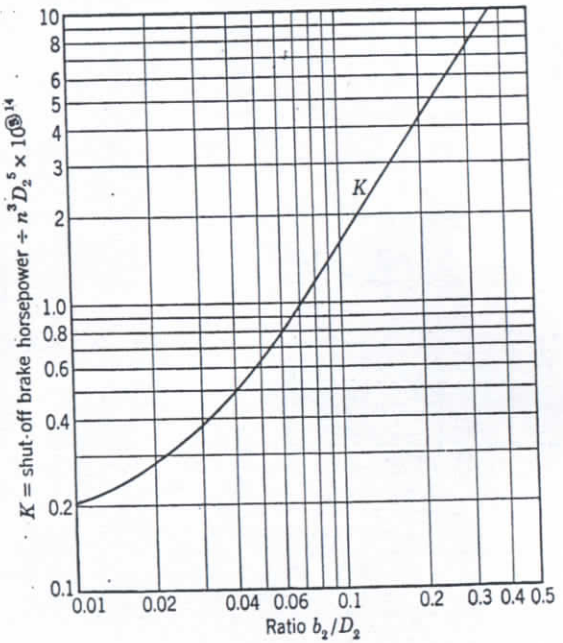

FIG. 10.13. Shut-off brake horsepower versus b_2/D_2 (Mockridge [9]).

capacities lower than normal. These power losses cannot be hydrauli losses because then the hydraulic efficiency would be too low, or th input head H_i too high; in fact H_i would be higher than u_2^2/g, whic is an absurdity. These unaccounted-for losses of power could not b an error in calculation of disk, mechanical, or leakage losses, as the would be out of proportion. *Thus it is necessary to assume another lo of power which is zero at the b.e.p. and increases toward zero capacit This loss of power is caused by the exchange of momentum of liquid part cles in the impeller passages at the periphery with those in the volute casi moving with much lower velocities. It is somewhat similar to the disk fri*

tion losses. It is believed that a major part of this loss is caused by recirculation of the high pressure liquid from the leading face of the vane into the low pressure zone near the underside of the vane, thus again absorbing energy from the impeller and losing it on the next drop from the high pressure face of the vane into the low pressure zone. Wide impellers and a small number of vanes waste more power by recirculation, thus increasing the brake horsepower near zero capacity. Mockridge [9] has plotted

$$\frac{\text{bhp at shut-off} \times 10^{14}}{n^3 D_2{}^5} \text{ versus } \frac{b_2}{D_2}$$

to study the trend of variation of brake horsepower at zero capacity as a function of specific speed or b_2/D_2 (Fig. 10.13). As the specific speed approaches zero the brake horsepower is approaching the disk friction loss.

Existence of a recirculation loss was realized by Daugherty [10] and called a churning loss. Pfleiderer also mentions the recirculation loss in his book.[11] No formulas have been offered to express the recirculation loss in terms of known variables.

(*a*) Remarks on Losses in Centrifugal Pumps. In reviewing the progress in design and improvements in efficiencies of centrifugal pumps in the course of the last two decades, the following factors can be pointed out, in the order of their importance, as being responsible for the improvements in performance.

1. Use of more favorable specific speed types to meet a given set of conditions. Factors contributing to this step were the use of high speed motors (3600 rpm or higher), an increasing demand for higher capacities in every field, and the splitting up of the head into a greater number of stages. Increased size and brake horsepower of pumps increased the importance of efficiency, thus permitting more expensive patterns and manufacturing procedure.

2. A general perfection of the hydraulic design of all types of pumps, accomplished primarily through better streamlining of all parts taking part in the generation of head (this becomes apparent by a comparison of catalog cuts of 20 years ago with modern sectional drawings), and secondly through establishing optimum proportions of various pump passages, or velocity ratios, to obtain a maximum efficiency at the desired point. Elimination of cavitation by better design is an important factor contributing to a better initial and sustained efficiency.

3. Increased competition and importance of high efficiency, which demanded better manufacturing methods.

To obtain optimum efficiency, clean and smooth liquid passages are absolutely essential. Since a part of the casing and most of the impeller passages are not accessible for cleaning, the importance of a good quality of castings cannot be overemphasized. In small sizes, cleaning of the volute passages alone may show a difference of two to four points in efficiency. In the more competitive line of vertical deep-well turbine pumps, porcelain enameling on the cases and impellers (cast iron) is in wide use. The gain in efficiency due to porcelain enameling of cases varies from two to three points and is dependent on the size and the specific speed. Porcelain coating of open impellers has little advantage over polishing, as all surfaces are accessible for cleaning. But with closed impellers, particularly of low specific speed (say 1500), the efficiency gain is about two points. Porcelain enameling is less advantageous with volute casings than with diffusion casings of vertical turbine pumps because of the accessibility for cleaning and relatively greater areas of passages. On a 3- or 4-in. pump this gain in efficiency may be about one point. Enameling of volute cases is not practiced commercially.

10.5 OPEN IMPELLER DESIGN

The introduction of open impeller construction in recent years was one of the major design features contributing to the improvement of performance of medium and high specific speed pumps. In addition to having hydraulic advantages, open impellers are capable of handling suspended matter with a minimum of clogging, and they permit restoration of the running clearance between the impeller vanes and the stationary casing, thus maintaining the original efficiency. The impeller passages are accessible for cleaning, and the manufacturing cost is lower.

The improvement in efficiency of the open impeller design results from reduction of disk friction loss by elimination of the front shroud. Hydraulic friction loss through an open impeller changes little or not at all. In a closed impeller there is friction loss due to the flow relative to the inner side of the outer shroud proportional to $w_2{}^2/2g$, where w_2 is the relative velocity through the impeller. In open impellers this loss is absent but, instead, there appears a hydraulic friction loss against a stationary casing wall while liquid is passing the impeller channel enclosed between two adjacent vanes. This loss is proportional to $c_2{}^2/2g$, where c_2 is the absolute velocity of flow through the impeller. For high specific speed pumps these two items approximately balance each other; thus the reduction in disk friction loss is a net gain. Omission of the front shroud improves the gross efficiency about two points for medium specific speed pumps (2500 to 6000). Kaplan [12] gives a gain in efficiency

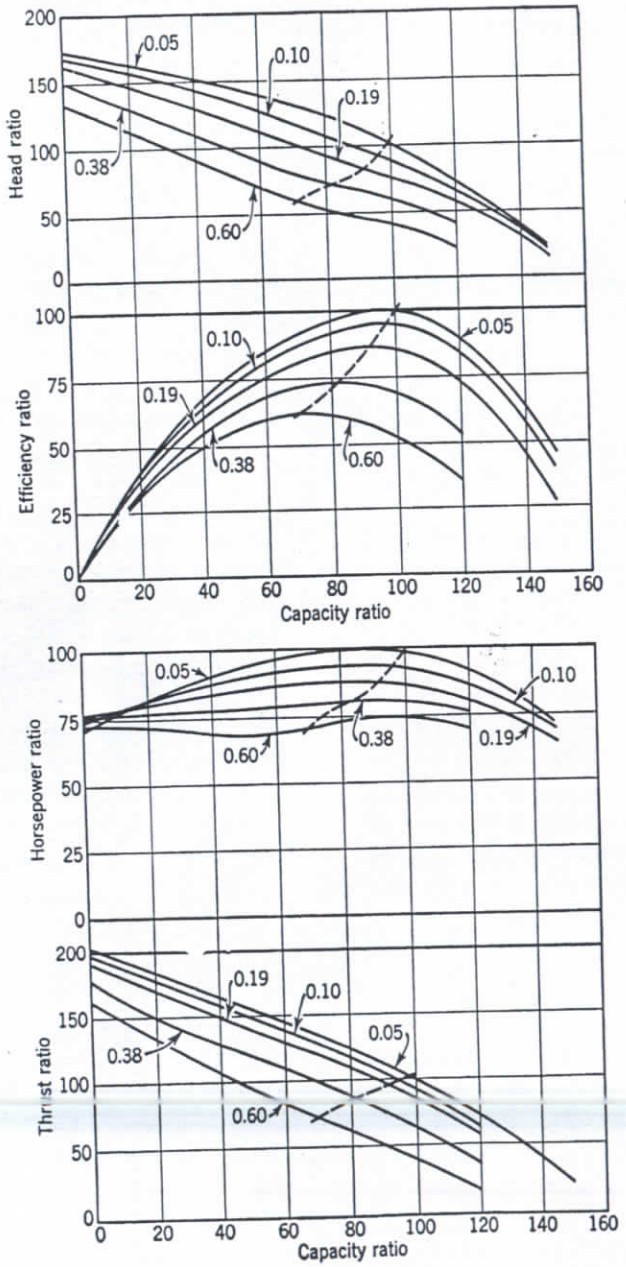

FIG. 10.14. Effect of clearance on the performance of open-impeller vertical turbine pumps (Folsom [13]).

for axial propeller turbines with shrouds removed five to ten points. By removing the front shroud the leakage through the wearing rings is eliminated, but instead leakage from the front side to the back side of impeller vanes is introduced. It is believed that the latter loss is no higher than the normal leakage loss of closed impellers, provided a minimum running clearance is maintained. If clearance is increased, the head, capacity, efficiency, and brake horsepower are reduced. Figure 10.14, obtained by Folsom,[13] shows the effect of the clearance on the pump performance. The clearances are given as ratios of clearance to the impeller width b_2. The rest of variables are given as percentages of the values at b.e.p. The decrease of brake horsepower obtained with increased clearance indicates that the impeller vanes at the open edge are not fully loaded. Note that the minimum clearance shown in Fig. 10.14 is about 0.020 in., which is excessive for normal operation.

REFERENCES

1. L. F. Moody, "Friction Factors for Pipe Flow," *Trans. A.S.M.E.*, Vol. 66, No. 8, p. 671, November 1944.
2. E. Schneckenberg, "Der Durchfluss durch Drosselspalte," *Z. Ver. deut. Ing.*, Vol. 74, p. 485, 1930.
3. A. J. Stepanoff, "Leakage Loss and Axial Thrust in Centrifugal Pumps," *Trans. A.S.M.E.*, p. 65, Aug. 15, 1932.
4. E. J. Blackwell and M. L. Murdock, "Leakage in High Pressure Centrifugal Boiler Feed Pumps," Allis-Chalmers Eng. *Bull.* B-6158, Current Trends No. 6, 1941.
5. A. H. Gibson, *Hydraulics and Its Application*, p. 186, New York, D. Van Nostrand Company, 1925.
6. Joseph N. LeConte, *Hydraulics*, p. 332, New York, McGraw-Hill Book Company, 1934.
7. F. Schultz-Grunow, "Der Reibungswiderstand rotierender Scheiben in Gehäusen," *Z. Angew. Math. Mech., Bull.* 4, Berlin, Verein Deutscher Ingenieure, pp. 194–204, July 1935.
8. C. Pfleiderer, *Die Kreiselpumpen*, p. 99, Berlin, Julius Springer, 1955.
9. C. R. Mockridge, discussion of "Centrifugal Pump Performance as a Function of Specific Speed," by A. J. Stepanoff, *Trans. A.S.M.E.*, p. 642, August 1943.
10. R. L. Daugherty, *Centrifugal Pumps*, p. 76, New York, McGraw-Hill Book Company, 1915.
11. C. Pfleiderer, *Die Kreiselpumpen*, p. 64, Berlin, Julius Springer, 1932.
12. Victor Kaplan and Alfred Lechner, *Theorie und Bau von Turbinen-Schnellläufern*, p. 142, Berlin, R. Oldenbourg, 1931.
13. R. G. Folsom, "Some Performance Characteristics of Deep-Well Turbine Pumps," *Trans. A.S.M.E.*, Vol. 63, No. 3, p. 245, April 1941.
14. E. Becker, "Strömungsvorgänge in ringförmigen Spalten," *Z. Ver. deut. Ing.*, Vol. 51, pp. 1133–1141, 1907.
15. M. D. Aisenstein, "Construction Details Need to be Considered in Choosing Suitable Centrifugal Hot Oil Pumps," *Oil Gas J.*, Vol. 32, pp. 49–50, April 5, 1934.

Chapter 11

Axial Thrust

11.1 SINGLE-STAGE PUMPS

(a) Balancing Axial Thrust. A double-suction impeller is balanced for axial thrust due to symmetry. If this balance is not destroyed by an unsymmetrical impeller approach, there really is no need for a thrust bearing. Older-type, slow speed, low head pumps were fitted with only a thrust collar to locate the rotating element axially. All modern double-suction pumps have a small thrust bearing to take care of any possible accidental thrust.

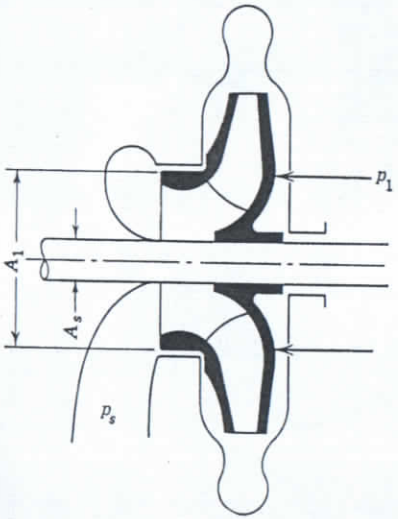

FIG. 11.1. Axial thrust on a single-suction impeller.

Single-suction impellers (Fig. 11.1) are subjected to an axial thrust because the area opposite the impeller eye is under suction pressure at the front of the back shroud and under discharge pressure at the rear of the back shroud. The magnitude of the axial thrust can be calculated from

$$T = (A_1 - A_s)(p_1 - p_s) \quad (11.1)$$

where T is the axial thrust in pounds.

A_1 is the area corresponding to the diameter D_r of the impeller wearing ring in square inches.

A_s is the area of the shaft sleeve through the stuffing box, in square inches.

p_s is the suction pressure in pounds per square inch.

p_1 is the pressure on the back shroud at diameter D_r in pounds per square inch.

The pressure difference $(p_1 - p_s)$ is less than the total head of the pump because the liquid behind the impeller is in rotation. It is more accurately expressed as $H_L/2.31$, where H_L is determined as shown in Chapter 10, equation 10.5. This can be assumed to be uniform over the whole unbalanced area. The actual thrust is somewhat less than the value given by equation 11.1, the reduction being caused by the change in momentum of the flow through the impeller eye, which in a straight centrifugal pump makes a 90° turn at this point. The opposing force is equal to

$$F = \frac{W}{g} c_1 = A_e {c_1}^2 \frac{\gamma}{g} = 2A_e\gamma \frac{{c_1}^2}{2g} \quad (11.2)$$

where A_e is the net impeller eye area, and c_1 is the meridional velocity through the impeller eye. When the axial thrust can be safely carried by a thrust bearing, this is the most efficient way to take care of it. Otherwise some means should be provided to reduce the thrust on the bearing. This can be done only at the expense of the pump efficiency.

One of two methods is usually employed to reduce or eliminate axial thrust in single-stage pumps. In the first a chamber on the back of the impeller is provided with a closely fitted set of wearing rings, and suction pressure is admitted to this chamber either by drilling holes through the impeller back shroud into the eye (Fig. 2.2) or by providing a special channel connecting the balancing chamber to the suction nozzle.

In the second method, radial ribs are used on the back shroud to reduce the pressure in the space between the impeller and the pump casing. *It is evident that the first method doubles the leakage loss of the pump which, in turn, increases as wearing rings are worn. The second method requires some additional power which, however, does not change with time. In addition it is cheaper and more effective than the first method. It will be shown later that this method requires no more power than is lost through leakage under normal conditions.*

The use of drilled holes through the impeller shroud to the balancing chamber is inferior to the arrangement using a special channel to connect the balancing chamber with the suction nozzle because leakage through the holes is directed against the flow in the impeller eye, causing disturbances. *The balance by this method is never complete. From 10 to 25 per cent of the axial thrust always remains, depending on the size of the holes.*[1] *For a complete balance the diameter of the wearing rings of the balancing chamber should be greater than that at the impeller eye.*

The axial thrust depends on the pressure distribution in the space between the impeller shrouds and the stationary casing walls. The pressure distribution depends in turn on the clearance between the

shrouds and the casing walls. These clearances are made small in special pumps handling solids in suspension, such as dredge pumps, to keep solids from these spaces. To promote circulation between the shrouds and casing, radial ribs are attached to both front and back shrouds. The axial thrust can be reduced or reversed by reducing the clearances between the back shroud and the casing and increasing the clearance between the front shroud and the casing.[2]

Modern pumps are made with ample clearance between the casing and the impeller so that if the impeller is placed ⅛ or ¼ in. from the plane of symmetry of the casing no appreciable axial thrust appears.

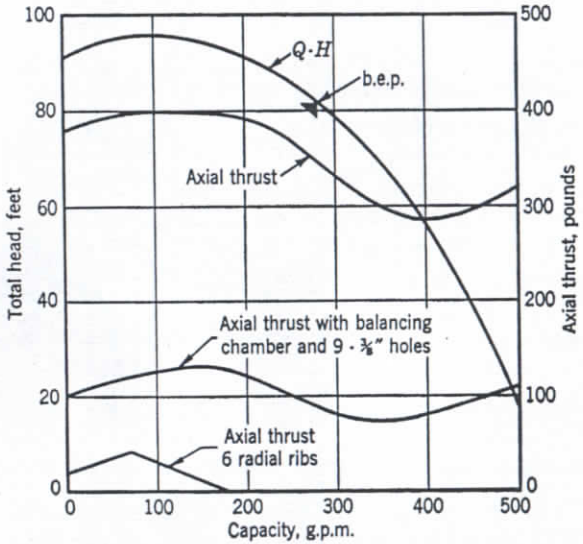

80-200 @ 2000 RPM

FIG. 11.2. Axial thrust; 3-in. pump, 2000 rpm, 8½-in. impeller, 4⅛-in. diameter of wearing ring.

The author has run extensive tests covering axial thrust measurements on horizontal single-stage and multistage pumps, complete report of which is given in reference 1. Figure 11.2 shows one typical test curve giving values of axial thrust for an unbalanced impeller, for an impeller with a balancing chamber on the back shroud using nine ⅜-in. holes through the impeller web, and for an impeller with radial ribs on the back of the impeller. In the latter case the thrust was reversed before the b.e.p. was reached.

The reason for the increase of axial thrust at capacities above normal is not entirely clear. Similar thrust curves were obtained by several investigators.[3] It is likely that at high capacities the heads produced

along the outer and inner shrouds are not equal, and this inequality produces different pressures in the volute and between the impeller shrouds and the casing walls. High velocities through the 90° turn in the impeller eye may also cause such conditions. Local cavitation at the impeller entrance may be another contributing factor. Vertical turbine pumps, with open or closed impellers, never show an increase of axial thrust at high capacities.

(b) Balancing with Radial Ribs. Figure 11.3 shows the pressure distribution between the impeller shrouds and the casing walls for an impeller with radial back ribs. All pressures are taken above the suction

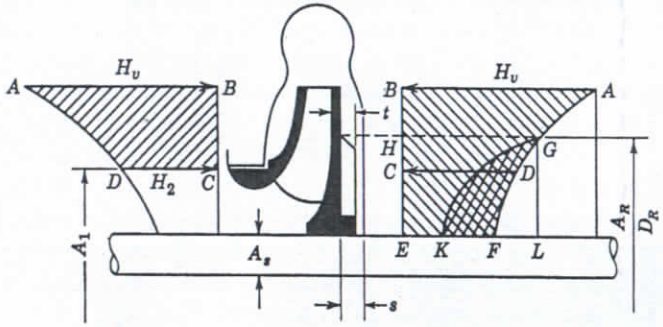

FIG. 11.3. Balancing axial thrust with radial ribs.

pressure. The axial forces on the impeller shrouds are represented by volumes enclosed by the surfaces of revolution *ABCD* on the front shroud and *ABEF* on the back shroud. The unbalanced axial thrust on the back shroud T_b is equal to the volume *CDEF*, which is expressed by

$$T_b = (A_1 - A_s)\left(H_L - \frac{1}{8}\frac{u_r^2 - u_s^2}{2g}\right)\gamma \approx (A_1 - A_s)\gamma H_L \quad (11.3)$$

where u_r is the peripheral velocity at the impeller wearing ring diameter, and u_s is the peripheral velocity at the shaft sleeve diameter. For practical purposes the head H_L can be assumed to act over the whole unbalanced area $(A_1 - A_s)$. The pressure distribution in the space between the impeller shrouds is based on the assumption that the angular velocity of rotation of the liquid in this space is equal to one half that of the impeller. This has been confirmed by Schultz-Grunow (reference 7, Chapter 10) and the author's own tests.[1] To balance the axial thrust T_b (equation 11.3), radial ribs are provided on the back shroud. With these ribs closely fitted to the casing walls the liquid will rotate approximately with full impeller angular velocity. This will

further reduce the pressure on the impeller back shroud over the area A_R, determined by the diameter of the radial ribs D_R. The reduction of the axial forces on the back shroud is given by the volume *GFKG* (Fig. 11.3, double cross-hatched) which is the difference of volumes of the two paraboloids *GKL* and *GFL*. Note that the volume of a paraboloid is equal to one half the volume of a cylinder of the same base and height.

$$T_{bR} = (A_R - A_s)\left(\frac{HG + EF}{2} - \frac{HG + EK}{2}\right)\gamma$$

$$= (A_R - A_s)\left(\frac{EF - EK}{2}\right)\gamma$$

$$= \frac{A_R - A_s}{2}\left[\left(H_v - \frac{1}{4}\frac{u_2^2 - u_s^2}{2g}\right) - \left(H_v - \frac{u_2^2 - u_R^2}{8g} - \frac{u_R^2 - u_s^2}{2g}\right)\right]\gamma$$

$$T_{bR} = \frac{3}{8}(A_R - A_s)\left(\frac{u_R^2 - u_s^2}{2g}\right)\gamma \qquad (11.4)$$

For a complete balance, $T_b = T_{bR}$. From this relationship the diameter of radial ribs can be determined. If radial ribs do not fit closely to the casing wall the angular velocity of the liquid in the space between the back impeller shroud and the casing will be lower than the impeller angular velocity ω, but higher than $\omega/2$. It can be assumed, approximately, that the angular velocity of the liquid can be represented by the relationship

$$\omega' = \frac{\omega}{2}\left(1 + \frac{t}{s}\right) \qquad (11.5)$$

where s is the average distance between the casing wall and the impeller back shroud and t is the height or thickness of the radial ribs (Fig. 11.3). The number of ribs varies from four for small pumps to six for large pumps.

Frequently, radial ribs are used to reduce pressure on the stuffing box. Following the same procedure, an expression can be developed for the pressure at the stuffing box (H_{sR} feet) represented by *EK* in Fig. 11.3.

$$H_{sR} = H_v - \frac{\text{rpm}/1000}{13.55}\left[D_2^2 - D_R^2 + \left(\frac{s + t}{s}\right)^2\left(D_R^2 - D_s^2\right)\right] \qquad (11.6)$$

where D_s is the shaft or sleeve diameter through the stuffing box. All diameters are in inches. Equation 11.6 applies to the b.e.p. The power absorbed by radial ribs varies as the square of the rib outside diameter and is directly proportional to the rib height (t).

For overhung impeller pumps there is an additional thrust component in a direction opposite to the impeller suction equal to the suction pressure p_s times the area of the sleeve through the stuffing box (A_s).

$$T_s = p_s A_s$$

Thus for overhung impeller pumps the diameter of the balancing ribs depends on the suction pressure.

11.2 MULTISTAGE PUMPS

(a) Balancing Axial Thrust. The problem of axial thrust becomes more important when dealing with multistage pumps because of the higher pressures involved and the combined thrust of several stages. Several methods are used to balance axial thrust in multistage pumps: (1) impellers with even numbers of stages may be arranged in two opposing groups (Fig. 11.7); (2) individual stages may be balanced by providing balancing chambers on the back of each impeller but this method is seldom used for modern pumps; (3) double-suction impellers may be used in all stages; (4) special balancing devices such as the automatic balancing disk and balancing drum may be used.

The automatic balancing disk operates on the following principle. All impellers are faced in the same direction (Fig. 11.4). On the back of the last-stage impeller a balancing chamber, connected through a throttle A to the first-stage suction, is formed. The balancing disk C is of larger diameter than the impeller wearing rings. The rotating element is free to move axially. Axial thrust tends to move the disk to the left, thus closing the gap between the disk and a stationary face B. This reduces the pressure in the balancing chamber behind disk C. At the same time the full pump pressure will move disk C to the right until a perfect balance is reached. The amount of leakage is controlled by the throttle A. When this is worn, the gap between the disk C and the face B increases in order to maintain the required pressure on the back of the disk.

To protect the disk C and face B from damage under any possible condition a spring-loaded bearing keeps the faces apart about $\frac{1}{32}$ in. when the pump does not develop full pressure. Under normal conditions the spring permits the rotating element to float freely with only a slight increase in pressure to overcome the spring tension. The calcu-

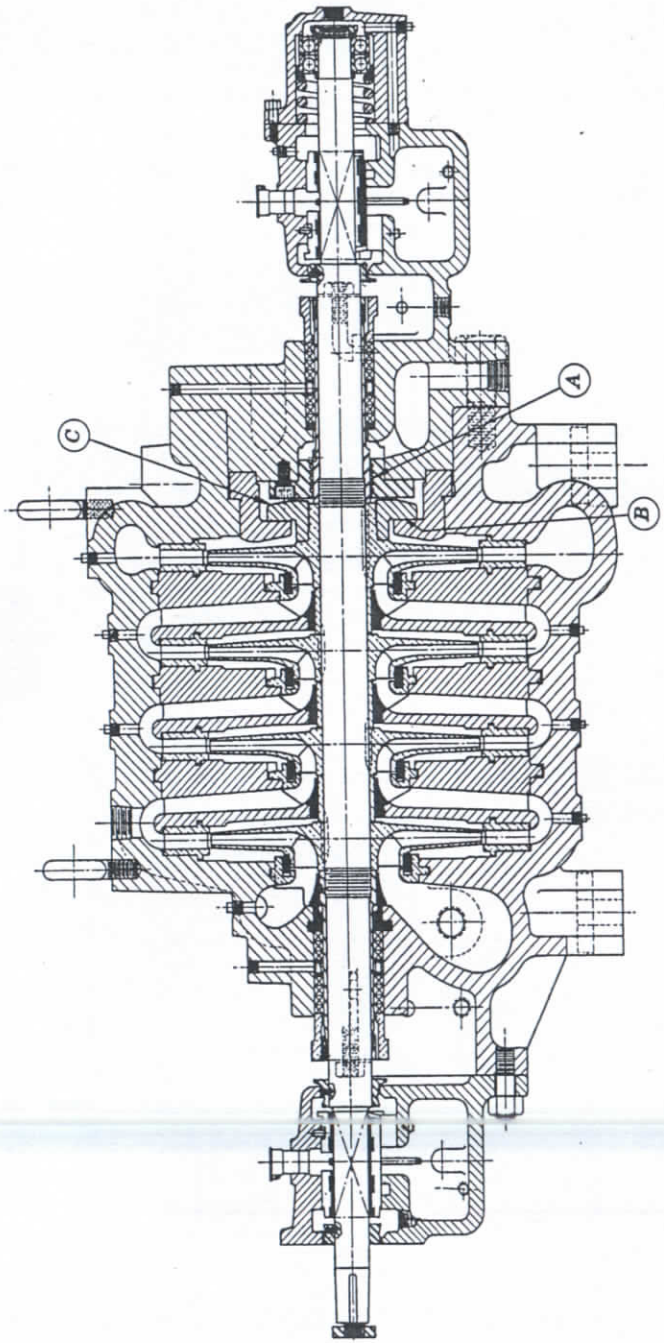

FIG. 11.4. DeLaval boiler feed pump with automatic balancing disk.

lation of the amount of leakage past the balancing disk is complicated by the uncertainty of actual clearances and pressures controlling the leakage. However, the leakage can easily be measured.

Figure 17.9 shows a combination of a balancing drum and an automatic balancing disk. It works on the same principle as the one described except that the fixed throttle is arranged ahead of the automatic

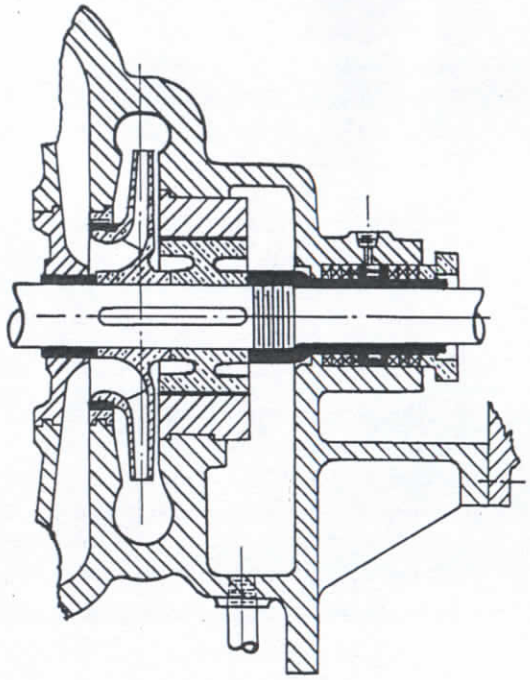

FIG. 11.5. Balancing drum, not used on modern pumps; widely used on multistage centrifugal blowers.

disk throttle. *The pressure ahead of the disk is fixed by the amount of unbalanced axial thrust, and when the auxiliary throttle becomes worn the disk gap increases in order to maintain the required pressure at the disk, thus increasing the amount of leakage. In every case the total pressure through the balancing device is split up by automatic throttle in the same ratio to balance the same axial thrust.*

When a balancing drum alone is used, the axial thrust is eliminated or reduced to the extent that it can be safely carried by the thrust bearing by means of a low pressure balancing chamber on the high pressure end of the pump (Fig. 11.5). This is separated from the last-stage casing by a drum closely fitted into the stationary casing bushing. Full

pump pressure acts on the drum and gives a force essentially equal to the axial thrust of all the impellers. The amount of leakage through the drum increases with drum and bushing wear. Normal leakage is 2 to 3 per cent. The balancing drum alone is seldom used on modern pumps.

(*b*) **Thrust Due to Shaft Shoulders and Impeller Hubs.** *Multistage pumps having impellers arranged in two opposing groups are balanced for axial thrust only if the pumps have two stuffing boxes, if the shaft is of a constant diameter throughout the pump, and if the impeller hubs do not extend through the casing walls separating two adjacent stages.* Modern high pressure, high speed pumps usually have shafts which are heavier in the middle portion, and the impeller hubs frequently extend through the casing walls of two adjacent stages. This produces considerable axial thrust. Figure 11.6 shows diagrammatically the principle involved. The thrust direction is indicated on this figure as well as the method of calculating the thrust.

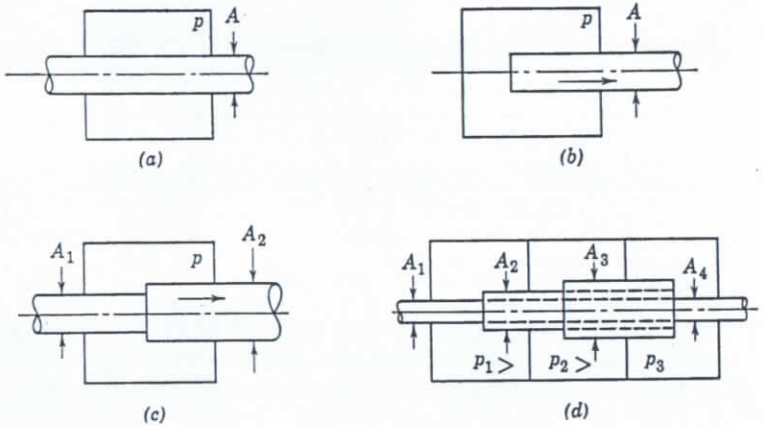

FIG. 11.6. (*a*) Axial force $T = 0$; (*b*) $T = pA$; (*c*) $T = p(A_2 - A_1)$; (*d*) $T = (p_1 - p_3)(A_2 - A_1) + (p_2 - p_3)(A_3 - A_2)$; direction of T is to the right.

Now consider as an example a four-stage pump with impellers arranged as in Fig. 11.7. The following notation will be used in this discussion:

p_s = suction pressure
p_1 = volute pressure in the first stage $= p_s + p$ where p is the pressure produced by one stage
p_2 = volute pressure in the second stage $= 2p + p_s$
p_3 = volute pressure in the third stage $= 3p + p_s$
p_4 = volute pressure in the fourth stage $= 4p + p_s$

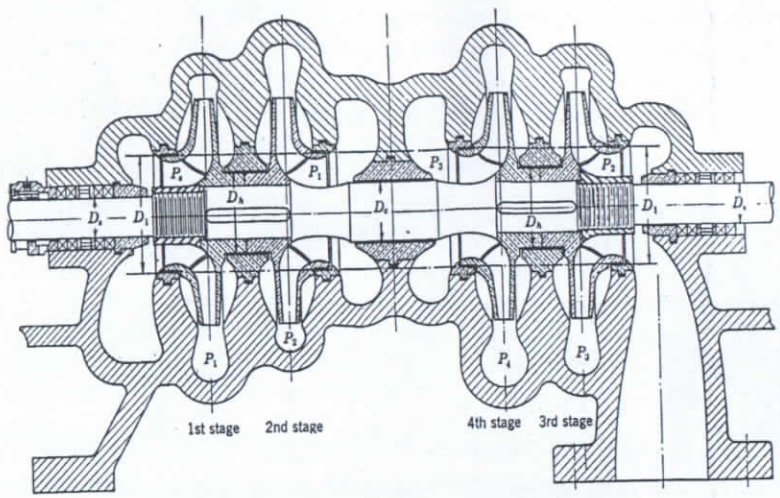

FIG. 11.7. Four-stage pump. Axial thrust due to shaft shoulders and impeller hubs.

D_s = diameter of shaft or shaft sleeve at the stuffing box, equal on both sides
D_h = impeller hub diameter
D_c = shaft diameter at the center
D_1 = impeller wearing ring diameter
A_1, A_s, A_h, A_c = areas of the circles corresponding to diameters D_1, D_s, D_h, and D_c

All pressures are in pounds per square inch and areas are in square inches.

Assume that the pressures in the clearances between the pump case and the impeller shrouds are uniform and equal to that of the corresponding volute pressure. Assume also that the suction pressure of the third stage is the same as the discharge pressure of the second, and so on. These assumptions do not affect the final result, since there is always a one-stage pressure difference p between two similar points in two successive stages.

It is evident that the pressures on both sides of the impeller shrouds from Diameter D_2 to diameter D_1 are equal and balanced. Consider now the pressures on each impeller after exclusion of the areas between D_2 and D_1. Call pressures to the left positive, those to the right negative. Then the forces on the rotating element are:

$$(A_1 - A_h)p_1 - (A_1 - A_s)p_s = \text{first-stage thrust}$$

$$(A_1 - A_c)p_1 - (A_1 - A_h)p_2 = \text{second-stage thrust}$$

$$(A_1 - A_h)p_4 - (A_1 - A_c)p_3 = \text{fourth-stage thrust}$$

$$(A_1 - A_s)p_2 - (A_1 - A_h)p_3 = \text{third-stage thrust}$$

The axial thrust is equal to the sum of these forces. Adding and rearranging,

$$T = A_1(2p_1 + p_2 + p_4 - p_s - p_2 - 2p_3) + A_h(p_2 + p_3 - p_4 - p_1) + A_s(p_s - p_2) + A_c(p_3 - p_1)$$

Substituting for p_1, p_2, p_3, and p_4 their values ($p + p_s$, and so on) and reducing,

$$T = 2p(A_c - A_s) = 2p(D_c^2 - D_s^2)0.785 \qquad (11.7)$$

It is seen that, owing to symmetry, D_1 and D_h do not appear in the final result. The whole system can be represented diagrammatically as equivalent to the simple case shown in Fig. 11.8. This result holds

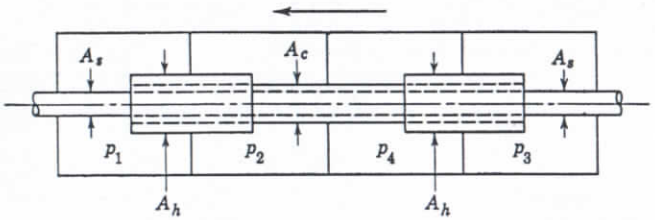

FIG. 11.8. Diagram of a four-stage pump. Axial thrust $T = (p_3 - p_1)(A_c - A_s)$.

for the arrangement of stages as shown (1, 2, 4, 3), which gives a minimum thrust.

To obtain an idea of the magnitude of the thrust produced in this way, take a numerical example. A 4-in. four-stage pump with an arrangement of stages like that in Fig. 11.7 and developing 100 psi per stage has the dimensions: $D_s = 1\frac{3}{4}$ in., $D_h = 3\frac{1}{4}$ in., and $D_c = 2\frac{5}{8}$ in. Substituting these values in equation 11.7, we get

$$T = 2 \times 100 \times 0.785[(2.625)^2 - (1.75)^2] = 597 \text{ lb}$$

In a multistage pump with one stuffing box and one internal bearing there is a thrust due to the pressure acting on the end of the closed shaft. This should be added to the thrust caused by shoulders on the shaft and impeller hubs. Suppose that, in the pump shown in Fig. 11.7, the right-hand stuffing box is replaced by a closed bearing. The pressure on this end of the shaft is $2p$, the area is A_s, and the additional thrust is

$$T' = p_2 A_s = A_s(2p + p_s) \qquad (11.8)$$

When p_s is equal to atmospheric pressure,

$$T_1 = 200 \times 0.785 \times (1.75)^2 = 480 \text{ lb}$$

From equation 11.8 it is seen that the thrust due to an internal bearing depends on the suction pressure on the first stage. Thus thrust increases as the suction pressure increases, and it may reach a high value if the pump is operating under a considerable positive head (for instance, if two pumps are working in series). The main object of pumps with one stuffing box is elimination of the high pressure stuffing box. The thrust due to this cause is always toward the first-stage suction, or in the same direction as the thrust due to shoulders on the shaft. The thrust on the enclosed shaft end may be reduced or eliminated by using an uneven number of stages and grouping them so that the thrust caused by one stage will balance that caused by the enclosed bearing.

Thrust due to shaft shoulders and impeller hubs can be balanced by making the hubs of different diameters and such that the resulting force opposes the axial thrust of the impellers. Thus, for example, if we assume that the impeller hubs on stages three and four are made larger than those on stages one and two (Fig. 11.7), and if we let D_{h1} denote the diameter of the impeller hubs for stages one and two and D_{h2} the diameter of the impeller hubs for stages three and four (A_{h1} and A_{h2} denoting the corresponding areas), we can repeat the calculations with these changes, and the following expression is obtained for the axial thrust.

$$T = 2p(A_c - A_s) - p(A_{h2} - A_{h1}) \qquad (11.9)$$

By equating the thrust to zero, we get:

$$2(A_c - A_s) = A_{h2} - A_{h1} \qquad (11.10)$$

For the same values of A_c and A_s, $D_{h1} = 3\frac{1}{4}$ in., A_{h2} is equal to 14.3 sq in., or $D_{h2} = 4.27$ in.

Axial thrust due to shaft shoulders and impeller hubs can be eliminated by making impeller ring diameters D_r, or impeller diameters D_2 (and stage pressure p) different for several stages, but both of these methods have several objections from a practical point of view.

Figures 11.9 and 11.10 show tests run by the author on a 4-in. four-stage pump, described in the above examples. The test proves the effectiveness of the described balancing method.

Equation 11.7 is based on the assumption that each stage develops the same pressure and that the balance should hold at all capacities. Figures 11.9 and 11.10 show that this is not true in practice. The discrepancy is caused by the inequality of stage pressures for different stages; apparently the difference varies with capacity.

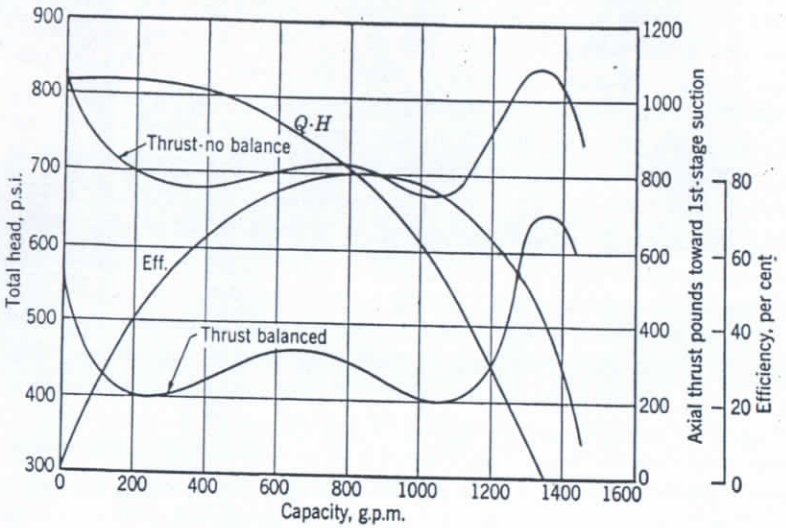

FIG. 11.9. Four-inch four-stage pump, 3560 rpm, suction pressure 60 psi.

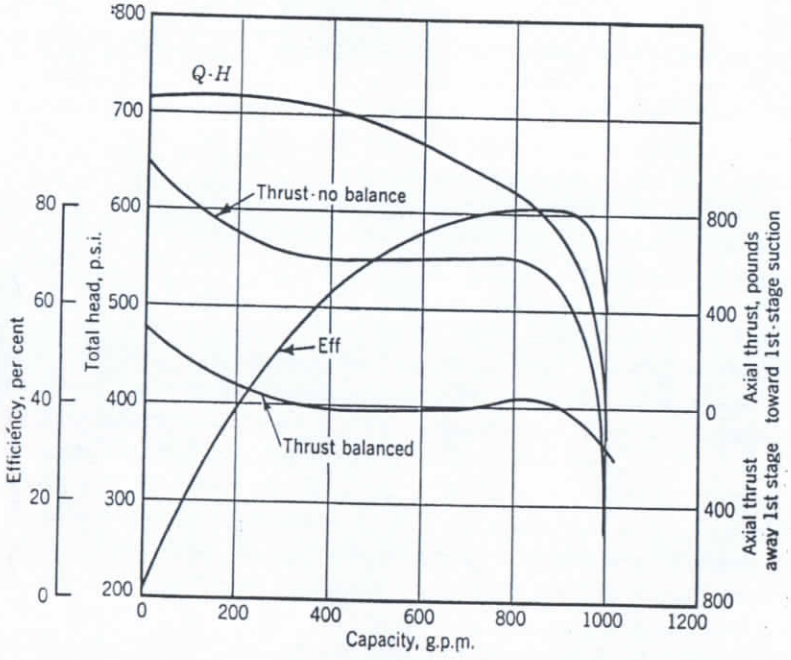

FIG. 11.10. Four-inch four-stage pump, 3560 rpm, suction lift 10 ft.

Interstage leakage is the principal cause of the difference in stage pressures in multistage pumps; it results in axial thrust with the opposed impeller arrangement. In general, with increasing leakage (worn wearing rings), the head drops for a given capacity. Because of interstage leakage across two adjacent stages, the head produced by the high pressure stage is lower than that produced by the low pressure stage. This follows from the fact that, for a measured pump capacity Q, the low pressure stage impeller capacity is $Q_1 = Q + Q_L$, where Q_L is the leakage

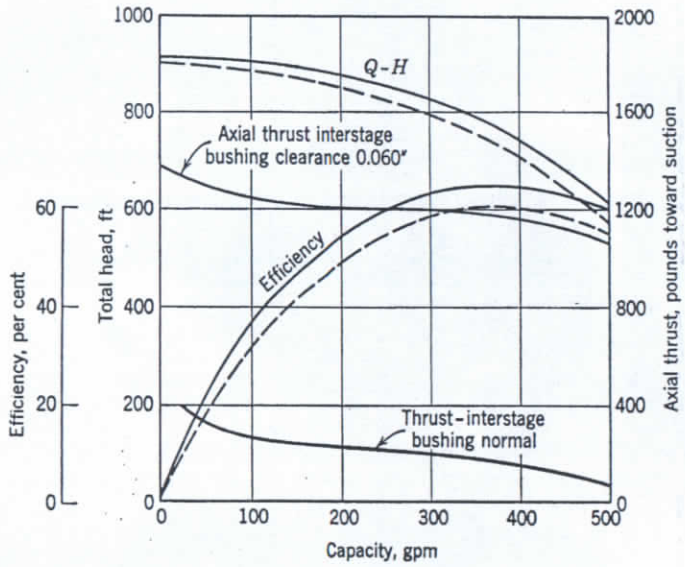

FIG. 11.11. Axial thrust due to interstage leakage; 2-in. two-stage pump, 3500 rpm, back-to-back impellers.

through the wearing rings. At the same time the high pressure stage impeller capacity is $Q_2 = Q + Q_L + Q_i$, where Q_i is the interstage leakage circulating between the high pressure and the low pressure casings. But since both impellers have identical head-capacity characteristics, the high pressure impeller working at a higher capacity will produce a lower head than the low pressure impeller.

Figure 11.11 shows a test of a 2-in. two-stage pump with normal and worn interstage clearances. The axial thrust increased about six times because of the increased interstage leakage.

Any difference in the leakage through the wearing rings at the impeller eye leads to a difference in head of individual stages and, hence, unbalance of axial thrust. When the pump handles capacities above normal under limited suction head, cavitation may set in at the first-

stage impeller, and thus reduce the head produced by this stage and upset the axial thrust balance. A displacement of impellers from the central position in their respective volute cases may be a contributing factor to the unaccounted-for axial thrust of multistage pumps with opposed impellers. Because none of the above causes of hydraulic thrust can be determined with certainty, a thrust bearing is always provided in multistage pumps with opposed impellers.

(*c*) **Condensate Pumps.** Pumps working under very low submergence, such as hot-well or condensate pumps, may be required to operate under a head considerably lower than normal, depending on the amount of liquid coming into the pump and the characteristics of the discharge system. In Fig. 11.12, assume that AB is the normal head-capacity characteristic and that CD is the discharge system curve. Point E is the normal operating point when sufficient submergence is available. When the rate of flow to the pump suction is reduced the submergence will fall, cavitation will set in, and the head-capacity curve will break off suddenly. The operating points will remain on curve CD. At point G the pump total head is less than the normal head for this capacity. *If the pump is a two-stage pump with two opposing single-suction impellers, the entire head GH will be produced by the second stage, as this stage is under discharge pressure from the system and is capable of maintaining this pressure alone without the aid of the first stage.* The first stage will produce no head. Therefore the axial balance will be destroyed. Since most condensate pumps are low speed with the large impellers, this unbalance may ruin the thrust bearing selected for normal operating conditions. Automatic liquid level controls will overcome this by maintaining the operating point on the normal characteristic. In this set-up the discharge valve is controlled by a float in the suction receiver which causes the valve to throttle as the liquid level tends to lower, thus changing the system characteristic to CJ or CK. The pump will operate at the intersection of such curves with the normal pump head-capacity curve. If both stages have double-suction impellers, no undue thrust develops under cavitation. Figure 11.13 shows a three-stage horizontal condensate pump with a double-suction first-stage impeller and two single-suction impellers for the second and third stages. These pumps are free from undue axial thrust under all load conditions. Two-stage condensate pumps are built with a double-suction first-stage impeller

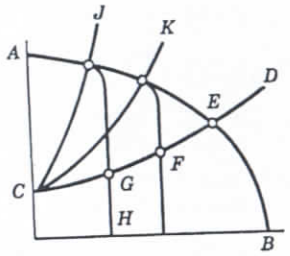

FIG. 11.12. Diagram of condensate pump performance.

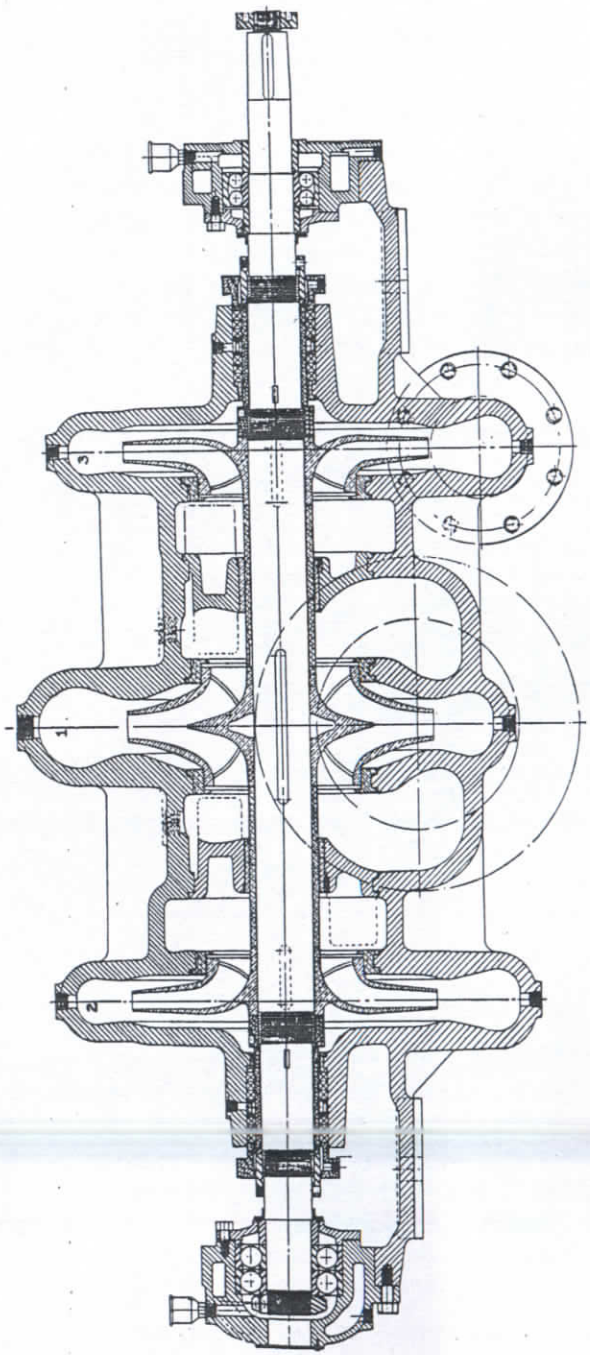

FIG. 11.13. Worthington three-stage condensate pump.

and two single-suction impellers in parallel for the second stage. In Chapter 16, condensate pumps of the vertical turbine type are described which have marked advantages over horizontal condensate pumps.

11.3 OPEN IMPELLERS

(a) Axial Thrust. Open impellers produce higher axial thrust than closed impellers. The thrust on the back shroud is only partly balanced by the pressure inside the impeller (Fig. 11.14). The thrust on the back shroud is given by equation 11.11.

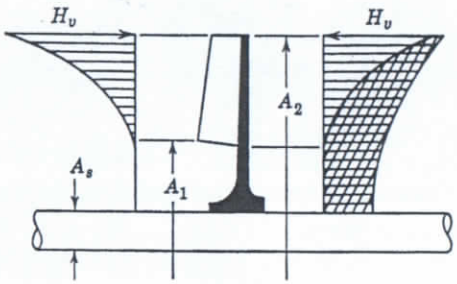

FIG. 11.14. Open impeller axial thrust.

$$T_b = (A_2 - A_s)\left[H_v - \frac{1}{8}\frac{(u_2^2 - u_s^2)}{2g}\right]\gamma \qquad (11.11)$$

The pressure inside the impeller is H_v at the periphery and the suction pressure at the diameter D_1. The thrust on the inside of the back shroud is

$$T_{bi} = (A_2 - A_1)\frac{H_v}{2}\gamma \qquad (11.12)$$

The net axial thrust is the difference between T_b and T_{bi} or

$$T = T_b - T_{bi}$$

$$= (A_2 - A_s)\left[H_v - \frac{1}{8}\frac{(u_2^2 - u_s^2)}{2g}\right]\gamma - (A_2 - A_1)\frac{H_v}{2}\gamma \qquad (11.13)$$

Radial ribs on the back shroud are the only practical means for the reduction of the axial thrust of open impellers. Multistage pumps with open impellers are always of the vertical turbine type, having impellers facing the same direction and the axial thrust taken up by the thrust bearing. Radial ribs are used to reduce the axial thrust if it is beyond the bearing capacity. However, this reduces the pump gross efficiency.

No accurate information is available on the power loss due to radial ribs. On tests of several vertical turbine pumps the author found that the pump gross efficiency dropped approximately two points when ribs were added on the back shrouds and the axial thrust was reduced to one half its normal value. The power loss due to ribs increases rapidly with the diameter of the ribs. Therefore, the rib diameter should be no greater than necessary to reduce the thrust by the desired amount.

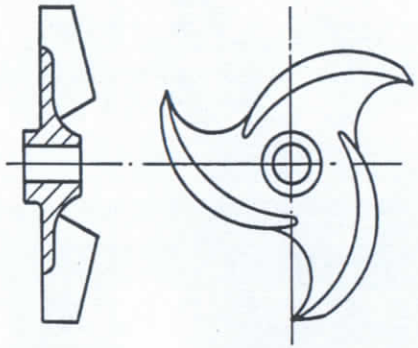

FIG. 11.15. Open impeller with back shrouds removed.

Single-stage pumps handling suspended material such as paper stock have impellers with part of the back shroud removed (Fig. 11.15). These impellers reduce the axial thrust and help impellers to clear themselves of stringy matters.

(b) Axial Thrust in Axial Flow Pumps. In radial impellers, open or closed, the axial thrust is produced by static pressure on the impeller shrouds, which do not take part in the generation of head. The flow takes place in a plane normal to the axis and the difference of pressure on the faces of impeller vanes does not contribute to the axial thrust. In axial impellers there are no shrouds, and the flow is in the axial direction; any difference in pressure on the two faces of the vanes register as axial thrust on the rotating element. There is also a small axial force due to the difference in pressure on the two faces of the impeller hub. The axial thrust of an axial flow impeller is equal to $T = A_e\gamma H/e_h$, where A_e is area of the annulus between the impeller hub and the casing, H is the total head of the pump in feet, γ is the specific weight of liquid, and e_h is the hydraulic efficiency. This expression can be obtained from the following consideration. The work per unit time done in lifting liquid by an axial impeller can be represented as Tc_1, where c_1 is the axial velocity and T is an axial force. This force is a liquid reaction on the impeller vanes and is equal to the axial thrust. On the other hand,

the same work per second is equal to the impeller input $Q\gamma H/e_h$. By equating the two we obtain the expression sought, or

$$Tc_1 = \frac{Q\gamma H}{e_h}$$

hence

$$T = \frac{Q}{c_1}\frac{\gamma H}{e_h} = \frac{A_e\gamma H}{e_h} \tag{11.14}$$

To this thrust T must be added a force due to the static difference in pressure on the two faces of the hub.

(*c*) **Axial Thrust in a Mixed Flow Pump.** Mixed flow impellers have axial thrust due to both vane dynamic action and static pressure on the impeller hub. The method of calculation thrust for axial flow pumps can be applied here also, but instead of the axial velocity c_1, the axial component of the meridional velocity $c_1 \cos\theta$ (Fig. 11.16) is used. The axial thrust due to static pressure on the impeller hub is greater than that in the axial flow pump. Note that there is an upward component of thrust due to pressure on the conical part of the hub. This is variable and is applied on area $(A_{h2} - A_{h1})$.

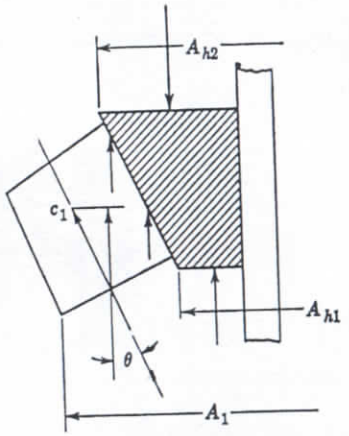

FIG. 11.16. Axial thrust on a mixed flow impeller.

For practical purposes great accuracy of thrust calculations is seldom required as there is always a thrust bearing to take care of the unbalanced thrust. For that reason simple experimental formulas are in use which permit quick thrust calculations. One of these has the form

$$T = A_e p K_t$$

where T is thrust in pounds, A_e is the impeller eye area in square inches, p is the total head in pounds per square inch, and K_t is an experimental factor which is equal to 1.0 for axial flow pumps and increases for mixed flow and radial impellers. The value of K_t for different specific speeds is given in Fig. 7.26.

In a vertical pump of the propeller or turbine type, when the hydraulic thrust is carried by the motor bearing, the thrust does not impose any load on the motor support in addition to the dead weight of the pump and the liquid in the column if the motor support is integral with the pump discharge column (Fig. 11.17). This is because the thrust is an

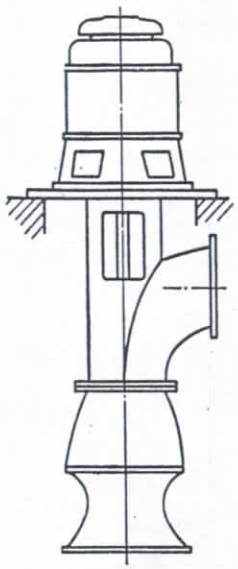

FIG. 11.17. Motor support does not carry impeller axial thrust.

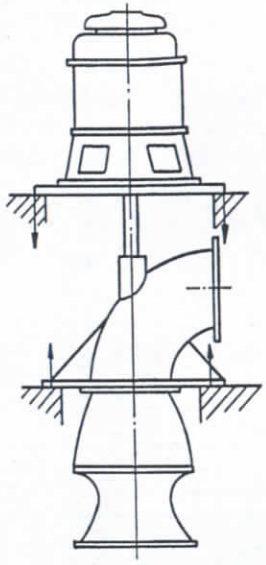

FIG. 11.18. Motor support carries full axial thrust.

internal force in a self-contained system comprising the pumping element, the discharge column, and the motor. The hydraulic thrust imposes some internal stresses on certain parts of the system and can be

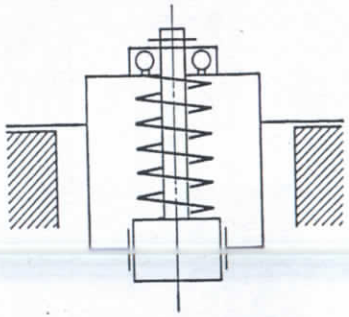

FIG. 11.19. Supports do not carry spring load.

compared to a spring in a box (Fig. 11.19). However, if the pump and motor have independent supports (Fig. 11.18), then the motor support carries full downward hydraulic thrust in addition to the weight of the

rotating element, and the pump support carries an equal upward casing hydraulic reaction.[4]

(*d*) **Thrust Bearing Lock.** *In horizontal pumps having no axial thrust, the outer race of the thrust bearing should be prevented from rotating. Otherwise, while floating within the available axial clearance, the outer race may acquire sufficient momentum to hit and grind the end stops of the ball bearing. Large high speed thrust bearings have been damaged in this way.*

REFERENCES

1. A. J. Stepanoff, "Leakage Loss and Axial Thrust in Centrifugal Pumps," *Trans. A.S.M.E.*, Vol. 54, No. 15, pp. 100–101, Aug. 15, 1932.
2. J. H. Polhemus and J. Henly, "Dredge Pump Pressures and Thrust Loads," *Trans. A.S.M.E.*, Vol. 51, No. 6, p. 33, Jan.–Apr. 1929.
3. F. G. Switzer, discussion in reference 1, p. 104.
4. A. J. Stepanoff, "Propeller Pumps for Circulation of Molten Salt," *Refiner Natural Gasoline Mfr.*, Vol. 19, No. 12, p. 474, December 1940.

Chapter 12

Cavitation in Centrifugal Pumps

12.1 INTRODUCTION AND DEFINITION

In the last decade no other phase of hydraulic machinery design and operation has been given so much attention in technical literature as cavitation. The reason for this was the use of higher specific speeds, for both hydraulic turbines and centrifugal pumps, with the increased danger of cavitation. To cope with the problem, experimental and theoretical studies of cavitation were made on hydraulic turbines, centrifugal pumps, and apparatus without moving parts, such as venturi-shaped water conduits. As a result of the study and accumulated experience, pumps now operate at higher speeds and are safer against cavitation damage than they used to be.

The term cavitation refers to conditions within the pump where, owing to a local pressure drop, cavities filled with water vapor are formed; these cavities collapse as soon as the vapor bubbles reach regions of higher pressure on their way through the pump. In order to form such vapor cavities, the pressure first has to drop to the vapor pressure corresponding to the prevailing water temperature. The liberation of air or the formation of air- or gas-filled cavities, however, is not sufficient to produce cavitation because the effect of air bubbles on the performance and behavior of the pump is different.

Cavitation should be distinguished from separation, which is a separation of the streamlines from the low pressure side of the vane and the formation of a turbulent wake behind the vane. Separation is possible only with real viscous fluids, whereas cavitation is possible with hypothetical perfect liquids too. Experimentally, separation has been found to exist without cavitation, and cavitation without separation. Although centrifugal fans work on the same principle as centrifugal pumps, the former can have separation whereas the latter can have both separation and cavitation. Cavitation can appear along stationary parts of a hydraulic machine or along a moving vane, as in centrifugal pump impellers.

The reduction of the absolute pressure to that of vapor tension may

be either general for the whole system or merely local; the latter may be realized without a change of the average pressure. A general pressure drop may be produced by one of the following means: (1) an increase in the static lift of the centrifugal pump; (2) a decrease in the atmospheric pressure with a rise in the altitude; (3) a decrease in the absolute pressure on the system, as in the case of pumping from vessels under vacuum; and (4) an increase in the temperature of the pumping liquid, which has the same effect as a decrease in the absolute pressure of the system.

A local decrease in pressure is produced by one of the following dynamic means: (1) an increase in velocity by speeding up the pump; (2) a result of separation and contraction of flow (viscosity); and (3) a deviation of streamlines from their normal trajectory, such as takes place in a turn or in a passing obstruction to the flow.

Low absolute pressures and cavitation may also be caused by a sudden starting and stopping and recoil of the water column, such as occur during water-hammer phenomena. This type of cavitation is transient in character and is of little importance in centrifugal pump practice.

12.2 SIGNS OF CAVITATION

Cavitation is manifested by one or several of the following signs, all of which adversely affect the pump performance and may damage pump parts in severe cases.

(*a*) **Noise and Vibration.** This is caused by the sudden collapse of vapor bubbles as soon as they reach the high pressure zones within the pump; the bigger the pump, the greater the noise and vibration. Although these signs of cavitation may appear in the normal operating range of the pump only if the suction head is not sufficient to suppress cavitation, noise and accompanying vibration are present in all pumps to a varying degree when they are operated at points far removed from the b.e.p. because of a bad angle of attack at the entrance to the impeller. By admitting small amounts of air into the pump suction, noise can be almost completely eliminated. In this way the air serves as a cushion when the vapor bubbles collapse. This method, however, is not often used to eliminate noises in centrifugal pumps, although it is an established procedure with water turbines and large butterfly valves where air is admitted automatically at partial loads.[1,2,3] The beneficial effect of air admission to the pump suction under cavitation conditions is not limited to the elimination of noise and mechanical vibration, for the impeller vane pitting is also reduced if not entirely eliminated, as it is caused by the mechanical shock accompanying the collapse of the vapor bubbles.

(*b*) **Drop in Head-Capacity and Efficiency Curves.** This appears in varying degrees with pumps of different specific speeds. With low specific speed pumps (up to 1500), the head-capacity, the efficiency and the

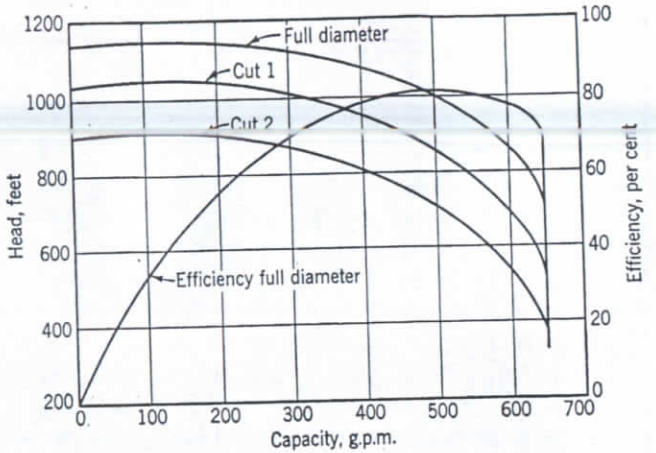

FIG. 12.1. Effect of impeller diameter on cavitation; 4-in. four-stage pump, 3550 rpm, $n_s = 1200$.

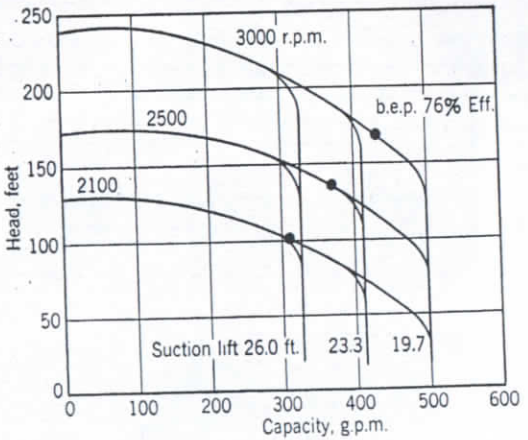

FIG. 12.2. Effect of speed and suction lift on cavitation; 3-in. single-suction pump, $n_s = 1000$.

brake-horsepower curves drop off suddenly when Q is increased to the point where cavitation is reached (Figs. 12.1 and 12.2). With higher specific speed pumps (1500–5000), however, the head-capacity and the efficiency curves begin to drop along the whole range gradually before

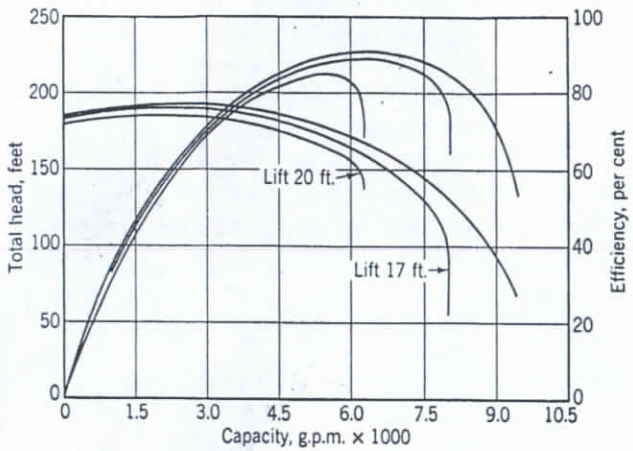

FIG. 12.3. Twelve-inch double-suction pump, 1200 rpm, $n_s = 2100$.

the point of sudden break-off is reached (Fig. 12.3). The degree of drop in the head-capacity and efficiency curves depends on the specific speed and on the suction pressure, increasing for higher specific speed and lower suction pressure.

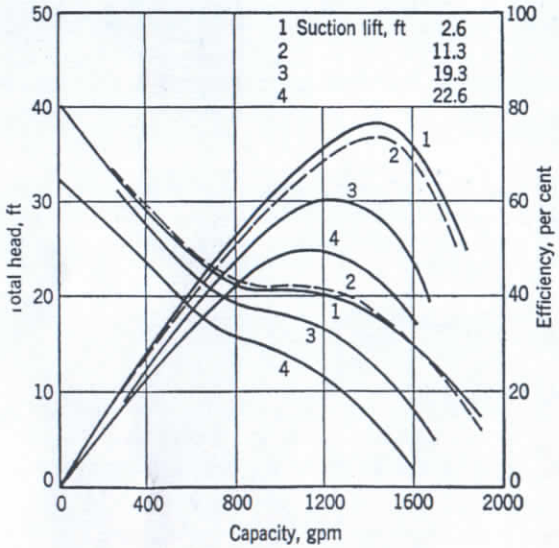

FIG. 12.4. Axial flow pump performance, 6½-in. impeller diameter, 2250 rpm, $n_s = 9750$ (Tenot [27]).

With very high specific speed pumps (above 6000) of the propeller type, there is no definite break-off point on the curves (Fig. 12.4); instead, there is a gradual drop in the head-capacity and the efficiency curves along the whole range. In this type of pump, the drop in the efficiency appears before there is a perceptible drop in the head-capacity curve. Therefore, a drop in the efficiency is a more reliable criterion of approaching cavitation conditions. Even the objectionable noise may not appear until cavitation has progressed beyond the point where the efficiency becomes unsuited commerically.

The difference in the behavior of pumps of different specific speed results from the difference in the impeller design. Low specific speed impeller vanes form a definite channel, the length of which depends on the vane angles, the number of vanes, and the ratio of the impeller eye diameter D_1 to the impeller outside diameter D_2 (Fig. 12.5). When

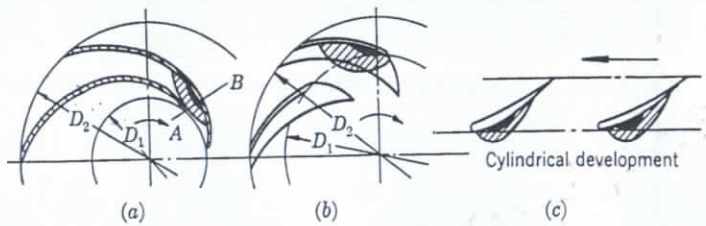

FIG. 12.5. Low pressure zones on back side of impeller vanes: (*a*) low specific speed; (*b*) medium specific speed; (*c*) propeller pump.

the pressure at the impeller eye reaches the vapor pressure, usually on the back side of the vane entrance tips, it extends very rapidly across the whole width of the channel, A–B, Fig. 12.5(*a*)—with a small increase in capacity and decrease in head. A further drop in the discharge pressure does not produce any more flow because the pressure differential moving water to the impeller eye cannot be increased any more. This differential is fixed by the suction pressure outside the pump, and the vapor pressure across the whole channel between any two vanes at the impeller entrance.

With high specific speed impellers, the channel between two vanes is wider and shorter; see Fig. 12.5(*b*). More drop in head and a greater increase in capacity are required to extend the vapor pressure zone across the whole channel. Therefore, the drop in the head-capacity curve extends through a wider range before the sudden break-off occurs. With propeller pumps the vanes do not overlap; see Fig. 12.5(*c*). Therefore, although the low pressure zone extends when the pump head is reduced, there are always parts of the channel which remain at pressures higher than vapor pressure, and the flow through the impeller will steadily increase even though cavitation has definitely set in.

In multistage pumps cavitation affects only the first stage; therefore

the drop in head capacity and efficiency is less pronounced than in a single-stage pump. The cut-off capacity is determined by the first stage.

The drop in the head-capacity and the efficiency curves may begin before the vapor pressure is reached in certain parts of the impeller suction. This is caused by the liberation of air or light fractions in petroleum oils at reduced pressures in the impeller eye. The absolute

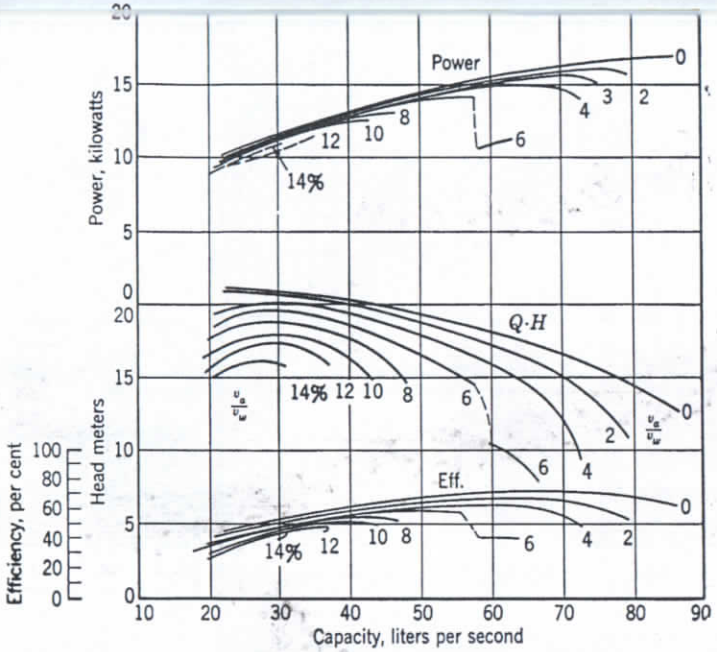

FIG. 12.6. Effect of admission of air into pump suction (Siebrecht [4]).

pressure in the vacuous pockets is the sum of all the partial pressures of the gases occupying this space, in accordance with Dalton's law of partial pressures.

The drop in the head-capacity and the efficiency curves due to liberation of free air in the water is followed by a reduction in the brake horsepower also. This method has been suggested [4] as a means of reducing the head and at the same time saving power instead of throttling the pump discharge, as done ordinarily. Figure 12.6 shows test results obtained by Siebrecht, namely, the head-capacity, efficiency, and brake-horsepower curves of a pump with different volumes of air admitted to the pump. The author does not know of any case where this method was employed in actual installations, but a modification of this method,

whereby the pump suction is throttled instead of the discharge to reduce the head, is frequently employed. At reduced suction pressures, air or gases begin to be liberated from the liquid, producing a lower head-capacity curve and lower brake horsepower. However, this method is not recommended because, if suction throttling is carried too far, cavitation will start with all its bad effects—noise, pitting, and vibration. Figure 12.7 shows a test of a 5-in. pump with the suction and the discharge throttled. A comparison of the brake-horsepower curves shows the power saved by suction throttling.[5]

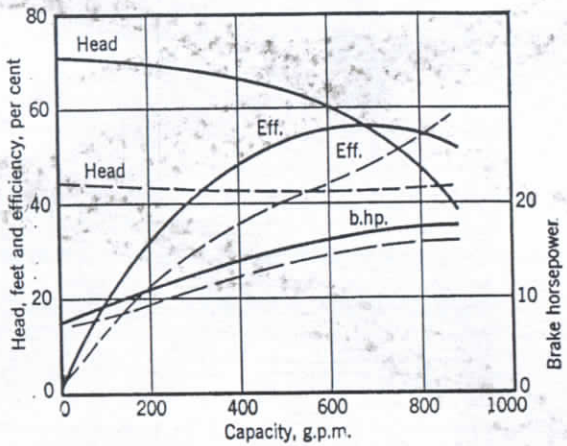

FIG. 12.7. Throttling of pump suction instead of discharge to save power may be a dangerous procedure; 5-in. pump, 1160 rpm, $n_s = 1500$ (Van Leer [5]).

On several occasions it has been found by careful tests on centrifugal pumps and water turbines that the efficiency may show a slight increase shortly before cavitation sets in. This is explained by a reduction of friction at the beginning of separation, just before the disturbing water hammering begins.[6-9]

(c) Impeller Vane Pitting and Corrosion Fatigue Failure of Metals If a pump is operated under cavitation conditions for a sufficient length of time, impeller vane pitting appears, the amount of metal lost depending on the material in the impeller and the degree of cavitation. *Foettinger [6] showed very conclusively that vane pitting is caused solely by the mechanical (water-hammer) action of collapsing vapor bubbles, and that electrolytic and chemical action is entirely insignificant in this process.* He proved this by producing cavitation in a venturi-shaped channel made of neutral glass which was pitted in the same manner as the metal in a centrifugal pump or water turbine impeller vanes. *If electrolytic*

or chemical reaction is active, it should affect all the parts of the same material and not only the spots subject to cavitational water hammer.

The fact that air or gases may be more active at the instant of liberation has been stated in the past. However, the places affected by pitting are always beyond the low pressure points where the vapor bubbles are formed. Another corroboration of the mechanical nature of the metal destruction has been shown by the damage of a lead plate without any loss of weight.[10]

By experience it has been found that the collapse of vapor bubbles is harmless when it takes place entirely surrounded by the stream of liquid.[10] *In addition to metal destruction caused by the fatigue of the metal surface as a result of repeated water-hammer blows, Poulter* [11] *has shown that metal particles can be torn off and carried away by liquid penetrating into and escaping from the pores of the metal under successive pressure waves.* In that case, more porous materials are most readily affected by such destruction. The degree of destruction depends on the length of time the specimen is under pressure, or the time between two successive pressure waves.

There seems to be no correlation between the hardness and the cavitation erosion of metals, but apparently the molecular size and the viscosity of liquids play an important part in cavitation pitting.

Cavitation pitting should be distinguished from corrosion and erosion. The first is caused exclusively by chemical and electrolytic action of the pumped liquids; the second is the wearing away of the metal parts in a pump by foreign bodies carried by the pumped liquids, such as sand, grit, coke, and coal. There is no difficulty in distinguishing these three kinds of pitting by the appearance of the attacked parts and their location in the water passages of the pump.

Frequencies of hammering were recorded from 600 to 1000 cycles per second by Hunsaker [10] and up to 25,000 cycles per second by de Haller.[12] The intensity of hammering depends on the velocity. Pressures of 300 atm were measured by de Haller. Local pressures confined to very small areas (the piston area of de Haller's pressure-measuring device was 1.5 mm) may be considerably higher than those recorded. A satisfactory explanation of how such high pressures may arise in the case of cavitation has been lacking.

In the light of Poulter's investigation,[11] *it may appear possible that high destructive pressures are derived from the elastic forces of metal parts extending over areas larger than those actually attacked by cavitation. These parts are under fluctuating forces of large magnitude, so large that often the whole foundation supporting the pump is set in vibration under cavitation conditions. Under fluctuating stresses liquid is drawn in and squeezed*

from the pores, and it is during this squeezing phase that tremendous pressures may be produced in small restricted areas.

A similar process may be a partial explanation of what is known as corrosion fatigue of metals, or metal failure under repeated stresses in presence of liquids. The corrosive effect of water as compared with oils in the case of corrosion fatigue is due to the fact that water molecules are smaller than those of oil; therefore, water penetration of metals would be deeper than that of oil; hence the destructive effect on the metal is greater where it is subjected to rapidly fluctuating stresses. *This will explain the failure by corrosion fatigue of non-corrosive high chromium steels in the presence of water.* Another illustration and proof that the penetration of metals by liquid plays an important part in metal destruction by corrosion fatigue are furnished by results of laboratory tests by McKay and Worthington.[13] They have found that the endurance limit depends not only on the stress level and the total number of cycles but also on the frequency of stress reversals. For the same total number of cycles, the low frequency gives a much lower endurance limit because more time is allowed for liquid penetration of metal with consequently higher destructive pressures developed in the metal pores when the liquid is compressed on the stress reversal. Rheingans [14] has found that cast materials (iron, bronze, and steel) absorb water, and his test showed that castings actually increase in weight during the first 30 minutes of cavitation tests.

12.3 MATERIALS TO RESIST CAVITATION PITTING

(*a*) Experimental Study. Different materials resist cavitation pitting in varying degrees. In addition to the chemical composition, the heat treatment of metals and also the surface conditions control the amount of material destroyed by cavitation. The behavior of metals under cavitation parallels that under corrosion fatigue conditions. Any notches, nicks, scratches, flaws, or sharp corners on the surface of metals attacked by cavitation accelerate the beginning of pitting. Protective coats do not improve the resistance of metals to cavitation pitting.

Schroeter [15] has run tests on different materials under cavitation in a venturi-shaped conduit built for the purpose. A velocity of 197 ft per sec was maintained throughout these tests. Figure 12.8 shows some materials tested by Schroeter.

Hardening decreases the rate of metal destruction although the hardness alone (for different materials) is not a determining factor as far as resistance to cavitation is concerned.

To prolong the life of runners of large Kaplan turbines working under

high heads (over 50 ft), the turbine manufacturers protect with welded stainless steel the places subject to cavitation pitting.[16] Propeller pumps of the same type are not built in sizes justifying such procedure, nor are they operated at such high heads.

Although covering the surface of metals with rubber helps them to resist the impact of water hammering very well, its bond to the metal fails after a short time. No practical method of rubber protection of

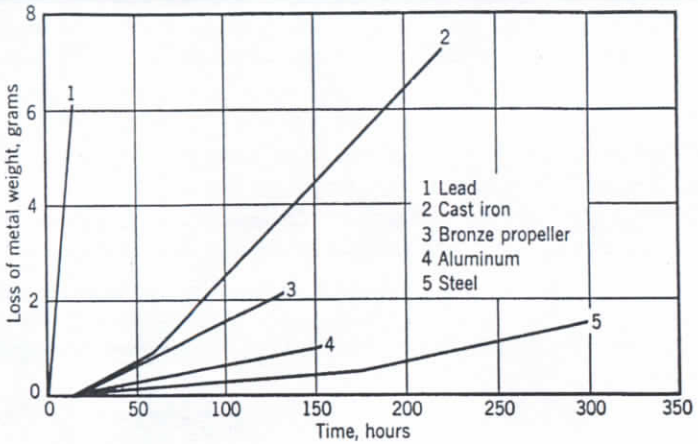

FIG. 12.8. Loss of metal due to cavitation (Schroeter [15]).

metals against cavitation has yet been developed. Tests with rubber again corroborate the mechanical nature of the destruction of materials by cavitation.[15]

Schroeter's tests have definitely established the fact that the beginning of cavitation and its extent depend on the velocity of the flow. This must be expected as all the destructive blows by water hammer derive their energy from the kinetic energy of the flow.

De Haller [12] has found that the behavior of various metals is analogous during tests with direct drop-impact and with cavitation. In both cases the metal destruction is caused by water hammering. Although the mechanism of water blows against metals is different, the result is quite similar. In a special apparatus resembling a steam turbine wheel, de Haller ran erosion tests on a number of materials, and his results, reproduced in Fig. 12.9, are in agreement with Schroeter's. De Haller's method of testing materials for cavitation resistance requires only a short time to produce cavitation pitting.

Kerr [17] has tested 80 materials for cavitation in sea water in a special vibratory apparatus developed by the Massachusetts Institute of Tech-

nology. These tests show that cavitation damage was slightly greater by sea water than by fresh water. It has been found also that the temperature of water has a marked effect upon the metal loss by cavitation, the loss increasing with temperature. *At higher temperatures the amount of air dissolved in water is reduced, and thus the cushioning effect of water-hammer blows is reduced, while at the same time the increased vapor pressure tends to increase the vapor bubble formation.*

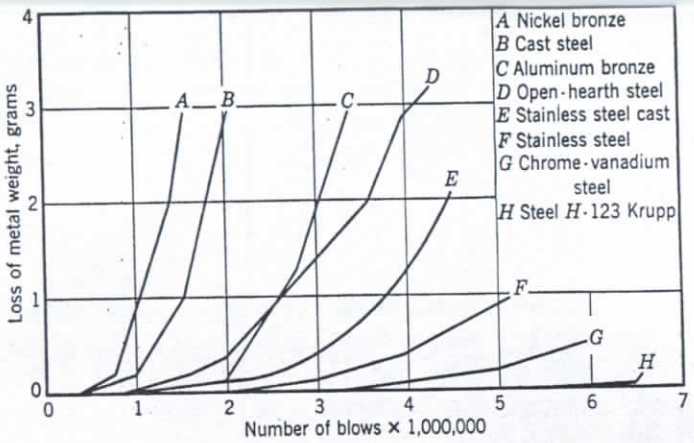

FIG. 12.9. Loss of metal by jet drop-impact (de Haller [12]).

Mousson [18] has found that loss of metal by cavitation is approximately proportional to vapor pressure. He also demonstrated the beneficial effect of admission of small amounts of air upon the metal damage by cavitation. Mousson and Kerr give extensive test data which are very useful in the selection of materials when cavitation is expected.

(*b*) Examples of Metal Attack by Cavitation. In pumps of normal design, the lowest pressure occurs on the back side of the impeller vane slightly beyond the suction edge. The cavitation pitting appears somewhat farther downstream where the vapor bubbles collapse; Figs. 12.10(*a*), 12.11(*a*), and 12.11(*b*). However, if the pump is operating continuously at a capacity considerably higher than normal, the pitting may appear on the front side of the vane at the suction vane tips; Fig. 12.12(*a*). Cavitation in this case accompanies separation resulting from a bad angle of attack.

Figure 12.10(*b*) shows vane and shroud pitting near the outer shroud due to lack of streamlining.

Figure 12.10(*a*) shows vane pitting at the impeller discharge caused by the vane's blunt discharge tips.

Figure 12.10(*c*) shows a marginal cavitation observed on propeller pumps and also on centrifugal pumps with open impellers. Local high velocity through the clearance and separation due to a sudden change in direction produced the marginal cavitation and pitting. Rounding off of

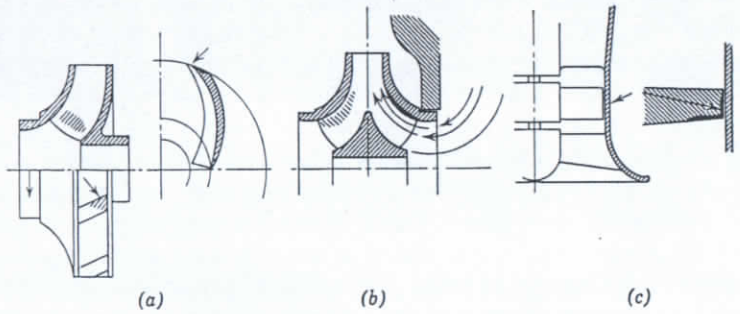

FIG. 12.10. Examples of impeller cavitation.

the high pressure side corners of vanes eliminates the marginal pitting at the expense of increased leakage through the clearance.[8]

Figure 12.11(*a*) shows pitting of the volute casing of a propeller pump caused by a lack of streamlining.

Figure 12.11(*b*) shows a diffusion casing vane pitting due to a discrepancy between angles of incoming flow and diffusion vane.

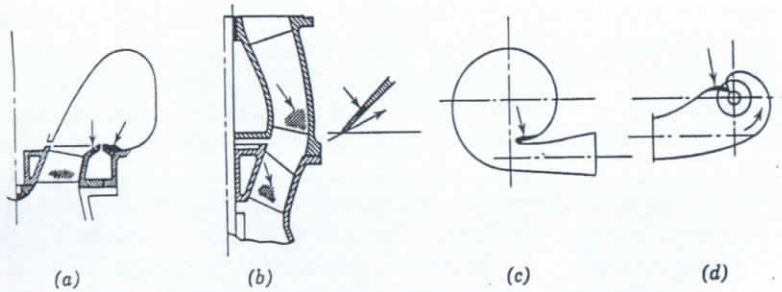

FIG. 12.11. Examples of casing cavitation.

Figure 12.11(*c*) shows pitting of the tongue of a volute casing observed when a pump is operated continuously at capacities above normal.

Figure 12.11(*d*) is an example of pitting of the baffle in the suction nozzle, which permits excessive prerotation of the flow before it enters the impeller eye.

In general, sudden change in direction, sudden increase in area, and lack of streamlining are responsible for local pitting of pump parts.

This may appear only if the suction pressure is reduced below a certain minimum. On the other hand, pitting of pump parts on the discharge side of the pump has been observed when the pump pressure is not high enough to suppress cavitation.

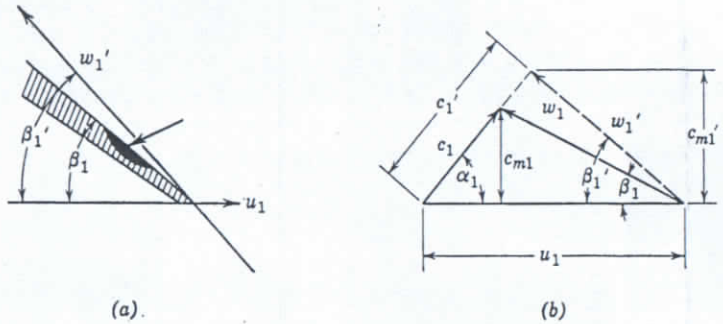

FIG. 12.12. (*a*) Entrance vane pitting at capacities above normal; (*b*) entrance velocity triangle at capacity above normal.

(*c*) Cavitation Due to Vibration. Destruction of metal parts by cavitation can take place when there is no apparent local drop in pressure due to high velocity flow. It is possible for cavitation conditions to appear as a result of vibration of parts in contact with water. Water is unable to follow the frequency of a vibrating body and, at each reversal of the deflection, vapor-filled cavities are formed between the water and the vibrating body and these collapse upon each reversal of the deflection. This principle has been used in the building of material-testing machines for cavitation studies.[17] Pitting of metal parts, typical of cavitation and caused by vibration, has been observed on such parts as diesel engine cylinder liners on the water jacket side or, locally, on ship hulls in spots which respond to the vibration of the machinery inside the hull. In centrifugal pumps, evidence of cavitation due to vibration of parts was never definitely established. However, it may be responsible for, or contribute to, the pitting of parts on which cavitation is difficult to explain from the standpoint of local dynamic depression or lack of streamlining.

(*d*) "Air Impingement Attack of Metals." In literature dealing with corrosion of condenser tubes another method of metal destruction is frequently mentioned, that of "impingement of air bubbles" on the tube surface. This conception contradicts the theory and test results of metal destruction by cavitation in hydraulic machinery, as described by many authentic reports quoted in this chapter. The physical side of the air impingement attack of metals is not easy to visualize when it

is borne in mind that air bubbles in a condenser tube move at the same velocity as the water, and particles of air are 800 times lighter than particles of water.

Air bubbles do not carry sufficient energy to make any appreciable effect by impingement on the stationary boundary layer of liquid attached to the tube walls. The effect of such attack would be somewhat similar to the hitting of the bottom of a swimming pool with a toy balloon or a tennis ball. The experimental proof of the metal damage by air impingement, such as that carried out by May,[19] lacks conclusiveness, because in every case when samples of metal were subjected to a jet of air-water mixture the sample was free to vibrate. The fact that metal destruction could be accomplished only with a fixed air-water ratio and with a certain size of air bubbles suggests that, apparently, those were the necessary conditions for exciting vibration of the sample. It is believed that in the de Haller tests,[12] which were performed with a water jet impact against revolving plates, vibration of the samples was an important factor in producing the cavitation effect.

Where conditions are favorable to chemical corrosion, cavitation may accelerate the damage because the products of corrosion and protective films are removed more rapidly and new and fresh surfaces are exposed to action.

12.4 THEORETICAL RELATIONSHIP AT CAVITATION CONDITIONS

The flow to the impeller of a centrifugal pump following the energy gradient is determined by the existing pressure difference between the suction pressure and the pressure established by the flow at the impeller eye. The latter is not uniform at any section of the impeller passages, and even determination of the average pressure inside the impeller presents difficulties. For that reason, the theoretical relationship for the flow through the impeller eye, although easy to establish, does not give a reliable tool for an accurate predetermination of cavitation conditions. An examination of the theoretical formulas for the flow through the impeller eye, however, enables one to learn the effect of several factors upon cavitation. A study of theoretical relationship has also resulted in the introduction of simplified formulas incorporating experimental coefficients which permit prediction of a pump's behavior with regard to cavitation if experimental data are available on similar pumps.

Let

H_a be the absolute pressure prevailing at the surface of the pump suction supply. This will be atmospheric pressure if the suction vessel is open to the atmosphere. If the suction is taken from an enclosed vessel, H_a is the absolute pressure in this vessel.

h_s be the static head in the suction vessel above the pump center line. If it is suction lift, it is negative.

h_v be the vapor pressure at the prevailing water temperature.

h_l be the head loss in the suction pipe and impeller approach.

c_1 be the average absolute velocity through the impeller eye; Fig. 12.12(*b*).

$\lambda w_1^2/2g$ be the local pressure drop below the average at the point of cavitation. Hence w_1 is the average relative velocity at entrance, and λ is an experimental coefficient.

This local pressure drop is caused by the difference in pressure on the leading and trailing sides of the vane. When pressure is applied by the vane on water, the water exerts an equal reaction in the opposite direction, which exists as a pressure difference on the two faces of vanes. This is frequently referred to as a dynamic depression. Figure 3.20 shows a typical pressure distribution inside an impeller channel obtained by Uchimaru [26] under actual operating conditions.

Evidently cavitation starts when

$$H_a + h_s = h_l + h_v + \frac{{c_1}^2}{2g} + \lambda \frac{{w_1}^2}{2g} \tag{12.1}$$

When liquid in the suction vessel is boiling, the pressure in the vessel H_a is equal to the vapor pressure, or $H_a = h_v$, and equation 12.1 becomes

$$h_s = h_l + \frac{{c_1}^2}{2g} + \lambda \frac{{w_1}^2}{2g} \tag{12.1a}$$

meaning that a positive suction head h_s is necessary to produce the flow. To prevent vaporization, an excess of suction head is necessary above h_s.

Equation 12.1 is not suitable for determining the maximum permissible suction lift for a given pump capacity (c_1 and w_1), because the true value of maximum c_1 is not known, and also because the value of λ varies for pumps of different specific speed. Even for a given pump at constant speed, λ varies with capacity, being a minimum near the b.e.p. and increasing on both sides of this point. Figure 12.13 shows a typical curve of λ variation obtained by Krisam.[21] Similar curves were published by von Widdern.[22] The increase of λ on both sides of the b.e.p. shows the effect of the angle of attack [see Fig. 12.12(*a*)] between the direction of relative velocity and the vane angle at the impeller entrance.

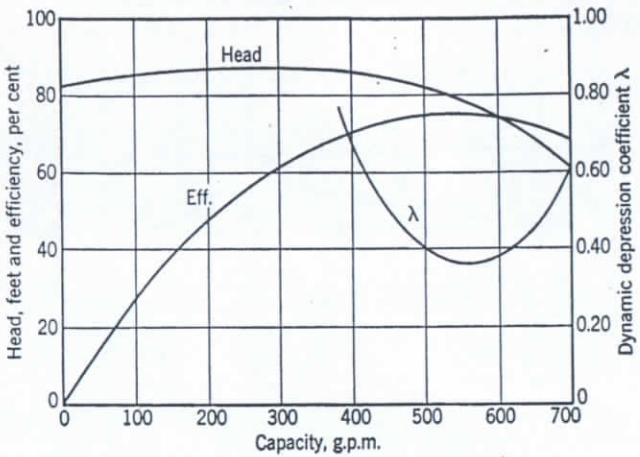

FIG. 12.13. Dynamic depression coefficient λ (Krisam [21]).

12.5 FACTORS AFFECTING CAVITATION

A study of equation 12.1 permits a number of conclusions which hold in practice for, at cavitation conditions, a change in one term of the equation is always followed by a change in another to satisfy the relationship. Thus:

1. If atmospheric pressure is decreased because of an increased elevation (about 1 ft per 1000 ft of elevation), the pump maximum capacity will decrease (c_1 and w_1 will decrease).

2. If suction lift is increased ($-h_s$ greater), or if vapor pressure rises as a result of the higher temperature of water, pump maximum capacity will decrease.

3. Higher suction lifts may be possible with low velocities (c_1 and w_1) or with a minimum loss h_l in the suction pipe.

4. Note that H_a expressed in feet of liquid depends on the specific gravity of the liquid. Thus, when molten salt (used as a heating medium in the petroleum refinery process) of specific gravity 1.75 is being pumped and the suction vessel is under atmospheric pressure, $H_a = 19.4$ ft. Therefore the danger of cavitation is much greater with heavier liquids.[23] Vapor pressure should not be overlooked with liquids other than water.

5. For given average velocities, c_1 and w_1, the approach of cavitation is affected by the casing and impeller design because they affect the velocity distribution. Thus, pump suction design permitting more prerotation in the impeller eye will decrease the maximum capacity for a fixed

suction pressure. Any lack of streamlining in the suction passages of the pump and impellers results in the formation of dead water pockets (separation), which increase local velocities beyond the average of those obtained from the velocity triangle.

6. With pumps of high specific speed of the axial flow type, the beginning of cavitation is indicated by a gradual drop of pump efficiency without any sudden drop in the head-capacity curve. In this case a further reduction in the suction pressure extends to the region affected by cavitation and equation 12.1 does not apply, as the vapor pressure is reached locally only; the impeller vanes do not form an entirely enclosed channel, and Bernoulli's equation (12.1) cannot be used.

7. The presence of gases in the liquid does not affect the validity of equation 12.1 except that, according to Dalton's law of partial pressures, the vapor will behave as if it occupied the voids alone, and vaporization will begin at an absolute pressure higher than its normal boiling point and corresponding to the existing temperature. Petroleum oils represent the most complicated example of this. Being mixtures of different individual hydrocarbons, each of which has its own vapor pressure, light fractions will vaporize at pressures far above their normal boiling points, but the vaporization will affect only a small portion of the total flowing volume. As a result, the drop in the Q-H curve is more gradual with oils than with water, and the mechanical disturbance is not so violent. The fact that vaporization and condensation during cavitation require a heat exchange tends to slow down the bubble formation in oils as compared with water on account of the lower heat conductivity of oil.

In dealing with petroleum products the "bubble point" pressure should be used and not Reid vapor pressure, as the latter gives a summary pressure of several fractions and not the beginning of vaporization of the lighter fraction.[24]

8. In the study of cavitation, the suction pressure should be specified or measured at the pump suction nozzle. In this way the loss in the suction pipe and the entrance loss are eliminated. The loss in the suction nozzle is negligibly small, owing to a low velocity, a short distance, and accelerated flow in a normal nozzle design.

9. In small pumps of low specific speed, the term $c_1^2/2g$ is predominant in setting up cavitation conditions, and the term $\lambda(w_1^2/2g)$ is of little significance. In high specific speed pumps approaching propeller pump type the term $\lambda(w_1^2/2g)$ is the controlling factor, and $c_1^2/2g$ is of secondary importance. $\lambda(w_1^2/2g)$ depends on the pump head (and hence speed) and the number of impeller vanes, and it decreases with a smaller head or a lesser speed and a greater number of vanes.

With low specific speed pumps the maximum capacity for a given suction head can be increased by cutting away part of the vane in the

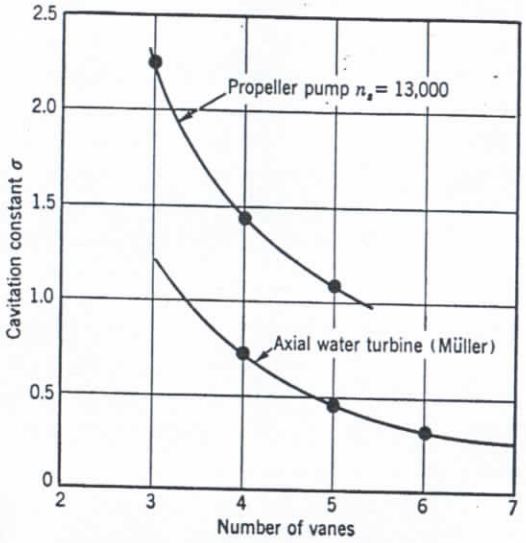

FIG. 12.14. Effect of number of vanes on σ.

impeller eye and filing the vane tips, thus increasing the available area for c_1 and making c_1 smaller. On the other hand, with propeller pumps, increasing the number of vanes will lower the vane loading and will improve the cavitation conditions of the pump (Fig. 12.14) for a given submergence, and thus permit higher head without noise or drop in efficiency.

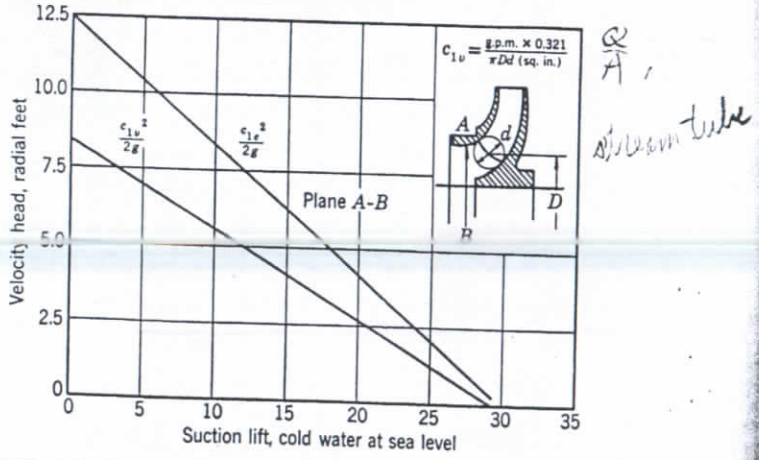

FIG. 12.15. Meridional velocity versus suction lift at cavitation conditions.

10. With low specific pumps the maximum absolute velocity c_1 may be reached either at the impeller eye (plane A–B, Fig. 12.15), or at the vane entrance. The actual effective area of both sections is greatly affected by the impeller approach design. In the study of cavitation test data, both sections should be investigated.

12.6 PREDETERMINATION OF CAVITATION CONDITIONS FROM VELOCITY CONSIDERATIONS

From a great number of observations on pumps of low and medium specific speeds (up to 1500), the author has found that for cold water (70°F), equation 12.1 can be simplified to

$$30 - h_s = 2.4 \frac{c_{1e}^2}{2g} \tag{12.2}$$

where c_{1e} is the meridional velocity through the impeller eye at cut-off capacity (plane A-B, Fig. 12.15) at suction lift h_s taken at the suction nozzle and referred to the pump shaft center line. The same relationship is represented by a curve on Fig. 12.15

A similar curve, plotted for meridional velocities at the vane entrance tips, is shown in Fig. 12.15. This curve can be expressed by

$$30 - h_s = 3.5 \frac{c_{1v}^2}{2g} \tag{12.3}$$

A comparison of equations 12.2 and 12.3 with equation 12.1 leads to the following conclusions:

1. The difference between atmospheric pressure $H_a = 34$ and $H_a = 30$ in equations 12.2 and 12.3, or 4 ft, includes: a vapor pressure of 0.85 ft at 70°F water temperature; the loss of head (h_l) in the suction nozzle, a local drop in pressure due to uneven velocity distribution in the impeller approach, and a small margin of safety.

2. The right-hand term in equation 12.2 can be expanded as follows.

$$2.4 \frac{c_{1e}^2}{2g} = \frac{c_1^2}{2g} + \lambda \frac{w_1^2}{2g} = \frac{c_{1e}^2}{2g} \left(\frac{1}{(\sin \alpha_1)^2} + \frac{\lambda}{(\sin \beta_1)^2} \right) \tag{12.4}$$

where α_1 is the absolute velocity angle and β_1 is the vane angle at the entrance; Fig. 12.12(*b*). Similarly, in equation 12.3 the right-hand terms can be represented as follows.

$$3.5 \frac{c_{1v}^2}{2g} = \frac{c_1^2}{2g} + \lambda \frac{w_1^2}{2g} = \frac{c_{1v}^2}{2g} \left(\frac{1}{(\sin \alpha_1)^2} + \frac{\lambda}{(\sin \beta_1)^2} \right) \frac{1}{\delta^2} \tag{12.5}$$

δ is a contraction coefficient to account for the vane thickness because this was disregarded when c_{1v} was calculated.

3. Since curves on Fig. 12.15 have been plotted for low specific speed pumps where the term $\lambda(w_1^2/2g)$ is of secondary importance, the cut-off capacity is determined by the impeller eye velocity, c_{1e} or c_{1v}, and is independent of the impeller diameter or pump speed as long as the cut-off capacity occurs at or near the b.e.p., as shown on Figs. 12.1 and 12.2. (Similar tests were published by von Widdern.[22]) Within the range specified for a fixed suction head, the cut-off capacity is independent of the specific speed and is governed by the absolute velocity through the impeller eye. Either the term $\lambda(w_1^2/2g)$ is small or it varies little with the specific speed and bears an approximately constant ratio to $c_1^2/2g$, thus leaving the experimental numerical constant in the right-hand terms of equations 12.2. and 12.3 essentially constant.

With pumps of medium and high specific speed (1500 to 4000), the cut-off capacity will increase somewhat with the speed if the cut-off

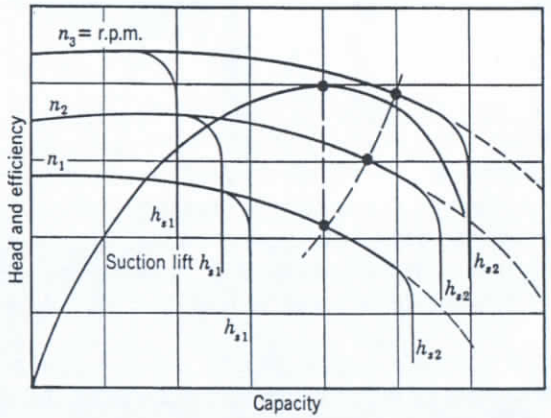

FIG. 12.16. Cut-off capacities at several speeds.

takes place to the right of the b.e.p. The cut-off capacity will decrease at higher speeds if the cut-off takes place at capacities smaller than normal (Fig. 12.16). The reason for this is the variation of the coefficient λ in the term $\lambda(w_1^2/2g)$. Figure 12.13 shows that this is a minimum near the b.e.p. When the cut-off takes place at capacities above normal, the b.e.p. moves nearer to the cut-off capacity at a higher speed where λ is smaller, and thus $\lambda(w_1^2/2g)$ is smaller; hence $c_1^2/2g$ or pump capacity will increase. At partial capacities the peak efficiency moves away from the cut-off capacity at higher speeds, while λ is increasing and the cut-off capacity is decreasing.

Looking at the same phenomena from a different point of view, it will be noticed that where the cut-off capacity is nearer the peak efficiency at higher speed, the angle of attack of the incoming flow at the impeller entrance is smaller, the extent of separation is reduced at the vane tips, and the effective area available for the flow is increased. Thus, at the same suction pressure, a higher capacity is possible at a higher speed. When the cut-off takes place at partial capacity and the b.e.p. is moving farther at a higher speed, the angle of attack is increasing, separation is more pronounced, the effective area is reduced, and the cut-off capacity is lower at a higher speed.

Since the best angle of attack may not coincide with the b.e.p., the effect of the angle of attack upon the maximum capacity at several speeds may not be apparent if the cut-off capacity is not sufficiently removed from the b.e.p.

12.7 THOMA'S CAVITATION CONSTANT

The experimental relationship between the impeller eye velocity at cut-off capacity and the suction pressure gives a satisfactory means for predicting cavitation for low specific speed pumps.

For higher specific speed pumps this connection becomes inaccurate and, moreover, with high specific speed pumps, the drop in efficiency may appear much sooner than the pump capacity cut-off. There is no simple way to predict the beginning of cavitation in high specific speed pumps.

Thoma [25,26] has suggested that the dynamic depression, including the velocity head at the impeller eye can be expressed as a fraction of the total head, or

$$\frac{c_1^2}{2g} + \lambda\frac{w_1^2}{2g} = \Delta h = \sigma H \tag{12.6}$$

The coefficient σ is determined experimentally. If, for the dynamic depression, its value in terms of σ and H are substituted, equation 12.1 takes the form

$$H_a + h_s - h_v - h_l = \sigma H \tag{12.7}$$

or

$$\sigma = \frac{H_a + h_s - h_v - h_l}{H} \tag{12.8}$$

The use of the cavitation coefficient σ became quite general among water turbine designers and is coming into wide use among centrifugal pump builders.

The use of the cavitation constant σ is subject to a number of considerations:

1. For the same pump at different speeds or similar pumps operated at the corresponding points (the same specific speed), all velocities vary as $\sqrt{H}$, and hence

$$\sigma = \frac{\Delta h}{H} = \text{constant} \tag{12.9}$$

This presupposes that λ in equation 12.6 remains constant. This relationship is the basis of all model testing for cavitation. If σ is determined by test for a certain design, equation 12.8 or equation 12.9 can be used to determine the required suction head for a given pump total head.

2. *Equation 12.9 holds only at conditions approaching cavitation while the affinity laws still hold. When cavitation sets in, the laws of similarity are not fulfilled and the relationship, σ = constant, expressing similarity of conditions regarding cavitation, becomes approximate only.*

3. Tenot [27] gives the following relationship for the similarity regarding cavitation when it has progressed beyond the incipient stage.

$$\frac{\sigma_1 - \sigma_c}{\sigma_2 - \sigma_c} = \frac{H_2}{H_1} \tag{12.10}$$

where σ_c is the critical sigma coefficient which is constant for both model and prototype, $\sigma_c = \sigma_{c1} = \sigma_{c2}$.

$$\sigma_1 = \frac{\Delta h_1}{H_1} \quad \text{is sigma for the model}$$

$$\sigma_2 = \frac{\Delta h_2}{H_2} \quad \text{is sigma for the prototype}$$

H_1 and H_2 are the operating heads of the model and prototype respectively.

Tenot has demonstrated the validity of this relationship by high speed (1/1,000,000 sec) photography of a small propeller pump, operated at several speeds with different suction heads.

Equation 12.10 can be transformed as follows. Multiply both sides by H_2H_1:

$$\frac{\sigma_1 - \sigma_{c1}}{H_2} = \frac{\sigma_2 - \sigma_{c2}}{H_1}$$

$$(\sigma_1 - \sigma_{c1})H_1 = (\sigma_2 - \sigma_{c2})H_2$$

$$\Delta h_1 - \Delta h_{c1} = \Delta h_2 - \Delta h_{c2} \tag{12.11}$$

Equation 12.11 shows that, for cavitation similarity in two pumps, the absolute pressure at the points of minimum pressure in the impellers is equally removed from the critical pressures (vapor pressure) existing at the incipient cavitation conditions. This means that if two pumps operate at different heads ($H_1 \neq H_2$) but if the suction pressures are such that $\sigma_1 = \sigma_2$, the pump with the higher head will have cavitation developed to a smaller degree than that prevailing in the low head pump.

If both model and prototype are tested at the same head, ($H_1 = H_2$),

$$\frac{\sigma_1 - \sigma_c}{\sigma_2 - \sigma_c} = 1 \quad \text{and} \quad \sigma_1 = \sigma_2 \tag{12.12}$$

and consequently, if equation 12.10 holds and $H_1 \neq H_2$, $\sigma_1 \neq \sigma_2$.

4. It has been pointed out already that it is very difficult to detect incipient cavitation, and any σ_c determined as a sigma for the critical cavitation conditions really may represent the state of cavitation progressed sufficiently to be measured by the available testing equipment. Therefore the relationships discussed under (3) are of particular importance.

Again, with wider use of high specific speed water turbines and pumps, it frequently becomes uneconomical to provide sufficient submergence to suppress cavitation completely under all operating conditions; therefore, unless the heads are reproduced in the model testing the conditions, $\sigma_1 = \sigma_2$ will only approximately represent the cavitation similarity. In water turbine practice, when it is impossible to provide a proper submergence due to the high cost of excavation, the runner vanes are protected with stainless steel in the places subject to cavitation pitting.[28]

5. *To make the discussion of cavitation more definite, the criterion of incipient cavitation should be stated—whether it is the breaking off of the head-capacity curve, or the drop in efficiency, or noise and vibration, or the pitting of the impeller vane. The drop in efficiency is more general because it applies to pumps irrespective of the specific speed and may be found while other signs of cavitation are not yet apparent.* Depending on the testing facilities and requirements, a drop of 1 per cent or even just a fraction of a point in the efficiency may be taken to indicate that cavitation has already set in.

During cavitation tests, σ variation is obtained either by changing the suction pressure (mostly by throttling), or by changing the pump speed and hence the head at the same static suction pressure.

Although the first method is simpler to arrange, better results are obtained with the variable head tests. For laboratory testing a special

testing equipment has been used to a limited extent. With this method the pump suction is taken from a vessel which can be kept under different pressures. With a variable speed drive this procedure is ideal for accurate σ determination.[29]

Although the same σ value may be obtained either with low head and low suction pressure (high suction lift), or with high head and correspondingly higher suction head (large pump or higher speed), the physical aspect of the phenomenon as far as cavitation is concerned is not exactly the same. In the first case the whole suction pipe is under suction lift and, with low velocities, ample time may be available for air or gases to liberate and accumulate in quantities sufficient to impair the pumps' efficiency and reduce the head-capacity before actual formation of vapor bubbles starts. In the second case the pressure drop is mostly dynamic and is limited to a small part of the impeller passages. In addition, with high velocities through the impeller, the time required for the water particles to cross the low pressure zone is shorter and, since in all thermodynamic changes time is an essential factor, the relative volume of vaporization and its effect on the pump performance is smaller for high head pumps.[22]

Even for two similar pumps of different sizes operating at the same head and the same σ value (which in this case means the same suction pressure), the extent of cavitation is not in proportion to the pump size, and the bad effects of cavitation will be less pronounced in the large unit.[30]

Although the velocities at similar points in the impellers are the same in both pumps under such conditions, the effect of the curvature of the impeller profile or suction approach upon the velocity distribution (the maximum local velocity) is not the same in the small model and the large prototype because the Reynolds numbers are different. The centrifugal forces which are instrumental in the distortion of the velocity distribution along the curved path are inversely proportional to the radius of curvature; therefore, negotiating the curves through the impeller eye and suction approach in a large pump results in lower maximum local velocities, as compared with the average, than in a small model.

On the other hand, the path of the flow through the low pressure zone of the impeller of the prototype is longer than that in the model, therefore more vapor will be produced in the prototype. This effect of time on cavitation volume may partly or entirely compensate for the above effect of the curvature of the impeller profile on cavitation.

Figures 12.17 and 12.18 show test results by Krisam [31] of two pumps at different speeds. The values of the cavitation criterion σ for the b.e.p.

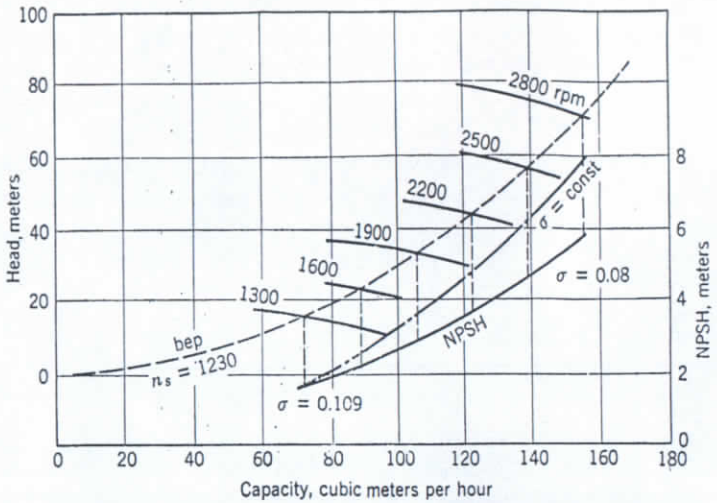

FIG. 12.17. Effect of speed on the value of σ for the b.e.p. (Krisam [31]).

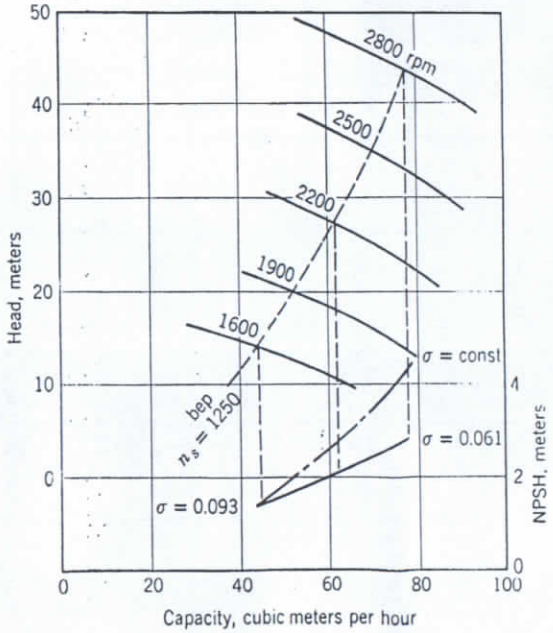

FIG. 12.18. Effect of speed on the value of σ for the b.e.p. (Krisam [31]).

observed on the test (full lines) are considerably below those calculated from the dynamic relation σ = constant (dash and dot lines). The effect of Reynolds number and time (thermal effect) are additional contributing factors causing a reduction of NPSH or σ value at higher speeds as discussed later in this chapter.

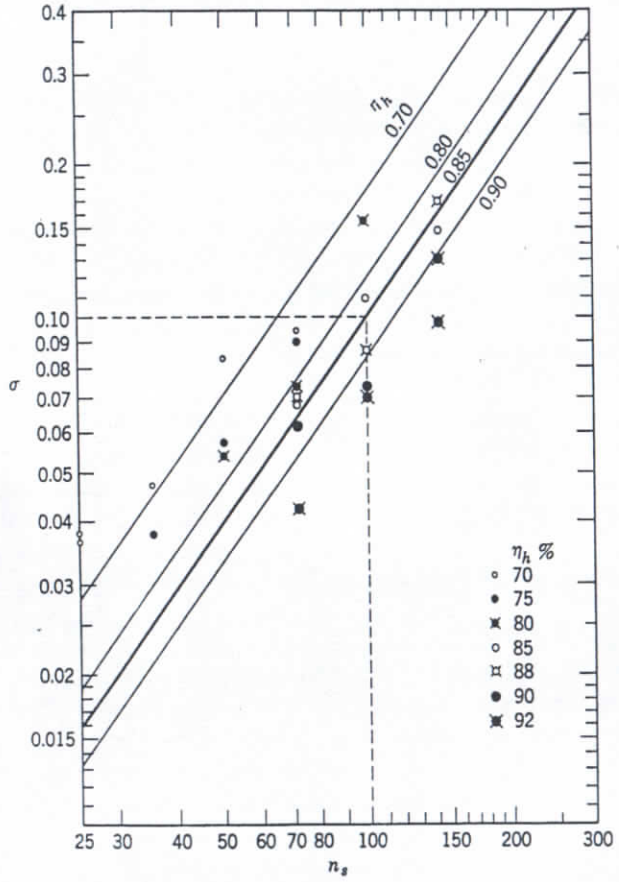

FIG. 12.19. Cavitation constant σ versus specific speed (metric units) for different efficiencies. To convert n_s to English units multiply by 14.15; η_h is hydraulic efficiency (Rütschi [32]).

6. For similar pumps higher Reynolds numbers mean lower hydraulic friction losses in the impeller approach, through the impeller and in the volute casing. Thus for a measured value of NPSH the absolute pressure in the low pressure zone of the impeller will be higher, and cavitation is less pronounced at higher Reynolds numbers. Furthermore, at

higher Reynolds numbers the ratio of the local high velocities to the average velocity is lower, hence the dynamic depression is smaller at the same value of measured NPSH. Besides, at higher Reynolds numbers a reduction of hydraulic losses leads to a better efficiency, which appears

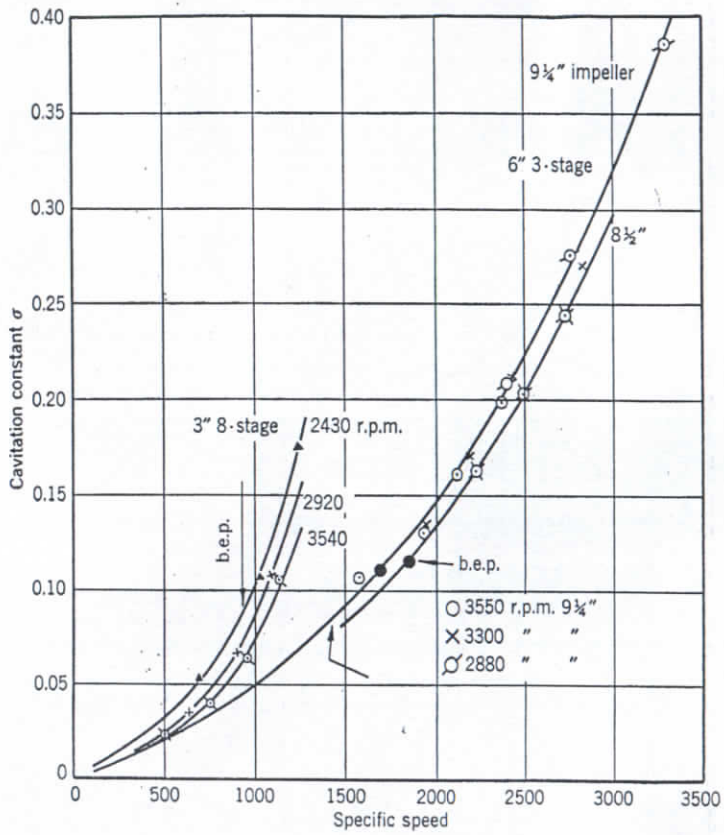

FIG. 12.20. Cavitation constant σ versus specific speed for a constant speed head-capacity curve.

as an increase in head. This would lead to a reduction of the value of σ = NPSH/H, in addition to the above-mentioned reduction of NPSH for the same cavitation effects.

In general it can be stated that for pumps of the same specific speed the σ value is a function of efficiency, more efficient pumps requiring lower values of σ. Figure 12.19 shows a plot σ versus specific speed compiled by Rütschi [32] which shows definitely the effect of efficiency. Specific speeds on this figure are based on capacity measured in cubic meters per second

and head in meters. To obtain specific speed in term of gallons per minute and feet, it should be multiplied by 14.15.

7. There are several ways to represent graphically the results of cavitation tests. In one of them σ is determined for several points on the head-capacity curve and plotted versus specific speed of the same points. Figure 12.20 shows curves for two pumps plotted on this basis. These curves give complete cavitation characteristics of the pump irrespective of size and speed.

In another method, efficiency or head is plotted against σ or suction head, at a constant speed and capacity, the drop in efficiency and head curves indicating the beginning of cavitation (Fig. 12.21). These curves

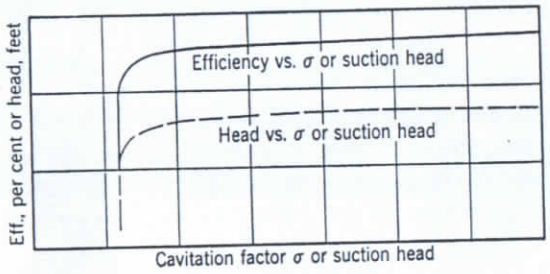

FIG. 12.21. Cavitation characteristics at constant speed and capacity.

give cavitation information for one point on the head-capacity curve, and this method is used mostly for model testing when head-capacity conditions are fixed and safe suction head is determined from model testing.

The general trend of σ variation for the b.e.p. of pumps of different specific speeds is shown in Fig. 12.22 and is discussed further under 8 below.

When the plant's pumping capacity, head, and suction head are given, the plant's σ is fixed. By selecting the proper pump speed, pumps of different specific speed may be used to meet the plant's requirements with a desired degree of protection from cavitation. Frequently, the speed is also fixed by the specifications. In that case the specific speed of the plant is fixed. Only a slight variation in pump design is possible in such a case by placing the operating point to the right or left of the b.e.p. The pump's rated normal specific speed at the b.e.p. will be different from the plant's specific speed, but special designs may be used to obtain the desired degree of protection against cavitation. With pumps of high specific speed, where the dynamic depression $\lambda(w_1^2/2g)$ plays an important part in setting up cavitation conditions, the number of impeller vanes is a very effective means of reducing the critical σ value without changing the specific speed materially (Fig. 12.14).

8. From theoretical consideration, it is possible to establish a relationship between the σ factors and specific speed for b.e.p.[22,33]

$$\frac{\sigma_2}{\sigma_1} = \left(\frac{n_{s2}}{n_{s1}}\right)^{4/3} \tag{12.13}$$

The general trend of σ variation as a function of specific speed as found by actually plotting experimental results agrees very well with

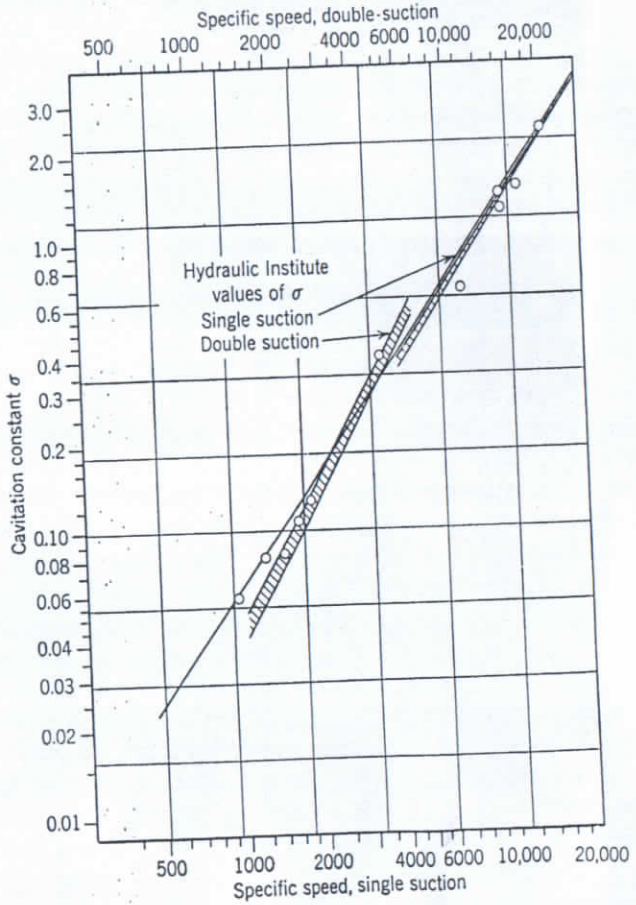

FIG. 12.22. Cavitation constant σ versus specific speed for b.e.p.

equation 12.13, as evidenced, for instance, by the curve published by Wislicenus, Watson, and Karassik [34] which follows exactly equation 12.13. For a series of pumps of consistent design, a continuous curve of σ values versus specific speed should be obtained, as all design fac-

tors governing cavitation (eye area, number of vanes, and so on) are continuous functions of specific speed. The σ curve on Fig. 12.22 can be expressed by the following equations.

$$\sigma = \frac{6.3 n_s^{4/3}}{10^6} \qquad \text{for single-suction pumps} \qquad (12.14)$$

$$\sigma = \frac{4.0 n_s^{4/3}}{10^6} \qquad \text{for double-suction pumps} \qquad (12.15)$$

Figure 12.22 also shows σ values obtained from the Hydraulic Institute charts of the upper limits of specific speeds for double-suction and single-suction pumps. This chart gives a belt of σ values for several specific speeds rather than a single curve, higher values of σ applying to lower head pumps. Such arrangement resulted from the superimposition of performances of pumps of different makes.

9. Suction condition of pumps in respect to cavitation can be expressed by another criterion known as suction specific speed,[34, 35] and defined as

$$S = \frac{\text{rpm}\sqrt{\text{gpm}}}{\Delta h^{3/4}} \qquad (12.16)$$

The development of this equation is based on the use of similarity relations (affinity laws) at conditions approaching cavitation, and it does not establish any new relationship between the variables entering into this expression which cannot be determined from the affinity laws or σ consideration. There is a fixed connection between the factor S, σ, and specific speed.

$$\frac{n_s}{S} = \sigma^{3/4} \qquad (12.17)$$

Substituting the values of σ from equations 12.14 and 12.15 into equation 12.17 shows that

$$S = 7900 = \text{constant} \qquad \text{for single-suction pumps} \qquad (12.18)$$

$$S = 11{,}200 = \text{constant} \qquad \text{for double-suction pumps} \qquad (12.19)$$

With special design suction specific speeds approaching $S = 15{,}000$ were realized for single-suction pumps at b.e.p. At partial capacity, S values up to 20,000 are possible at some sacrifice of efficiency. For special services (the rocket engine fuel pumps), still higher values of $S = 40{,}000$ were contemplated by providing an axial-flow booster impeller ahead of the regular impeller entrance. The booster impeller

operates by cavitating at partial capacity, thus greatly reducing the efficiency of the combination.

By analogy from the performance specific speed n_s, a physical meaning for the suction specific speed can be attached, that of: rpm of a geometrically similar impeller to produce a capacity of 1 gpm at NPSH of 1 ft. However, this has no practical application. The number S is used only for labeling impellers in regard to their NPSH requirements. This is independent of the pump size and its operating specific speed n_s. If lines of constant suction specific speeds are drawn on Fig. 12.22, these will be parallel to the line $S = 7900$ shown in the figure, higher values of S being below this line. Such lines would be a part of the scale network not dependent on any experimental observation.

A constant value of S is associated with similar entrance velocity triangles, i.e., $c_{m1}/u_1 = \tan \beta_1 = \text{constant}$ and $c_{m1}/\sqrt{\text{NPSH}} = \text{constant}$. Where c_{m1} is the meridional entrance velocity, u_1 is the impeller eye peripheral velocity, and β_1 is the impeller vane entrance angle at the impeller eye diameter D_1. Higher values of S lead to lower values of β_1 and c_{m1}.

10. *When using a model for testing performance and cavitation conditions, the similarity of the model and the prototype should be extended to the suction approach to the impeller and the discharge piping.*

12.8 THERMODYNAMIC ASPECTS OF CAVITATION

(*a*) **Introduction.** The boiling of liquid in the process of cavitation is a thermal process and is dependent on the liquid properties: pressure, temperature, latent heat of vaporization, and specific heat. During cavitation conditions, damage to the pump performance (head-capacity and efficiency) is caused by the appearance and disappearance of vapor cavities in the low pressure zone which disrupt the dynamic conditions existing during normal pump operation when the flow is all solid liquid. To make the boiling possible the latent heat of vaporization must be derived from the liquid flow. This necessary flow of heat from the liquid can only take place when the liquid temperature is above that corresponding to the saturation temperature at the prevailing pressure in the low pressure cavitation zone. This is the same as to say that the pressure in the cavitation region must fall below the saturation pressure corresponding to the liquid temperature.

The extent of damage to the head-capacity characteristics of a pump depends upon the amout of liquid vaporized and the vapor specific volume at the existing pressure in the cavitation zone. The effect of the liquid properties on cavitation will be observed by comparing the per-

formance of a given pump, at a given speed, handling water at various temperatures. In this way identical dynamic conditions are assured inside the impeller passages. The performance of a centrifugal pump, when it is not affected by cavitation, is independent of the fluid properties, be it liquid, vapor, or gas.

(b) Thermal Cavitation Criterion. The effect of properties of liquids on the behavior of a centrifugal pump under cavitation conditions can be studied analytically as follows.

On Fig. 12.23, curve $ABCD$ is the normal H-Q characteristic established under ample NPSH so that no cavitation occurs. Curve $ABC'E$

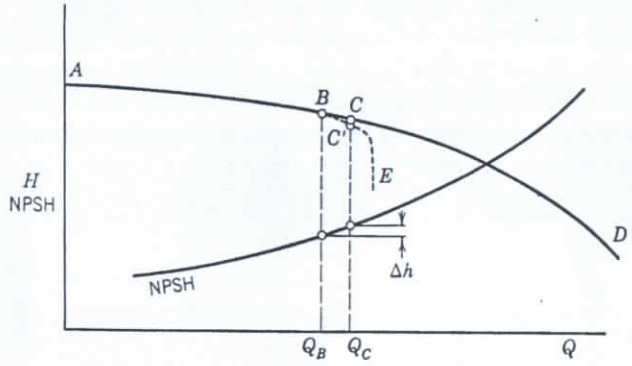

FIG. 12.23. Definition of the depression Δh.

is a typical H-Q curve under limited NPSH. The NPSH curve shown represents minimum values for incipient cavitation as determined by such points as B on the curve $ABC'E$. Suppose now that the NPSH value for capacity Q_C is reduced by Δh and sufficient to produce a measurable effect on the performance (point C'). The saturation temperature corresponding to the new reduced pressure in the low pressure zone of the impeller will be lower than the original temperature by ΔT. If a sufficient time is allowed, Δh_f Btu per pound of liquid passing through the low pressure zone will be available for vaporization of liquid. The value of Δh_f is the difference between the enthalpy of the liquid at original conditions of thermal equilibrium and the new conditions at a pressure Δh less than original. This increment of enthalpy can be expressed as

$$\Delta h_f = C_L \, \Delta T \tag{12.20}$$

where C_L is the specific heat of the liquid.

If it is assumed that thermal equilibrium is restored, the following heat balance equation can be written for each pound of liquid passing

through the low pressure zone. The liquid not passing through the low pressure zone need not be considered as it takes no part in the cavitation process.

$$1 \times \Delta h_f = r_v L \tag{12.21}$$

where $r_v < 1$ is a fraction of 1 pound of liquid boiled per each pound of liquid and L is the latent heat at vaporization. Introducing specific volumes of liquid and vapor instead of their weights, equation 12.21 becomes after arrangement:

$$\frac{V_v}{V_L} = \frac{v_v}{v_L} \frac{\Delta h_f}{L} = B \tag{12.22}$$

Here V represents volumes, v represents specific volumes, subscript L is for liquid, subscript v for vapor, and

$$V_L = 1 \times v_L; \qquad V_v = r_v v_v \tag{12.23}$$

For a given pump operated at the same speed and capacity when pumping two different liquids, the same value of V_v/V_L would mean the same extent of cavitation and the same damage to the performance. Thus this ratio may serve as a criterion of the pump behavior under cavitation conditions when handling different liquids. It will be given a symbol B. The value of the liquid thermal criterion B can be calculated from equation 12.22, repeated below,

$$B = \frac{v_v}{v_L} \frac{\Delta h_f}{L} \tag{12.24}$$

in terms of properties of the liquid for an assumed value of the depression Δh. When a comparison is made of the behavior of a pump under cavitation conditions pumping two different liquids, the value of the thermal criterion B should be calculated for the same assumed value of the depression Δh.

For practical use of the thermal criterion B complete cavitation performance, such as Fig. 12.24, of a given pump (or similar pump) should be available for different liquids or for water at various temperatures. Water has an advantage in that its properties are known for a wide range of temperatures and pressures. To estimate the performance of the given pump or similar pump when pumping a different liquid under limited NPSH, the value of B is first calculated for an assumed value of Δh. Then the available test of the pump which gives the same or approximately the same, value of B for the same Δh will apply to the new liquid.

When the criterion B is applied in this manner its absolute value is not important. The value of B depends upon the value of Δh used for its calculation. The value of the depression Δh does not have to conform to the definition used for the development of expression for B. The absolute value at B does not enter into consideration when B is used as proposed here.

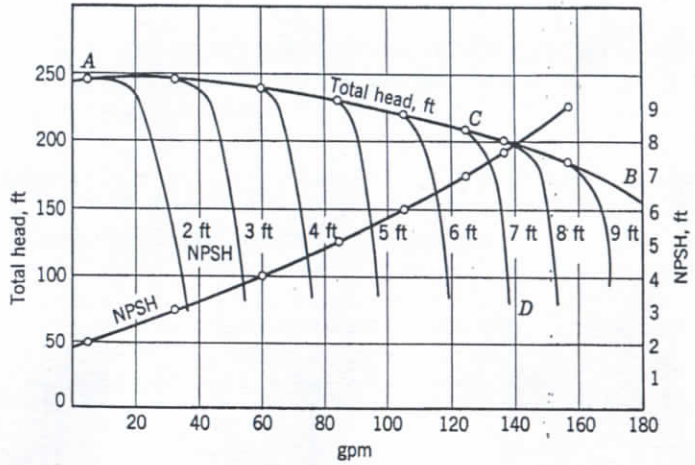

FIG. 12.24. Test of a 1½-in. single-stage pump at 3470 rpm, on water, 70°F.

(c) Remarks. 1. The heat balance equation 12.21 is based on the assumption that the thermal equilibrium under the reduced pressure Δh is restored. This theoretically would require infinite time. However, when comparing the performance of the same or similar pump handling two different liquids at the same value of the criterion B, the effect of time will be the same in both cases. Equation 12.22 really means that, for the same value of B, the rate of increase of the volume of flow through the low pressure zone (or the impeller channel) is the same for two liquids and, hence, the damage to the head-capacity characteristics is the same.*

(d) Test Results and Numerical Illustrations. Figure 12.25 shows the performance of a 1½-in. pump at 3470 rpm pumping deaerated water of different temperatures under the same net positive suction head (NPSH) of 4 ft. These curves were compiled from a series of tests with water at stated temperatures and different NPSH values. Figure 12.24

* A similar method of attack on the same problem was presented by R. C. Fisher, *Proc. Inst. Mch. Engrs.*, Vol. 152, 1945, and also by E. E. Breault of Ingersoll-Rand Company in private correspondence with the author in 1947.

Also by R. B. Jacobs, K. B. Martin, C. J. Van Wylen, and B. W. Birmingham "Pumping Cryogenic Liquids," *Report 3569*, National Bureau of Standards, 1956.

is one of such tests with water at 70°F. For a given pump operated at the same speed with an ample suction head (no cavitation), the dynamic conditions within the impeller are identical at the same rate of flow. With a limited NPSH identical dynamic conditions will prevail at the point of incipient cavitation for all liquids (point B on Fig. 12.25). A given dynamic depression below the pressure prevailing at the low pressure zone for point B will produce different amounts of vapor for different liquids. The difference in the form of the head-capacity and efficiency curves at capacities higher than those corresponding to the point B depends on the physical properties of liquids.

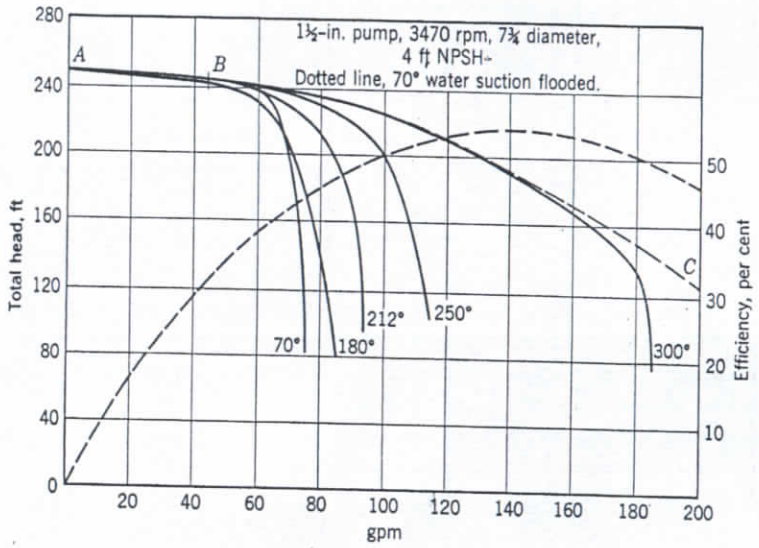

FIG. 12.25. Test of a 1½-in. pump at 3470 rpm on water at different temperatures and saturation pressures.

TABLE 12.1. PHYSICAL PROPERTIES OF WATER AND VAPOR

Temperature, °F	Press., psia	Vapor: Specific Volume, cu ft/lb	Vapor: Latent Heat, Btu/lb	Enthalpy of Liquid, Btu/lb
65	0.3056	1021.4	1057.1	33.05
70	0.3631	867.9	1054.3	38.04
180	7.510	50.23	990.2	147.92
212	14.696	26.80	970.3	180.07
250	29.825	13.82	945.5	218.48
300	67.013	6.466	910.1	269.59

The properties of water and its vapor are tabulated in Table 12.1 for several temperatures. The following observations can be made from an inspection of this table:

1. The specific volume of vapor decreases rapidly as pressures and temperatures are increased. At the critical pressure and temperature the specific volume of liquid and of saturated vapor is the same, thus it would appear that no cavitation can occur under these conditions.

2. A depression of only 0.0575 psi at 70°F (equivalent to a head of 1.6 in.) results in a temperature differential ΔT of 5°F; but for 300°F water, the same depression corresponds to a temperature difference of only 0.0533°F. The difference in enthalpy of water per °F is essentially the same at 70°F and at 300°F. Thus for the same depression of 1.6 in. of water more heat is available for vaporization at 70°F than at 300°F. At the same time the specific volume of vapor at 70°F is 134 times greater than that of vapor at 300°F, thus the difference in behavior under cavitation conditions for water at 70°F and at 300°F is easy to visualize.

Table 12.2 shows calculations of the thermal cavitation criterion B for water at five different temperatures. The last column gives the same variables for butane at 70°F. The value of the criterion B for butane is essentially the same as that for water at 300°F (slightly lower); thus it is expected that the pump performance on water at 300°F will apply to butane.

Since the criterion B by definition (equation 12.22) represents the ratio of volume of vapor to the volume of liquid per pound of the liquid (V_v/V_L), for the same depression Δh lower values of B mean less pronounced effects of cavitation. High values of B shown in Table 12.2 at low temperatures ($B = 253$ at 70°F) merely mean that the assumed value of $\Delta h = 1.6$ in. was too high for this liquid, and the value of the temperature differential (5°F at 70°F) is not realistic under actual operating conditions. Considering the very short time it takes for the liquid to traverse the impeller channel (0.025 sec in the test pump), only a small fraction of the available heat is utilized for vaporization, the liquid passing the low pressure zone in a superheated state. The fraction of liquid in a vapor state given by equation 12.21, $r_v = \Delta h_f/L$, is never realized in actual pumps for that reason.

When pumping petroleum products which are mixtures of various hydrocarbons, under limited NPSH, it is expected that the lightest fraction will determine the cavitation behavior of the mixture. This follows from the fact that, even in the case of water at 70°F under the exaggerated conditions assumed in Table 12.2, the amount of vapor is

TABLE 12.2. CALCULATION OF THERMAL CAVITATION CRITERION B FOR SEVERAL LIQUIDS FOR $\Delta h = 1.6$ IN.

Liquid Properties	Water, 70°	Water, 180°	Water, 212°	Water, 250°	Water, 300°	Butane, 70°
1. Temperature difference ΔT, °F	5.0	0.34	0.194	0.1058	0.0533	0.0645
2. Specific volume of vapor v_v, cu ft/lb	867.9	50.53	26.80	13.82	6.466	2.88
3. Specific volume of liquid v_L, cu ft/lb	0.01606	0.01651	0.01672	0.01700	0.01745	0.02773
4. $v_v/v_L = (2)/(3)$	54,000	3050	1603	812	369	103.5
5. $v_L/v_v = (3)/(2)$	0.0000185	0.000328	0.000625	0.00123	0.00272	0.00967
6. Enthalpy difference Δh_f, Btu/lb	4.99	0.340	0.196	0.1065	0.055	0.0322
7. Latent heat L, Btu/lb	1054.1	990.2	970.3	945.5	910.1	157.5
8. $\Delta h_f/L = r_v$, (6)/(7)	0.00468	0.000344	0.000204	0.000115	0.00006	0.000198
9. $B = (4) \times (8)$	253	1.048	0.324	0.0915	0.0223	0.0202

less than ½ per cent of the weight of the liquid. The actual amounts of the vapor produced in the low pressure zone may be a fraction of those tabulated if the effect of time is allowed. The values of r_v, as small as they appear in Table 12.2, are not unreasonable as can be seen from dynamic considerations. The head-capacity characteristic of a pump at a given speed does not depend upon the nature of the fluid, and is the same for liquids and vapors or gases. Assume that the pump will handle vapor only without any liquid. Then the weight of the vapor handled will be only a small fraction of the weight of the solid liquid. The ratio of the two is equal to the ratio of specific volumes (v_L/v_v) and is given in Table 12.2, item 5. It is interesting to note that the figures are of the same order as those in item 8 of the same table.

(*e*) **Deviation from Thoma's Law.** By applying equation 12.22 to similar pumps operated at different speeds pumping the same liquid (cold water), the thermal criterion B reduces to

$$B = \Delta h_f \times \text{constant} = V_v/V_L \tag{12.25}$$

indicating that the same damage to the performance (value of V_v/V_L) is caused when Δh_f is the same, and not at the same value of $\sigma = \text{NPSH}/H$. The same thought is expressed by equation 12.11, derived from equation 12.10, established by Tenot [27] with the aid of high speed photography. This means that the value of NPSH necessary to produce measurable cavitation effects consists of two parts: one is the value corresponding to the incipient cavitation (this follows the dynamic laws of similarity σ = constant), the second part is a depression Δh (negative) necessary to produce a thermal depression ΔT sufficient to cause vaporization. This is independent of the dynamic conditions (head, or speed) and is determined by the physical properties of liquid. However, an analysis of Krisam's test results (Figs. 12.17 and 12.18) indicates that these considerations are not sufficient to explain completely the deviation from σ = constant relation. This suggests that the effects of Reynolds number and particularly time are contributing factors responsible for the flow deviation from the laws of dynamic similarity under cavitation conditions.

(*f*) **NPSH Correction for Liquids Other than Water.** The NPSH requirements for cold-water pumps of different types are either known from previous tests, or can be very closely estimated from the available test data on similar pumps. The NPSH requirements for liquids other than water, such as petroleum products, can be calculated by means of equation 12.22 if the value of the vapor/liquid ratio V_v/V_L has been previously established experimentally. By definition the ratio V_v/V_L

produces a measurable effect on the pump performance and does not depend on the nature of the liquid. Equation 12.22 permits calculation of the enthalpy increment Δh_f for cold water Δh_{f1} and any other liquid Δh_{f2}. The pressure drop below the saturation pressure corresponding to these enthalpy increments can be determined from tables or charts of the physical properties.

The difference between these depressions is the difference between the NPSH requirements for water and the other liquid.

$$\Delta h_2 - \Delta h_1 = (\text{NPSH})_1 - (\text{NPSH})_2 \tag{12.26}$$

The method for the experimental determination V_v/V_L is the reverse procedure of that outlined for calculation of the NPSH correction as presented above. If performance of the same pump under cavitation conditions for the whole range of capacities is established experimentally, both for water and some other liquid (curves similar to Fig. 12.24), then the difference in NPSH for the same capacity will represent the difference between the depressions below the saturation point as they appear in equation 12.26. The values of $B = V_v/V_L$, equation 12.22 should be equal for water and the tested liquid. By selecting several values of Δh_{f1} for water, Δh_{f2} values for the tested liquid are calculated. The corresponding values of depressions Δh_1 and Δh_2 should satisfy equation 12.26. Presently no experimental data are available to prove or disprove the above deduction.

Although the expression for V_v/V_L, equation 12.22, contains only values of the physical properties of liquids, it cannot be indiscriminately applied to pumps of different sizes, types, and speeds because its value may be affected by the time it takes the liquid particles to traverse the cavitation zone. Thus the method of NPSH corrections depends for its accuracy on the available test information of a reference pump operated under dynamically identical conditions. In this respect this method is only a different way of using the basic thermal relationship developed in the first article of this chapter.

(*g*) **Thermal Cavitation Criterion for Mixture of Liquids.** Pumping petroleum products is next in importance to pumping water. Many petroleum products are mixtures of two or more hydrocarbon components. When such a mixture boils in the process of cavitation, all components of the mixture vaporize at different rates, depending on the proportions (mole fraction) of each component in the mixture, their temperature, and their vapor pressures. The performance of a pump handling mixtures of liquids under cavitation conditions can be estimated by comparison with the performance of a reference pump for the same value of

the thermal cavitation criterion. For an assumed NPSH reduction Δh, the value of the thermal cavitation criterion B is calculated for a mixture of liquids as follows:

1. By referring to equation 12.22, the value of the specific volume of the vapor mixture v_v is calculated on the basis that each component contributes to the value of the specific volume of the vapor mixture in proportion to its mole fraction, which for gases and vapors is equal to the fractions by volume.

$$v_v = v_{v1}m_1 + v_{v2}m_2 + v_{v3}m_3 \tag{12.27}$$

where v_v are specific volumes.

m are mole fractions, or fraction by volume of different components in the vapor mixture so that $m_1 + m_2 + m_3 = 1$.

Subscripts 1, 2, and 3 indicate components 1, 2, and 3.

2. The value of the specific volume of the liquid mixture v_L is calculated in the same manner, by taking mole fractions (not fractions by volume) of specific volumes of components.

$$v_L = v_{L1}m_1' + v_{L2}m_2' + v_{L3}m_3' \tag{12.28}$$

where $m_1' + m_2' + m_3' = 1$.

3. The value of heat furnished by the liquid to cause vaporization (Δh_f) is calculated by using mole fractions of the values of the enthalpy increments of the component liquids m_1', m_2', m_3'.

$$\Delta h_f = \Delta h_{f1}m_1' + \Delta h_{f2}m_2' + \Delta h_{f3}m_3' \tag{12.29}$$

The value of the latent heat L is calculated as a sum of the mole fractions of latent heats of vapor components, or m_1, m_2, m_3.

$$L = L_1m_1 + L_2m_2 + L_3m_3 \tag{12.30}$$

Composition of Vapor. Usually the composition of the liquid to be pumped, its pressure, and temperature are known. Also, the physical properties of the component liquids must be available. The composition of the vapor can be calculated by application of Raoult's or Henry's laws. In the case of a mixture of two liquids the procedure is straightforward, but for a mixture of three or more liquids, reference 36 can be consulted.

If y_1 and y_2 are the volume or mole fractions of the component 1 and 2 in a vapor mixture, so that $y_1 + y_2 = 1$ and x_1 and x_2 are the mole fractions of the same components in the liquid ($x_1 + x_2 = 1$), Raoult's law states that

$$y_1 = \frac{P_1}{P}x_1 \quad \text{and} \quad y_2 = \frac{P_2}{P}x_2 \tag{12.31}$$

where P_1 is the vapor pressure of pure component 1 at the same temperature.

P_2 is the same for pure component 2.

P is the vapor pressure of the mixture $P = p_1 + p_2$, where p_1 is partial vapor pressure of component (1) and p_2 is the same for component (2); $p_1 = p_1x_1$ and $p_2 = p_2x_2$.

Raoult's law applies to mixtures of chemically similar components which do not interact together in any way. In the case of complex hydrocarbon mixtures, the deviation from the law depends upon the similarity and dissimilarity of the components. An accuracy of from 5 to 15 per cent is quite common when the law is applied to such mixtures.

Henry's law gives a more general relationship between the liquid and vapor mole fractions.

$$y = Kx$$

where K is an experimental constant dependent on the pressure and temperature. The values of K for a majority of hydrocarbons are available in the form of charts.[36, 37, 38]

12.9 MEANS OF AVOIDING OR REDUCING CAVITATION

1. *A knowledge of the cavitation characteristics of pumps is the most important prerequisite of any cavitation problem study.*

2. *Second in importance is the knowledge of existing suction conditions of the plant at the time the pump selection is made.*

3. An increase of suction pipe size, reduction of suction pipe length, elimination of turns, provision of a good suction bell—in other words, reduction of losses in the suction pipe—improve the suction conditions of a pump with regard to cavitation.

4. An increase in the number of vanes in high specific speed pumps, or the removal of parts of the vanes and opening the passages in the impeller eye of low specific speed pumps, will reduce the minimum suction head to meet fixed head-capacity conditions.

5. An ample suction approach area without excessive prerotation and a better streamlining of impeller approach are essential to obtain optimum cavitation characteristics of a pump.

6. Special materials may be used to reduce the pitting of pump parts due to cavitation, when justified, or when it is impossible to eliminate cavitation by any other means.

7. The noise and vibration caused by cavitation can be reduced or eliminated by the admission of a small amount of air to the pump suction.

8. The impeller velocities, impeller vane load, and head per stage should be low for minimum suction head. All these factors lead to a bigger pump operated at a low speed, and possibly to location of the operating point to the left of the b.e.p.

9. A low impeller inlet angle β_1 leads to a reduction of NPSH requirements particularly at partial capacities.

10. A uniform velocity distribution through the impeller eye is important to obtain a minimum NPSH condition. Figure 12.26 shows a test

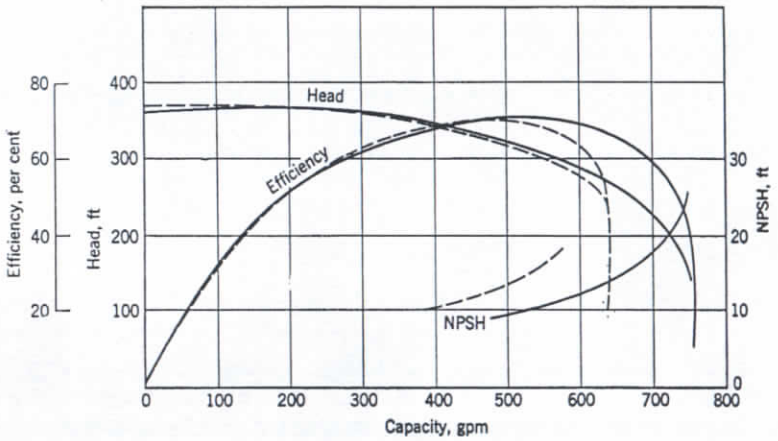

FIG. 12.26. Effect of suction nozzle on NPSH requirements. 3-in. pump, 3500 rpm. Full lines, straight end suction; dotted lines, flat elbow suction nozzle.

of the same impeller in two casings; one has a straight tapered suction nozzle (full lines), the other has a flat elbow inlet nozzle similar to that shown on Fig. 7.2 (dotted lines). The advantages of the straight suction nozzle as to cavitation are quite obvious.

REFERENCES

1. I. A. Winter, "Hydraulic Turbine Development," *Proc. A.S.C.E.*, Vol. 65, pp. 1553–1589, 1939; abstracted in *Mech. Eng.*, Vol. 62, p. 27, 1940.
2. R. L. Mahon, "Hydraulic Butterfly Valves," *Trans. A.S.M.E.*, Vol. 54; *Hydraulics*, 54–2, 1932.
3. R. V. Terry, "Development of the Automatic Adjustable Blade-Type Propeller Turbine," *Trans. A.S.M.E.*, Vol. 63, pp. 394–409, 1941.
4. W. Siebrecht, "Untersuchungen über Regelung von Kreiselpumpen," *Z. Ver. deut. Ing.*, Vol. 74, p. 87, 1930.
5. B. R. Van Leer, "Throttling Suction Changes Pump Characteristic," *Power Plant Eng.*, Vol. 31, p. 1133, 1927.

6. H. Foettinger, "Untersuchungen über Kavitation und Korrosion," *Hydraulische Probleme*, Berlin, Verein Deutscher Ingenieure, p. 14, 1926.
7. A. J. Stepanoff, "Leakage Loss and Axial Thrust in Centrifugal Pumps," *Trans. A.S.M.E.*, Vol. 54, *Hydraulics*, 54–5, 1932.
8. Hans Mueller, "Spalt Kavitation an schnelllaufenden Turbomaschinen," *Z. Ver. deut. Ing.*, Vol. 79, p. 1165, 1935.
9. C. Pfleiderer, *Die Kreiselpumpen*, p. 169, Berlin, Julius Springer, 1955.
10. J. C. Hunsaker, "Cavitation Research," *Mech. Eng.*, Vol. 57, p. 211, 1935.
11. T. C. Poulter, "The Mechanism of Cavitation Erosion," *Trans. A.S.M.E.*, Vol. 9, pp. A-31–A-37, 1942.
12. P. de Haller, "Investigation of Corrosion Phenomena in Water Turbines," *Escher-Wyss News*, p. 77, May–June 1933.
13. Battelle Memorial Institute, *Prevention of the Failure of Metals under Repeated Stress*, p. 164, New York, John Wiley & Sons, 1941. (Out of print.)
14. W. J. Rheingans, "Accelerated Cavitation Research," *Trans. A.S.M.E.*, Vol. 72, p. 705, 1950.
15. H. Schroeter, *Versuche zur Frage der Werkstoffsanfressung durch Kavitation*, Munich, R. Oldenbourg, 1935.
16. E. B. Sharp, "Cavitation of Hydraulic Turbine Runners," *Trans. A.S.M.E.*, Vol. 62, p. 569, 1940.
17. S. L. Kerr, "Determination of the Relative Resistance to Cavitation Erosion by the Vibratory Method," *Trans. A.S.M.E.*, Vol. 59, p. 373, 1937.
18. J. M. Mousson, "Pitting Resistance of Metals under Cavitation Conditions," *Trans. A.S.M.E.*, Vol. 59, p. 399, 1937.
19. "Eighth Report to the Corrosion Research Committee," *J. Inst. Metals*, Vol. XL, No. 2, 1928.
20. Saichiro Uchimaru, "Experimental Research on the Distribution of Water Pressure in a Centrifugal Pump Impeller," *J. Faculty Eng., Tokyo Imp. Univ.*, Vol. 16, 1925.
21. Fritz Krisam, "Versuche und Rechnungen zum Kavitations Problem der Kreiselpumpen," Mitt. Inst. Strömungsmaschinen Tech. Hochschule, Karlsruhe, February 1930.
22. H. Cardinal von Widdern, "On Cavitation in Centrifugal Pumps," *Escher-Wyss News*, p. 15, January–March 1936.
23. A. J. Stepanoff, "Propeller Pumps for Circulation of Molten Salt," *Refiner Natural Gasoline Mfr.*, Vol. 19, pp. 474–476, 1940.
24. C. D. Bower and P. H. Brown, "Prediction of Suction Limitations when Pumping Volatile Liquids," *Calif. Oil World and Petroleum Ind.*, p. 15, April 1943.
25. D. Thoma, "Bericht zur Weltkraftkonferenz, London, 1924," *Z. Ver. deut. Ing.*, Vol. 79, p. 329, 1935.
26. D. Thoma, "Verhalten einer Kreiselpumpe beim Betrieb im Hohlzog Bereich," *Z. Ver. deut. Ing.*, Vol. 81, p. 972, 1937.
27. M. A. Tenot, "Phénomènes de la Cavitation," *Mém. soc. ing. civils France, Bull.*, pp. 377–480, May and June, 1934.
28. R. E. B. Sharp, "Cavitation of Hydraulic Turbine Runners," *Trans A.S.M.E.*, Vol. 62, p. 569, 1940.
29. G. F. Wislicenus, "Test Stand for Centrifugal and Propeller Pumps," *Trans. A.S.M.E.*, Vol. 64, No. 6, p. 619, 1942.
30. F. H. Rogers, *Trans. A.S.M.E.*, Vol. 58, p. 317, 1936.
31. F. Krisam, "Neue Erkenntnisse im Kreiselpumpenbau," *Z. Ver. deut. Ing.*, Vol. 95, No. 11–12, p. 320, April 1953.

32. K. Rütschi, "Untersuchungen an Spiralgehäusepumpen verschiedener Schnellläufigkeit," *Schweiz. Arch. angew. Wiss. u. Tech.*, p. 33, February 1951.
33. A. J. Stepanoff, *Trans. A.S.M.E.*, Vol. 62, pp. 158, 164, 1940.
34. G. F. Wislicenus, R. M. Watson, and I. J. Karassik, "Cavitation Characteristics of Centrifugal Pumps," *Trans A.S.M.E.*, Vol. 61, p. 17, 1939.
35. Paul Bergeron, Discussion, *Trans. A.S.M.E.*, Vol. 62, p. 162, 1940.
36. W. L. Nelson, *Petroleum Refinery Engineering*, New York, McGraw-Hill Book Company, pp. 244–256, 1936.
37. Technical Manual, *Natural Gasoline Supply Men's Association*, 1946, pp. 64–107.
38. J. W. Maxwell, *Data Book on Hydrocarbons*, New York, D. Van Nostrand Company, Inc., 1950.

Chapter 13

Special Operating Conditions of Centrifugal Pumps

13.1 INTRODUCTION

This chapter deals with operating conditions of centrifugal pumps beyond their normal head-capacity and speed range. If head-capacity and speed are assumed as positive for normal pump operation, the head-capacity characteristics are confined to one quadrant on the head-capacity coordinates. All the unusual head-capacity characteristics occupy the remaining three quadrants for a positive rotation, and all four quadrants for a negative rotation. Some of the special operating conditions are unavoidable, others occur accidentally, and still others can be reproduced only in the laboratory or they develop during a transient period while changing from one state to another. Operation of a centrifugal pump as a hydraulic turbine, behavior of a pump in the event of power failure, or starting a pump running in reverse are examples of unusual operating conditions.

In Fig. 13.1(*a*), quadrant *A* shows normal head-capacity curves at several speeds. These are expressed as percentage of the normal head capacity (at b.e.p.) for a certain speed selected as normal. It is possible to extend the head-capacity curves beyond zero head and zero capacity lines. In the first case—Fig. 13.1(*a*), quadrants *G* and *H*—water has to be forced through the pump, or the head is higher at the suction nozzle than at the discharge. Such a head is defined as negative. In the second case—Fig. 13.1(*a*), quadrant *B*—a head higher than the pump shut-off head is applied to the discharge nozzle and the flow through the pump is reversed; thus the flow becomes negative.

Figure 13.1(*c*) shows similar head-capacity curves with the pump speed reversed, or negative. Figure 13.1(*b*) shows the torque curves for all possible conditions appearing on Figs. 13.1(*a*) and 13.1(*c*). Obtained experimentally, such curves represent complete pump characteristics. A considerable interest has been aroused in the study of such complete pump characteristics by several articles published in Germany by Thoma,[1] Engel,[2] and Kittredge.[3] In the United States, several in-

vestigations conducted at the California Institute of Technology have been reported by Knapp.[4]

Prediction of pump behavior from theoretical considerations alone is impossible. Therefore, for solutions of such problems one has to rely on experimental results or complete pump characteristics covering all possible cases or combinations of head, capacity, torque, and speed.

13.2 COMPLETE PUMP CHARACTERISTICS; REPRESENTATION OF TEST RESULTS

This discussion is based on test results appearing in the publications listed as references and is supplemented with some test data by the author. To make the data applicable to all similar pumps, irrespective of pump size and speed, the head, capacity, torque, and speed are expressed in percentages of those values at the b.e.p., a certain speed being selected as normal.

To show all test values of the four variables involved, that is, head H, capacity Q, torque T, and speed n, on one chart, two of these can be taken as independent coordinates and the remaining two as parameters. Evidently, six combinations of pairs of independent variables are possible. By actual trial it has been found that speed versus capacity gives the best chart.

Figures 13.2, 13.3, and 13.4 are such charts for a centrifugal, mixed flow, and axial flow pumps. These charts will be used for the solution of several typical problems dealing with some unusual pump operating conditions.

13.3 MECHANICAL PROBLEMS CONNECTED WITH PUMP OPERATION OUTSIDE THE NORMAL HEAD-CAPACITY AND ROTATION RANGE

(*a*) **Mechanical Damage.** Opinions have been expressed [1,2,3] that, should power suddenly fail on a pump and reverse flow develop (no check valve in the discharge line), dangerous pressure surges may develop or the pump may reach a dangerous runaway speed in the reverse direction. These dangers are not founded when pumping cold water or any liquid far removed from the boiling point. *Although pressure surges do result from a sudden reversal of the flow and the motor may reach a speed exceeding the normal speed, the magnitude of both is such that no dangerous stresses develop in any standard part normally used for pumps or motors.*

It should be noted that at the time the studies of the complete pump characteristics were launched (about 1930), thousands of vertical pumps of the deep-well type had already been installed and were subjected to

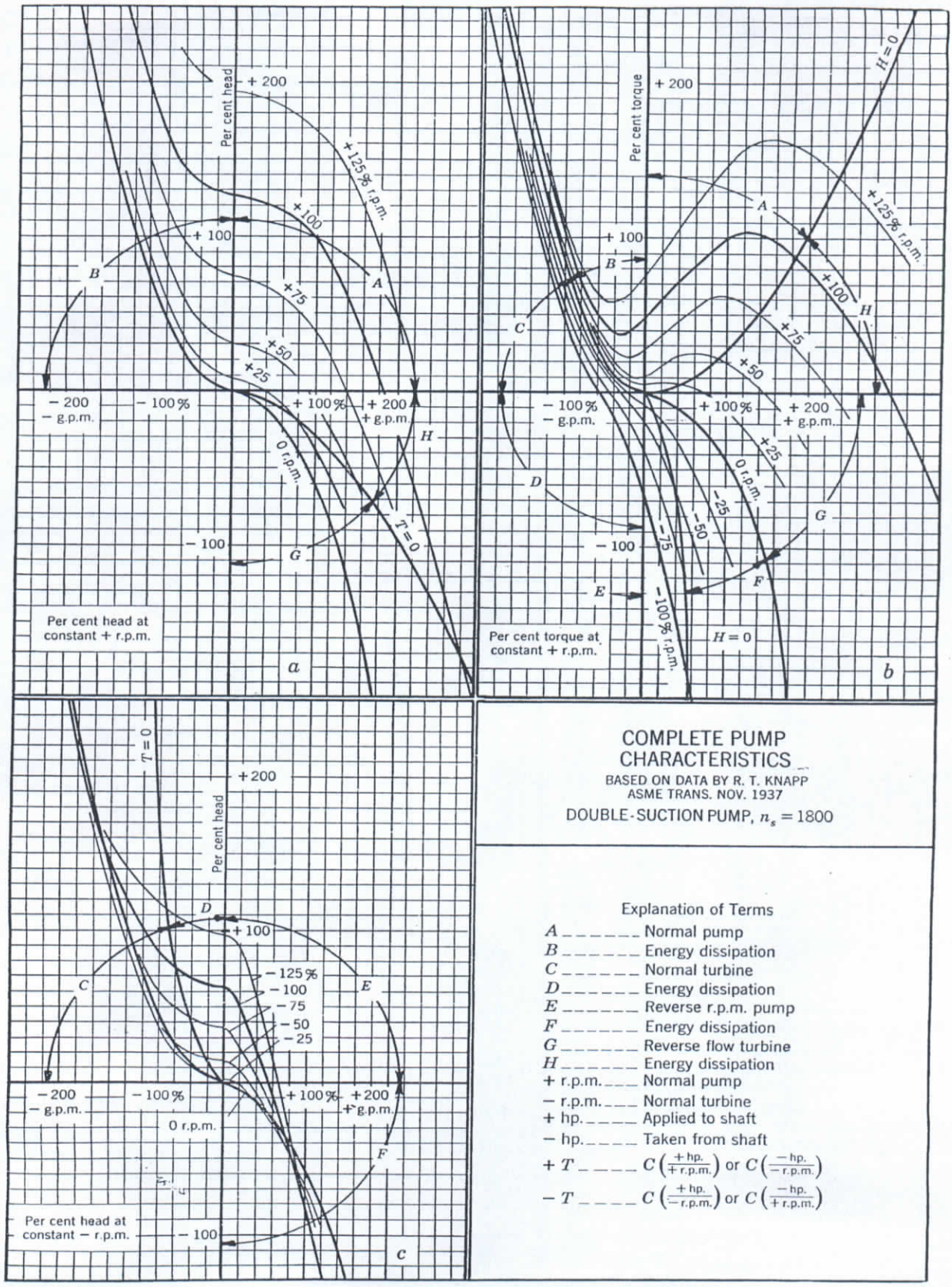

FIG. 13.1. Complete pump characteristics, double-suction pump; $n_s = 1800$.

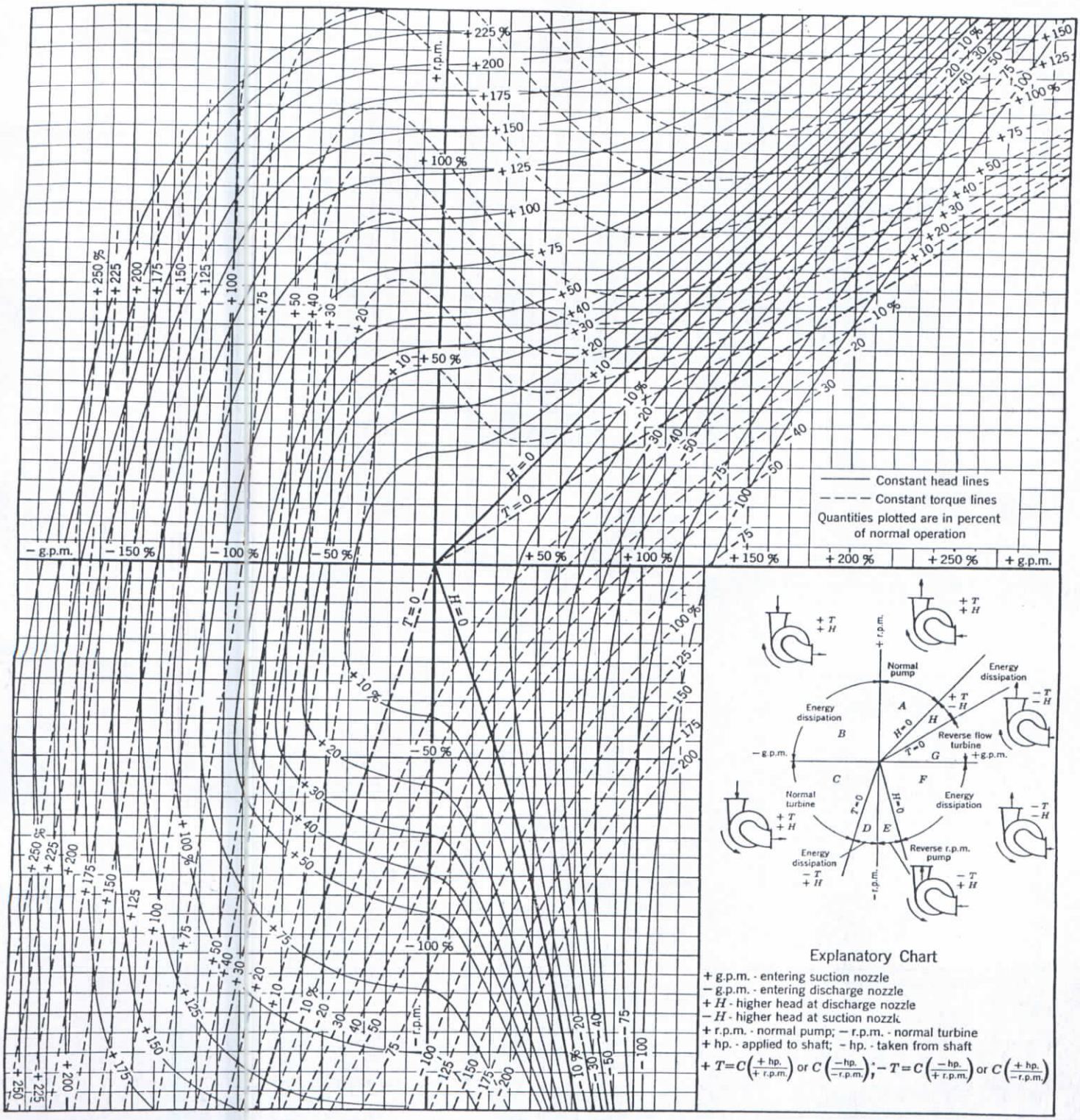

FIG. 13.2. Complete pump characteristics, double-suction pump; $n_s = 1800$.

FIG. 13.3. Complete pump characteristics, mixed flow pump; $n_s = 7500$. Data by W. M. Swanson.[3]

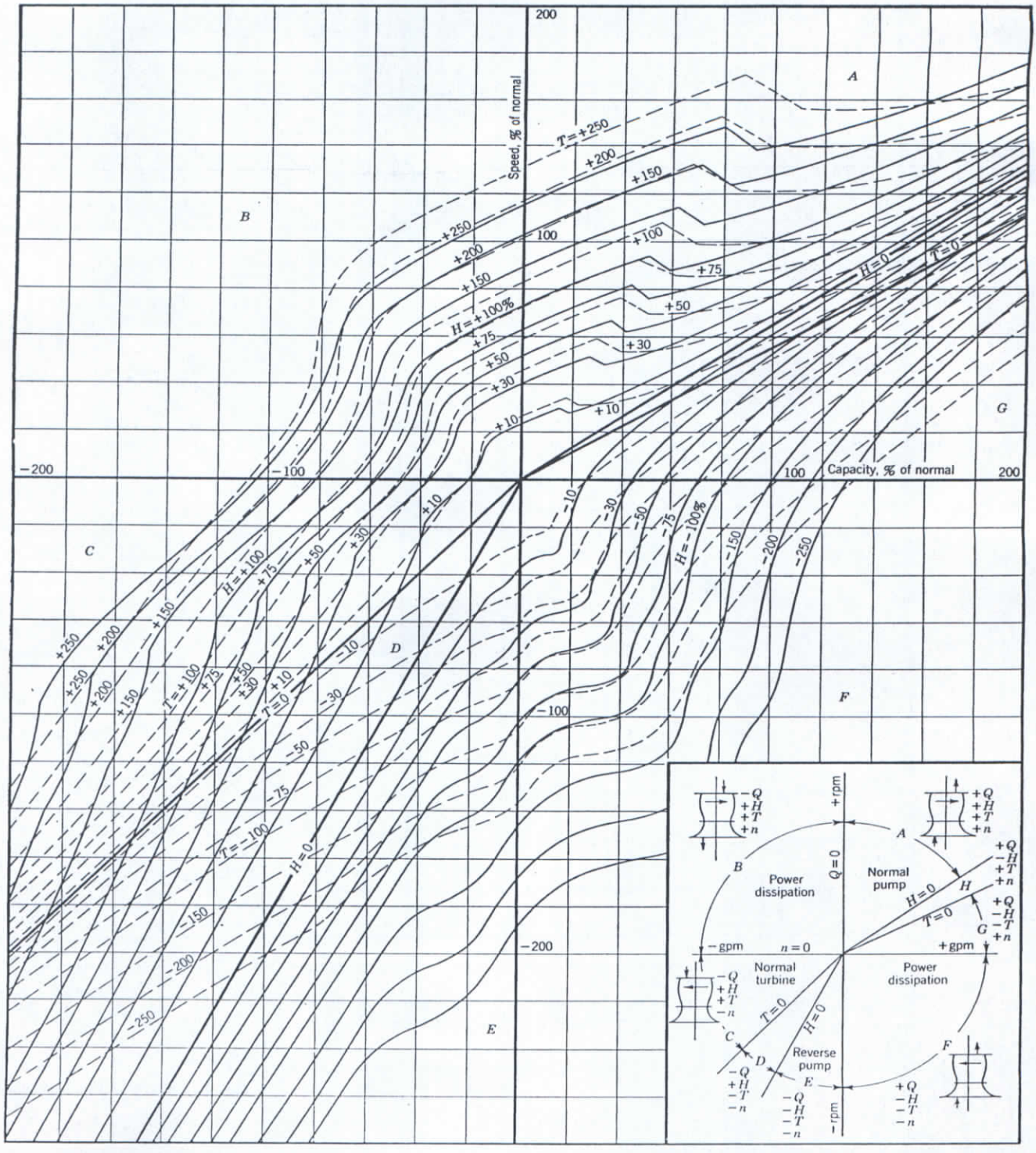

FIG. 13.3. Complete pump characteristics, mixed flow pump; $n_s = 7500$. Data by W. M. Swanson.[22]

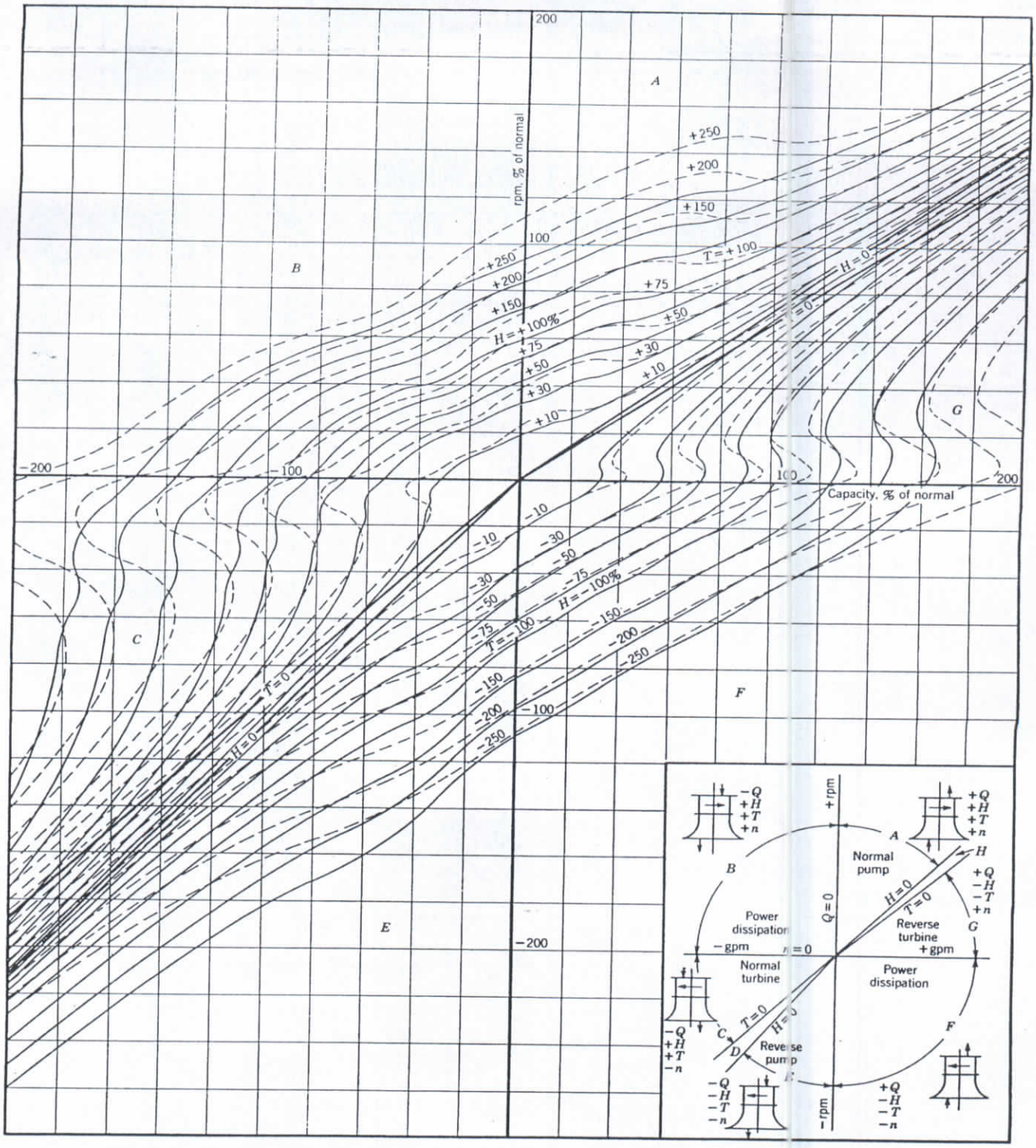

FIG. 13.4. Complete pump characteristics, axial flow pump; n_s = 13,500. Data by W. M. Swanson.[11]

reverse rotation under maximum heads approaching the pump total head every time they were stopped. The maximum reverse speeds recorded were in excess of 120 per cent of the normal pump speed. No dangerous speeds, pressure rise, or stresses in the pump shafts were observed.

When liquids approaching their boiling points, such as light hydrocarbons or boiler feed water, are being pumped, if the check valve fails (mechanical obstruction) in a sudden power failure, the liquid flowing from the discharge pipe will flash into vapor because of the sudden drop in pressure through the check valve. The reverse gas flow under the full discharge pressure in pounds per square inch will correspond to that under a head several hundred times the pump operating head expressed in feet of flowing gas. Under such conditions the pump reverse speed may exceed the normal speed a great many times, if not prevented by mechanical damage to the pump or driver. If only a small fraction of the total back-flow flashes into vapor it may be sufficient to ruin the pump or driver. Two cases of motor damage under such conditions have been called to the author's attention recently.

(*b*) Reverse Speed. Deep-well pumps have presented a number of problems connected with reverse rotation from the very early stages of their introduction; through the use of complete pump characteristics charts, solution of several problems has been simplified. Figure 7.25 shows a typical deep-well pump. In a great majority of cases the deep-well pumps used for irrigation lift water to the surface, and thus work against all static head. Every time the power is shut off, the pump is subjected to a full pump head and works as a turbine in a reverse direction at runaway speed or zero torque.

The experience of many years shows that no dangerous speed develops under these conditions and no mechanical damage results. By following the 100 per cent head line of Fig. 13.2 from the first quadrant through the second and to the intersection with the zero torque line in the third quadrant, it is found that this particular pump will develop 117 per cent reverse speed and 68 per cent capacity.

If part of the pump total head is friction, then the head on the pump when operating as a turbine at the runaway speed will be static head less friction head. If the speed and capacity are known at one head, the speed and capacity at any other head can be found by applying the affinity laws, that is, the speed and capacity vary directly as the square root of the head.

(*c*) Shaft Couplings. The screwed type of couplings is universally adopted for the column shaft deep-well pumps in this country. The hand of the threads is such that in normal pump operation the torque

exerted by the motor tightens the threads in the shaft couplings (Fig. 16.17). When the flow and speed are reversed, the pump becomes a driver and, although the direction of rotation is changed, the torque developed by the pump tends again to tighten the threads of the shaft couplings. For that reason no special means are employed to lock the threaded couplings on the shafts on vertical pumps. When power is applied to the shaft coupling, threads are tightened until the applied torque is equal the friction torque in the threads. The latter increases as the compression of the two shaft ends increases. To unscrew the coupling an equal torque is required. With large shafts this may present some difficulty. For large shafts, over 2 in. in diameter, it has been found helpful to insert a thin, plastic disk gasket between the shaft ends in the coupling. To take the coupling apart, heat is applied to the coupling until the gasket begins to melt. This relieves the tension between threads and the coupling starts unscrewing with less effort.

(*d*) **Motor-Disengaging Clutch.** If the motor of a deep-well pump is not wired to the power lines correctly and the pump is started in the wrong direction, the column shaft will unscrew in one of the couplings. Motor-disengaging clutches are used to prevent damage to the pump shaft or motor in such a case. Without the clutch the shaft would unscrew entirely and damage the threaded shaft ends, and would require the removal of the pump until the loose joint is discovered.

The disengaging clutch is now a standard part of all hollow shaft motors. Evidently, to avoid trouble, the motor rotation should be checked before it is connected to the pump. The possibility of reversal of rotation due to power phase crossing on the power lines is very remote and can be disregarded.

(*e*) **Wrong Rotation of Horizontal Pumps.** Use of locking devices (such as lock nuts and set screws) on deep-well shafts proved to be impractical. They increase the cost of parts and delay in assembly of deep-well pumps, without providing foolproof protection. However, on horizontal pumps, locking devices for parts mounted on the shaft are considered a necessity. Although checking of the motor rotation before it is coupled to the pump is prescribed by all pump manufacturers, all pumps are built so that no damage occurs if a pump is started in the wrong direction. What happens if these precautionary measures are neglected will be seen from the following illustration.

A 16-in. double-suction pump of conventional design, shown in Fig. 13.5, was installed at an industrial plant. Before starting the pump it was decided to test the whole piping system hydrostatically, including the pump. During this process, leakage was observed from the stuffing box and from under the shaft sleeves. Accordingly, the set screws

were removed from the shaft sleeves, and the sleeves and the stuffing box glands were tightened. After the completion of the hydrostatic test, the pump was started and after a few seconds the bracket supporting the outboard bearing was broken off. The motor rotation happened to be wrong and, since the stuffing boxes had been tightened, one of the sleeves started to unscrew until the shoulder on the inboard sleeve

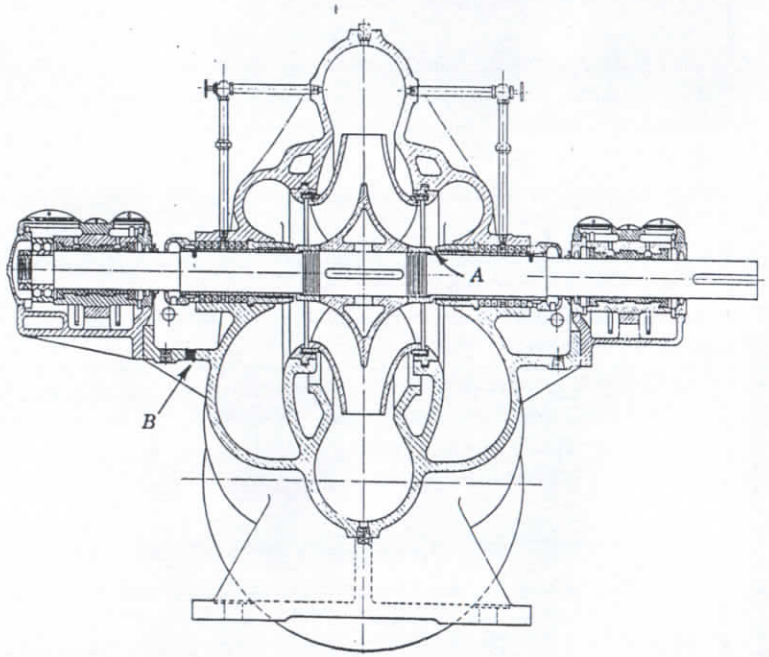

FIG. 13.5. Broken bearing bracket resulted from wrong rotation.

butted against the stuffing box bushing at *A*. Then the rotating element started to move outward, breaking off the thrust bearing support at *B*.

(*f*) **Motor Rotation.** There is no way to determine the rotation of a three-phase induction motor except by trial and observation of the exposed shaft end of the motor. The motor rotation should be ascertained before the motor is connected to the pump. However, in special designs the motor may be enclosed into a common cell with the pump so that no moving part of the pump or motor can be observed (submersible motor pumps). In that case all parts mounted on the pump shaft should be securely locked. The correct rotation of such units can be found by observing the pump head developed by the pump with discharged valve closed. By referring to Figs. 13.1(*a*) and 13.1(*c*) it will

be noticed that at the same speed (say 100 per cent) the pump shut-off head under correct rotation is in excess of the pump rated head (125 per cent), whereas at reversed speed the shut-off head is only about 60 per cent of the pump rated head. In every case when the motor rotation is checked with the pump coupled to the driver the pump should be filled with liquid before the motor trial to avoid seizure in closely fitted parts.

(*g*) **Non-Reversing Ratchets.** A great number of deep-well pumps are driven by tractor engines through a power take-off and a quarter-turn belt. It has been found that the driving belt has a tendency to

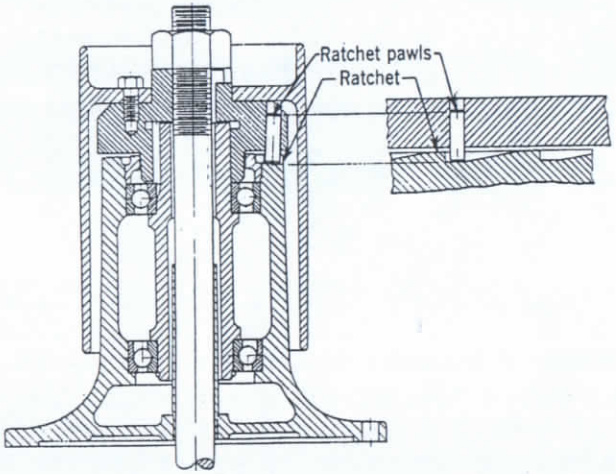

FIG. 13.6. Deep-well belt-drive head with non-reverse ratchet (Peerless Pumps).

slip off the pulleys when the pump rotation is reversed after stopping. All deep-well belt-drive heads are equipped now with non-reversing ratchets. These permit the pump pulley to be driven in only one direction. Figure 13.6 shows a belt-drive deep-well head. In this the upper half of the clutch carries several loose vertical pins. These are pushed up and held in their position by centrifugal force when the pump starts rotating in the right direction. When the power is cut off and the pump pulley slows down to almost zero speed the pins drop down and engage the teeth of the stationary ratchet. Evidently, the ratchet will prevent the pump rotation if the belt quarter-turn is made in the wrong direction.

(*h*) **Pressure Surges during Reverse Rotation.** *With the introduction of the open impeller construction into the deep-well pump field it was discovered that, with long settings, pressure waves developed in the discharge column when the flow is reversed which caused impeller hammering against*

their seats. With closed impellers such pressure waves did no harm and passed unnoticed because there was sufficient axial clearance between the rotating element and the stationary pump casing to prevent interference between the two. However, with open impellers, the axial thrust was greater than with the closed impellers, and the running axial clearance was reduced to a minimum to obtain a maximum efficiency. *The impeller pounding against the casing while revolving in the reverse direction resulted in the impeller vane grinding to such an extent that it was impossible to maintain normal pump efficiency.* It should be borne in mind that the pump shaft extension due to the hydraulic thrust in average deep-well pumps with over 200-ft setting is of the order of ¼ or ½ in. Pressure waves cause variation in the shaft extension. This could be observed on the surface by a violent vibration of the pump support.

Motors with non-reversing ratchets are used also with long deep-well settings to prevent damage to water-lubricated rubber bearings after water has receded from the bearings.

To eliminate the wear of the impeller vanes and reduce the mechanical disturbance during reverse flow of water through the pump, some of the deep-well motors are provided with non-reversing ratchets similar to that shown in Fig. 13.6. These prevent rotation of the shaft in the reverse direction, although they do not eliminate the pressure waves or mechanical vibration during the reverse flow of water through the pump.

In all non-reversing ratchets, the ratchet is engaged when the pump speed is approaching zero, but the torque developed by the pump is not zero, as can be seen from Fig. 13.2. The torque is applied suddenly and, therefore, all parts subject to stress due to this torque, such as keys and pins, should be able to stand the imposed stresses under such conditions.

Several pump manufacturers used check valves in the discharge column to prevent or reduce the bad effects of the pressure surges during reverse flow but with a limited degree of success.

The bad effects of the pressure surges in a deep-well pump with open impellers are pronounced with high head pumps, long discharge columns, and relatively small shafts. However, the advantages of open impellers (better hydraulic efficiency, possibility of adjusting for wear, freedom from sand locking, and accessibility for cleaning) make this construction more popular than the closed impeller design.

13.4 HYDRAULIC PROBLEMS ARISING DURING UNUSUAL PUMP OPERATING CONDITIONS

(*a*) **Centrifugal Pumps Operating as Turbines.** When the flow in a centrifugal pump is reversed by applying head to the discharge nozzle, the pump becomes a hydraulic turbine. In centrifugal pump practice this may happen unintentionally when the motor is stopped and no means are used to prevent the reverse flow. Since no power is being utilized from the shaft, the pump is operated as a turbine at what is known as runaway speed. The question of speed and capacity under such conditions has been discussed already.

Special tests conducted to operate centrifugal pumps as hydraulic turbines throughout the head-capacity-speed range [3,4,5] show that a good centrifugal pump makes an efficient hydraulic turbine. To establish the relationship between the head and capacity (at the b.e.p.) of a unit when operated as a hydraulic turbine at the same speed in terms of the head and capacity when it is operated as a pump is of interest and practical importance. From the theoretical considerations [2] it is possible to state that at the same speed

$$H_t = \frac{H_p}{e_{ht}e_{hp}} = \frac{H_p}{e_h^2} \tag{13.1}$$

$$Q_t = \frac{Q_p}{e_h} \tag{13.2}$$

$$n_{st} = n_{sp}e_h \tag{13.3}$$

where H is the total head at the b.e.p.
Q is the capacity.
n_s is the specific speed.
e_h is hydraulic efficiency, taken the same for the turbine and the pump.

Subscripts t and p refer to operation as a turbine and a pump respectively. Since the exact value of the hydraulic efficiency is never known $\sqrt{e}$ can be taken as an approximation, where e is the gross pump efficiency. These relationships hold approximately in practice.

If torque, head, capacity, and speed values are taken from the turbine section, C in Fig. 13.2, the calculated turbine efficiency is considerably lower than the pump efficiency, which is not a true turbine efficiency. To obtain the latter the first should be divided by the pump efficiency or

$$\text{True } e_t = \frac{e_t \text{ (from chart)}}{e_p \text{ (true)}} \tag{13.4}$$

This is because all variables for the turbine are expressed in terms of those for the pump. Thus

$$\text{True turbine efficiency } e_t = \frac{T_t n_t}{Q_t H_t} \times \frac{3960}{5250} \tag{13.5}$$

$$\text{True pump efficiency } e_p = \frac{Q_p H_p}{T_p n_p} \times \frac{5250}{3960} \tag{13.6}$$

By multiplying the two and rearranging, we get

$$e_t e_p = \frac{(T_t/T_p)(n_t/n_p)}{(Q_t/Q_p)(H_t/H_p)} = e_t' = \text{turbine efficiency in terms of pump variables} \tag{13.7}$$

Hence

$$e_t = e_t'/e_p \tag{13.8}$$

For the reverse-speed abnormal pump or turbine operation, zones E and G, efficiency is of little interest. Table 13.1 shows values of efficiency for the b.e.p. for four types of pumps for the zones of operation A, E, C, and G.

TABLE 13.1. VALUES OF EFFICIENCY

		Best Efficiency, Per Cent			
Type	n_s	Zone A Pump Normal	Zone E Pump Reverse	Zone C Turbine Normal	Zone G Turbine Reverse
Radial	1,800	83	9	70	9
Mixed	7,500	82	9	78	9
Axial	7,500	77	25	..	..
Axial	13,500	80	34	78	50

The idea of using the same unit as a turbine and pump has atrracted considerable attention in connection with pumped storage plants.

The difficulty in using the same hydraulic machine for both a turbine and a pump lies in the fact that at the same speed the pump will deliver only a portion of its rated turbine capacity at a reduced efficiency when pumping against a head equal to the turbine head. For that reason when the same hydraulic machine is used as a pump-turbine, a two-speed electric machine is used as a pump operating at a higher speed. A number of pumped storage plants have separate units for pump and turbine, the same electric machine being used as a generator and motor.[6] Others have two entirely independent generating and pumping sets.

The first two pumped storage systems in the United States both have separate pumps and turbines. The first one is the Connecticut Light and Power Company plant at Rocky River, consisting of two pumps

of 8100 hp each, built in 1930.[7] The other plant of the same type is the Colorado River Authority plant at Buchanan Dam in central Texas, 13,450 hp, built in 1949.[8]

Figure 13.7 shows the sectional drawing of the Flatiron Power and Pumping Plant built as a part of the Colorado-Big Thomson Project

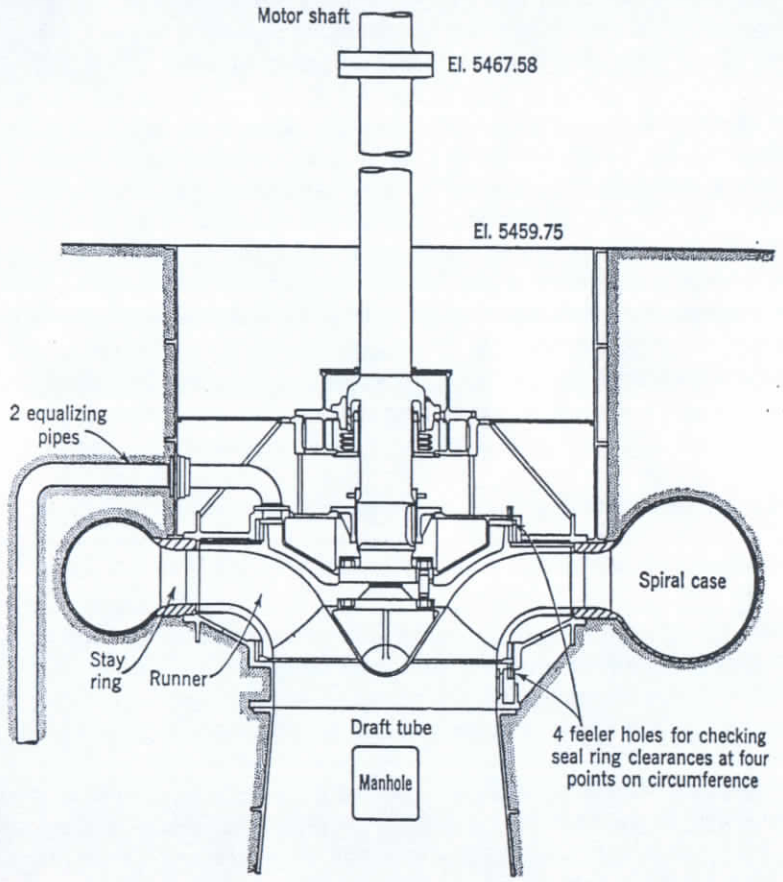

FIG. 13.7. Flatiron pump turbine, 166,000 gpm, 240-ft head, 300 rpm, 13,000 hp.

which was completed in 1953.[9] As a motor the electric unit is rated at 13,000 hp at 300 rpm. As a turbine the same electric machine develops 10,700 hp at 257 rpm. The same hydraulic unit is used as a pump and turbine. Operated as a pump the field test efficiency was found to be 91.0 per cent, and 88.8 per cent when operated as a turbine.

It has been observed experimentally on several occasions that a good pump always makes a good water turbine; however, a number of good

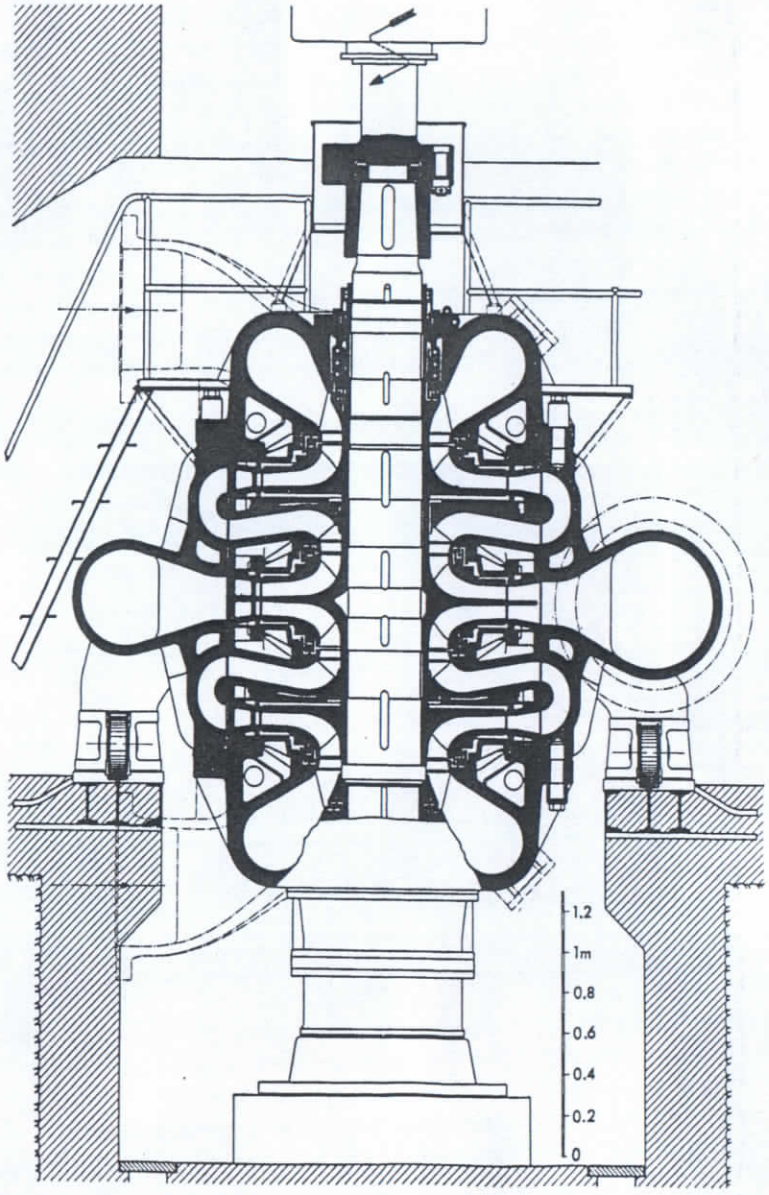

FIG. 13.8. Two-stage Sulzer pumped-storage pump at Zentrale Grimsel Oberaar Power Plant, 25,100 hp, Switzerland.

turbines have shown a much lower efficiency when operated as pumps. The reason for this is that in a water turbine the flow toward the impeller and through the impeller is accelerated. A high rate of acceleration does not entail large losses. But when the flow is reversed in a turbine, the high rate of deceleration is followed by an appreciable diffusion loss. In a good pump the rate of deceleration is small, making it almost equally efficient for flow in both directions.

The world's largest storage pump is that of the Tennessee Valley Authority at Hiwassee Dam in southwestern North Carolina.[10] As a motor the electric unit is rated 102,000 hp; as a generator the same unit is rated 120,000 hp. The speed in either direction is 106 rpm, which is a compromise between the optimum speed of operation of the pump and that of the turbine at some sacrifice in efficiency. The use of adjustable guide-diffuser vanes in this pump-turbine casing brings closer together the optimum conditions for both modes of operation. The capacity of the unit as a pump is 1,750,000 gpm at 205-ft head. The impeller diameter is 22 ft.

Construction of pumped storage plants in the heavily industrialized areas where hydroelectric plants have reached the saturation point is justified economically because of a difference in power rates (four to one in one case) during the peak load and low-demand periods. Such conditions did not exist in the United States until recently. The above listed plants are the only ones in this country built to date.

Figure 13.8 shows a cross section of a Sulzer two-stage pump, rated 64,000 gpm, 1312-ft head at 1000 rpm, requiring 25,100 hp to drive. The dual-flow arrangement with inlets on both ends and discharge in the middle is typical for large, high pressure pumps and blowers in Europe. The field test peak efficiency was found to be 88.2 per cent.[11] The same design is used for horizontal pumps.

Multistage pumps operated as turbines behave in the same manner as single-stage pumps. Vertical multistage pumps of the deep-well type show the same efficiency when operated either as turbines or as pumps (unpublished tests by University of California).

(*b*) Two Pumps in Parallel; Power of One Cut-Off. When two pumps operate in parallel and power of one of them fails while the other continues to operate, the flow in the first will be reversed and it will operate as a turbine at runaway speed. The following questions arise under these conditions: (1) What portion of the pump capacity will go into the discharge system and what portion will go back to the suction sump through the idle pump? (2) What will be the reverse speed of the idle pump? (3) What can be accomplished by preventing the reverse rotation of the idle pump?

To show the method of attack in solving this problem, an illustration will be taken of two propeller pumps circulating cooling water through a condenser. The total pump head is used to overcome the friction of the system. Figure 13.9 shows the head-capacity curves of one and two pumps in parallel each delivering 100 per cent of their rated capacities when in parallel. The condenser resistance curve AB is also shown. To answer the above three questions the pump characteristics under reversed flow should be known. This is shown in Fig. 13.9 for a free

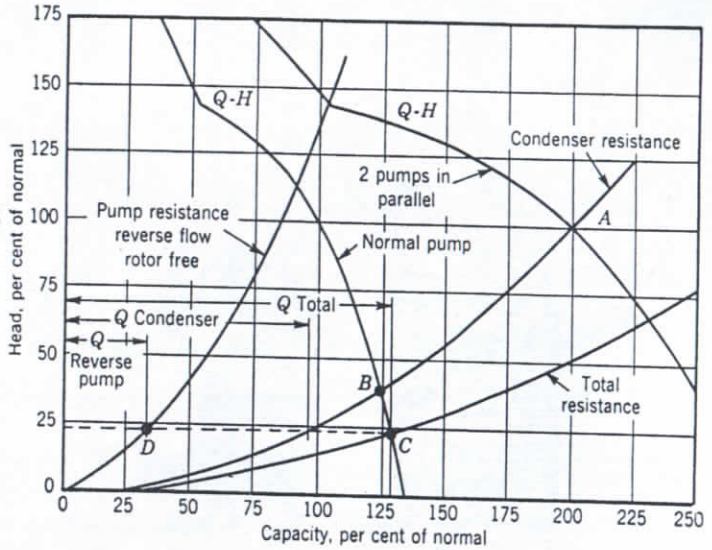

FIG. 13.9. Two pumps in parallel, power failure on one pump.

rotor. To determine how the capacity of one pump will be divided between the condenser and the idle pump, a combined (total) resistance of both should be plotted. This is done by adding capacities for the same heads. The intersection of this curve with the head-capacity curve of a single pump (point C) will give the pump operating point. From this it is seen that with the rotor free (Fig. 13.9) the active pump will operate at 129 per cent of its normal capacity, delivering 96.5 of its normal capacity per cent to the system; the rest will be wasted through the idle pump. By similar procedure it has been found that, with the rotor locked, the pump will deliver 127.5 per cent of its normal capacity, 108 per cent being delivered to the system and the rest being returned to the suction through the idle pump.

Figure 13.9 shows that, when the rotor is free, the idle pump operates at 23 per cent of its normal head (point D). Its reverse speed under

100 per cent head is 128 per cent (see Table 13.3), and at 23 per cent head the speed is 61 per cent of normal speed. The pump characteristics under reversed flow have to be determined experimentally at least for one point and the curve then has to be plotted by applying affinity laws.

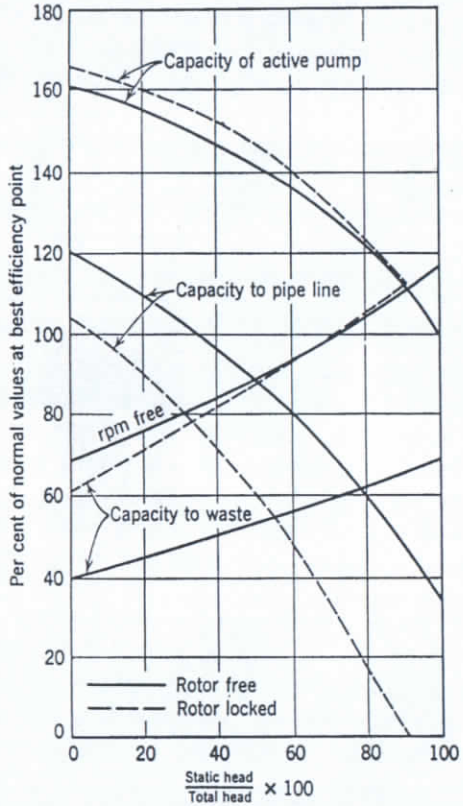

FIG. 13.10. Two pumps in parallel, power failed in one; $n_s = 1800$, double-suction pumps.

Note that both with free and locked rotor the operative pump works at 129 and 127.5 per cent of its rated capacity. With propeller pumps, the brake horsepower at these points is lower than at the normal capacity; therefore, the motor will be unloaded. With pumps of lower specific speed the brake-horsepower curve rises with increasing capacity and, under such conditions, the motor may be overloaded beyond the safe limit.

Figure 13.10 shows the capacity division between the useful discharge and the waste through the idle pump for a centrifugal pump at different

ratios of static head to total pump head with both free and locked rotor. This curve was calculated in the same manner as that in Fig. 13.9. *For a given head a greater portion of the capacity goes to waste with the rotor locked. This is similar to the induction motor, which draws more current with the rotor locked than with the rotor free. A motor generates counter-electromotive force which reduces the current through the rotor. In centrifugal*

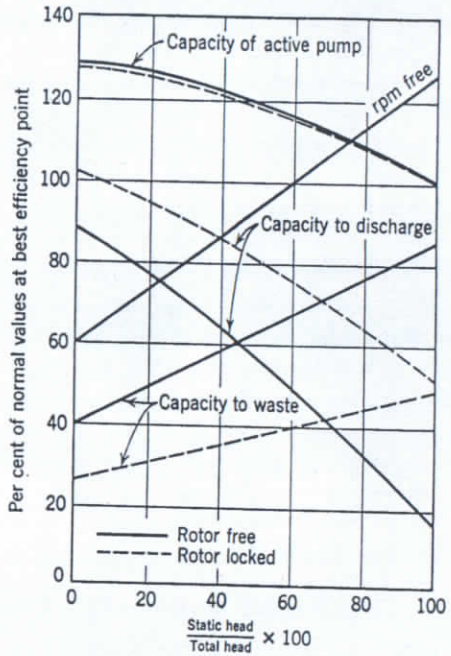

FIG. 13.11. Two pumps in parallel, power failed in one; $n_s = 7500$, propeller pumps.

pumps with the rotor free, part of the applied head is used to overcome the head generated by the pump, and the remaining part produces the reverse flow which is less than with the rotor locked.

Figure 13.11 shows similar curves for a propeller pump. *Note that here a greater capacity is returned to the suction sump with the rotor free than with the rotor locked. In propeller pumps no centrifugal head is generated by rotation; on the other hand, rotation permits the impeller to move enough to reduce the absolute path of the water, and thus to increase the flow.*

(c) Two Pumps in Series. Frequently, in order to increase the capacity during extremely low river level, booster pumps of the propeller type are installed in series with pumps taking their suction from a river. To simplify the piping these pumps are left in line when not in operation. In this connection it is important to know what the pump

resistance will be with the rotor free and with the rotor locked; also at what speed the idle pump will rotate. In this case the capacity is positive and the head is negative. Using the chart in Fig. 13.2 ($n_s = 1800$) for convenience, at 100 per cent capacity and zero torque the speed is 33 per cent of normal, the head is 25 per cent. This falls into section *G*, and the pump is operated as a turbine with reversed flow and at runaway speed. *If the rotor is locked the same chart shows that at 100 per cent capacity and zero speed the head is 56 per cent, thus showing that the pump resistance is greater with a locked rotor when full capacity is drawn through the pump.*

For a propeller booster pump of 7500 specific speed operating with a free rotor at full capacity, following the zero torque line in Fig. 13.3, zone *G* shows that the resistance to the flow is 25 per cent and the speed is 55 per cent of normal. With the rotor locked the resistance is 150 per cent of the pump normal head.

For an axial flow pump of 13,500 specific speed (Fig. 13.4), with a free rotor, the resistance is 12 per cent, and the speed is 68 per cent. With the rotor locked the resistance to the flow is 96 per cent.

Note that when a propeller pump is used as a booster and water is drawn through it (the power is off) when the rotor is locked, the torque developed tends to unscrew the threaded shaft couplings. With the rotor free no such danger exists as the torque is zero.

When two pumps are operated in series, if the power should fail on the high pressure pump and the flow reverse (all or part of the total head static and no check valve in the pipe line), the booster pump will operate as shown in the second quadrant, *B* on Figs. 13.1(*a*), 13.1(*b*), and 13.2; that is, the speed is positive, the flow is negative, and the head is positive and higher than the booster shut-off head. If the head applied from the pipe line, through the idle main pump, is high in comparison with the booster's own head, dangerous overload will develop on the booster pump motor, and it probably will be cut off by the overload protection relays.

(*d*) Pump Operation under Negative Head, Section *H*, Fig. 13.1(*a*). In this section the flow is positive, rotation is positive, and head is negative. If two pumps are operated in series and the booster pump is of much larger capacity than the high pressure pump, the discharge valve on the latter can be opened until the differential pressure across the pump will reach zero and then become negative. The capacity will increase beyond the maximum capacity at zero head. Evidently, under such conditions the pump not only does not generate any head but it also absorbs some of the head produced by the booster pump.

The author knows of a case where similar conditions prevailed with one pump taking its suction from a high pressure oil well. When the valve was operned wide the pump discharge pressure gradually fell below that on the suction. The pump happened to be of the double-casing type. In this kind of pump the outer barrel is under full discharge pressure, which keeps the inner casing halves tight. Only small bolts hold the inner casing halves when assembled. When the discharge pressure fell below the suction pressure, these bolts were not strong enough to keep the pump halves together, and mechanical damage to the rotating element resulted. The cause of the damage was not easily established at that time as the conceptions about the pump operation outside its normal head-capacity range were only beginning to attract the attention of pump engineers.

13.5 STARTING OF CENTRIFUGAL PUMPS

A knowledge of complete pump characteristics is very helpful for solving some problems connected with starting centrifugal pumps. In general, the torque requirements of centrifugal pumps during the starting period are easily met with standard motors, induction or synchronous. However, conditions may arise, depending on the pumping arrangement, which impose severe requirements on the motor during the starting period, calling for high motor starting and pull-in torques. In special cases, a definite starting procedure is prescribed to permit the motor to pull in into its normal operating speed. Several typical cases will be considered, including the most difficult ones. In every instance it will be assumed that the same relationship exists between the head capacity and the speed during the transient period of acceleration as that at the same speed with a steady established flow. Knapp [4] has shown that this assumption gives results in close agreement with an actual test in his calculations of the time-speed relation during the reverse rotation after the power failure of a pump.

(*a*) Speed-Torque Curve. When a centrifugal pump of low and medium specific speed (below 3500) is started, the power at shut-off, or zero capacity, is lower than the normal brake horsepower. Figure 13.12 shows constant speed head-capacity and torque curves for $n_s = 1800$. If started against the shut-off head the torque-speed curve for such pumps is a square parabola as torque varies as the square of the speed $A'B'D'$ (Fig. 13.13). While pumping torque is zero at zero speed, the starting torque of the motor should overcome the static mechanical friction in the bearings and stuffing boxes. This varies greatly with the size and speed of the pump, and also with the stuffing box size and pressure.

A horizontal pump with two stuffing boxes packed to hold 250 lb with a 3.375-in. shaft sleeve, two sleeve bearings, and a ball thrust bear-

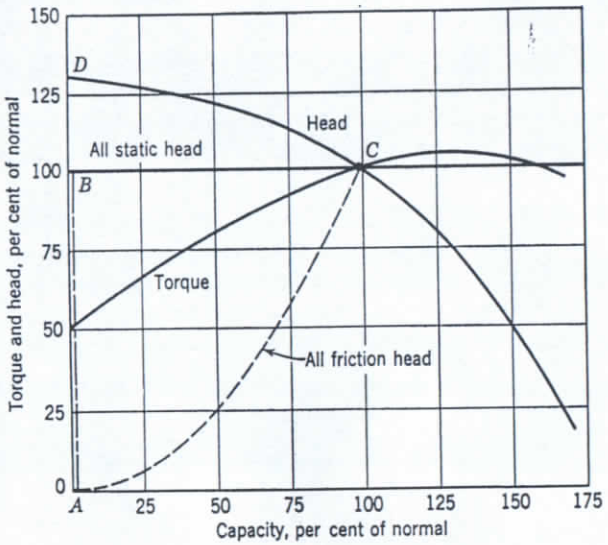

FIG. 13.12. Constant speed pump characteristics.

ing requires 430 lb-in. starting torque. This constitutes 1.25 per cent of the pump normal torque at 3600 rpm, 5.0 per cent at 1800 rpm, and 11.25 per cent at 1200 rpm. The portion EF of the speed-torque curve

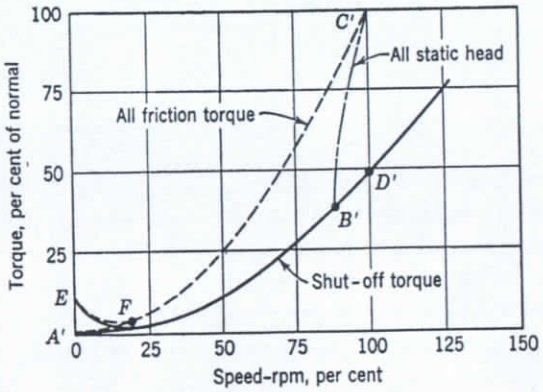

FIG. 13.13. Speed-torque curves.

in Fig. 13.13 near zero speed is drawn arbitrarily and its exact form is not important. From this example it is seen that the starting torque

is higher for low speed pumps, but is low enough to be met by any standard motor.

If a centrifugal pump is started with the discharge valve open the speed-torque curve depends on the head-capacity characteristics of the system into which the pump is delivering. Suppose a pump with head-capacity and torque characteristics as shown on Fig. 13.12 is pumping against a static head only. The system characteristic will be ABC. In this case, when started the pump will work near the shut-off head until the total static head is reached at B; then the pump will begin to discharge into the system along the constant head line BC. The speed-torque curve is plotted by finding the speed to obtain head-capacity points along BC and reducing the torque for the same points from the constant speed torque curve.

As another example consider the case when the total head is all friction head, AC in Fig. 13.12, and the pipe length is short, as with a condenser circulating pump. The head-capacity point during the starting period will move along the system characteristic curve AC and, when the corresponding points (of the same specific speed) on the constant head-capacity curve are located, the speed and torque can be determined and plotted, $A'C'$ in Fig. 13.13, the procedure outlined above being followed.

If the pipe line is long (several miles) the mass of the liquid to be moved becomes so great that the time required to accelerate the liquid in the pipe line is much greater than the time required to bring the motor up to speed, and the pump behavior during the starting period will approach that when operating against a closed discharge valve. Cases intermediate between these two extremes will have their speed-torque curves lying between $A'C'$ and $A'D'$ in Fig. 13.13. Similarly, if the total head consists partly of static and partly of friction, curves similar to $A'C'$ and $A'B'C'$ can be plotted; if the pipe line is long, the speed-torque curve will approach that with shut-off discharge.

(*b*) **Starting a Pump Running Backwards.** For centrifugal pumps having brake-horsepower curves either flat or decreasing toward zero capacity, the torque never exceeds 100 per cent of normal with any possible method of starting and any system characteristics as long as the pump is not allowed to run backwards under the head from the system. But, if a part or all of the total head is static and if there is no provision to prevent back-flow through the pump, the opposing torque may exceed the normal torque when starting with the discharge valve open and it depends on the head applied to the pump. Assume a case when the pump is running backwards under 100 per cent head from the system. As long as an equilibrium is reached the pump is operating at

runaway speed and generating no torque. However, if the motor is put on the line and the reverse speed of the unit begins to drop, the pump will develop opposing torque, as can be seen from Fig. 13.2 when following the 100 per cent head line from the zero torque line through sections C and B, to A. Figure 13.14 shows the torque-speed curve plotted from Fig. 13.2 for 100 per cent head from full reverse speed to 100 per cent forward speed. Prevention of reverse rotation by mechanical means, such as a non-reversing ratchet (a spring solenoid-operated brake applied to the coupling between motor and pump has been used

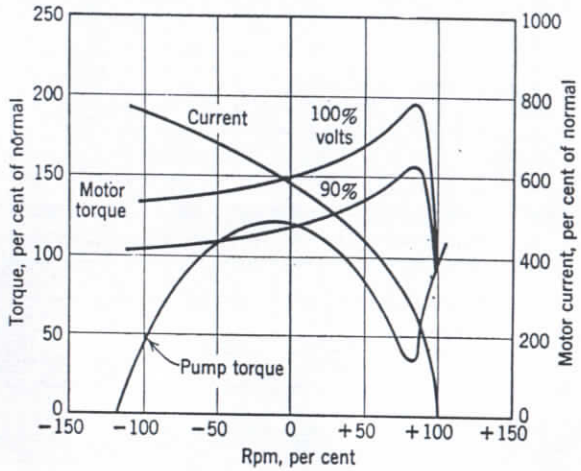

FIG. 13.14. Speed-torque curves; pump $n_s = 1800$; four-pole motor.

on condenser circulating pumps to prevent reverse rotation) does not change the speed-torque curve from zero speed to full positive speed; thus high motor starting torque is required to overcome pump torque at zero speed, which is 120 per cent in Fig. 13.14. Attention is called to the fact that, for cases where the pump may be started while running backwards, the motor speed-torque curve should be known for a negative rotation, that is, the positive torque developed by the motor when put on the line while rotating in the opposite direction.

Figure 13.14 shows motor torque-speed curves for a typical four-pole induction motor. *It will be noticed that although a standard motor will be able to accelerate the pump from 120 per cent reverse speed, the starting time will increase, and the starting current will increase, and this may result in excessive heating of the motor. At a slightly reduced voltage the motor may not be able to pull into full speed, and may be cut out of the line by the overload relays.* Evidently, it is impossible to establish a general

rule on pump and motor behavior under such conditions, and each case should be studied individually.

(*c*) **Starting Propeller Pumps.** The peculiar feature of these pumps is that they have a brake-horsepower curve rising toward zero capacity. The brake horsepower at shut-off may be twice (or more) that of the normal for the higher specific speed pumps of this group.

Evidently, if started with the discharge valve shut these pumps will require a pull-in torque twice (or more) the normal. Standard motors cannot develop such pull-in torque. Instead of going to special motor design several schemes have been devised to start propeller pumps with standard motors.[12] These include:

1. Using a check valve in addition to a gate valve in the discharge line. With the gate valve open the pump is started against static head only.
2. A small by-pass back to the suction sump, open during the starting period; locating the by-pass as close as possible to the pumping element will increase the by-passed capacity for a given size of by-pass.
3. Starting with discharge valve partially open, allowing the pump to rotate backwards.
4. Placing the impeller above the suction level and starting the pump dry, then priming the pump after the motor pulls into step.[13] A similar effect is obtained by depressing the water level in the pump below the impeller by compressed air during the starting period.

With a variable speed driver the pump can be started at a reduced speed to produce a head slightly above the normal, when the discharge valve can be opened and the pump brought up to normal speed.

The torque-speed curves for propeller pumps are plotted in the same manner as those for centrifugal pumps, particular attention being given to the peculiarities of the brake-horsepower curves.

Frequently propeller pumps are used for lifting water from one level to another over the crest of a levee (drainage or irrigation plants). The discharge pipe of such pumps forms a siphon. To start a siphon the pump has to fill it with water, and this requires a static head higher than the pump normal head. The torque requirements during the starting period of the pump should be studied, the pump being considered as working at or near the shut-off point until the siphon is primed, whereupon the pump head will fall suddenly to its normal static head.

Priming the siphon by extracting air with a special primer may lead to complications during starting because, as soon as the siphon is primed, a reverse flow through the pump starts under full pump head, and start-

ing conditions become similar to those with pumps running in reverse direction as described above.

In addition to torque requirements for pumping during the starting period shown on speed-torque curves, the motor has to furnish the torque for accelerating the mass of the rotating element of the pump. Although the impellers are filled with water, the acceleration of the latter is already taken care of by the pumping speed-torque curve, as pumping is produced by water acceleration.

Starting large pumps, even with a flat brake-horsepower curve, against a closed valve and with the pipe empty has been found undesirable, as the shock of the water column against the valve may cause mechanical damage to the pump or column parts. This has been actually observed on pumps circulating molten salt in catalytic oil-cracking processes. The high specific gravity of this material (1.75 to 1.90) increases the intensity of the shock during the starting period.

13.6 EFFECT OF SPECIFIC SPEED UPON THE BEHAVIOR OF CENTRIFUGAL PUMPS UNDER SPECIAL OPERATING CONDITIONS

When complete pump characteristics are available, questions connected with any possible operating conditions outside the normal head-capacity and speed range can be easily answered. Unfortunately, experimental determination of complete pump characteristics requires equipment usually not found among commercial testing facilities of the pump manufacturers. As a result, only a few complete pump characteristics are available.

In addition to the complete pump characteristics shown in Fig. 13.2, 13.3, and 13.4, below are listed several references giving the pump performance for the zones A, B, and C which are the most important for water-hammer studies. All pumps are of the single-suction type and specific speeds are tabulated in Table 13.2.

TABLE 13.2. REFERENCES FOR PUMP PERFORMANCE OUTSIDE THE NORMAL ZONE

Reference no.	4	5	5	14	15	16	17
Specific speed n_s	1700	2150	1850	1425	1350	1285	2150

In Table 13.3 are compiled from various sources, test results of several pumps of different specific speeds obtained at $T = 0$ or revolutions per minute = 0, and recalculated to $H = 100$ or $Q = 100$. A comparison of the figures in the tabulation would indicate the trend of the effect of specific speed on the pump behavior under the specified conditions.

TABLE 13.3. SPECIAL OPERATING CONDITIONS OF PUMPS OF DIFFERENT SPECIFIC SPEEDS

No.	Specific speed, single-suction	Negative Flow: Rotor-free, $H = +100$, $T = 0$		Negative Flow: Locked, $H = +100$, rpm = 0		Positive Flow: Rotor-free, $Q = +100$, $T = 0$		Positive Flow: Locked, $H = -100$, rpm = 0		Remarks: Values of head (H), capacity (Q), and torque (T) are percentages of normal pump operation		
		$-Q$	$-$ rpm	$-Q$	$+T$	$-H$	$+$ rpm	$+Q$	$-T$	Size	Type of pump	Source
1	1,190	85	104	164						1½	Multistage	Stepanoff
2	1,220	76	108	117	96					2	Multistage	Stepanoff
3	1,270	68	117	118	120	25	32	133	80	4	Double-suction	Knapp
4	1,285		117							4	Four-stage	Stepanoff
5	1,700	58	125	115	146					8	Single-suction	Knapp
6	1,760	52	106	103	110	37	30	117	73	2	Single-suction	Kittredge
7	1,940	75	125	108	130	40	30	105	60	8	Single-suction	Kittredge
8	2,140	60	123	95	125						Single-suction single-volute	Knapp
9	2,140	50	123	108	140					8	Single-suction double-volute	Knapp
10	3,500	80	125	84	116	40	50	84	93	12	Double-suction	Stepanoff
11	6,700	112	126	79	88	33	66	55	67	16	Propeller	Stepanoff
12	7,200	85	128	37	74	34	65	50	63	16	Propeller	Stepanoff
13	13,500	121	128	66	37	40	70	72	54	16	Propeller	Stepanoff

NOTES. To find operating conditions other than those shown apply affinity laws except for propeller pumps with rotors locked.

Pumps 8 and 9 have the same impeller.

Pumps 11 and 12 have the same casing but the impellers are different.

REFERENCES

1. D. Thoma, "Vorgänge beim Ausfallen des Antriebes von Kreiselpumpen," Mitt. Hyd. Inst. Tech. Hochschule, München, Vol. 4, pp. 102–104, 1931, Munich, R. Oldenbourg; also in English translation: C. P. Kittredge and D. Thoma, "Centrifugal Pumps Operated under Abnormal Conditions," *Power*, pp. 881–884, June 2, 1931.
2. Ludolf Engel, "Die Rücklaufdrehzahlen der Kreiselpumpen," doctoral dissertation, Tech. Hochschule zu Braunschweig.
3. Clifford P. Kittredge, *Vorgänge bei Zentrifugalpumpenanlagen nach plötzlichem Ausfallen des Antriebes*, Munich, R. Oldenbourg, 1933.
4. R. T. Knapp, "Complete Characteristics of Centrifugal Pumps and Their Use in the Prediction of Transient Behavior," *Trans. A.S.M.E.*, pp. 683–689, November 1937.
5. R. T. Knapp, "Centrifugal Pump Performance as Affected by Design Features," *Trans. A.S.M.E.*, Vol. 63, No. 3, April 1941.
6. R. W. Angus, *Trans. A.S.M.E.*, Vol. 64, No. 8, November 1942.
7. *Engineering*, pp. 33–38, Jan. 10, 1930, and pp. 97–100, Jan. 24, 1930.

8. C. L. Powell, "Pump at Buchanan Dam Adds Peak Capacity to Power System," *Power*, pp. 95–98, August 1951.
9. J. Parmakian, "Flatiron Power and Pumping Plant," *Mech. Eng.*, pp. 677–680, August 1955.
10. F. E. Jaske, "Pump-Turbines," *Allis-Chalmers Elec. Review*, 4th quarter, 1954.
11. A. Weibel and J. Sprecher, "Sulzer Speicherpumpen," special publication, from *Sulzer Tech. Rev.*, No. 1, 1955.
12. C. B. Tuley, "Propeller Pumps in Parallel," *Power*, p. 187, April 1934.
13. M. F. Wagnitz, "Stormwater Pumping Station at Detroit," *Eng. News-Record*, July 30, 1931.
14. H. C. v. Widdern, "Tests on Turbo-Pumps," Escher-Wyss Research on Turbo-Machinery, pp. 36–40, 1939.
15. J. Sprecher, "The Hydraulic Power Storage Pumps," *Sulzer Tech. Rev.*, No. 3, pp. 1–14, 1951.
16. J. Duc, "Die Berechnung der Druckschwankungen in Pumpenleitungen," "Sulzer Speicherpumpen," special publication from *Sulzer Tech. Rev.*, No. 1, pp. 22–32, 1955.
17. Takeshi Kobori, "Experimental Research on Water-hammer in Pumping Plant of the Numazawanuma Pumped Storage Power Station," *Hitachi Rev.*, pp. 65–74, February 1954 (in English).
18. Robert Zobel, "Versuche an der hydraulischen Rückstromdrossel," Mitt. Hyd. Inst. Tech. Hochschule, München, Vol. 8, pp. 1–47, Munich, R. Oldenbourg.
19. R. M. Peabody, "Typical Analysis of Water Hammer in a Pumping Plant of the Colorado River Aqueduct," *Trans. A.S.M.E.*, p. 117, February 1939.
20. Oskar Spetzler, "Die Turbinenpumpe im Stauwerk Baldeney," *Z. Ver. deut. Ing.*, Vol. 78, No. 41, p. 1183, Oct. 13, 1934.
21. R. V. Terry, "Development of the Automatic Adjustable Blade-Type Propeller Turbine," *Trans. A.S.M.E.*, pp. 398, 405, 406, July 1941.
22. W. M. Swanson, "Complete Characteristics Circle Diagram for Turbo-Machinery," *Trans. A.S.M.E.*, Vol. 75, pp. 819–826, 1953.

Chapter 14

Special Problems of Pump Design and Application

14.1 UNSTABLE HEAD-CAPACITY CHARACTERISTICS OF CENTRIFUGAL PUMPS

A theoretical investigation has shown that the actual head-capacity curve is a parabola with its apex displaced to the right of the zero capacity axis (Fig. 14.1). The shut-off head is lower than the maximum head ($H_s < H_{max}$). Actual test curves of low specific speed pumps ($n_s \approx 1000$) approach this form. Under certain operating conditions part AB of the head-capacity curve is unstable, and this instability results in head-capacity fluctuations or failure to pump entirely. This happens if the capacity is reduced to Q_b or less. At certain conditions, such as when two pumps work in parallel, head-capacity swings may start at capacity Q_d. Fluctuations of head capacity are followed by fluctuations in the power and speed of the unit and, if the frequency of such swings coincides with that of the adjoining piping system, severe mechanical vibrations of the piping are induced.

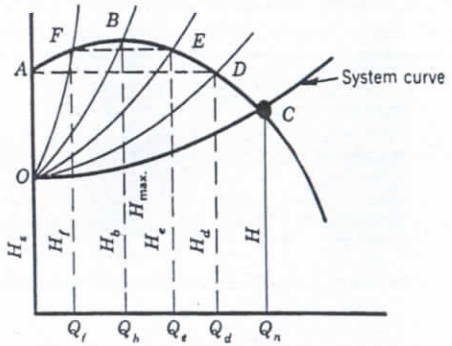

FIG. 14.1. Unstable Q-H characteristic.

(a) Conditions for Head-Capacity Swings. *The following conditions must exist to develop head-capacity and power swings in a system including a pump:*

1. *The mass of water must be free to oscillate.* This condition exists when the water mass is suspended between two free surfaces, as in boiler-feed and condensate pumping cycles. In both, the suction is taken from a vessel that has a free surface, and the water is discharged into another vessel with a free surface.

2. *There must be a member in the system which can store and give back the pressure energy or act as a spring in a water system.* The static water column in a water system, having two free surfaces, serves this purpose. In a boiler-feed pump cycle, the elastic steam cushion in the boiler also serves the same purpose. Long piping, with or without a vessel having a vapor or air cushion, may provide the necessary spring effect to produce oscillations. When compressible fluids, air, or gases are being pumped, the fluid itself serves as an elastic member of the system. As a result, air blowers with unstable head-capacity characteristics cannot be operated near the maximum head point. The blower head-capacity swings produce a peculiar pulsating sound similar to that of plunger pumps and is referred to as pumping.

3. *There must be some member that will provide impulses at regular intervals to start the swings.* When the head-capacity curve is unstable, such conditions appear when the capacity is as low as, or lower than, that corresponding to the maximum head or that at capacity Q_b. Even with stable head-capacity curves, capacity surges may be induced by excessive rotation in the impeller approach.

(*b*) **Analogy to Water Turbine Experience.** It should be pointed out that hydraulic water turbine installations contain all the conditions necessary for head-capacity and power swings, and surges have been observed on a great many installations during part-load operation. These conditions are aggravated by the fact that power swings of such magnitude are induced in the electric system that some of the units cannot be kept in parallel operation with other units on the line. An investigation by Rheingans [1] and several discussions of his original article on the subject have shown that the power swings originate in the water turbine draft tube (corresponding to the pump suction). At partial loads, the residual component of the tangential velocity sets up a whirl in the draft tube which, because it is not symmetrical about the axis of rotation, causes the runner to discharge against a fluctuating head. When the fluctuation frequency equals that of the system, the swings appear at their maximum value.

The whirl occurring in the draft tube of a water turbine at partial loads appears also in centrifugal pumps to a different degree, depending on the suction and impeller design, provided the rest of the conditions necessary for oscillation are existent. Power swings in water turbines

may be eliminated or reduced to the point that they do no harm by providing baffles in the draft tubes and by changing the runner design so that rotation of water in the draft tube is reduced. Similar means are used in pump design to achieve the same goal. More specifically, *the suction nozzle should provide a gradually accelerated flow and have proper baffling to suppress the prerotation in the impeller approach, and the impeller should have plain vanes in preference to the extreme Francis type to reduce churning in the impeller eye.*

(*c*) **Stable Curves for Boiler-Feed Service.** All modern boiler-feed pumps are designed with a stable head-capacity curve, that is, the head is constantly increasing toward zero capacity. Frequently the shut-off head is specified to be not lower than a certain minimum as, for example, 117 per cent of the normal operating head. Such limitation in itself does not guarantee a stable head-capacity curve. In many instances a maximum shut-off head instead of a minimum is stipulated. Such a request is usually inspired by considerations of power saving, presuming that a flatter head-capacity curve will result in less loss due to throttling at partial capacities. This is not necessarily true because: (1) *the slope of the brake-horsepower curve is affected by the shape of the efficiency curve and* (2) *if the shut-off head limit is too low (110 per cent) the requirement must be met by locating the full-load condition to the left of the best efficiency capacity of the pump, thus defeating the purpose of reducing power over a wide range.* Furthermore, setting the minimum shut-off head too low reduces the margin of safety against surges in discharge lines.

The ratio of H_s/H is in general a measure of stability of the head-capacity curve and is an important factor in reducing the hunting of governing devices.[2]

The effect of heat due to internal hydraulic losses, including disk friction, on the fluid density is observed on high pressure boiler feed pumps. For instance, the water temperature rise due to losses in pumping 250°F water against 1800-psi pressure is about 50°F, resulting in a reduction of density 2.7 per cent and a reduction of discharge pressure (the head remaining constant) of 50 psi. Thus a pump which has a steadily rising head-capacity curve on cold water will show a drop of pressure near shut-off when pumping hot water if the change in density is disregarded. The head-capacity curve remains rising and perfectly stable under such conditions.

(*d*) **Cause of Surges.** During each cycle of the swinging conditions the pump goes through the following steps. When the pump capacity is reduced from the normal Q_n (Fig. 14.1) by throttling the pump discharge, new system curves, *OD*, *OE*, and *OB*, are produced by additional resistance in the throttle valve requiring higher heads at each

capacity Q_d, Q_e, Q_b. Until capacity Q_b is reached, the pump is able to furnish increasing head demand. At the instant the capacity is reduced below Q_b, the pump head H_f will be lower than the pressure in the system and there will be a tendency for the flow to reverse with the operating point moving from B to F and A. But as soon as the flow is reduced the pressure in the system begins to drop and the pump will again begin to discharge into the system until the pressure is built up to H_b at capacity Q_b. Since the demand from the system is only for a capacity Q_f, there will again be a tendency to reverse the flow and the cycle will be repeated. Fluctuations in head and capacity are accompanied by power and speed oscillations. This makes the phenomenon more complicated. However, *the origin of the pressure variation lies in the fact that, at certain times, the pressure in the discharge line is higher than the pump head and a tendency to reverse flow appears.*

The compressibility of a column of high temperature water is an important factor in the swinging systems of a boiler-feed pump. *If the throttle valve is placed next to the pump discharge nozzle, the oscillations do not appear as the water column is too short to provide the necessary compressibility, and the turbulence set up by the throttle valve destroys the regularity of impulses from the pump.*

It may be mentioned here that if a pump is operating under cavitation conditions, such as self-regulating condensate pumps (points F and G, Fig. 11.12), oscillations do not appear because the irregular water-hammer blows resulting from cavitation destroy the regularity of impulses which may be present otherwise.

In the majority of applications, the friction head is a major portion of the total head and the capacity is varied by throttling a valve next to the discharge flange. Under such conditions no swings appear, even with unstable head-capacity characteristics.

(e) Parallel Operation. A stable head-capacity characteristic is essential for parallel operation of several boiler-feed pumps. If a set of pumps have unstable head-capacity curves and the operating pressure happens to be at a point E (Fig. 14.1), which is higher than the shut-off head H_s, a pump cannot be put on the line as the zero capacity head H_s is not sufficient to open the check valve in a common discharge manifold. Also, if several pumps work at a head H_e some pumps may be working at a point F beyond the maximum head H_b, while others are working at point E on the rising part of the head-capacity curve. If the throttle valve is opened under such conditions, a pump working at point E will increase their capacity and those working at F will decrease their capacity. The latter group of pumps may cease to deliver entirely. Fluctuations in capacity and pressure will result. When one of a group of

pumps working on the same boiler begins to surge, the rest of the pumps respond immediately with swings of the same frequency, thereby increasing the total oscillating mass. The swings stop immediately when the faulty pump is stopped.

(f) Rising Characteristics. A rising head-capacity curve is essential for boiler-feed service and other applications where conditions for setting up pressure surges exist. Theory gives only one hint of how to produce a rising head-capacity curve, that is, making the discharge angle β_2 smaller. In actual pumps this condition is not sufficient, as the number of vanes, the vane angle at entrance β_1, and the vane development between β_1 and β_2 have a marked effect on the shape of the head-capacity curve near shut-off. For a selected vane angle β_2 the number of vanes z is determined by the experimental rule $z = \beta_2°/3$ given on page 78, which gives six vanes for $\beta_2 = 18°$ and seven vanes for $\beta_2 = 21°$. These are the values mostly used in practice.

By referring to Fig. 9.13 it will be noticed that lower impeller discharge vane angles β_2 and higher specific speeds produce a steeper head-capacity curve. Usually specific speed is selected from economic and mechanical considerations by fixing the number of stages for a specified head.

Schröder [3] has studied the form of the head-capacity curve as a function of the vane angle β_2, and the number of vanes. Figure 14.2 shows

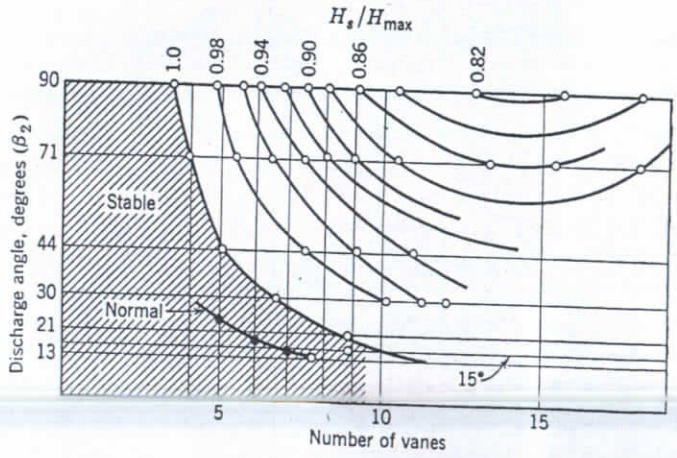

FIG. 14.2. Conditions for a stable Q-H curve (Schröder [3]).

a summary of his results. The shape of the head-capacity curve near zero capacity is represented by the ratio H_s/H_{max}. For a ratio less than unity the curve is unstable. Lower angles and fewer vanes tend to produce a more stable curve. Points marked "normal" added by the author.

(g) Means to Reduce or Stop Head-Capacity Swings.

1. By-passing part of the capacity to the suction supply tank. This step is also recommended as a precautionary measure to protect the pump from overheating in case the discharge is shut off.

2. With the automatic capacity governor near the boiler, very slight throttling at the pump will stop head-capacity swings.

3. All piping to and from the pump should be braced except for a provision for heat expansion. The mechanical vibration can be checked in this way.

4. Operation near the critical point should be avoided. In large stations the total capacity is split between several pumps. Units are put on and off the steam to meet the load instead of depending entirely on the governor for the capacity variations.

Dzialas [4] has studied swings of head-capacity curves of centrifugal pumps with unstable characteristics experimentally. His testing arrangement included an air chamber for an elastic member in the systems. These tests have definitely connected the swings in the systems to the unstable form of the head-capacity characteristics of the pump.

14.2 DETERMINING OPERATING POINTS OF CENTRIFUGAL PUMPS WORKING ON PIPE LINES

When a pump has to overcome the pipe line resistance in addition to a static head, the head against which the pump has to work varies with the capacity, pipe line resistance increasing with the capacity. The operating conditions of the pump in that case are best determined graphically by plotting, on the same sheet and to the same scale, both the pump head-capacity curve and the pipe line resistance curve. The operating point is obtained by the intersection of the two. The procedure is very simple when only one pump and one pipe line of a constant diameter are involved. However, when more than one pump is used to produce the total head or when the pipe line consists of several sections of different diameters going through points at different elevations, or when the flow from a main pipe line is divided, the plotting of the pipe line resistance curve becomes more complicated.

In every case, the operating point is obtained as an intersection of the pump head-capacity curve and the pipe line characteristics curve. When the total head is produced by more than one pump operating in series, the pump head-capacity curve is obtained by adding the heads for a given capacity. Figure 14.3 shows the head-capacity curve for two pumps in series. When the total capacity is divided between the two pumps, the combined head-capacity curve is obtained by doubling

the capacities for given heads. Figure 14.3 also shows the head-capacity curve for two pumps in parallel. The same procedure is followed if the pumps are not alike. When two pumps are available and are to operate against pipe line resistance, it is not always possible to say offhand whether the maximum capacity will be obtained when the pumps are being operated in series or parallel. This depends on the characteristics of the pumps and pipe line. Only by plotting head-capacity curves for series and parallel operation and determining the points of intersection of these with the pipe line resistance curve is the correct answer obtained.

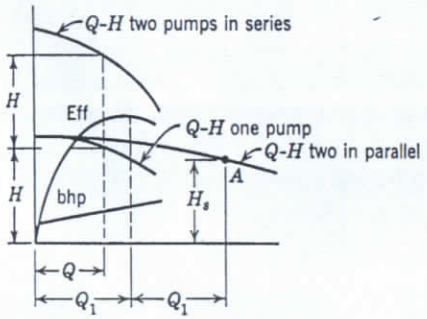

FIG. 14.3. Characteristics of two pumps in series and in parallel.

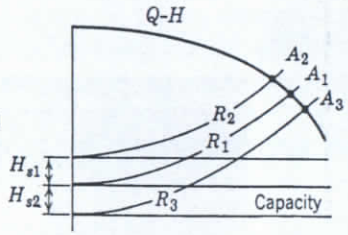

FIG. 14.4. Characteristics of a single pipe line.

(a) Pipe Line Resistance Curve. It is the plotting of the pipe line resistance curve that may present difficulties in some complicated cases. In every case the problem is broken up into several simple ones, and the final pipe line resistance curve is plotted by combining the pipe line resistance curves of the several elements comprising the given pipe line. Several cases will be considered, starting from the simple and working up to more complicated cases.

When a pump is working against the static head H_s only, the pipe line resistance curve is a horizontal line drawn at a distance equal to the static head H_s from the zero head on the head-capacity scales (Fig. 14.3). When the pump is discharging into a pipe line laid out on a perfectly flat surface, the pump total head is used to overcome the pipe line friction. The pipe line friction increases with the capacity going through the pipe line approximately as the square of the capacity, and the pipe line characteristics curve is a parabola with the apex going through the zero head point of the head-capacity curve. In Fig. 14.4 curve R_1 represents the pipe line resistance curve for such a case. Operating point A_1 is obtained as the intersection of the pipe line resistance curve

and the pump head-capacity curve. When, in addition to pipe line resistance, the pump has to overcome a static head H_{s1}, the combined pipe line characteristics curve is obtained by plotting the pipe line resistance curve (R_2, Fig. 14.4) as the sum of the static head and the pipe line resistance curve. When the final point of destination is located below the pumping station, the pump total head required to force the liquid through the pipe line is less by the difference in elevation, as this would assist the flow, and at small capacities the flow will take place by gravity. The pipe line characteristics curve in that case is obtained by subtraction of the difference in elevation between the pumping station and the end of the pipe line, which results in shifting the pipe line resistance curve (R_3, Fig. 14.4) by the static head H_{s2} below the zero head line. The pump operating point in every case is obtained as an intersection of the pipe line resistance curve, and the pump head-capacity curve (points A_1, A_2, A_3, Fig. 14.4).

When the pipe line consists of two sections of different diameters, the combined pipe line resistance curve is obtained by adding the pipe line resistance for a given capacity of the component parts of the pipe line. In Fig. 14.5(a), suppose pumping takes place from point B to point D, point D being higher than point B by H_s feet. The pipe line from B to C is of diameter d_1 and from C to D is of diameter d_2. In

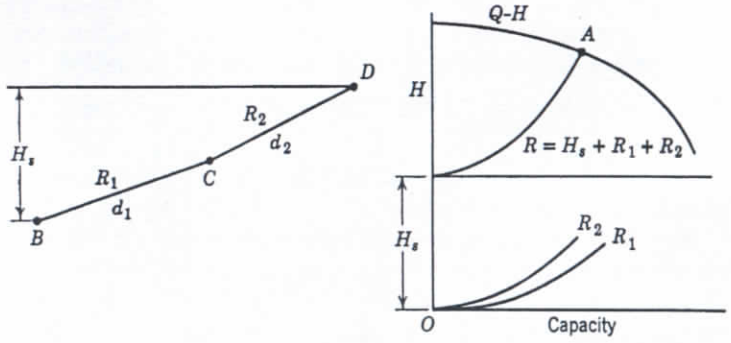

FIG. 14.5. Two pipe lines in series.

Fig. 14.5(b), curve R_1, the pipe line resistance curve is plotted for section BC, and curve R_2 is plotted for section CD. The combined pipe line resistance curve R is obtained by adding the ordinates for curves R_1 and R_2 and the static head H_s. The operating point A is obtained as an intersection of the combined pipe line resistance curve R and the pump head-capacity curve Q-H.

(b) **Two Parallel Lines.** When the pump is working on two pipe lines discharging either at two different points or at the same point, the operating point is obtained as an intersection of the pump Q-H curve and the pipe line resistance curve, which is obtained by adding the capacities for given heads of the individual pipe lines. In Fig. 14.6(a), suppose pump is at point B and pumping into two pipe lines to points

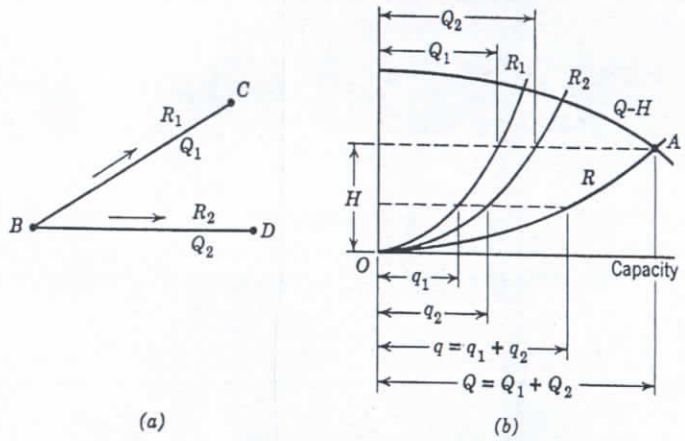

FIG. 14.6. Two pipe lines in parallel.

C and D, located at the same elevation as point B. In Fig. 14.6(b), R_1 is a pipe line characteristic for the line BC; R_2 is a pipe line resistance curve for the line BD. The combined pipe line resistance curve R is obtained by adding capacities for the same head. The operating point A is obtained as an intersection of pipe line resistance curve R and pump head-capacity curve Q-H. The pump capacity Q will be a sum of the capacities Q_1 and Q_2 going through the lines BC and BD respectively, which are obtained by reference to the curves R_1 and R_2 for a given head H.

In Figs. 14.7(a) and 14.7(b) an example similar to the one shown in Figs. 14.6(a) and 14.6(b) is presented, but points C and D are located higher than point B by H_{s1} and H_{s2} feet respectively. The procedure is the same. In Fig. 14.7(b) curve R_1 is the pipe line resistance for line BC. Curve R_2 is the pipe line resistance for line BD, plotted in the manner previously explained. The combined pipe line resistance curve R is obtained by adding the capacities for given heads from the curves R_1 and R_2. The pump-operating point A is obtained as an intersection of the combined pipe line resistance curve R and the pump head-capacity curve Q-H. Of the total capacity Q, Q_1 would go to point C, Q_2 to point D, which are read off from the curves R_1 and R_2 at the head H.

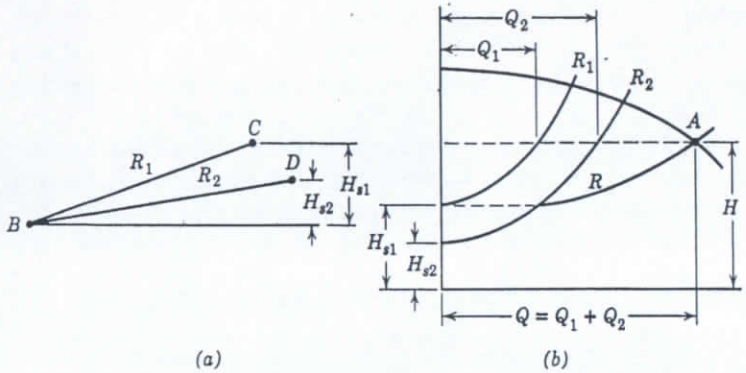

FIG. 14.7. Two pipe lines in parallel at different elevations.

As another example, suppose we are to pump from point B to point D, Fig. 14.8(a). At point C a constant quantity of liquid Q_3 is taken off. To find the operating point of the pump, proceed as follows. The pipe line resistance for the section of pipe line BC is plotted in the regular way, curve R_1, Fig. 14.8(b). The pipe line resistance for section CD is plotted with the zero point displaced with respect to head-capacity zero point by the capacity Q_3, which is going through pipe section BC but is not going through pipe section CD, curve R_2, Fig. 14.8(b). The

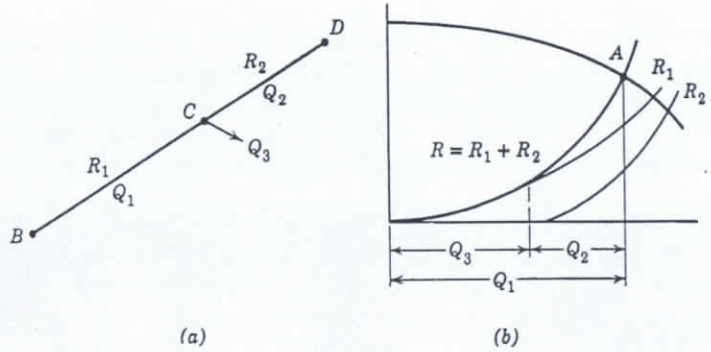

FIG. 14.8. Two pipe lines in series with a side outlet.

resistance of the complete pipe line BD is obtained by adding the pipe line resistances for the same capacity from curves R_1 and R_2; curve R, Fig. 14.8(b). Operating point A is obtained as the intersection of curve Q-H, with curve R in Fig. 14.8(b). Of the total quantity, Q_1 going through section BC, Q_3 is discharged at point C and Q_2 is going through section CD.

(*c*) **Pipe Line Throttling.** The determination of the operating point of centrifugal pumps working on pipe lines as treated in this article gives the maximum capacity possible with the existing pipe line and selected pumps. Very often this maximum capacity is not available when the pipe line is put in operation, and the flow must be throttled to reduce the throughput of the pipe line. When several stations are working in series, the throttling of the pumps requires great care. Thus, if all the throttling is done at the last station, the pipe line pressure at this station

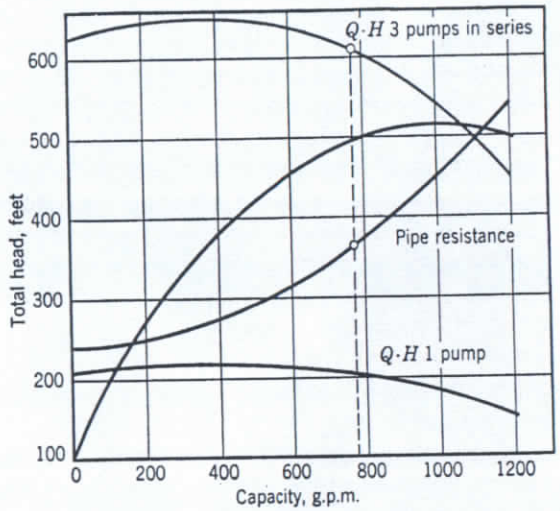

FIG. 14.9. Performance of 5-in. double-suction pump at 1760 rpm, efficiency 83 per cent.

may exceed the safe limits for the pipe line or the pump itself. Therefore, the throttling is divided uniformly among the stations in such a way that the suction pressures at each station are kept at the required minimum. If too much throttling is done at some intermediate station, the suction pressure at the next station may drop below the safe minimum and the pump may start cavitating, reducing the flow below the required capacity. This may also result in some abnormal operating conditions at some stations above the one causing the trouble. This case is illustrated in one example taken from actual experience.[5]

Three pumps with head-capacity characteristics as shown in Fig. 14.9 were installed to operate in series on a pipe line with pipe line characteristics as shown in the same figure. The expected capacity obtained by intersection of the combined head-capacity curve of the three pumps in series and the pipe line resistance curve was 1110 gpm. The first pump took suction from a tank, and several feet of static

liquid head were available above the pump center line. The last pump discharged into a tank located 240 ft above the location of the first pump. The liquid pumped was gasoline, of specific gravity 0.73. The following readings were obtained when all three pumps were operating in series.

	Suction Pressure	Discharge Pressure, lb	Differential Pressure, lb
First pump, A	7 in. Hg	60	64
Second pump, B	46 lb	33	−13
Third pump, C	23 lb	87	64

The capacity going through the pipe line was 770 gpm instead of the expected 1110 gpm.

Attention is called to the behavior of the second pump B, which not only did not produce any head but also wasted 13 lb of the head produced by the first station. However, the trouble was caused not by

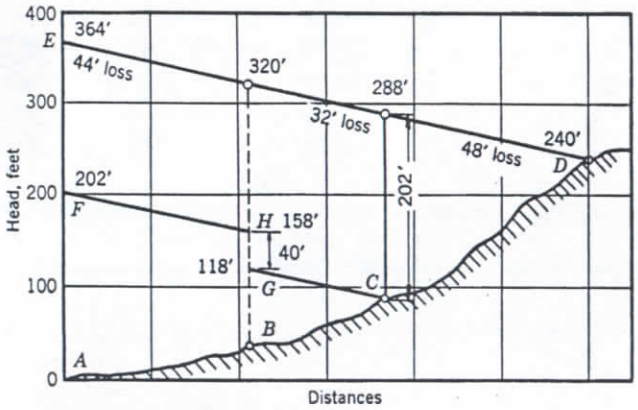

FIG. 14.10. Hydraulic gradient of the system represented in Fig. 14.9.

the second pump but by the first pump, which by all appearances and by comparison with pump C gave the impression of normal operation. However, 7 in. of vacuum on the first pump, when it was pumping gasoline, caused this pump to cut off at 770 gpm, thus fixing the capacity for the whole pipe line at 770 gpm. With this capacity the pipe line resistance is only 364 ft, including the 240 ft of static head, and two pumps were more than enough to produce this head. Thus, there was no work to be done by the second pump. Just why this pump and not the third pump had to loaf can be seen from Fig. 14.10, which gives the hydraulic gradient of the pipe line. The slope of the hydraulic

gradient is given by line ED. The first and third pumps produced 202 ft of head. Pump C had 154 ft of static head to overcome in addition to 48 ft of pipe line friction. The first pump produced 202 ft of head, corresponding to 770 gpm capacity. By drawing the hydraulic gradient lines from points C and F, points G and H are obtained, indicating that the pressure available at station B was more than required to overcome the pipe line friction and static head without the operation of station B.

If the profile of the pipe line were such that the major portion of the static head was between stations B and C, then station B would have to overcome this static head, and the excess of head available at station C would have to be destroyed by the third pump.

14.3 VARIABLE SPEED ENGINE DRIVE

With the engine throttle wide open or in a fixed position the engine output (brake horsepower) increases with the speed. If the head of an engine-driven centrifugal pump is changed so that the brake horsepower is increased, the engine will slow down. This will cause the pump brake horsepower to drop; this brake horsepower decreases much faster than the engine brake horsepower, and the unit will operate at a point where both engine and pump brake horsepower meet. If the head on the pump is changed so that the brake horsepower is decreased, the engine will speed up until, at a certain speed, again the pump brake horsepower becomes equal to the engine brake horsepower.

If the engine has sufficient power to meet any brake-horsepower requirement at a constant speed, a constant speed governor may take care of any possible variation of the brake-horsepower requirement by changing the engine throttle opening. However, in practice, it is frequently desired to utilize all the power available from the engine at any speed, for example, with fire engines. Then the determination of the variation of capacity with head becomes more complicated, as a change in head will result in a speed change, which in turn will change the head and capacity. Determination of the operating point by trial and error is a tedious and slow procedure. Below is offered a direct and simple method of plotting the variable speed head-capacity curves of engine-driven centrifugal pumps for a given engine rating.

Use is made of the unit head $h_{1n} = H/n^2$ and the unit capacity $q_{1n} = Q/n$. The unit brake horsepower can be defined in a similar manner: $(\text{bhp})_{1n} = \text{bhp}/n^3$, where n is revolutions per minute. In Fig. 14.11 the performance of a given pump is plotted in terms of the unit capacity, unit head, and unit brake horsepower. Suppose the engine is

directly coupled to the pump; then the engine horsepower can also be reduced to the unit speed by dividing the engine output by the corresponding (revolutions per minute)^3. This is plotted in Fig. 14.11 to the right of the pump curve, a common scale for the unit brake horsepower being used.

The operating points of the pump are determined by the condition that the unit brake horsepower of the pump is equal to the unit brake horsepower of the engine. Then, for any unit capacity A, the unit head is B, the pump unit brake horsepower is C and is equal to that of the

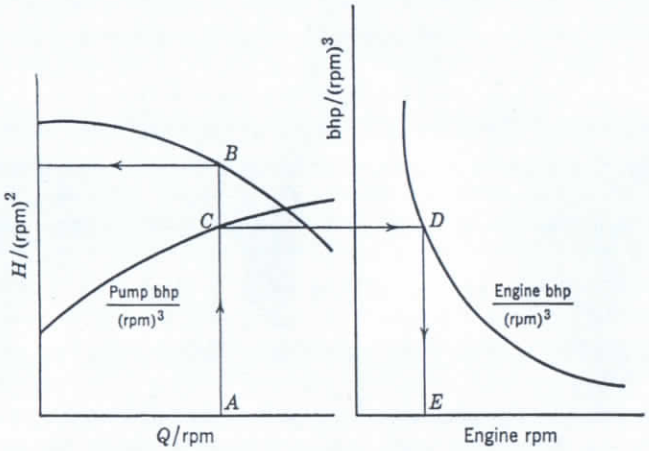

FIG. 14.11. Determination of the operating point of an engine-driven pump.

engine (point D), and the engine speed at which this unit brake horsepower is available is given by point E, which is the pump speed.

To find the capacity in gallons per minute multiply the unit capacity by the speed; the head is obtained by multiplying the unit head by n^2.

If the engine speed differs from that of the pump because of a gear reducer or increaser between the pump and the engine, the pump speeds are used for plotting the engine unit brake-horsepower curve. In other words, the gear reducer or increaser is considered a part of the engine, with a power output at the pump speed.

Figure 14.12 shows the performance of a 3-in. two-stage pump of $n_s = 1000$, engine-driven, with the throttle wide open. Constant speed head-capacity and brake-horsepower curves are also shown. The variable speed head-capacity curve is much steeper than the constant speed characteristic. Pumps having increasing brake horsepower toward shutoff, when engine-driven, have a flatter variable speed head-capacity curve than the constant speed curve. Figure 14.13 shows a variable

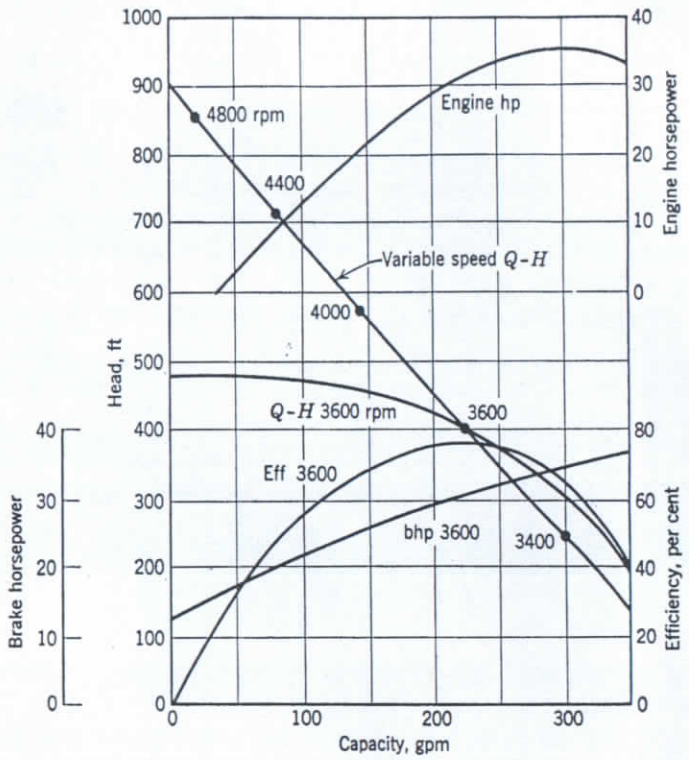

FIG. 14.12. Three-in. two-stage engine-driven pump with throttle wide open.

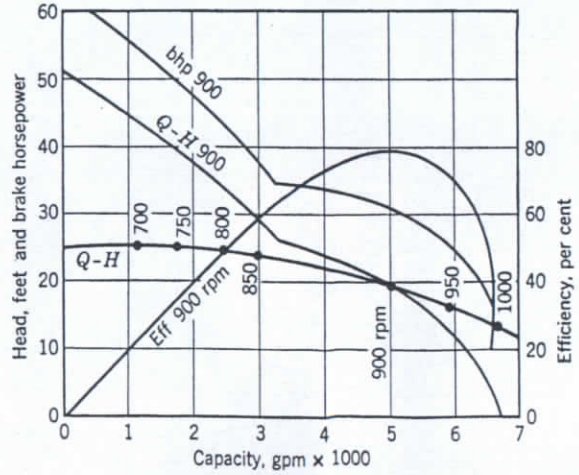

FIG. 14.13. Sixteen-in. propeller pump, engine-driven, with throttle wide open.

speed 16-in. propeller pump of $n_s = 7000$, engine-driven through a right-angle geared head. Constant speed head-capacity and brake-horsepower curves are also shown for comparison.*

14.4 PUMPING VISCOUS LIQUIDS WITH CENTRIFUGAL PUMPS

(*a*) **Pump Characteristics.** Pumping petroleum products is next in importance to pumping water. In general, in pumping viscous liquids the head and capacity at the b.e.p. are reduced by additional frictional losses and the brake horsepower increases, owing primarily to increased disk friction loss. The performance of a pump handling viscous oils is generally estimated by means of corrections applied to the water performance, because test facilities of the pump manufacturers provide only for water tests and most of the accumulated data and experience refer to water performance.

It is impossible to establish the performance of a pump handling viscous oil by purely theoretical deductions, even when the water performance is known. An analysis of the problem with the aid of dimensional analysis (Chapter 5) makes it evident that the relationship between head and capacity at constant speed is an experimental one, each viscosity producing a different head-capacity curve. However, the same analysis establishes certain relationships between variables describing the operation of centrifugal pumps which are confirmed by experiments. These constitute important guides in correlating the experimental test data for liquids of various viscosities and provide means for predicting pump performance for viscous liquids when water performance data are available. The following deductions suggested by the theory have been proved experimentally:

1. *The affinity laws hold for all viscosities but with less accuracy than those for water. This means that when speed varies the capacity varies directly as the speed, and the head varies directly as the square of the speed. Usually the efficiency is better at higher speeds; therefore when the speed is increased the brake horsepower increases less than the cube of the speed and the head increases more than the square of the speed (Fig. 14.14).*† When speed is varied the specific speed at b.e.p. remains unchanged when viscous liquids are being pumped, irrespective of the deviation from the affinity laws stated above.

* A direct method of determining the performance of engine-driven centrifugal pumps without the use of unit capacity, unit head, and unit brake horsepower is described in the author's article.[6]

† From unpublished tests by Lehigh University for Ingersoll-Rand Company.

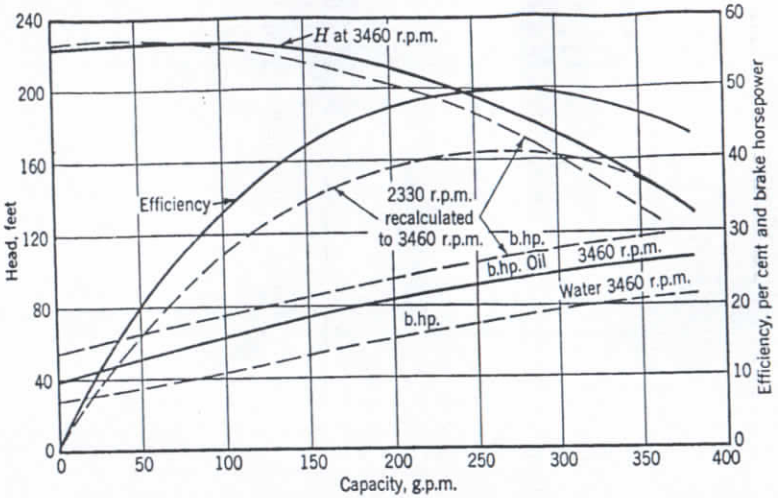

FIG. 14.14. Performance of 2-in. pump at two speeds pumping oil 825 S.S.U. ($\nu \times 10^5 = 195$), $D_2 = 7\frac{1}{4}$ in., $n_s = 1160$ (Ingersoll-Rand).

2. *At a constant speed the head-capacity decreases, as the viscosity increases, in such a way that the specific speed at b.e.p. remains constant (Fig. 14.15).*

$$n_s = \frac{n\sqrt{Q_1}}{H_1^{3/4}} = \frac{n\sqrt{Q_2}}{H_2^{3/4}} \tag{14.1}$$

where Q_1 and H_1 are the capacity and head at one viscosity and Q_2 and H_2 the same at another viscosity. From equation 14.1 it follows that

$$\frac{Q_1}{Q_2} = \left(\frac{H_1}{H_2}\right)^{1/2} \tag{14.2}$$

This is an important relationship. Thus to estimate the b.e.p. when viscous oil is being pumped, only one experimental correction factor is necessary, either that for the head or that for the capacity; the other will follow from the relationship of equation 14.2.

The following equations are used for conversion of the oil viscosities from S.S.U. to kinematic viscosity in square feet per second.

For S.S.U. > 100 $\quad \nu \times 10^5 = 0.237\,\text{S.S.U.} - (145/\text{S.S.U.})$ (14.3)

For S.S.U. < 100 $\quad \nu \times 10^5 = 0.244\,\text{S.S.U.} - (210/\text{S.S.U.})$ (14.4)

To convert the kinematic viscosity from metric units in stokes (square centimeters per second) to English units (square feet per second), divide

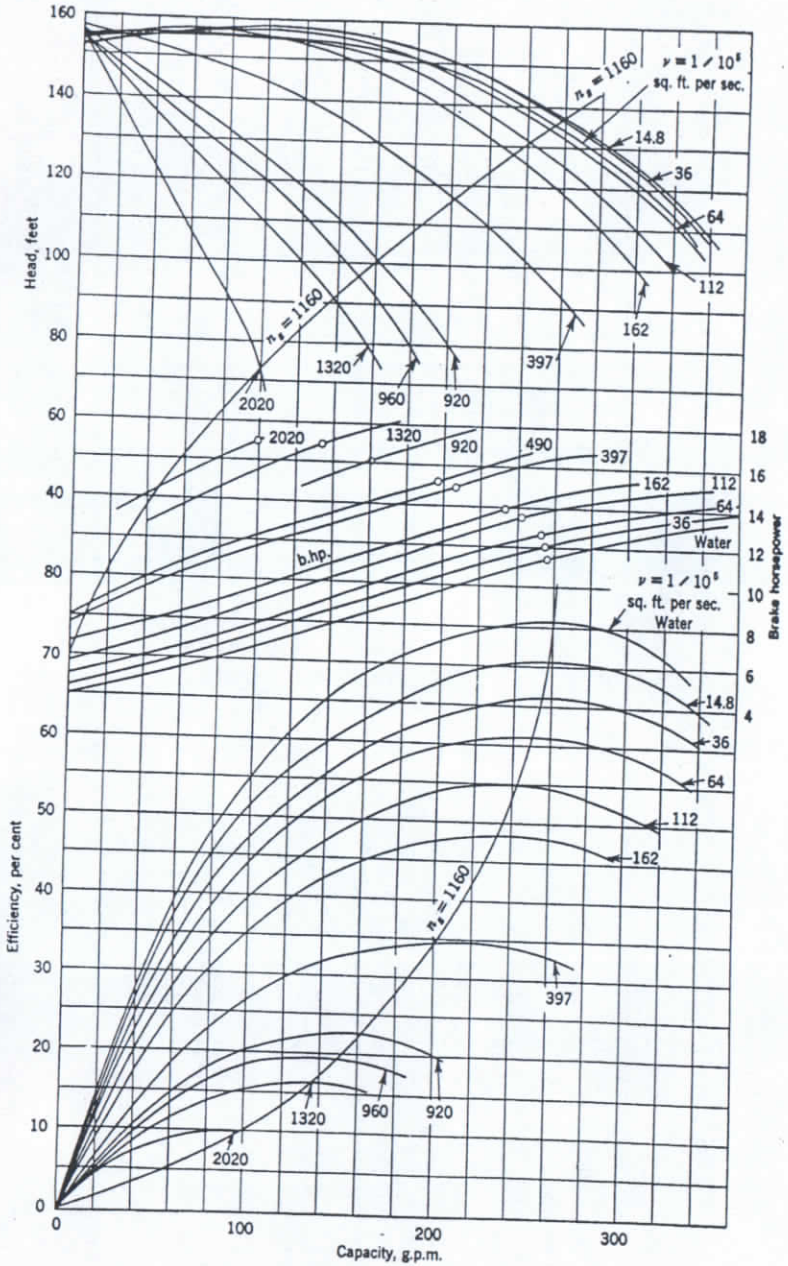

FIG. 14.15. Performance of 2-in. pump, pumping oil at 2875 rpm (Ingersoll-Rand).

the value in stokes by $929.03 = (2.54 \times 12)^2$. Note that in metric units the kinematic viscosity of water at 68°F = 1 centistoke. In English units the kinematic viscosity of water at 75°F = $1/10^5$ sq ft per sec.

3. *At constant speed and variable viscosity the head-capacity decreases as the viscosity increases, but the head at zero capacity remains essentially the same, thus resulting in steeper head-capacity curves for higher viscosities. Therefore, it can be generalized that the shut-off head does not depend on the impeller discharge angle and viscosity of the liquid.* However, it is affected appreciably by the pump casing, more so when pumping viscous liquids than when pumping water. *For instance, if the impeller diameter is too small for the pump casing (cut impeller diameter) and there is a large gap between the impeller periphery and the volute casing cut-water, the shut-off head will be lower for higher viscosities, and the head drop at b.e.p. will be greater than for the same impeller in a normal casing.* This is due to the fact that the impeller cannot maintain a normal velocity distribution in the pump casing, because most of the shear takes place at the impeller periphery and a lower generated head results. *On the other hand, if an impeller pumping a viscous liquid is fitted too closely to the cut-water in the casing, it will build up excess head—higher than with water at low capacities—because of the viscous drag.*

It has been observed on lower specific speed pumps with closed impellers that the head, even at the b.e.p., will increase above that for water upon a slight increase of viscosity before the head begins to drop upon a further increase of viscosity. This is caused by the fact that a slight increase in viscosity suppresses the relative circulation within the impeller channels, Fig. 3.15, sufficiently to increase the generated head more than is necessary to compensate for the increased hydraulic losses through the pump. With open impellers, owing to the absence of one of the shrouds, no such effects have been noticed. Also, in high specific speed impellers, the shrouds are relatively small and the impellers wide, and the effect of the shrouds on the head is negligible.

4. *For a constant viscosity and variable speed, efficiency at the b.e.p. is higher at higher rotative speeds* (Figs. 14.16 and 14.14). The reason for this is that when the speed is varied the disk friction increases as the 2.5 power of the speed for viscous flow and the 2.8 power for turbulent flow, whereas the pump output varies directly as the cube of the speed. It will be noticed in Fig. 14.14 that the reduction in brake horsepower at 3460 rpm is constant for all capacities. Hydraulic losses expressed as a percentage of the total head are also lower at higher speeds; thus a higher head than would follow from the affinity laws results. This contributes to the higher efficiency at higher speeds.

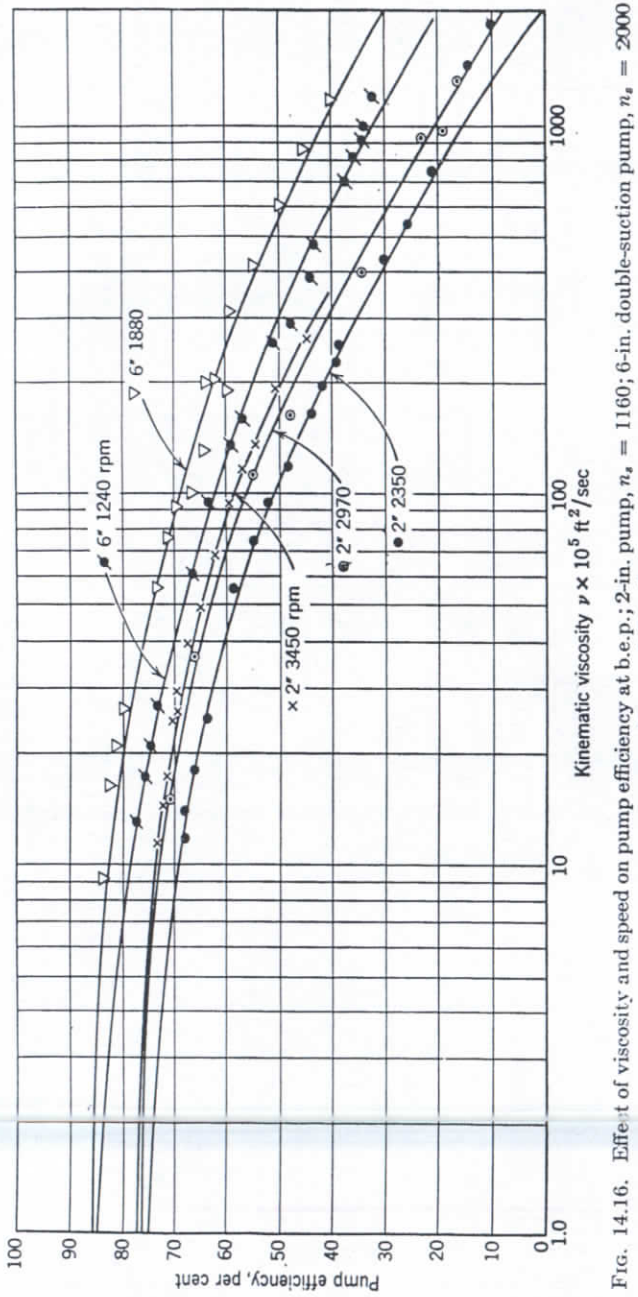

FIG. 14.16. Effect of viscosity and speed on pump efficiency at b.e.p.; 2-in. pump, $n_s = 1160$; 6-in. double-suction pump, $n_s = 2000$ (Ingersoll-Rand).

5. *From Figs. 14.14 and 14.15 it will be noticed that when viscous oils are being pumped the brake horsepower increases the same amount for a wide capacity range, the increase being the increase in disk friction loss.* A slight reduction in the disk friction loss power is observed near and at the shut-off and at capacities over normal. The first is caused by a reduction of viscosity due to the temperature rise of the liquid at low capacities. The reduction of the power at capacities above normal shows the approach of cavitation at the higher rates of flow. With increasing viscosity the friction in the closely fitted running clearances between the rotating element and the stationary parts becomes increasingly important. But even an approximate determination of this loss is difficult because of the uncertain temperature of the oil in the clearance. Since leakage through the running clearances becomes negligible at high viscosities, liquid confined between the impeller shrouds and casing walls and adjacent to the running clearances may be at a higher temperature than the pumped liquid.

Also, it is important to note that the brake horsepower at b.e.p. increases with viscosity. This means that, although the head and capacity drop with viscosity, the efficiency decreases more rapidly than the product of the head and capacity, as seen from the simple relationships below.

For water

$$\frac{QH}{3960 \times e} = \text{bhp} \tag{14.5}$$

For an oil of specific gravity s_1 and viscosity ν_1,

$$\frac{Q_1 H_1 s_1}{3960 \times e_1} = (\text{bhp})_1 \tag{14.6}$$

Then

$$\frac{QH}{e} < \frac{Q_1 H_1 s_1}{e_1} \tag{14.7}$$

Hence

$$\frac{Q_1}{Q} \times \frac{H_1}{H} \times s_1 > \frac{e_1}{e} \tag{14.8}$$

Letting the ratio $Q_1/Q = F_Q$ denote the capacity correction factor, and $H_1/H = F_H$ the head correction factor, and $e_1/e = F_e$ the efficiency correction factor, from equation 14.8, we find

$$F_Q F_H s_1 > F_e \tag{14.9}$$

Or, utilizing the relationship from equation 14.2,

$$F_H{}^{\frac{5}{6}} s_1 > F_e \tag{14.10}$$

Equations 14.2 and 14.10 give the relative values of the correction factors for head, capacity, and efficiency, when viscous liquids are being pumped, in terms of those when pumping water. The absolute values of these factors have to be determined experimentally.

(*b*) **Estimating Performance for Viscous Liquids.** Performance of centrifugal pumps for viscous liquids is usually estimated only for the b.e.p., correction factors based on test data being used. Two such factors are sufficient, one for the head and one for the efficiency. The capacity correction factor is determined from equation 14.2. The head and capacity for the b.e.p. having been established, the head-capacity curve is drawn by eye through the shut-off head point, which remains the same irrespective of viscosity. To complete the efficiency curve, the brake horsepower is calculated for the b.e.p., then the brake-horsepower curve is drawn by eye, the general slope of the brake-horsepower curve for water being followed. The efficiency curve is calculated from the brake-horsepower and head-capacity curves.

Figure 14.17 shows the head correction factor and efficiency (not a factor) plotted against Reynolds number defined as follows:

$$R = Q_o n/\nu\sqrt{H_w} \tag{14.11}$$

where Q_o is oil capacity, cubic feet per second.
n is revolutions per minute.
ν is kinematic viscosity, square feet per second.
H_w is water head, feet.

This form of Reynolds number is adopted in preference to that defined by equation 5.8.

$$\Pi_4 = Q/\nu D \tag{5.8}$$

because it does not contain the impeller diameter and permits converting the pumping requirements for oil to those of water after the speed is assumed. For the first approximation the oil head instead of the water head can be used for calculation of the Reynolds number. There is a fixed relationship between the two forms of Reynolds number.

$$R = \frac{60\sqrt{2g}\,K_u}{\pi} \times \Pi_4 = 153.4 \times \Pi_4 \tag{14.12}$$

where K_u is the speed constant defined by equation 5.21 $\approx$ 1.0.

For viscosity S.S.U. > 100 the expression for Reynolds number can be given the form

$$R = 941.6\,\frac{(\text{gpm})_o \times \text{rpm}}{\text{S.S.U.}\sqrt{H_w}} \tag{14.13}$$

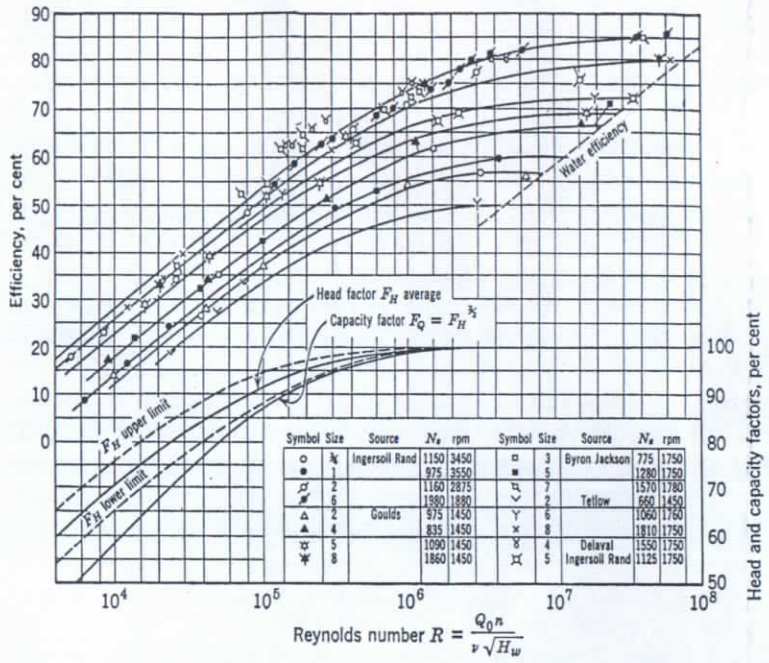

Q_0 = oil capacity cu ft/sec = gpm/448
N = rpm
N_s = specific speed
H_w = water head ft
ν = kinematic viscosity sq ft/sec

For S.S.U. < 100 $\quad \nu \times 10^5 = 0.244\,\text{S.S.U.} - 210/\text{S.S.U.}$
For S.S.U. > 100 $\quad \nu \times 10^5 = 0.237\,\text{S.S.U.} - 145/\text{S.S.U.}$
For S.S.U. > 100 $\quad R = 941.6\,\frac{(\text{gpm})0 \times \text{rpm}}{\sqrt{H_w} \times \text{S.S.U.}}$

FIG. 14.17. Head and efficiency corrections for viscosity at best efficiency points.

For the same Reynolds number the efficiency drop is smaller for smaller, less efficient pumps, because of accumulative heating effect due to power loss in hydraulic and disk friction. The efficiency drop for Reynolds numbers lower than shown on Fig. 14.17 is smaller than extrapolation of the curves would indicate. This again is caused by the increased heating effect on viscosity at low efficiencies.

(*c*) **Special Pumps for Viscous Liquids.** Experimental data on pumping viscous liquids were obtained with standard water pumps, some of obsolete design. Specially designed pumps can have special design features which would show better performance than normal pumps when pumping viscous liquids; however, their performance on water may be impaired. The following design elements are suggested for pumps to handle viscous liquids:

1. Use of high impeller discharge angles, perhaps up to $\beta_2 = 60°$, will reduce the impeller diameter necessary to produce the same head

and, hence, reduce the disk friction loss. Impeller hydraulic friction will be reduced at the same time as impeller passages become shorter.

2. Elimination of close-clearance wide sealing rings at the impeller eye and providing knife edge seals (one or two) similar to those used on blowers. Leakage loss becomes secondary when pumping viscous liquids.

3. Providing a similar axial seal at the impeller outside diameter to confine the liquid between the impeller and casing walls. The temperature of the liquid in this confined space may be considerably higher than that of the liquid going through the impeller because of the accumulation of heat resulting from disk friction. Thus the disk friction loss may be reduced. When pumping petroleum oils of high viscosities, feeding of light (or heated) oil into the confined space may prove an effective means to reduce further the disk friction power.

4. It is essential to have an ample gap (twice the normal) between the casing tongue or cut-water and the impeller outside diameter. Otherwise impeller shrouds will produce head by viscous drag at low capacities, which is not an efficient way of pumping.

5. It has been pointed out already that high rotative speed and, hence, high specific speed types show a better efficiency and more head-capacity output than the low specific speed pumps on viscous liquids.

(*d*) **Theoretical Considerations.** For a given capacity the input head H_i and Euler's head H_e are the same for all viscosities, and they depend on the impeller discharge angle only. This means that for a given capacity (for instance, the b.e.p. at a given viscosity) the impeller power input does not depend on the viscosity, and the increase in power, as compared to the power at the same capacity when pumping water, is caused solely by the increased external friction of the rotating element. If the latter could be calculated the brake horsepower and the efficiency, when viscous liquids are being pumped, could be obtained. In this way only one correction factor for the head would be necessary to predict the performance. However, accurate calculation of the disk friction and ring friction losses presents great difficulties, as temperature of the liquid in the ring and the space between the impeller shrouds and the casing walls may differ considerably from that of the pumped liquid. Therefore, in practice, estimation of the pump efficiency, when viscous liquids are being pumped, will depend on experimental data such as shown in Fig. 14.17.

Attention is called to the fact that when viscous liquids are being pumped for a given capacity, Euler's and the input velocity triangles remain the same as for water. However, for b.e.p. both Euler's and the input triangles are different for each viscosity although specific speed n_s remains the same. Thus a complete dynamic similarity is not possible under these conditions because n_s = constant and R = constant cannot both be satisfied at the same time. When pumping water the effect of Reynolds number is negligible, and the laws of similarity hold; but when pumping viscous liquids Reynolds number becomes a predominant factor and dynamic similarity is impaired as viscosity is increased.

14.5 REGULATION OF CAPACITY OF CENTRIFUGAL PUMPS

Pump capacity may vary for one of the following reasons: (1) change in total head, which is quite common with low head pumps taking their suction from, or discharging into, rivers, lakes, or oceans; (2) variation in the demand, such as in boiler-feed systems; and (3) variation in supply at the pump suction, as on condensate pump service.

In the first case, particularly with low and medium specific speed pumps, there is a danger of the motor overloading if the head decreases since the brake horsepower increases with the capacity. Throttling of the pump discharge is necessary to protect the motor. On propeller pumps, the brake horsepower increases as the head is increased; therefore the motor should be selected to handle the load at the highest possible head. On the other hand, a decrease in operating head on a propeller pump will result in decreased power, and throttling will not be necessary to protect the motor.

When the demand is variable, throttling of the discharge is used to adjust the capacity to meet the demand. With low and medium specific speed pumps, power is saved when the discharge is throttled. With propeller pumps, reduction of the pump capacity by throttling will increase the load on the motor and, evidently, it will be more economical to by-pass the excess capacity back to the suction sump. Some power can be saved by throttling the pump suction instead of the pump discharge, but the danger of cavitation makes this method unpractical.

When the supply on the pump suction is limited there is always a danger that the pump will lose prime or cavitate. Therefore it is advisable to throttle the discharge so that a minimum submergence is maintained on the pump suction. Vertical condensate pumps of the turbine type (Fig. 16.22) can operate without control of the discharge and without bad effects of cavitation.

Variable speed drives, such as steam turbines or gasoline engines, permit capacity variation by changing speed. This entails very little or no power loss, whereas throttling always wastes power. A number of means have been developed to vary pump capacity with a power saving as compared with throttling. These will be briefly described here.

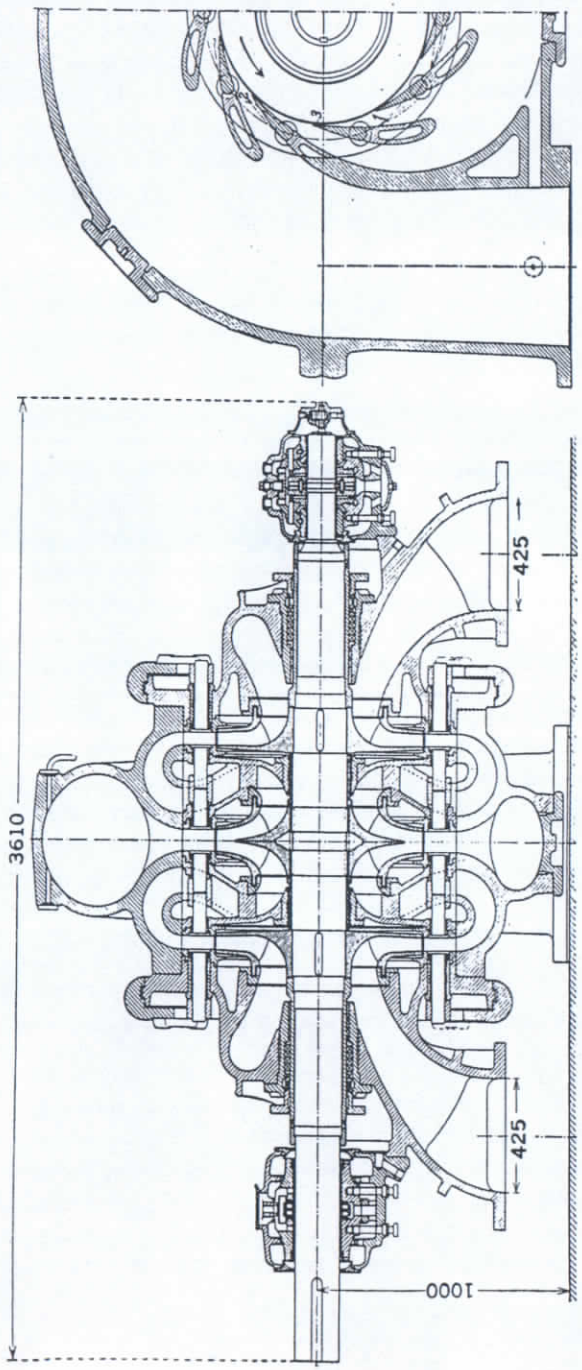

FIG. 14.18. Seventeen-in. two-stage pump with adjustable diffusion vanes; 17,400 gpm, 755 ft., 1000 rpm, n_s = 1540. Storage pumping at Schwarzenbachwerks (Escher, Wyss). (Dimensions in millimeters.)

Siebrecht [7] has studied a number of methods of varying the pump capacity, all of which proved to be unpractical for various reasons, although some of them had shown some power saving as compared with discharge throttling. The schemes tested by Siebrecht included the following:

1. *Adjustable Diffusion Casing Vanes.* This arrangement shows an appreciable gain in efficiency at reduced capacity. The saving in power,

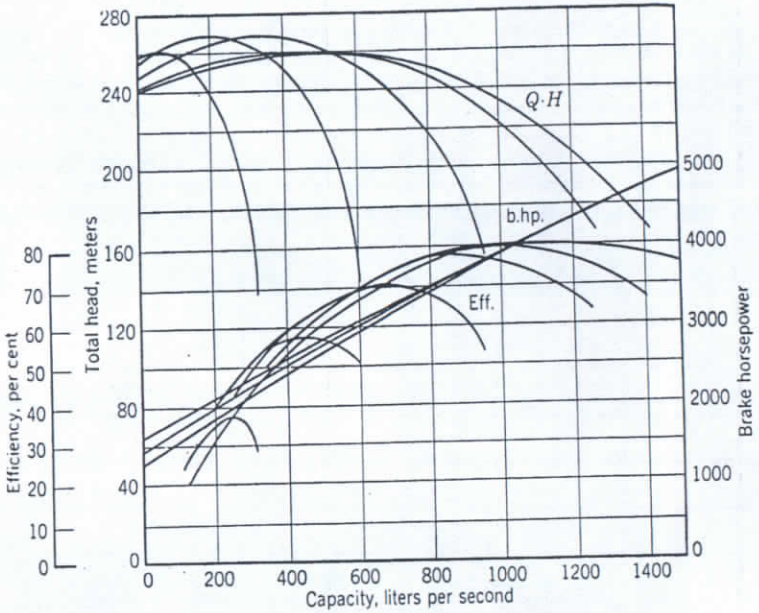

FIG. 14.19. Performance of pump shown in Fig. 14.18.

however, is not in proportion to the gain in efficiency, as the head increases at partial capacities and the discharge must be throttled. The mechanical complications make this method unpractical in the United States. However, there are several large installations of this type in Europe. Figures 14.18 and 14.19 show the sectional drawing and performance of one unit of this type.

2. *Throttle between the Impeller and Diffusion Vanes.* The impeller discharge was throttled in this scheme by a cylindrical throttle inserted between the impeller discharge and the diffusion casing vane. There was no improvement in efficiency with the impeller throttled at any capacity. However, a small saving of power was effected by this method, as the head at partial capacities was reduced more than the efficiency. This method was never tried on commercial pumps.

3. *Admission of Air to Pump Suction.* Figure 12.6 reproduces Siebrecht's tests wherein small amounts of air were admitted to the pump suction. Danger of losing prime and objection to air in the system make this method undesirable. The author knows of isolated cases where automatic admission of air into the suction bell of vertical pumps was used to maintain the submergence as the supply to the suction sump was decreased.

(*a*) **Capacity Regulation at Constant Speed.** Variable capacity demand at constant motor speed can be met in one of the following ways:

1. By providing a storage capacity and by intermittent pump operation.
2. By dividing the maximum capacity demand among several units, and operating one or more units at a time.
3. By throttling the pump discharge or by-passing part of the capacity. The latter method is used in preference to throttling to protect the pump when capacity varies from zero to a maximum.

Pump throttling is by far the most frequently used means to vary the pump capacity. With large units a considerable power saving can be effected by a proper selection of the pump characteristic to suit the existing requirements of the plant. Depending on whether the head on the pump varies with the capacity, and on the amount of time the pump has to operate at several capacities, location of the b.e.p and selection of the proper slope of the head-capacity curve may make an appreciable difference in the total power cost. In the majority of cases the best characteristics can be determined only by trial calculations.

(*b*) **Variable Speed Drive.** This can be realized by the use of one of the following arrangements:

1. Steam turbine or engine drive.
2. Variable speed electric motors.
3. Constant speed electric motors with variable speed coupling.

The first method is the best as it does not involve any waste of power. Since the driver and pump efficiency vary with the speed and location of the operating point, selection of the best speed for the driver and location of the pump b.e.p. require consideration to obtain a minimum yearly power expenditure to meet the variable capacity demand. Speed increasers or reducers between the driver and the pump frequently provide the best solution.

The direct-current electric motor is the most efficient electric drive for variable speed conditions and is widely used for marine service.

Direct-current motors are not available at high speed owing to commutation difficulties.

The wound-rotor induction motor is the most common and the simplest of the electric variable speed drives. Its efficiency varies approximately directly as the speed but, since the pump output varies directly as the cube of the speed, a considerable power saving can be effected

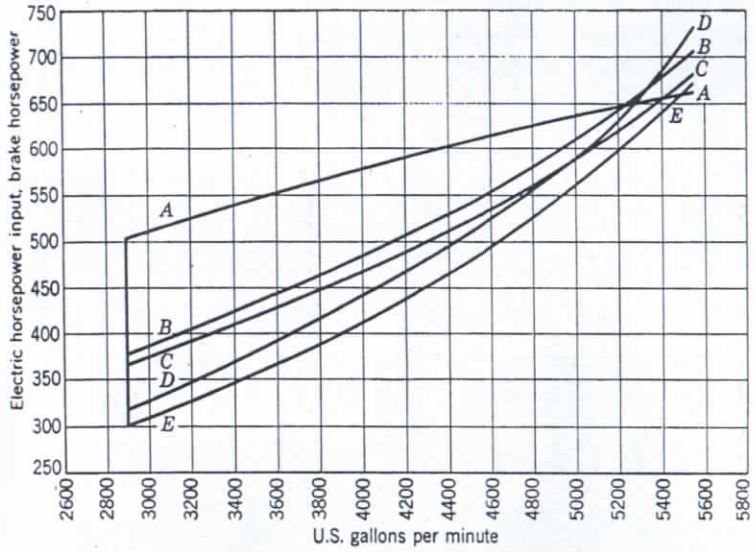

FIG. 14.20. Two double-suction pumps in series; 382-ft total head at 1800 rpm; variable capacity; constant head. Comparison of adjusting pump speed with throttling discharge. Curve *A*, horsepower input constant speed, throttling for reduced capacity; *B*, horsepower input variable speed, synchronous motor hydraulic coupling both pumps; *C*, horsepower input variable speed, wound-rotor induction motor; *D*, horsepower input variable speed, direct-current motor and rectifier using shunt field control; *E*, horsepower input variable speed, synchronous motor with variable speed, constant efficiency mechanical speed reducer.

with this type of drive. The shape of the head-capacity curve has some bearing on the power demand at reduced speeds, as a flat *Q-H* curve requires less reduction in speed to meet the reduced capacity.

Speed variation of wound-rotor motors is not continuous but in steps, usually six for large motors. By selecting the speed steps to suit the requirements some saving in power can be realized.

Variable speed couplings can be of the magnetic or the hydraulic type. The economy of both types is approximately the same. The magnetic coupling needs direct current for excitation, requiring either a synchronous motor with an oversize exciter for a drive, or special excitation

equipment. The hydraulic coupling speed reduction is not over 20 per cent and is less efficient than the wound-rotor induction motor.

Richardson [8] has made a study of comparative costs and relative power savings with constant and variable speed electric motor-driven units for variable capacity. Figure 14.20 is reproduced from his article. Note that curve D represents a direct-current motor drive through a rectifier from an alternating-current power source. When direct-current power is available, direct-current motors provide the most efficient variable speed drive. Curve B shows the electric horsepower input with a synchronous motor drive through a hydraulic coupling, both pumps operating at a reduced speed. However, a cheaper and more efficient arrangement is obtained by operating one pump at constant speed and the second pump at variable speed through a coupling between the pumps. The power input will be almost exactly as shown by curve B, the power saving resulting from the smaller initial slip loss of a smaller coupling.

Variation of capacity of axial flow pumps with a variable pitch impeller is discussed in Chapter 16.

14.6 MODEL TESTING

Models of pumps are built to obtain the desired information about the hydraulic performance of a given type of pump with a minimum expense of time and money. Model testing is resorted to in the following cases.

1. As part of the general development of a new type of pump to be built in different sizes.
2. To determine the pump behavior under special conditions, reproducing those existing in a new proposed plant, such as the cavitation characteristics of the pump and the effect of different arrangements of several pumps within the pumping station.
3. For use on acceptance tests where tests on the full-size pump are impossible owing to physical limitations of the plant or economic considerations.

In general, laboratory testing of a model is more accurate than field tests on a large pump because measuring large quantities of water accurately presents some difficulties. To arrive at the head and capacity of the prototype from the model tests, affinity laws are used. It has been pointed out that the cavitation conditions are best approached by the model if the pump is tested at the same head and submergence as the prototype. If this is impossible then the model can be operated

at any head and the submergence is so adjusted as to obtain the same value of the cavitation constant σ. Where a model is operated at the same head as the prototype, capacity varies as the square of the multiplier (ratio of impeller diameters of the model and prototype) and the speed varies inversely as the multiplier, or

$$\frac{Q_m}{Q} = F^2 \qquad \text{and} \qquad \frac{n_m}{n} = \frac{1}{F}$$

where Q_m and n_m are model capacity and speed, and F is a multiplier.

For accurate results, field suction and discharge conditions should be reproduced for the model testing. When this is impossible the suction and discharge should be so arranged as to make their effect negligible on the pump performance.

Experience has shown that the efficiency of large units is higher than that of their models, but there are no set rules to predict the efficiency of the prototype from the model efficiency. The Hydraulic Institute recommends that the efficiency guarantee should be made on the basis of a model acceptance test. In that case the estimated efficiency of the full-size pump may be used for estimating the motor size only.

Moody's equation [9]

$$\frac{1 - E}{1 - e} = \left(\frac{d}{D}\right)^{1/4}\left(\frac{h}{H}\right)^{1/10} \tag{14.14}$$

is in use in water turbine practice to estimate efficiency of a large unit from the model efficiency, and it is used occasionally by pump engineers. If the model is tested at the same head as the prototype Moody's equation reduces to

$$\frac{1 - E}{1 - e} = \left(\frac{d}{D}\right)^{1/4} \tag{14.15}$$

where E is the efficiency, D is the impeller diameter, and H is the head of the prototype, and e, d, and h are the same variables for the model. The same equation can be used for estimating efficiency from a reduced speed test of the full-size pump, in which case $d/D = 1$. Although a good agreement between efficiencies obtained with Moody's equation and actual field tests were observed on many occasions, there are cases on record when the discrepancy between the two efficiencies was 1.4 points.[10] On one recent installation of a large centrifugal pump the prototype efficiency determined by the field test did not exceed that of the 8-in. model, which was more than six times smaller than the prototype.

REFERENCES

1. W. J. Rheingans, "Power Swings in Hydraulic Power Plants," *Trans. A.S.M.E.*, p. 171, April 1940.
2. Karl Grün, *Dampfkessel-Speisepumpen*, Vienna, Julius Springer, p. 77, 1934.
3. Erich Schröder, "Das Förderhöhenverhältnis einer radialen Kreiselpumpe," Tech. Hochschule zu Braunschweig, doctoral dissertation, 1933; chart plotted by C. Pfleiderer and published in *Z. Ver. deut. Ing.*, Vol. 82, No. 9, p. 263, Feb. 26, 1938.
4. R. Dzialas, "Schwingungen bei Kreiselpumpen mit labiler Kennlinie," *Arch. Wärmewirt. und Dampfkesselwesen*, Vol. 22, *Bull.* 3, p. 63, March 1941.
5. A. J. Stepanoff, "Determining Operating Points of Centrifugal Pumps Working on Pipe Lines," *Oil Gas J.*, Dec. 4, 1941.
6. A. J. Stepanoff, "How to Determine Performance of Engine Driven Pumps," *Power*, p. 84, November 1940.
7. Wilhelm Siebrecht, "Beitrag zur Regelung der Kreiselpumpen," *Bull.* 321, Berlin, Verein Deutscher Ingenieure, 1929.
8. C. A. Richardson, "Economics of Electric Power Pumping," *Allis-Chalmers Elec. Rev.*, p. 20, June 1944.
9. L. F. Moody, "The Propeller Type Turbine," *Trans. A.S.C.E.*, Vol. 89, pp. 625, 690, 1926.
10. F. H. Rogers and R. E. B. Sharp, "45,000 HP Propeller Turbine for Wheeler Dam," *Mech. Eng.*, Vol. 57, p. 500 August 1935.
11. N. Tetlow, "A Survey of Modern Centrifugal Pump Practice," *Inst. Mech. Eng.*, pp. 121–134, 1942.
12. "A Further Investigation of the Performance of Centrifugal Pumps when Pumping Oils," Goulds Pump Inc., *Bull.* 130, 126.
13. Arthur T. Ippen, "The Influence of Viscosity on Centrifugal Pump Performance," *Trans. A.S.M.E.*, Vol. 68, No. 8, p. 823, 1946.

Chapter 15

Shaft Design for Critical Speeds

15.1 THEORETICAL RELATIONSHIPS

The pump shaft is designed to transmit the required power without vibration. Besides the torque and rotor's own weight, axial thrust and side thrust from the single-volute casing must be considered.

Theoretically, the shaft deflection should always be less than the radial clearance between the closely fitted parts of the rotating element and the stationary casing parts. In practice, however, owing to the inevitable eccentricity of the several running fits inside the pump, this condition is never fulfilled and some of the closely fitted parts serve as internal bearings. *In pumps having proper selection of materials, it has been found that, when liquids such as water and hot petroleum products are being pumped, they serve as a lubricating and cooling medium for such internal bearings.*

Shaft vibration usually appears as a result of dynamic deflections which reach their maximum value at critical speeds. Even with carefully balanced rotors, there is always a residual unbalance which develops a centrifugal force, and the latter causes a dynamic shaft deflection in addition to the static deflection due to the rotor's own weight. The centrifugal force increases with the increase of deflection at higher speeds until some internal parts are damaged or the shaft fails.

(a) Critical Speed of a Single Impeller on a Weightless Shaft. A disk of weight W and mass $m = W/g$ is fastened on a weightless shaft so that its center of gravity S is displaced a distance e from the axis of the vertical shaft (Fig. 15.1). If the center of the disk is deflected a distance y from the axis of rotation, then the center of gravity of the disk is displaced a distance $y + e$ from the axis of rotation, and the centrifugal force is

$$P = m(y + e)\omega^2 \qquad (15.1)$$

where ω is the angular velocity in radians per second.

Since there is proportionality between the force and the deflection,

$$P = Ky \tag{15.2}$$

where K is a constant for a given type of load and support and is defined as a force to give a unit deflection.

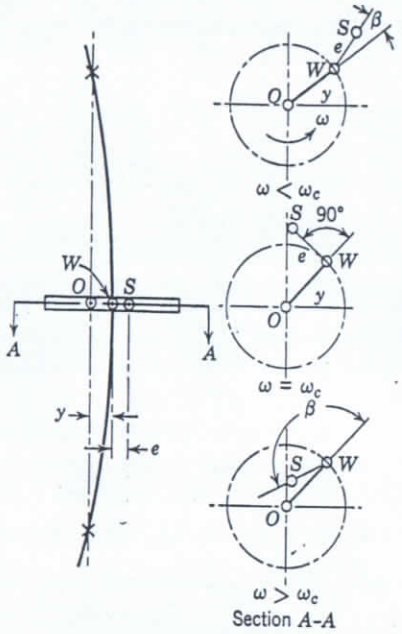

FIG. 15.1. Single load on a vertical weightless shaft.

Substituting equation 15.2 into equation 15.1, we get

$$m(y + e)\omega^2 = Ky \tag{15.3}$$

and

$$y = \frac{me\omega^2}{K - m\omega^2} \tag{15.4}$$

If ω is increased so that the denominator becomes equal to zero or

$$K - m\omega^2 = 0 \quad \text{and} \quad \omega_c = \sqrt{\frac{K}{m}} \tag{15.5}$$

then y becomes infinite, $y = \infty$, and the shaft should theoretically break. In practice, violent vibration is observed only as the value of y is limited by the close internal fits inside the pump. *Even in machines*

having no closely fitted internal parts, the shaft deflection at the critical speed stays limited because (1) *the critical speed, mathematically, is a point on both sides of which the shaft regains rapidly its ability to resist deflection;* (2) *time is necessary for the shaft to develop its maximum deflection, which may not be available when the critical speed is passed rapidly;* (3) *the surrounding medium causes external friction and damping;* (4) *internal friction of shaft material causes energy dissipation.*

ω_c is called the critical angular velocity to which a critical speed in revolutions per minute corresponds:

$$n = \frac{30\omega_c}{\pi} = \frac{30}{\pi}\sqrt{\frac{K}{m}} \tag{15.6}$$

The value of K depends on the shaft dimensions, its material, method of support, and load distribution. Thus, if I is the moment of inertia of the shaft, a and b are the distance of the disk from support, and E is the modulus of elasticity of the shaft material, then, for a freely supported shaft,

$$y = \frac{Pa^2b^2}{3EI(a + b)} \tag{15.7}$$

and

$$K = \frac{3EI(a + b)}{a^2b^2} \tag{15.7a}$$

Combining equations 15.4 and 15.5

$$y = \left(\frac{\omega^2}{\omega_c^2 - \omega^2}\right)e = \left(\frac{n^2}{n_c^2 - n^2}\right)e \tag{15.8}$$

If the operating speed n is above n_c, y becomes negative and its value decreases. In other words, the shaft again approaches the straight line joining the two points of support. At $n = \infty$, $y = e$, or the center of gravity S is on the axis of rotation (Fig. 15.1). The location of the point of disk fastening and the center of gravity have exchanged their positions. Thus the mass m has a tendency to balance itself in the sense that, above critical speed, the rotating body tends to rotate about the center of gravity.

Note that equation 15.8 gives for critical speed ($y = \infty$ or large) not a point but a belt. This is confirmed by the actual behavior of pump shafts near the critical speed (Fig. 15.2). Vibration-free operation of pumps is possible on both sides of the critical speed. A great majority

of multistage pumps with mechanical seals (no support at stuffing boxes), operating at 3000 or 3600 rpm, operate above the critical speed.

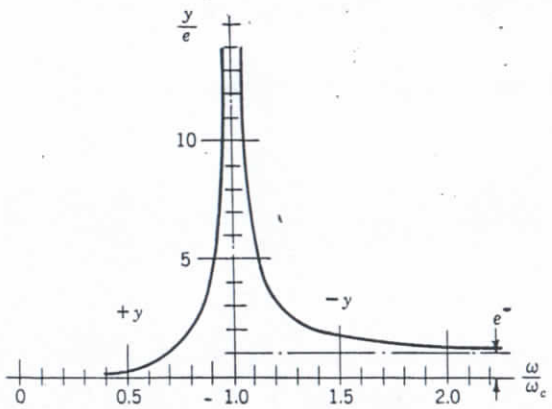

FIG. 15.2. Shaft deflections at different speeds.

(*b*) **Effect of Disk's Weight.** With a horizontal shaft, there is always a deflection y_0 due to the disk's weight W directed downward (Fig. 15.3). The center of gravity S of the disk describes now a circle with a center O' below the line connecting the two shaft supports by y_0. The radius of the circle is $y + e$, and the result of the above deductions remains the same. *Thus, a given shaft has the same critical speed when operated horizontally, vertically, or at any angle. The dynamic deflection due to centrifugal force is superimposed upon the static deflection of a horizontal shaft.*

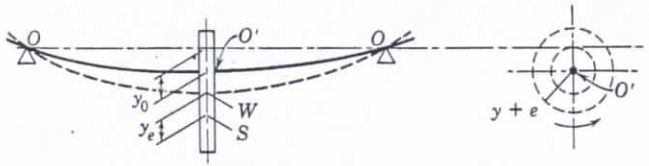

FIG. 15.3. Single load on a horizontal shaft.

(*c*) **Connection between the Shaft Deflection Due to the Disk Weight and the Critical Speed.** The deflection due to the disk's weight can be found from equation 15.2.

$$W = Ky_0 \tag{15.9}$$

From this the value of the shaft constant K can be found.

$$K = \frac{W}{y_0} \tag{15.10}$$

By substituting this value of K in equation 15.5, we obtain

$$\omega_c = \sqrt{\frac{W}{y_0 m}} = \sqrt{\frac{g}{y_0}} \tag{15.11}$$

where W is the disk weight, and m is the disk mass, $m = W/g$. *Note that the value of the shaft's static deflection y_0 due to the weight of the disk is a measure of the shaft elastic properties only. The actual value of the shaft's static deflection under operating conditions may be different, but the critical speed remains the same. Thus, if the same shaft is operated vertically, $y_0 = 0$. There may be an additional deflection due to belt pull or, if the shaft is operated submerged, as in a centrifugal pump, there is a force of buoyancy directed upward reducing the actual shaft deflection, but in all cases the critical speed is the same as that given by equation 15.11. Also, if the actual deflection of the shaft is limited inside the pump by the internal running clearances to less than y_0, the critical speed remains the same, unless the clearance is so small that it becomes an internal bearing.*

In a centrifugal pump there are a number of factors which reduce the amplitude of vibration at the critical speed. A number of closely fitted running clearances act as dampers. If the clearance of one of them, say at the middle of the shaft, is gradually reduced, the amplitude of vibration will be reduced further until it disappears entirely. At this point, this part becomes an internal bearing, and the critical speed is found as in the case of a three-bearing shaft.

(*d*) **A Perfectly Balanced Shaft.** In a perfectly balanced shaft the center of gravity of the rotor coincides with the axis of rotation; thus $e = 0$. Then equation 15.3 becomes

$$my\omega^2 = Ky \tag{15.12}$$

Conditions represented by equation 15.12 show that the shaft is in indifferent equilibrium, a state in which the centrifugal force developed is balanced by the elastic forces at any value of y, or the smallest force may, if allowed sufficient time, deflect the shaft to infinity or break it. The deflecting force is usually supplied by the unavoidable deviation of the centers of gravity of the various loads from the center line of the shaft. Conditions of indifferent equilibrium represented by equation 15.12 can occur only at the critical speed, because equation 15.12, when $y \neq 0$ reduces to

$$m\omega^2 = K \tag{15.13}$$

which is the same as equation 15.5 defining the critical speed.

(*e*) **The Period of Natural Vibration and the Critical Speed.** From equation 15.5 the number of revolutions per second at the critical speed is

$$n_c = \frac{1}{2\pi}\sqrt{\frac{K}{m}} \tag{15.14}$$

This is also the equation for the period of natural transverse vibration of the same rotor. *Thus, at the critical speed, the shaft vibrations are synchronized with the natural period of vibration of the shaft.* It is possible to determine the critical speed of a rotor by observing the natural period of transverse vibration of the rotor with some vibration-indicating device, and setting up vibration by a hammer blow.

(*f*) **Several Disks on a Weightless Shaft.** The following simple case will be considered (Fig. 15.4). A shaft of length $4l$ carries two disks,

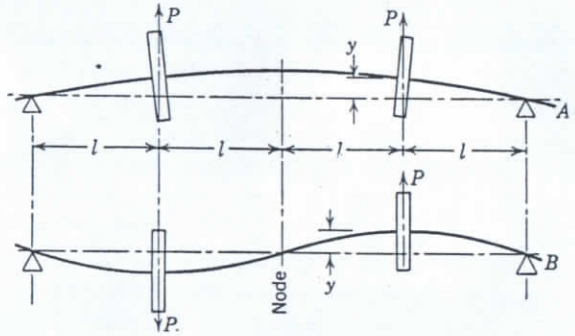

FIG. 15.4. Elastic curves with two loads.

each a distance l from the nearest bearing. Apparently both forms of the elastic curve, A and B, are possible. For the first critical speed, the rotating masses arrange themselves so that the deflection is a maximum (curve A). The points of zero deflection can occur only at the bearings. In other words there are no nodes (points of zero deflection, curve B) between the bearings at the first critical speed. These are dynamic deflections due to centrifugal forces which are superimposed upon the static deflection of the shaft. Evidently centrifugal forces are different in two cases, and the values of K are different for the two deflection curves. Owing to symmetry, equations developed for a single disk can be applied.

Case A.:

$$y = \frac{4Pl^3}{3EI} \qquad K_1 = \frac{3EI}{4l^3} \qquad {\omega_{c1}}^2 = \frac{K_1}{m} \tag{15.15}$$

Case B:

$$y = \frac{1Pl^3}{6EI} \qquad K_2 = \frac{6EI}{l^3} \qquad {\omega_{c2}}^2 = \frac{K_2}{m} \tag{15.16}$$

$$\frac{{\omega_{c1}}^2}{{\omega_{c2}}^2} = \frac{K_1}{K_2} = \frac{1}{8} \tag{15.17}$$

Thus with two loads two critical speeds are possible. Their ratio is $1:\sqrt{8}$ for load locations, as in Fig. 15.4.

The result is not changed provided eccentricity of the center of gravity of the loads is provided for, if the eccentricity is small in comparison with the shaft deflection.

In the case of two disks of different weights and mounted in any possible way, the numerical values will change, but in every case there will be two critical speeds, the first and the second with deflection curves similar to A and B on Fig. 15.4. Similarly, with three loads there will be three critical speeds and with twelve loads, twelve critical speeds. In multistage pumps, if the weight of the shaft is considered in addition to the impellers, an unlimited number of critical speeds is possible. In practice it is possible to observe only a few.

In general, irrespective of the number of loads on the shaft and their distribution, the first critical speed always corresponds to the period of natural transverse vibration of the rotating element. At speeds above the first critical speed, the center of gravity of the rotor approaches the axis of rotation, and thus the shaft tends to straighten itself. Also, at the first critical speed, the shaft's dynamic deflection is a maximum and there are no nodes between the two supports of the shaft.

With several loads the value of the critical speed does not depend on the magnitude and on the location of the eccentricities of the individual loads (Stodola[1]).

15.2 MAIN FACTORS AFFECTING THE CRITICAL SPEED

(*a*) **Effect of Liquid.** Practically all textbooks and treatises on critical speeds deal with steam turbine or gas blower rotors. The operation of centrifugal pumps differs from that of these machines in that (1) the pumped liquid exerts a definite damping effect on the shaft vibrations; (2) there are a number of closely fitted parts inside the pump which reduce, or limit, the amplitude of vibrations or serve as bearings; (3) *stuffing boxes of modern pumps serve as perfect bearings, and thus reduce the span of the shaft between the supports.* Everyday experience has shown that a great many pumps which vibrate when the running clearances are worn stop vibrating when the clearances are restored.

(*b*) **Force of Buoyancy.** Although the weight of the rotating element when submerged in water is reduced by the amount of the displaced water, its mass is not changed. Therefore, the critical speed (equation 15.5) stays the same. The force of buoyancy should be considered an external force, like belt pull, which does not change the properties of the revolving mass or the shaft elastic constant.

(*c*) **Damping Effect of Liquid.** The liquid in the pump casing presents some resistance to the vibration of the rotating element. Part of the kinetic energy of the vibrating shaft is continuously absorbed by the surrounding liquid. As a result, the amplitude of vibrations is reduced. The closely fitted parts, if they do not serve as bearings, tend to dampen the vibrations since at each cycle liquid is squeezed from one side and drawn in at the other. Special tests run by Stodola [1] have shown that a shaft having appreciable vibration at the three observed critical speeds had its amplitude reduced as soon as the flume containing the shaft was gradually filled with water, and finally vibration could hardly be detected.

(*d*) **Stuffing Boxes.** By far the greatest effect on the critical speed of pumps is due to stuffing boxes. A number of pumps which vibrated at the critical speeds when operated with mechanical seals (no shaft support at stuffing box) stopped vibrating entirely when operated with the stuffing boxes packed. If the stuffing boxes are considered as bearings, the calculated critical speeds are usually found to be above the operating speeds in the majority of cases (above 3600 rpm) and no other vibrations appear.

As a result of the factors just discussed, centrifugal pumps are essentially trouble-free from critical speeds or vibrations; however, introduction of mechanical seals, increase of operating speeds (6000 rpm and over), reduction of shaft sizes, and the like may create conditions in which critical speeds may appear. *Sometimes these critical speeds are of secondary nature and are induced by a number of factors not entering into calculation of the first or higher critical speeds and, therefore, they are difficult to predict. Solutions of such cases present some difficulties, as there is no easy way to identify some of the causes, and some of them are not easily removed.* Some of the factors causing secondary vibrations are discussed later.

15.3 CALCULATION OF CRITICAL SPEEDS

(*a*) **The First Critical Speed.** The first critical speed can be calculated by using equation 15.5.

$$\omega_c^2 = \frac{K}{m} \tag{15.18}$$

where m is the mass of the rotating element and K is the shaft elastic constant which depends on the shaft dimensions, material, and method of support and loading. From equation 15.2

$$K = \frac{P}{y}$$

For concentrated loads on a weightless shaft, K can be found by substituting for P the weight of the rotating masses and for y the static deflection y_0 under these weights. By substituting the value of K thus found, equation 15.5 becomes

$$\omega_c^2 = \frac{g}{y} \tag{15.19}$$

With uniformly distributed loads (shaft weight) the load on the shaft due to centrifugal forces is different from the static load distribution; therefore, the value of K is different, and is higher than for static loads only. Also, with a two-bearing shaft, an overhung load, such as a coupling, increases the dynamic deflection whereas the static deflection is reduced by the overhung load.

These cases demonstrate that the static deflection is used for determination of the shaft elastic constant only for concentrated loads and has nothing to do with the critical speeds. With distributed loads, the dynamic deflection is used only for calculating the shaft elastic constant. Its absolute value varies with the speed as shown by equation 15.4 and Fig. 15.2, whereas the shaft constant K and the critical speed are fixed quantities. Equation 15.19 can be used for any kind of loading with an experimental factor, the maximum static deflection, y_0 being used.

$$\omega_c = \sqrt{C\frac{g}{y_0}} \tag{15.20}$$

For a two-bearing supported shaft the coefficient C is

$$1 < C < 1.2685 \tag{15.21}$$

The higher value is applied to a uniformly loaded shaft (shaft's own weight), and $C = 1$ for concentrated loads, a maximum value of the shaft deflection being used. For multistage centrifugal pumps, $C = 1.08$ according to Bauman (Holba,[2] p. 19). The factor C accounts for the difference between the static and dynamic load distribution resulting from the fact that near the bearings centrifugal forces have a smaller effect on the shaft deflection.

Static deflections can be determined by methods found in the textbooks on strength of materials. Solution of simple cases is given in

Use is made of the conditions prevailing at the critical speed, namely, that in a balanced shaft centrifugal forces balance the shaft elastic forces at all deflections. This equilibrium is reached for a definite elastic curve. It is also maintained when the deflections for all points are either increased or reduced in the same ratio, as internal stresses and centrifugal forces are proportional to the deflections.

The static shaft deflection curve is used as a first approximation for the calculation of centrifugal forces. However, the static deflection curve, as obtained by graphical statics methods, should be modified if there is an overhanging load such as a coupling.

For the first critical speed calculations the zero deflections (nodes) can occur only at the bearings, so that, with a two-bearing shaft, if

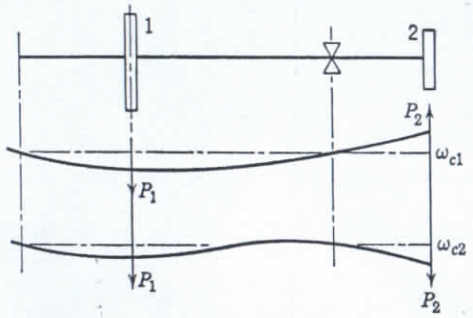

FIG. 15.6. Elastic curves with overhung load.

there is an overhanging load (a heavy coupling on a long shaft extension), it must be replaced with one acting in an opposite direction from the loads between the bearings. Figure 15.6 shows the dynamic deflection curves for two loads. The first one, corresponding to the first critical speed ω_{c1}, shows a greater deflection than the second curve which occurs at the second critical speed ω_{c2}. At the first critical speed, the dynamic deflections due to loads between the bearings and overhung loads are 180° apart. This curve prevails between the first and second critical speeds.

The graphical determination of the first critical speed includes the following steps:

1. A moment diagram is drawn by Mohr's method, used in graphical statics. For this, several concentrated loads are substituted for the shaft's weight.
2. The moment diagram is corrected for variation of the shaft diameter.

	$\omega_{c1}^2 = \frac{3EIL}{ma^2b^2}$	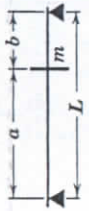
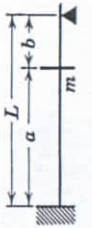	$\omega_{c1}^2 = \frac{6EI}{ma^2(3L-4a)}$ $\frac{\omega_{c1}^2}{\omega_{c2}^2} = \frac{(L-2a)^2}{L(3L-4a)}$	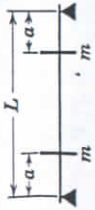
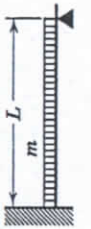	$\omega_{c1}^2 = \frac{98EI}{mL^3}$ $\omega_{c1} : \omega_{c2} : \omega_{c3} = 1 : 4 : 9$	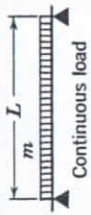
	$\omega_{c1}^2 = \frac{3EI}{mL^3}$	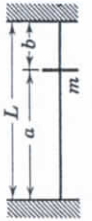
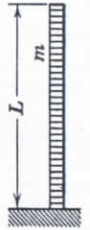	$\omega_{c1}^2 = \frac{12{\cdot}4EI}{mL^3}$ $\omega_{c1} : \omega_{c2} : \omega_{c3} = 1 : 6{\cdot}3 : 17{\cdot}5$	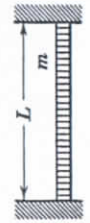
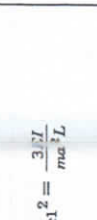	$\omega_{c1}^2 = \frac{3EI}{ma^2L}$	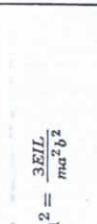
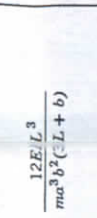	$\omega_{c1}^2 = \frac{12E/L^3}{ma^3b^2(3L+b)}$	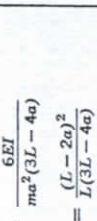
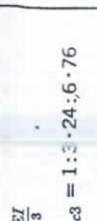	$\omega_{c1}^2 = \frac{237EI}{mL^3}$ $\omega_{c1} : \omega_{c2} : \omega_{c3} = 1 : 3{\cdot}24 : 6{\cdot}76$	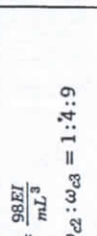
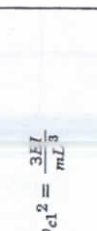	$\omega_{c1}^2 = \frac{3EI}{mL^3}$	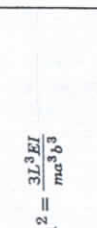
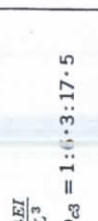	$\omega_{c1}^2 = \frac{12{\cdot}4EI}{mL^3}$ $\omega_{c1} : \omega_{c2} : \omega_{c3} = 1 : 6{\cdot}3 : 17{\cdot}5$	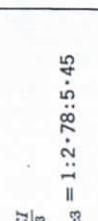

Fig. 15.5. Critical speeds for simple loadings.

Fig. 15.5. *With one or two impellers and a symmetrical shaft of uniform section, the maximum deflections due to shaft weight and impellers occur in the middle of the shaft. Therefore, y_0 can be found separately for the shaft and impellers and added to obtain the maximum static shaft deflection.*

When shafts are of variable diameter and the load distribution is not uniform, it is very laborious to calculate the static deflection of the shaft. Graphical methods developed by strength of material studies are used. However, for a general case, the use of maximum static deflection is not accurate for critical speed calculation; and the constant K is determined for dynamic loading at an arbitrary speed, the static shaft deflection for calculation of centrifugal forces being used as a first approximation.

(*b*) **Dunkerley's Equation.** Dunkerley in England has found by extensive experiments that for several concentrated loads and a shaft freely supported on two bearings the critical speed is very accurately expressed by the following equation (15.22).

$$\frac{1}{\omega_c^2} = \frac{1}{\omega_s^2} + \frac{1}{\omega_1^2} + \frac{1}{\omega_2^2} + \text{etc.} \qquad (15.22)$$

where ω_c is the critical speed of the system.
ω_s is the critical speed of the shaft alone.
ω_1 is the critical speed of the weight (1) on a weightless shaft.
ω_2 is the critical speed for the disk (2), and so on.

By using equation 15.19 for the individual loads and dividing the shaft into several concentrated loads, Dunkerley's equation reduces to

$$\omega_c^2 = \frac{g}{\Sigma y} \qquad (15.23)$$

Evidently, the critical speed of the system is lower than the critical speed due to individual loads.

If the shaft diameter is variable, Dunkerley's equation is applied either by substituting a shaft of uniform section (which will reduce the accuracy of the results) or by dividing the shaft into a number of parts and substituting concentrated loads for the several sections of the shaft.

15.4 EXAMPLE OF GRAPHICAL DETERMINATION OF THE CRITICAL SPEED

When the problem involves several concentrated loads and a stepped shaft freely supported on two bearings, a general solution is possible by a graphical method employing successive approximations.

3. The static deflection curve is drawn, the corrected moment diagram being used.

4. Centrifugal forces are calculated on the basis of an assumed arbitrary speed; with these centrifugal forces being used as concentrated loads, the dynamic deflections are found by following the same procedure.

5. The critical speed is calculated by making use of the equilibrium conditions between the centrifugal forces and the shaft elastic forces for a balanced shaft at the critical speed.

(*a*) Static Curve-Moment Diagram (Fig. 15.7). Choose a suitable scale for drawing the essential features of the shaft. In the example, 1 in. = 4 in. is used. Vectors are used to represent the loads and reactions as shown. If the weight of the shaft is to be included, it is subdivided into sections and the weights of these sections are considered as concentrated loads located at their respective centers of gravity. The direction of the vectors representing overhung loads are reversed to get the maximum shaft deflection used for calculation of the first critical speed. The loads are lettered *BA*, *BC*, *CD*, and so on, starting from the left and proceeding in a clockwise direction until the extreme right end load is labeled. Next the reactions are lettered in a similar fashion, the clockwise direction around the length of the shaft (*AR* and *RQ*) being maintained.

Beneath the shaft and to the right, locate a vertical line (*AQ*) on which to place the load vectors. Using a force scale that will give a conveniently sized diagram (1 in. = 100 lb), the loads are scaled off on the vertical line (*AQ*) in alphabetical order and labeled. The diagram is completed by measuring a pole distance to the right of *AQ* (pole distance = 5 in.) and drawing the rays *AO*, *BO*, *CO*, and so on. The pole distance may be any convenient length that will give a convenient scale for the moment diagram which follows. The moment scale is equal to the shaft scale times the force scale times the pole distance (moment scale 1 in. = 4 × 100 × 5 = 2000 lb-in.).

From the loads and the reactions on the shaft drawing, vertical lines are extended down. Then starting with ray *AO*, a line parallel to it (*A'*) is drawn between reaction *AR* and load *BA*. Next *BO* is transferred and placed between *AB* and *BC* and adjoining *A'*. Following the clockwise rotation, the rest of the rays are transferred until *QO* is drawn between load *PQ* and reaction *QR*. The figure is now closed by drawing a line between reactions *AR* and *RQ* to the ends of the exposed rays.

The value of the moment at any point on the shaft is the vertical distance between the boundaries to the scale as determined before.

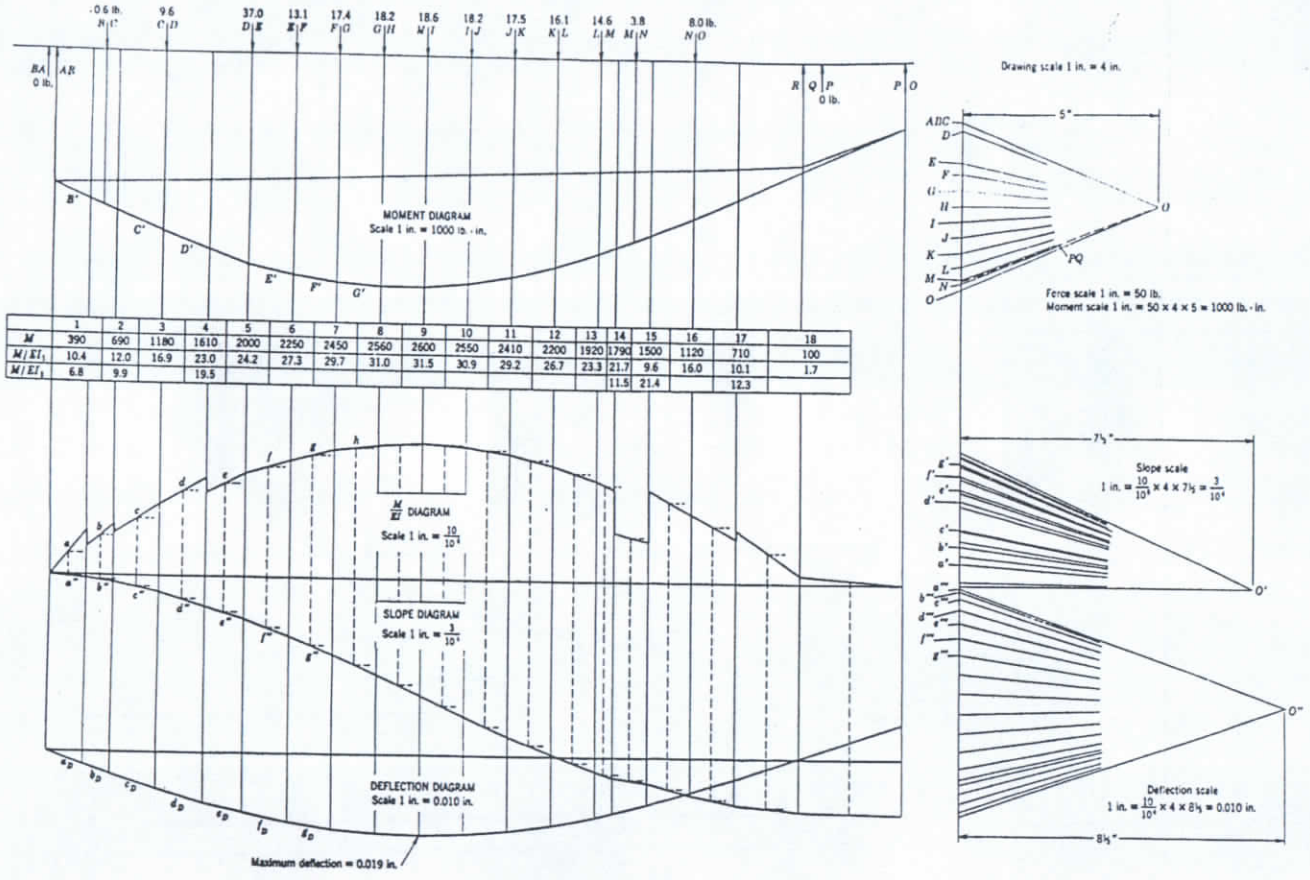

	1	2	3	4	5	6	7	8	9	10	11	12	13	14	15	16	17	18
M	390	690	1180	1610	2000	2250	2450	2560	2600	2550	2410	2200	1920	1790	1500	1120	710	100
M/EI_1	10.4	12.0	16.9	23.0	24.2	27.3	29.7	31.0	31.5	30.9	29.2	26.7	23.3	21.7	9.6	16.0	10.1	1.7
M/EI_2	6.8	9.9		19.5										11.5	21.4		12.3	

FIG. 15.8. Dynamic deflection curve due to centrifugal forces.

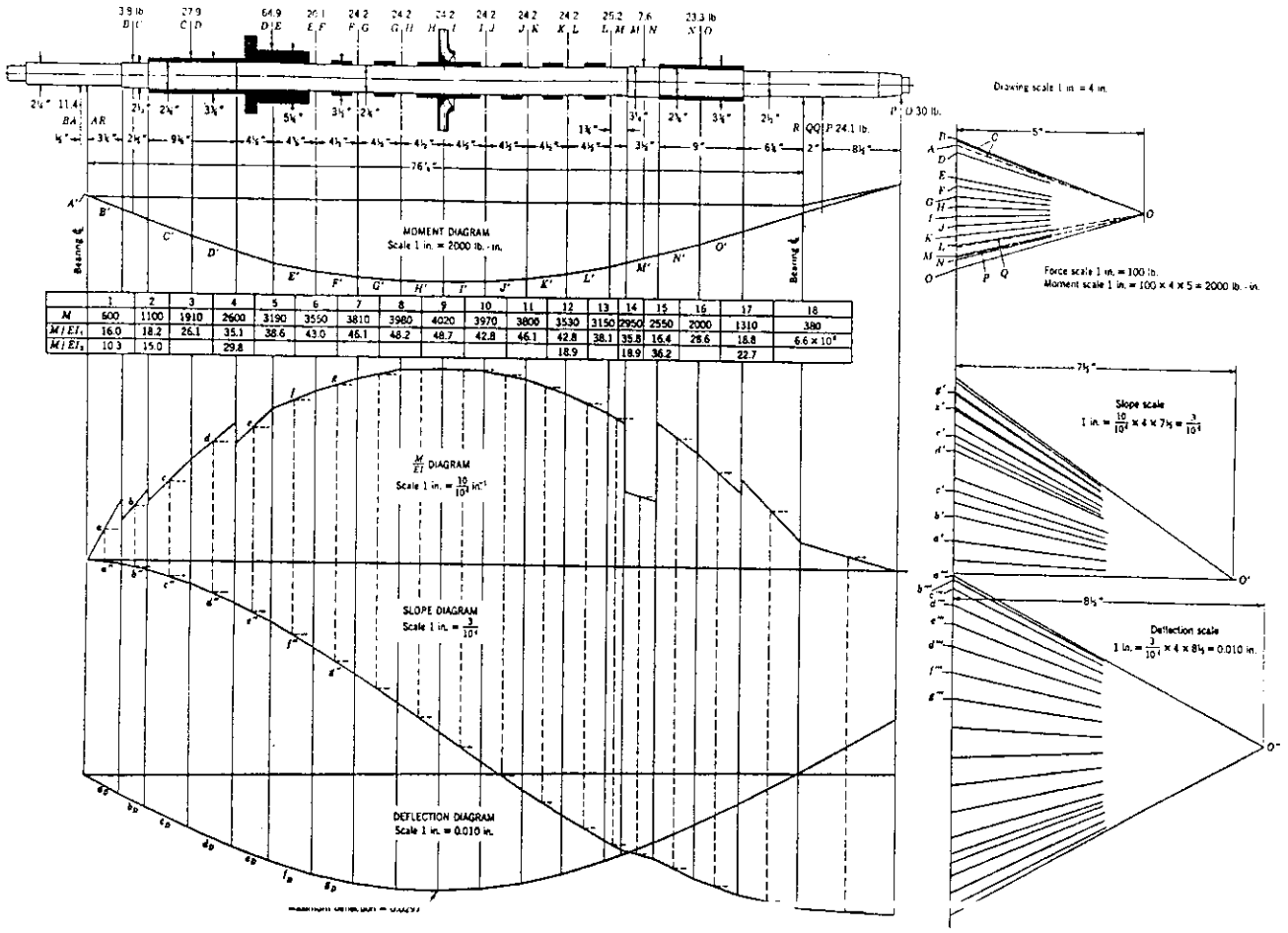

	1	2	3	4	5	6	7	8	9	10	11	12	13	14	15	16	17	18
M	600	1100	1910	2600	3190	3550	3810	3980	4020	3970	3800	3530	3150	2950	2550	2000	1310	380
M/EI_1	16.0	18.2	26.1	35.1	38.6	43.0	46.1	48.2	48.7	42.8	46.1	42.8	38.1	35.8	16.4	28.6	18.8	6.6 × 10⁴
M/EI_2	10.3	15.0		29.8								18.9		18.9	36.2		22.7	

FIG. 15.7. Deflection curve under static load.

The critical speed in the example is calculated by using equation 15.26.

$$\omega_c = 100\sqrt{\frac{0.0297}{0.019}} = 125 \text{ rad per sec} \quad \text{or} \quad 1195 \text{ rpm}$$

Experimentally the critical speed was observed to be about 1300 rpm.

The discrepancy between the observed and calculated critical speeds is explained by the stiffening effect of the shaft sleeves and the impeller hubs although the shaft nuts were loose during these tests.

(*f*) The Same Example Using Dunkerley's Equation. The weight of the shaft is distributed among the loads in the same manner as for the graphical solution. An average diameter is found for calculations by

$$d = \frac{d_1 l_1 + d_2 l_2 + \cdots}{L} \tag{15.27}$$

where d and l are diameter and length of shaft sections with constant diameter.

d	l	dl
2¼	3¾	8.44
2½	2¾	6.87
2⅝	9¼	24.25
2¾	41¾	115.0
3⅛	3½	10.93
2⅝	9⅛	23.95
2½	6⅝	16.55
=		
L	76⅞	205.99

$$d = \frac{206}{76\frac{7}{8}} = 2.68$$

To get the individual deflections use the equation from the first example in Fig. 15.5:

$$y = \frac{Wa^2b^2}{3EIL} \tag{15.28}$$

The critical speed is obtained from equation 15.23. Calculations of Σy are tabulated below.

W	a	b	$(ab)^2$	$W(ab)^2$
3.8	5	71⅞	129,000	0.50×10^6
27,9	11⅛	65¾	535,000	15.0
64.9	19¾	57⅛	1,270,000	82.5
20.1	24¾	52½	1,540,000	30.9
24.2	28⅞	48	1,920,000	46.5
24.2	33⅜	43½	2,110,000	51.1
24.2	37⅞	39	2,190,000	53.0
24.2	42⅜	34½	2,140,000	51.8
24.2	46⅞	30	1,980,000	48.0
24.2	51⅜	25½	1,650,000	40.0
25.2	55⅞	21	1,380,000	34.8
7.6	59⅜	17½	1,080,000	8.2
23.3	65⅝	11¼	544,000	12.7
348.0	76⅞	76⅞		475.0×10^6

$$I = \frac{\pi}{64} \times (2.68)^4 = 2.53$$

$$\Sigma y = \frac{\Sigma W a^2 b^2}{3EIL} = \frac{475 \times 10^6}{3 \times 30 \times 10^6 \times 2.53 \times 76.875} = 0.0271 \text{ in.}$$

$$\omega_c = \sqrt{\frac{386}{\Sigma y}} = 119 \text{ rad per sec} \quad \text{or} \quad 1140 \text{ rpm}$$

(*g*) Approximate Equation for Pump Shafts. When the method of support, load distribution, and the shaft diameter varies little, as in a multistage pump, it is possible to obtain a quick approximation of the first critical speed by using an equation with an experimental factor of the type

$$y = \frac{WL^3}{CEI} \quad \text{and} \quad \omega_{c1} = \sqrt{\frac{g}{y}} \tag{15.29}$$

where W is total weight of the rotating element in pounds.
L is the bearing span of the freely supported shaft in inches.
E is 30,000,000 lb per sq in. for steel.
I is the average moment of inertia of shaft section in inches^4.
C is a numerical constant to account for the method of support, load distributions, and so on.

For a single load, $C = 48$ (from Fig. 15.5); for a uniformly loaded shaft, $C = 98$; for all intermediate cases values of C lie between these limits. Figure 15.9 shows values of C calculated for a different ratio

of the weights of the shaft and the impellers, and for different impeller spacings (L_1, the distance between two extreme impellers) and the shaft span. The weight of all impellers is assumed to be uniformly distributed along L_1. Evidently the more impellers there are on the shaft, the more

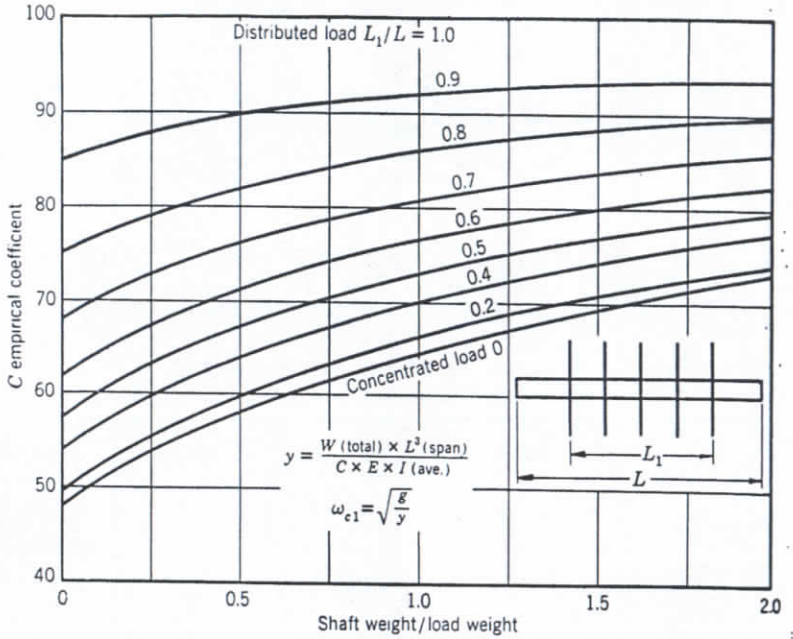

FIG. 15.9. Dynamic deflection coefficient for symmetrical rotors.

accurate are the results obtained from the chart. The chart cannot be used for pumps with packed stuffing boxes.

15.5 CRITICAL SPEED TESTS

To check the first critical speed with stuffing boxes packed, a special light shaft and heavy dummy impellers were built for a 2-in. six-stage pump. With this shaft the first critical speed was brought within the range of pump operating speeds. Tests with this rotor and also with a standard pump-rotating element revealed the following:

1. *With stuffing boxes packed, the first critical speed took place at a speed corresponding to that for a shaft with shaft ends fixed at the middle of the stuffing boxes.*

2. When the pump-rotating element operated in air and without packing in stuffing boxes, it vibrated through a wide range of speeds

above the first critical speed. When assembled with mechanical seals and pumping water the rotor operated satisfactorily.

3. With the light shaft, vibrations were observed above the first critical speed with stuffing boxes packed. *It was found that the driver's vibrations, including the coupling, increasing gear, and dynamometer, superimpose their amplitudes of vibration upon the shaft's own.* By eliminating the gear box and using a smaller driver and coupling, these vibrations were reduced, but not entirely eliminated. *When operated in water and with closely fitted casing rings, no objectionable vibrations were observed.*

Note that the power to drive the dummy rotor was negligibly small; therefore the coupling and gear box were not properly loaded. Also, the mass of the rotor was very small in comparison with that of the large test drivers. Under these conditions the effect of driver vibrations on the light rotor was exaggerated.

15.6 THE THREE-BEARING SHAFT

A three-bearing, freely supported shaft is seldom, if ever, used in centrifugal pumps. Occasionally three-bearing systems are encountered

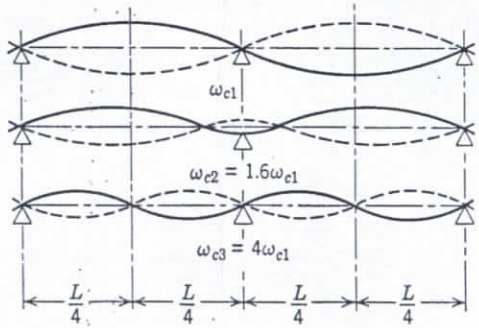

FIG. 15.10. Elastic curve with uniform shaft and three bearings.

when the pump and the driver use a common shaft and one intermediate bearing is omitted. In this case, the driver manufacturers should check the shaft for critical speeds because they usually furnish the shaft and have more experience in dealing with critical speeds. With closely fitted internal parts, conditions may arise where the pump shaft may be considered as having three or more supports.

A few remarks will be made on the three-bearing shaft. Figure 15.10 shows the deflection curves for the first three critical speeds of a uniform shaft supported at three bearings.

In this case the first critical speed is the same as for a two-bearing set of half the length of the three-bearing set, as though the shaft were cut at the middle (Kimball,[3] p. 75).

The second critical speed is a direct result of the presence of the middle bearing, which supports a vibration reaction and at which there is a point of maximum flexure. The third critical speed corresponds exactly to the second critical speed for a single span of half the length. Like the first critical speed, the frequency of the third would not be altered if the shaft were cut at the middle bearing. Thus, the frequency of the third critical is four times that of the first, but that of the second is about 1.6 times the first. With three-bearing sets it is very seldom that second or higher critical speeds are observed. Determination of the first critical speed as outlined above gives quite accurate results if the shaft and loading are symmetrical about the middle bearing.

In general, the critical speed of the three-bearing shaft is higher than the individual critical speed of the shaft part obtained by bisecting the shaft at the middle bearing. These individual critical speeds of shaft parts never appear; neither does the critical speed of the whole shaft with the middle bearing removed. Higher critical speeds for the whole shaft as compared with two halves are explained by the stiffening effect of one part upon the other (Holba,[2] p. 131).

15.7 HIGHER CRITICAL SPEEDS

With a weightless shaft there may appear as many critical speeds as there are individual loads on the shaft. To each critical speed corresponds a different form of the elastic curve and a different value of K in equation 15.5. With a distributed load an infinite number of critical speeds are possible, theoretically. However, in pump design, critical speeds of higher order very seldom come into consideration. The graphical method of critical speed determination previously described cannot be applied for calculation of the second critical speed because it is not convergent. Instead of approaching a certain limit, the deflection lines move farther apart with each successive approximation. Other methods are more complicated and will not be discussed here. *However, in a great many cases when the pump shaft is approximately symmetrical about its middle, the second critical speed can be determined by using the first critical for one-half of the shaft obtained by bisecting the shaft in the middle and replacing the node (zero deflection point) with a free supporting bearing. This is the same method that was used in the determination of the first critical speed of a three-bearing shaft.* The method is quite general; that is, if the location of the node is known, substitution of a third bearing

at this point reduces the problem to the finding of the first critical speed for a three-bearing shaft (Hohenemser method, in Holba,[2] p. 129). *In some simpler cases the second critical speed can be approximated by comparing the shaft loading and support with some cases for which solutions are known, such as those given in Fig. 15.5, where ratios of critical speeds of higher order to the first critical speed are given.* It will be noticed that the second critical speed is at least about three times the first critical speed.

15.8 SECONDARY CRITICAL SPEEDS

Under this heading will be considered critical speeds caused by forces other than centrifugal. A number of these have been observed and studied. All of them occur seldom and, for that reason, are difficult to recognize as there are not sufficient signs to identify each, and some of them are not easy to remove.

(a) Weight Disturbances. The alternate rise and fall of the center of gravity in respect to the center of rotation induce speed variation and minute disturbances of the circular path. Under some critical conditions this may produce a "secondary" critical speed at half of the first critical speed. Noticeable disturbances are possible only with a considerable eccentricity of the center of gravity, or if the rotor is badly out of balance.

According to Föppl, a similar secondary critical speed appears as a result of the fluctuation of rotative speed caused by the type of drive.

(b) Friction between the Shaft Sleeves, the Impeller Hubs, and the Shaft. At the critical speed centrifugal forces are balanced by the shaft stresses at all deflections and a vertical shaft is whirled bodily as though it had a permanent set with the same side out. Thus, there is no relative slipping of the impeller hubs on the shaft. At speeds higher than the critical, even if there is whirling of the shaft, the shaft sides are alternately extended and compressed. Thus there is relative motion between the shaft and the shaft sleeves or impeller hubs, resisted by whatever friction develops during such slipping. It has been proved (Kimball,[3] p. 126) that as result of such friction a component of frictional forces develops which tends to whirl the shaft in the same direction as the shaft revolves when operated above the first critical speed. This whirling speed may reach the critical speed at which a condition vibration develops due to synchronism between the whirling speed and the natural period of vibration. Thus the frequency of vibration is the same as the first critical speed, and operating speed is higher than the latter.

Vibration of this type was obtained experimentally. With horizontal shafts, extension and compression of the outer filaments occur every revolution and, when impellers and sleeves are shrunk on the shaft, such shaft may develop vibration due to friction between the shaft and the impeller hubs, if operated above the critical speed.

It may be of interest to mention that the shaft's own internal friction during the process of extension and compression of its outer filaments of material will develop similar tangential components contributing to the whirling of the shaft. But, with steel shafts, tests show that such internal friction forces alone are unable to build up and maintain such a whirl.

This cause of vibration of the rotors caused manufacturers of centrifugal compressors and steam turbines to mount their disks with a narrow ring contact between the disks and the shaft. Long flexible laminated rotors of electric motors may vibrate as a result of internal friction between laminations regardless of a careful dynamic balance of the rotors.

(*c*) **Oil Whip.** It has been found experimentally and was observed on actual machines that, with oil-lubricated sleeve bearings, the oil wedge travels around at half the shaft speed. If this speed falls near the shaft's first critical speed, the shaft whirling produces vibration, which does not die down even when the shaft speed is increased more than twice the critical speed. The oil wedge continues to stay at the same speed, having all the encouragement from the shaft. With horizontal shafts the weight of the rotor is not sufficient to suppress the oil whip vibrations. In general these vibrations are not easily eliminated. The following steps have been tried with different degree of success: (1) change to ball bearing; (2) decrease bearing length to increase the load on the oil film; (3) deliberately put bearing out of line with the shaft.

The best way to avoid vibrations due to oil whip is not to run the pump above twice the critical speed.

(*d*) **Reverse Synchronous Precession.** Stodola[1], has studied and shown experimentally that under certain conditions disturbing moments can arise which produce reverse synchronous precession. This may result in vibrations at an operating speed twice the first critical speed. To eliminate vibration of this nature the impeller positions on the shaft can be changed and the rotor rebalanced (Holba,[2] p. 46).

(*e*) **Sleeve Bearings versus Ball Bearings.** *With sleeve bearings small disturbances from the coupling, the driver, or any other cause easily produce secondary vibrations of the pump shaft, as the weight of the shaft is not sufficient to maintain a continuous contact between the shaft and the bearings.* During tests of the 2-in. six-stage pump shaft referred to previously the shaft ran smoothly with stuffing boxes packed and with no water in the pump casing. Replacing the packing with a closely fitted bushing with normal bearing clearances, grease-lubricated, produced vibration. Ball bearings provide a positive support for the shaft, and have an advantage over sleeve bearings in this respect. Grün[4] advocates ball bearings in preference to sleeve bearings to reduce a tendency to vibration for boiler feed pumps. Stodola[1] (p. 956) states that on several occasions vibration disappeared when sleeve bearing clearances were reduced below normal, thus indicating that the sleeve bearing was not functioning properly. Note that shaft vibration due to oil whip, described above, also is characteristic of sleeve bearings and cannot occur with ball bearings.

(*f*) **Effect of the Coupling on Secondary Vibrations.** The disturbing effect of the coupling comes as a result of either misalignment or transmission of disturbance from the driver. Even with elastic couplings, if the shaft runs above the first critical speed, a slight misalignment between the pump and driver shafts produces periodic disturbing forces which may induce secondary vibrations (Holba,[2] p. 168). Vibrations induced or transmitted by the coupling are not easily eliminated. If no other means are available a substitution of a rigid coupling may either remove secondary vibrations or bring them outside the operating speed range. Rigid couplings are universally used with vertical propeller or turbine pumps, and also on horizontal turbo-generating units.

(*g*) **Summary of Secondary Critical Speeds.** *A general conclusion from the study of secondary critical speeds is that operation of the pump should be avoided at speeds which are even fractions* ($\omega_c/2$; $\omega_c/3$) *or multiples of the first critical speed. Considering that the first critical speed is not a point but a belt and that its calculations are more or less approximate, the above rule imposes a great limitation on the speed selection.*

In spite of the vast experience and knowledge accumulated on critical speeds, some puzzling cases of shaft vibration are encountered which do not fall into any of the above descriptions. (Stodola,[1] p. 956.) Fortunately, such examples are rare in centrifugal pump practice.

15.9 SECONDARY FACTORS AFFECTING CRITICAL SPEED

Under this heading a number of factors which affect the critical speed in general will be considered, although in the case of centrifugal pumps their effect may be neglected.

(*a*) **Axial Forces.** In some designs of multistage pumps and in all vertical pumps, besides transmitting torque, the shafts carry a considerable axial force due to axial thrust. It has been found that axial forces

tend to increase the critical speed. This tendency is more pronounced in shafts having a low critical speed. This is in agreement with experience with strings used for musical instruments, where tension determines the frequency of vibration of the string (tone). However, axial forces encountered in centrifugal pump shafts are too small to produce any appreciable differences in the critical speed (Holba,[2] p. 27).

(*b*) **Torque.** Theoretically, a shaft transmitting higher torque should have a lower critical speed, as shaft stiffness decreases when the torque increases. However, this effect is negligible in general (Holba,[2] p. 31).

(*c*) **Friction.** Mechanical friction of the impellers and the shaft tends to reduce the amplitude of vibration without any effect on its frequency. This, in addition to the internal molecular friction of the shaft, results in a finite shaft deflection at the critical speed. The time element is also a contributing factor in limiting the amplitude of the shaft at and near the critical speed.

(*d*) **Shaft Moment of Inertia.** If the shaft moment of inertia about two axes is different, for instance, if it is a result of keyways in the shaft, there will be two critical speeds of the first order. The region between the two is unstable. The author does not know one case where two critical speeds due to keyways being in one plane were observed.

(*e*) **Gyroscopic Action.** When there are several impellers on the shaft, all impellers except the middle ones revolve in planes not normal to the line joining two bearings. Under such conditions gyroscopic action causes a restoring force in addition to the shaft elastic stiffness. This results in increasing the frequency of vibration. However, in centrifugal pumps the mass of the impellers is too small to have any noticeable gyroscopic effects. In large steam turbines gyroscopic action may increase the critical speed 2 to 3 per cent (Kimball,[3] p. 25).

(*f*) **Elasticity of Bearings.** All critical speed calculations are based on the assumption of perfectly rigid bearing supports. In horizontal pumps this condition is approached practically in every case. In vertical pumps with long shafts, bearings are either supported by the inner tubing enclosing the shaft or mounted on horizontal beams. Both have a marked degree of flexibility. Under such conditions, reduction of as much as 25 per cent in the first critical speed is possible; under extreme conditions reduction to below one-half the critical speed with rigid bearings is possible. With long vertical pumps of the deep-well type, it is common practice to provide spiders to steady the inner tube and bearings.

(*g*) **Elasticity and Mass of the Foundation.** If a pump is mounted on a support which in itself is not sufficiently rigid, a compound vibrating system results with two or more critical speeds, depending on the degree of freedom of the support. With only up-and-down motion of the base-

plate two critical speeds will appear, one when the shaft and the support frequencies of vibration are in phase, and the other when they are 180° out of phase. There is no way to calculate the critical speeds under such conditions. A solid foundation is the main prerequisite for vibration-free operation of pumps.

(*h*) **Stiffening by Impeller Hubs and Shaft Sleeves.** When impellers are individually mounted without spacer sleeves between them, the stiffening effect of the hubs on the shaft can be disregarded. However, if all impellers are assembled on the shaft with spacers between the hubs and nuts on both ends outside the stuffing box shaft sleeves, the stiffening effect of the parts mounted on the shaft is appreciable. A considerable difference in the critical speed was observed experimentally (1800 versus 1400 in one case), by running the shaft with nuts tight and loose. To calculate the critical speed, only part (50 to 65 per cent) of the moment of inertia of sections of impeller hubs or sleeves should be added to the shaft moment of inertia to account for the stiffening effect of all parts mounted on the shaft.

(*i*) **Effect of Temperature.** Centrifugal pumps are employed at present for liquids at temperatures up to 850°F. At such temperatures the modulus of elasticity E drops considerably, as shown by the tabulation below for low-carbon steels; it is given in millions of pounds per square inch.

$E = 30$	0 to 300°F
28	480
25	750
20	930
13	1100

Shaft deflection is inversely proportional to the modulus of elasticity,[5] and hence the critical speed will be lower at high temperatures.

Another effect of temperature on critical speeds is observed when the degree of stiffening of the shaft by the impeller hubs and sleeves changes as a result of difference in the heat expansion of the shaft and parts mounted on the shaft.

(*j*) **Wear.** On several occasions it has been found that pumps begin to vibrate after being in service for some time. Several causes may contribute to such conditions: (1) worn internal closely fitted parts which acted as bearings or provided enough damping effect for quiet operation when new; (2) loss of balance by rotor owing to clogging of one of the impeller passages; or (3) wearing out of bearings.

(*k*) **Torsional Vibrations.** Special test run by Stodola [1] (p. 470) failed to show any effect of torsional vibrations on the first critical speed of the shaft.

15.10 SELECTION OF CRITICAL SPEED

Extensive experiments by several investigators have proved a very satisfactory agreement between the calculated and the observed values of critical speeds. Therefore, it is possible to select shaft dimensions in such a way as to reduce the possibility of shaft vibration to a minimum. Operation below the critical speed gives a maximum assurance of vibration-free operation. However, this frequently leads to designs unpractical from a commerical point of view.

From the considerations discussed in previous articles, the selection of the shaft sizes for critical speed should be guided by the following considerations:

1. The operating speed should not be an even fraction ($\frac{1}{2}$, $\frac{1}{3}$, $\frac{1}{4}$) or multiple (2, 3, 4, $\cdots$) of the first critical speed.
2. The operating speed should not be too close to the critical speeds, first or second.

$$n < 0.8n_{c1} \text{ where } n = \text{operating speed.}$$

$$n > 1.3n_{c1} \text{ where } n_{c1} = \text{first critical speed.}$$

$$n < 0.7n_{c2} \text{ where } n_{c2} = \text{second critical speed.}$$

3. Satisfactory operation above the second critical speed is impossible according to Eck (Holba,[2] p. 169).

At high speed and especially above the critical speed, the deflection of the shaft may have a considerable effect on balancing. As a result of this, the rotor can be balanced only for one definite speed and, under certain conditions, it cannot be balanced at all (Holba,[2] p. 179). This can be seen from the following simple example (Fig. 15.11). Consider a shaft of uniform cross section with a single unbalance m in the middle. This can be

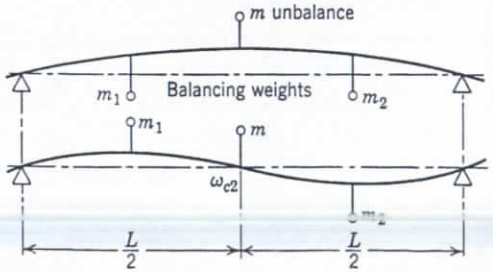

FIG. 15.11. Flexible shaft is dynamically balanced at one speed only.

balanced by adding corrective weights m_1 and m_2 in any two balancing planes at the first critical speed. However, at the second critical speed the unbalance happens to be at a node, and the corrective weights m_1 and m_2 become unbalanced.[6]

Owing to the simplicity of mass distribution, static balancing of the individual impellers of a multistage pump is sufficient for an average job but, in doubtful cases, complete rotors should be checked on the dynamic balancing machine at the operating speed.

REFERENCES

1. A. Stodola, *Steam and Gas Turbines*, New York, McGraw-Hill Book Company, 1927 (translation of the sixth German edition).
2. J. J. Holba, *Berechnungsverfahren zur Bestimmung der kritischen Drehzahlen von geraden Wellen*, Vienna, Julius Springer, 1936.
3. Arthur L. Kimball, *Vibration Prevention in Engineering*, New York, John Wiley & Sons, 1932.
4. Karl Grün, *Dampfkessel-Speisepumpen*, p. 68, Vienna, Julius Springer, 1934.
5. S. Timoshenko and J. M. Lessells, *Applied Elasticity*, Westinghouse Tech. Night School Press, 1925.
6. R. P. Kroon, "Balancing of Rotating Apparatus," *Trans. A.S.M.E.*, Vol. 65, No. 4, p. 228, 1943.
7. J. P. Den Hartog, *Mechanical Vibrations*, New York, McGraw-Hill Book Company, 1947.
8. S. P. Timoshenko, *Vibration Problems in Engineering*, New York, D. Van Nostrand Company, 1948.
9. W. T. Thomson, *Mechanical Vibrations*, New York, Prentice-Hall, Inc., 1948.

Chapter 16

Special Problems and Applications of Vertical Turbine and Axial Flow Pumps

16.1 BRAKE HORSEPOWER AT ZERO CAPACITY

The most desirable form of brake-horsepower curve for any application is one which has a maximum value at the b.e.p. Such a curve eliminates the danger of overloading the motor at any point on the head-capacity curve. Pumps of medium specific speeds (3000 to 4000, single-suction) have brake-horsepower characteristics of this type. At lower specific speeds the brake horsepower continues to increase at capacities greater than that at the b.e.p., the minimum being at zero capacity. Such brake-horsepower curves are satisfactory for a great majority of applications as they permit the starting of pumps under minimum load with the discharge valve closed, and it is not often that such pumps have to operate at capacities much in excess of normal.

High specific speed pumps, particularly of the axial flow type, have brake-horsepower curves which rise sharply toward zero capacity. The brake horsepower at shut-off may be twice (or more) that at the b.e.p. This is a very undesirable feature because, as a rule, the head on propeller pumps varies with water level variations in the suction or discharge reservoirs, and thus requires an oversize motor to permit operation at higher heads than the normal. Also, to permit starting of the pump with the discharge valve closed, an oversize motor and starting equipment are required. Attention of designers has been directed toward developing types of propeller pumps having a lower value of horsepower at shut-off. In high specific speed pumps of the axial flow type, very little has been accomplished to date and prospects are not bright. In the range of specific speeds from 6000 to 8000, pumps have been produced which have a value of shut-off horsepower lower, or only slightly higher, than that of the power at the b.e.p. Such a shut-off horsepower permits operation of the pump at any point on the head-capacity curve without overloading the motor. The best of these new types of pumps show efficiencies equal to those of "standard" older design. In some cases, the efficiency at part loads has been improved and, in all cases,

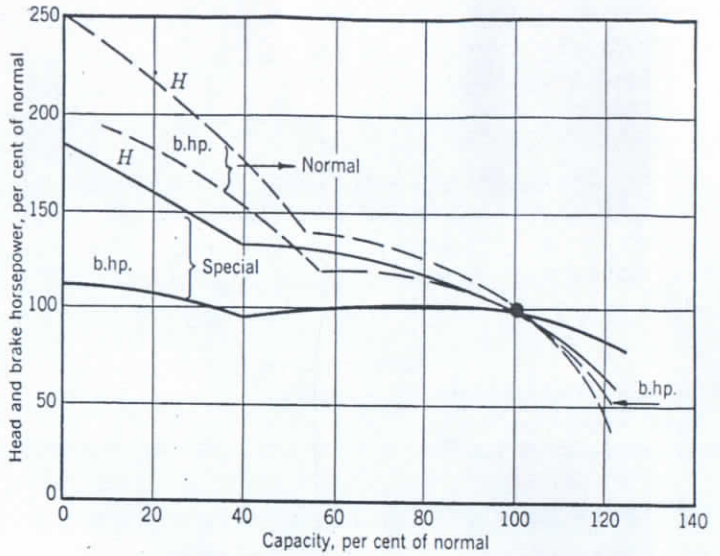

FIG. 16.1. Reduction of brake horsepower at zero capacity of propeller pumps of $n_s = 7500$.

the head-capacity curve is flatter. Figure 16.1 shows representative curves of normal and special designs at the same specific speed.

(a) Factors Leading to a Flat Brake-Horsepower Characteristic. If at zero capacity the liquid contained in the impeller rotates at the same speed as the impeller, the brake horsepower is a minimum. These conditions are approached with low specific speed centrifugal impellers where, owing to narrow impeller passages, the exchange of momentum between the liquid inside the impeller and that in the casing is limited. On the other hand, in mixed flow and particularly in axial flow pumps the exchange of momentum at zero capacity between the liquid in contact with the impeller vanes and liquid in the pump casing takes place most freely. As a result power is wasted in eddies and the brake horsepower increases towards shut-off. Note that pumps of the impulse type, working on the principle of exchange of momentum between the liquid in the impeller cells and the casing channel, have a rising brake-horsepower characteristic toward zero capacity similar to that of axial flow pumps.

The shape of a brake-horsepower curve can be best described by a ratio of the brake horsepower at zero capacity to that at the b.e.p. Reduction of this ratio can be accomplished by a reduction of the brake horsepower at shut-off, and by an increase of the brake horsepower at the b.e.p., by increasing the pump output without increasing the shut-off

brake horsepower appreciably. The effect of several design elements upon the brake-horsepower ratio will be discussed below.

(*b*) **Number of Vanes.** For the same impeller profile and impeller vane an increase of the number of vanes reduces the brake horsepower at shut-off with hardly any effect upon the brake horsepower at b.e.p., thus the brake-horsepower ratio is reduced. For a given impeller profile (vane length) and impeller discharge angle, there is an optimum number of vanes above which the pump efficiency drops appreciably. Table 16.1 obtained with a mixed flow pump of $n_s = 8000$ may serve as an illustration.

TABLE 16.1. EFFECT OF NUMBER OF VANES ON SHUT-OFF BRAKE-HORSEPOWER RATIO, $n_s = 8000$

	Number of Vanes			
	3	4	6	8
Brake-horsepower ratio	1.53	1.275	1.06	1.00
Efficiency, per cent	86.5	85.0	75.5	70.0
Ratio H_s/H	2.2	2.1	2.0	1.85

A reduction of the brake-horsepower ratio is usually accompanied with a reduction of the ratio of the shut-off head H_s to the normal head H.

(*c*) **Impeller Discharge Angle.** Higher impeller discharge angles increase the pump output so that the specific speed remains essentially

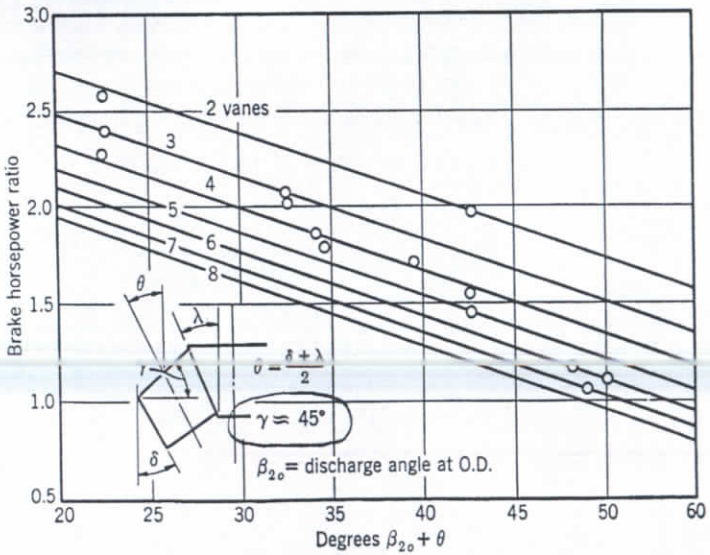

FIG. 16.2. Brake-horsepower ratio in terms of design elements.

the same. The shut-off head does not change; the brake horsepower at shut-off increases only slightly and the brake-horsepower ratio is reduced. Figure 16.2 shows the effect of the number of vanes and impeller discharge angle on the brake-horsepower ratio for a constant impeller profile angle. There is an optimum impeller angle above which a discontinuity in the head-capacity curve appears before the peak efficiency begins to fall off, Fig. 16.3. Such discontinuity takes place between 50 to 60 per cent of the pump rated capacity and, in a moderate degree, is not objectionable for satisfactory pump operation. Propeller pumps normally are not operated in this range of capacities.*

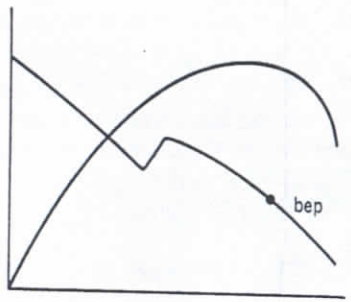

FIG. 16.3. Discontinuity in *Q-H* curve.

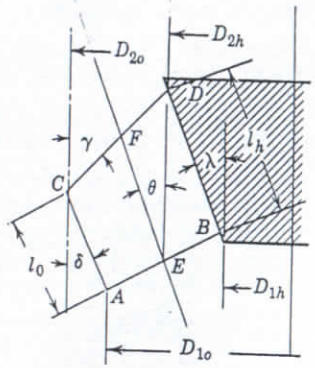

FIG. 16.4. Mixed flow impeller profile.

(*d*) **Impeller Profile.** The impeller profile of a mixed flow pump contains the following elements, each having a bearing on the specific speed and brake-horsepower ratio of the pump.

1. *The impeller hub ratio* could be expressed as a ratio of the hub diameter to the impeller outside diameter at the discharge or to the diameter at the inlet. The effect of these ratios on the specific speed cannot be established as simply as has been done for the axial flow pump because it is closely interlocked with two other elements described in the following.

2. *Impeller profile angle* at the outside diameter (δ on Fig. 16.4) and the hub profile angle (λ in Fig. 16.4) will be combined into one profile angle θ at the average inlet and outlet diameters for this discussion. Higher impeller profile angles lead to a lower brake-horsepower ratio

* It has been pointed out [14] that discontinuity in head-capacity curve could be reduced or eliminated by providing two concentric bell-shaped baffles at the pump suction to distribute the inlet flow uniformly across the impeller inlet area.

and lower specific speed. To maintain specific speed at the rated point some compensating changes in design should be made, such as more liberal casing areas or a smaller hub.

3. *The impeller profile depth* (l_0 on Fig. 16.4) is proportional to the impeller vane length for a fixed value of β_2 and β_1. Long impeller vanes, or a deeper impeller profile, result in a lower brake-horsepower ratio, because longer vanes cause liquid to rotate with the impeller more than short ones, thus reducing the brake-horsepower ratio. Cutting impeller vanes to reduce the head capacity, as shown on Fig. 5.12, increases the brake-horsepower ratio.

It will be noticed that the *combined effect* of the number of vanes, impeller discharge angle, and vane length (vane profile depth l_0, Fig. 16.4) determine the vane overlap or vane "solidity." This can be expressed as the chord/spacing ratio l/t in the similar manner as has been done for axial flow impellers. Taking, for simplicity, the vane length l along the outer edge of the impeller vane and the vane spacing $t = \pi D_{20}/z$, where z is the number of vanes, the values of l/t ratio for a number of successful designs fall within a narrow range (1.0 to 1.05) for specific speeds from 6000 to 8000 and four impeller vanes.

(*e*) **Prerotation.** In Art. 3.5 it has been pointed out that, at partial capacities, liquid following a path of least resistance acquires prerotation in direction of impeller rotation. This tendency is more pronounced with mixed and axial flow pumps than with straight centrifugal pumps. The immediate effect of prerotation is unloading of the impeller and reduction of shut-off head and brake horsepower, because the subtractive term in the input-head equation 3.5 is not equal zero. Thus for low brake-horsepower ratios it is important to encourage prerotation in the impeller approach. If vertical pumps have a bottom bearing, the ribs supporting the bearing body should be as far as possible from the impeller. A number of mixed flow pumps are built without bottom bearings for the same reason.

Note that if prerotation is induced by the shape of the channel of approach to the pump, it may overload or unload the impeller depending on the direction of prerotation. However, this increase or decrease of head and brake horsepower takes place at all capacities and cannot be utilized as a means of reducing the brake-horsepower ratio.

(*f*) **Casing.** The effect of the casing design on the brake-horsepower ratio is indirect. A greater number of diffusion vanes and lower diffusion vane angles tend to reduce the brake-horsepower ratio, but result in a reduction of specific speed, since the b.e.p. moves toward lower capacities while no appreciable change takes place in the shape of the brake-horsepower or head-capacity curves. A reduction of space between the impellers and the diffusion vanes of the casing also tends to reduce the brake-horsepower ratio as the volume of liquid involved in the energy waste at shut-off is reduced.

It is left to the skill of the designer to manipulate the various design elements in the sense indicated above to obtain a flat brake-horsepower characteristic and to stay within the prescribed specific speed range without undue sacrifice in efficiency and shape of the head-capacity curve. The best combination of the several design elements to meet all these conditions can be determined only experimentally.

In straight axial flow pumps or mixed flow pumps with high shut-off brake horsepower, several methods have been devised to start the pumps without overloading the motors. On a great many installations, pumps can be started with the discharge wide open; in such cases the advantages of a flat brake-horsepower curve are minimized.

16.2 SUCTION SUMP DESIGN

Owing to the features of propeller pumps—high relative velocities, short impeller passages, few vanes, and little guiding action from the suction bell—their performance is affected markedly by the flow in the suction sump. Therefore particular attention should be paid to the sump design in order to obtain optimum performance of propeller pumps. The sump design is frequently beyond the control of the pump designer. Although it is impossible to foresee all the possible field conditions which would adversely affect pump performance, several well-established principles cover the minimum requirements which should be met in laying out a pumping station to assure normal pump performance. These include: (1) submergence; (2) clearances from the floor and walls; (3) sump intake, or flow distribution in the sump; (4) spacing of several units; and (5) strainers and trash racks.

Only vertical turbine pumps, or diffusion-casing-type propeller pumps, will be considered here, as these have replaced entirely the volute-type vertical pumps used in the past. Also, wet-pit construction is now used universally, the dry-pit station layout having been used mostly in connection with volute propeller pumps.

(*a*) **Submergence.** Submergence is selected with due regard for cavitation limits. Hydraulic Institute Standards give the recommended submergence in terms of pump head and specific speed for an average design. Individual designs of several manufacturers may require different submergences. Another point in setting a minimum submergence is the prevention of vortexes in the suction sump which may permit air

to be drawn into the pump suction. This depends on the sump layout, velocity of approach, suction bell design, effect of adjacent pumps, and the like. For these reasons the submergence on an average job should not be less than 5 ft above the suction bell edge. With low suction bell velocity (2 to 3 ft per sec) and small units, this can be reduced to $D/2$, where D is the suction bell diameter which, on an average pump, should be not less than twice the diameter of the impeller eye. In every case the minimum water level in the suction sump should cover the impeller hub to keep the pump self-priming. When vortices appear in an existing station they can be checked by providing wooden floats around the pump discharge pipe or baffles in the suction sump. All vortices originate from the impeller; for that reason pumps having a bottom bearing with radial supporting baffles in the suction bell are less likely to set up vortices in the suction sump. Submergence also has an important bearing on the velocity distribution in the suction bell approach, particularly if there are several pumps in the same sump. With ample submergence, water can approach the suction bell from all directions with a uniform velocity and with a minimum of disturbance from the flow toward several units in the same pit.

(b) Floor Clearance. The free area between the suction bell and the sump floor should be at least equal to the area of the bell itself. This

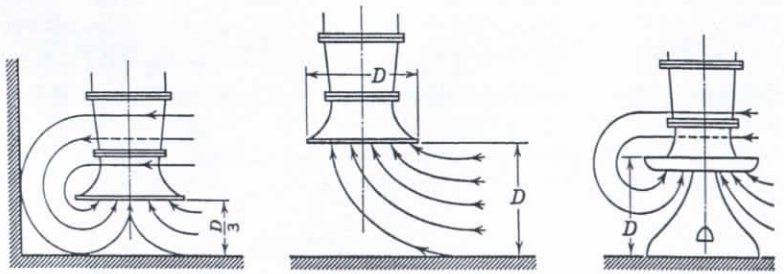

FIG. 16.5. Pattern of flow with suction bell distance to floor $D/3$ and D.

requires a distance between the bell and the floor equal to $D/4$, where D is the bell outside diameter. But this will cause the water to make a sharp turn inside the bell. *It has been found that a distance $D/3$ between the bottom of the pit and the suction bell is ample for normal pump performance. A further increase in this distance may even impair, rather than improve, the velocity distribution in the suction bell approach.* Tests at the University of California [1] have shown that the best performance is obtained with a clearance of $D/2$. An increase of the clearance to D

reduced the gross pump efficiency about one point. This has been confirmed by later tests by Kerr and Moyer.[2] The possible patterns of flow are shown in Fig. 16.5. When the bottom clearance is $D/3$, a more uniform velocity distribution in the suction bell is obtained. With the

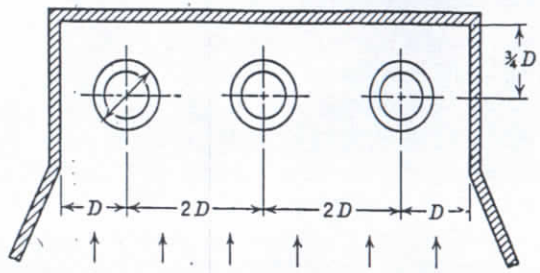

FIG. 16.6. Pump spacing with a uniform approach—best.

distance between the suction bell and the floor D or more, a guide cone on the floor and suction bell design as shown in Fig. 16.5(*c*) will improve velocity distribution in the impeller approach. Guide cones have been found beneficial also when pumping from high velocity channels.[3] The wall clearances for normal performance should be at least $D/2$. If the sump intake is such that the flow is equally divided among several units, the minimum spacing between the units should be $2D$ (Fig. 16.6).

(c) Sump Design. When water is brought to the suction sump by means of a tunnel, equal distribution of the flow among several units

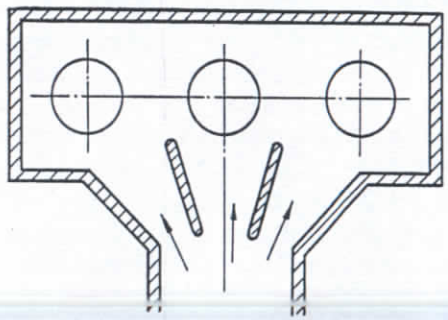

FIG. 16.7. Tunnel inlet to a suction sump—satisfactory.

becomes very important. Baffling may be necessary to assure minimum interference between the flow to several units (Fig. 16.7).

Cases are on record [4] where normal pump performance in the field could not be realized on account of a suction sump design which did not permit equal distribution of flow among three pumps. However, after

proper baffling and change in the inlet tunnel, all determined by model testing, normal performance of all pumps was restored.

The sump plan arrangement shown in Fig. 16.8, where the sump intake is at one end of the sump, will inevitably result in an uneven flow distribution and mutual interference of the several units. The units nearest

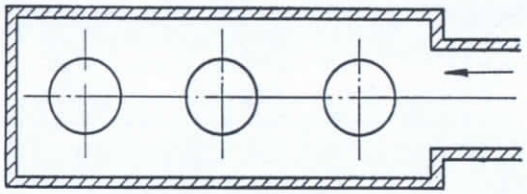

FIG. 16.8. A suction sump arrangement to be avoided.

to the intake will be affected most. The example shown in Fig. 16.9 was called to the author's attention. Each pump, A and B, worked satisfactorily when operating alone. When both were operating, A would run normally whereas B would develop mechanical vibration and drop in capacity (and possibly in efficiency). *When local conditions do not permit a favorable station layout to assure an equal distribution of flow among several pumps, the adverse effects of inadequate sump design are minimized if the velocity of approach to each pump is kept as low as possible and if spacing between the pumps is increased above the minimum stated above.*

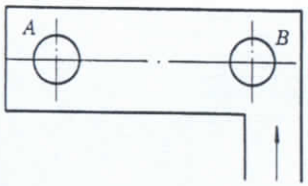

FIG. 16.9 A suction sump and pump arrangement proved unsatisfactory.

All modern pumping stations are provided either with manually cleaned trash racks or moving screens. These are preferred to the individual suction strainers as the latter, even when clean, result in an appreciable loss of head. When clogged up with trash, the resistance may increase to the extent that cavitation may appear. The velocity through the trash rack should not exceed 1 ft per sec.

(*d*) Design of Discharge Column. Although the discharge columns of propeller pumps are usually short, the loss in the column should be kept to a minimum for low head pumps. All high speed propeller pumps need an increaser next to the pump diffusion casing. The total angle of the increaser should be about 8° for efficient conversion of velocity into pressure. Fabricated steel elbows should be laid out with at least five sections, and a minimum radius of curvature of at least $1.25d$, where d is the pipe diameter. In no case should a tee be substituted for an elbow.

(Refer to Fig. 1.12 for relative losses of several elbow designs and tees.) The size of the discharge column is selected so that the velocity head in the column does not exceed 4 to 5 per cent of the pump total head.[5] When discharging into an open canal or lake, the discharge pipe outlet should be submerged, and velocity at the discharge should be reduced to a minimum. When there is no valve on the discharge pipe, a flap valve will serve the same purpose. Nagler [6] has found that resistance of freely suspended flap valves does not exceed 0.10 ft if their weight is light or if the weight is balanced.

In irrigation and drainage plants the discharge pipe is frequently put over a levee. To recover the extra lift over the levee a siphon action is provided by submerging the discharge end of the pipe. In that case no valve is necessary on the discharge pipe, but an automatic vacuum-breaking valve should be provided in the discharge pipe to prevent backflow through the siphon. When the pump is started to prime the siphon the pump should be able to lift water over the hump. With rising brake-horsepower curve and synchronous motor drive the pull-in torque of the motor should be sufficient to produce the head necessary to prime the siphon.

(*e*) Sump Model Testing. In connection with the extensive postwar expansion of power plants a number of hydraulic problems were encountered with the installation of vertical condenser circulating pumps of the propeller type. The basic difficulty was that the capacities required were considerably greater than those for which the existing intake tunnels or pump cells were designed. In a number of new plants having high tunnel velocities and sharp turns into the individual cells, similar trouble has been experienced, namely, hydraulic noise and mechanical vibration.

There was general agreement in these cases that vibration was caused by vortices at the pump intake induced by a sharp turn in the channel of approach to the pump and uneven flow distribution in the suction bell. This has been proved by testing scale models of the complete installation including the inlet tunnel and pump intake pipe through which water was withdrawn. There was no need to reproduce the pump itself. The velocity distribution could be observed through lucite channel bottoms (and through the top if the tunnel was under pressure) with the aid of a mirror and addition of sawdust to water. Installation of small, free-revolving flags in strategic places was found helpful for the purpose of photographing the flow in the channel.

From consideration of Froude's number, or the expression for the centrifugal forces which upset the velocity distribution, the test velocity should be reduced in the ratio of the square root of the model size factor.

However, since the sense of forces does not change with the rate of flow, it is advantageous to run tests with exaggerated velocities to intensify the visual characteristics of the flow.

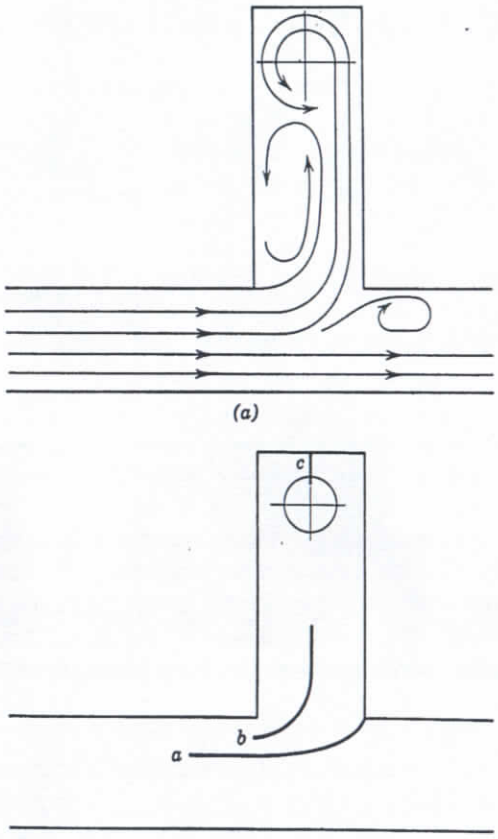

FIG. 16.10. Suction sump with 90° turn; *a*, *b*, *c* are baffles.

There are a number of principles suggested by model testing and confirmed by experience with existing plants which should be observed for satisfactory operation of vertical pumps:

1. Maintaining the suction bell clearance to the floor at $D/3$ is the most effective means to stabilize the flow to the impeller. In special cases this could be reduced to $D/4$, with hardly any effect on the pump hydraulic performance.
2. In the individual cells the clearance between the bell edge and the dead-end wall should not exceed $D/4$.

3. A symmetrical approach to the suction bell is essential for uniform velocity of approach to the impeller. With the channel width equal to $2D$, and clearances as stated above, if the channel length is $7D$ or more, no special means are necessary to stabilize the flow. With shorter channels some baffling may be necessary for smooth operation of the pumps. Figures 16.10 and 16.11 show the baffling which was necessary in one case to eliminate hydraulic noise and vibration.

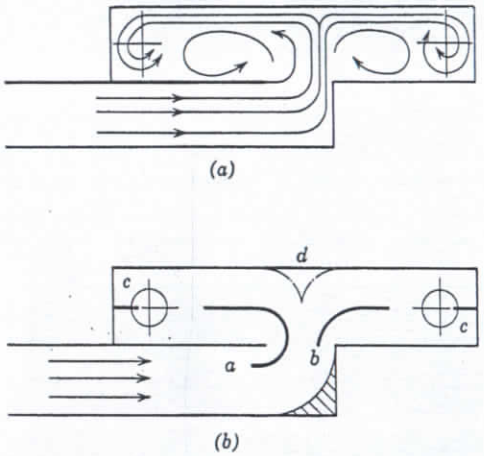

FIG. 16.11. Suction sump with 180° turn; *a*, *b*, *c* are baffles; tunnel under pressure.

Figures 16.10(*a*) and 16.11(*a*) show a general appearance of the vortices before the baffling. In a majority of cases it was not necessary to install the baffle *c*. In every case baffles are so arranged that they cut off from the flow in a tunnel its share for each pump. The individual pump flow is also divided in two by a baffle. In this way, when two streams meet at the dead end of the cell, there is no tendency for vortex formation.[7,8]

16.3 VERTICAL PROPELLER PUMPS VERSUS HORIZONTAL PUMPS

(*a*) Hydraulic Performance. By referring to Fig. 16.12 it will be noticed that, at specific speeds above 5000, vertical mixed flow and axial flow pumps have a better efficiency than horizontal pumps. The difference is caused mostly by the adverse effect of the suction approach on the impeller performance. The relative performance of vertical pumps is even better than it appears from this chart as the entrance loss and loss in the discharge column, including the elbow, are charged against the pump, whereas in horizontal pumps the head is measured between the

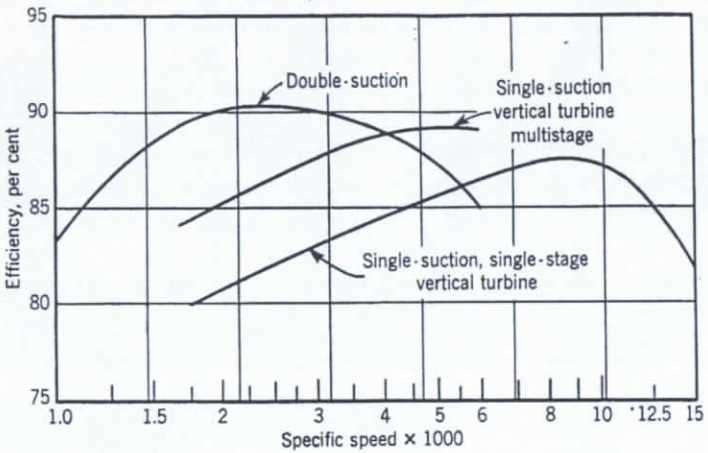

FIG. 16.12. Pump efficiency is affected by the casing design.

suction and discharge flanges, and the loss in the suction pipe should be charged to the pump to put the comparison on the same basis.

Moreover, horizontal pumps usually require an increaser on the discharge nozzle, thus incurring additional loss of head, whereas in propeller pump discharge elbow velocities are already reduced to what they are in the discharge pipe.

Horizontal propeller pumps lose part of their advantages if there is an elbow on the suction or if the pump has to work under a suction lift. In the past, horizontal propeller pumps were invariably used for engine-driven jobs. This resulted in a slow speed pump operating under suction lift, and required a deep excavation to reduce the static lift of the pump. *The recent trend is to use vertical submerged pumps driven through a right-angle geared head. This permits freedom of speed selection for the pump, and gives all the advantages of vertical pumps as to submergence and impeller approach. The engine floor can be located at any convenient level, and the over-all cost of the pumping station is lower.*

(*b*) **Variable Head-Capacity Performance.** The efficiency curve of a low specific speed centrifugal pump, when plotted against capacity, is flatter than that of propeller pumps. When capacity is varied by throttling, this has a definite advantage. But low head pumps are used mostly where head varies as a result of suction level variation (tide, seasonal change in river levels, and so on) and maximum capacity is wanted at any head. In this case propeller pumps with a steep head-capacity curve have a definite advantage and they will deliver more water within a given head range, and at a better efficiency, than the centrifugal pump. The fact that the efficiency is better is more evident

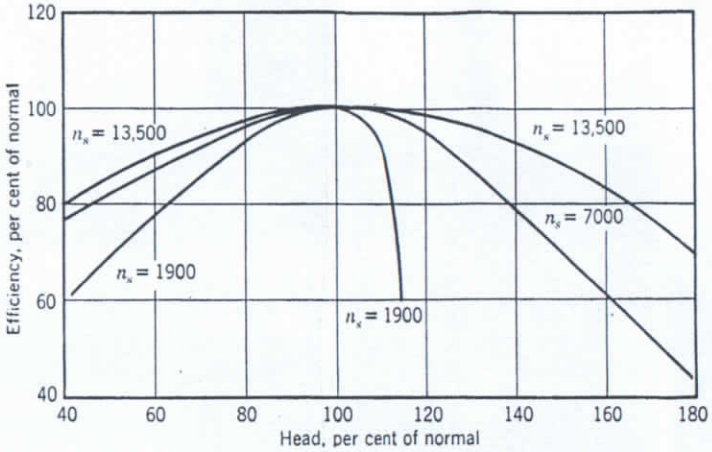

FIG. 16.13. Efficiency versus head of one centrifugal and two propeller pumps.

if the efficiencies of both centrifugal and propeller pumps are plotted against the head (Fig. 16.13). On this basis the propeller pump efficiency curve is flatter than that of the centrifugal pump.

16.4 FIELD PERFORMANCE OF VERTICAL TURBINE PUMPS

The field performance of vertical pumps with a long discharge column may differ materially from the laboratory or shop performance. Since the motor is selected to meet the field brake-horsepower requirement, and the user of the pump is mostly interested in the field performance of the pump, it is important to be able to estimate the field performance of the vertical turbine pump from the shop test or pump rating.

Calculation of the field performance involves the following steps and is better arranged in a tabular form with column headings as shown below.

1 Capacity, gpm	2 Field Head, ft	3 Hydraulic Loss, ft	4 Shop Total Head, ft	5 Shop Efficiency, %	6 Shop, bhp	7 Field, bhp	8 Field Efficiency, %

1. Specified capacity is entered in column 1, to be followed by other capacities to complete the performance curve.

2. Field head is equal to the static head plus the specified discharge nozzle pressure plus the discharge nozzle velocity head.

3. Hydraulic friction loss for the total length of discharge column (excluding the discharge elbow) is calculated by using Chart D-3.[9]

4. Shop total head equals field head (step 2) plus hydraulic friction loss (step 3). The pump is selected to meet the shop head at the specified capacity. Next, columns 1, 4, and 5 are filled out for several capacities from the selected rating curve. Also column 3 is filled out by assuming that the friction loss varies directly as the square of capacity. Column 2 is then filled in by subtracting column 3 from column 4.

5. Shop rated efficiency is obtained from the rating curves.

6. Shop brake horsepower

$$= \frac{\text{gallons per minute} \times \text{shop total head}}{3960 \times \text{shop efficiency}} = \frac{(1) \times (4)}{3960 \times (5)}$$

7. Field brake horsepower = shop brake horsepower plus column shaft friction loss, Chart D-4.[9]

8. Field efficiency $= \dfrac{(1) \times (2)}{3960 \times (7)}$

When testing or estimating the performance of vertical turbine pumps used for irrigation service it is customary to charge the discharge velocity head as a loss against the pump. Thus the velocity head is not included in calculating the field head. However, when used for industrial installations, vertical turbine pumps are credited with the velocity head at discharge according to the A.S.M.E. test code.

16.5 ADJUSTABLE IMPELLER VANE AXIAL FLOW PUMPS

When adjustable impeller vanes are provided on axial flow pumps it is possible to vary the head and capacity over a wide range with good efficiency by changing the position of the impeller vanes in the hub. This type of construction is widely used in Kaplan water turbines but has been applied to pumps only recently. As used in water turbines, the cost of this design was prohibitive considering the size of pumps. Early pumps with adjustable impeller vanes were built in accordance with the water turbine practice.[10,11] In these the rod operating the mechanism inside the impeller hub was brought out through hollow pump and motor shafts. The author has designed an adjustable vane axial flow pump in which the adjusting mechanism was arranged externally to the pump, as shown in Fig. 16.14. The details of the impeller hub design are shown in Fig. 16.15.

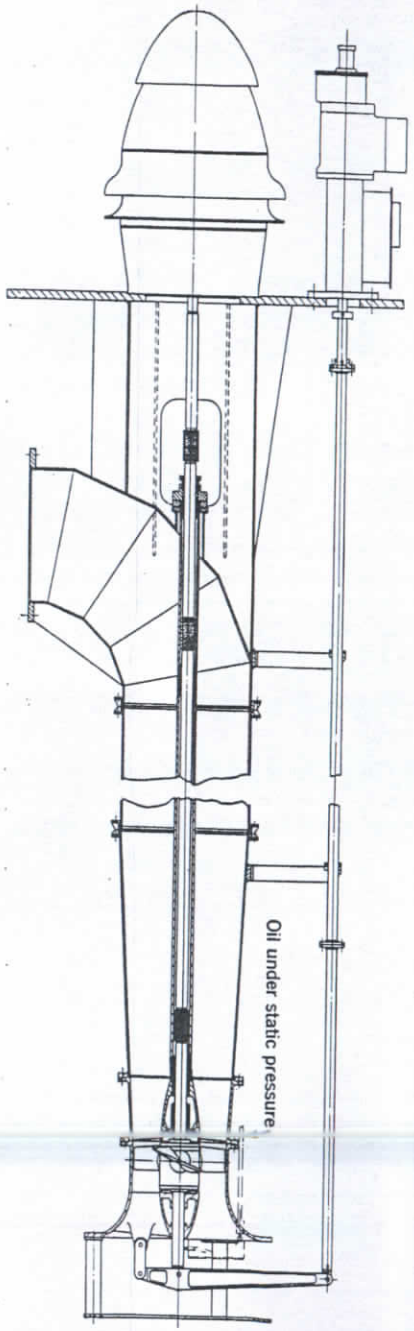

FIG. 16.14. 24-in. Ingersoll-Rand adjustable impeller vane axial flow pump at Central Illinois Electric and Gas Company; 22,000 gpm, 24.8-ft head, 880 rpm.

of the installation, the life of condenser tubes is appreciably prolonged as minimum velocities through the condenser are maintained at all loads.

For manual control of the vanes, especially where the change in the vane setting is not frequent and the pump can be stopped for the change (irrigation, drainage), this design becomes particularly simple. All the external leverage is omitted and vanes are moved by reversing the procedure; that is, by moving the pump shaft and holding the lower stub shaft rigidly attached to the suction bell. A hollow-shaft motor is employed and the pump shaft is moved by means of the adjusting nut on top of the motor in the same manner as for the adjustment of running clearance of regular vertical turbine pumps with open impellers.

The Ingersoll-Rand Company has built a 16-in. mixed flow pump of $n_s = 7000$ with adjustable diffusion casing vanes to be used with a standard impeller. This has shown marked improvement in efficiency at reduced capacities. However, the head increased at the same time and there was little or no reduction in brake horsepower.

16.6 EXAMPLES OF PROPELLER AND VERTICAL TURBINE PUMPS

Figure 16.17 shows a "pull-out" type of a mixed flow propeller pump as built in large sizes for condenser circulating service. The pumping element can be removed through the opening in the discharge elbow without disturbing the discharge flange and the outer column. The pumping element is identical with that normally bolted directly to the discharge column except that a portion of the suction bell is attached to the outer column. Clear water can be fed to the bottom bearing through the inner column and a drilled hole through the lower section of the shaft. Figure 16.18 shows an enlarged view of the pumping element. To release the pressure in the inner column the impeller is provided with closely fitted wearing rings and a drain port to the suction.

Figure 16.19 shows a horizontal volute mixed flow propeller pump. In sizes up to 24 in. such pumps are used widely for brine circulation through evaporators in chemical processes at a low head and very limited NPSH, operating at a very low speed. Pumps of the same type are used also in paper mills. In large sizes volute propeller pumps become too bulky and cannot compete with vertical propeller pumps with straight diffusion casings (Fig. 16.18) in cost and efficiency. The same impeller will produce essentially the same head-capacity curve regardless whether it is used in a diffusion casing or a volute casing. The b.e.p., however, moves to a lower capacity (about 90 per cent) in a volute casing. This can be attributed to a lower through-flow ability (specific capacity) of the volute casing (90° turn) as compared with a straight vaned casing.

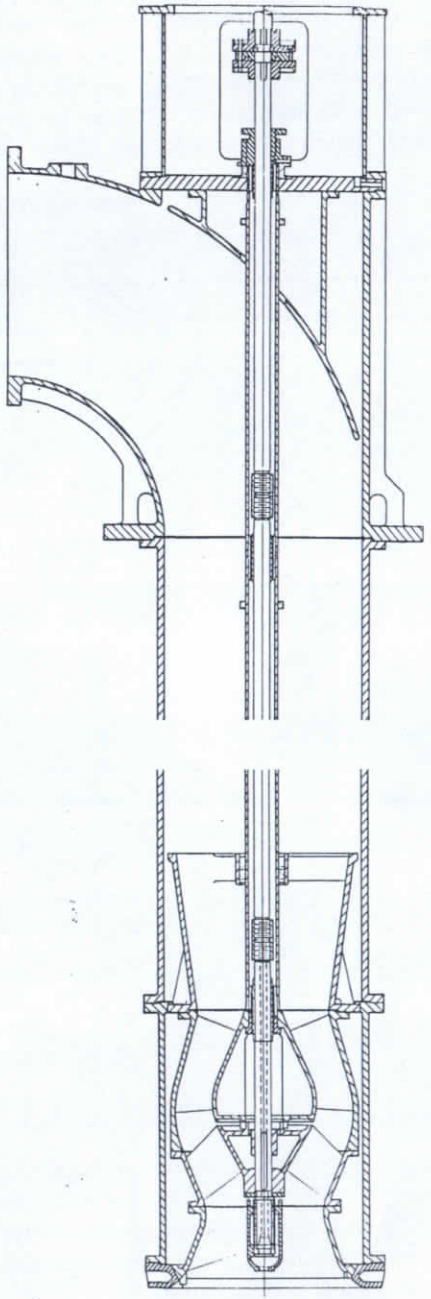

FIG. 16.17. Mixed flow propeller pump of $n_s = 7500$, pull-out type (Ingersoll-Rand).

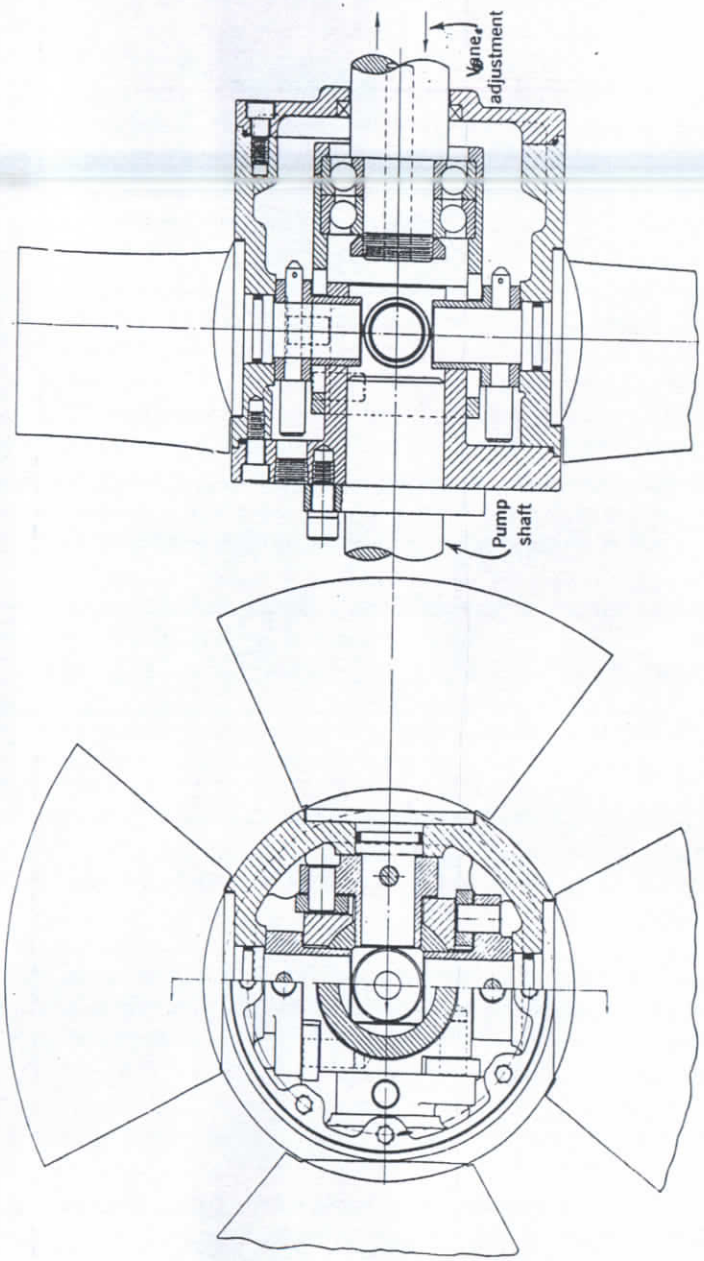

FIG. 16.15. Impeller hub detail of pump in Fig. 16.14 (Ingersoll-Rand).

Except for the impeller the rest of the pump parts are the same as those of pumps which have one-piece standard impellers. The mechanism is operated electrically by remote control from a switchboard. The performance of this pump is shown in Fig. 16.16. The system charac-

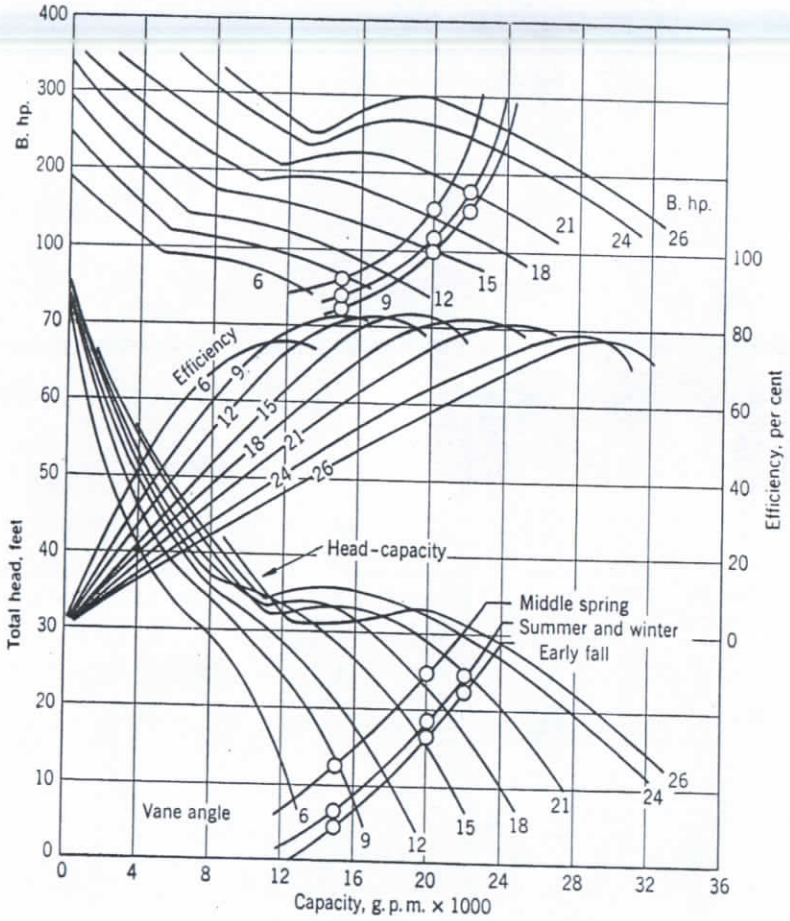

FIG. 16.16. Test curve of pump shown in Fig. 16.14.

teristics of the plant vary with the season of the year. Note that a 25 per cent reduction in capacity results in over 50 per cent saving in power. *The pump can be started with the discharge valve closed and, when the impeller vanes are flat, the pump requires about 25 per cent of the maximum rated brake horsepower. In condenser circulating service the variation in capacity is caused not only by the load on the condenser but also by the water temperature. By adjusting the pump capacity to the actual needs*

3.9 PREVIOUS STUDIES OF NPSH REQUIREMENTS

.Pfleiderer [5] has offered the following method for calculation of the minimum NPSH requirements in terms of the inlet-velocity triangle elements using the formula

$$\text{NPSH} = \lambda_1 \frac{w_1^2}{2g} + \lambda_2 \frac{c_{m1}^2}{2g} \tag{3.15}$$

where λ_1 is a numerical constant with values from 0.25 to 0.35 and λ_2 is a numerical constant which lies between 1.1 and 1.3. Equation (3.15) can be presented in the form similar to equation (3.8).

$$\text{NPSH} = K_1 c_{m1}^2/2g \tag{3.16}$$

where

$$K_1 = \lambda_1/\sin^2 \beta_1 + \lambda_2 \tag{3.17}$$

By expressing NPSH in equation (3.17) in terms of the several elements of the inlet-velocity triangle and assuming that NPSH is a function of β_1 only (the rest of the variables remaining constant) the value of the minimum NPSH was found by differentiation of equation (3.17) with respect to tan β_1. Solving tan β_1 Pfleiderer arrived at the following expression

$$\tan \beta_1 = \sqrt{\frac{1 + \lambda_2(R_1 - 1)^2}{2(\lambda_1 + \lambda_2)}} \tag{3.18}$$

Since in Pfleiderer's development the leakage loss and the reduction of the effective area due to vane thickness were neglected, a value of $R_1 = 1.2$ should be used for the radial inlet flow without prerotation. Using $\lambda_1 = 0.25$ and $\lambda_2 = 1.1$ equation (3.18) yields

$$\beta_1 = 18 \text{ degrees}$$

and

$$K_1 = 3.64$$

This result is in agreement with the chart in Fig. 3.4. On the same chart several values of K_1 are shown for different β_1 values, according to equation (3.17). These show that if λ_1 and λ_2 are constant the value of R_1 has to increase for lower values of β_1. Conversely, if the value of R_1 is selected, the value of λ_1 and λ_2 will vary, to locate the points on their respective lines of β_1 values.

Krisam [4] has expressed serious doubts about the validity of the equations (3.15) and (3.18), indicating that there was ample experimental evidence that lower values of NPSH and higher values of the suction

specific speeds were obtained with β_1 as low as 12 degrees. T
sistency of equation (3.18) also becomes apparent when higher
R_1 (allowing prerotation) are used. Thus, for $R_1 = 1.5$, the ar
24 degrees, and for $R_1 = 2.0$, $\beta_1 = 35$ degrees. It has been stat
that higher values of R_1 up to $R_1 = 2.0$ were resorted to in c
with a minimum value of $\beta_1 = 15$ or 16 degrees. All the above
ations lead to a conclusion that λ_1 and λ_2 do not remain cor
different values of β_1 and R_1 and hence the whole method of
mination of the minimum values of NPSH by differentiatio
applicable.

REFERENCES

1. Stepanoff and Stahl, "Dissimilarity Laws in Centrifugal Pumps and *Journal of Engineering for Power, Trans, ASME*, Series A, vol. 83, 1961, p
2. Stepanoff, *Centrifugal and Axial Flow Pumps*, John Wiley & Sons, New pp. 47, 60. (Omitted from the second edition, 1957.)
3. Stepanoff, *Centrifugal and Axial Flow Pumps*, John Wiley & Sons, New p. 249.
4. Krisam, "Neue Erkenntnisse im Kreiselpumpenbau," Z. Ver. Deut. Ir no. 11–12, p. 320, April, 1953.
5. Pfleiderer, *Die Kreiselpumpen*, Springer, 1955, p. 174.
6. Horie and Kawaguchi, "Cavitation Tests on an Axial Flow Pump," *Japanese Society of Mechanical Engineering*, vol. 2, no. 5, 1958, p. 1 English).
7. Reference [3], p. 228 (Tenot data).
8. Mullan, "An Investigation of Cavitating Inducers," Report No. 53, Ma Institute of Technology, Cambridge, Mass., May, 1959.
9. Acosta, "An Experimental Study of Cavitating Inducers," Second Syn Naval Hydrodynamics, 1958, Office of Naval Research, Washington, California Institute of Technology.
10. Rütschi, "Die Pfleiderer-Saugzahl als Gütegrad der Saugfähigkeit v pumpen," Schweizerische Bauzeitung Heft 12, 24 Marz 1960.
11. Blom, "Development of the Hydraulic Design for the Grand Coul *Trans. ASME*, vol. 72, 1950, p. 53.

An alternate procedure: from equation (3.10*b*)

$$M = \frac{4.67 \times 14.8}{54.0} = 1.28$$

$$S = 13{,}000/1.28 = 10{,}150$$

hence NPSH

$$10{,}150 = \frac{1750\sqrt{2100}}{(\text{NPSH})^{3/4}}$$

and

$$\text{NPSH} = 15.8 \text{ ft}$$

Example 4. Figure 3.10 shows variation of NPSH, S' and D_1 for different values of β_1 and R_1 calculated for a 1000-gpm 3500-rpm pump,

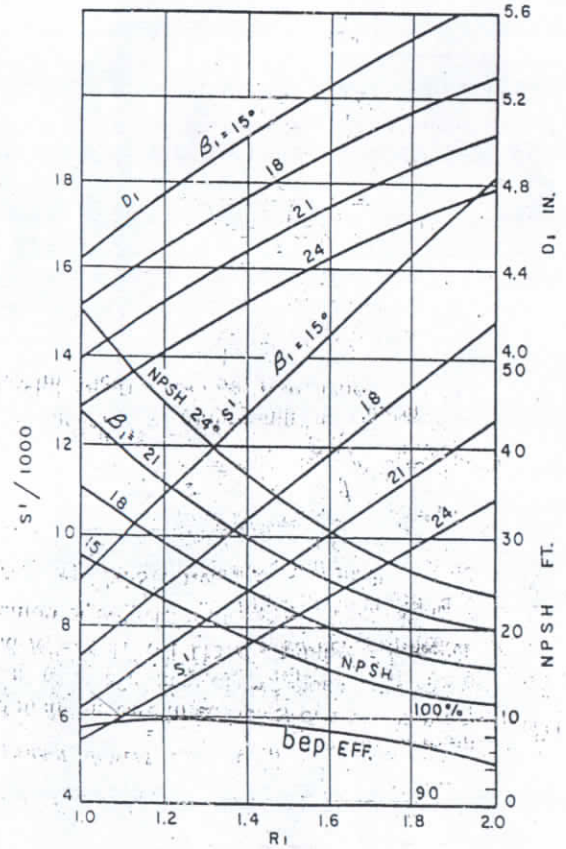

Figure 3.10 Example: 1000 gpm, 3500 rpm. $F = 1.0$; $f = 1.1$; $SM = 13{,}000$.

assuming $F = 1.0$, $f = 1.1$, and $S'M = 13{,}000$. Note that the imp eye diameter D_1 is completely defined for each value of β_1 and R_1, equ (3.7*a*), and thus is independent of the choice of $S'M$ value.

Higher value of $S'M$ (13,500 instead of 13,000 for instance) result higher NPSH and lower S' values, thus increasing the margin of s Equation (3.14) indicates that K_1, and hence NPSH, varies directly fourth power of $S'M$ value. In Example 1 NPSH value will inc from 17.5 to 20.7 ft, when $S'M$ is changed from 13,000 to 13,500.

3.8 AXIAL-FLOW PUMPS AND INDUCERS

In Fig. 3.9 are collected experimental values of the multiplier M for flow pumps and inducers extending the range of suction-specific s up to 48,000. The inducers were tested as independent pumps and r boosters for centrifugal pumps. The points in the figure refer to the ditions of incipient cavitation (noncavitating).

The great variation of the suction specific speed of three grou impellers, with a small difference in β_1 and hub ratio, is explained b method of NPSH measurement and the effect of the casing o impeller performance. Three points in the upper left corner of the were obtained from normal axial flow pumps where the suction (NPSH) includes the inlet bell loss. Furthermore the curved im approach tends to create high local velocities at impeller inlet. second group of points by Mullan [8], $S' \approx 23{,}000$, were obtained a long straight inlet pipe of the same diameter as the impeller. The su pressure was measured a short distance ahead of the impeller. This discharged into a circular collecting chamber (not a volute). W greatly improved impeller approach the specific capacity (bep) incr as compared with the first group of pumps.

The third group of points by Acosta [9], $S' \approx 50{,}000$, were ob with a straight pipe both on suction and discharge. The NPSH is mized, and specific capacity is increased still further as compared the second group. Neglecting any losses of head in the impeller app the value of $K_1 = 1.5$ for this inducer can be accounted for by the of the maximum local velocity in the low-pressure zone which i times the average inlet radial velocity.

Although the suction specific speed of a pump with an inducer of a centrifugal impeller is determined by that of the inducer, s specific speeds shown by inducers when tested alone cannot be rea without cavitation, when these are used as boosters to the n centrifugal impellers.

1.2 resulted in an increase in efficiency of 1.4 points. Blom [11] obtained an improvement in efficiency of two points by reducing $\beta_1 = 28$ to 21 degrees, and $R_1 = 1.41$ to 1.115 of a pump with overhung impeller.

3. Estimation of NPSH for an existing impeller.

Example 1. Design an impeller inlet for a 3-in. pump, 1000-gpm, 3500-rpm, low NPSH, overhung impeller construction. Select:

$$\beta_1 = 16 \text{ degrees} \qquad f = 1.1$$
$$R_1 = 1.6 \qquad S'M = 13{,}000$$

To allow for impeller holding nut obstruction estimate $F = 0.90$, subject to a check later from the actual impeller layout. From Fig. 3.8 read

$$K_1 f^2 = 6.5, \text{ hence } K_1 = 5.37$$

From the equation (3.10*c*)

$$M = \frac{5.37 \times 0.286}{1.6} = 0.96$$

Then

$$S' = \frac{13{,}000}{0.96} = 13{,}560$$

and

$$S = 13{,}560 \times \sqrt{0.90} = 12{,}900$$

NPSH value is obtained from

$$S = 12{,}900 = \frac{3500\sqrt{1000}}{(\text{NPSH})^{3/4}}$$
$$\text{NPSH} = 17.5 \text{ ft}$$

c_{m1} is obtained from equation (3.8)

$$17.5 = 5.37 \times c_{m1}^2/2g$$
$$c_{m1} = 14.5 \text{ ft/sec}$$

Impeller-eye diameter is obtained from (3.10*b*).

$$\frac{5.37}{0.96} = \frac{u_1}{14.5}$$
$$u_1 = 81.2 \text{ ft/sec}$$
$$D_1 = 5.32 \text{ in.}$$

D_1 could be found directly from the equation (3.7*a*).

Example 2. Design impeller inlet for a 12-in. double-suctio 6800 gpm, 175-ft head, 1775 rpm, $n_s = 3040$ for the best performance.

Select

$$\beta_1 = 22\tfrac{1}{2}^\circ, \qquad f = 1.1$$
$$R_1 = 1.25 \qquad S'M = 13{,}000$$

Tentatively take $F = 0.85$.

Following the same procedure

$$K_1 f^2 = 6.5$$
$$K_1 = 5.37$$
$$M = \frac{5.37 \times 0.414}{1.25} = 1.78$$
$$S' = \frac{13{,}000}{1.78} = 7300$$
$$S = 7300 \times \sqrt{0.85} = 6730$$

NPSH is determined from

$$6730 = \frac{1775\sqrt{3400}}{(\text{NPSH})^{3/4}}$$

NPSH = 38.0 ft or about 5.5-ft positive head.

$$c_{m1} = 21.0 \text{ ft/sec}$$
$$u_1 = 63.3$$
$$D_1 = 8.34 \text{ in.}$$

From equation (3.11), $D_1 = 8.3$ in. The impeller-eye diameter be obtained from the equation (3.6).

Example 3. Estimate NPSH of a 6-in. pump, 2100 gpm, 175 which the impeller drawing is available, but β_1 and R_1 are not k Calculate

$$c_{m1} = 14.8 \text{ ft/sec}$$
$$u_1 = 54.0$$
$$f = 1.18$$
$$F = 1.0$$

From Fig. 3.8 for $S'M = 13{,}000$

$$K_1 = 4.67$$

From equation (3.8)

$$\text{NPSH} = 4.67 \times (14.8)^2/64.4 = 15.8 \text{ ft}$$

may affect the cavitation characteristics of the impeller: (1) form of impeller approach (casing); (2) impeller profile; (3) number of impeller vanes; (4) the degree of the impeller-vane finish (sharpening of the inlet edges). Thus deviations from equations can be expected. Besides, accurate testing of pumps for cavitation requires special equipment and an elaborate procedure, not always available for commercial testing. Therefore, a tolerance of, perhaps, plus 10 per cent should be allowed when estimating NPSH value by the procedure outlined in this article.

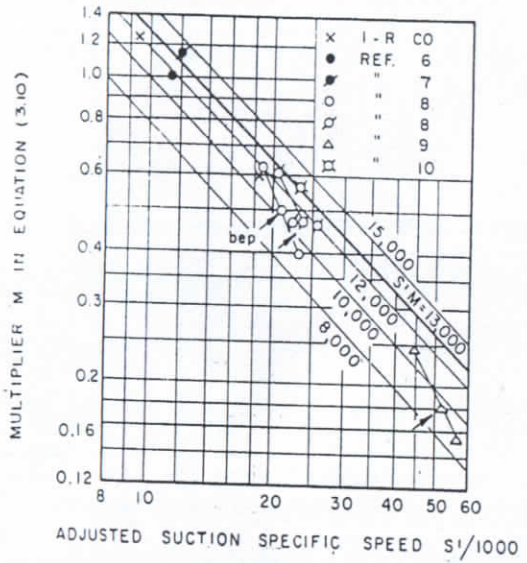

Figure 3.9 Axial flow pumps and inducers.

Examples: One 4-in., 650-gpm, 3500-rpm pump has shown 15-ft NPSH requirement with a six-vane impeller and 12.5-ft NPSH with a four-vane impeller of the same pattern.

A 3-in., 450-gpm, 3500-rpm pump required 14.0-ft NPSH with top suction nozzle (flat elbow) as compared with 12.0-ft NPSH with a straight axial suction (end suction) with the same impeller and volute casing.

One 1-in., 55-gpm, 3500-rpm pump has shown a reduction of NPSH from 11.7 to 6.5 ft by replacing a hexagonal impeller holding nut with a turned streamlined nut.

(*f*) The test points obtained at partial capacities following the general direction of $S'M$ lines on Figs. 3.6, 3.7, and 3.9 shift markedly toward lower $S'M$ lines. Figure 3.9 shows three examples of this type. Also in Fig. 3.7 two points obtained with impellers of the same profile but different

values of β_1 show the same tendency—point corresponding to lowe of β_1 shifting toward lower $S'M$ lines.

Also anything in the design of the pump casing that leads to the tion of NPSH value and an increase of specific capacity of the shifts test points to higher specific speeds and lower $S'M$ lines. 3.9, discussed later, furnishes illustrations to this deduction.

(*g*) Although equation (3.11) was originally established as an em relationship between NPSH and the inlet-velocity triangle, it is b that it has a theoretical background. Thus, for $M = 1.0$, equation shows that NPSH is equal to the area of the inlet-velocity triangle (Fig. 3.3) expressed in ft of liquid and representing the dynamic depr from the suction nozzle to the low-pressure zone. When this is ec NPSH, cavitation begins. A similar interpretation of the im discharge-velocity triangle area has been used in a previous publicati

(*h*) In all equations connecting the cavitation properties of in with its inlet-velocity triangle elements $R_1/\tan\beta_1 = u_1/c_{m1}$ always a as a ratio. For a given u_1 the value of c_{m1} is the same. Selection o desirable values of R_1 and β_1 is guided by considerations of efficienc NPSH requirements.

(*i*) The test results presented in the paper indicate that the cavi factor K_1 can be expressed in terms of a "criterion" $S'M$ (Fig. 3. dissimilar pumps. The practical use of this criterion is illustrated b

3.7 PPLICATION

In practice problems dealing with NPSH can be divided into groups:

1. Designing for a minimum NPSH within the prescribed ph limitations and with acceptable pump efficiency. For these $\beta_1 = 15$ de and $R_1 = 1.8$ are widely used by the industry. This leads to $S' \approx 1$ at bep. At partial capacities higher values of S' are realized. With pumps a reduction of capacity, increase in leakage, and effect o (Reynolds number) result in lower values of S' for the same valu β_1 and R_1.

2. Pumps designed for best hydraulic performance. For these usually selected equal to the impeller-discharge angle β_2 and $R = 1$, 1.25, and suction specific speed of about $S = 8000$ (single suctio obtained with this design. Special test on a 12-in. double-suction p has shown a gain of 1.5 points in efficiency when $R_1 = 1.85$ was cha to 1.35. On another 6-in. double-suction pump change of $R_1 = 1$.

3.5 EXPERIMENTAL RESULTS

Figure 3.4 represents a plot of equation (3.10*a*) for $M = 1.0$. Great many low NPSH pumps are of $S' \approx 13{,}000$. For these $M = 1.0$ and Fig. 3.4 gives $K_1 = 6.6$ for $R_1 = 1.8$ and $\beta_1 = 15$ degrees. For this group of

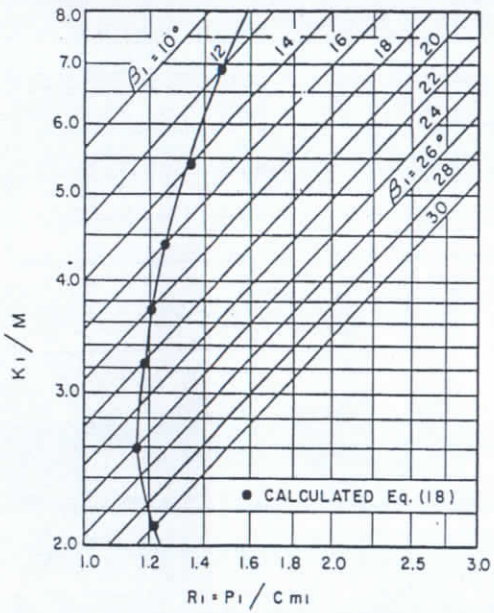

Figure 3.4 K_1 versus R_1 at bep (equation 3.10*a*).

pumps ($M = 1.0$), Fig. 3.5 gives NPSH in terms of u_1 and c_{m1} according to equation (3.11).

Figure 3.6 shows a plot of the test values of M for single-stage pumps of the end-suction type and double-suction pumps. For the latter group M values are plotted against the adjusted suction-specific speed (S') based on one-half of the measured capacity.

Figure 3.7 represents a collection of test values of M for multistage pumps with the hub ratio D_h/D_1 up to 0.765 plotted versus S'. On both figures the median drawn through the points is represented by $S'M = 13{,}000$ line. An analytical expression for $S'M$ in equation (3.12) can be obtained by substituting for $R_1/\tan\beta_1$ in equation (3.9) its value from equation (3.10*a*).

$$S'M = 8147K_1^{1/4}f^{1/4} \quad \text{or} \quad (S'M/8147)^4 = K_1 f^2 \qquad (3.14)$$

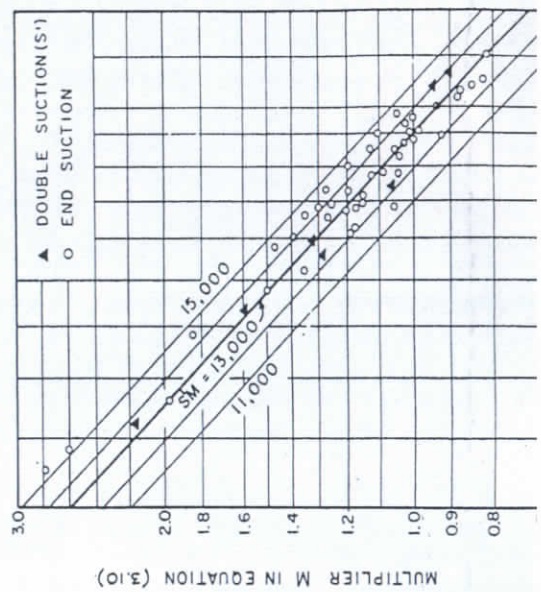

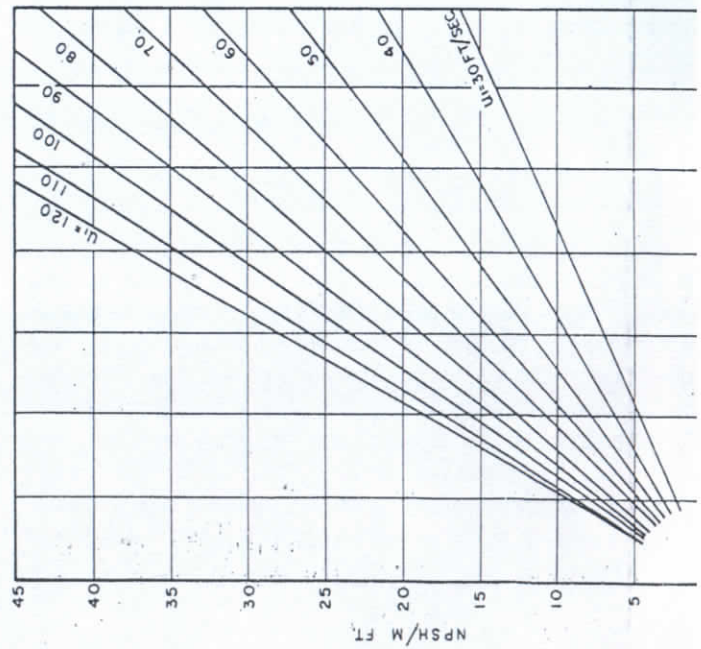

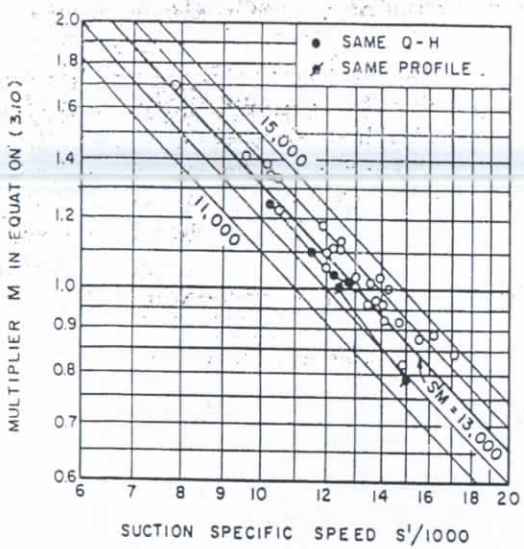

Figure 3.7 Multistage pumps.

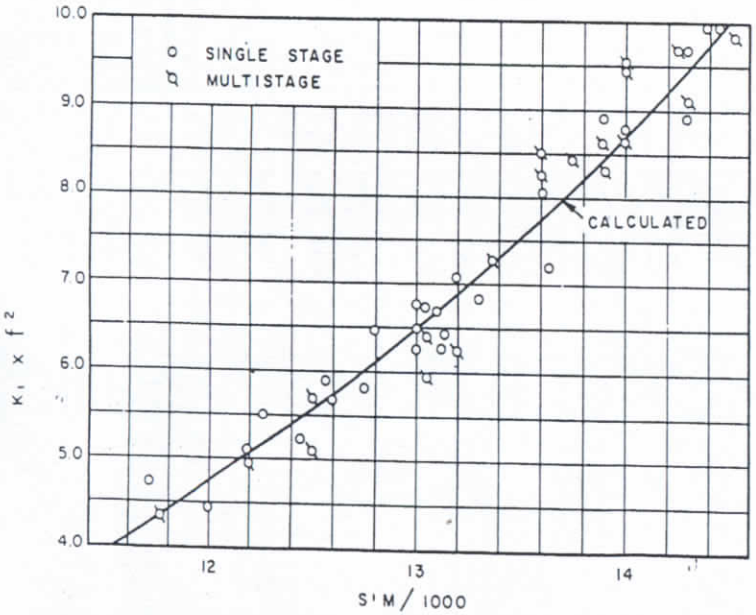

Figure 3.8 Single and multistage pumps (equation 3.14).

Figure 3.8 shows a plot of the test values of K_1 and actual valu against $S'M$. The solid line represents calculated values of $(K_1 f^2$ sidering that the values of f are selected rather arbitrarily in pract have no direct effect on the design elements represented in th velocity triangle the test points show a definite trend to line up al calculated line. For the majority of single-stage pumps represe Fig. 3.8 the value of f varied from 1.10 to 1.15. For multistage with large shafts through the eye the average value of $f = 1.2$ believed that when there are no physical limitations imposed the $f = 1.0$ is preferable, allowing some acceleration of the flow ente impeller channels.

3.6 DISCUSSION OF RESULTS

(*a*) Since equations (3.7) to (3.11) contain dimensionless ratios o follow affinity and Thoma's cavitation laws, thus are independent and size of pumps.

(*b*) There is ample experimental evidence that measured ca effects are observed when cavities appear in the vicinity of the i eye outside diameter (area *G* Fig. 3.2). For that reason the inlet triangles at the diameter D_1 were only considered. Such a pa events in the process of cavitation would suggest that the prese shaft through the impeller eye should not have any effect on the b of cavitation and NPSH requirements. This has been confirmed data on many multistage pumps having a hub ratio Dh/D_1 up t as is evidenced by the data on Fig. 3.7 as compared to that on

(*c*) The majority of the test points for this investigation were at or near the best efficiency points (bep). However, all formula applied to partial capacities down to, perhaps, one-half of the pacity. Since S in equation (3.9*a*) contains c_{m1} in the denomina M in equation (3.10*d*) has c_{m1} in the numerator their produc independent of c_{m1}. Figures 3.7 and 3.9 contain several poin along the same Q-H curve, all of which follow the general dire SM lines, S increasing as c_{m1} is decreased.

(*d*) Similarly it can be shown that impellers with different val follow the same SM direction, higher values of β_1 producing low of S. In Fig. 3.7 there are two points to illustrate this case. Not partial capacities the value of R_1 varies approximately inversel thus if $R_1 = 1.8$ at bep, $R_1 = 3.60$ at half-capacity.

(*e*) There are a number of pump design elements which do n into the development presented in this article. Among these the f

a higher value (18 degrees) is preferred. Reduction of β_1 below these values does not reduce NPSH values and may reduce the efficiency. A further reduction of NPSH is possible by reducing the radial velocity c_{m1} by increasing the impeller-eye diameter, which means higher values of the R_1 factor. However, this is done at the expense of pump efficiency. Values of $R_1 = 1.80$ are quite common and a value of $R_1 = 2.0$ is occasionally found in low NPSH pumps. The physical meaning of such values is that the impeller suction and inlet is designed for a larger pump and it is operated at partial capacities with a smaller output pump.

3.3 GENERAL NPSH EQUATIONS

The following equations enter into the development of the expression for NPSH in terms of the design elements: R_1 and β_1. From Fig. 3.3

$$R_1 c_{m1}/u_1 = \tan \beta_1 \tag{3.5}$$

$$c_{m1}' = f c_{m1} = \frac{\text{gpm} \times 0.321}{0.785(D_1^2 - D_h^2)} \tag{3.6}$$

Where D_h is the impeller-hub diameter, Fig. 3.2, c_{m1}' is the velocity through the eye, and $f > 1.0$ is a ratio of the area at impeller vane to the net impeller-eye area

$$f = \frac{D_m\, d\pi}{0.785(D_1^2 - D_h^2)}$$

Eliminating D_1 between equations (3.5) and (3.6) and rearranging we obtain

$$\frac{n\,(\text{gpm})^{1/2}}{(c_{m1}^2/2g)^{3/4}} = \frac{8147 R_1 F^{1/2} f^{1/2}}{\tan \beta_1} \tag{3.7}$$

where $F = 1 - D_h^2/D_1^2$ is the ratio of the free eye area to the gross impeller-eye area, $0.785 D_1^2$.

Solving equations (3.5) and (3.6) for D_1 and rearranging yields

$$\frac{\text{gpm}}{n D_1^3} = \frac{F f \tan \beta_1}{93.7\, R_1} \tag{3.7a}$$

Equation (3.7*a*) permits a direct determination of D_1 when R_1 and β_1 are selected.

Expressing NPSH in terms of c_{m1} at which cavitation appears we obtain

$$\text{NPSH} = K_1 c_{m1}^2/2g \tag{3.8}$$

where $K_1 > 1$ is a numerical constant accounting for the pressure drop from the suction nozzle to the low-pressure zone where cavitation appears.

Its value depends upon R_1 and β_1. Making use of equation (3.8) (3.7) can be given the form

$$S = \frac{n\,(\text{gpm})^{1/2}}{(\text{NPSH})^{3/4}} = \frac{8147 R_1 F^{1/2} f^{1/2}}{\tan \beta_1 (K_1)^{3/4}}$$

or making use of equation (3.4) gives

$$S = \frac{8147 F^{1/2} f^{1/2} u_1}{(K_1)^{3/4} c_{m1}}$$

Equations (3.9) and (3.9*a*) connect the impeller-inlet design (β_1, R_1, F, f) and the cavitation characteristics of the impelle K_1, S).

3.4 CAVITATION FACTOR K_1

From test data on a great many pumps of different performar speed, including axial flow pumps and inducers it has been f the cavitation factor K_1 in equation (3.8) can be conveniently by the following relationships:

$$K_1 = M \frac{R_1}{\tan \beta_1} \quad (a); \qquad K_1 = M \frac{u_1}{c_{m1}} \quad (b)$$

hence

$$M = K_1 \frac{\tan \beta_1}{R_1} \quad (c); \qquad M = K_1 \frac{c_{m1}}{u_1} \quad (d)$$

Then equation (3.8) takes the form

$$\text{NPSH} = M \frac{u_1 c_{m1}}{2g}$$

where M is a numerical multiplier for centrifugal impellers from the empirical relationship

$$MS/F^{1/2} = 13{,}000$$

For pumps of the overhung impeller construction $F = 1.0$. with the shaft through the eye

$$S/F^{1/2} = S'$$

where S' will be termed the "adjusted" suction-specific sp impeller having the same impeller-eye diameter D_1 and no sha the eye. It is assumed that capacity increases in direct rat increase, i.e., $1/F$, and the suction specific speed in the ratio 1/

3

Cavitation Criterion for Dissimilar Pumps

A method is presented of expressing Net Positive Suction Head for centrifugal pumps in terms of the impeller-design elements as they appear in the inlet-velocity triangle. The procedure is applicable to pumps of different specific speeds, of different suction-specific speeds, and to pumps having impellers of either the overhung type or with a shaft through the eye. The suggested relationship represents another "dissimilarity law" to supplement those discussed in Chapter 4.

3.1 DEFINITIONS AND FORMULAS

The hydraulic design of an impeller is completely determined by the inlet- and discharge-velocity triangles. To exclude the effect of size and speed these can be made dimensionless by using ratios of velocities to their respective peripheral velocities. Thus the impeller characteristics are really completely fixed by the impeller-vane angles and the absolute-velocity angles. Figure 3.1 shows an inlet-velocity triangle for the case of radial (meridional) inlet velocity c_{m1}. This is based on the measured capacity (gpm) plus leakage and with inlet area corrected for vane thickness. In practice, for simplicity, leakage and vane interference are neglected and the inlet velocity c_{m1} is determined from

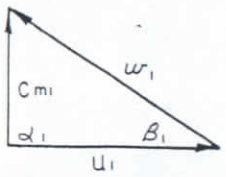

Figure 3.1 Inlet-velocity triangle.

$$c_{m1} = \frac{\text{gpm} \times 0.321}{D_m\, d\pi} \qquad (3.1)$$

where D_m and d are in inches and measured at the impeller-inlet vane edge (Fig. 3.2). To establish the inlet-vane angle the velocity c_{m1}

for normal design is multiplied by an experimental factor

$R_1 = 1.15$ for end suction
$R_1 = 1.25$ for flat elbow suction

The latter figure applies to double-suction pumps and horizontall multistage pumps with the suction nozzle shaped so that some prer

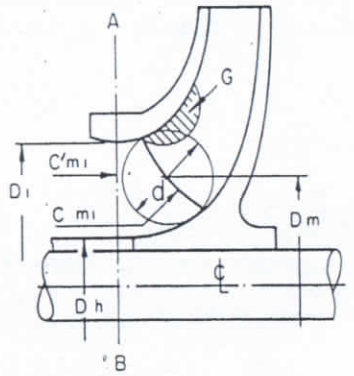

Figure 3.2 Impeller inlet.

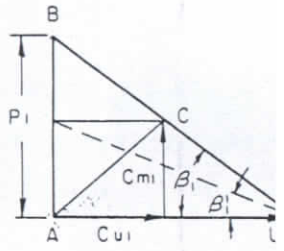

Figure 3.3 Inlet-velocity dia

is induced. Figure 3.3 shows the inlet-velocity triangle, where defined as

$$R_1 = \frac{P_1}{c_{m1}} \quad (a); \text{ or } \quad R_1 = \tan\beta_1 \frac{u_1}{c_{m1}} \quad (b)$$

or

$$R_1 = \frac{\tan\beta_1}{\tan\beta_1'} \quad (c)$$

hence

$$\frac{R_1}{\tan\beta_1} = \frac{u_1}{c_{m1}}$$

The numerical values of the constant R_1 given above apply to design for the best efficiency point with zero-incidence angle at t capacity. The gross area normal to c_{m1} as given by equation greater than the impeller-eye area in plane AB by about 10 per allow for the vane thickness.

3.2 MINIMUM NPSH REQUIREMENTS

It is a well-established fact that a low impeller-inlet angle β_1 ar large impeller-eye diameter D_1 leads to a minimum NPSH valu minimum practical value of the inlet angle is 15 degrees. For smal

PUMPS AND BLOWERS

Selected Advanced Topics

TWO-PHASE FLOW

Flow and Pumping of Solids in Suspension and Fluid Mixtures

A. J. Stepanoff
Ingersoll-Rand Company

ROBERT E. KRIEGER PUBLISHING COMPANY
Huntington, New York
1978

$$D_2 = \frac{K u_2 \times 1840 \sqrt{H}}{rpm}$$

4. R. S. Quick, "Comparison and Limitations of Various Water-Hammer Theories," *Mech. Eng.*, Vol. 49, pp. 524–530, 1927.
5. Lorenzo Allievi, "Air Chambers for Discharge Pipes," *Trans. A.S.M.E.*, Vol. 59, p. 657, 1937.
   Louis Bergeron, Discussion, *Trans. A.S.M.E.*, Vol. 61, p. 444, 1939.
6. L. Bergeron, "Étude des coups de belier dans les conduits," *Tech. mod.*, Vol. 28, No. 2, p. 33, January 1936; also, *ibid.*, Vol. 27, No. 5, pp. 8–20, 1935.
7. "Flywheel on Pumps Soft-Pedals Pipe Line Surges," *Power*, Vol. 84, p. 57, January 1940.
8. E. Bruce Ball, "Methods Employed to Remedy Water Hammer, Etc.," *Trans. A.S.M.E.*, Vol. 61, p. 6, 1939.
9. R. W. Angus, "Water-Hammer Pressures in Compound and Branched Pipes," *Trans. A.S.C.E.*, Vol. 104, p. 340, 1939.
10. Joseph N. Le Conte, "Experiments and Calculations on the Resurge Phase of Water Hammer," *Trans. A.S.M.E.*, Vol. 59, p. 691, 1937.
11. Vance C. Lischer, "Water Hammer," *J. Am. Water Works Assoc.*, Vol. 29, No. 3, pp. 343–361, March 1937.
12. A. J. Stepanoff, "Elements of Graphical Solution of Water-Hammer Problems in Centrifugal Pump Systems," *Trans. A.S.M.E.*, p. 515, July 1949.
13. J. Parmakian, "Pressure Surges at Large Pump Installations," *Trans. A.S.M.E.*, Vol. 75, p. 995, 1953.
14. L. Bergeron, *Du coup de belier en hydraulique au coup de foudre en électricité*, Paris, Dunod, 1950.
15. R. M. Peabody, "Typical Analysis of Water Hammer in a Pumping Plant of the Colorado River Aqueduct," *Trans. A.S.M.E.*, Feb. 1939.
16. J. Parmakian, *Water-Hammer Analysis*, New York, Prentice-Hall, Inc., 1955.

Index

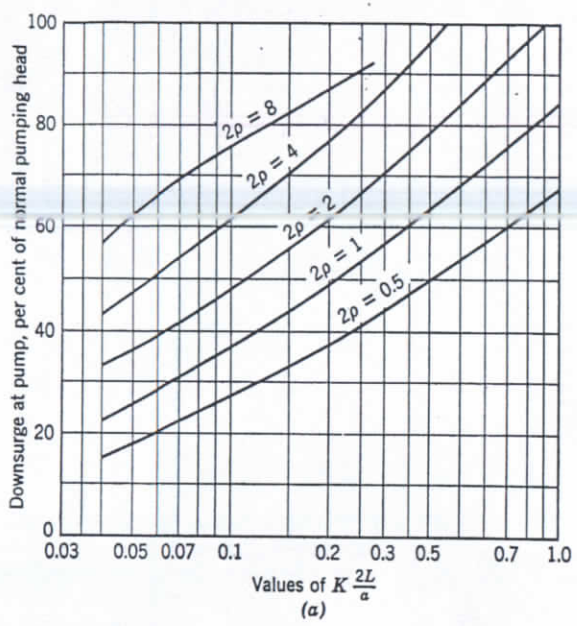

FIG. 19.20. Water-hammer effects in pump discharge lines due to a power failure at the pump motors.

exact determination of the maximum pressure rise is required. Mer recognition of the existence of conditions leading to water hammer i sufficient to arrive at a procedure of starting or stopping a pump, o providing the discharge valve controls to avoid objectionable pressur rise in the case of power failure.

(e) Water-Hammer Chart. For an approximate determination o pressure rise and drop, in the case of power failure when no control valve are present at the pump, Parmakian [13] has prepared a chart, reproduce on Fig. 19.20. This chart represents results of a large number of water hammer solutions based on the data appearing on Fig.13.2 for the pump performance outside its normal operating zone, since such information was not available for the pumps considered. The pressure rise above the normal head and the pressure fall below the normal are given in per cen of the normal head in terms of two parameters ρ and $K\mu$ defined below

$$2\rho = \frac{aV_0}{gH_0} = \frac{h_{max}}{H_0} \tag{19.20}$$

where a is velocity of the pressure wave in feet per second.
V_0 is initial pipe velocity in feet per second.
H_0 is initial pumping head in feet, mostly static.
h_{max} is defined by equation 19.1.

The parameter used as the abscissa contains a factor K defined as follows

$$K = \frac{810{,}000 \times (\text{bhp})}{WR^2(\text{rpm})^2} \tag{19.21}$$

where bhp is brake horsepower at the initial operating conditions.
WR^2 is moment of inertia of the rotating element including pump and motor, in terms of weight, pound-feet^2.
μ is the interval of time for the pressure wave round trip, $\mu = 2L/a$, where L is pipe length in feet.

The pressure rise and fall at the middle of pipe line are approximately one half of the values at the pump as given by the chart.

REFERENCES

1. S. Logan Kerr et al., "New Method for Bulk Modulus Determination," *Trans. A.S.M.E.*, Vol. 72, p. 1143, 1950.
2. Lewis F. Moody, "Simplified Derivation of Water-Hammer Formula," *Symposium on Water Hammer*, New York, A.S.M.E., p. 25, 1933.
3. E. B. Strowger, "Water-Hammer Problems in Connection with Design of Hydroelectric Plants," *Trans. A.S.M.E.*, Vol. 67, pp. 377, 389, 1945.

When started with the discharge valve closed and the discharge pipe (20 in.) air- or steam-filled, a violent shock was produced which resulted in a bent 4-in. pump shaft. The difficulty was eliminated by starting the pump with the valve partly open and the shaft rotating in the reverse direction. For an average installation filling the discharge column with liquid (priming) is sufficient to eliminate dangerous water hammer during the starting operation. Stopping of vertical turbine open-impeller pumps used for deep-well service is always followed by pressure surges which cause the impellers to hammer against their seats while revolving backward. It is impossible to maintain close running clearances between the impeller and the casing under these conditions. Introduction of non-reversing clutches in connection with hollow-shaft motors eliminated impeller grinding but not the surges and vibration.

Stopping of pumps with the discharge valve open (automatic or due to power failure) may produce objectionable water hammer which may damage the check valve, loosen the bell-and-spigot lead joints, cause stuffing-box troubles or endanger other equipment connected to the discharge system. Sometimes noise and vibration alone, due to check slamming, may be objectionable. It is common belief that water hammer is accompanied invariably by a clearly audible blow. Severe surges have been observed when a high pressure rise was built up after the valve had closed quietly.

(*b*) **Water Hammer Originated by the System.** In certain types of systems such as hydraulic descaling systems on strip mills, hydraulic presses, refinery loading stations, and boiler-feed installations, the delivery from centrifugal pumps may be shut off suddenly while the pump is running. Destructive water hammer will result if no precautionary measures are provided by the installation. In the case of descaling and hydraulic-press systems, pneumatic accumulators serve as protective air chambers.† With long suction lines, air chambers are also used on the suction to prevent breaking the water column at the pump suction. A by-pass from the discharge pipe to suction (or atmosphere), while protecting the pump from overheating at zero discharge, also alleviates the hydraulic shock. Open-impeller pumps of the vertical-turbine type enclosed in a suction barrel, when used for petroleum-products loading service, are particularly vulnerable to hydraulic shock. In several instances pump shafts were bent (by compression) and the pump-discharge piping (cast-iron increaser) was ruptured as a result of sudden

† It should be pointed out that the friction in the system and not the cushioning effect of the air chamber is primarily responsible for the reduction of pressure in the pipe. For systems with little or no friction the air chambers are a very ineffective means of protection against water hammer.[12]

closure of the discharge valve. Closed impeller pumps having a axial play between the rotating element and the casing are better s for services where hydraulic shocks are expected.

Instances in which volute pumps with closed impellers deve cracked casings when used on loading service are numerous. A su rupture of the discharge pipe produces the same effect as a sudden opening, resulting in a high pressure rise, as discussed previously.

(*c*) **Means to Reduce Water Hammer.** The pressure rise ca reduced only by reduction of the rate of velocity destruction in the This can be accomplished by one or several of the following means

1. Designing pipe systems with low original velocities.
2. Positively controlled valves combining functions of both a and gate valve. The slower the closing rate, the less is the resulting sure rise. Loss of water and reverse rotation of pumps are seldon jectionable.
3. Use of special check valves such as "balanced," and "loaded," by-pass around a check valve which can be closed slowly (manual automatically) after the check valve is closed.
4. Use of air chambers, accumulators, or surge tanks. The latte the most expensive and hardly ever justified under ordinary cir stances.
5. Relief valves are widely used for protection of various typ hydraulic equipment. When provided with a positive control, thes known as surge suppressors.
6. When water-column parting is unavoidable in a pipe line, vac breakers are installed to admit air which cushions the shock when th parts of the water column join together.

(*d*) **Remarks.** The graphical solutions of water-hammer prob are just as accurate as the analytical solutions. There are numerou perimental proofs of the soundness of the basic water-hammer th The irregular shape of pressure-rise curves plotted from theore calculations was reproduced with surprising accuracy by accurate re ing instruments. The accuracy of solutions depends entirely upo accuracy of the information about the rate of flow during the v closure time and the information necessary to establish the sy characteristics. A clear visualization of the sequence of events lea to water hammer and the mechanism of the pressure wave propag and reflection are essential for the intelligent application of the grap (or analytical) method of solution of water-hammer problems. drawing of the diagram then becomes a simple mechanical proce

In the field of centrifugal pump application it is not often tha

height of the peak and time spacing between the peaks is reduced as the energy of the water column is wasted. Such curves were obtained experimentally by Le Conte.[10]

From the inspection of Fig. 19.19(*b*) it is evident that the maximum pressure rise at time $t = 4\mu$ is approximately equal to the pressure rise

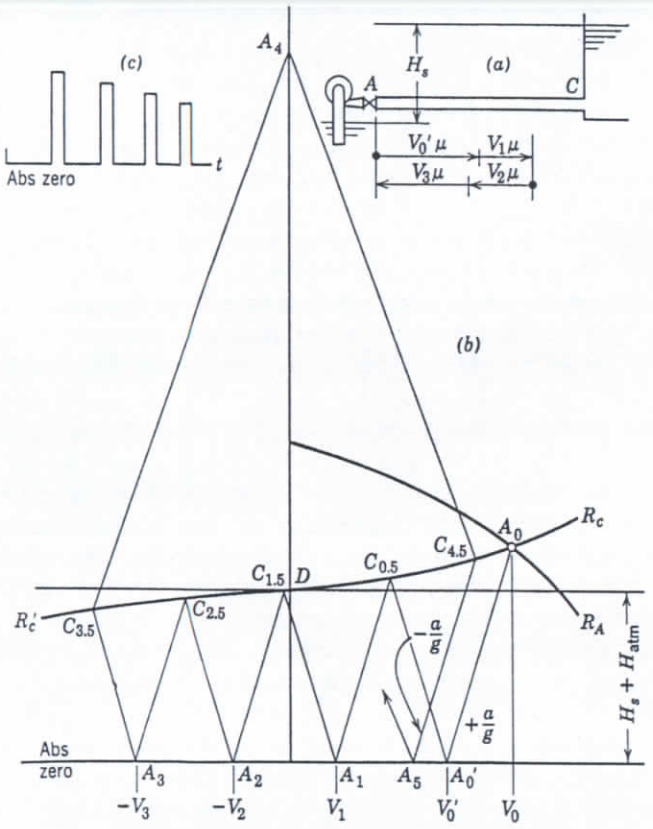

FIG. 19.19. Parting of water column.

due to a sudden destruction of the initial velocity V_0, reduced only by hydraulic losses during the first cycle of events. For a frictionless flow the maximum pressure rise will be exactly equal to that due to a sudden extinguishing of the original velocity V_0. The maximum velocity in the reverse direction will be exactly equal to V_0, and the time of recoil of water column would be exactly the same as the time to retard the water column to zero from its original velocity V_0. This is because the reverse flow is produced by the force due to a pressure $H_s + H_{atm}$ which is the same force that caused the deceleration of the initial flow in the pipe.

The kinetic energy of the water column in the pipe is converted into th energy of position at the level $H_s + H_{atm}$ during the deceleration of th initial flow, which is converted back into the kinetic energy of the flo in the reverse direction during the second half of the cycle. If the instan of the closing of the vacuous space does not coincide with the end of on complete interval, the shape of the pressure-rise peaks in Fig. 19.19(c becomes irregular. If the valve is closed gradually in a time less tha one interval μ, the same pressure rise will result, but the curve become sharp-pointed.

Admission of air at point A in Fig. 19.19 will limit the pressure dro to atmospheric pressure. This will increase the deceleration time an time of recoil of the water column, because the force on the column i that due to static head H_s only. The air cushion will further delay th joining of the water columns and thus reduce the pressure rise again.

Lischer [11] reports damage to three cast-iron pipes, 20, 24, and 36 in leading from the pumping plant to the reservoir over the crest of a hi as a result of water column parting at the top of the hill each time th power supply failed. After quick-opening–slow-closing air valves wer placed at the top of the hill and quick-opening and slow-closing reli valves installed near the pumping station, no failures occurred.

Since the decelerating and accelerating force in Fig. 19.19 ($H_s - H_{atm}$) is constant, one might expect that the velocity change should b gradual, as Newton's law for a rigid body states

$$\text{Force} = \text{mass} \times \text{acceleration}$$

However, in the case of a solid body, force is applied instantaneously t the whole body (mass center) and, since the mass remains constant, th body will move with ever-increasing velocity. While with a compressibl mass, like water, there is no mechanism by which a force can be applie to the mass center (or to the whole mass instantaneously), therefore th acceleration or velocity change occurs in jumps of ΔV each interval time μ, while the same increment of velocity is applied to an ever-increa ing mass of water along the pipe at a rate equal to the velocity of soun

19.5 EXAMPLES OF WATER-HAMMER DAMAGE

(*a*) Starting and Stopping Pumps. Water hammer caused by cer trifugal pumps themselves can take place in the process of stopping an starting them. Vertical turbine pumps with open impellers running i close vertical clearances with the casing seat furnish examples of dan age to a pump by water hammer. In one case, a vertical pump of th type was used to circulate hot molten salt in an oil-refinery proces

damage are on record.[8] The author knows a number of cases where pump casings cracked on gasoline loading pumps because of a sudden closure of a quick-closing valve at the end of the discharge pipe. In several cases vertical turbine pumps (in a suction barrel), used for a similar service, developed buckled shafts (by compression) in addition to cracked discharge nozzles, thus indicating a higher pressure in suction than in discharge. Angus [9] mentions cases in which the entire rotating element of a hydraulic turbine has been lifted by the pressure rise in the draft tube, which corresponds to the suction of centrifugal pumps.[3]

Suction pipes, including the pump up to the discharge flange, can be investigated for water hammer in the same manner as that used for discharge pipes. The end conditions are fixed by the system characteristics. The suction level for the intake end of the suction pipe (point S in Figs. 19.11, 19.17, and 19.18) and the other end (A in these figures) is common for both the suction pipe (including pump) and the discharge pipe; thus the same characteristics apply. The starting point A_0 is given by the initial conditions and is also common for both pipes.

Evidently, if the object of a study is a determination of the maximum pressure rise, there is no need to draw a water-hammer diagram for the suction pipe because the maximum rise will appear in the discharge pipe. However, the pressure rise produced on the discharge end of the pump will travel through the pump casing and into the suction pipe (reduced only by hydraulic losses) when not prevented by a check valve or positively controlled valve. In the case of a sudden valve closure, Fig. 19.18, the pressure rise C_1' will travel the full length of the suction pipe undiminished (except for hydraulic losses), the duration of supernormal and subnormal pressure decreasing from μ sec at C to zero at the free end of the suction pipe. Reference to Fig. 19.2 will illustrate the point. Note on this figure that, at certain times (for instance μ to 1.25μ), the pressure at a point C', the point most removed from the valve A, is higher than at the valve by the amount of the full pressure rise h. This may help to visualize how pressure at the pump suction, with pump running, can be higher than at the pump discharge if the pressure rise is higher than the pump generated head. If the discharge valve at C, Fig. 19.18, is closed gradually, the pressure rise in the suction pipe and the pump casing will be lower than at the valve (see Fig. 19.3), depending upon the relative length of the suction and discharge pipes.

When the subnormal pressure wave passes through the pump it may reduce the pressure at the impeller eye to the vapor pressure, thus producing a cavity. If this occurs a severe blow can develop upon arrival of the supernormal pressure wave which would cause an instantaneous collapse of the vapor cavity in the same manner as that during cavitation.

Formation of the cavity will interfere with the propagation of press waves, thus complicating matters considerably. Cavitation and part of the water column may also take place on the discharge side of pump if the topography of the pipe layout is such that the subnorr pressure wave is greater than the absolute pressure (above the va pressure) at some points on the pipe line. Bergeron [5] and Angus [9] g graphical solutions for such systems, but experimental verification results is lacking. The sequence of events and the manner in which high pressure rise appears under cavitation conditions are illustrated the example which follows.

(b) Parting of Water Column or Cavitation. Suppose in a syst as shown in Fig. 19.19(a), the valve at the discharge flange A is sudde closed, and we want to investigate water hammer in the discharge pi On the diagram, Fig. 19.19(b), A_0 is the initial operating point, and is the initial pipe velocity. The sudden valve closure will cause a sud pressure drop at A to absolute zero (vapor pressure) and a sudden vel ity drop from V_0 to V_0', as determined by the slope coefficient a/g the line A_0A_0'. From that instant to the time $t = \mu$, water will conti to move at A with a velocity V_0' and the column moves a distance V_0 leaving a vacuous space $V_0'\mu$ long. At time μ the velocity at A dr suddenly to V_1, and water will continue to move away from the va an additional length $V_1\mu$. Velocity V_1 is determined by the surge li $A_0'C_{0.5}A_1$ drawn in the usual manner. However, in the case of a sud valve closure the physical meaning of these surge lines is different; th do not represent the pressure variation along the pipe line, as press travels undiminished, and pressure and velocity changes occur sudden But the surge lines give a time scale for the velocity variation during retardation time and the acceleration of the water column in the oppos direction (toward the valve). At time $t = 2\mu$, the velocity at A change suddenly from $+V_1$ to $-V_2$ and the water column will start m ing toward the valve. At time $t = 3\mu$, the vacuous space between valve and water column will have been reduced by the length $V_2\mu$. Al at time $t = 3\mu$, the velocity will increase suddenly from $-V_2$ to $-V_3$, a the vacuous space will be reduced by an additional length $V_3\mu$ dur the fourth interval of time. It is assumed, for simplicity, that vacuous space is reduced to zero exactly at time $t = 4\mu$ when veloc $-V_3$ is suddenly arrested, causing a pressure rise to A_4 following surge line $A_3C_{3.5}A_4$. This pressure will prevail at A for μ sec, then fall suddenly to A_5, after which the cycle will repeat itself at redu velocities until all the energy in the water column is absorbed by the draulic losses, and the final point for settled conditions is reached at The pressure variation at A with time is shown in Fig. 19.19(c). T

pump running in the reverse direction at zero torque; R_{V1} is the valve resistance curve at time μ, R_{V2} is the same at time 2μ. At time 3μ the valve is completely closed. In order to construct the surge diagram, the

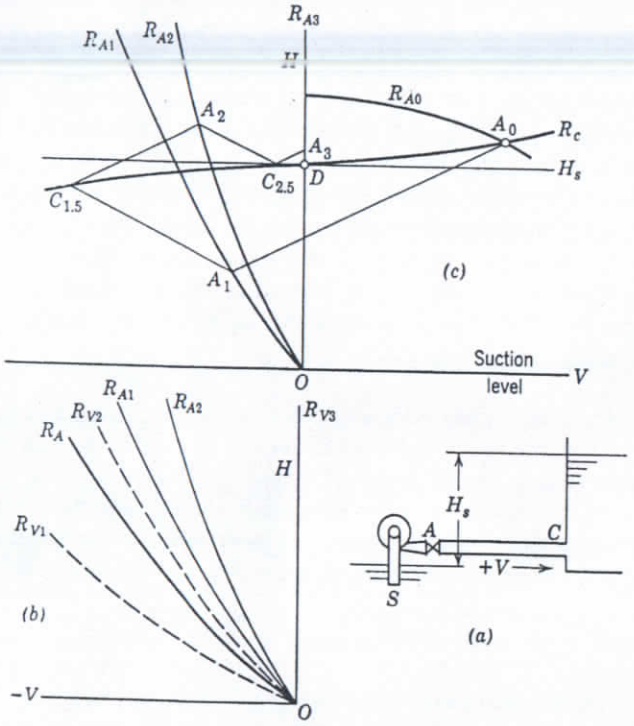

FIG. 19.17. Positively controlled valve closure.

system characteristics are drawn for time μ and time 2μ by combining R_{V1} and R_A, and R_{V2} and R_A, to obtain R_{A1} and R_{A2} respectively. R_{A3} coincides with the axis of heads. In Fig. 19.17(*c*) the surge characteristics are then drawn following the usual procedure. Points A_0, A_1, A_2, A_3, $\cdots D$ give pressures at A at one interval of time spacing.

(*b*) **Valve Closure at End of Discharge Pipe.** In Fig. 19.18 a centrifugal pump at A delivers water against a static head H_S to the tank at C. The pipe resistance characteristics R_{C0} determine the operating point C_0. Now suppose the valve at C is closed in a time $t = 3\mu$, while the pump is running. The system characteristics for the point C with the valve throttled at times μ, 2μ, and 3μ are R_{C1}, R_{C2}, and R_{C3} respectively. The pump characteristic for positive flow will remain R_{A0} and for negative flow it is represented by R_{A1}. The surge characteristic $A_{0.5}\ C_1$

$A_{1.5}\ C_2\ A_{2.5}\ C_3$ is drawn in the usual manner, the maximum pressu rise being at C_3. If the valve at C is closed in a time $t \leq \mu$, the surg characteristic will be $A_{0.5}\ C_1'\ A_{1.5}'\ C_2'$ as shown by the dotted line.

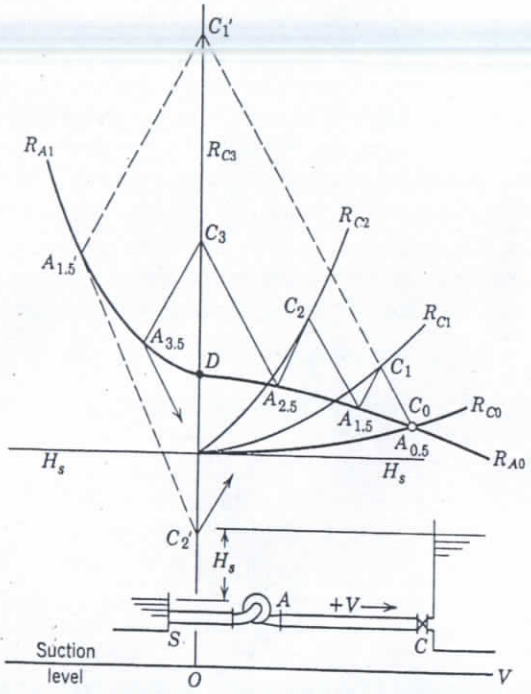

FIG. 19.18. Valve closed in $t = 3\mu$ (full line); sudden valve closure, pump runnin (dotted line).

19.4 SPECIAL PROBLEMS

(*a*) **Water Hammer in Suction Pipe.** In all examples thus far con sidered, attention has been confined to water hammer in the discharg pipe between the points A at the pump-discharge flange and C at the open end of the pipe, as in Figs. 19.11, 19.17, and 19.18. However, al velocity changes in the discharge pipe are followed by a corresponding velocity change in the suction pipe; thus water hammer is also produced in the suction pipe and pump casing.

Mechanically, the suction pipe and pump casing may be the most vulnerable parts of the whole installation. It is not often that long suction pipes are used and, as a rule, suction velocities are lower than those in the discharge pipe. Thus dangerous pressure rises due to water hammer in suction pipes are not frequent. However, cases of suction-pipe

retardation and reversal of the pump speed in event of power failure to a time greater than one interval of time μ. The author knows of instances when centrifugal pumps were provided with flywheels so that in case of electric power failure a steam turbine could take over the load with a minimum drop of the discharge pressure. In this case, at the end of the first interval, the pump characteristic will be a regular head-capacity curve at a reduced speed (R_{A1}, Fig. 19.15). Several such characteristics

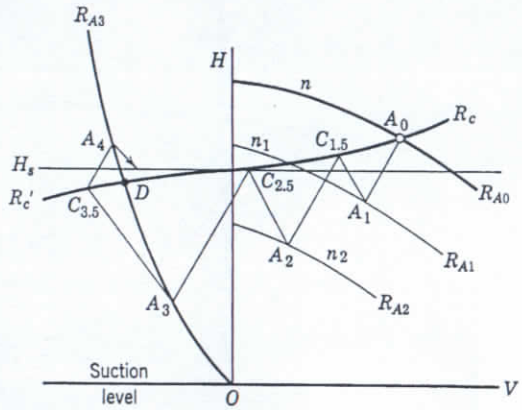

FIG. 19.15. Pump with flywheel effect; arrangement of Fig. 19.11(*a*).

may be drawn at speeds corresponding to times μ, 2μ, etc., from the instant of power failure.

To draw such characteristics, pump speeds at times μ, 2μ, etc., are determined from the relationship

$$T_0 = I\frac{\delta\omega}{\delta t} \tag{19.19a}$$

Torque T_0 is known at the time $t = 0$; I is the moment of inertia of the revolving mass, including the motor rotor;* $\delta\omega$ is the increment of angular velocity reduction during an increment of time δt. Using $\delta t = \mu$, $\delta\omega$ is determined and thus the speed n_1, at time μ is established. The pump characteristic R_{A1} at speed n_1 is drawn. Point A_1 is determined and torque T_1 can be calculated. The pump speed at time 2μ can be determined in the same manner and lines $A_1C_{1.5}$ and $C_{1.5}A_2$ are drawn.

The pump will reach the zero speed point between times 2μ and 3μ. After that the pump will run in a reverse direction, gradually increasing its speed and always remaining on its zero torque characteristic R_{A3}.

* Note that motor manufacturers usually give WR^2 of the motor rotor in lbs-ft^2; this should be divided by 32.2 to obtain (mass) ft^2 which has dimensions (lb-ft sec^2).

The rest of the diagram is drawn in the same manner as in the first ample.

If more points for a pressure-time curve at the pump are wanted head-capacity curves are drawn for $\mu/2$ intervals and the pressure of two pressure waves is observed; one starting from A at time t and the other at time $t = \mu/2$. Two pressure waves will furnish po of pressure rise at A and C at $\mu/2$ intervals of time.

As a means for reduction of pressure rise, the use of a flywheel is very effective. For instance, in one case, an 800-hp, 1200-rpm pum unit having a WR^2 of 1450 lb in.^{2} and delivering 9400 gpm at 284 ft in 42-in. pipe 900 ft long reversed in 0.8 sec and produced a pressure ris 108 ft. When supplied with a flywheel with $WR^2 = 5500$, the tim reversal increased to 2.42 sec, and the pressure rise reduced to 48 Thus, to reduce the pressure rise to 44.5 per cent, the moment of ine of rotating mass (WR^2) had to be increased 3.8 times.

(*f*) **Valve Opening.** Figure 19.16 shows a water-hammer diagram a pump started with the discharge valve closed, and then the v

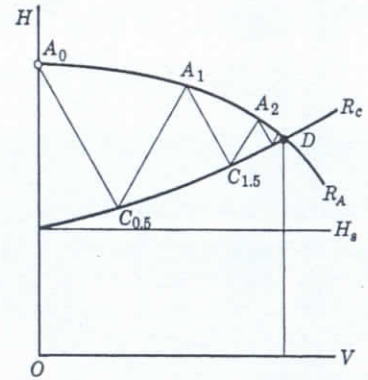

FIG. 19.16. Sudden valve opening.

suddenly opened. The surge diagram is drawn starting from the p A_0 and zigzagging between the pump characteristic R_A and the characteristic R_C until the final point D is reached.

(*g*) **Positively Controlled Valves.** To avoid surge pressures du a sudden check valve closure when a pump is shut off or when the po fails, valves with automatically controlled closure time are used. most advantageous valve-closing time can be established from a st of the water-hammer diagrams.

In Fig. 19.17(*a*) the pump at A discharges against a static head H_S pipe-line resistance R_C. In Fig. 19.17(*b*), R_A is the characteristic of

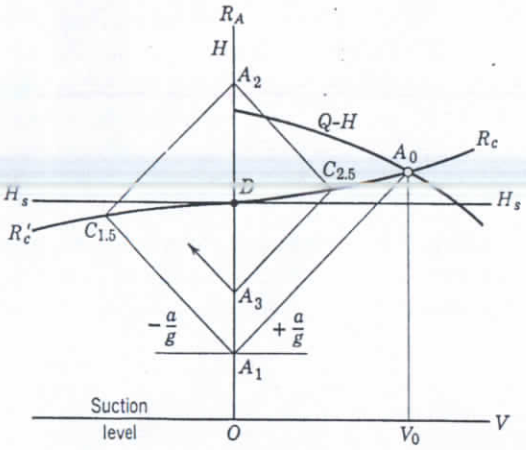

FIG. 19.12. Power failure with a check valve.

Depending on the value of a/g, the surge characteristic A_0A_1 may intersect the axis of velocities before it does the axis of heads, Fig. 19.13. This means the pressure has dropped to the pump suction pressure and cannot drop any lower as the check would open and let water flow through

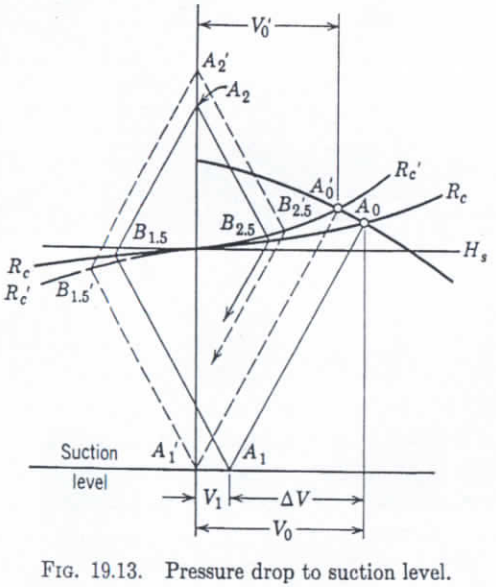

FIG. 19.13. Pressure drop to suction level.

the pump. At the end of the first time interval μ only part of the original velocity ΔV is destroyed, and the flow will continue with a velocity V_1 in the same direction. The check valve is still open. Con-

struction of the rest of the diagram is evident from the figure. Note tha a greater pressure rise is obtained if the pump operates at a lower origina velocity $V_0{}^1$, because the velocity destroyed is greater, being a maximur when A_1' coincides with the zero head-capacity point. In that case th whole original velocity V_0' is destroyed.

(*d*) Relief Valves and Surge Suppressors. A surge suppressor con sists of a special relief valve of adequate capacity arranged to open at predetermined rate under conditions which would produce a surge an before check-valve closure, after which the relief valve slowly close

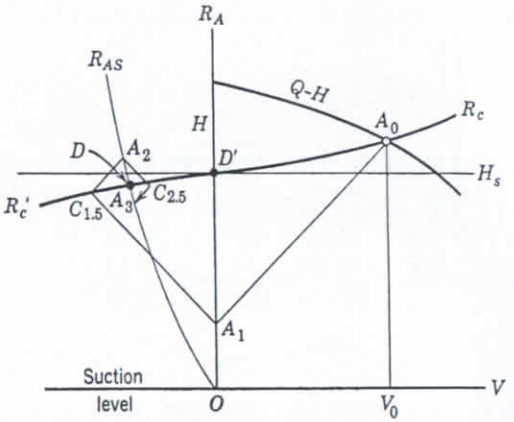

FIG. 19.14. Pump with a check valve and surge suppressor.

Surge suppressors may be arranged to be actuated hydraulically, m chanically, or electrically. A number of installations were equipped wi surge suppressors, partly to prevent reverse rotation, partly to redu the pressure rise in the pipe in case of power failure. The method operation of the surge suppressor will be illustrated in the example Fig. 19.14, showing a pump with a check valve and surge suppress The system curve of the surge suppressor is shown by a parabola R_A The suppressor is set to open at a time between μ and 1.5μ. The A_0 $C_{1.5}$ part of the surge characteristics is drawn in the same manner as Fig. 19.12. Point A_2 is placed on the parabola R_{AS}, so is A_3. In th way the pressure rise is almost entirely eliminated. After the flo settles at the point D, the surge suppressor is gradually closed and t final point of the system moves from D to D' on the axis of heads.

In recent installations positively controlled valves combine the fun tions of both a check valve and a surge suppressor.

(*e*) **Flywheel Effect.** If the pump in the first example has an a preciable rotating mass, the inertia of the rotating element will delay t

pump. In event of power failure assume that the pump will slow down, stop, and reverse in less than one interval of time, μ. The pump will then operate as a hydraulic turbine under head H_s at runaway speed. The pump characteristic under these conditions is R_{A1} and the operating point for final equilibrium is D. Prior to the power failure, the system

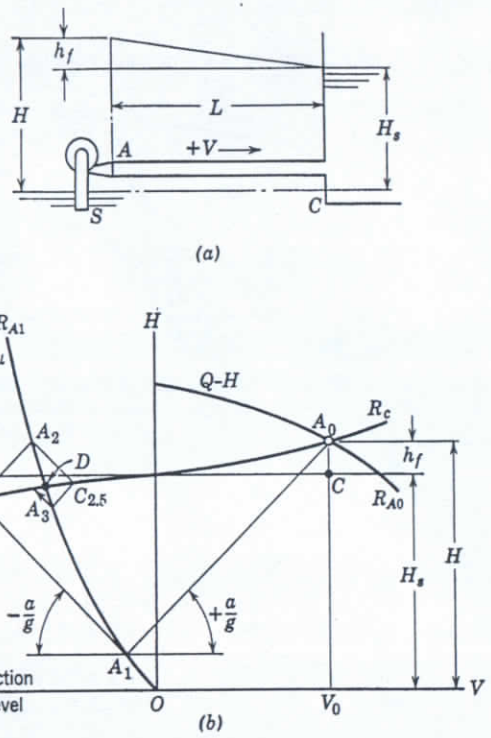

FIG. 19.11 (*a*) and (*b*). Power failure without a check valve.

curves are the pump head-capacity curve R_{A0} and the pipe resistance curve R_c, which fix the operating point A_0. The pipe velocity V is used to represent capacity. At the instant of power failure and for one interval of time, the pressure and velocity at point A drop. Starting with the point A_0 the surge characteristic is drawn with a slope $+a/g$. The surge velocity a is calculated by means of equation 19.4.

The pump will stop and reverse in a time of one interval μ (or less), after which the pump characteristic becomes R_{A1}, and all points for A on the diagram lie on this curve.

The first point is given by intersection of R_{A1} with the surge characteristic A_0A_1.

After the pump reversal, the velocity in the pipe is negative and the characteristics for the point C are given by the curve R_c'.

All points for C on the diagram for different times will lie on the R_c' characteristics.

The procedure in drawing the surge diagram is as follows:

1. The pressure drop at point A for one interval of time μ is drawn (line A_0A_1).
2. After that, pressure variation of one particular pressure wave, that leaving point A at time μ, is followed as it travels from A to C back and forth, changing its direction at points A and C.
3. The slope of the surge line is negative or $-a/g$ when the pressure wave travels in the direction of the original flow (from A to C), and the slope a/g becomes positive when the pressure wave is traveling in the opposite direction.
4. Thus from point A_1 a line is drawn with a slope $-a/g$ to intersect curve R_c' at point $C_{1.5}$ and to represent the pressure rise as the pressure wave moves from A to C. From $C_{1.5}$ draw a line $C_{1.5}A_2$ to intersect curve R_{A1}, and so on.

Experience has shown that, even with little or no pipe friction, no dangerous pressure rise occurs. With a long suction pipe its resistance should be added to the pump characteristic for the reverse flow R_{A1}, making it steeper. This will result in a higher pressure rise in the system.

(*b*) Level Receding in Tank. If the static level in the tank C is receding as the flow is reversed in the pump, the levels at times 1.5μ, 2.5μ, etc., should be known or estimated, and system characteristics for the point C are drawn for times 1.5μ, 2.5μ, etc., using different characteristics each time the pressure wave reaches point C. Otherwise the procedure remains the same as in the foregoing example.

(*c*) A Check Valve at Pump. If the check valve closes instantaneously, no water can flow past it. This means that the system characteristic R_A for the point A coincides with the axis of heads, Fig. 19.12. The surge characteristic $A_0A_1C_{1.5}A_2C_{2.5}$, etc., is drawn as in the previous example, and the operating points (pressures at A and C) are obtained as intersections of the surge characteristics and the system characteristics. If the check valve fails to close fast enough to prevent back-flow through the pump, the surge line A_0A_1 is extended to the left to intersect a parabola of the combined characteristics of the pump running backward and the check valve partly open, and higher pressure rise will result.

will rise during a complete interval μ, and will reach the point $A_3{}^1$ along the dotted line $A_2{}^0A_3{}^1$ which is higher than the maximum pressure rise previously obtained. When starting from wide open (A_0), the pressure rises during a complete interval μ (A_0A_1) but the slope of the parabola μ is such that the pressure rise is lower than for closure from any intermediate position.

(e) Effect of Pipe Friction. There are several methods used to take care of pipe friction loss in the graphical solutions of water-hammer problems. All are approximate but sufficiently accurate for the determination of maximum pressure rise at one of the extremities of the system:

1. In the problem shown in Figs. 19.5(*a*) and (*b*), suppose the pipe friction loss from A to C is h_f, Fig. 19.9. This plotted against velocity in

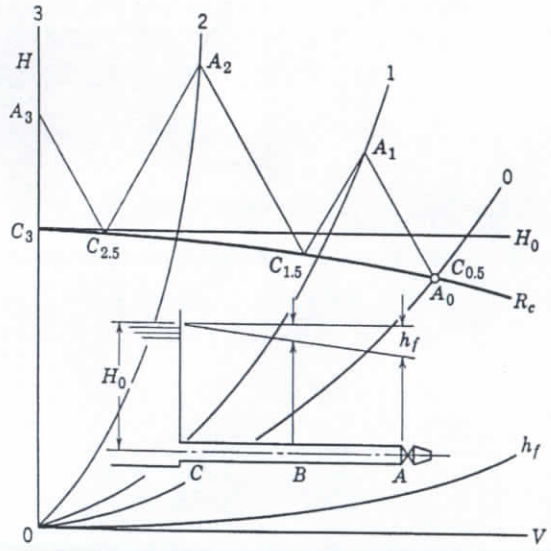

FIG. 19.9. Pressure rise with friction allowed at C.

the pipe is represented by the curve h_f. In one method (Schnyder's) the pipe friction loss is subtracted from the system characteristics H_0 for the point C, and the resultant (curve R_c) is used for the construction of the surge diagram as shown in Fig. 19.9. This method is equivalent to an assumption that all pipe friction is concentrated at point C (for instance, a local obstruction).

2. In the second method it is assumed that all friction loss is concentrated at the valve at point A. This means that pressures on all system curves for A (parabolas 0, 1, 2, $\cdots$, Fig. 19.10) are raised by the amount

of friction to produce the same velocities (curves 0′, 1′, 2′). Using these new system curves for A and H_0 = const for the point C, the diagram is completed following the same procedure. This method in essence is the same as that used by Bergeron.[5,6]

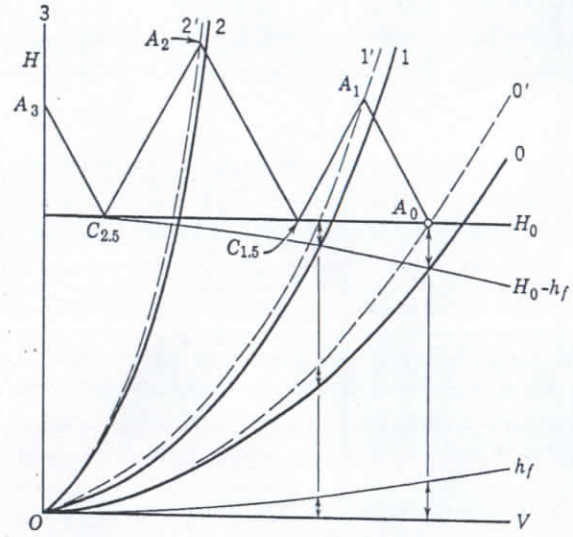

FIG. 19.10. Pressure rise; all friction at valve A.

For an established flow, or a given initial pipe velocity, if the valve is closed suddenly or in a time less than one interval, the pressure rise will be the same with or without friction. However, for a fixed head the initial velocity will be smaller, and the initial pressure at the valve lower. For a valve closure in a time greater than one interval, some of the energy will be consumed by pipe friction during each round trip of the pressure wave.

Placing all friction loss at one end of the pipe (instead of uniformly spreading the loss along the whole pipe length) introduces an error of pressure-rise determination at any intermediate points. The pressure rise at either end of the pipe is affected very little by this approximation.

19.3 EXAMPLES OF WATER-HAMMER PROBLEMS IN CENTRIFUGAL PUMP SYSTEMS

(a) Power Failure—No Check Valve. A pump A in Fig. 19.11 is discharging into a tank C under static head H_s and friction head h_f. The system curve for point A (pump) is R_{A0} for steady conditions before power failure. There is no check valve between the reservoir and the

Note the notation in the diagram, Fig. 19.5(*b*). Capital letters A and C show the pressures at points A and C on the pipe, Fig. 19.5(*a*), at times indicated by subscripts given them such as A_0, A_1, A_2, A_3, A_4, and $C_{0.5}$, $C_{1.5}$, $C_{2.5}$, $C_{3.5}$, and which are expressed as fractions or multiple of one interval of time $\mu = 2L/a$.

Figure 19.7 shows the pressure-time curve for the point A at the valve plotted from the data in Fig. 19.5(*b*).

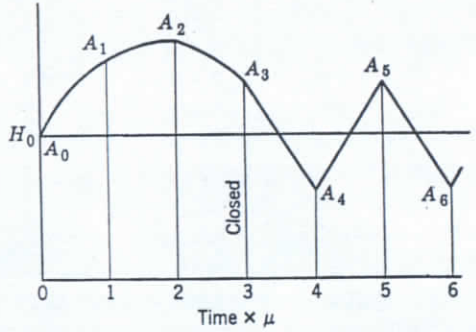

FIG. 19.7. Pressure at valve A versus time.

If more points are desired, the system characteristics for the point A are drawn at half of one interval of time, Fig. 19.8, and the pressure variation of two pressure waves is followed up: one leaving A at time $t = \mu$ (full line), and the other leaving A at time $t = \mu/2$ (dotted line). The surge characteristics for this wave are A_0, $A_{0.5}$, C_1, $A_{1.5}$, C_2, $A_{2.5}$, C_3, drawn in the same manner, i.e., the wave changing its direction each time it strikes the C characteristics, or A—parabolas at one interval of time spacing. Thus we have obtained additional points $A_{0.5}$, $A_{1.5}$, and $A_{2.5}$. In general we could follow up any pressure wave leaving point A at any instant between 0 and μ and draw its surge characteristics. For that we would need time parabolas drawn at μ intervals from the pressure-wave departing time to locate the points of change in the slope of the surge characteristics. In this way it is possible to determine the pressure at point A at any desired instant.

Note that the slope of the surge characteristics is positive $(+a/g)$ when the pressure wave travels in the direction opposite to the original flow velocity or from A to C; the slope is negative $(-a/g)$ when the pressure wave travels in the direction from C to A.

(*c*) **Pressure Rise at Any Point on Pipe.** For practical purposes only the maximum pressure rise is of importance. In our example it takes place at the valve. However, to illustrate the flexibility and general properties of the graphical solution, the method used to determine the

pressure at some point between A and C will be shown. For simplicity take point B, Fig. 19.8, midway between A and C. Note that the pressure rise created by the valve closure at A will not be felt at B until time $\mu/4$ sec. Therefore point A_0 can represent the pressure at B until time 0.25μ (marked $B_{0.25}$). Thereafter, when the pressure wave travels from A to C, it will reach $B_{0.25}$ μ sec later. But, on its way from C to A, the pressure wave will reach $B_{0.25}$ μ before it reaches A. On the diagram, Fig. 19.8, the points representing pressures at B are placed between A

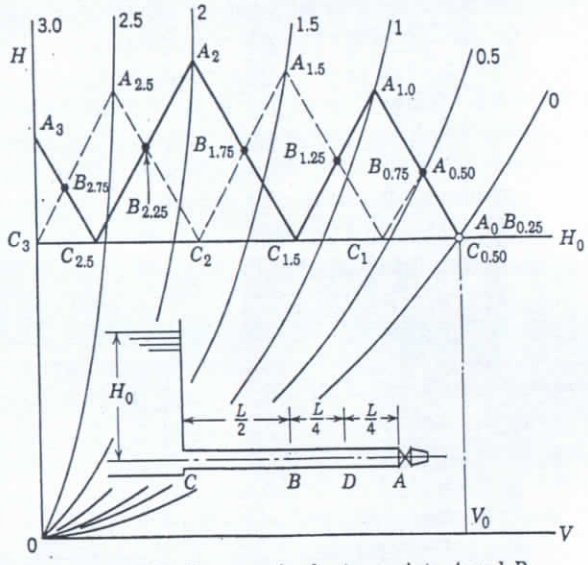

FIG. 19.8. Pressure rise for two points A and B.

and C points at 0.25μ sec from either one, and are marked $B_{0.75}$, $B_{1.25}$, $B_{1.75}$, $B_{2.25}$, $B_{2.75}$, which are intersections of the two surge characteristics of the two pressure waves at 0.5μ time spacing. For any other point, say, D at $L/4$ from A, a surge characteristic should be drawn starting on line A_0A_1 and parabola 0.75μ (nearer to A_1) and change its directions at $H_0 = \text{const}$, and parabolas 1.75μ, 2.75μ. Evidently the pressures at D will be higher than at B and lower than at A.

(*d*) **Valve Closure from Some Intermediate Position.** If a valve is closed completely or partially from some intermediate position, the pressure rise may be considerably higher than that produced by a complete valve closure at the same rate from the wide-open position. In Fig. 19.5(*b*), suppose the original position of the valve is two-thirds closed, the operating point A_2^0 is on the intersection of the curve 2μ and H_0. If the valve is now closed in a time μ (the same rate as before), the pressure

straight-line equation where $-a/g$ is a "slope coefficient." The expression $-a/g$ is not a tangent of the angle α between the straight line, equation 19.17, and the positive direction of axis of V, because V and H are not of the same dimensions. Therefore $-a/g$ is not dimensionless as a tangent should be. The actual slope of the line depends upon the scales used for V and H and does not affect the results. This is determined from

$$\tan \alpha = \frac{H - H_0}{V_0 - V} \tag{19.18}$$

where the numerator is the pressure rise for an arbitrary velocity drop $V_0 - V$; both expressed in inches to the scale used for the diagram. Equation 19.17 is a surge characteristic and represents pressure rise in terms of pipe velocities at the valve (point A, Fig. 19.5).

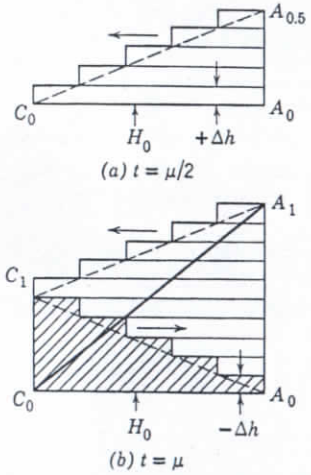

FIG. 19.6. Pressure rise for gradual valve closure.

Point A_0 in Fig. 19.5(b), represents the initial conditions. The pressure rise will continue during the first interval μ, until point A_1 is reached on the parabola μ. At this instant the first reflected negative wave (or pressure drop) will arrive at point A, Fig. 19.1(d).

Figure 19.6(a) shows a simplified diagram of the pressure-wave positions at time $\mu/2$, assuming that velocity is extinguished instantaneously by the valve at equal increments at a uniform rate. Figure 19.6(b) shows a diagram of pressures along the pipe at time μ. The broken line A_1C_1 shows the supernormal pressures produced at A. These are partially canceled by the reflected negative pressure waves arriving from C. The latter are represented by a broken line C_1A_0. All the pressure waves produced during time $\mu/2$ in Fig. 19.6(a) are reflected at C and moving toward A. The net pressures along the pipe are equal to the difference between the two and are represented by a line C_0A_1. The pressure rise A_0A_1 is the same as that due to a sudden valve closure destroying the same velocity instantaneously. It is easy to see from Figs. 19.6(a) and (b) the effect of the pipe length on the maximum pressure rise at the valve. The longer the pipe, the longer the pressure at the valve will be built up until the first negative wave arrives at A, as μ is directly proportional to the pipe length.

It is also evident from Fig. 19.6(b) that the maximum pressure rise is obtained if the valve is closed in a time equal to or smaller than one interval of time μ. The pressure rise in that case is equal to that caused by a sudden valve closure which, in general, is the maximum pressure rise possible in a system.

Actually, events at the valve are complicated by the fact that, even with a uniform valve closure, the velocity through the nozzle (and pipe) is affected by the pressure rise at the valve which varies with time. However, the linear relationship between velocity and pressure rise holds irrespective of time or space.

From the beginning of the second interval it is easier to follow up the pressure variation of the pressure wave leaving A at $t = \mu$, than to keep a record of the pressure at point A. Leaving point A at this instant and moving in direction C the pressure wave will meet the negative waves reflected at C. The negative pressures are appearing at C at the same rate as positive pressures were created at A. Therefore the pressure of the traveling wave will be reduced at the same rate. The surge characteristic will change its direction, but the linear relation between pressure drop and velocity in the pipe is maintained. Its equation will become

$$H_0 - H = \frac{a}{g}(V_0 - V) \tag{19.19}$$

In Fig. 19.5(b), equation 19.19 is represented by the line $A_1C_{1.5}$. The pressure continues to decrease for one half of interval, while the pressure wave travels from A to C. At time 1.5μ, it will reach point C, and will change its direction moving from C to A. Now the traveling wave will meet supernormal pressure waves, hence its pressure will increase, or the slope of the surge characteristics will change again. Thus the surge characteristic will change its direction each half of interval or at intersections with parabolas μ, 2μ, 3μ producing points A_1, A_2, A_3, and points $C_{1.5}$, $C_{2.5}$, $C_{3.5}$ as intersections with the system characteristics for the point C. Velocity in the pipe is decreasing from V_0 to 0, or until the surge characteristic intersects the axis of H. Hereafter the pressure at A will fluctuate between A_3 and A_4 in the same manner as after a sudden valve closure. The surge characteristic, if continued after the valve closure, will be represented by $A_3C_{3.5}A_4C_{2.5}$ with A_3 still changing its slope each half interval of time $\mu/2$. The velocity becomes negative and positive alternately each interval of time, as illustrated in Fig. 19.1. Points A_1, A_2, A_3, and A_4 show the pressures at the valve (point A) at times 1, 2, 3, and 4 intervals from the beginning of the valve closure.

variation of some arbitrary pressure wave as it travels back and forth from the valve to the open end of the pipe. The latter is the principle employed in the graphical method by Bergeron.[5,6] In the graphical method the pressure rise at end points is determined as an intersection of the "surge characteristics" with the system characteristics given by the end conditions of the pipe, somewhat in the manner used for the determination of the operating point of a centrifugal pump discharging into a pipe line.

The graphical method is more flexible and easier to grasp than the analytical method. It permits solution of a variety of water-hammer problems not possible analytically.

(*a*) **System Characteristics.** In any closed conduit to be investigated for water hammer, the system characteristics either are known or are estimated. This means that the relationship between the head and capacity, or velocity, at both ends of the conduit is known for a steady condition prior to the valve closure. Such a relationship can also be established for any partial valve opening. The same relationships hold at any instant during the gradual valve closure. Taking as an example a nozzle discharging freely under a head H_0, Fig. 19.5(*a*) with the nozzle wide open, the system characteristics for the point A, is a square parabola, marked 0 in Fig. 19.5(*b*), representing velocity in the pipe (not a velocity through the nozzle) in terms of head in the reservoir H_0. This applies to a steady flow prior to valve closure or at time $t = 0$. Such characteristics can be drawn for any valve position.

For instance, if the valve is gradually and uniformly closed in time $t = 3\mu$, the nozzle will be $\frac{2}{3}$ open at time $t = \mu$ and, under the same head, the pipe velocity will be $\frac{2}{3}$ of the original velocity V_0. This is expressed by a parabola marked μ, with abscissas $\frac{2}{3}$ of their original values at any head. Similarly, at time $t = 2\mu$, the nozzle is $\frac{1}{3}$ open, and the system characteristic is a parabola 2μ. At time 3μ the flow is zero and the system characteristics coincide with the axis of heads. A uniform valve closure was assumed for simplicity.

There is no added complication in the procedure of the graphical method for other rates of valve closure as long as the discharge through the valve is known as a function of time. This results only in a different spacing of parabolas 0, μ, 2μ, etc. Another property of the system is that the pressure at the point C always remains equal to H_0 at all rates of flow and is not affected by the valve closure. The line $H_0 = \text{const}$ is a system characteristic for the point C. Parabolas 0, μ, 2μ, and 3μ represent a time scale on the diagram for the events occurring at point A. Such a time scale can be drawn at each $\mu/2$ or $\mu/4$ interval, or a parabola of time can be drawn for any specified time from the moment the valve

closure starts. Both system characteristics, parabolas μ, 2μ, 3μ for A, and $H_0 = \text{const}$ for C, give the "end conditions" for the pipe at any given time. Pipe friction and velocity head will be neglected for the time being for simplicity and will be discussed later.

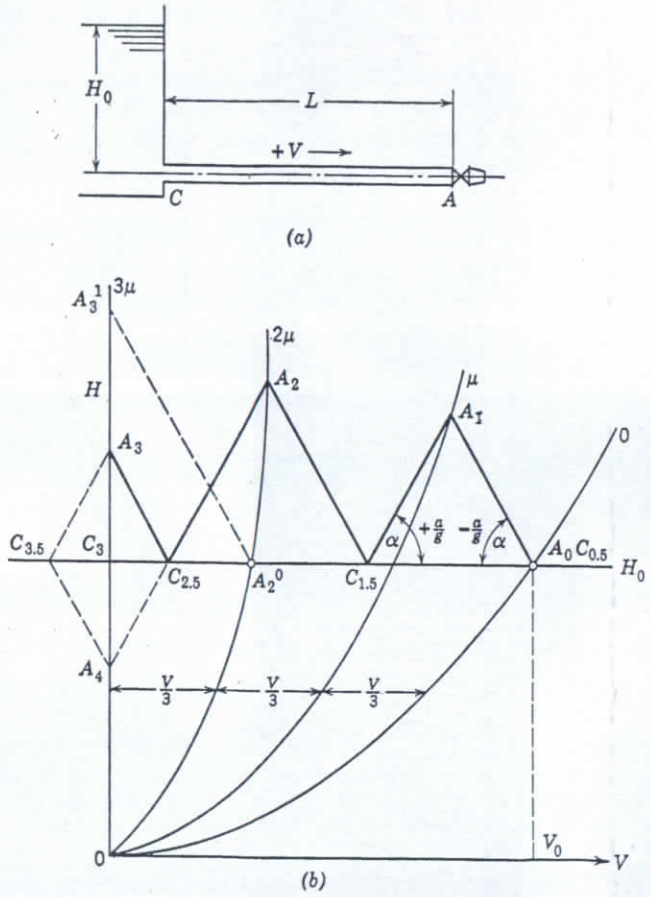

FIG. 19.5 (*a*) and (*b*). Valve closure in three-time intervals.

(*b*) **Surge Characteristics.** Applying Joukowsky's equation to a partial valve closure the pressure rise becomes

$$H_0 - H = -\frac{a}{g}(V_0 - V) \tag{19.17}$$

which shows that the pressure rise is proportional to the velocity drop; $-a/g$ being the factor of proportionality. Equation 19.17 is a typical

complete closure of the valve. This follows from equation 19.3 for, if k and E are infinite, a becomes infinite and, hence, h_{max} becomes infinite.

(h) Pipe of Variable Diameter. In the case of a compound pipe consisting of several sections of different diameters in series an "equivalent velocity" is used for calculation of the maximum pressure rise with equation 19.1. The equivalent velocity is defined as

$$V = \frac{L_1V_1 + L_2V_2 + \text{etc.}}{L} \tag{19.12}$$

where L_1 is the length and V_1 is velocity of one section of pipe, L_2 and V_2 the same for the second section, etc., and L is the total length of the pipe. Equation 19.12 is obtained by equating the total kinetic energy of several pipes to that of one pipe with an equivalent section area A producing the equivalent velocity V.

$$LA\gamma\frac{V^2}{2_g} = L_1A_1\gamma\frac{V_1^2}{2_g} + L_2A_2\gamma\frac{V_2}{2_g}, \text{ etc.} \tag{19.13}$$

but

$$A = \frac{Q}{V}; \qquad A_1 = \frac{Q}{V_1}; \qquad A_2 = \frac{Q}{V_2}, \text{ etc.} \tag{19.14}$$

where A, A_1, and A_2 are the pipe sectional areas for pipes L, L_1, and L_2 respectively and Q is the volume of water flowing through the pipes. Substituting into equation 19.13 for A, A_1, A_2, etc., their values from equation 19.14, we obtain

$$LV = L_1V_1 + L_2V_2 + \text{etc.} \tag{19.15}$$

which is equivalent to equation 19.12.

The value of the pressure wave velocity for a compound pipe is determined by the following equation:

$$\frac{L}{a} = \frac{L_1}{a_1} + \frac{L_2}{a_2} + \text{etc.} \tag{19.16}$$

where a_1, a_2, etc., are the values of the velocity of sound in the first, second, etc., portions of the pipe. The value of a is referred to as "effective" velocity of the pressure wave. Equation 19.16 expresses that the total time to travel the total length of pipe L with a velocity of sound a is equal to the sum of times to travel pipe lengths L_1, L_2, etc., with their respective velocities of sound a_1, a_2, etc. If the closure time is appreciably greater than one interval (over four intervals), accurate results are obtained by using "equivalent" velocity of flow and "effective" pressure wave velocity.

(i) Pipe Friction and Velocity Head. In all discussions it has been assumed that the pipe velocity is so low that the pipe friction loss and velocity head are very small in comparison with the head H_0. Therefore the head H_0 prevailed at all points of the pipe before the valve closure. With water turbines such conditions are approximated, and the rate of flow may be varied by wicket gates with very little or no change in pressure in the penstock.

When the pipe is not horizontal (as shown in Fig. 19.1), then the original head H_0 is the total head, or neglecting the friction loss and

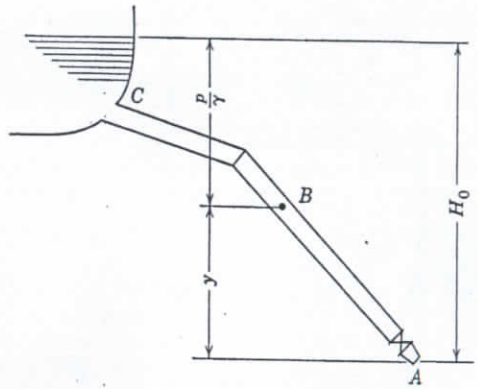

FIG. 19.4. Total head on nozzle.

velocity head $H_0 = p/\gamma + y$, where y is the elevation of the point of pressure measurement above the nozzle, Fig. 19.4.

19.2 GRAPHICAL SOLUTION

In the cases of sudden valve closure and closure in a time equal to or smaller than one interval of time, Joukowsky's equation 19.1 gives accurately the maximum pressure rise in a simple conduit which takes place at the valve. In the latter case negative (reflected) waves will not have reached the valve in this time, and the pressure rise is built up gradually to the same value as it would reach after a sudden valve closure. If the total closing time is greater than one interval, the pressure rise at the valve is equal to the sum of the supernormal pressure waves created by the valve closure and the negative waves arriving from the open end of the pipe. The maximum pressure rise can be found by determination of pressures at a fixed point (at the valve) at some arbitrary interval of time, like in the arithmetical integration method of Gibson [3] or Quick [4] and analytical method of Allievi,[5] or by following the pressure

(g) Velocity of Pressure Wave. Knowing the pipe size, thickness, material, and the bulk modulus of the liquid, the velocity of the pressure wave can be calculated by using the equation

$$a = \frac{1}{\sqrt{\frac{\gamma}{g}\left(\frac{1}{k} + \frac{d}{eE}\right)}} \tag{19.3}$$

where γ = specific weight of liquid.
k = bulk modulus of liquid.
d = pipe diameter.
e = pipe thickness.
E = pipe material modulus of elasticity.

For cold water k = 294,000 psi for pressures up to 500 psi; this increases as the water temperature and pressure are increased. For steel pipe E = 29,400,000 psi. Using these values for cold water and steel pipe equation 19.3 becomes

$$a = \frac{4660}{\sqrt{1 + \frac{d}{100e}}} \tag{19.4}$$

Petroleum oils are next in importance to water in pumping problems. The bulk modulus of elasticity for crude oil at 60°F and 500 psi varies from 235,000 to 250,000 psi depending on the type of crude. The bulk modulus of gasoline is 150,000 psi. The bulk modulus of petroleum oils decreases as temperature is increased and increases slightly with pressure.[1]

The development of equation 19.3 is of interest.[2] After the instantaneous closure of the valve a region of compressed water is created adjacent to the valve and extending a distance x upstream at a time t seconds after closure (Fig. 19.1(a)). At the same time the pipe in the same region is expanded under the pressure rise h_{max} from a diameter d to d_1. From the instant of the valve closure to time t through a section of pipe A (original) at a point a distance x from the valve, a volume of liquid passed is AV_0t. Since there is no outlet from the pipe this volume must be accommodated by compression of water and by stretching of the pipe walls, so that

$$AV_0t = \frac{xAp}{k} + \frac{x\pi(d_1^2 - d^2)}{4} \tag{19.5}$$

where p is pressure rise h_{max}/γ and xAp/k is the reduction in volume of water due to compression.

The last term of the equation 19.5, which is the increase of pipe volume x feet long due to pipe expansion, will be transformed by expressing the pipe diameter increase in terms of the tensile modulus of the pipe material E, and the pressure increase p

$$\frac{S}{E} = \frac{d_1 - d}{d} \tag{19.6}$$

where S is the unit stress in the pipe material determined from

$$pd = 2eS \tag{19.7}$$

where e is the pipe thickness. Then combining equations 19.6 and 19.7, we obtain

$$\frac{pd}{2eE} = \frac{d_1 - d}{d} \tag{19.8}$$

In equation 19.5 $(d_1^2 - d^2)$ can be written as $(d_1 - d)(d_1 + d)$ and, since $d_1 - d$ is very small in comparison with d_1 or d, we put $d_1 + d = 2d$. Then the last term of the equation 19.5 can be transformed by making use of equation 19.8 to

$$\frac{x\pi(d_1^2 - d^2)}{4} = \frac{xApd}{eE} \tag{19.9}$$

Substituting this into equation 19.5, we get

$$V_0t = xp\left(\frac{1}{k} + \frac{d}{eE}\right)$$

Hence the velocity of the pressure wave is

$$a = \frac{x}{t} = \frac{V_0}{p\left(\frac{1}{k} + \frac{d}{eE}\right)} \tag{19.10}$$

Substituting for V_0 its value from equation 19.1, $V_0 = pg/\gamma a$, we obtain equation 19.3.

$$a = \frac{1}{\sqrt{\frac{\gamma}{9}\left(\frac{1}{k} + \frac{d}{eE}\right)}} \tag{19.11}$$

It should be noted that the elasticity of the pipe and water serves to cushion the shock due to a sudden change in velocity of flow. Without this, or considering the water column as a solid rod, the rise of pressure would be greater and, in fact, theoretically infinite in the case of a sudden

stant velocity (V_0) while the mass is changing at a constant rate (a/g). In mechanics of solid bodies the mass is fixed and change in momentum can be realized only by a velocity change.

The time to complete a round trip for the pressure wave $\mu = 2L/a$ is called variously "period of pipe," "reflection time," "critical time," "one interval of time." The latter term will be used in this chapter. The negative pressure wave originated at the open end of the pipe is referred to as a "reflected" wave.

(*c*) **Sudden Opening of Valve.** The sequence of events can be similarly traced for a sudden valve opening. The magnitude of the pressure drop and rise is given by Joukowsky's equation 19.1, and is the same as in the case for a sudden valve closure. However, during the first interval of time μ, pressure at the valve remains subnormal, whereas during the second interval the pressure is above the normal. The velocity fluctuates from 0 to $2V$, about its average velocity V, which is the final velocity of the established flow.

(*d*) **Partial Valve Closure.** An instantaneous partial valve closure produces the same cycle of events as a complete valve closure. The pressure rise and fall is given by the equation

$$h = \frac{a}{g}(V_0 - V) = \frac{a}{g}\Delta V \qquad (19.2)$$

where V_0 is the initial velocity of flow and V is the final velocity. The pressure diagram for the two intervals will be the same as in Fig. 19.1, but the velocity will fluctuate from V_0 to $V_0 - 2\Delta V$ about its average value $V = V_0 - \Delta V$, which is the final velocity of established flow.

(*e*) **Gradual Valve Closure.** This case is usually considered as the equivalent of a series of consecutive instantaneous partial closure movements, each producing a pressure wave proportional to the increment of velocity destroyed and traveling between the valve and open end of the pipe. The pressure at any point of the pipe is the algebraic sum of all pressure waves, direct and reflected. Thus the pressure will continue to rise at the valve during the whole first interval $2L/a$ until the reflection wave arrives at the valve at this instant.

(*f*) **Variation of Pressure Rise Along Pipe.** If a valve closure occurs instantaneously the pressure wave will travel undiminished up the pipe to the open end, as shown in the diagram of Fig. 19.1. Figure 19.2 shows the variation of pressure with time at the valve A, near the open end of the pipe C, and at an intermediate point B. At the open end C the original pressure H_0 prevails. For a gradual valve closure, when the total time of closure T is equal to or greater than one interval of time,

the maximum pressure rise occurs at the valve, and from there to the open end it reduces to zero uniformly along the length of the pipe (Fig. 19.2, full line). Note that although the pressure wave travels undiminished along the pipe after each partial instantaneous closure of the valve, at points other than the valve there are times when pressure remains unchanged. Thus in Fig. 19.2 at point B in the middle of the pipe, the original pressure H_0 prevails during time $\mu/2$ between each positive and negative pressure wave. When series of pressure waves are traveling along the pipe as a result of successive partial valve closures some of the waves will fall in the gaps between the positive and negative pressure waves; pressure waves of opposite sign will cancel each other and, as a result, a pressure distribution as shown in Fig. 19.3 is obtained. If the closure time is less than one interval of time, $2L/a$, the maximum pressure rise will be transmitted undiminished to an intermediate point (a distance $Ta/2$ from the open end), and from that point to the open end the pressure rise reduces uniformly to zero (Fig. 19.2 dotted line).

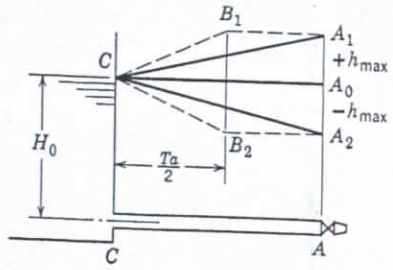

FIG. 19.2. Pressure variation with time along pipe ($\mu = 2L/a$, one-time interval).

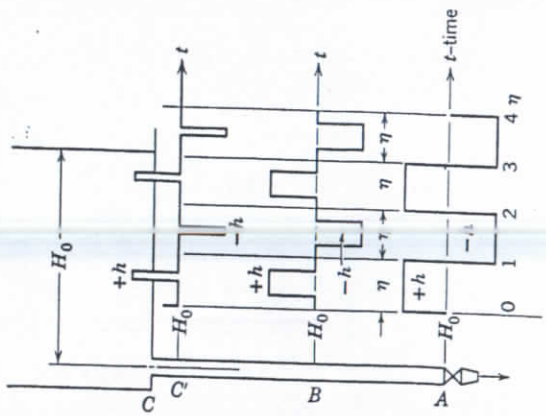

FIG. 19.3. Pressure distribution along pipe (full line, $T \geq \mu$; dotted line, $T < \mu$).

As soon as the valve movement ceases, the supernormal pressure at the valve will be succeeded by subnormal pressure and the pressure will fluctuate between these limits until damped out by friction, Fig. 19.7.

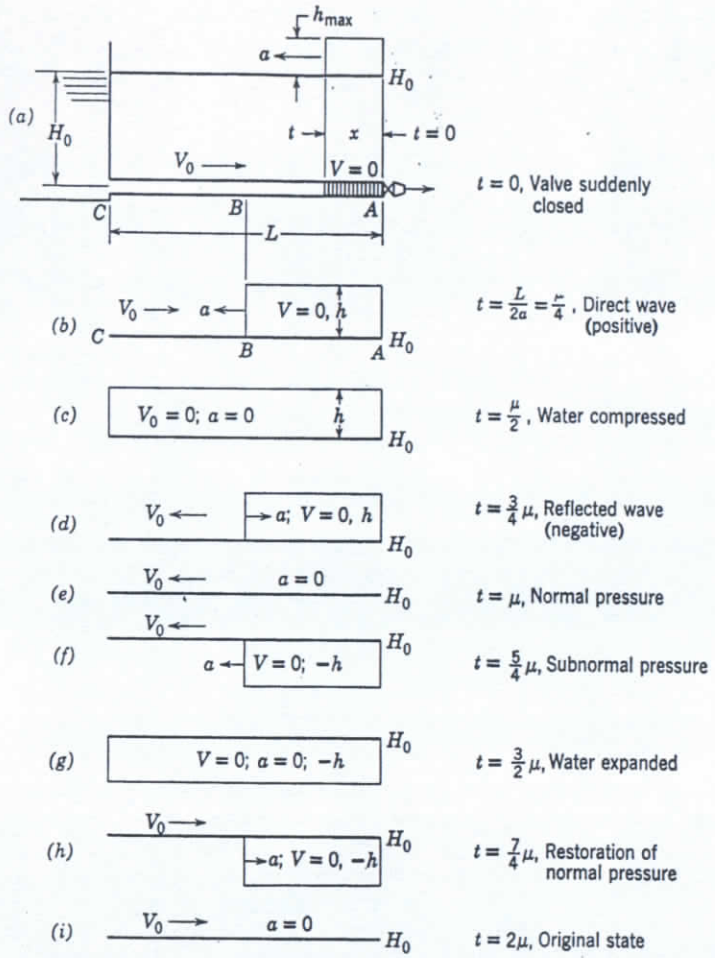

FIG. 19.1. Sequence of events after sudden valve closure.

where A is the area of pipe, and γ is specific weight of water; hence

$$h_{max} = \frac{aV_0}{g} \tag{19.1}$$

Here x/t is the rate at which the pressure wave travels along the pipe, and this is equal to the velocity of sound in the water within the pipe. Since the velocity V_0 in the pipe prior to the valve closure was constant and velocity of the pressure wave a is constant, the pressure at the valve remains constant. The pressure rise does not depend upon the pipe

size and original pressure in the pipe. The water between the valve A, Fig. 19.1(b), and the wave front will be at rest under a state of uniform compression under the head h_{max} (in addition to initial compression due to H_0), whereas water between the wave front point B, Fig. 19.1(b), and the open end of the pipe (point C) is under its original pressure at every point and moves with a constant velocity V_0 toward the valve. When the wave front reaches the open end of the pipe C, the whole pipe is completely filled with water at rest under an additional pressure head h_{max} uniform along the whole pipe length, Fig. 19.1(c). At this moment the whole kinetic energy of flow is stored in the elastic energy of strain of pipe and water column.

However, the instant the pressure wave reaches the open end, water in the pipe will begin to expand through the open end, creating a velocity V_0 in the pipe in the opposite direction and relieving the pressure back to its original pressure, Fig. 19.1(d). This pressure drop travels backward from the open end to the valve with the same velocity a, and reaches the valve in a time $2L/a$ from the time of valve closure. At this instant the pipe is again under the normal pressure and the water moves with velocity V_0 toward the reservoir, Fig. 19.1(e). In the next instant water will continue to move toward the reservoir, bringing the slug of water adjacent to the valve to rest; at the same time the pressure at the valve will drop below its normal pressure H_0 by $-h_{max}$, exactly equal to the pressure rise during the first interval of time $2L/a$ as the same velocity is destroyed at the same rate. The wave of subnormal pressure $-h_{max}$ now starts from the valve, Fig. 19.1(f), and reaches the open end at time $3L/a$, when all water in the pipe is at rest under reduced compression due to a negative head of $-h_{max}$, Fig. 19.1(g). During the next instant water will flow into the pipe with velocity V_0 restoring the pressure in the pipe to the original value H_0, Fig. 19.1(h). At the end of the second interval $2L/a$, or total time from the valve closure $4L/a$, the conditions will be the same as before the valve closure, Fig. 19.1(i). After that the new cycle begins and repeats itself continuously until the original kinetic energy of flow is dissipated in pipe friction, internal water friction (due to velocity rearrangement), and energy rejected into reservoir. However, the damping has little effect on the pressure of several cycles under usual conditions.

It will be noticed that while part of the water column is expanded or compressed, the rest of it is at rest (or moving with a constant velocity). Thus there is no mass oscillation as a whole as has been observed, for instance, on boiler feed pumps with unstable characteristics, producing pressure surges in the discharge lines. It should be pointed out that in water-hammer phenomena change in momentum takes place at a con-

REFERENCES

1. "Manual of Water Supply Equipment," The National Association of Domestic and Farm Pumping Equipment, pp. 37–47, 1946.
2. J. E. Gosline and M. P. O'Brien, "The Water Jet Pump," *Univ. of Calif. Publ.*, Vol. 3, No. 3, pp. 167–190, 1934.
3. W. S. Weeks, "The Air Injector for Auxiliary Ventilation Underground," *Eng. Mining J.*, Vol. 138, pp. 196–199, 1937.
4. G. E. McElroy, "Design of Injectors for Low-Pressure Air Flow," *Paper 678*, U. S. Dept. of Interior, Bureau of Mines, 1945.
5. R. G. Cunningham, "The Jet Pump as a Lubrication Scavenge Pump for Aircraft Engines," *Report, Penn. State Univ.*, July 20, 1954.
6. K. R. Lung, *Patent No. 2,457,388*, Dec. 28, 1948.
7. Andor v. Okolicsanyi, "Bemessung des Windkessels bei selbsttätigen Pumpenanlagen," *Z. Ver. deut. Ing.*, Vol. 75, No. 21, p. 657, 1931.
8. H. Nickelsporn, "Hydropneumatic Tank Operation," *Power Engr.*, April 1951.

Chapter 19

Water-Hammer Problems in Centrifugal Pump Systems

19.1 WATER HAMMER IN SIMPLE CONDUITS

(a) Introduction. Water hammer is defined as the change in pressure in closed conduits above or below normal caused by sudden changes in velocity of flow. Although the analytical solution of water-hammer problems is rather involved, the graphical method presented here does not require an exact knowledge of the theoretical background and, at the same time, gives a clear mental pattern of the events which enables one to use the method with confidence for solution of practical problems. An understanding of the mechanism of pressure waves, their propagation, reflection, and addition, is essential for the intelligent use of the graphical method even in its simplest form.

(b) Joukowsky's Law. Joukowsky has found that the maximum pressure rise h_{max} above the normal pressure H_0 in a conduit due to instantaneous closure of the valve is given by the expression known by his name

$$h_{max} = \frac{aV_0}{g} \tag{19.1}$$

where V_0 is the normal velocity in the conduit before the closure of the valve, a is the velocity of sound in water under the conditions existing in the pipe, which is the velocity of propagation of the pressure wave, and g is acceleration due to gravity.

This equation follows from the application of the second Newton's law, which states that the force (increase in pressure at the valve) is equal to the time rate of change of momentum of the moving mass. In Fig. 19.1(*a*) consider a long pipe flowing full with a uniform velocity V_0 under the head H_0. If the valve at its end is closed instantaneously, then at time t a portion of the column of length x will have its velocity reduced to zero; then

$$F = A\gamma h_{max} = \frac{A\gamma x}{gt} V_0$$

not as simple. Thus with zero demand and the tank at low pressure there will be only one pump starting, the whole useful storage volume being delivered in t minutes, or

$$\frac{v_1 - v_2}{Q} = t \tag{18.30}$$

where v_1 in gallons is the volume of air cushion at the pressure p_1 lbs/sq in. absolute (Fig. 18.16), v_2 the same at p_2 pressure, and Q is pump capacity in gallons per minute at the average tank pressure $(p_2 + p_1)/2$. On the other hand, when the tank is full of water and the demand is a maximum (equal to pump capacity), the whole useful tank capacity will be expended in t minutes, the pump will start and run continuously, maintaining the average tank pressure. It follows that the maximum number of starts per hour will occur at some intermediate water demand. It can be shown that for a *constant rate* of consumption, the highest frequency of starting will happen at half of the maximum demand. Then the pump will fill the tank in $2t$ minutes, as half of the pump capacity will be used up during pumping. After the pump stops the amount of water stored will last also $2t$ minutes. Thus the cycle will be completed in $4t$ minutes and the frequency of starting per hour under these assumed conditions will be $f = 60/4t$.

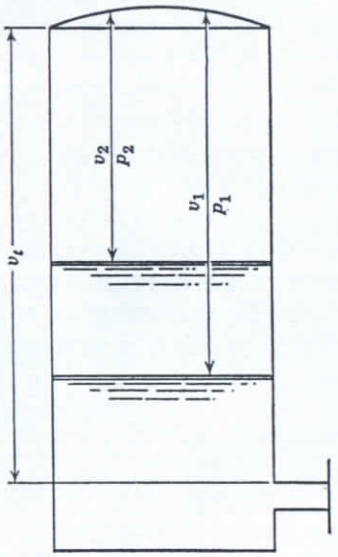

FIG. 18.16 Air tank size calculations.

With a *variable consumption* the most unfavorable case is when the demand varies from zero, with pump running to a maximum with pump idle. In that case the cycle is completed in $2t$ minutes and the frequency of starting per hour becomes $f = 60/2t$.

For the average conditions, therefore, with any possible rate of consumption, it is reasonable to assume a frequency

$$f = 60/3t \tag{18.31}$$

for the tank size calculations.

(*c*) **Tank Size.** In determining the tank size the maximum demand, equal to pump capacity Q, and the pressure limits p_1 and p_2 in pounds per square inch are specified. The number of startings per hour or frequency of starting f is selected. Five startings per hour are a good number to assume. Then the minimum tank total volume v_1 above the discharge nozzle is obtained in terms of the above variables as follows.

The air cushion volumes and pressures are connected by a relationship

$$v_1 p_1 = v_2 p_2$$

hence

$$\frac{v_1 - v_2}{v_1} = \frac{p_2 - p_1}{p_2} \tag{18.32}$$

Combining with equations 18.30 and 18.31 and solving for v_1 gives

$$v_1 = \frac{20 Q p_2}{f(p_2 - p_1)} \tag{18.33}$$

This value of the minimum calculated tank volume above the discharge nozzle should be increased by, say, 25 per cent to provide a margin of safety for a possible fluctuation in the starting of automatic switches and to prevent rushing of air into the discharge pipe.

Then assuming five startings per hour, or $f = 5$, equation 18.33 becomes

$$v_t = \frac{5 Q p_2}{p_2 - p_1} \tag{18.34}$$

where v_t is tank volume above the discharge nozzle (Fig. 18.16).

If $p_2 = 2p_1$, equation 18.34 becomes

$$v_t = 10Q \tag{18.35}$$

This is a rule of thumb widely used in the industry.

Some of the air in the tank is dissolved by water and some is entrained into the discharge pipe; for that reason pumps for domestic water systems are provided with simple automatic air-charging devices to maintain a minimum of air volume necessary for a satisfactory operation. Any reduction of the air volume below that results in a greater number of startings per hour than originally planned. If a water system is using a vertical deep-well pump without a foot valve the tank will receive a charge of air each time the pump is started. An automatic air release of the float type is provided in this case to maintain the predetermined minimum water level in the tank.

$$
\left.
\begin{aligned}
H_d &= H_c \frac{N}{1 + B(N+1)} \\
H_1 &= H_c \frac{N+1}{1 + B(N+1)} \\
H_p &= H_c \frac{(N+1)(B+1)}{1 + B(N+1)} = H_1(B+1) \\
h_1 &= H_c \times \text{constant} = Q^2 \times \text{constant} \\
h_2 &= BH_1
\end{aligned}
\right\} \tag{18.28}
$$

$$
\left.
\begin{aligned}
Q_1 &= \sqrt{H_c} \frac{CA_1\sqrt{2g(N+1)}}{\sqrt{1 + B(N+1)}} = CA_1\sqrt{2gH_1} \\
Q_2 &= Q_1 M \\
Q &= Q_1(M+1)
\end{aligned}
\right\} \tag{18.29}
$$

When centrifugal pump speed or impeller diameter is changed M and N values remain the same, and it can be stated from equations 18.28 that the net system head H_p and the other heads H_1, H_d, h_1, and h_2, vary directly as the square of the speed or impeller diameter, or directly as the centrifugal head H_c. Similarly from equations 18.29 the capacity of the jet-centrifugal pump combination Q_2, and also Q_1 and Q, vary directly as the speed or impeller diameter of the centrifugal pump or directly as $\sqrt{H_c}$.

(*b*) **Change in Size of Jet Pump.** If, for a given centrifugal pump, a larger jet pump of the same design (R = constant) is used, M and N remain the same except for the effect of change in peak efficiency. $Q/\sqrt{H_c}$ will increase directly as the nozzle area A_1 (equation 18.25). This means that the operating point of the centrifugal pump will move to a higher capacity and lower head. Since M remains the same Q will be split in the same ratio, or Q_1 and Q_2 will change directly as Q. All the heads, H_p, H_d, H_1, h_1, and h_2, will change directly as $\sqrt{H_c}$.

(*c*) **Increase of Throat Size.** If, for a given centrifugal pump, the nozzle/throat ratio R is changed, for instance, by increasing the throat area by reboring, R will decrease. For b.e.p., $MN = e_j$ will essentially remain constant but M will increase and N will decrease. Thus, from equation 18.25, the centrifugal pump unit capacity $Q/\sqrt{H_c}$ will increase (for simplicity assume $B = 0$); this means that the operating point of the centrifugal pump will move to a higher capacity Q and lower head H_c; therefore H_p and all heads will decrease because of the decrease of both N and H_c, as shown by equations 18.28. Capacity Q_2 will increase, but Q_1 will decrease because of the decrease of the driving head H_1.

(*d*) **Increase of the Nozzle Size.** If the nozzle ratio R is increased by reboring the nozzle diameter, variation of heads and capacities will be in the opposite direction to that in case (*c*); that is, all heads will increase, Q_1 will increase, Q_2 will decrease, and Q will decrease.

(*e*) **Change in Size or Length of Pipes.** If the size or the length of the centrifugal pump suction pipe is changed so that the hydraulic loss h_1 in this pipe is increased, H_c will be lower (Fig. 18.15). The decrease in H_c will be followed by a decrease in all heads and capacities. If the size or length of the drive capacity pipe is so changed as to increase its resistance h_2, the constant B will increase, and both heads and capacities will drop as indicated by equations 18.28 and 18.29.

For a shallow-well unit when the jet pump is built into the centrifugal pump assembly the pipe losses h_1 and h_2 are absent, and $H_c = H$, and $B = 0$ in the equations 18.28 and 18.29.

18.5 DETERMINATION OF TANK DIMENSIONS FOR AUTOMATIC WATER SYSTEMS

Jet-centrifugal pump combinations are mostly used for domestic water supply systems in connection with a tank partly filled with air under pressure for water storage. For this service such units are particularly suited because of their steep head-capacity characteristics. Determination of the most practical size of the tank involves adjusting several conflicting requirements: pump capacity, pressure range, water demand, and maximum number of pump startings per hour. All of these vary and a solution aims at a satisfactory compromise among these conditions at a minimum cost.[7] The large tank assures more reliable service, with less motor startings per hour and greater water storage for emergency.

(*a*) **Pump Size.** The pump size (capacity) is selected to meet the maximum demand. This capacity should be referred to the average tank pressure. This will permit building up of pressure in the tank to the average at the time of maximum demand. A pump with a higher capacity will result in too frequent starting and stopping of the motor.

(*b*) **Frequency of Starting.** Frequency of pump starting depends on the pump capacity, tank pressure variation, tank size, and variation of the water demand and is assumed from the following considerations. The volume of useful water in the tank is in direct proportion to the difference between the pressures and tank size. Therefore, a small pressure difference and small tank result in a greater number of startings per hour. The effect of water demand on the frequency of starting is

3. $$Q_1 = CA_1\sqrt{2gH_1} \tag{18.16}$$

This is the discharge through the nozzle under the net head H_1, since $H_s = 0$, the small velocity head in the jet pump suction chamber being neglected. C is the nozzle discharge coefficient, selected from available data.

4. $$H_c = \frac{H_1}{N+1}[1 + B(N+1)] \tag{18.17}$$

where B is a numerical constant expressing the head loss h_2 as a fraction of H_1. The development of the relationship between H_c and H_1 as given by equation 18.17 follows:

From inspection of Fig. 18.2 it can be established that

$$H_p = H_1 + h_2 = H_d + H - h_1 = H_c + H_d \tag{18.18}$$

$$H_c = H_1 - H_d + h_2 \tag{18.19}$$

The value of the friction loss h_2 can be expressed as a fraction of H_1.

$$h_2 = f\frac{LV_1^2}{d2g} = f\frac{16L}{2gd^5\pi^2}Q_1^2 \tag{18.20}$$

where f is the friction coefficient, L is the length, and d is the diameter of the driving pipe.

From equation 18.16

$$H_1 = \frac{Q_1^2}{2gC^2A_1^2}$$

Combining the two,

$$\frac{h_2}{H_1} = \frac{16fLC^2A_1^2}{d^5\pi^2} = B = \text{constant} \tag{18.21}$$

$$h_2 = BH_1 \tag{18.22}$$

Then equation 18.19 becomes

$$H_c = H_1(1 + B) - H_d \tag{18.23}$$

Substituting for H_d its value from equation 18.3 gives the equation

$$H_c = \frac{H_1}{N+1}[1 + B(N+1)] \tag{18.17}$$

Now the number of variables is reduced by combining equations 18.14, 18.16, and 18.17:

$$Q = CA_1\sqrt{2gH_1}\,(M+1) \tag{18.24}$$

Squaring this and dividing by equation 18.14,

$$\frac{Q^2}{H_c} = \frac{2gC^2A_1^2(M+1)^2(N+1)}{1 + B(N+1)} \tag{18.25}$$

For an arbitary point on the centrifugal pump head-capacity curve (Q, H_c) equations 18.15 and 18.25 are two simultaneous equations with M and N unknowns. Solution of these for M or N leads to a cubic equation, which cannot be solved algebraically. For a solution by trial it is more convenient to use equation 18.25 and reverse the procedure, that is, to substitute M and N values for an arbitrary point on the M-N curve (A in Fig. 18.5). Then equation 18.25 becomes

$$\frac{Q}{\sqrt{H_c}} = \text{constant} \tag{18.26}$$

This means that equation 18.25 can be satisfied by a given centrifugal pump at any speed or impeller diameter. To find Q and H_c for a fixed revolutions per minute of the pump an arbitrary value is assigned to Q, and H_c is obtained (point B). Points of the same unit capacity $(Q/\sqrt{H_c})$ lie on a square parabola with its apex at the origin of Q-H_c coordinates. To determine its intersection with the Q-H_c curve (point D) another point C is located at an arbitrary capacity and connected with point B by the affinity relations. A straight line BC is drawn to intersect the Q-H_c curve at point D. Q and H_c being known, the system head H_p and capacity Q_2 (point E) are found by using the relationships already established (or equations 18.28 and 18.29). The efficiency of the jet-centrifugal combination e_c (point J) is obtained by dividing the output of the system by the brake horsepower of the centrifugal pump (points F and G):

$$e_c = \frac{Q_2H_p}{3960 \times \text{bhp}} \tag{18.27}$$

Any required number of points for the Q_2-H_p curve can be obtained by this method by selecting different points on the M-N curve.

18.4 AFFINITY RELATIONS

(a) Change in Pump Speed. Equations 18.28 and 18.29 express all heads and capacities in terms of the centrifugal pump head H_c and the jet pump constants M and N.

18.3 PERFORMANCE OF A CENTRIFUGAL-JET PUMP COMBINATION

To proceed to the determination of the head-capacity characteristics of the combination when both centrifugal and jet pump performances are known, a number of additional notations should be made. From Fig. 18.2,

H_p = centrifugal pump discharge head, which is the net head of the combination.
H = centrifugal net head.
H_1 = head on the jet pump nozzle, driving head.
H_d = discharge head of the jet pump.
h_1 = friction loss head in the centrifugal pump suction pipe, which is the discharge pipe of the jet pump.
h_2 = friction loss head in the driving capacity pipe.

All heads are taken above the jet pump suction level, which for simplicity is taken at the center of the jet pump suction nozzle: $H_s = 0$.

When the submergence of the jet pump H_s does not equal zero in the final results of the development (equation 18.28), the heads H_p, H_d, and H_1 will have an additive term H_s. The head H_c is not affected by the jet pump submergence.

It is convenient to consider the pipe between the jet pump discharge and the centrifugal pump suction as part of the centrifugal pump to reduce the net centrifugal head H by the amount of loss in that pipe h_1, and to denote the difference between the two by

$$H_c = H - h_1 \tag{18.13}$$

This will be the net centrifugal head available to the system and, for a given length and size of suction pipe, it can be established for the whole head-capacity range (Fig. 18.15). In this way the friction loss in the centrifugal pump suction pipe will be taken care of automatically.

The operating point of the system is determined by four conditions:

1. $$Q = Q_1 + Q_2 = Q_1(M + 1) \tag{18.14}$$

2. $$\frac{M}{M_0} + \frac{N}{N_0} = 1 \tag{18.15}$$

This is the equation of the jet pump head-capacity line, which is selected for a given nozzle/throat ratio and efficiency.

Here M_0 is M value at $N = 0$; N_0 is N value when $M = 0$; and M and N are any values on M-N straight line.

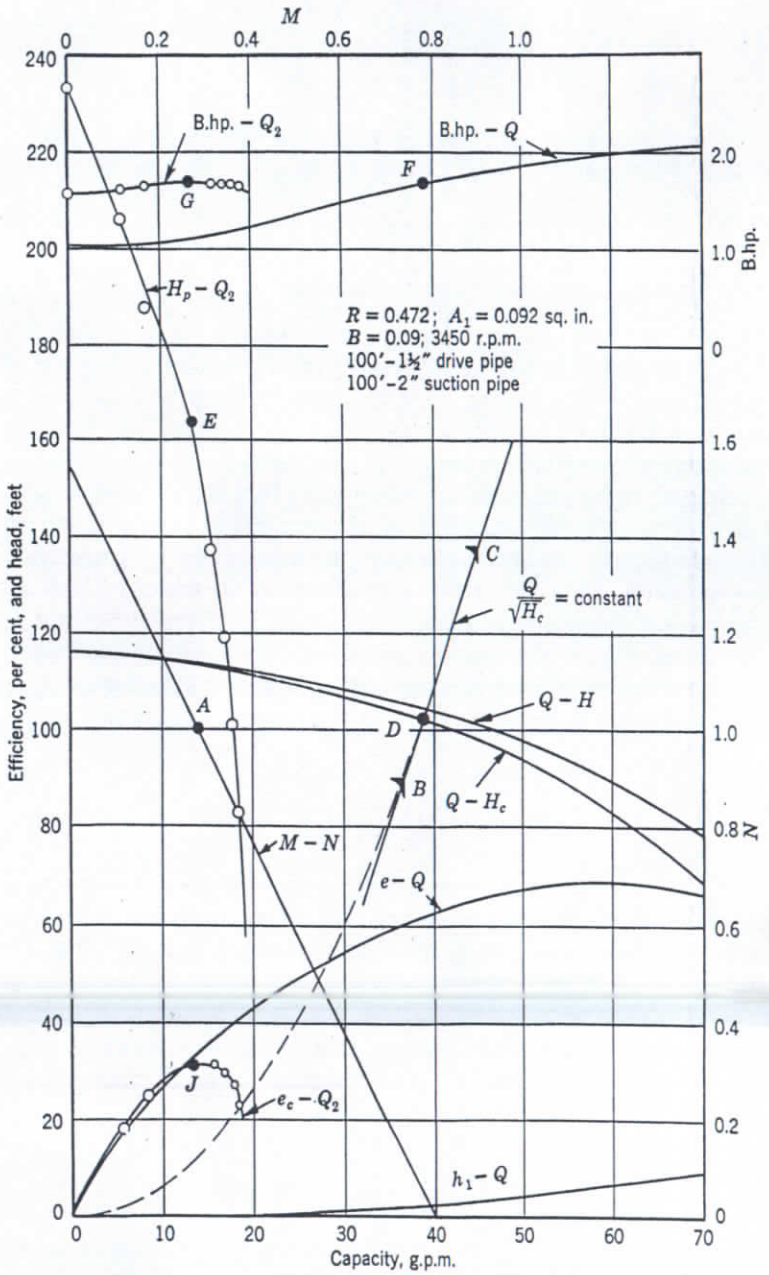

FIG. 18.15. Example of calculation of jet-centrifugal pump performance.

per cent, indicating that part of the secondary flow in immediate contact with the nozzle jet moves at a higher velocity than the net suction head would produce.

Note that with adjustable nozzle the maximum suction flow Q_2 is higher than with fixed nozzle at the same throat area because A_1 is reduced by the needle valve.

(*d*) **Design Procedure.** The normal design procedure aims are to design a jet pump at best efficiency to meet the required head-capacity requirements. Normally, the driving head H_1, the jet pump head H_d, and the suction head H_s are fixed by the conditions, and the quantity to be pumped (Q_2) is known. The quantity to be calculated is the driving capacity Q_1. The size of the nozzle and the size of the throat can be determined by straightforward procedure:

1. The value of N is calculated according to equation 18.3.
2. From Fig. 18.9 the value of R and M are read off for the b.e.p. and 30 per cent efficiency. If efficiency different than 30 per cent is expected, the value of N should be reduced according to equation 18.9 to enter the chart of Fig. 18.9. Then the value of M obtained from the chart is revised upward or downward to comply with the efficiency expected.
3. The value of Q_1 is now determined for the known values of Q_2 and M; $Q_1 = Q_2/M$. If instead of Q_2 the value of $Q = Q_1 + Q_2$ is specified, then $Q_1 = Q/(M + 1)$; and $Q_2 = Q - Q_1$.
4. The nozzle size A_1 is given by equation 18.16 using $C = 0.95$.
5. The throat area A_2 can now be determined from

$$A_2 = A_1/R$$

This should be checked by Weeks' rule, equation 18.8.

6. The dimensionless characteristics M-N can be drawn as a straight line with a slope $\tan \alpha = N/M$. The Q_2-H_d curve can be drawn point by point. The capacity $Q_2 = Q_1 M$, Q_1 remaining essentially constant. The values of H_d for a selected N is found from equation 18.3, where H_1 and H_s are very nearly constant.
7. If the design capacity (Q_b in Fig. 18.14) cannot be realized because of a limited suction head H_s, the head-capacity curve breaking off at some smaller capacity Q_c, a larger throat and nozzle will be necessary to produce the required capacity. The larger jet pump will be designed for a greater capacity Q_d but will deliver only capacity Q_b, which is a partial capacity for the larger unit, the operating point being to the left of the peak efficiency.

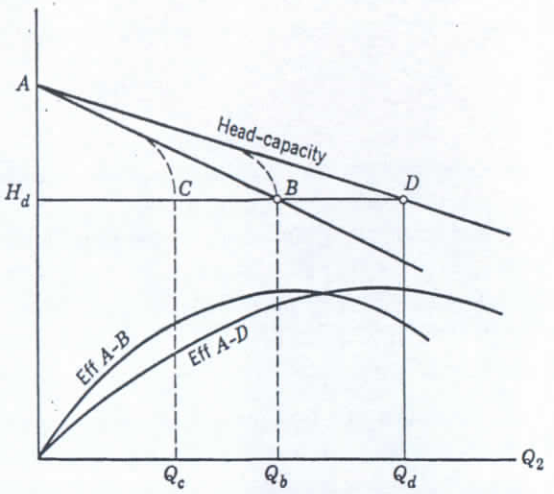

FIG. 18.14. Effect of submergence on jet pump performance.

The larger jet pump will have the same values of M and R at the design point Q_d because both these characteristics depend on the value of N only, which remains unchanged. Equation 18.10 and the ratio $R = A_1/A_2$ enable one to determine the required throat and nozzle areas. A larger driving capacity Q_1 will be required to lift the same capacity Q_2 as a result of moving the operating point off peak in the larger pump. Note that limited submergence (NPSH) requires use of a larger pump to meet the specified capacity, a procedure similar to that practiced with centrifugal pumps under cavitation conditions.

Remarks. Note that for a given value of N, values of M and R are uniquely defined by Fig. 18.9, indicating that M and R are not independent. Their relation is given by the equation 18.7

$$1 + M = 1/\sqrt{R}$$

or

$$1 + M = D_t/D_n \qquad (18.11)$$

where D_t is the throat diameter and D_n is the nozzle diameter. But since M and N are related to jet pump efficiency,

$$MN = e_j \qquad (18.12)$$

and as efficiency should be known or estimated prior to the actual design of the jet pump, values of M and R can be calculated directly from equations 18.11 and 18.12 without resorting to Fig. 18.9. The consistency of the points plot on Fig. 18.9 in reality is a proof of equations 18.7 and 18.8 found first experimentally.

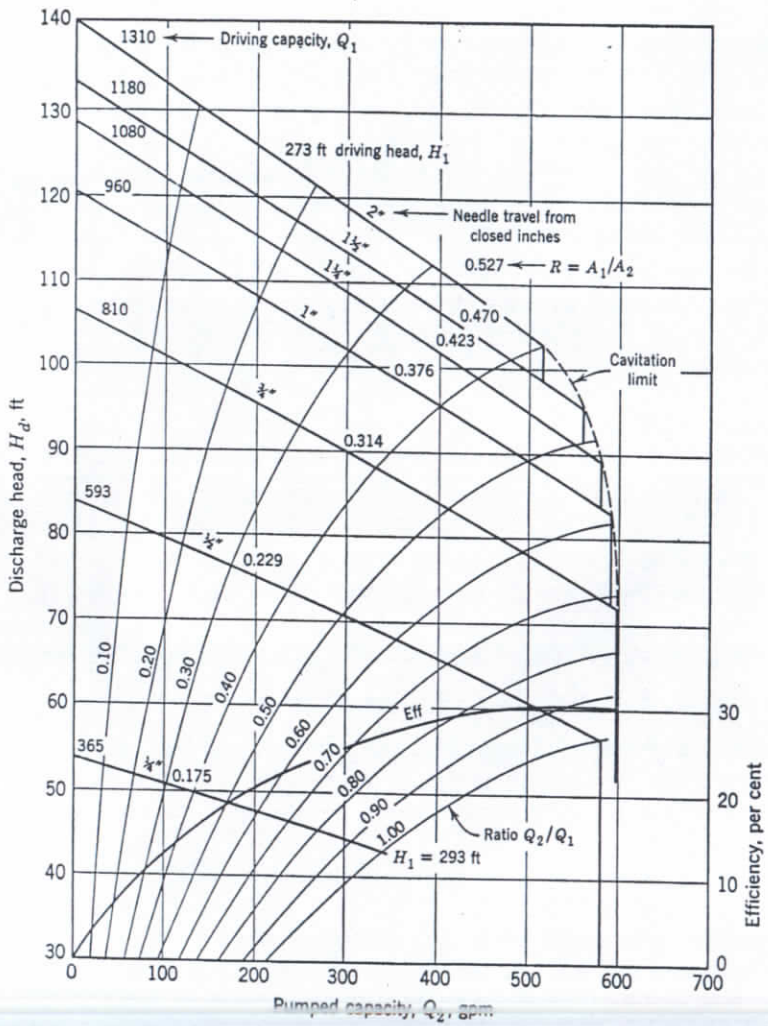

FIG. 18.13. Eight-in. jet pump performance. $A_2 = 6.35$ square in., $H_s = 6$ ft (lift) (Bureau of Reclamation).

shown in Fig. 18.11.[6] In the latter when the jet pump discharge pressure is reduced, the nozzle area is reduced, thus reducing the nozzle/throat ratio, shifting to a flatter M-N curve, greater capacity, and a better efficiency. By referring to Fig. 18.5, the dotted lines show envelopes of M-N and efficiency curves of four jet pumps of different nozzle/throat ratio. Such characteristics are approached by jet pumps with an automatic needle valve.

When used in combination with a centrifugal pump the adjustable nozzle results in an increase of the capacity range for a given submergence, an improved efficiency, and a reduced power demand for the centrifugal pump motor (Fig. 18.12). The performance of a similar unit with a fixed nozzle is shown for comparison.

Figure 18.13 shows the performance of an 8-in. jet pump shown on Fig. 18.10. This is one of several large jet pumps built by the U. S. Bureau of Reclamation * in sizes up to 72 in. for auxiliary services in large hydroelectric plants. Some applications for these jet pumps are: water supply for generator cooling, water stream for fish trap, drainage of water turbine casings, emergency sump service, and others. An examination of performance of large jet pumps is of interest particularly in comparison with small jet pumps.

The following observations are based on a study of performance of 8-, 12-, 24-, and 72-in. discharge nozzle sizes.

1. The peak efficiency of large jet pumps is of the same order as that of small pumps (up to 3 in.).
2. There are indications that the optimum nozzle/throat ratio shifts to a lower value than that appearing on Fig. 18.6. This suggests that with large nozzles the middle part of the jet cannot exchange its momentum very effectively.
3. The M and N values of large jet pumps plot satisfactorily on Fig. 18.9.
4. The individual M-N curves are more nearly straight lines without showing any tendency to higher values of N as zero M is approached.
5. Equation 18.8 holds very accurately for large jet pumps.

(c) Cavitation. Jet pumps are subject to cavitation in the same manner as the centrifugal pumps. Cavitation limits the maximum capacity possible for a given suction head, irrespective of the reduction of the discharge head, as it appears on Fig. 18.12. Cavitation in jet pumps is accompanied with typical cavitation noise and pitting of the throat walls. Actual measurements of pressure at the throat under cavitation condition show the vapor pressure corresponding to the liquid temperature. Under this condition the maximum suction flow is given by

$$Q_2 = (A_2 - A_1)\sqrt{2g(H_s - h_s)} \qquad (18.10)$$

where h_s is the losses in the suction pipe. The actual measured suction flow is greater than that given by this equation by approximately 10

* U. S. Dept. of Interior, Bureau of Reclamation, Denver, Colorado, Hydraulic Machinery Branch.

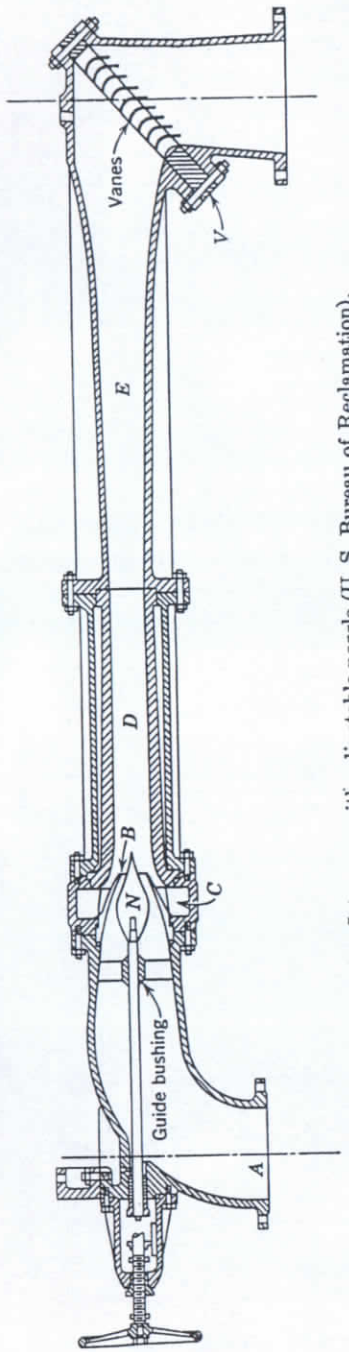

FIG. 18.10. Jet pump with adjustable nozzle (U. S. Bureau of Reclamation).

nozzle/throat spacing ratio below one leads to a reduction of head capacity and efficiency due to obstruction of the secondary flow to the throat.

Since the M-N characteristics of jet pumps approach a straight line for the useful range of their performance, such characteristics can be drawn if the values of M and N are known for the b.e.p. The slope of the straight line M-N is given by $\tan \alpha = N/M$, where α is the angle between the M-N line and the positive direction of the M axis. The fact that the M-N line is straight results in the peak efficiency taking place at the $M = M_0/2$ and $N = N_0/2$.

Figure 18.9 shows the plot of M and N values for the b.e.p. for jet pumps of different nozzle/throat ratios and a peak efficiency of 30.0 per cent. For values of efficiency e_j, different than 30.0 per cent, the M and N values were reduced directly as the square root of efficiencies, or

$$M' = M\sqrt{0.30/e_j} \quad \text{and} \quad N' = N\sqrt{0.30/e_j} \qquad (18.9)$$

where e_j is the actual measured peak efficiency $e_j = MN$, and M' and N' are values plotted in Fig. 18.9.

(b) Adjustable Nozzle. By providing a needle valve for the nozzle (Figs. 18.10 and 18.11) the nozzle/throat ratio can be varied and, in this way, the operating range of the jet pump (or jet-centrifugal combination) can be increased. The needle valve adjustment can be made either manually, as shown in Fig. 18.10, or automatically by a membrane, as

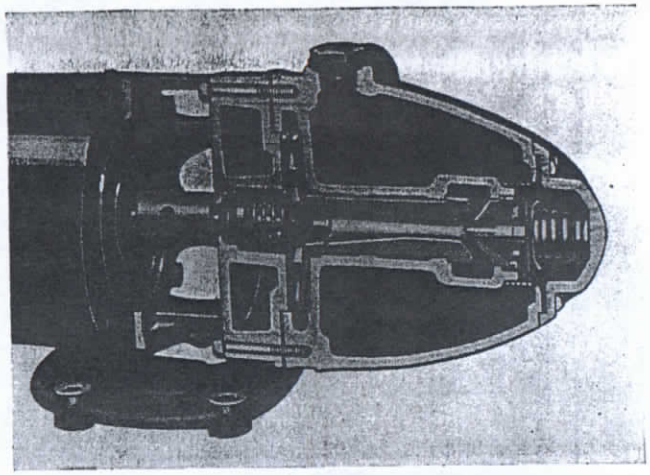

FIG. 18.11. Centrifugal-jet pump combination with an adjustable nozzle (Flint & Walling).

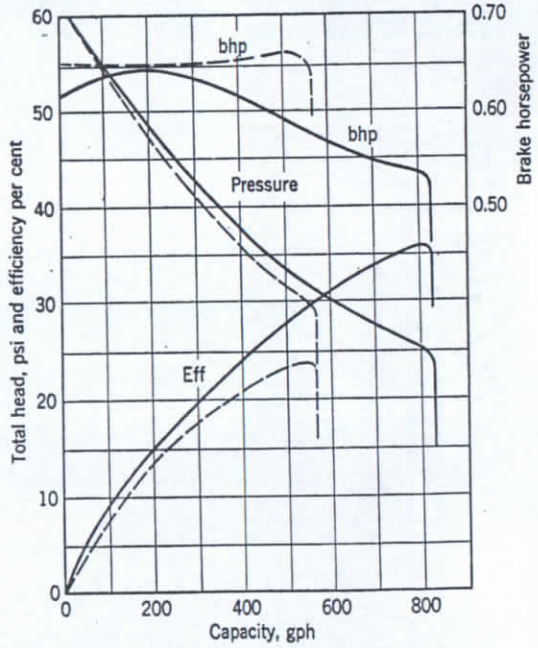

FIG. 18.12. Centrifugal-jet performance. Full line, variable nozzle; dotted line, fixed nozzle (Flint & Walling).

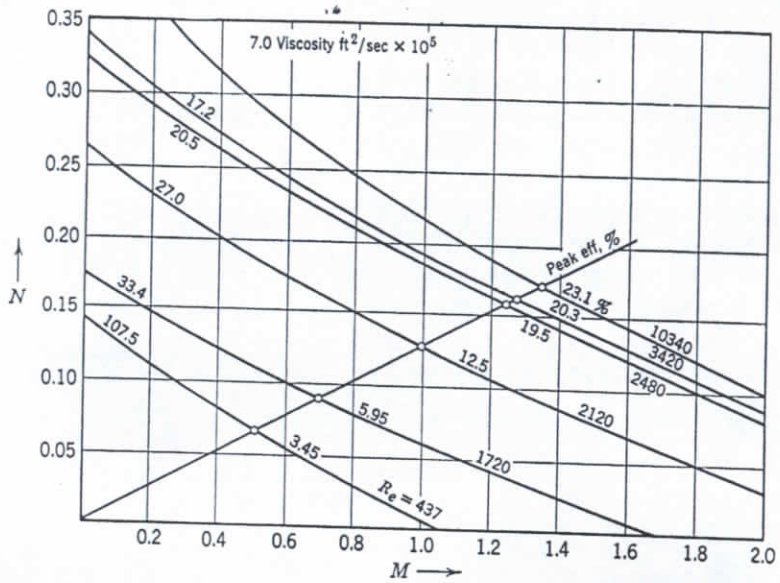

FIG. 18.8. Performance of a jet pump on viscous oil. $R = 0.174$; $D_1 = 0.10$ in.; R_e = Reynolds number.

and viscosity of the liquid. Effect of viscosity is seen better on Fig. 18.8 which shows that the shape of M-N lines remains the same for several Reynolds numbers, being a characteristic for a given nozzle/throat ratio. Reynolds numbers are based on the nozzle size and nozzle velocity. There is a fixed relationship between the Reynolds number for nozzle flow R_n and that for the throat flow R_t.

$$R_t = R_n\,(1 + M)\sqrt{R} \tag{18.6}$$

It so happens that at the b.e.p. $R_t = R_n$. This means that for the b.e.p.

$$(1 + M)\sqrt{R} = 1 \tag{18.7}$$

It can be shown by algebraic transformation that equation 18.7 is equivalent to

$$Q_1 v_1 = (Q_1 + Q_2) v_t \tag{18.8}$$

where v_1 is the nozzle velocity and v_t is the throat velocity. Equation 18.8 states that the momentum of the flow through the nozzle is equal to the momentum of the flow through the throat. This means that momentum lost by the nozzle flow is gained by the pumped secondary flow, assuming that the latter has a zero velocity of approach

$$Q_1(v_1 - v_t) = Q_2 v_t \tag{18.8a}$$

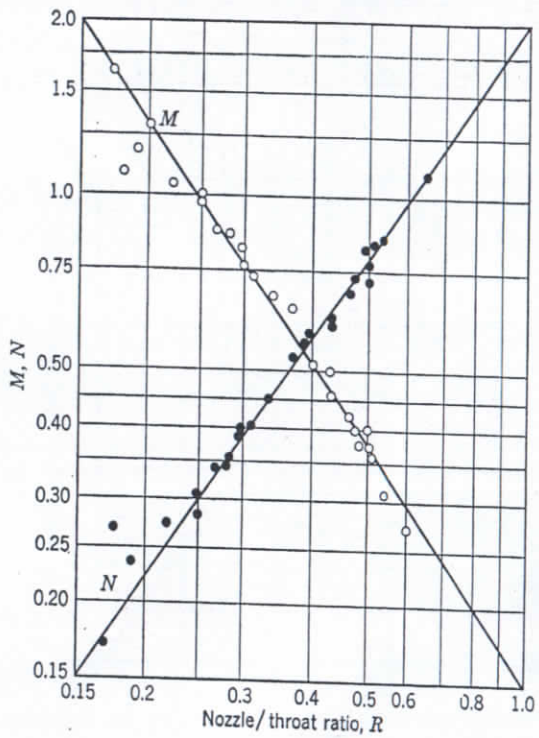

FIG. 18.9. M and N in terms of nozzle/throat ratio for 30 per cent peak efficiency.

The relationship expressed by equation 18.8 was established experimentally by Weeks [3,4] on air and led to the method of design of air jet pumps for mine ventilation service. The scatter of the points on Fig. 18.7 is caused by the effect of the nozzle/throat ratio and the lack of physical similarity of detail. In general, it should be realized that the Reynolds number for the flow through the nozzle or throat of the jet pump does not possess the properties of the Reynolds numbers associated with the straight pipe flow and, therefore, cannot serve as an all-including criterion of performance of the pump.[5]

3. For small jet pumps as used in connection with centrifugal pumps for the domestic water supply the spacing between the nozzle and throat is equal to one nozzle diameter. The length of the throat is about six throat diameters. These ratios are functions of the velocities through the nozzle and the throat, and the size of the unit, higher velocities and larger sizes requiring larger spacing between the nozzle and the throat and a longer throat. Although an increase of both of the above ratios has only minor effect on the jet pump performance, a reduction of the

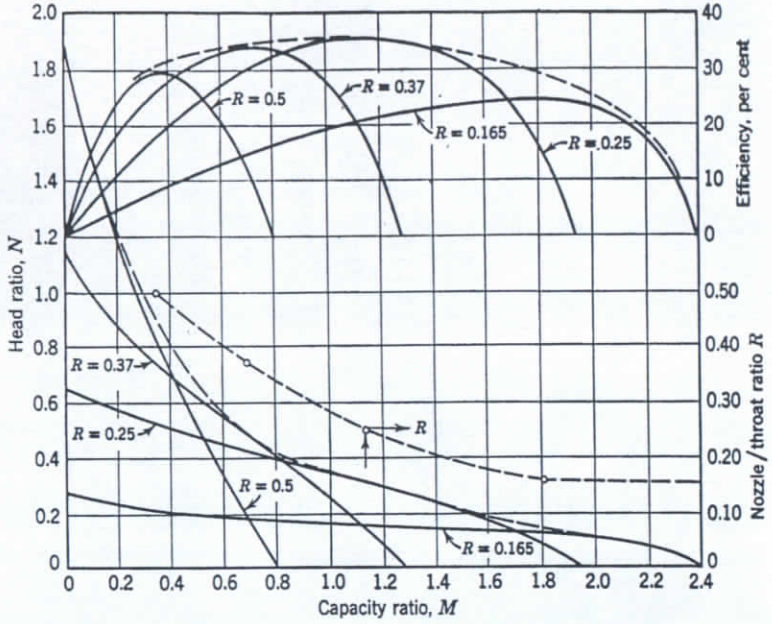

FIG. 18.5. Jet pump characteristics (Flint & Walling). Dotted line, adjustable nozzle performance.

The fact that the M-N curves are approaching straight lines for the useful range of head capacity results in the peak efficiency taking place at the values of M and N equal to half of values of M_0 and N_0 respectively, where M_0 is the M value for $N = 0$ and N_0 is the N value for $M = 0$. When the M-N curve is established an efficiency curve can be easily plotted, and it is symmetrical about its peak.

The efficiency of jet pumps is affected by the following factors:

1. The nozzle/throat ratio is the most important design element for jet pumps and serves as a type criterion in the same manner as specific speed does for centrifugal pumps. Figure 18.6 shows jet pump efficiency for different nozzle/throat ratios compiled from tests of commercial jet pumps in sizes from 1- to 3-in. discharge. The sizes of nozzles are marked on the figure. The maximum 35 per cent for $R = 0.28$ is the highest efficiency known to the author ever attained by jet pumps irrespective of size. The scatter of points on Fig. 18.6 reflects the effects of size and minor variations in details of component parts of the jet pumps.

2. Figure 18.7 shows jet pump efficiency as a function of the Reynolds number, which accounts for nozzle size, pressure range or jet velocity,

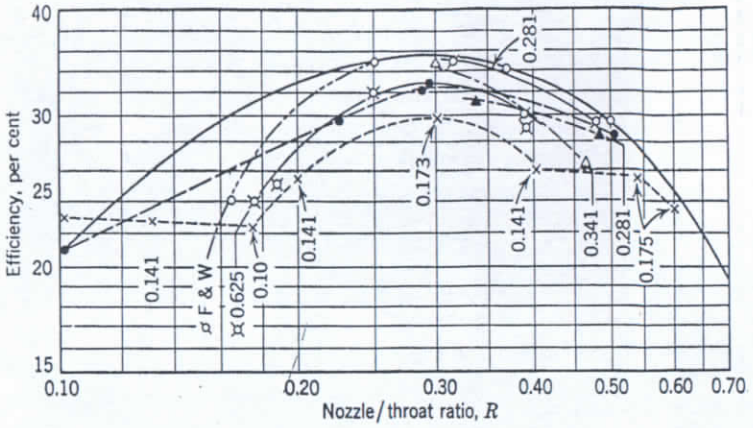

FIG. 18.6. Efficiency of jet pumps.

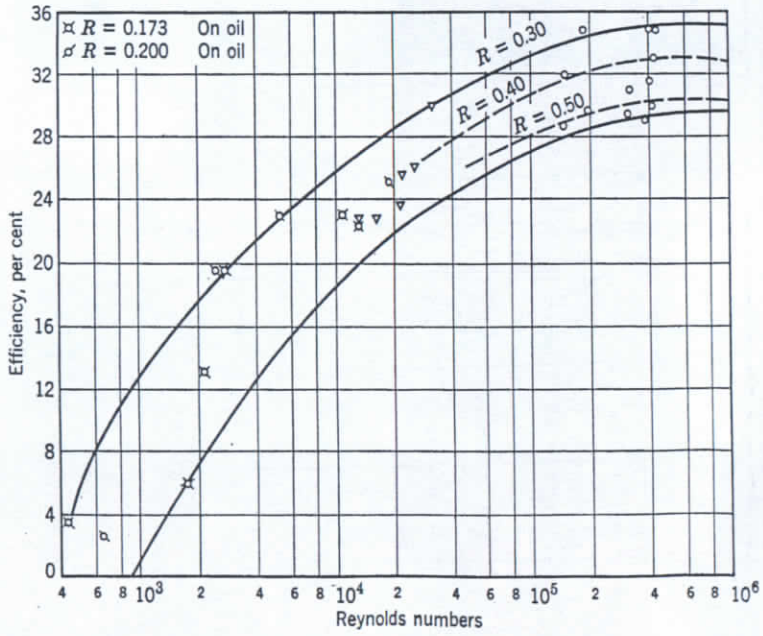

FIG. 18.7. Efficiency of jet pumps for different Reynolds numbers.

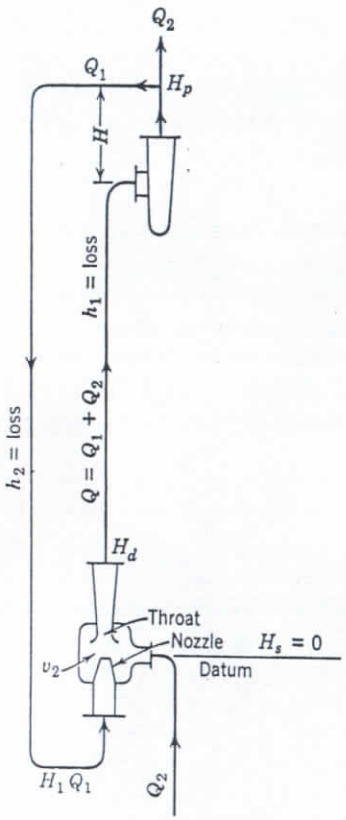

FIG. 18.2. Jet-centrifugal pump combination.

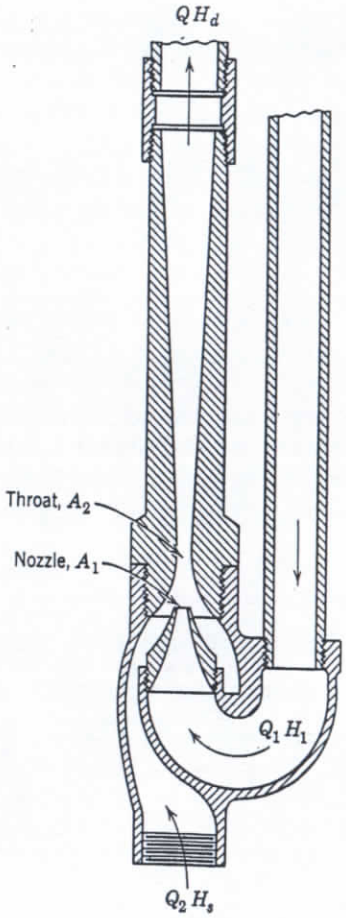

FIG. 18.3. Jet pump.

speeds. According to Gosline and O'Brien [2] the characteristics of jet pumps can be described by three ratios:

$$R = \frac{A_1}{A_2} = \frac{\text{nozzle area}}{\text{throat area}} \tag{18.1}$$

$$M = \frac{Q_2}{Q_1} = \frac{\text{pumped capacity}}{\text{driving capacity}} \tag{18.2}$$

$$N = \frac{H_d - H_s}{H_1 - H_d} = \frac{\text{net jet pump head}}{\text{net driving head}} \tag{18.3}$$

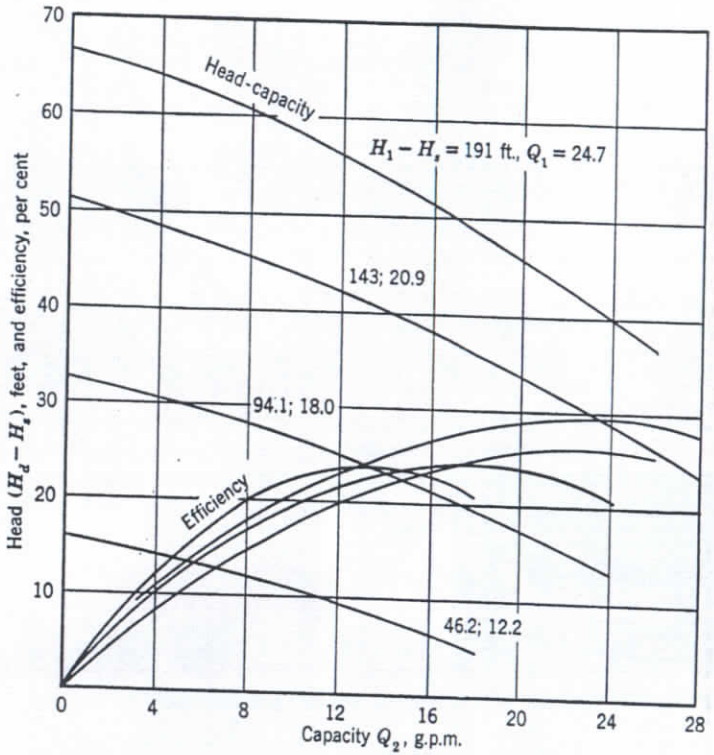

FIG. 18.4. Jet pump performance (Gosline and O'Brien [2]).

The driving head H_1 and the driving capacity Q_1 are furnished from the outside source. Capacity Q_2 enters the jet pump suction under the head H_s. The capacity leaving the jet pump discharge equals the sum of the driving capacity and the jet pump capacity:

$$Q = Q_1 + Q_2 \tag{18.4}$$

Figure 18.5 shows several typical characteristics of jet pumps in terms of M and N for four values of R. Except for the extreme values of R the M-N curves approach straight lines for the major part of the range and apply to all similar jet pumps. The slope of the M-N lines ($\tan \alpha = M/N$) is determined by the value of R. The position of the M-N lines is governed by the efficiency of the jet pumps, more efficient pumps giving higher values of M and N, as is evident from the definition of efficiency of jet pumps.

$$e_j = \frac{Q_2(H_d - H_s)}{Q_1(H_1 - H_d)} = MN \tag{18.5}$$

Chapter 18

Centrifugal-Jet Pump Water Systems

18.1 GENERAL ARRANGEMENT

For small capacities and low lifts (up to 125 ft) a special type of pumping unit has been developed which consists of a combination of a centrifugal pump and a jet pump or ejector. The first is mounted next to the motor at the ground surface and furnishes the driving head and capacity for the jet pump placed in the well below the water surface (Fig. 18.1). For shallow wells up to 25 ft the jet pump can be placed on the surface of the ground or built into the centrifugal pump casing.[1] The mechanical advantage of this arrangement is evident as there are no moving parts in the well, and the centrifugal pump, with its motor, can be placed at some convenient point. The hydraulic advantages are: steep head-capacity characteristics with operating head about 50 per cent higher than that of the centrifugal pump alone and a brake-horsepower curve which is non-overloading. The peak efficiency of the combination is equal to or better than that of the jet pump but is lower than that of centrifugal or vertical turbine pumps. However, at the operating capacity the efficiency is equal to or better than that of the centrifugal pump at the same capacity. In small sizes, this type of pumping unit is widely used for the domestic water supply. According to U. S. Department of Commerce Census ("Facts for Industry," Series M31B-116) over 360,000 jet-type water systems were sold each year (average for 1946 to 1952) representing a value over $30,000,000.

18.2 JET PUMPS

(*a*) **Performance Characteristics.** Figure 18.2 shows a diagram of the jet-centrifugal combination and the notation for several terms used for discussion. Figure 18.3 shows an enlarged view of the jet pump, and Fig. 18.4 gives the performance of a jet pump under several driving heads, kept constant for each head-capacity curve. Note the resemblance of these curves to centrifugal pump characteristics at several

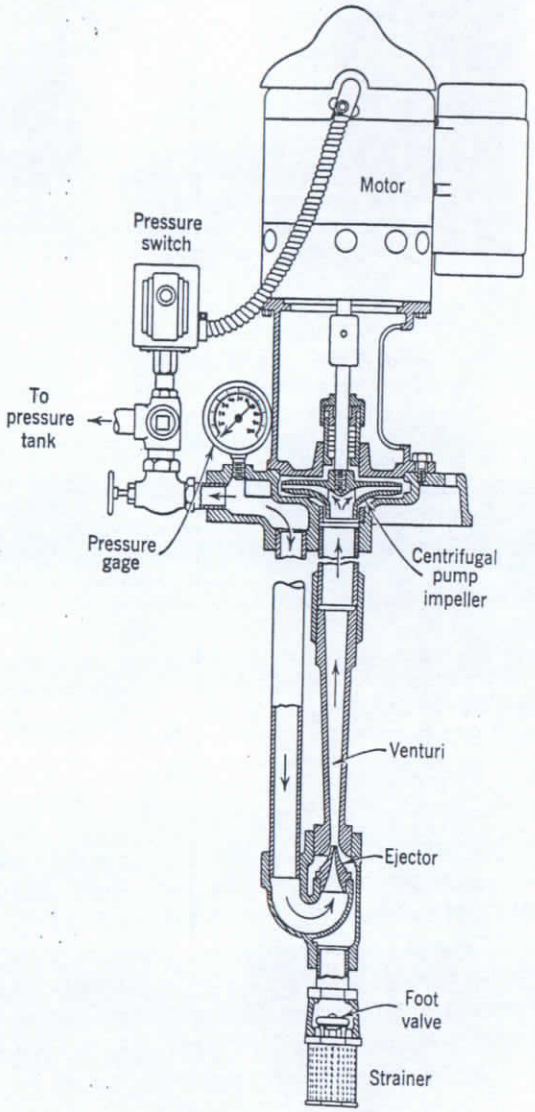

FIG. 18.1. Jacuzzi jet pump water system.

the cut-water or tongue (Fig. 17.22). The upper part is not submerged in liquid during the priming period and the cut-water is closely fitted to the impeller, thus preventing the air from recirculating. A chamber

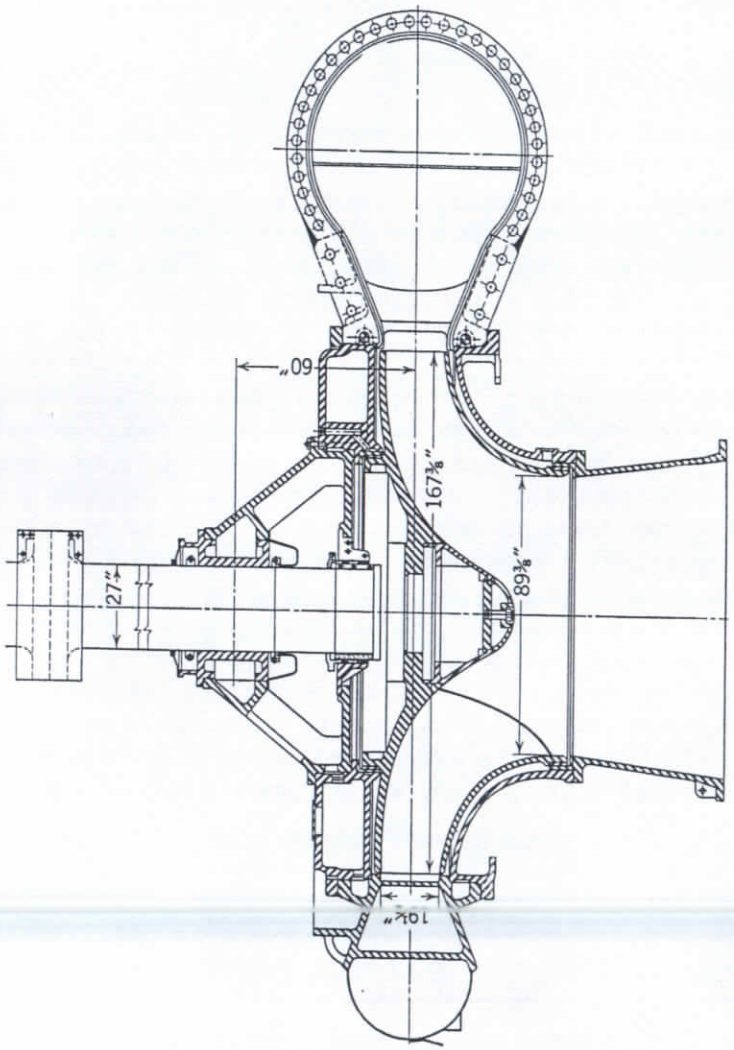

Fig. 17.23. Grand Coulee vertical pump, 607,000 gpm, 310 ft, 200 rpm, 65,000 hp (Byron Jackson).

built around the volute-proper and surrounding the suction nozzle is so arranged that there is enough liquid stored in the pump casing for the priming operation. The self-priming casing is interchangeable with a standard casing when self-priming is not wanted. An 800-gpm pump of this design at 1750 rpm when handling cold water will prime 30 ft

of 6-in. pipe at a 20-ft static lift in less than 2 minutes. Efficiency of this pump approaches that of the conventional end-suction pump of the same rating.

Figure 17.23 shows the Grand Coulee pump, referred to in Art. 2.3, rated at 607,000 gpm, 310-ft head, and driven by 65,000-hp motor at 200 rpm. The size of the pump was determined by the size of available forgings for the pump shaft. Two of these pumps are driven by a single 165,000-hp water turbine. The hydraulic design of these pumps is given in detail by the pump manufacturer.[10] The full-size units had presented a number of mechanical and hydraulic problems which could not be predicted from the model testing or previous experience (reference 7, Chapter 7).

REFERENCES

1. A. Hollander, "Stuffing Box for Refinery Pumps," *Calif. Oil World and Petroleum Ind.*, March 1944.
2. Hanns Hornschuch, "Why Mechanical Seals Improve Centrifugal Pump Operation," *Power*, August 1943.
3. A. J. Stepanoff, "Mechanical Performance of Hot Oil Centrifugal Pumps," *Petroleum Refiner*, December 1942.
4. J. B. Godshall, "Materials for Central-Station Pumps," *Corrosion*, January 1954.
5. L. W. Cadwallader and H. S. Frederick, "Design Features, Operating Experience and Performance of 100,000 KW Reheat Installation at Potomac River Station," *Combustion*, p. 38, May 1955.
6. *Standards of the Hydraulic Institute*, New York, 1955.
7. Igor Karassik, "So You Are Going to Buy a Boiler Feed Pump," *Southern Power and Ind.*, pp. 55, 57, April 1942 to July 1943 (a series of twelve articles distributed by Worthington Pump and Machinery Corporation).
8. J. B. Godshall, "Prevention of Feed-Pump Corrosion," New York, Edison Electric Institute Report, 1941–1942; reprinted by Ingersoll-Rand Company.
9. L. H. Roddis, Jr., and J. W. Simpson, "The Nuclear Propulsion Plant of the USS Nautilus," *Westinghouse Eng.*, March and May 1955.
10. Carl Blom, "Development of the Hydraulic Design for the Grand Coulee Pumps," *Trans. A.S.M.E.*, Vol. 72, No. 1, p. 33, January 1950.
11. A. J. Stepanoff, "Testing Hot Oil Pumps under Actual Operating Conditions," *Oil Gas J.*, Oct. 31, 1940.

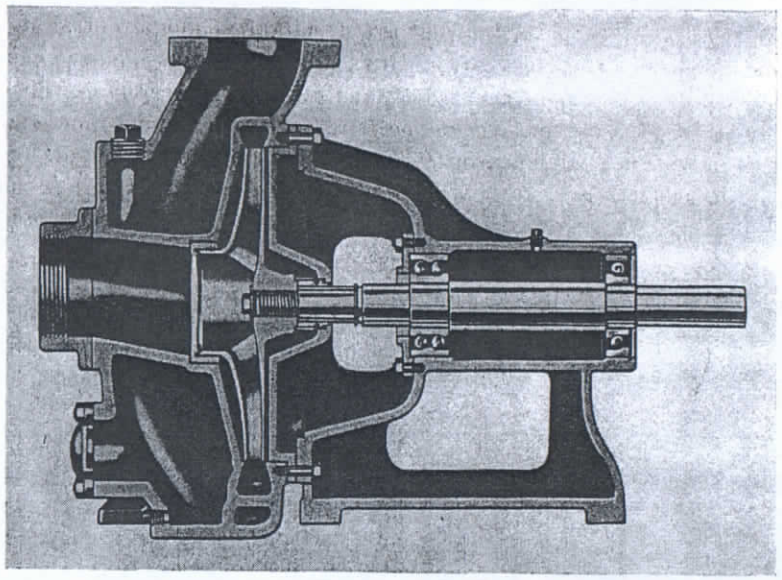

FIG. 17.21. Gorman-Rupp self-priming pump.

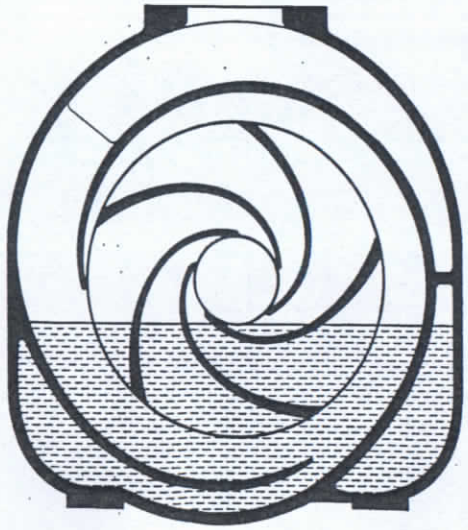

FIG. 17.22. A section through the double volute of pump in Fig. 17.21.

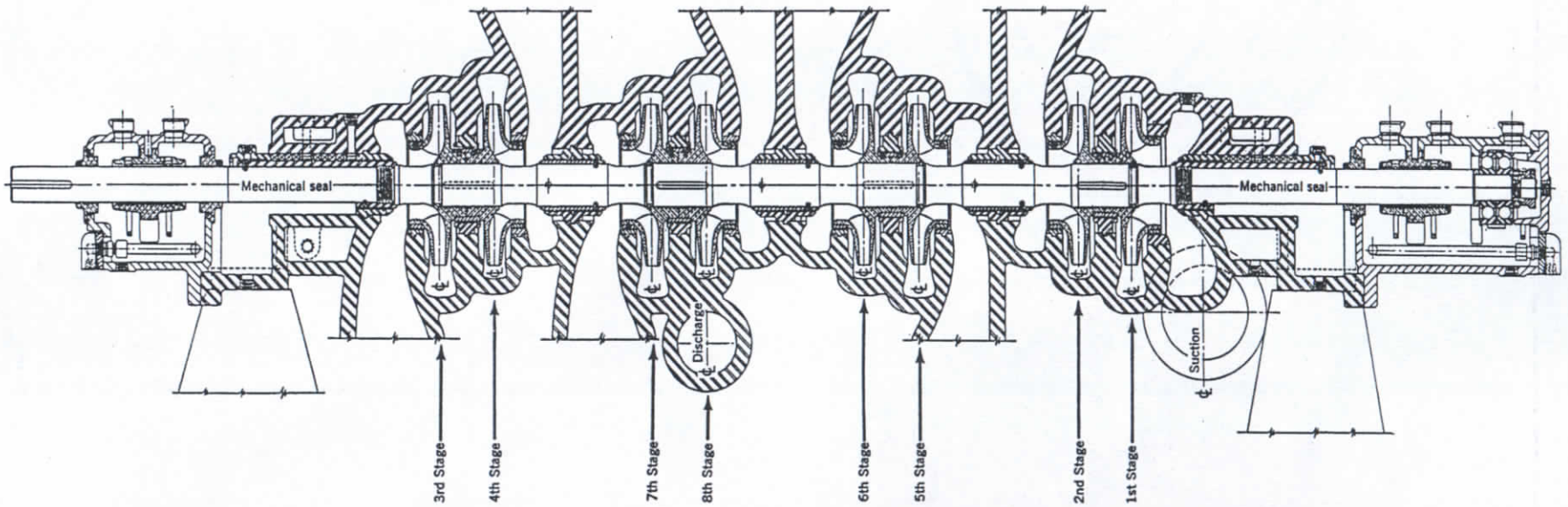

FIG. 17.20. Eight-stage pump with all-external crossover cast on the casing (United Centrifugal Pumps).

Figure 17.19 shows a very compact design of a single-stage pump widely used in the petroleum industry for transfer and pipe line booster service in sizes from 2 to 20 in. Installed outside, this pump does not require a baseplate or heavy foundation and weather protection. In locations subject to floods the motor is placed above the flood level requiring a special pump shaft rigidly coupled to the motor.

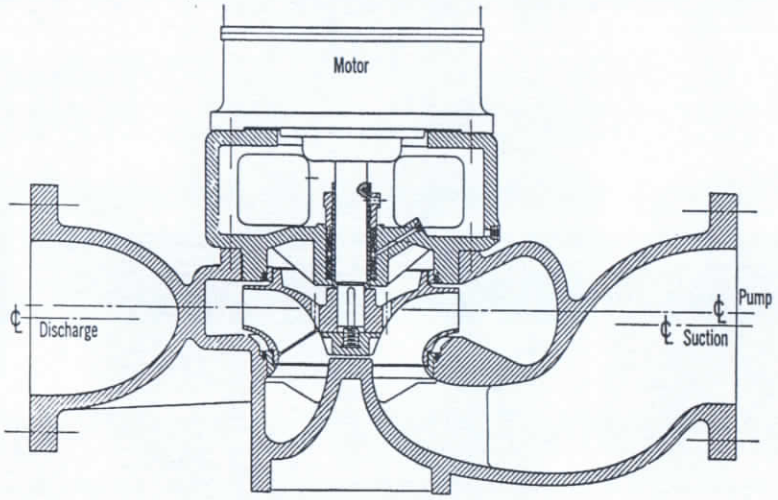

FIG. 17.19. Single-stage pipe line booster pump (United Centrifugal Pumps).

Figure 17.20 shows an eight-stage pump with seven external crossovers as shown on Fig. 7.14. Impellers are arranged in four opposing pairs, thus, theoretically, there should be no axial thrust due to symmetry. The stage arrangement is 1–2–5–6–8–7–4–3. With crossovers cast integral with the casing halves, this presents a major foundry problem. Originally the multistage pump with external crossovers, bolted on or cast on, were developed in this country for oil pipe line service where efficiency evaluation was extremely high. Recent improvement in the vaned diffuser and return channel design here and in Europe has practically wiped out any advantages the external crossover multistage pumps had years ago. There were no pumps with external crossovers built in Europe; as all multistage pumps, they are of the vaned diffuser type.

Figure 17.21 shows a simple self-priming pump. † The double-volute casing is so arranged that the lower part of the volute is always submerged in the liquid and provides ample gap between the impeller and

† H. F [illegible]pp, *U. S. Patent No. 2,461,925*, Feb. 15, 1949.

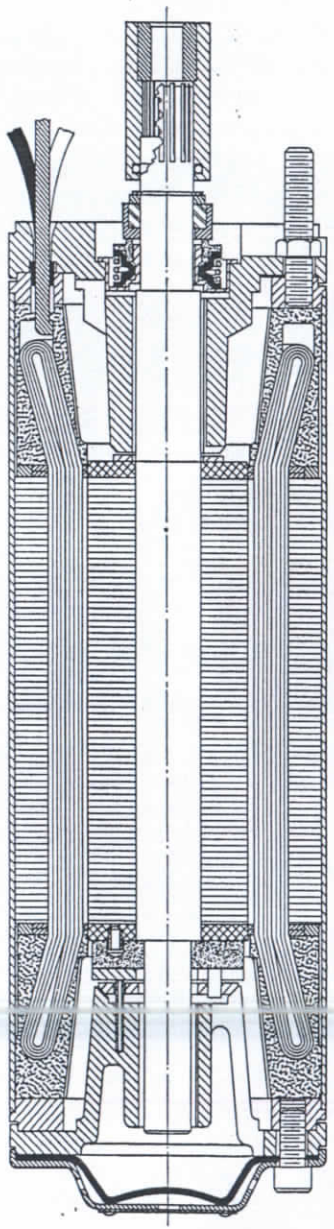

FIG. 17.17 A wet type of submersible motor (U. S. Motors).

Figure 17.17 shows a submersible motor of the wet type specially designed for deep-well pumping. The windings are protected with a special plastic insulation, impervious to water, which remains elastic under the temperatures it is subjected to in deep-well service application. To prevent corrosion within the motor it is filled with a water-oil emulsion. A mechanical seal prevents a free exchange between motor contents and the well water or sand. The outer shell and shaft are stainless. The thrust bearing is of the tilting shoe type with a graphite

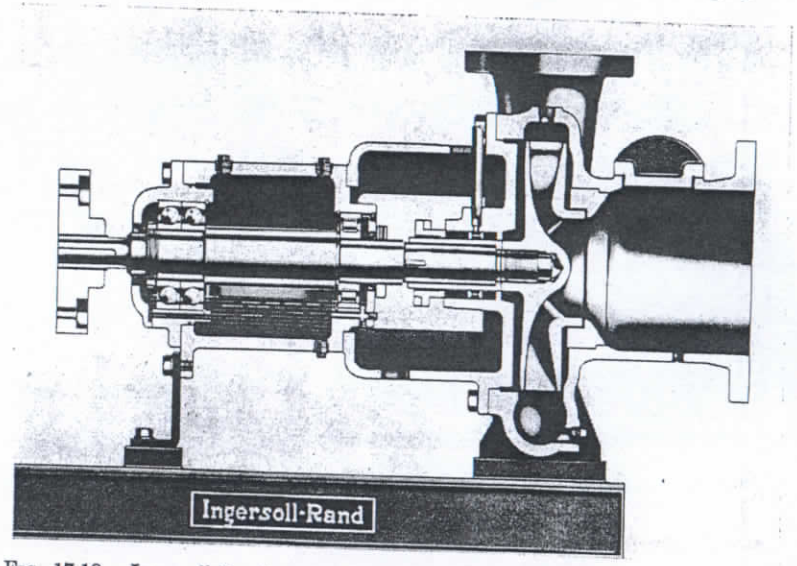

FIG. 17.18. Ingersoll-Rand paper stock pump (Emil Egger, *U. S. Patent No.* 2,566,795, 1951).

thrust disk. There is an elastic diaphragm at the bottom of the shell to allow for heat expansion of the emulsion.

Wet-type submersible motors for 4-in. wells are now available in small ratings (up to 5 hp) from several manufacturers here and abroad. Higher ratings and larger sizes are expected to follow.

Figure 17.18 shows a pump of special design particularly adapted for handling paper stock (up to 10 per cent concentration), and liquids containing up to 50 per cent of entrained gases or vapor without vapor-binding or losing prime. The impeller of this pump has a few (three to five) non-overlapping vanes and profile with an increasing width from the impeller eye to the impeller outside diameter. In spite of such a marked deviation from the normal pump design the pump performance on solid water with adequate NPSH does not differ much from that of the ordinary centrifugal pump.

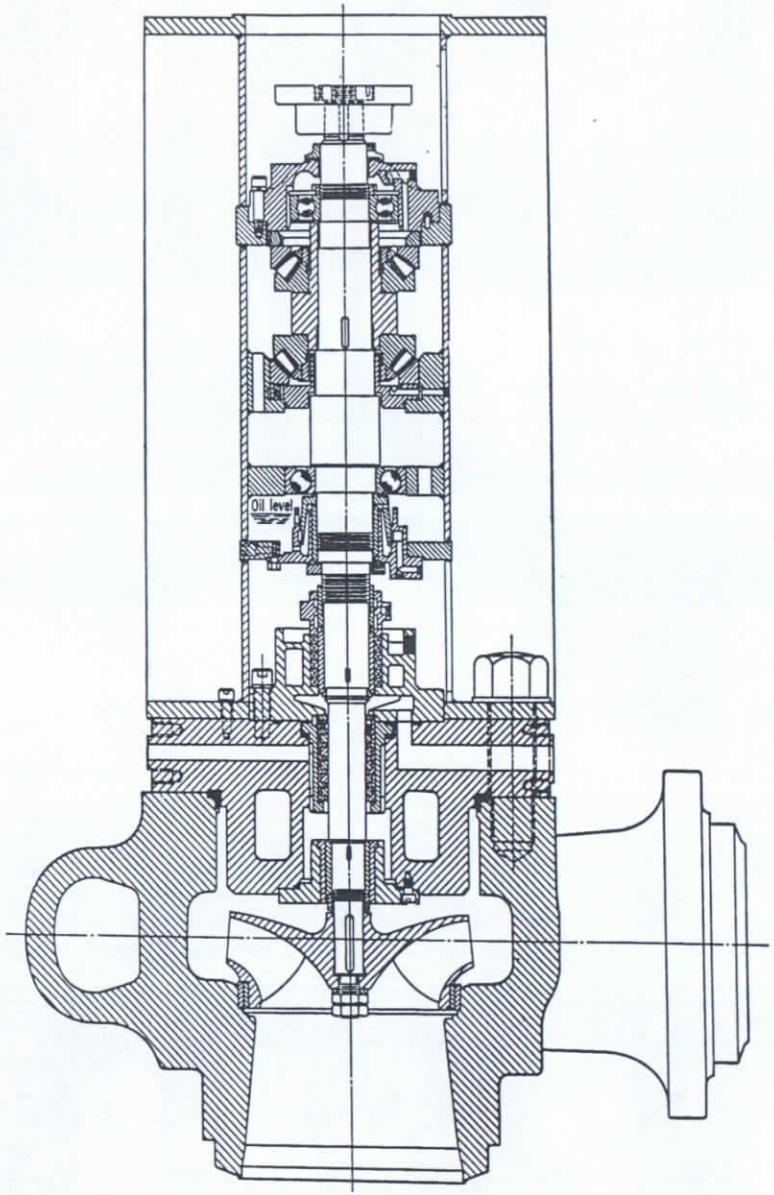

FIG. 17.15. Boiler circulating pump, 4250 gpm, 40 psi at 1750 rpm (Ingersoll-Rand).

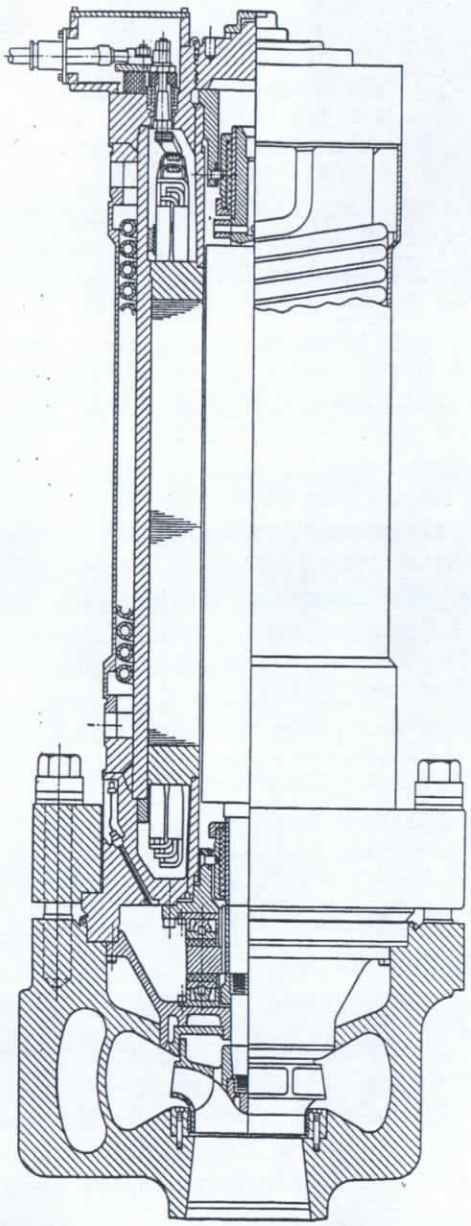

FIG. 17.16. Nuclear reactor primary coolant pump, 4000 gpm, 310 ft at 3550 rpm (Westinghouse Electric Corporation).

long bleed-offs, with leakage precooled to below 212°. The high pressure joints in the barrel are protected with an overlay of stainless steel.

The double-case high pressure pumps in the United States are perhaps evenly divided between the double-volute and diffusion casing designs. In Europe all multistage designs are of the vaned diffuser type because of higher valuation of efficiency there.

17.3 EXAMPLES OF CENTRIFUGAL PUMPS AND INSTALLATIONS

Figure 17.15 shows a boiler circulating pump rated at 4250 gpm at 40 psi differential pressure at 1750 rpm. Three pumps are used per boiler, any two of which are capable of circulating adequate water for full-steam output. The inlet pressure is 1945 psig. Suction and discharge nozzles are arranged for welding to the boiler circulating piping which supports the pumps. The sealing arrangement consists of a throttle bushing and sleeve between the injection water chamber and the back of the impeller. The function of this seal is to prevent high temperature boiler water from entering the pressure breakdown device. A floating seal pressure breakdown is provided between the injection water chamber and the stuffing box. A differential pressure control valve maintains 40 psi across the pump seal. Under this condition the total injection water supply for three pumps is 50 gpm and the total leak-off for three pumps is 37 gpm.[5]

Figure 17.16 shows a pumping unit for the primary coolant circulation of the type used on the nuclear propulsion plant of the U.S.S. *Nautilus*. The pump handles water of extreme purity under 2000-psig pressure, which is used for heat transfer from the reactor into a steam generator. The pump is driven by a "canned" motor enclosed into a container to withstand full pressure of the circuit. The motor stator windings are protected with a nickel-alloy liner or "can." The rotor is sealed in a similar manner. All parts are made of corrosion-resistant materials. The bearings are made of a carbon-graphite compacted material (graphitar) and are water lubricated by means of an auxiliary impeller forcing cooled primary water through the motor gap and two radial and thrust bearings. A low pressure, fresh water heat exchanger, a part of which is built integral with the motor, is used to remove the heat generated within the motor. A detailed description of the primary coolant pump is given in reference 9.

A similar unit rated 4700 gpm at 1800 rpm, 150 hp, 440 volts, has been installed for high pressure boiler circulation of water at 605°F at 1725 psig at the Possum Point Generating Station of the Virginia Electric Power Company.

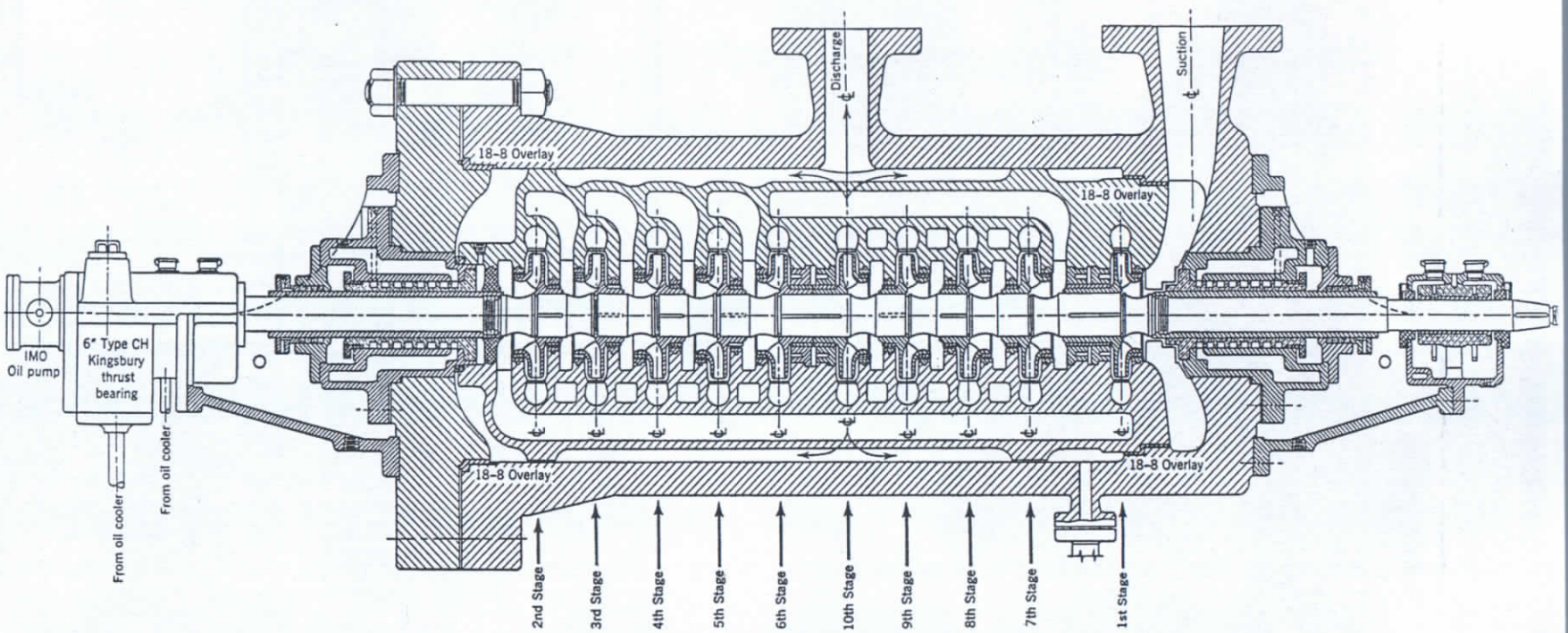

FIG. 17.14. High pressure boiler feed pump with horizontally split inner casing (United Centrifugal Pumps).

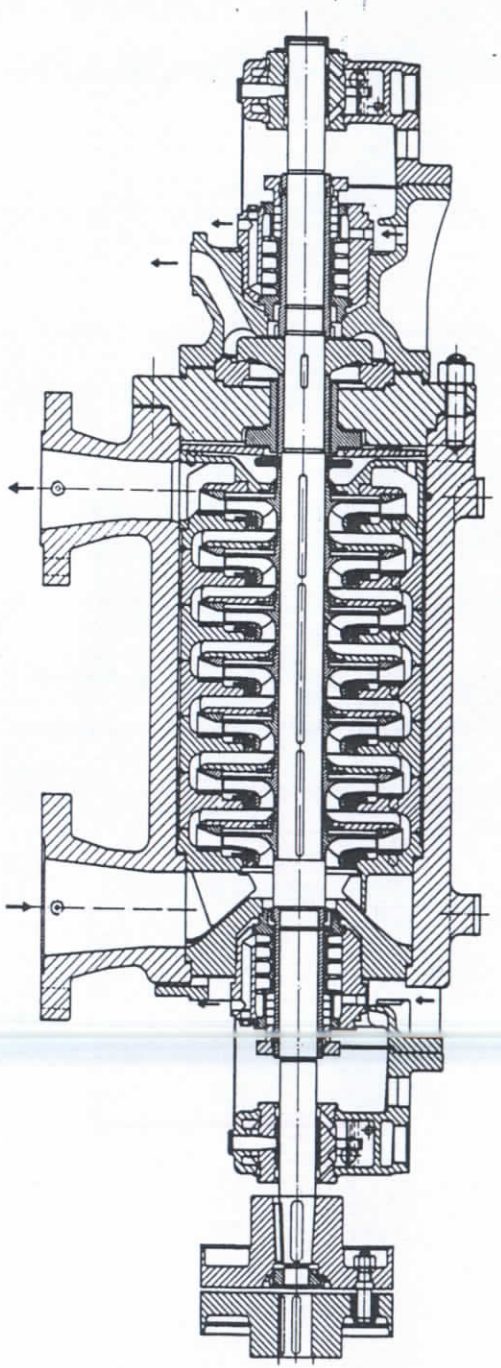

FIG. 17.13. Sulzer high pressure boiler feed pump.

means of corrosion-resistant sealing rings. Axial thrust is taken up with a flanged balancing drum, accessible without opening the outer casing. Any residual thrust is taken up by a Kingsbury thrust bearing which carries the load during starting and stopping. Stuffing boxes can be equipped with single or double mechanical seals. This design is available for capacities of 125 to 1600 gpm. For higher pressures, up to 2800 psi, the pumping element is assembled within a steel-forged barrel vertically split with a circular joint between the cover and the casing.

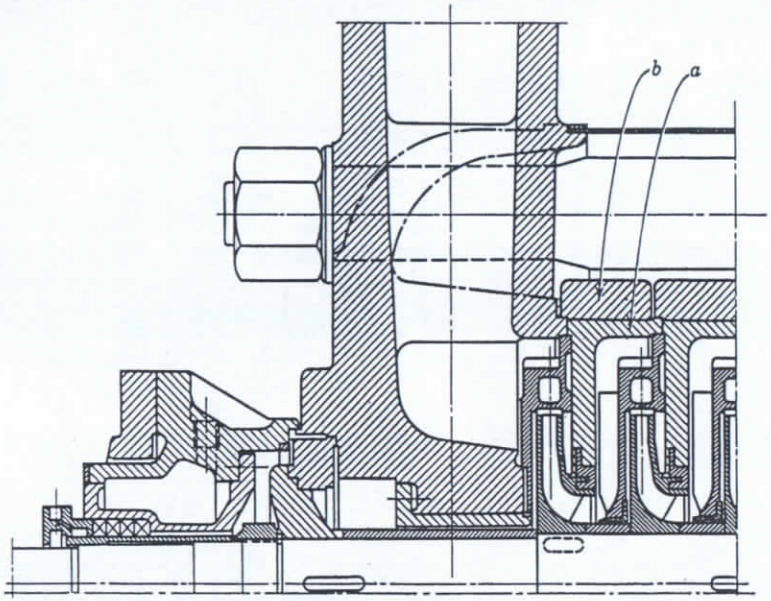

FIG. 17.11 Detail of high pressure Klein, Schanzlin & Becker boiler feed pump.

Figure 17.10 shows a Klein, Schwanzlin & Becker boiler feed pump, consisting of individual stage casings bolted together without gaskets by heavy anchor bolts. Axial thrust is taken up by the automatic balancing disk preceded by a closely fitted throttle. There is no thrust bearing. Until recently all European boiler feed pumps were of similar design. For high pressures (up to 4600 psi) the stage elements (*a* in Fig. 17.11) are surrounded with alloy steel rings (*b* in Fig. 17.11) shrunk on the individual stages to take up the stress due to internal pressure. The joints between the stages are ground and held tight by heavy anchor bolts.

Figure 17.12 shows a single-stage boiler feed pump built integral with the steam turbine, intended primarily for locomotive and marine

service. These pumps are built for capacities up to 300 gpm, pressures up to 750 psi or 1800 ft of head, water temperatures up to 300°F, and speeds of 7400 rpm.

Figure 17.13 shows a Sulzer high pressure boiler feed pump of double-casing design. The outer barrel is open on both ends. Axial thrust is taken up by the automatic disk without any thrust bearing. The

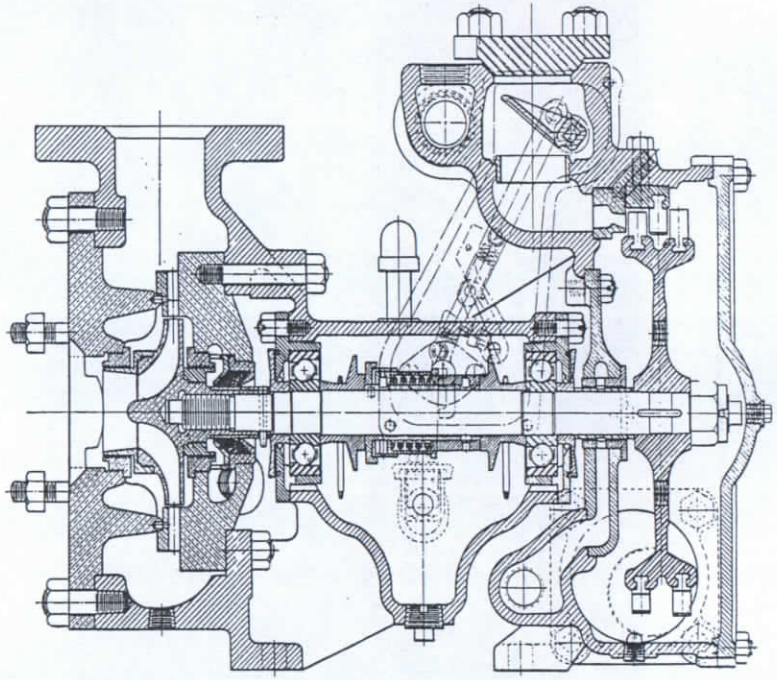

FIG. 17.12. Coffin boiler feed pump.

difference in expansion between the pumping element and the outer barrel is taken up with two elastic members. Effective cooling of stuffing boxes keeps the leakage in liquid form rather than steam.

Figure 17.14 shows a double-case boiler feed pump with inner casing horizontally split, and is of double-volute design, two halves of the casing being identical. Having two outlets from the inner casing tends to equalize the temperature of the outer barrel and to minimize the distortion. The axial thrust is balanced by arranging impellers in two opposing groups. There is a Kingsbury thrust bearing to carry any residual thrust. The stage arrangement from right to left is 1–7–8–9–10–6–5–4–3–2. There are two high pressure breakdowns with six- and four-stage pressure across them. Both stuffing boxes are provided with

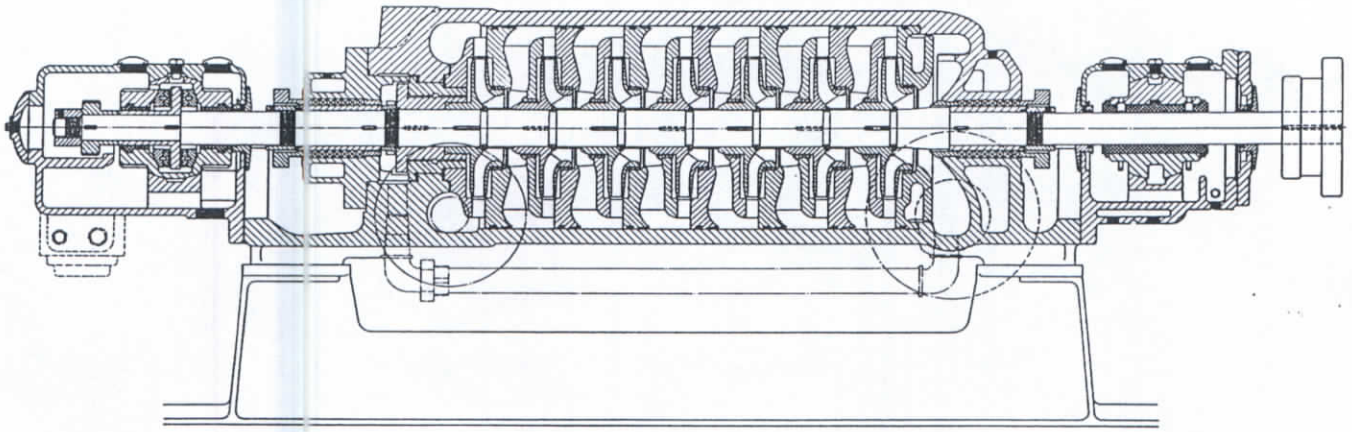

FIG. 17.9. Ingersoll-Rand boiler feed pump for pressures up to 1200 psi.

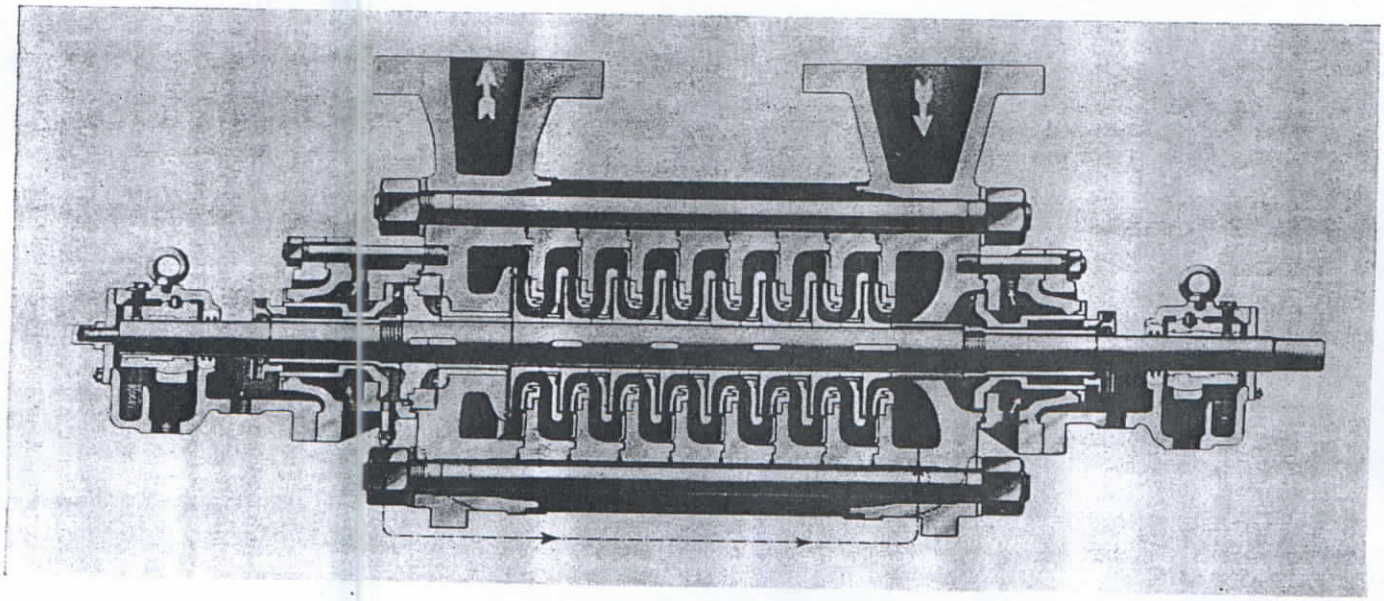

FIG. 17.10. Klein, Schanzlin & Becker high pressure boiler feed pump.

where h_2 is enthalpy of water at pump discharge conditions.
h_1 is enthalpy at suction conditions.
w is power input per pound of water pumped equal to brake horsepower $\times$ 2545/W, where W is the rate of flow in pounds per hour.
q is heat loss from the system through radiation, bearing, and external seal losses.

The last term q usually is very small in comparison with the brake horsepower and can be omitted. Add the enthalpy rise thus obtained to the inlet enthalpy to get h_2. The inlet enthalpy can be read off from Ellenwood and Mackey charts (plate B, p. 24).* For the value of h_2 and known discharge pressure, the discharge temperature T_2 can be read off from the chart. At the same time specific volume (and hence water density) of water at discharge conditions is obtained. This should be used for an accurate calculation of the pump total head in feet for a known pressure when testing the pump on hot water. If this change in density is neglected the head-capacity curve approaching shut-off may show a slight droop, although the true head-capacity curve as tested on cold water is steadily rising toward zero capacity.

If the governing devices are actuated by the boiler feed pump discharge pressure (in pounds), to be effective such controls require a steadily rising discharge pressure curve. Herein lies the justification of the requirements to have a shut-off head *not less* than a certain fixed value (115 per cent of the rated head according to U. S. Navy specifications). When there is a booster pump ahead of the boiler feed pump the above considerations apply to their combined discharge pressure. At and near the rated capacity, water compressibility under discharge pressure and water expansion due to internal heat addition very nearly compensate each other and, as a result, there is hardly any change in specific volume of water from inlet to discharge conditions.

(e) Selection of Materials. This selection is governed by the following factors: pressure, temperature, water treatment, and cost of material. Figure 17.8(*a*) shows materials for boiler feed pumps in terms of pressure and temperature alone. Final selection depends on the nature of the boiler feed water. Figure 17.8(*b*) gives material selections based on *p*H values of boiler feed water.[7] When feed water is pure condensate, the *p*H value does not accurately describe the corrosiveness of water, and corrosion-resisting materials (stainless steel) should be used.[8]

* Frank O. Ellenwood and Charles O. Mackey, *Thermodynamic Charts*, New York, John Wiley and Sons, 1944.

Although the speed of 60-cycle motor-driven boiler feed pumps is limited to 3600 rpm, steam-turbine-driven pumps in smaller sizes are operated at speeds up to 7500 rpm. Higher speeds permit the use of

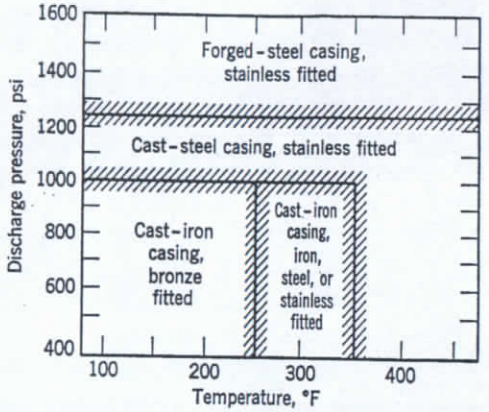

FIG. 17.8(*a*). Boiler feed pump materials in terms of pressure and temperature.

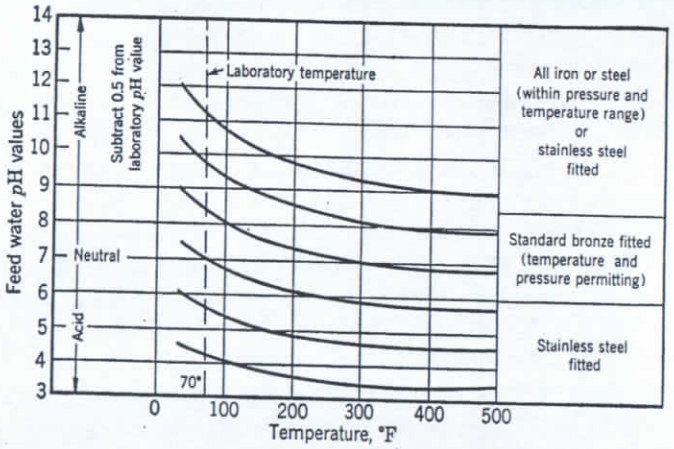

FIG. 17.8(*b*). Boiler feed pump materials based on *p*H values of feed water (Karassik [7]).

centrifugal boiler feed pumps for low capacities and high heads because the resulting specific speed produces more efficient types than those possible at 3600 rpm.

Figure 17.9 shows an Ingersoll-Rand boiler feed pump for pressures up to 1200 psi. The outer casing shell is horizontally split, permitting removal of the complete pumping element. Interstage sealing is by

Figure 17.7 shows an interstage bushing of a boiler feed pump. The bore of the bushing was scored and discoloration indicated high local temperatures. Although the body of the bushing could not expand under heat, being closely fitted into the stage piece, the bushing flange was free to expand. As a result the flange was sheared off from the bushing body. The effect is the same as if the cold body of the bushing were compressed uniformly beyond the elastic limit until it sheared off from the flange.

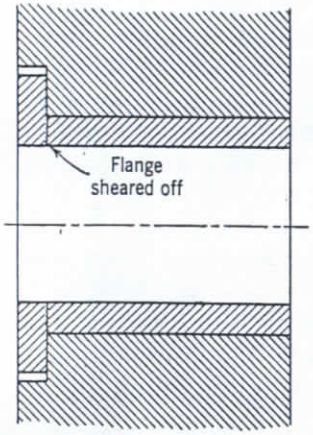

FIG. 17.7. Bushing failure due to thermal stresses.

It can be stated that modern hot-oil centrifugal pumps are just as simple, efficient, and reliable as cold-water pumps. Their higher cost is governed by special materials and the design necessary to meet the service requirements of the refinery.

17.2 BOILER FEED PUMPS

(*a*) **Requirements.** Application of centrifugal pumps to boiler feed service presented a number of problems not encountered in any other field of application involving high pressure and high temperature pumps. These may be listed as follows:

1. Requirement of a stable head-capacity characteristic throughout the whole range of capacities. (See discussion in Chapter 14.)
2. The NPSH requirements are in excess of those given by the cavitation constant σ to prevent vapor binding as a result of sudden reduction of electric load, or sudden increase of pump capacity.
3. Protection against overheating when operating at zero or low capacities.
4. Material selection to suit the feed water composition to assure normal life of pump parts.

Hydraulic and mechanical problems connected with high pressures and temperatures are not different from those of hot-oil charging pumps described above.

(*b*) **Minimum NPSH.** In Chapter 12 it has been shown that the NPSH above the vapor pressure does not depend on the temperature or pressure of the liquid if the liquid is in the boiling state. However, in boiler feed service it has been found by experience that there is a

danger of flashing in the pump suction whenever the load on the steam turbine is dropped suddenly. The sequence of events in this case is as follows. As the electric load on the generator is reduced, the steam turbine tends to speed up. The constant speed controls act to throttle the steam supply to the steam turbine; as a result the pressure drops in all stages of the steam turbine, including the stage feeding steam to the direct contact heater. The water in the storage space of the heater and suction piping is then at a higher temperature than that corresponding to the reduced pressure, and violent vaporization of the water will take place until the pressure-temperature equilibrium is established. A sudden "dynamic" pressure drop may occur in the suction pipe when the throttle on the discharge pipe is opened suddenly. This action requires that the mass of water in all piping be accelerated in a short interval of time. The pressure differential in the suction line may not provide sufficient force to accelerate the liquid in the suction line as rapidly as that of the discharge system, and a severe pressure drop results.[4,5]

The Hydraulic Institute Standards give NPSH recommendations in terms of pump capacity and speed for water at 212°F; see Charts BF–11 and 12.[6] The additional suction head required for water of higher temperature is given in Chart BF–17.[6] These values do not represent absolute minimum values of NPSH fixed by the pump design, but are safe values derived from successful practice in power plant design.

(*c*) **Minimum Flow.** In order to protect boiler feed pumps from overheating (vapor binding and scoring may follow) when the capacity is reduced below a safe limit, provision is made to by-pass a small portion of the pump capacity back to the water heater. The amount of water by-passed varies from 5 to 10 per cent of the normal capacity. The minimum volume of water to be by-passed is determined by the NPSH available on the pump suction, which determines the permissible water temperature rise. If this limit is exceeded, flashing will take place at the throttling surfaces of balancing devices. Such by-passes are either operated manually or automatically from the feed water flowmeter. In some cases they are left open continuously. The leak-off from the balancing devices can be used as a portion of by-passed capacity; in every case the leak-off is piped to the heater storage space rather than to the pump suction.

(*d*) **Temperature Rise.** To calculate the temperature rise for any rate of flow the following procedure is outlined:

The enthalpy rise of the boiler feed water from suction to discharge is found from the enthalpy equation which holds for liquids as well as for gases.

$$h_2 - h_1 = w - q$$

perature difference and, hence, the casing distorts if special means are not provided to prevent it.

There are several ways to eliminate or reduce casing distortion:

1. Hot oil is circulated through the casing of a spare pump to keep it ready for starting on hot oil in case of an emergency.
2. Oil circulation is provided through the bottom of the barrel during the starting period, even when starting on cold oil, by means of by-passes from the bottom of the barrel to the pump suction.
3. The discharge from the inner casing is divided so that one half of it is directed upward and the other half downward.
4. The pump casing is well insulated to reduce and equalize loss of heat from the outer casing to the atmosphere.

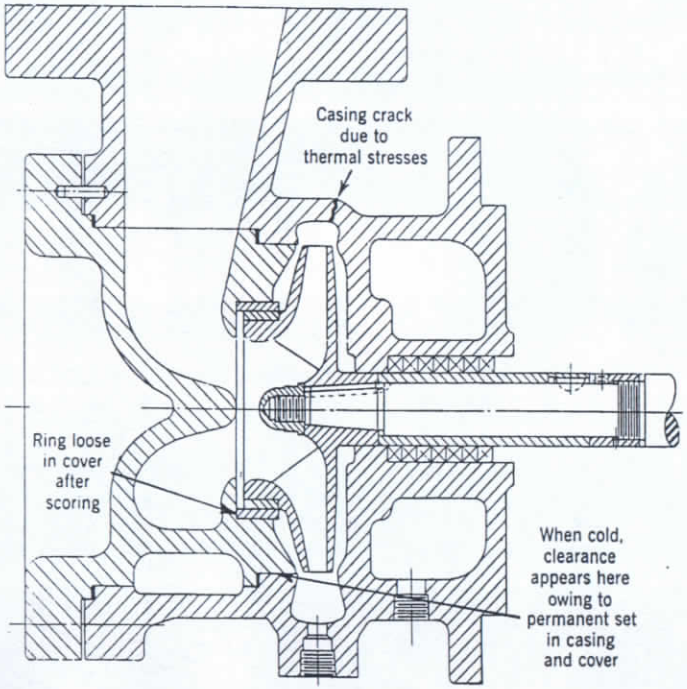

FIG. 17.5. Effect of temperature difference inside and outside of pump.

Evidently heat distortion imposes a severe strain on a pump shaft and bearings and usually results in permanent damage. A self-aligning radial bearing reduces the chances for shaft damage under such conditions.

Still another example damaging a pump mechanically will be presented.[3] The cause in this case may affect even sm all single-stag pumps; it lies in the temperature difference between the internal parts and the outside casing when the latter is not insulated. Figure 17.5 shows a single-stage, hot-oil pump with a vertically split casing sealed with a circular confined gasket. The diaphragm separating the suction chamber from the discharge casing is closely fitted into the casing. In a pump of this type, when oils are being pumped at a temperature of about 800°F with the casing uninsulated, the temperature of the diaphragm will be equal to that of the hot oil, and that of the casing will be several hundred degrees lower. The expansion of the diaphragm, being restricted by the cooler casing, may result in compression of the diaphragm and tension in the casing beyond the elastic limit, and both will receive a permanent deformation. When cold, the diaphragm will be loose in the casing. If the joint between the volute casing and suction chamber is made without a gasket (metal-to-metal fit), loss of capacity will result when the pump is operated at a temperature lower than the maximum to which the casing was subjected. The magnitude of stresses developed under such conditions can be judged by the fact that steel casings made from perfectly sound steel castings of normal wall thickness were found cracked under such conditions.

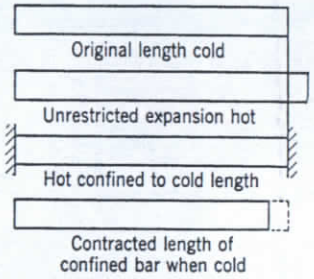

FIG. 17.6. Steel bar crushed by restricted heat expansion.

Calculations show that if a steel bar is heated and its expansion is prevented by an outside force a temperature of only 100°F is required for the bar to reach its elastic limit of 50,000 per square inch. If heating is continued the bar will get a permanent deformation and will be crushed (Fig. 17.6). Upon cooling, the bar will contract in a regular manner but will be shorter than it was originally. This is independent of bar section or length.

These examples emphasize again the importance of insulation on hot-oil pumps, not to conserve heat but to assure satisfactory mechanical operation of the pump.

It is well to mention here that scored casing wearing rings of pumps handling cold liquids are frequently found loose in the casing although they were originally tightly fitted. The reason for this is that the ring is subjected to heat expansion from the heat generated by rubbing or scoring and, since the ring is held in a confined space, it receives a permanent set in a manner similar to that of the diaphragm described in the preceding example.

of heat absorption by different parts of the casing during the starting period and a difference in the heat dissipation when thermal equilibrium of all the pump parts is reached.

Water cooling of the pump bases or supporting pedestals, as used on the early pumps, can do more harm than good under certain conditions, as the following considerations show. Without water cooling, the pedestals are seldom hotter than 120° to 140°F. Motors and most steam turbines are bottom-mounted, and their frames reach about the same temperature as the pump pedestals. Steam turbines, even when center-mounted, are never provided with water-cooled supports. Thus it is evident that

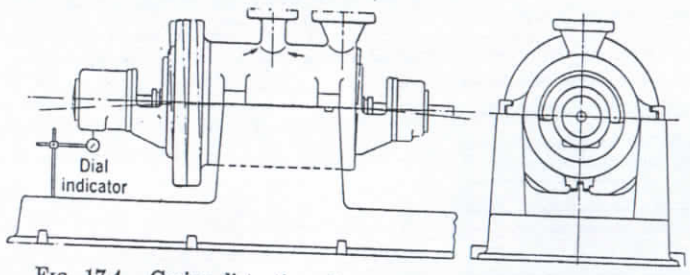

FIG. 17.4. Casing distortion when starting cold pump on hot oil.

if the pump and the driver are aligned when cold they will maintain the alignment better without water cooling of the pump supports.

Uneven heat expansion of the pump casing is the most serious cause of mechanical failures. This is more pronounced in large multistage pumps of the double-case type, such as used for charging service (Fig. 17.4). If the pump is put on stream cold when starting a run and is brought up to temperature gradually during several hours, there is sufficient time for all parts to reach the same temperature, and no casing distortion results. However, if hot oil is charged to the pump suddenly, the various pump parts do not reach the same temperature at the same time. Usually, the upper part of the outer casing reaches its highest temperature an hour or more before the bottom. This is because both the suction and discharge nozzles, which carry hot liquid, are on top, whereas at the bottom there are dead spaces filled with cold oil (between the inner and outer pump casings). Under these circumstances the pump casing is distorted as shown in Fig. 17.4. The amount of distortion actually observed on a pump with a bearing span of 80 in. was in excess of $\frac{3}{16}$ in. This was measured with a dial indicator at the outboard bearing. Calculations indicate a difference in temperature, between the top and the bottom of the outer casing, of about 350°F. Even after thermal equilibrium is reached there is an appreciable tem-

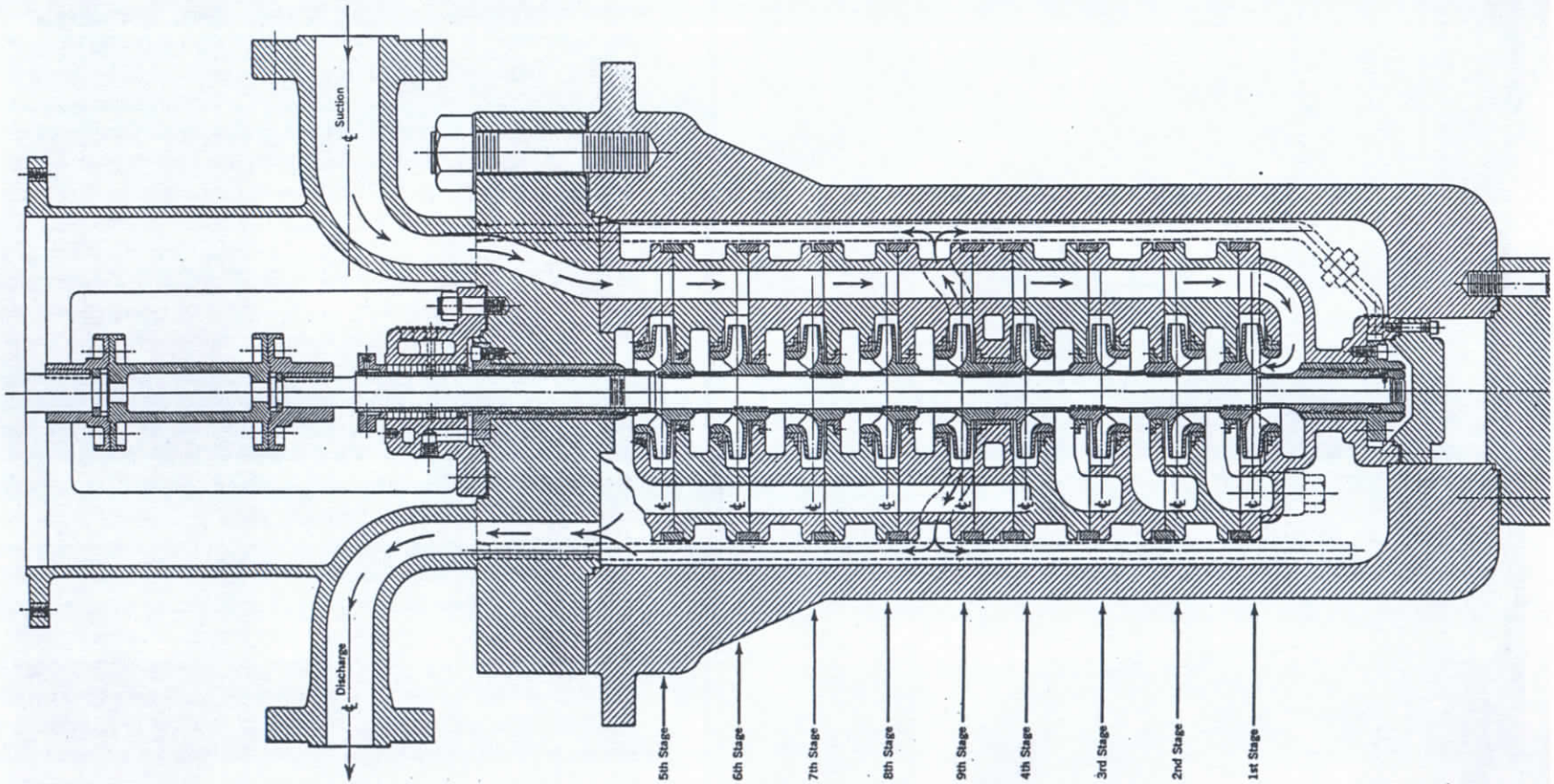

Fig. 17.3. Vertical multistage pump (United Centrifugal Pumps).

tion is still used on the small capacity, high head pumps having a great number of stages. In these, the pumping element is enclosed in a barrel, under full discharge pressure, which is mounted below the floor level (Fig. 17.3).

The inner casing is made up of one-stage sections and can be assembled in any number of stages. Stages can be added or removed if the head requirements change. To obtain a complete balance of radial forces on the rotating element, adjacent stages are turned through 180°. Axial balance is obtained by dividing the total number of stages into two groups, the impellers of each group facing in opposite directions. The number of stages in each group may or may not be equal.

The problem of corrosion is most effectively taken care of by using special materials which will resist the corrosive action of chemicals carried by the pumped oil. The practice of lining pump barrels with stainless-steel sheets or bars, and use of stainless welding, has been used to a limited extent. In all other cases a corrosion allowance is made for the decrease of metal thickness to assure the required years of service. For the majority of pumps (single-stage and two-stage) this allowance requires no excess of metal thickness over that necessary to obtain a satisfactory steel casting.

The heat expansion of pump parts can affect the mechanical performance of the pump in several ways:

1. If the parts of the rotating element are of different materials than the pump casing, the running clearances may be reduced below a safe minimum owing to a difference in the coefficients of expansion and a difference in temperature.

2. Such parts as shaft sleeves, impeller rings, and casing wearing rings, which are tightly fitted when cold, may become loose when hot owing to a difference in temperature or coefficient of expansion. For example, *if the impeller expands more than the impeller wearing ring, the latter may be stretched beyond the elastic limit when hot, and become loose on the impeller when cold; also, if the casing wearing ring expands more than the casing, the ring may be compressed beyond the elastic limit when hot, and become loose in the casing when cold.* In both cases the running clearance is reduced below the original when the pump is cold.

3. The rotating element, in perfect alignment when cold, may get out of alignment when the casing is hot owing to heat distortion of the casing. To prevent misalignment the pump casings are supported near the center plane of the rotating element and are keyed to the baseplate in the vertical central plane (Fig. 17.4). *However, this is not sufficient to assure freedom from casing distortion caused by a difference in the rate*

are used with injection of suitable oil for cooling and lubricating the sealing elements.

In order to withstand high pressures at high temperatures, hot-oil casings are designed so that the case openings have circular confined gaskets. Figure 17.1 shows the design of a single-stage pump. The spacer-type coupling used with this construction permits removal of

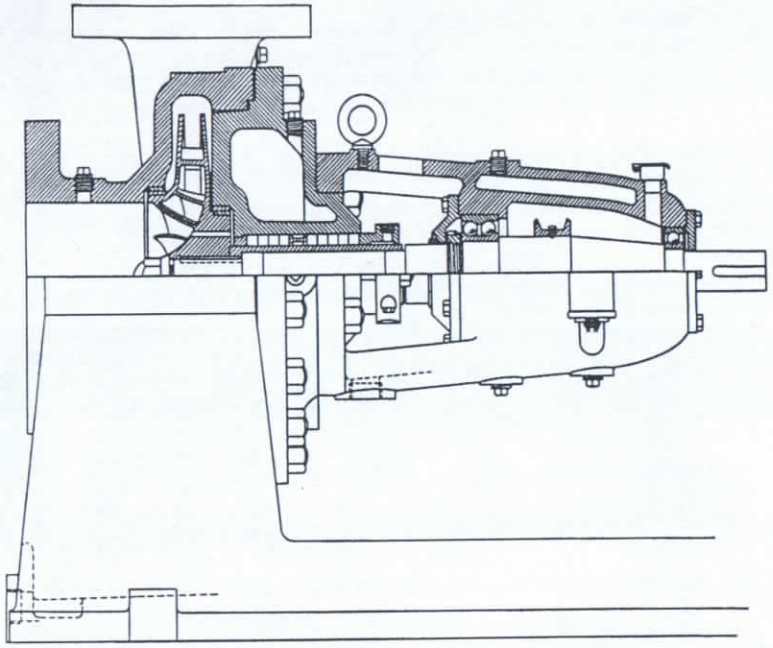

FIG. 17.1. Single-stage hot-oil pump (Wilson-Snyder).

the rotating element, including the ball bearing bracket, without disturbing the piping or alignment of the units. Pumps with more than two stages are designed with an internal casing placed inside a cylindrical shell having one or two end covers (Fig. 17.2). The inner casing is split vertically or horizontally and is under compression because of full discharge pressure existing between the shell and the inner casing. The design of the outer shell is made in the same manner as that for any unfired pressure vessel, except that the stresses are kept low because any deflection of the casing affects the alignment of the rotating element with respect to the stationary parts. As a rule, the pump casing carries the bearing supports; thus any distortion of the outer shell is reflected in the location of the rotating element. Pumps having independent bearing supports proved impractical. The vertical construc-

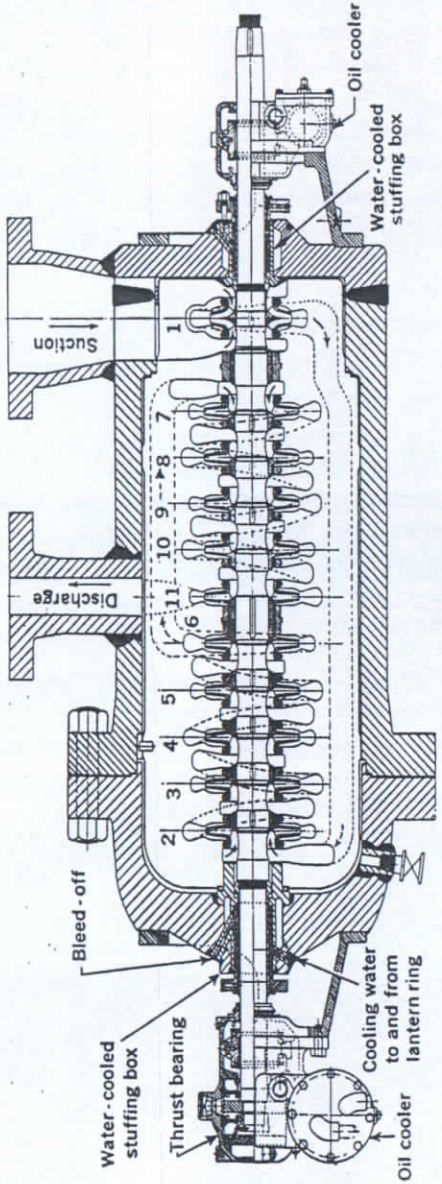

FIG. 17.2. Byron Jackson hot-oil charging pump.

vibration when operated without governing of the pump discharge; (4) better gross efficiency resulting from a better hydraulic type with less head per stage. As a rule all horizontal pumps are selected oversize because of a limited available submergence.

Vertical turbine condensate pumps with proper materials and stuffing box arrangement are widely used for pumping petroleum distillates at high temperatures. In Art. 19.5(*b*) it has been pointed out that when water-hammer shocks are expected (petroleum products loading stations), the open impeller construction of vertical turbine condensate pumps proved to be mechanically unsatisfactory.

REFERENCES

1. *Univ. of Calif. Tech. Memo.* VI, HP-14, 1940.
2. S. Logan Kerr and Stanley Moyer, "Hydraulic Engineering Problems at Southwark Generating Stations," *Trans. A.S.M.E.*, Vol. 64, No. 6, p. 539, August 1942.
3. J. W. McNulty, "Propeller-Type Pump Shows High Efficiency," *Power*, p. 63, Jan. 13, 1931.
4. Richard W. Allen, "Some Experiences of the Use of Scale Models in General Engineering," *Engineering*, Sept. 9, 1938.
5. M. Medici, "Versuche an Propeller- und Kaplanpumpen," *Z. Ver. deut. Ing.*, Vol. 87, No. 21/22, p. 331, May 29, 1943.
6. Floyd A. Nagler, "Hydraulic Tests of Flap Valves on Drainage Pipe Outlets," *Eng. News-Record*, Vol. 91, No. 26.
7. W. H. Iversen, "Studies of Submergence Requirements of High-Specific-Speed Pumps," *Trans. A.S.M.E.*, Vol. 75, No. 4, May 1953. Discussion by A. J. Stepanoff, p. 639.
8. G. A. Wauchope, "The Design of Large Pumping Installations for Low and Medium Heads," *Proc. Inst. Mech. Eng.*, Vol. 165, 1951. Discussion by A. J. Stepanoff, p. 250.
9. *Standards of the National Association of Vertical Turbine Pump Manufacturers*, Los Angeles, 1948.
10. L. N. Reeve and J. D. Scoville, "Adjustable-Blade Axial-Flow Pumps for Circulating Water," *Combustion*, pp. 30–37, May 1943.
11. J. D. Scoville, "Comparative Characteristics of Fixed and Adjustable-Blade Axial-Flow Pumps," *Trans. A.S.M.E.*, Vol. 64, No. 6, pp. 599–605, August 1942.
12. J. Zaba, "Characteristics of the Submersible Electric Pumps," *Oil Gas J.*, June 3, 1944.
13. C. Pfleiderer, "Der Entwicklungsstand der Tauchpumpen," *Z. Ver. deut. Ing.*, Vol. 80, No. 9, pp. 253–256, Feb. 29, 1936.
14. A. I. Ponomareff, "Axial Flow Compressor for Gas Turbines," *Trans. A.S.M.E.*, Vol. 70, No. 4, p. 299, May 1948.
15. "Specifications for Deep-Well Vertical Turbine Pumps," *ASA Standard B-58.1*, New York, American Standards Association, 1955.

Chapter 17

Special Problems and Applications of Centrifugal Pumps

17.1 HOT-OIL PUMPS

The application of centrifugal pumps to the pumping of petroleum oils under high pressures and temperatures presented several very difficult problems, some of which took many years to solve. The development of modern hot-oil pumps depended on a satisfactory solution of the following problems:

1. A suitable stuffing box design capable of sealing such pumps operating at high rotative speeds with minimum attention and maximum packing life.
2. The selection of materials to withstand high pressures, temperatures, and the corrosive action of petroleum oils.
3. A suitable mechanical design to counteract uneven heat absorption and radiation by the pump casing and to prevent seizure and scoring of internal parts.

Experience has shown that good metallic packing, hard rustless shaft sleeves, and freedom from vibration are the prerequisites for successful stuffing box operation. Water-jacketing of the stuffing boxes is universal on hot-oil pumps.

The application of centrifugal pumps to the pumping of light hydrocarbons presented somewhat different stuffing box problems. In this case, the liquid is cold while the stuffing box pressures are high, and the liquid flashes into gas at atmospheric pressure; thus, it is impossible to lubricate stuffing boxes with the pumped liquid. In most cases, the stuffing boxes are sealed with a heavier oil at a pressure slightly above the vapor pressure of the pumped liquid. In many cases, the stuffing boxes are heated through the jackets to counterbalance the refrigerating effect of the escaping gas.

In recent years mechanical seals have been used successfully for sealing high pressure stuffing boxes up to 600 psi and at temperatures above 350°F.[1,2] For higher pressures and temperatures double seals

let pipe has a marked effect on the pump performance at partial capacity. Thus, if a baffle is installed in the suction pipe to prevent liquid spinning in the impeller approach, the shut-off head and brake horsepower will increase, approaching those of a normal pump with a vaned diffuser casing.

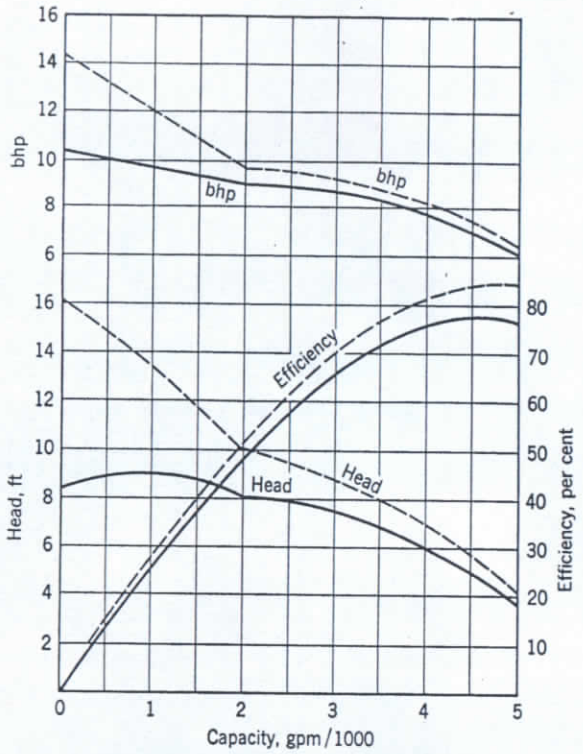

FIG. 16.21. Performance of 14-in. elbow-type axial flow pump, 690 rpm; dotted line, axial pump with a vaned diffuser casing.

Figure 16.22 shows a vertical turbine pump arranged for condensate pumping. The pump is mounted as close as possible to the discharge head, and the pumping element proper is placed in a barrel which is long enough to provide the necessary submergence for normal operation at the rated capacity. Placing the pump barrel in the basement floor hole does not complicate the construction problem; on the contrary it permits bringing the basement floor closer to the condenser hot-well, thus reducing the size of the building. The hydraulic advantages of the vertical turbine condensate pumps can be summarized as follows: (1) freedom from cavitation at the rated capacity; (2) minimum adverse effects from cavitation at reduced rates of flow; (3) no excess axial thrust, noise, or

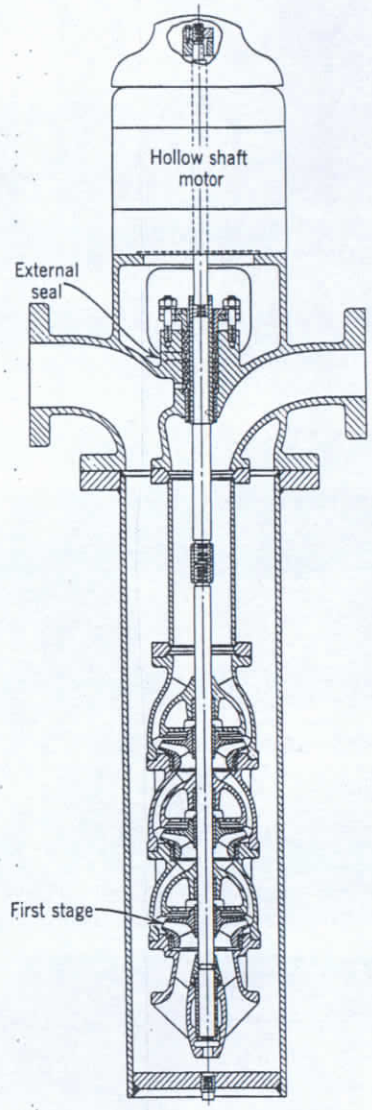

FIG. 16.22. Vertical multistage condensate pumps of the turbine type (Ingersoll-Rand).

Figure 16.20 shows an axial flow propeller pump in its simplest form. The pump casing is no more than a discharge elbow, with no diffusion vanes. This type of pump in sizes up to 24 in. is also used for brine

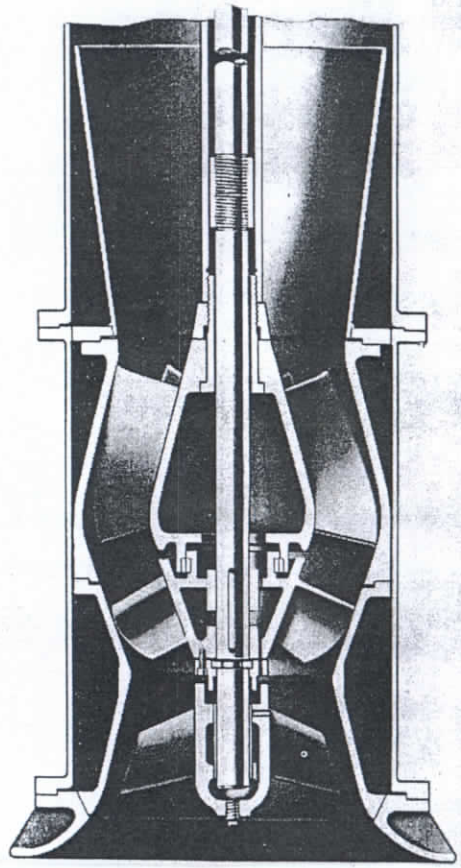

FIG. 16.18. Detail of the pumping element from Fig. 16.17.

circulation in chemical processes at total heads as low as 3 ft. In view of the low power involved, efficiency is secondary to mechanical simplicity. Figure 16.21 shows a typical performance curve. The dotted curve shows the performance of an axial flow pump with vaned diffuser. Note the reduction of head and brake horsepower at partial capacities caused by the fact that in an elbow-type axial flow pump liquid rotation is not prevented by the pump casing. In this respect the shape of the in-

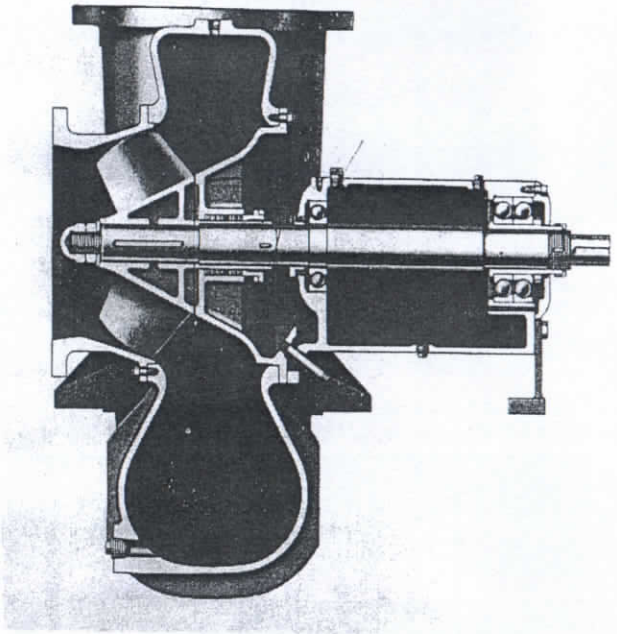

FIG. 16.19. Horizontal volute propeller pump (Ingersoll-Rand).

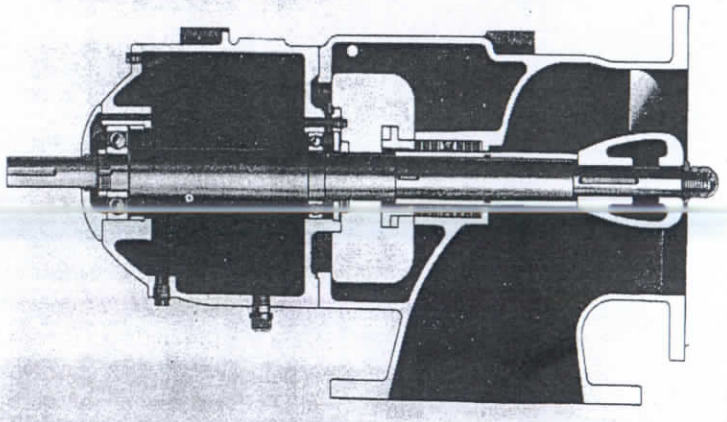

FIG. 16.20. Axial flow pump of the propeller type (Ingersoll-Rand).